Evaluation Of Prestressed Concrete Beams In Shear

MDOT ORBP Reference Number: OR10-040

FINAL REPORT

September 30, 2014

Prepared For:

Michigan Department of Transportation
Research Administration
8885 Ricks Rd.
P.O. Box 30049
Lansing MI 48909

Prepared By:

Wayne State University
5050 Anthony Wayne Drive
Detroit, MI 48202

Authors:

Christopher D. Eamon
Gustavo Parra-Montesinos
Alaa Chehab

MDOT Research Advisory Panel:

Sudhakar Kulkarni
Steve Kahl
Michael Townley
Rebecca Curtis
Creightyn McMunn
Christal Larkins
Raja Jildeh
Jose Garcia

1. Report No. RC-1615	**2. Government Accession No.** N/A	**3. MDOT Project Manager** Sudhaka Kulkarni
4. Title and Subtitle Evaluation of Prestressed Concrete Beams in Shear		**5. Report Date** 9/30/2014
		6. Performing Organization Code N/A
7. Author(s) Christopher D. Eamon, Gustavo Parra-Montesinos, and Alaa Chehab		**8. Performing Org. Report No.** N/A
9. Performing Organization Name and Address Wayne State University Dept. of Civil and Environmental Engineering 5050 Anthony Wayne Drive Detroit, Michigan 48202		**10. Work Unit No. (TRAIS)** N/A
		11. Contract No. 2010-0298
		11(a). Authorization No. Z5
12. Sponsoring Agency Name and Address Michigan Department of Transportation Research Administration 8885 Ricks Rd. P.O. Box 30049 Lansing MI 48909		**13. Type of Report & Period Covered** Final Report 10/1/2011 to 9/30/2014
		14. Sponsoring Agency Code N/A
15. Supplementary Notes		

16. Abstract

This research investigates possible design-related causes of apparent shear cracks on MDOT prestressed concrete (PC) bridge girders; assesses the adequacy of PC shear design and rating methods; and recommends changes to these procedures. It involved a field survey, laboratory testing, FEA modeling, and bridge field testing. The field survey included sixteen PC bridges with potential shear cracks, and the shear capacities of the girders were analyzed and compared to various shear load demands. The laboratory testing consisted of six tests on full-scale beam specimens of different shear span-to-depth ratios and stirrup spacings. An FEA model was developed and validated using the experimental data. Using the model, a parametric analysis was conducted on a variety of PC bridge girder configurations. A regression analysis was performed to modify existing shear capacity procedures to best-fit the FEA results. Field tests of two PC bridges constructed continuous for live load were conducted to determine interior joint continuity and girder distribution factors.

17. Key Words Bridges, Prestressed Concrete, Beams, Shear, Finite Element Analysis, Field Testing	**18. Distribution Statement** No restrictions. This document is available to the public through the Michigan Department of Transportation.

19. Security Classification - report	**20. Security Classification - page**	**21. No. of Pages**	**22. Price**
Unclassified	Unclassified	324	N/A

DISCLAIMER

This publication is disseminated in the interest of information exchange. The Michigan Department of Transportation (hereinafter referred to as MDOT) expressly disclaims any liability, of any kind, or for any reason, that might otherwise arise out of any use of this publication or the information or data provided in the publication. MDOT further disclaims any responsibility for typographical errors or accuracy of the information provided or contained within this information. MDOT makes no warranties or representations whatsoever regarding the quality, content, completeness, suitability, adequacy, sequence, accuracy or timeliness of the information and data provided, or that the contents represent standards, specifications, or regulations.

TABLE OF CONTENTS

LIST OF TABLES

LIST OF FIGURES

ACKNOWLEDGEMENTS

The authors would like to thank several students at WSU and the University of Michigan for their help on this project. In particular, we greatly appreciate the assistance of Thai Dam; Alexander Lamb; Kapil Patki; Vahid Kamjoo; Emira Rista; and Hadi Salehi.

EXECUTIVE SUMMARY

The primary objectives of this research were to investigate possible design-related causes of apparent shear cracks on MDOT prestressed concrete (PC) bridge girders; to assess the adequacy of PC shear design and rating methods; and to recommend changes to these procedures if necessary. The project began with a thorough investigation of the design and rating methods that were used for the PC bridge girders found to have potential shear distress. In particular, the AASHTO Standard Code, the AASHTO LRFD Code, and the 1979 AASHTO Interim Specifications, as well as the supporting technical literature, as summarized in Chapter 2.

The next stage of the project involved a field survey of PC bridge girders that were identified in previous inspection reports to have shear cracks. Sixteen such MDOT PC bridges in southeast Michigan were visited and studied, and the girders on eight of these structures were found to have possible shear cracks. The shear capacities of the girders on the 16 bridges were analyzed according to the 2002 Standard, 2010 LRFD, and 1979 Interim AASHTO provisions, and compared to various shear load demands. It was found that shear load/capacity ratios, the code method used to design the girders, as well as various other bridge girder characteristics could not be clearly linked to cracked girders in all cases. However, a weak pattern emerged in which cracked girders tended to be associated with longer spans, larger girders, and higher average prestress stresses. Also, no structures with end blocks were observed to have cracking. Of the methods considered, it was found that the best predictor of cracking was the ratio of $V_n/V2$, with V_n found from the 1979 Interim Specifications and $V2$ the shear force due to a unfactored HS20 truck and dead load only. In light of these findings, of the methods studied, the method used to design or analyze the girder does not appear to be a primary factor contributing to potential shear cracking.

A major portion of the research involved the laboratory testing of two full-scale beam specimens. The purpose of the testing was to gather reliable experimental data that could be used to validate numerical (finite element analysis; FEA) models to be used later in the project. Each girder was tested three times in different regions of the span by adjusting support locations, to generate data for different critical shear span-to-depth ratios and stirrup spacings. For each beam, the portion of the span which was to be preserved for subsequent testing was externally clamped with steel bars to prevent any significant damage in this region during the first two tests. Beams had stirrup spacings from 8-12 in and shear span/depth ratios from 2.0 to 3.5.

Once the test beam data were available, FEA models were constructed and validated. The developed FEA models could well-match the majority of the test beam results as well as the three PC beam shear tests found in the technical literature that were chosen for validation. Using the validated FEA modeling technique, a parametric analysis was then conducted on a variety of PC bridge girder configurations relevant to MDOT design practice. Varied parameters included beam type; load position; strand profile; concrete strength; prestress level; stirrup spacing; and

longitudinal steel reinforcement ratio, for a total of 414 analyses. The analyses revealed that, of the three code procedures considered (AASHTO LRFD, 1979 Interim, and AASHTO Standard), the AASHTO Standard code could best predict the FEA results of shear capacity in terms of accuracy as well as consistency. It was also found that it was not possible to fail the analysis beams in shear prior to a moment failure using the vehicle configurations considered.

A regression analysis was then performed to modify the LRFD and Standard shear capacity procedures to best-fit the FEA results. For both procedures, adjustment functions were developed with girder concrete compressive strength, average stress due to prestress force, stirrups spacing, and beam height as input variables. Application of the adjustment expressions resulted in significant improvement in the predictive capability of the code procedures for the shear capacities found in the FEA analysis. Therefore, to best estimate the shear capacity of MDOT PC girders within the range of beam parameters considered in this study, it is recommended that the developed linear regression function is used in conjunction with the modified AASHTO LRFD procedure as described in this document. Alternatively, a significantly simpler procedure can be obtained from using the Standard Code and its associated adjustment expression with only a minor loss of accuracy. If further verification of girder shear capacity is desired, it is recommended that a field load test, in the form of a monitoring or proof load test, is considered. Several existing MDOT reports detail the field load testing of bridges.

Based on the results of the field study, associated analysis, and FEA modeling, it appears highly unlikely that any diagonal cracks observed on the field study bridges were due to live load overloads. Consequently, it does not appear that the presence of these cracks, which were observed to be relatively tight where aggregate interlock is preserved, poses significant concern for significant loss of shear capacity. It is thus recommended that cracks are monitored and repaired if necessary to prevent penetration of water and corrosion of reinforcing steel. Various other references are available to guide this process. If crack growth and opening continues and strength loss becomes a concern, external strengthening may be achieved with the use of fiber reinforced composite fabric, an MDOT guideline for which is currently under development.

As part of this project, field tests of two PC bridges constructed continuous for live load were conducted. The purpose of the field testing was to determine the degree of moment continuity between adjoining spans of PC bridges designed continuous for live load. This information could then be used to determine the proper assumption for joint continuity for shear analysis of these bridges. Two nearly identical bridges of this type were tested, where bridge girders were instrumented with strain gages at different locations along their spans to monitor positive and negative moment strains during the tests. Test data were recorded as two test trucks moved across each bridge. A total of 15 tests were conducted for each bridge, by varying the positions of the test vehicles. Single, side-by-side, and following vehicle configurations were included in the tests. It was found that overall girder strains as well as positive moments from the tests are best predicted in analysis using a joint stiffness approximately mid-way between a simple and fully-continuous condition. It was also found that AASHTO LRFD and Standard Code girder distribution factors were conservative for all positive moment cases considered.

From these test results, it is recommended that for the analysis of positive bridge girder moments for these types of bridges, results from a simple span and a continuous span assumption are averaged. An easier and more conservative estimation is to use the simple span moment only. It

was also found that a reasonable estimation of negative moment is to reduce that found from a continuous analysis assumption by half. For the analysis of shears, it is similarly recommended that the results from a simple span and a continuous span assumption are averaged. For end supports, a slightly conservative assumption is to assume a simple span case, while for the interior support, a slightly conservative assumption is to assume a continuous span case. A simpler alternative is to treat the spans as simple, and increase the interior support shear found from the simple span analysis by approximately 5%.

CHAPTER 1: INTRODUCTION

Statement of the Problem

In the last several decades, there have been significant changes to the AASHTO Bridge Design Specifications with regard to shear design. These changes include how the shear strength contributions attributed to the concrete and transverse steel are calculated, as well as limits on the maximum allowable shear stress. In 1983, the 12th edition of the AASHTO Standard Specifications (AASHTO 1983) presented a significantly revised shear design method for prestressed concrete (PC) bridges from that previously found in the 1979 Interim Specifications (AASHTO 1979). Revisions included a new method for calculating the concrete shear strength that explicitly accounts for web-shear cracking and flexural-shear cracking (Fig. 1.1); a change in location of the critical shear section near supports; and a reduction of 50% in the calculated shear strength contribution from the transverse reinforcement, as compared to the 1979 Interim Specifications. These 1983 shear provisions have remained unchanged up to the latest, 17th edition of the Standard Specifications, which were last published in 2002 (AASHTO 2002). A second significant change in shear design was presented in the 1st edition of the AASHTO Load and Resistance Factor Design (LRFD) Specifications, released in 1994 (AASHTO 1994). Based on the Modified Compression Field Theory (Fig. 1.2), the shear design provisions in the AASHTO LRFD Specifications are significantly more complex than those in the Standard Specifications, with major changes in calculation of the concrete shear strength contribution, horizontal projection of diagonal cracks, and maximum allowable shear stress. Although some revisions have been made, the 1994 LRFD shear design approach is essentially the same method presented in the most recent 5th edition of AASHTO LRFD, published in 2010 (AASHTO 2010).

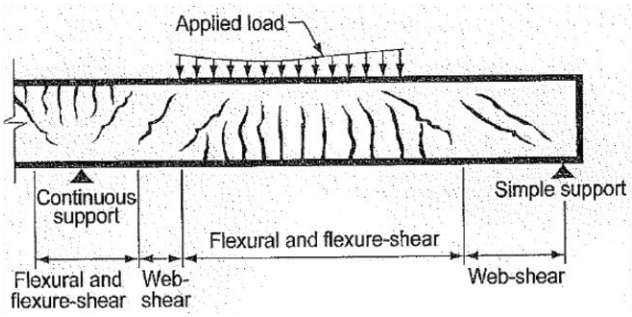

Figure 1.1. Web-Shear And Flexural-Shear Cracking (ACI 318-11).

The major differences in PC bridge shear design methods have possibly resulted in bridges that behave differently under service conditions. Correspondingly, a number of MDOT PC bridge beams have been found with potential shear cracks; these cracks may be contributed to designs under one or more of the several different AASHTO code provisions that have been used for design. This observation has led to three questions of concern: 1) are these cracks due to unacceptably high shear stresses under service conditions that may be associated with the use of one or more of the shear design procedures?; 2) are these cracks due to an under-design for shear?; and 3) how can these cracks, which may be associated with high service shear stresses and/or under-design for shear, be prevented in future PC bridges?

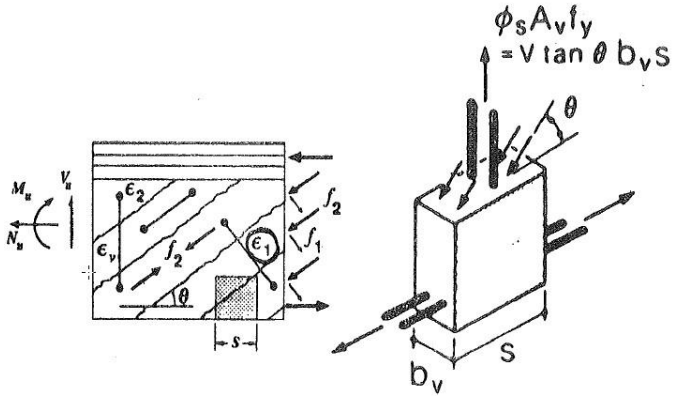

Figure 1.2. Principal Components Of Modified Compression Field Theory (Collins et al. 1996). The leftmost diagram shows a beam section with moment (M_u), shear (V_u) and axial force (N_u) load effects, with diagonal cracks in the web of width b_v at angle θ. Principal tensile and compressive stresses f_1 and f_2 are normal and parallel to the cracks, with corresponding strains are ε_1 and ε_2 and vertical strain ε_v. The rightmost diagram shows the force developed in a vertical shear reinforcement bar at yield, which is given as the area of the steel (A_v) times yield stress (f_y), or average shear stress (v) times $tan\theta b_v s$.

Since the several shear design methods that have been used by MDOT provide significantly different requirements for the amount of steel required, which could translate in significant differences in shear stress at service conditions, it is possible that the cause of possible shear cracks observed in MDOT PC girders is related to an insufficient consideration of service stresses when designing for shear. At present, the adequacy of the current MDOT shear design and evaluation procedure is not well known. As shear failures tend to be brittle, coupled with the identification of possible shear cracks on some MDOT PC bridges, a safety and/or serviceability concern may exist.

Background

Shear Resisting Mechanisms in Prestressed Concrete Beams

PC beams are known to resist shear through various mechanisms. These include aggregate interlock across diagonal cracks, shear carried in the compression zone, dowel action of the longitudinal reinforcement, transverse reinforcement, and the vertical force in draped prestressing strands. For design purposes, the first three terms are lumped into a "concrete" shear strength contribution, while the shear strength contributions from transverse reinforcement and the vertical component of the prestress force are treated separately. Determination of the latter strength component is straightforward. However, mechanisms involved in the "concrete" and transverse steel reinforcement contributions to beam shear strength are somewhat more complex.

"Concrete" Shear Strength Contribution, V_c

Shear carried through the member compression zone, aggregate interlock, and dowel action are typically lumped, for shear design purposes, into a single shear resisting component attributed to the concrete, V_c. Relative contributions from each of these three mechanisms are difficult to estimate and could vary significantly depending on the amount of longitudinal and web reinforcement provided, as well on the level of prestressing force. While some researchers (Richart 1927; Bresler and Pister 1958; Tureyen and Frosch 2003) have argued that most of the "concrete" contribution to beam shear strength is provided by shear carried in the beam

compression zone, others (for example, Vecchio and Collins 1986) have claimed that most of this shear is resisted by the member web through aggregate interlock. This is the approach typically followed when designing beams using the Modified Compression Field Theory (Vecchio and Collins 1986) and thus, this same assumption is implicit in the AASHTO LRFD General Sectional design method.

Shear Strength Contribution from Steel Transverse Reinforcement, V_s

The role of beam transverse reinforcement (e.g. stirrups) in resisting beam shear has long been explained through the use of a truss analogy (Fig. 1.3) (Ritter 1899; Mörsch 1909). Idealizing a reinforced (or prestressed) concrete beam as a truss, shear is resisted by a combination of diagonal concrete members and steel vertical members (for the case of vertical stirrups). In order to calculate the shear strength of a beam using the truss analogy, however, it is necessary to estimate the angle of inclination and compression strength of the concrete diagonal elements, as well as the strength of the steel members. In his development of the truss analogy, Mörsch (1909) assumed a 45-degree angle for the concrete diagonal elements and a failure mode governed by the steel members (i.e. a possible compression failure of diagonal concrete members was neglected).

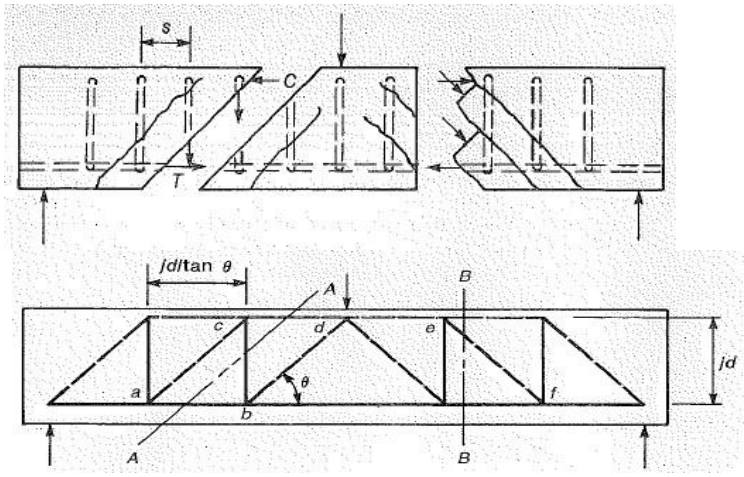

Figure 1.3. Truss Analogy (Wight and MacGregor 2012).
The cracked reinforced concrete beam is modeled as a truss with top chord as the concrete compression zone, bottom chord as longitudinal steel, web ties as vertical shear reinforcement, and diagonal struts as concrete in compression between shear cracks.

The 45-degree truss analogy has long been adopted in the ACI Building Code (2008) and the AASHTO Standard Specifications. However, in order to ensure that yielding of the steel transverse reinforcement would occur prior to either a web-crushing or a shear-compression failure, the AASHTO Standard Specifications (2002) limit the contribution of steel transverse reinforcement to beam shear strength to a stress of $8\sqrt{f_c'}$, where f'_c is the specified concrete strength in psi. Over the past several decades, the use of a truss analogy with angles shallower than 45 degrees has been explored (Ramirez and Breen 1991; Vecchio and Collins 1986). Reducing this angle implies a higher efficiency of the transverse reinforcement (as geometrically, more stirrups will cross a shear crack with a lower angle) and thus results in less shear reinforcement required for the same shear demand. While it may be argued that this

approach is more consistent with experimental observations, it is also less conservative than the 45-degree truss analogy, producing a design which may be more prone to shear distress under service conditions.

Review of Shear Design Provisions for Prestressed Concrete Bridge Girders

1979 Interim Specifications

Contrary to the AASHTO Standard and LRFD Specifications, the "concrete" contribution to shear strength V_c in the 1979 Interim Specifications was assumed to be linearly related to concrete compressive strength and was taken equal to $0.06\,f'_c$. This contribution, however, was limited to 180 psi, which in practice governed the design value of V_c for all PC girders, since this limit was reached with an f'_c of only 3000 psi. For comparison, for concrete compressive strengths of 4000 and 10000 psi, this shear stress limit corresponds to $2.8\sqrt{f_c'}$ and $1.8\sqrt{f_c'}$ (psi), respectively. In the 1979 Interim provisions for PC, the shear strength contribution of the transverse steel reinforcement is given as (Eq. 1.1):

$$V_s = 2A_v f_y \frac{jd}{s} \tag{1.1}$$

where A_v is the area of steel transverse reinforcement spaced at a distance s, f_y is the yield strength of the transverse steel reinforcement, and jd is the distance between the resultant normal tension and compression force couple in the section (i.e. truss depth). Although the angle of inclination for the diagonal elements to be used in the truss analogy was not explicitly specified, the number of layers of steel transverse reinforcement assumed to be crossed by a diagonal crack in Eq. (1.1) is effectively $2jd/s$, which leads to a truss angle of 29.1 degrees. This significantly shallower design angle compared to the typical 45-degree angle used in reinforced concrete was due to the effect of the prestressing force in PC beams, which lowers the principal compression angle. However, as will be discussed later, this beneficial effect is not accounted for in the 1983 nor the current 2002 AASHTO Standard Specifications. Other important provisions of the 1979 Interim Specifications are a minimum shear reinforcement requirement to provide a shear stress contribution of at least 100 psi, while maximum stirrup spacing was limited to ¾ of the member height. It should be noted that the 1979 Interim Specifications did not limit the maximum shear strength contribution that could be assigned to the steel transverse reinforcement. That is, no explicit provisions were provided to prevent web-crushing failures.

Another aspect of the 1979 Interim Specifications that deserves attention is the critical section used for design near the supports. In the case of simply supported beams, the shear calculated at a quarter of the span length from the support is used as the maximum shear design value; i.e. higher shear forces closer to the support are neglected.

AASHTO Standard Specifications

The shear design provisions in the 1983-2002 AASHTO Standard Specifications are based on research conducted at the University of Illinois (MacGregor 1960; MacGregor et al. 1965). In these provisions, the "concrete" shear strength is calculated as the smaller of the shear force associated with flexural shear cracking and the shear force that causes web-shear cracking. Flexural shear cracking will govern in sections with high moment and low shear, while web-

shear cracking will govern in sections subjected to high shear and low moment. In the case of flexural-shear cracking, the shear strength is calculated as the sum of the shear corresponding to flexural cracking and the shear required to turn a flexural crack such that it becomes a flexural-shear crack (Eq. 1.2):

$$V_{ci} = 0.6\sqrt{f_c}b_v d + V_d + \frac{V_i M_{cr}}{M_{\max}} \geq 1.7\sqrt{f_c}b_v d \qquad (1.2)$$

where b_v is the web width, d is the member effective depth (need not be taken less than 0.8 times the member depth, h), V_d is the shear force due to unfactored dead load, V_i is the factored shear that occurs simultaneously with the maximum factored moment at the section (M_{max}), while M_{cr} is the cracking moment due to external loads. The last term in Eq. (1.2) represents the factored shear due to external loads (in addition to dead load) that leads to flexural cracking in the section. For sections subjected to low moment, Eq. (1.2) will lead to very large shear strength values (infinity at points where M_{max}=0). In these cases, design shear strength is governed by the shear corresponding to web-shear cracking.

Shear corresponding to web-shear cracking is calculated assuming that the section is uncracked in flexure and that first diagonal cracking will develop on the member web when the principal tensile stress in the concrete, calculated including the effect of prestressing, reaches the assumed concrete tensile strength of $3.5\sqrt{f_c'}$ (psi). This shear force, combined with the vertical component of the prestressing force, V_p, is then taken as the web shear strength, V_{cw} (Eq. 1.3).

$$V_{cw} = (3.5\sqrt{f_c} + 0.3 f_{pc})b_v d + V_p \qquad (1.3)$$

where f_{pc} is the stress due to prestressing at the centroid of the cross section or at the web-flange interface when the centroid is in the flange.

In the AASHTO Standard Specifications, the shear strength provided by the steel transverse reinforcement is calculated based on the 45-degree truss analogy which, for a typical lever arm distance between the internal forces $jd = 0.9d$, represents only 56% of the steel shear strength V_s as calculated in the 1979 Interim Specifications (Eq. 1.1). Further, in order to prevent web-crushing failures, the strength provided by the steel transverse reinforcement is limited to $8\sqrt{f_c'}$ (psi). The minimum amount of transverse steel, however, is half that required in the 1979 Interim Specifications (corresponding to a minimum shear stress of 50 psi), while maximum spacing is limited to either 0.75h (or 24 in.) or 0.375h (or 12 in.), depending on the shear stress demand. Moreover, the critical section for shear in the Standard Specifications for PC girders is taken as h/2, which is substantially smaller than that in the 1979 Interim Specifications (a quarter of the span length), and correspondingly results in larger design shear forces near supports.

AASHTO LRFD Specifications

The General Sectional Method for shear design in AASHTO LRFD Specifications represents a significant departure from the traditional shear design methods applied to reinforced and prestressed concrete members in other design codes (e.g. ACI Building Code, AASHTO Standard Specifications). Based on the Modified Compression Field Theory (MCFT) developed at the University of Toronto in the late 1970s and early 1980s (Vecchio and Collins 1986), this

shear design method relies on the use of equilibrium, strain compatibility, and material constitutive relations to determine the "concrete" and steel reinforcement contributions to shear strength. In compression, the concrete behavior is assumed to "soften" (or become weaker) due to the presence of transverse tensile strains. Moreover, on average terms, concrete is assumed to carry some tension beyond cracking to account for tension stiffening (i.e. the tension carried by the concrete between cracks).

Contrary to the traditional approach of lumping the contributions from aggregate interlock, shear carried in the compression zone, and dowel action into a single term V_c, the AASHTO LRFD MCFT-based Sectional Method is based on the assumption that the entire "concrete" shear contribution is given by aggregate interlock. In this method, the web of a PC girder is idealized as a panel whose deformations are defined in terms of average strains calculated at member mid-depth. The "concrete" contribution V_c is then a function of the ability of the concrete to resist tension between cracks, defined by a factor β. This resistance depends on the average tensile strain in the concrete, and is limited by yielding of the reinforcement at the cracked section and/or the amount of shear that can be resisted through aggregate interlock along the crack. V_c is thus determined as:

$$V_c = \beta\sqrt{f_c}\, b_v d_v \tag{1.4}$$

where d_v is the effective shear depth, equivalent to jd in the 1979 Interim Specifications, and is taken as the greater of $0.9d$ and $0.72h$. The final determination of V_c is not straight forward. In order to facilitate the use of the MCFT for the shear design of PC girders, the AASHTO LRFD Specifications include tables that allow the determination of β and the principal compression angle θ based on the shear stress level, average longitudinal strain, and crack spacing. Because the longitudinal strain is a function of θ, iteration is required. Values of θ vary from approximately 25 to 45 degrees (often much less than 45 degrees), while β values range from approximately 1 to 6.5 for members with at least minimum shear reinforcement. Further, because the contribution from shear carried through the compression zone is neglected, very low values of V_c compared to those in the 1979 Interim and 1983-2002 AASHTO Standard Specifications are obtained when the strains in the steel tension reinforcement are large. This approach, therefore, encourages designers to add more longitudinal steel to reduce longitudinal strains and increase shear resistance, which may result in over-reinforced sections in flexure.

Once the principal compression angle θ is determined, the contribution from the steel transverse reinforcement is based on the truss analogy and is determined as:

$$V_s = A_v f_y \frac{d_v \cot\theta}{s} \tag{1.5}$$

Another major departure from the AASHTO Standard Specifications is the upper shear stress limit to prevent web-crushing failures. In the AASHTO LRFD Specifications, this limitation is given by:

$$V_c + V_s \le 0.25 f_c' b_v d_v \tag{1.6}$$

As will be shown in the next section, this limit is substantially higher than that in the Standard Specifications and could have important implications in the serviceability of PC bridge girders. Minimum shear reinforcement in the LRFD Specifications is required to provide a maximum shear stress equal to $\sqrt{f_c'}$ (psi), which is more conservative than the minimum shear reinforcement provision in the Standard Specifications. Finally, the location of the first critical section from the face of the support is located at a distance equal to the larger of d_v or $0.5d_v\cot\theta$, as opposed to the value of $h/2$ given in the Standard Specifications.

Comparison of Shear Design Methods: Practical Implications for Capacity and Serviceability

From the summary of the three design methods provided above, it is clear that substantial differences in the calculation of both V_c and V_s can be obtained depending on the method used. In terms of the "concrete" contribution V_c, the 1979 Interim Specifications tend to provide the lowest values, as V_c is limited to a maximum shear stress of 180 psi. For concrete strength of 4000 psi or greater, this stress limit represents less than $3\sqrt{f_c'}$ (psi), which is a low value for PC beams, particularly in regions where moment is low and shear is high, such as near the supports of simply supported beams. In these regions the "concrete" contribution to shear strength would normally be on the order of $4-5\sqrt{f_c'}$ (psi). In the AASHTO LRFD Specifications, V_c is also generally lower than that calculated in the Standard Specifications, because in LRFD, V_c is entirely based on shear resisted by the web through aggregate interlock. One exception may occur when the section mid-depth is in compression (i.e. there are compressive longitudinal strains at member mid-depth). In this case, values of V_c using the LRFD Specifications could be greater than those obtained using the Standard Specifications.

When calculating total member shear strength, the differences in calculated values of V_c for the three methods are often somewhat balanced by accompanying differences in V_s. For example, consider the 1979 Interim Specifications and the Standard Specifications. While the Interim provisions will often predict substantially lower V_c values compared to the Standard Specifications, the required area of steel for a given V_s in the Interim Specifications is nearly half that required for the same value of V_s in the Standard Specifications. The result is that unless the difference in V_c is extremely large (which could be the case near supports), the difference in the amounts of transverse steel required by these two methods is generally not significant. In the case of the LRFD Specifications, calculated values of V_c tend to be closer to those in the AASHTO Standard Specifications. An exception here is when calculated longitudinal tensile strains are large, for which the LRFD Specifications tend to assign low values to V_c, as shear carried through the member compression zone is neglected. In these cases, the calculated V_c values could be close to those obtained using the 1979 Interim Specifications. Figure 1.4 illustrates these trends and illustrates the differences in V_c and the transverse steel required for the case of a typical two-span continuous PC girder. As shown in the figure, the largest differences in the values of V_c occur near the supports, while differences in the required area of transverse steel, in general, are substantially smaller throughout the span.

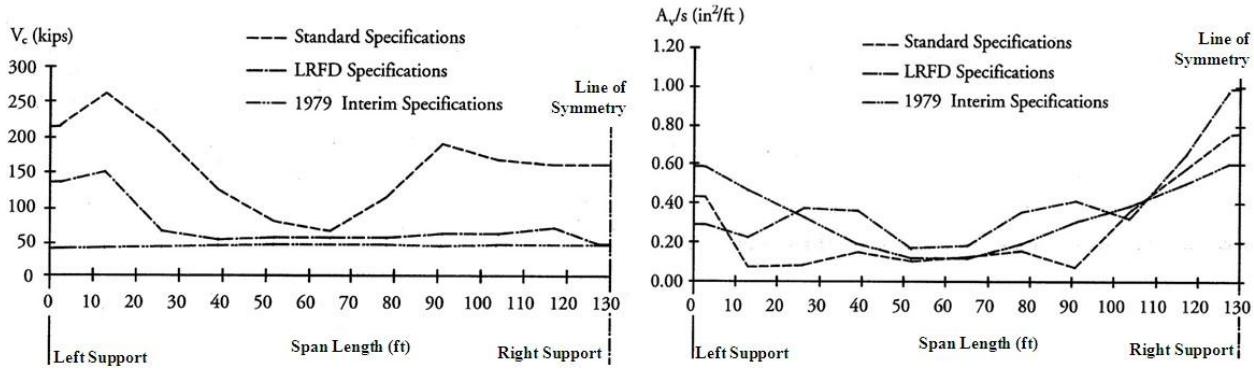

Figure 1.4. Differences In V_c And Shear Reinforcement Required (PCI Bridge Design Manual 2003). Concrete capacity V_c (left graph) and required shear stirrup steel (right graph) for a typical symmetric, two-span PC bridge made continuous over the middle support.

Another major difference between the three shear design provisions lies on the maximum shear stress limit which is set in order to prevent web-crushing failures. The 1979 Interim Specifications do not include an upper stress limit, while the Standard Specifications limit the shear strength contribution from the steel reinforcement to $8\sqrt{f_c'}$ (psi). The LRFD Specifications, on the other hand, place a stress limit of $0.25f'_c$ on the sum of the "concrete" and "steel" contributions to shear strength (i.e. $v_c + v_s \le 0.25 f_c'$). The difference between the Standard and LRFD Specifications for various concrete compressive strengths is illustrated in Figure 1.5. To facilitate comparison, two limits to the shear stress corresponding to $v_c + v_s$ are shown for the Standard Specifications, which correspond to reasonable concrete shear stresses of $2\sqrt{f_c'}$ and $4\sqrt{f_c'}$ (psi). As can be seen, the LRFD Specifications allow PC girders to be designed for a much higher shear stress at ultimate compared to the Standard Specifications. The difference in shear stress limits between the Specifications increases as the concrete compressive strength increases, with the LRFD provisions allowing approximately twice the maximum shear stress for concrete strengths between 8000 and 10000 psi.

The difference in shear stress limit between the Standard and LRFD Specifications, and the lack thereof in the 1979 Interim Specifications, could potentially lead to substantial differences in the behavior, at service conditions, of PC girders designed following these three approaches. This is because the higher the design shear stress, the more likely diagonal cracks will develop under service conditions. To illustrate this point, consider an example PC girder with f_c' = 8000 psi concrete designed for a factored shear stress equal to 50% of the upper shear stress limit in either the Standard Specifications (i.e. $v_u = 0.5[v_c + (v_s)_{max}]$, where $(v_s)_{max} = 8\sqrt{f_c'}$ in psi), or LRFD Specifications [i.e. $v_u = 0.5(v_c + v_s)_{max} = 0.5(0.25 f_c')$]. Assuming a typical ratio between factored and unfactored shear of 1.5 and a reasonable "concrete" shear stress $v_c = 3.5\sqrt{f_c'}$ (psi), the PC girder designed according to the Standard Specifications would be subjected to an unfactored shear stress of 340 psi, while the unfactored shear stress in the PC girder designed according to the LRFD Specifications would be 670 psi (nearly 100% difference).

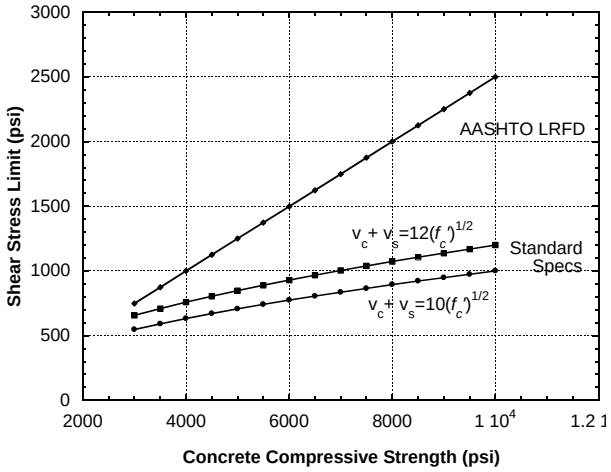

Figure 1.5. Comparison Of Maximum Shear Stress Limit In AASHTO Standard And LRFD Specifications.

It would therefore not be surprising to find PC girders designed according to the LRFD Specifications to be more prone to diagonal cracking under service conditions than girders designed to the Standard Specifications. The same potential for shear cracking under service loads could be found for structures designed using the 1979 Interim Specifications, given the lack of an upper shear stress limit for design.

In addition to shear capacity, shear force demands are calculated differently between the Standard and LRFD Specifications, and these differences involve changes in nominal traffic live load (HS-20 versus HL-93) and impact load, as well as girder distribution and load and resistance factors. In general, these differences in shear design loads act to decrease the effective differences in final shear designs between the codes. However, these differences are far from uniform, and depend greatly on bridge geometry, with the final LRFD design shear resistance varying from about 1.0 to 1.4 times the design shear resistance calculated from the Standard Specifications (Nowak 1999). Relative to LRFD, shear designs by the Standard Specifications are generally less conservative (in terms of ultimate strength) as girder spacing increases and span decreases. These differences are detailed in NCHRP Report 368 (Nowak 1999) and must be considered along with capacity to assess differences and problems among the design approaches. Ultimate capacity comparisons, however, do not account for the fact that, as illustrated above, shear stresses at service conditions in girders designed according to the LRFD Specifications can be substantially higher than those in girders designed following the Standard Specifications, and which may be the most probable cause of visible shear cracking.

Continuous Bridge Girders

Another issue that complicates the shear design of PC bridges is that, based on the results of NCHRP Report 322, *The Design of Precast, Prestressed Bridge Girders Made Continuous* (Oesterle et al. 1989), depending on the construction sequence and reinforcement detailing, some continuous PC bridges have been flexurally-designed to act as simply supported spans under some load conditions and continuous under others. For example, when precast girders are brought to the construction site, the girders must carry self-weight for simple span conditions,

but with the addition of proper joint construction over the supports, act as continuous spans for additional dead and live loads, as well as restraint moments caused by creep and shrinkage. However, shear design in bridges made continuous through the bridge deck was not studied in NCHRP 322, but only recommended for future research. Further, potential complications in the calculation of the shear corresponding to flexural-shear cracking (Eq. 1.2) were reported, particularly due to the numerous loading conditions to be considered in the analyses. In fact, the 2003 PCI Bridge Design Manual does not recommend the calculation of the "concrete" strength contribution based on the AASHTO Standard Specifications because it was derived from tests of simply supported beams. The same manual indicates, however, that there are no known problems associated with the application of this method to continuous bridge girders.

Objectives of the Study

The specific research objectives of this study are to:

- Identify MDOT PC bridges with potential shear cracks, attempt to determine their cause, and evaluate whether these cracks are associated with the application of a particular shear design method.
- Conduct laboratory tests to generate experimental data that can be used to validate numerical models of PC beam shear capacity.
- Develop a validated numerical (finite element) modeling approach that can be used to investigate the effect of critical parameters on the shear capacity of PC girders.
- Conduct field tests to determine the degree of joint moment fixity for continuous-span PC girders, and estimate the effect that joint fixity has on shear distribution.
- Determine the most appropriate analysis method to determine MDOT PC beam shear capacity, and validate the use of current code procedures to evaluate shear capacity.
- Develop a calibration procedure such that the AASHTO shear capacity analysis procedure can be most accurately applied to MDOT PC bridges.

Summary of Research Tasks

Task 1. Conduct a comprehensive review of the state-of-the-art technical literature.
Task 2. Identify MDOT PC bridges that show signs of potential shear distress.
Task 3. Determine the cause of cracking.
Task 4. Conduct laboratory tests of PC beams to generate high-quality, controlled data for model development and calibration.
Task 5. Develop a finite element model of PC girders and conduct a parametric analysis of critical shear capacity-affecting factors using the laboratory results for validation and calibration.
Task 6. Conduct field tests of two MDOT PC bridges to determine the degree of continuous joint fixity.
Task 7. Evaluate the effectiveness of existing code procedures to predict the shear capacity of PC beams, and recommend a shear design and evaluation procedure specifically suited for MDOT PC bridges.
Task 8. Prepare project deliverables.

CHAPTER 2: LITERATURE REVIEW

Shear Design Methods

AASHTO 1979 Interim Design Specifications

As noted in Chapter 1, In the 1979 Interim provisions, contrary to the AASHTO Standard and LRFD Specifications, the "concrete" contribution to shear strength V_c was assumed to be linearly related to concrete compressive strength and was taken equal to 0.06 f'_c. This contribution, however, was limited to 180 psi, which in practice governed the design value of V_c for all prestressed concrete (PC) girders, since this limit was reached with an f'_c of only 3000 psi. For comparison, for concrete compressive strengths of 4000 and 10000 psi, this shear stress limit corresponds to $2.8\sqrt{f_c'}$ and $1.8\sqrt{f_c'}$ (psi), respectively. In the 1979 Interim provisions for PC, the shear strength contribution of the transverse steel reinforcement is given as:

$$V_s = 2A_v f_y \frac{jd}{s} \tag{2.1}$$

where A_v is the area of steel transverse reinforcement spaced at a distance s, f_y is the yield strength of the transverse steel reinforcement, and jd is the distance between the resultant normal tension and compression force couple in the section (i.e. truss depth).

Although the angle of inclination for the diagonal elements to be used in the truss analogy was not explicitly specified, the number of layers of steel transverse reinforcement assumed to be crossed by a diagonal crack in Eq. (2.1) is effectively $2jd/s$, which leads to a truss angle of 29.1 degrees. This significantly shallower design angle compared to the typical 45 degree angle used in reinforced concrete was due to the effect of the prestressing force in PC beams, which lowers the principal compression angle. However, this beneficial effect is not accounted for in the 1983 nor the latest 2002 AASHTO Standard Specifications. Other important provisions of the 1979 Interim Specifications are a minimum shear reinforcement requirement to provide a shear stress contribution of at least 100 psi, while maximum stirrup spacing was limited to ¾ of the member height. It should be noted that the 1979 Interim Specifications did not limit the maximum shear strength contribution that could be assigned to the steel transverse reinforcement. That is, no explicit provisions were provided to prevent web-crushing failures.

Another aspect of the 1979 Interim Specifications that deserves attention is the critical section used for design near the supports. In the case of simply supported beams, the shear calculated at a quarter of the span length from the support is used as the maximum shear design value; i.e. higher shear forces closer to the support are neglected.

AASHTO Standard Specifications

The shear design provisions in the 1983-2002 AASHTO Standard Specifications are based on research conducted at the University of Illinois (MacGregor 1960; MacGregor et al. 1965). In these provisions, the "concrete" shear strength is calculated as the smaller of the shear force associated with flexural shear cracking and the shear force that causes web-shear cracking.

Flexural shear cracking will govern in sections with high moment and low shear, while web-shear cracking will govern in sections subjected to high shear and low moment.

Section 9.20.1 (General) in the 2002 AASHTO Standard Specifications states that prestressed concrete flexural members shall be reinforced for shear and diagonal tension stresses. Shear reinforcement may be omitted if the factored shear force, V_u is less than half the shear strength provided by the concrete. It also states that web reinforcement shall consist of stirrups perpendicular to the axis of the member or welded wire fabric with wire located perpendicular to the axis of the member. This web reinforcement is to extend to a distance *d* from the extreme compression fiber and is to be placed as close to the compression and tension surfaces of the member as cover requirements and the proximity of other reinforcement permits. Moreover, web reinforcement is to be anchored at both ends in accordance with the provisions of Article 8.27. Member shear strength must satisfy:

$$V_u \leq \phi (V_c + V_s) \tag{2.2}$$

where V_u is the factored shear force at the section considered, V_c is the nominal shear strength provided by the concrete, and V_s is the nominal shear strength provided by web reinforcement. When the reaction to the applied loads introduces compression into the end regions of the member, sections located at a distance less than *h/2* from the face of the support may be designed for the same shear V_u as that computed at a distance *h/2*.

Section 9.20.2 (Shear Strength Provided by Concrete) in the 2002 AASHTO Standard Specifications states that the shear strength provided by the concrete, V_c, is to be taken as the lesser of the values V_{ci} or V_{cw}. The shear strength, V_{ci}, is given by:

$$V_{ci} = 0.6\sqrt{f_c'}\, b_v d + V_d + \frac{V_i M_{cr}}{M_{max}} \tag{2.3}$$

However, this value need not be less than $1.7\sqrt{f_c'}\, b' d$, and d need not be taken less than $0.8h$. Here, b_v is the web width, d is the member effective depth, V_d is the shear force due to unfactored dead load, V_i is the factored shear that occurs simultaneously with the maximum factored moment at the section (M_{max}), while M_{cr} is the cracking moment due to external loads. The last term in Eq. (2.3) represents the factored shear due to external loads (in addition to dead load) that leads to flexural cracking in the section. For sections subjected to low moment, Eq. (2.3) will lead to very large shear strength values (infinity at points where M_{max}=0). In these cases, design shear strength is governed by the shear corresponding to web-shear cracking. The web shear strength V_{cw} is computed by assuming that the section is uncracked in flexure and that the first diagonal cracks will develop on the member web when the principal tensile stress in the concrete, calculated including the effect of prestressing, reaches the assumed concrete tensile strength of $3.5\sqrt{f_c'}$ (psi). This shear force, combined with the vertical component of the prestressing force, V_p, is then taken as the web shear strength, V_{cw}:

$$V_{cw} = \left(3.5\sqrt{f_c'} + 0.3 f_{pc}\right) b_v d + V_p \tag{2.4}$$

where f_{pc} is the stress due to prestressing at the centroid of the cross section or at the web-flange interface when the centroid is in the flange, and d need not be taken less than 0.8h.

Section 9.20.3 (Shear Strength Provided by Web Reinforcement) in the 2002 AASHTO Standard Specifications states that the shear strength provided by web reinforcement shall be taken as:

$$V_s = \frac{A_v f_{sy} d}{s} \tag{2.5}$$

where A_v is the area of web reinforcement within a distance s. V_s is not to be taken greater than $8\sqrt{f_c'}b_v d$, and d need not be taken less than 0.8h. The spacing of web reinforcing is not to exceed 0.75h or 24 inches. When V_s exceeds $4f_c'b'd$, this minimum spacing is reduced by 50%. The minimum area of web reinforcement shall be determined as:

$$A_v = \frac{50b's}{f_{sy}} \tag{2.6}$$

where b_v and s are in inches, and f_{sy} (the design yield strength of web reinforcement) does not exceed 60,000 psi.

AASHTO LRFD Design Specifications

The General Sectional Method for shear design in the AASHTO LRFD Specifications represents a significant departure from the traditional shear design methods applied to reinforced and prestressed concrete members in other design codes (e.g. ACI Building Code, AASHTO Standard Specifications). Based on the Modified Compression Field Theory (MCFT) developed at the University of Toronto in the late 1970s and early 1980s (Vecchio and Collins 1986), this shear design method relies on the use of equilibrium, strain compatibility, and material constitutive relations to determine the "concrete" and steel reinforcement contributions to shear strength. In compression, the concrete behavior is assumed to "soften" (or become weaker) due to the presence of transverse tensile strains. Moreover, on average terms, concrete is assumed to carry some tension beyond cracking to account for tension stiffening (i.e. the tension carried by the concrete between cracks).

The shear resistance of a concrete member may be separated into a component, V_c that relies on tensile stresses in the concrete, a component V_s, that relies on tensile stresses in the transverse reinforcement, and a component V_p, that is the vertical component of the prestressing force.
Section 5.8.3.3 (Nominal Shear Resistance) in AASHTO LRFD states that the nominal shear resistance, V_n, shall be determined as the lesser of:

$$V_n = V_c + V_s + V_p \tag{2.7}$$

$$V_n = 0.25f_c'b_v d_v + V_p \tag{2.8}$$

in which:

$$V_c = 0.0316\beta\sqrt{f_c'}b_v d_v \tag{2.9}$$

where b_v is the effective web width taken as the minimum web width, measured parallel to the neutral axis, between the resultants of the tensile and compressive forces due to flexure (in), d_v is the effective shear depth taken as the distance, measured perpendicular to the neutral axis, between the resultants of the tensile and compressive forces due to flexure (and need not be taken less than the greater of $0.9d_e$ or $0.72h$), s is the spacing of transverse reinforcement measured in a direction parallel to the longitudinal reinforcement, β is a factor indicating the ability of diagonally cracked concrete to transmit tension and shear, θ is the angle of inclination of diagonal compressive stresses, and α is the angle of inclination transverse reinforcement to longitudinal axis. The concrete contribution is controlled by the value of the coefficient β. The value of 0.0316 is used to convert the relationship for V_c from psi to ksi units. Note that V_c is taken as the lesser of V_{ci} and V_{cw} if the procedures of Article 5.8.3.4.3 (Simplified Procedure) are used. V_s is in general given as:

$$V_s = \frac{A_v f_y d_v (cot\theta + \cot\alpha) sin\alpha}{s} \tag{2.10}$$

When α = 90 degrees (shear reinforcement placed vertically), Eq. 210 reduces to:

$$V_s = \frac{A_v f_y d_v \cot(\theta)}{s} \tag{2.11}$$

The expressions V_c and V_s apply to both prestressed and non-prestressed sections, with the terms β and θ depending on the applied loading and the properties of the section. The upper limit of V_n given (discussed above) is intended to ensure that the concrete in the web of the beam will not crush prior to yield of the transverse reinforcement. A variable angle truss model is used to calculate the contribution of the shear reinforcement. The angle of the field of diagonal compression, θ, is used in calculating how many stirrups, $[d_v cot(\theta)/s]$, are included in the transverse tie of the idealized truss. The parameters β and θ may be determined either by the General Procedure or the Simplified Procedure.

The actual section is represented by an idealized section consisting of a flexural tension flange, a flexural compression flange, and a web. After diagonal cracks have formed in the web, the shear force applied to the web concrete, $(V_u - V_p)$ will primarily be carried by diagonal compressive stresses in the web concrete. These diagonal compressive stresses will result in a longitudinal compressive force in the web concrete of $(V_u - V_p)cot\theta$. Equilibrium requires that this longitudinal compressive force in the web be balanced by tensile forces in the two flanges, with half the force, that is $0.5(V_u - V_p)cot\theta$, being taken by each flange. For simplicity, $0.5cot\theta$ may be taken as 2.0 and the longitudinal demand due to shear in the longitudinal tension reinforcement becomes $(V_u - V_p)$, without significant loss of accuracy. After the required axial forces in the two flanges are calculated, the resulting axial strains ϵ_t and ϵ_c can be calculated based on the axial force-axial strain relationship.

For the General Procedure, for sections containing at least the minimum amount of transverse reinforcement specified in Article 5.8.2.5, the value of β is taken as:

$$\beta = \frac{4.8}{(1+750\varepsilon_s)} \tag{2.12}$$

When sections do not contain at least the minimum amount of shear reinforcement, the value of β is taken as:

$$\beta = \frac{4.8}{(1 + 750\varepsilon_s)} \frac{51}{(39 + s_{xe})} \tag{2.13}$$

The value of θ in both cases is:

$$\theta = 29 + 3500\varepsilon_s \tag{2.14}$$

where ε_s is the net longitudinal tensile strain in the section at the centroid of the tension reinforcement:

$$\epsilon_s = \frac{\left(\frac{M_u}{d_v} + 0.5N_u + 0.5|V_u - V_p| - A_{ps}f_{po}\right)}{(E_s A_s + E_p A_{ps})} \tag{2.15}$$

The crack spacing parameter s_{xe} , is:

$$s_{xe} = s_x \frac{1.38}{a_g + 0.63} \tag{2.16}$$

where 12.0 in $\leq s_{xe} \leq$ 80.0 in, A_c is the area of concrete on the flexural tension side of the member, A_{ps} is the area of prestressing steel on the flexural tension side of the member, A_s is the area of non-prestressed steel on the flexural tension side of the member at the section under consideration, a_g is the maximum aggregate size, f_{po} is a parameter taken as modulus of elasticity of prestressing tendons multiplied by the locked-in difference in strain between the prestressing tendons and the surrounding concrete. For the usual level of prestressing, a value of $0.7f_{pu}$ is appropriate for both pretensioned and post-tensioned members. N_u is the factored axial force, taken as positive if tensile and negative if compressive, $|M_u|$ is the factored moment, s_x is the lesser of either d_v or the maximum distance between layers of longitudinal crack control reinforcement, where the area of the reinforcement in each layer is not less than $0.003b_v s_x$, and V_u is the factored shear force.

In using the General Procedure, some additional considerations are:

- $|M_u|$ shall not to be taken less than $|V_u - V_p| d_v$
- In calculating A_s and A_{ps}, the area of bars or tendons terminated less than their development length from the section under consideration should be reduced in proportion to their lack of full development.
- If the value of ε_s is negative, it should be taken as zero or the value should be calculated using $(E_s A_s + E_p A_{ps} + E_c A_{ct})$ as the denominator. However, ε_s should not be taken less than -0.40×10^{-3}.

- For sections closer than d_v to the face of the support, the value of ε_s calculated at d_v from the face of the support may be used in evaluating β and θ.

- If the axial tension is large enough to crack the flexural compression face of the section, the value calculated by the denominator for ε_s should be doubled.

- It is permissible to determine β and θ using a greater value of ε_s than calculated by the equation above, however, ε_s should not be taken greater than 6.0×10^{-3}.

The relationships for evaluating β and θ in the previous equations are based on calculating the stresses that can be transmitted across diagonally cracked concrete. As the cracks become wider, the stress that can be transmitted decreases. For members containing at least the minimum amount of transverse reinforcement, it is assumed that the diagonal cracks will be spaced about 12.0 in apart. For members without transverse reinforcement, the spacing of diagonal cracks inclined at θ degrees to the longitudinal reinforcement is assumed to be $s_x/sin\theta$. Hence, deeper members having larger values of s_x are calculated to have more widely spaced cracks and therefore cannot transmit as high shear stresses. Also, the ability of the crack surfaces to transmit shear stresses is influenced by the aggregate size of the concrete. Members made from concretes that have a smaller maximum aggregate size will have a larger value of s_{xe} and thus, if there is no transverse reinforcement, will have lower shear strength.

As an alternative to the General Procedure, a Simplified Procedure may be used in some cases. The Simplified Procedure is based on the recommendations of NCHRP Report 549 (Hawkins and Kuchma 2005). These concepts are compatible with ACI 318-05 and the AASHTO Standard Specifications for Highway Bridges (2002) for evaluation of the shear resistance of concrete members. For nonprestressed sections, Section 5.8.3.4.1 (Simplified Procedure) states that for concrete sections not subjected to axial tension and containing at least the minimum amount of transverse reinforcement, or having an overall depth of less than 16 in, β can be taken as 2.0 and θ can be taken as 45°. Section 5.8.3.4.3 (Simplified Procedure) addresses prestressed sections as well. Here, for concrete beams not subject to significant axial tension, prestressed or non-prestressed, and containing at least the minimum amount of transverse reinforcement, V_n may be determined with V_p taken as zero and V_c taken as the lesser of V_{ci} and V_{cw}, where V_{ci} is the nominal shear resistance provided by the concrete when inclined cracking results from combined shear and moment, and V_{cw} is the nominal shear resistance provided by the concrete when inclined cracking results from excessive principal tension in web. In this case, V_{ci} shall be determined as:

$$V_{ci} = 0.02\sqrt{f_c'}b_v d_v + V_d + \frac{V_i M_{cre}}{M_{max}} \geq 0.06\sqrt{f_c'}b_v d_v \qquad (2.17)$$

where V_d is the shear force at the section due to the unfactored dead load, V_i is the factored shear force at section due to externally applied loads occurring simultaneously with M_{max}, M_{cre} is the moment causing flexural cracking at section due to externally applied loads, and M_{max} is the maximum factored moment at section due to externally applied loads. M_{cre} hall be determined as:

$$M_{cre} = S_c\left(f_r + f_{cpe} - \frac{M_{dnc}}{S_{nc}}\right) \qquad (2.18)$$

where f_{cpe} is the compressive stress in the concrete due to the effective prestress forces only at the extreme fiber or section where tensile stress is caused by externally applied loads, M_{dnc} is the total unfactored dead load moment acting on the monolithic or noncomposite section, S_c is the section modulus for the extreme fiber of the composite section where tensile stress is caused by externally applied loads, and S_{nc} is the section modulus for the extreme fiber of the monolithic or noncomposite section where tensile stress is caused by externally applied loads. V_{cw} shall be determined as:

$$V_{cw} = \left(0.06\sqrt{f_c'} + 0.30f_{pc}\right)b_v d_v + V_p \tag{2.19}$$

where f_{pc} is the compressive stress in the concrete at the centroid of the cross section resisting the externally applied loads or at the junction of the web and flange when the centroid lies within the flange.

For the simplified procedure, the angle θ used to calculate V_s can be determined as follows:

If $V_{ci} < V_{cw}$: $\cot\theta = 1.0$

If $V_{ci} > V_{cw}$: $\cot\theta = 1.0 + 3\left(\frac{f_{pc}}{\sqrt{f_c'}}\right) \leq 1.8$ (2.20)

Transverse reinforcement is required in all regions where there is a significant chance of diagonal cracking. A minimum amount of transverse reinforcement is required to restrain the growth of diagonal cracking and to increase the ductility of the section. A larger amount of transverse reinforcement is required to control cracking as the concrete strength is increased. According to the 2010 AASHTO LRFD Code (Section 5.8.2.4; Regions Requiring Transverse Reinforcement), for beams, transverse reinforcement must be provided where:

$$V_u > 0.5\phi\left(V_c + V_p\right) \tag{2.21}$$

Here, V_u is the factored shear force, V_c is the nominal shear resistance of the concrete, V_p is the component of prestressing force in direction of the shear force (V_p = 0 when the simplified method of Section 5.8.3.4.3 is used), and ϕ is the resistance factor specified in Article 5.5.4.2. For shear (normal weight concrete), ϕ is taken as 0.90, but for compression in strut-and-tie models, ϕ is taken as 0.70.

Section 5.8.2.5 (Minimum Transverse Reinforcement) states that the area of steel shall satisfy:

$$A_v \geq 0.0316\sqrt{f_c'}\frac{b_v s}{f_y} \tag{2.22}$$

where A_v is the area of transverse reinforcement within distance s, b_v is the width of web adjusted for the presence of ducts, s is the spacing of transverse reinforcement, and f_y is the yield strength of transverse reinforcement. Section 5.8.2.7 (Maximum Spacing of Transverse Reinforcement)

states that the spacing of the transverse reinforcement shall not exceed the maximum permitted spacing, s_{max}, determined as:

If $v_u < 0.125f'_c$, then $s_{max} = 0.8d_v \leq 24.0$ in (2.23)

If $v_u > 0.125f'_c$, then $s_{max} = 0.4d_v \leq 12.0$ in (2.24)

where v_u is the shear stress calculated in accordance with 5.8.2.9, and d_v is the effective shear depth.

Section 5.8.3.2 (Sections near Supports) states that where the reaction force in the direction of the applied shear introduces compression into the end region of a member, the location of the critical section for shear is to be taken as d_v from the internal face at the support.

In the case where a beam is loaded on its top surface and the end of the beam is not built integrally into the support, shear force must travel to the end bearing. In this case, if the beam has a thin web so that the shear stress in the beam exceeds $0.18f'_c$, there is a possibility of a local diagonal compression or horizontal shear failure along the interface between the web and the lower flange of the beam. In this case, strut-and-tie models are useful for analysis.

ACI 318-11

The calculation for nominal shear capacity in ACI-318 (2011) is similar to previous versions (1980 to 2002) of the AASHTO Standard Specifications for Highway Bridges. ACI-318 divides the nominal shear strength into contributions from concrete and steel transverse reinforcement. They are computed using the following equations:

$$V_{ci} = 0.6\sqrt{f'_c}\, b_w d_p + V_d + \frac{V_i M_{cre}}{M_{max}} \quad (2.25)$$

$$V_{ci} = \left(3.5\sqrt{f'_c} + 0.3f_{pc}\right) b_w d_p + V_p \quad (2.26)$$

$$V_s = \frac{A_v f_y d_v}{s} \quad (2.27)$$

where V_{ci} is the concrete shear capacity when cracking results from combined shear and moment, V_{cw} is the concrete shear capacity when cracking results from high principal tensile stress, V_s is the shear capacity of steel web reinforcement, M_{cre} is the moment causing flexural cracking at the section due to externally applied loads, V_d is the unfactored shear due to dead load, V_i is the factored shear at the section due to externally applied loads, M_{max} is the factored moment at the section due to externally applied loads, f_{pc} is the compressive stress in the concrete at the centroid of the gross section resisting externally applied loads including effective prestressing force, b_w is the width of the web adjusted for ducts, d_v is the effective shear depth (in), A_v is the total area of shear stirrups, f_y is the yield stress of the web reinforcement, s is the spacing of shear stirrups, and V_p is the vertical component of prestressing force.

The nominal shear resistance of concrete is taken as the lesser of V_{ci} or V_{cw}. Typically, V_{cw} will control near the supports and V_{ci} will control closer to midspan. The effective prestressing force

is included directly in the equation for V_{cw} as the vertical contribution of prestressing force and in the term f_{pc} which includes only the uniform axial compression due to the effective prestressing force. It is important to note that, although not shown explicitly in the equations above, the effective prestressing force is used in V_{ci} as it must be considered when determining M_{cre}.

The minimum shear reinforcement area is determined as follows:

$$A_v \geq \frac{0.75\sqrt{f_c'}b_w s}{f_{yt}} \tag{2.28}$$

where f_c' is the compressive strength of concrete, b_w is the effective width of the web, s is the spacing of shear reinforcement, and f_{yt} is the tensile strength of shear reinforcement.

Strut and Tie Modeling

Both AASHTO and ACI allow strut and tie models. Strut and tie models can be used when beam theory is not applicable, such as in beam D-regions. Here, the girder is modeled as a truss where concrete struts take the compressive loads and steel ties take the tension loads (Kuchma et al. 2008). A proper truss model should show how forces are distributed throughout the girder. Schlaich et al. (1987) states that the model producing the least strain energy is the most appropriate. In almost all cases where a point load is applied with a shear span to depth ratio less than 2.0, the least strain energy occurs when a compressive strut connects the load and support (Brown and Bayrak, 2008). Nominal strut and tie capacities for AASHTO LRFD are determined as follows, respectively:

$$P_n = f_{cu}A_{cs} \tag{2.29}$$

$$P_n = f_y A_{st} + A_{ps}(f_{pe} + f_y) \tag{2.30}$$

Nominal strut and tie capacities for ACI 318 are determined by the following equations:

$$F_{ns} = f_{ce}A_{cs} \tag{2.31}$$

$$F_{nt} = f_y A_{ts} + A_{tp}(f_{se} + \Delta f_p) \tag{2.32}$$

These equations are very similar as both codes use a limiting stress for the concrete strut capacity and include both conventional steel reinforcement and prestressing strands in the calculation of tie capacity. The development of stress in the steel ties must be considered in evaluating the tie capacity and the main difference between the codes is how the limiting stress of the concrete struts is calculated. For AASHTO LRFD, limiting concrete strengths are given as:

$$f_{cu} = \frac{f_c'}{0.8+170\varepsilon_1} \leq 0.85f_c' \tag{2.33}$$

$$f_{ce} = 0.85\beta_s f_c' \tag{2.34}$$

(2.35)

$$\varepsilon_1 = \varepsilon_s + (\varepsilon_s + 0.002)cot^2\alpha \qquad (Eq.35)$$

The value for ε_1 is based on the tensile strain in the strut due to the adjoining tie and the angle between the strut and tie. The ε_s factor is determined by the type of strut. For a bottle shaped strut (i.e. a strut taken to have a larger width at its midsection) the ε_s factor is taken as 0.6 or 0.75, depending on whether the minimum transverse reinforcement requirement is met. The strength of nodal regions is also considered. AASHTO LRFD applies a factor of 0.85, 0.75 and 0.65 to f_c' for nodes containing no ties, ties in one direction and ties in more than one direction, respectively. ACI uses similar equations.

Shear Models

Most traditional shear design procedures are derived from a parallel chord truss model developed by Ritter (1899) and Mörsch (1920 and 1922). In this model, for any member under shear, there are four unknowns (diagonal compressive stress, stress in stirrups, stress in longitudinal reinforcement, and the angle of the diagonal compression), but only three equations of statics to determine the unknowns. The angle of the diagonal compression strut is an important factor in deciding the shear reinforcement contribution to shear resistance. In early parallel chord truss models, θ was taken as 45 degrees. However, it was determined by various researchers that this angle often poorly estimated capacity, and thus over the past several decades, the use of a truss analogy with angles shallower than 45 degrees has been explored (Ramirez and Breen 1991; Vecchio and Collins 1986; Hsu 1988). Reducing this angle implies a higher efficiency of the transverse reinforcement (as geometrically, more stirrups will cross a shear crack with a lower angle) and thus results in less shear reinforcement required for the same shear demand. The concrete shear strength contribution can be considered as well, and in early formulations, it was based on a limiting shear stress. Later it was taken to be the diagonal cracking strength (i.e. the concrete contribution at ultimate, based on test data). Code provisions such as those of ACI 318 and the AASHTO Standard Specifications take into account the effect of flexure, axial force, and prestressing into the diagonal cracking strength. However, they also make the assumption that the concrete shear strength contribution is independent of shear reinforcement. In contrast, some European design methods take θ as the angle defined by a plasticity-based model, for which values may result as low as 21.8 degrees. In AASHTO LRFD, the angle θ is often taken between 20 and 25 degrees, consequently providing a larger shear strength contribution from the shear reinforcement than that found from a 45 degree model. The concrete shear strength contribution is defined as the ability of the cracked concrete to carry diagonal tension in the web of the member, and it depends on the longitudinal strain, the reserve capacity of the longitudinal reinforcement at a crack location, and the shear-slip resistance of concrete. The Tureyen and Frosch model takes the angle θ as 45 degrees and bases the concrete strength contribution on the limiting capacity of the uncracked section (Kuchma and Hawkins 2008).

Traditional provisions for shear capacity such as those of the ACI code do not explicitly take into account shear friction as a contributor to shear strength, but rather lump it together with other contributors such as the dowel effect and the shear strength capacity of the compression zone of the beam. This term is referred to as the concrete contribution to shear strength V_c. In the last 20 years, more rational methods for shear strength calculation (such as AASHTO LRFD and the Canadian Code CSA) have been able to explicitly account for the contribution of shear friction

across cracks to resist shear, by referring to concepts of the Modified Compression Field Theory (MCFT). The MCFT also provides a way to study the softening of concrete (effect of tensile stress in lowering the compressive strength of concrete below its uniaxial strength). The MCFT (Vecchio and Collins 1986) satisfies the equilibrium of forces and moments, compatibility of displacements, and stress-strain relationship of concrete and steel to predict the shear strength of RC and PC beams. It is assumed in MCFT that the principal direction of stress and strain coincide, and that shear strength is given as the sum of the steel reinforcement contribution (based on the truss model using strut angle θ) and the concrete contribution (shear resisted by the tensile stresses in the diagonally cracked concrete). While some researchers (Richart 1927; Bresler and Pister 1958; Tureyen and Frosch 2003) have argued that most of the "concrete" contribution to beam shear strength is provided by shear carried in the beam compression zone, others (Vecchio and Collins 1986) have claimed that most of this shear is resisted by the member web through aggregate interlock, which is the approach followed by MCFT. The ability of the crack interface to transmit shear stresses τ depends on the crack width w. According to MCFT,

$$V = V_s + V_c = \frac{A_v f_v}{s} jdcot\theta + f_{c1} b_w jdcot\theta \tag{2.36}$$

$$\frac{\tau}{\tau_{max}} = 0.18 + 1.64\frac{\sigma}{\tau_{max}} - 0.82(\frac{\sigma}{\tau_{max}})^2 \tag{2.37}$$

$$\tau_{max} = \frac{\sqrt{f_c'}}{0.3+\frac{24w}{c+16}} \tag{2.38}$$

where σ is the compressive normal stress across the cracks, c is the maximum aggregate size, and f_c' is the compressive strength of concrete.

Another expression developed later by Collins and Mitchell (1991) for τ is:

$$\tau = 0.18\tau_{max} \tag{2.39}$$

MCFT assumes a parabolic relationship between stress and strain of concrete in compression:

$$\frac{f_{c2}}{f_{c2max}} = 2\left(\frac{\varepsilon_2}{\varepsilon_0}\right) - \left(\frac{\varepsilon_2}{\varepsilon_0}\right)^2 \tag{2.40}$$

where ε_0 is the strain at peak uniaxial stress, and f_{c2max} is the compressive strength of concrete panels in biaxial tension-compression and depends on the transverse tensile strain ε_1. A softening parameter β was derived from tests with a mean value of 0.98 and coefficient of variation 0.16.

$$\beta = \frac{f_{c2max}}{f_c'} = \frac{1}{0.80+\frac{0.34\varepsilon_1}{\varepsilon_0}} \leq 1.0 \tag{2.41}$$

For ε_0=0.002,

$$\beta = \frac{1}{0.80+170\varepsilon_1} \tag{2.42}$$

f_{c2} is then a function of the principal compressive strain ε_2 and the principal tensile strain ε_1.

Two major research directions for the shear behavior in reinforced concrete are the characterization of shear friction, which controls the transfer of shear force across a crack, and the characterization of softening, which reduces the compressive strength of concrete when in a state of bi-axial compression and tension.

Walraven and Reinhardt (1981) and Walraven (1981) developed early equations for predicting the normal and shear stresses in cracked concrete. They based their expressions on experimental investigations of shear friction. It was observed that the behavior of externally reinforced beams loaded in shear was different from that of internally reinforced ones; the shape of the crack width vs. crack slip curve was more sensitive for externally reinforced beams. However, the same model for aggregate interlock was proposed for both types of beams. This model involved two components, a rigid plastic mortar component and a rigid spherical aggregate component. When the crack faces open and slide against one another, the portion of mortar in contact with the aggregates is assumed to yield and therefore creates normal and shear stresses that are related by a coefficient μ. Walraven and Reinhardt's equation for normal and shear stresses are given as:

$$\sigma = \sigma_{pu}(A_x - \mu A_y) \quad and \quad \tau = \sigma_{pu}(A_y - \mu A_x) \tag{2.43}$$

where A_x and A_y are the nondimensionalized sums of a_x and a_y (contact areas), and depends on crack width w, crack slip v, the maximum particle diameter, and the total aggregate volume per unit volume of concrete. The coefficient μ and strength of mortar σ_{pu} were found by fitting curves to experimental results:

$$\mu = 0.40 \quad and \quad \sigma_{pu} = 6.39(f_{cc})^{0.56} \tag{2.44}$$

An empirical expression for shear friction capacity of internally reinforced cracks as a function of concrete strength and amount of reinforcement was then developed as:

$$\tau_{max} = C_1(\rho_v f_y) \tag{2.45}$$

where $C_1 = 0.822(f_{cc})^{0.406} \quad and \quad C_2 = 0.159(f_{cc})^{0.303}$, ρ_v *and* f_y are the cross sectional area and yield strength of the steel reinforcement, and f_{cc} is the compressive strength of a concrete test cube.

Walraven and Reinhardt's expressions gave good approximations to their experimental data for a linear range. However, the equations require a limit so that shear and normal stresses do not increase indefinitely as the crack slip increases.

Other researchers investigated the same topic and derived expressions for the shear cracking capacity. Mau and Hsu (1988) derived an expression that works well for normal strength RC:

$$\frac{\tau_{max}}{f_c'} = 0.66\sqrt{w} < 0.3 \quad with \quad w = \frac{\rho_v f_y}{f_c'} \tag{2.46}$$

It was found that the cracks are smoother in high strength concrete (HSC), because cracks travel through the aggregates (as opposed to lower strength concrete, where cracks tend to travel

around the aggregates). This decreases shear friction decreases as concrete strength increases. It has been shown that shear friction at a crack slip of HSC is reduced by 35% of its value for lower strength concrete for externally reinforced specimens, and between 55-75% of its value for internally reinforced specimens. The expressions for crack-related stresses in the model are given as:

$$\sigma = k\sigma_{pu}(A_x - \mu A_y) \quad and \quad \tau = k\sigma_{pu}(A_y - \mu A_x) \tag{2.47}$$

where k = 0.35 or 0.65 for externally reinforced and internally reinforced concrete specimens, respectively.

Other authors derived expressions based on the experimental results of Walraven. Reineck (1982, 1991) used the following expressions for the friction of shear faces:

$$\tau = \tau_{f0} + 1.7\sigma = \tau_{f0}({}^{v - 0.24w}/_{0.096w + 0.01mm}) \tag{2.48}$$

The cohesion friction stress τ_{f0} is the limiting value of shear strength without the normal stress σ on the crack face, and is found as:

$$\tau_{f0} = 0.45f_t\left(1 - \frac{w}{0.9mm}\right) \tag{2.49}$$

where f_t is the concrete tensile strength.

Reineck's expressions also needed a limit for stresses. The expressions worked well for crack widths of 0.02 in, but lost accuracy for crack widths of 0.03 in. Kupfer and Bulicek (1991) used the following relationships based on Walraven and Reinhardt's (1981) work:

$$\tau_{max} = -\frac{f_{cc}}{30} + (1.8(w)^{-0.8} + (0.234(w)^{-0.707} - 0.20)f_{cc})v \geq 0 \tag{2.50}$$

$$\sigma = \frac{f_{cc}}{20} - (1.35(w)^{-0.63} + 0.191(w)^{-0.552} - 0.15)f_{cc})v \leq 0 \tag{2.51}$$

Earlier, Kupfer et al. (1983) had used:

$$\frac{\tau}{f_c'} = 0.117 - 0.085v \; for \; Case \; A: v = w \tag{2.52}$$

$$\frac{\tau}{f_c'} = 0.117 + 0.1\frac{v}{w} - 0.085v \; for \; Case \; B: v \neq w \tag{2.53}$$

These expressions were derived based on earlier work from Walraven, which considered concrete strengths of 3.5 ksi and v > 0.008 in. However, the relationships established by Kupfer et al. (1983) were based on weaker concrete and did not agree well with Walraven's original experimental data. Dei Poli et al. (1990) used a rough crack model to describe aggregate interlock stress as:

$$\sigma = 0.62\frac{r\sqrt{w\tau}}{(1+r^2)^{0.25}} \tag{2.54}$$

$$\tau = 0.25f_c'\left(1-\sqrt{\frac{2w}{c}}\right)r\frac{a_3+a_4|r|^3}{1+a_4r^4} \tag{2.55}$$

where $a_3 = 9.8/f_c'$, $a_4 = 2.44 - 39/f_c'$, and $r = \frac{v}{w}$

Various researchers have also explored the effect of concrete softening. The web in a reinforced concrete beam in flexure and shear is in a biaxial state of tension-compression. The existence of transverse tensile strains leads to a weakening of the cracked concrete compressive strength, or 'softening'. Different researchers derived softening expressions based on models and test panels. Vecchio and Collins (1993) expressed a softening parameter β as a function of the ratio of the principal strains:

$$\beta = \frac{1}{0.85-0.27^{\varepsilon_1}/_{\varepsilon_2}} \tag{2.56}$$

where ε_1 is the principal tensile strain averaged over several cracks. They used a parabola model for the uniaxial compressive stress-strain curve of concrete and multiplied both f_c' and its associated strain ε_0 by β. They found good agreement with experimental data.

Kollegger and Mehlhorn (1987, 1990) determined that the effective compressive strength did not reduce beyond $0.8f_c'$ and that the primary influencing factor was the tensile stress f_{c1} rather than the tensile strain ε_1. They determined the following for calculating β:

For $0 \le f_{c1} / f_t \le 0.25$, then $\beta = 1.0$

For $0.25 < f_{c1} / f_t \le 0.75$, then $\beta = 1.1 - 0.4^{f_{c1}}/_{f_t}$ (2.57)

For $0.75 < f_{c1} / f_t \le 1.0$, then $\beta = 0.8$

The tests were based on panels where the tension-compression loads were applied parallel to the reinforcement, and some on a 45 degree angle. Miyahara et al (1988) Proposed a softening model based on tensile strains, but predicted lesser degree of softening than the model by Vecchio and Collins:

For $\varepsilon_1 \le 0.0012,\ \beta = 1.0$

For $0.0012 < \varepsilon_1 < 0.0044,\ \beta = 1.15 - 125\varepsilon_1$ (2.58)

For $0.0044 \le \varepsilon_1,\ \beta = 0.60$

Shirai and Noguchi (1989) and Mikame et al. (1991) proposed the following expression for the softening parameter:

$$\beta = \frac{1}{0.27+0.96(\varepsilon_1/\varepsilon_0)^{0.167}} \quad (2.59)$$

It was noted that the softening is greater for HSC than for normal strength concrete (NSC). Ueda et al. (1991) proposed the following high strength concrete softening parameter:

$$\beta = \frac{1}{0.8+0.6(1000\varepsilon_1+0.2)^{0.39}} \quad (2.60)$$

Later, Vecchio and Collins updated the model that they had previously developed by basing the uniaxial stress-strain curve on Thorenfeldt's curve, which provided better linear correlation for HSC:

$$f_{c2base} = -f_p \frac{n\left(-\varepsilon_2/\varepsilon_p\right)}{n-1+\left(-\varepsilon_2/\varepsilon_p\right)^{nk}} \quad (2.61)$$

where

$$n = 0.80 + f_p/17 \quad (2.62)$$

$$k = 1.0 \; for - \varepsilon_p < \varepsilon_2 < 0;$$
$$k = 0.67 + f_p/62 \; for \;\; \varepsilon_2 < -\varepsilon_p \quad (2.63)$$

f_p = maximum compressive stress for softened concrete.

In these equations, $f_p = \beta f_c'$ and $\varepsilon_p = \varepsilon_0$ = strain in uniaxial compression at peak stress f_c'. Modifications to the base stress-strain curve were explored using two models. The first model used strength and strain softening (both peak stress and its appropriate strain decrease):

$$\beta = \frac{1}{1.0+K_c K_f} \quad (2.64)$$

where

$$K_c = 0.35\left(\frac{-\varepsilon_1}{\varepsilon_2} - 0.28\right)^{0.80} \geq 1.0 \; for \; \varepsilon_1 < \varepsilon_{1L} \quad (2.65)$$

$$K_f = 0.1825\sqrt{f_c'} \geq 1.0 \quad (2.66)$$

ε_{1L} is the limiting tensile strain at which value the reinforcement at a crack yields and the concrete experiences little additional cracking. The curve was divided into 3 parts depending on:

Prepeak: $For - \varepsilon_2 < \beta\varepsilon_0 \, , f_{c2} \; is \; calculated \; from \; f_p = \beta f_c' \; and \; \varepsilon_p = \beta\varepsilon_0$

Peak: $For \; \beta\varepsilon_0 \leq -\varepsilon_2 \leq \varepsilon_0, f_{c2} = f_p = \beta f_c'$

Postpeak: $For - \varepsilon_2 > \varepsilon_0, f_{c2} = \beta f_{c2base}$

Note: $K_f \geq 1.0$ when $f_c' \geq 4.4$ ksi and $K_c \geq 1.0$ when $-\varepsilon_t / \varepsilon_2 \geq 4$.

The second model considers strength softening only:

$$\beta = \frac{1}{1+K_c} \tag{2.67}$$

$$K_c = 0.27\left(\frac{\varepsilon_1}{\varepsilon_0} - 0.37\right) \tag{2.68}$$

$$K_f = 2.55 - 0.2629\sqrt{f_c'} \leq 1.11 \tag{2.69}$$

Vecchio and Collins repeated experiments with other panels reinforced with a reinforcement grid at a 45 degree angle and both models agreed well with the experimental data. It was also found that the compression-softening formulation worked well for NSC as well as HSC.

Belarbi and Hsu (1991) used Hognestad's parabola but suggested one softening parameter for stress and another for strain:

$$\beta_\sigma = \frac{0.9}{\sqrt{1+K_\sigma \varepsilon_1}} \tag{2.70}$$

$$\beta_\varepsilon = \frac{1.0}{\sqrt{1+K_\varepsilon \varepsilon_1}} \tag{2.71}$$

where K_σ and K_ε depend on the orientation ϕ of the cracks to the reinforcement and the type of loading, as shown in Table 2.1:

Table 2.1. Values Of *K* For Belarbi And Hsu's Model (1991).

	Proportional Loading		Sequential Loading	
ϕ	$K\sigma$	$K\varepsilon$	$K\sigma$	$K\varepsilon$
45 deg	400	160	400	160
90 deg	400	550	250	0

Later, after experimental testing, Belarbi and Hsu (1995) derived the following expressions for softening:

$$For\ \varepsilon_2 \leq \beta\varepsilon_0 \qquad f_{c2} = \beta f_c'\left[2\left(\frac{\varepsilon_2}{\beta\varepsilon_0}\right) - \left(\frac{\varepsilon_2}{\beta\varepsilon_0}\right)^2\right] \tag{2.72}$$

$$For\ \varepsilon_2 > \beta\varepsilon_0 \qquad f_{c2} = \beta f_c'\left[1 - \left(\frac{\frac{\varepsilon_2}{\beta\varepsilon_0} - 1}{\frac{2}{\beta} - 1}\right)^2\right] \tag{2.73}$$

$$\beta = \frac{0.9}{\sqrt{1+K_\sigma \varepsilon_1}} \tag{2.74}$$

where K_σ = 400 for proportional loading, and K_σ = 250 for sequential loading with some tension release immediately prior to failure.

The softening expression provided by Belarbi and Hsu is less severe than the one by Vecchio and Collins. This might be due to the angle of reinforcement (45 degrees in the case of Vecchio and Collins and parallel in the case of Belarbi and Hsu).

Based on measurements of reinforced cylindrical specimens under axial compression and internal pressure, Okamura and Maekawa (1987) developed the following expression for softening:

$$\beta = 1.0 \; for \; \varepsilon_1 < \varepsilon_a$$

$$\beta = 1.0 - 0.4\frac{\varepsilon_1 - \varepsilon_a}{\varepsilon_b - \varepsilon_a} \; for \; \varepsilon_a \leq \varepsilon_1 \leq \varepsilon_b \qquad (2.75)$$

$$\beta = 0.6 \; for \; \varepsilon_b < \varepsilon_1$$

where $\varepsilon_a = 0.0012 \; and \; \varepsilon_b = 0.0044$.

Shirai (1989) performed tests on small reinforced panels and derived the following:

$$\beta_1 = -\left(\frac{0.31}{\pi}\right) tan^{-1}(4820\varepsilon_1 - 11.82) + 0.84 \qquad (2.76)$$

$$\beta_2 = -5.9 - \frac{\sigma_1}{f_c'} + 1.0 \qquad (2.77)$$

$$\beta = \beta_1 \text{ x } \beta_2 \qquad (2.78)$$

Kupfer and Bulicek (1991) proposed a constant softening factor (0.85) coupled with a sustained load factor of 0.80:

$$f_{c2} = 0.80 \times 0.85 \times f_c' \approx \frac{2}{3} f_c' \qquad (2.79)$$

They also considered the following expression with a constant softening factor:

$$f_{c2} = f_c' \times 0.85 \times 0.75 \left(1 - \frac{f_c'}{250}\right) \qquad (2.80)$$

where 0.85 is the factor for sustained load, 0.75 is the factor for irregular crack trajectory, and $1 - \frac{f_c'}{250}$ is the difference between cylinder strength and uncracked concrete prism strength.

Reineck (1991) also proposed that the strength of the web struts be taken no lower than:

$$f_{cw} = 0.80 f_c' \qquad (2.81)$$

To account for the effects of transverse reinforcement in tension, Prisco and Gambarova (1995) proposed that the concrete strength be reduced by:

$$f_c = 0.75f_c' \ \ or \ f_c = \frac{0.90f_c'}{\sqrt{1+600\varepsilon_1}} \geq \frac{f_c'}{2} \tag{2.82}$$

Due to the presence of so many formulations for shear friction and concrete softening, a parametric study was performed by Duthinh (1999) to examine the effect that shear friction and concrete softening have on concrete shear strength, according to the Modified Compression Field Theory. The results indicated that:

1. The ratio of reinforcement is in inverse proportion with shear friction; as the reinforcement ratio decreases, the effect of shear friction increases.
2. The effect of stress normal to the interface (σ) were negligible regardless of which method was used.
3. Failure by concrete crushing was predicted to happen for very wide cracks, much higher than Walraven's experimental data ($v \leq 0.08$ in, $w \leq 0.06$ in).
4. The models of Kollegger, Okamura, Miyahara, and Shirai demonstrate significant postlinear strength and no concrete crushing. The models by Ueda and Noguchi also demonstrate concrete crushing after significant postlinear strength and wide cracks.
5. The models presented by Vecchio, Collins, and Hsu show no significant postlinear strength gained.

Depending on the method of estimation, the shear strength of beams with low shear reinforcement could be decreased by 15-25% if a decrease in shear friction occurs (according to MCFT). This has been experimentally observed in HSC beams.

Kuchma and Hawkins (2008) assembled a large experimental database and evaluated the accuracy of the different design methods to determine the shear-strength ratio of test results to code prediction (V_{test}/V_{code}). A total of 1359 beams were tested from which 878 were RC beams and 481 were PC beams. The majority of the PC beams were T-shaped and I-shaped and had depths less than 20 in, and were simply supported on bearings. Most members were subjected to four-point loading. Several design procedures that were used in design practice were studied and compared: ACI 318-02, AASHTO Standard Specifications (2002), AASHTO 1979 Interim Specifications, Canadian Standard Association (CSA) Design of Concrete Structures (1994 and 2004, respectively), AASHTO LRFD Specifications, Eurocode 1 and 2 (from 1991 and 2002, respectively), the German code DIN 1045-1, the Japanese specifications for design and construction of concrete structures, and the shear design approach by Tureyen and Frosch (2003). Kuchma and Hawkins summarized these results in NCHRP Report 549, "Simplified Shear Design of Structural Concrete Members", and recommended simplified provisions, which were implemented, to the existing Sectional Design Method in AASHTO LRFD. Prior to the implemented changes, AASHTO LRFD used a shear design procedure based on (and derived from) MCFT (Modified Compression Field Theory), in which the values for the critical parameters β and θ were obtained from tables. Note that the shear strength calculated using the AASHTO LRFD Sectional Design Method does not provide the same shear strength calculated by MCFT. An interesting observation was made by the authors regarding the minimum

transverse reinforcement, in that it was specified in AASHTO LRFD as 50% more than the minimum required reinforcement by the AASHTO Standard Specifications.

Some results from the evaluation and comparison of the codes were:

1. Most design procedures (Canadian Standard Association (CSA) Design of Concrete Structures 1994 & 2004, AASHTO 1979 Interim Specifications, AASHTO LRFD Specifications, Eurocode 1 and 2, and the German code) permit designers to use the angle θ as less than 45 degrees when calculating shear strength by shear reinforcement.
2. The AASHTO LRFD Specifications, Eurocode 1&2, and the German code allow the design of members that support much larger shear stresses than permitted in the traditional design approach. An important observation was made that the AASHTO Standard Specifications places a limit on the shear stress that can be supported by the concrete as $8\sqrt{f_c'}b_v d$ to prevent diagonal crushing of the concrete before the yielding of the reinforcement. However, MCFT has determined that such failures do not occur until shear stresses reach a level of ¼ of f'_c; this difference primarily affects concrete with 10 ksi or greater compressive strength.
3. From all methods evaluated, the CSA and the AASHTO LRFD methods provided the most accurate estimates for the shear strength ratio. The means were consistent and the COV (coefficient of variation) values were low. These two methods would be expected to result in conservative designs.
4. Based on the close mean and COV values for the CSA and AASHTO LRFD methods, it was determined that these methods would yield similar designs and therefore the design equations of CSA 2004 for β and θ could be adopted for the AASHTO LRFD method.
5. For members with shear reinforcement close to the minimum required by the ACI code, the shear strength ratios were often under 1.0, which emphasizes the fact that the higher minimum shear reinforcement imposed by AASHTO LRFD method is necessary.
6. Beams with a large amount of reinforcement were able to support high shear stresses (up to $0.25f'_c$), which indicates that the upper shear strength limit imposed by the ACI code is conservative compared with the higher strength limit in the AASHTO LRFD specifications.

These findings resulted in two main changes to the LRFD Design Specifications:

1. Development of the Simplified Method. The simplified provisions differed from the existing AASHTO LRFD specifications in several aspects; expressions for web shear cracking, the angle θ of the diagonal compression in the parallel chord truss model, the maximum allowed shear stress, the minimum required amount of reinforcement, the evaluation of shear depth, and the requirements for the amount of longitudinal reinforcement that must be developed at the face of the support. Moreover, new equations were developed for the web shear component V_w and the flexure shear strength V_{ci}. The shear strength contribution of concrete V_c was taken to be the smaller of the two. Therefore, the new provisions present the V_c as the lower bound of the possible concrete shear strength. The concrete shear strength contribution is comprised of the shear carried in the compression zone, shear carried along diagonal cracks due to shear friction (aggregate interlock), direct tension across diagonal cracks, dowel action, and arch action. However, accounting for all of these factors would complicate the procedure. Therefore, the simplified provisions accounted for the lower bound estimate of the diagonal cracking load that,

when summed with the stirrup contribution to shear resistance, resulted in a conservative estimate of the capacity.

2. Equations to calculate β and θ values. The second significant change involved using the expressions for calculating β and θ present in CSA method. This would eliminate the iterative aspect of the shear design in the AASHTO LRFD specifications. In addition, a new equation for the mid-depth strain was developed which assumed θ was 30 degrees when evaluating the influence of shear on longitudinal strain. The equations for these changes were presented in the AASHTO LRFD Bridge Design Specifications summary in Part 1 of this review.

Other researchers have conducted code comparisons for prestressed concrete girders as well, and in general, it was found that, relative to LRFD, shear design by the Standard Specifications is generally less conservative as girder spacing and span decrease. These differences are detailed in NCHRP Report 368 (Nowak 1999) and must be considered along with capacity to assess differences and problems among the design approaches. However, it should be noted that these differences are due to girder distribution factor approaches rather than assessment of shear strength. Kuchma et al. (2008) also recommend using the LRFD Sectional Design Model for high strength prestressed concrete girders.

Additional research has been conducted to develop new approaches to shear design in RC and PC beams. These approaches were mainly based on the MCFT method or the Strut and Tie model. Ramirez and Breen (1991) proposed a modified truss model with a variable angle of inclination for diagonal struts and a concrete contribution for beams with web reinforcement. The model includes a diminished concrete contribution to account for the variable angle truss model. For PC beams, the model utilizes a constant concrete contribution, but limits the compressive strength to $30\sqrt{f_c'}$, and lowered the angle of inclination from 30 degrees for RC beams to 25 degrees for PC beams. The provisions were compared with a large number of test results and were found satisfactory. Shahawy and Cui (1999) worked to develop a tied-arch model for the shear design of PC beams. This model was applied to predict the failure load and to study the interaction between the tie, the shear reinforcement, and the struts. Iteration is required to solve the equations and a few critical assumptions must be made. Experimental testing was conducted on 25 full scale AASHTO girders, and the proposed model was used to rate the girder capacities. The authors recommended use of the model due to its consistency, and suggested that, for deep beams and beam ends, the contribution of shear reinforcement, which is usually ignored in typical strut-and-tie models, should be included.

Cladera and Mari (2006) provide a revision of a previously proposed tension-shear model (intended for the shear design of reinforced concrete beams) and applied it to the design of PC beams with or without web reinforcement. For the beams with web reinforcement, the design procedure was based on a truss model with variable angle of inclination of the struts and a concrete strength contribution. The model was based on the MCFT method, where the angle of inclination is obtained by compatibility. The model includes the interaction of axial loads and bending moment. The procedure takes into account the influence of compressive strength on the size effect and limits the strength of beams without stirrups to 8.7 ksi. It also accounts for the non-linear relationship between the amount of shear reinforcement and shear strength. The procedure was found satisfactory for all tests done, and it appeared to correlate well with the ACI procedures. It provides one formulation for both RC and PC beams.

Wang and Meng (2008) developed a modified strut-and-tie model which is useful for the design of simply supported deep beams. The effects of prestressing is modeled with equivalent externally applied loads. The effect of concrete softening is taken into account (the model is based on the Kupfer-Gerstle biaxial tension-compression criterion) by adding an adjustment factor determined from consideration of force and moment equilibrium. The model was validated using the experimental results of 56 simply supported PC deep beams and found to be accurate, consistent, and conservative. Similarly, Ning and Tan (2007) worked to develop a modified strut-and-tie model for determining the shear strength of reinforced concrete deep beams based on the Mohr Coulomb failure criterion. More recently, Tuchscherer et al. (2011) proposed a modified strut-and-tie model based on experimental data from a database of 868 deep beam tests. The procedure was proposed for the strength design of deep-beam regions.

Other work of interest includes that of Esfandiari and Adebar (2009), who present a shear strength evaluation procedure similar to the AASHTO LRFD method (2008) without the need for iteration. The approach considers the failure modes of stirrup yielding, diagonal concrete crushing, and longitudinal reinforcement yielding. The approach was compared to the traditional MCFT model of a beam under uniform shear as well as to numerical models of beams under combined shear and bending. For validation, the shear strength predictions were compared to shear strength results from experimental results and provisions by ACI 318 and AASHTO LRFD. Laskar et al. (2010) present a simple shear design equation that was experimentally developed. Five PC beams were tested and several variables were considered: shear span-depth ratio (a/d), transverse steel ratio (ρ_t), the presence of harped strands in the web, and flexural shear capacity. Their developed expression is a function of shear span to depth ratio (a/d), concrete compressive strength $\sqrt{f_c'}$, web area $b_w d$, and the steel reinforcement ratio ρ_t. It was also shown that the prestressing force and the angle of failure crack had no effect on shear strength. The authors also derived a formula for the maximum shear strength to guarantee prevention of web crushing prior to reinforcement yielding. The proposed method was evaluated by comparing it to the provisions of the ACI 318 code and AASHTO LRFD 2007 Specifications. Most recently, Yang et al. (2011) proposed a mechanism analysis based on the upper-bound theorem of concrete plasticity to predict the critical failure plane and corresponding shear capacity of reinforced concrete dapped-end beams. Failure modes observed in physical tests of reinforced concrete dapped-end beams were idealized as an assemblage of two moving blocks separated by a failure surface of displacement discontinuity. The developed mechanism analysis represented the effect of different parameters on failure modes, and the predicted shear capacity was in good agreement with test results. Furthermore, it was observed that empirical equations specified by PCI as well as a strut-and-tie model based on ACI 318-05 highly underestimated test results.

Experimental Results

Early results include Mast (1964), who considered some of the most common girder shapes and analyzed them for shear and flexure according to the provisions of the ACI 318-63 code. The height-to-span ratio was found to be the crucial parameter in determining whether the member was controlled by shear or flexure. Nazir and Wilby (1964) tested the behavior and strength in shear of uniformly loaded, post-tensioned prestressed concrete beams without web reinforcement. Comparisons were made with tests on similar beams under different load

configurations and the results indicated that the shear strength was influenced by the type of loading. Beams with uniformly distributed loads failed at higher ultimate shears than similar beams tested under concentrated loadings.

Gustafson and Bruce (1966) present the results from tests conducted on eight PC beams and five smaller RC beams simply supported and equally loaded at third points of the span. The main variable of the test was shear reinforcement (including vertical, inclined and prestressed reinforcement—bonded or unbonded). Seven of the beams failed in shear and one had a transitional failure. The results were compared with the AASHTO and ACI code strength predictions. The study determined that the shear strength of full size PC girders can be predicted with reasonable accuracy from tests on smaller laboratory specimens. It was also observed that if failure occurred from flexural shear cracking, prestressing the web reinforcement did not add to the ultimate strength of the member. Inclination of the web stirrups also did not add to the ultimate shear strength, but it did better control the opening of inclined cracks than did vertical stirrups.

Fenwick and Paulay (1968) determined that shear may be resisted by beam and arch action, but at the diagonal cracking load, beam action breaks down. They also determined that, unless beams contain prestressed reinforcement, arch action cannot develop to a significant extent prior to diagonal cracking. It was also demonstrated that the shear strength of beam action strongly depends on the mechanisms of shear transfer across crack; by interlocking of aggregate particles and to a lesser extent, by dowel action of the reinforcement. At about the same time, Hanson and Hulsbos (1969) conducted laboratory fatigue tests on six prestressed concrete I-beams to determine their shear strength. Each beam was loaded statically to almost 80% of its ultimate flexural capacity and later subjected to repeated loads varying in magnitude between 20-45% of flexural capacity for about 2,000,000 cycles. The load range was increased until failure. The tests demonstrated that the prestressed concrete beams have a significant shear fatigue resistance. In addition, shear fatigue failures did not occur suddenly, but gave considerable warning with increasing deflection and shear crack widths before failure.

Later, Bennett and Mlingwa (1980) conducted tests on twenty-eight PC beams with prestressed web reinforcement and stirrups of mild or high strength steel. The results served to develop a formula to calculate the width of inclined cracks and ultimate shear capacity of beams with vertical prestressing. It was observed that the prestressing part of the web reinforcement increased the inclined shear and ultimate shear strengths. Hartmann et al. (1988) evaluated the adequacy of code provisions for shear capacity when considering high strength prestressed concrete girders. The results of shear testing of ten pretensioned girders made from concrete with compressive strength ranging from 10-13 ksi were summarized. Existing design approaches were found to be acceptable for concrete up to at least 12 ksi. It was observed that the three design methods studied displayed little variation from conservatism as a function of concrete strength. It was also shown that the maximum shear reinforcement limits could be significantly increased.

Libby and Konzack (1985) discussed the shortcomings of using ACI code provisions for the shear design of PC beams. An issue that complicates the shear design of PC bridges is that, based on the results of NCHRP Report 322, *The Design of Precast, Prestressed Bridge Girders Made Continuous* (Oesterle et al. 1989), depending on the construction sequence and reinforcement detailing, some continuous PC bridges have been flexurally-designed as if they were simply

supported spans under some load conditions, potentially resulting in under-design in some instances. Maruyama and Rizkalla (1988) studied the influence of slippage of prestressing strands on the behavior of pretensioned concrete T-beams. The effect of various shear reinforcement configurations, crack behavior, overall deformation, and mode of failure are investigated. Based on the test results, a proposed mechanism was introduced to describe the behavior of such beams, and design recommendations are presented.

Aboutaha and Burns (1991) studied how the mode of failure of prestressed composite flexural members could be changed from a sudden shear failure to a ductile flexural failure by utilizing external prestressing bars. This research studied the behavior of retrofitted prestressed composite beams that originally lacked shear reinforcement. Before retrofitting, these beams experienced sudden horizontal shear failures. However, ductile flexural failures occurred after the sections were retrofitted with external prestressing bars. Fagundo et al. (1995) studied the effects that shear span-to-depth ratio and moment-to-shear ratio have on the interaction between bond and shear forces in prestressed concrete girders. The study also focused on identifying parameters that affect the transfer length of the prestressing strands and evaluation of current code provisions. Two sets of four simply supported beams were tested. The beams tested at small shear span/depth ratios tended to fail in a brittle manner, where the behavior was governed by strut and tie action in the disturbed region. The beams tested at longer shear span/depth ratios (greater than 2.5) tended to fail in a more ductile manner, and it was found that the modified compression field theory provided a reasonable method of analysis for these beams. It was found that the presence of shear cracks deteriorated the bond between the tendons and the surrounding concrete. As the shear cracks formed, there were sudden increases in tendon slip in every case. The shear and bond forces did appear to be related, but premature shear failures due to excessive loss of bond were not experienced.

Cumming et al. (1998) performed four shear tests on high-strength concrete prestressed girders. The shear test results were compared with predicted results from the ACI 318-95 Simplified Method, the ACI 318-95 Detailed Method (AASHTO 1989), the Modified ACI 318-95 Procedure, Modified Compression Field Theory (AASHTO LRFD 1994), the Modified Truss Theory, Truss Theory, Horizontal Shear Design (AASHTO 1989), and the Shear Friction approach (AASHTO LRFD 1994). The calculated shear capacities were in all cases conservative compared to actual shear capacity.

Ranasinghe et al (2001) describe the effect of bond between the reinforcement and concrete on the shear behavior of reinforced and prestressed concrete beams. Seven beams with different bond conditions were tested to failure, while stress-slip relationships for these specimens were obtained from a parallel series of simple pullout tests. A numerical analysis was also conducted to simulate the beams tested. It was found that the bond condition of steel bars and prestressing bars highly influences the shear strength and failure mode of RC and PC beams. A reasonably good correlation was observed between the experimental and analytical results.

Higgins et al. (2003) investigated how shear capacity of reinforced concrete bridge beams is affected by stirrup corrosion damage, using accelerated corrosion tests and experimental testing. The authors describe the decrease in shear capacity as a function of stirrup corrosion. It was found that severely corroded rectangular beams typically experience a 10-30% capacity loss, but losses may be higher for T-beams. It was also found that existing shear capacity equations could

predict shear capacity for beams with corrosion damage provided that the section losses in steel and concrete are accounted for in the methods. Damage to the concrete from shear reinforcement corrosion is dependent upon stirrup spacing; as stirrup spacing decreases, the amount of corrosion required to crack the concrete also decreases. Moreover, diagonal cracking did not occur at lower loads for the corroded specimens, indicating that the cover concrete does not appear to be as significant as the core concrete contribution to shear strength. Later, Higgins et al. (2004) investigated the remaining capacity of cast-in-place reinforced concrete bridges with diagonal tension cracks. A database of 442 bridges constructed from 1947 to 1962 was developed. It was found that none of the bridge database parameters were prominent in predicting shear cracking. One of the subtle trends found was that bridges with greater crack damage tended to have larger girders and longer span lengths. A bridge with shear cracks was identified for field testing. Eight diagonal cracks were instrumented with LVDTs and stirrups near the cracks were instrumented with strain gages. A FEA model of the bridge was also constructed to investigate possible crack causes. In addition to dead and live loads, thermal loading, drying shrinkage, creep, and support displacement were considered. It was found that load distribution under service loads may be reasonably predicted using a linear finite element analysis, even when diagonal cracks are present. It was also found that better load distribution of shear forces across the girders is achieved as the slab thickness increased, and; diaphragm stiffness had little effect on the shear force distribution. The FE model considering dead and live loads, and loads due to drying shrinkage and nonuniform temperature changes, could predict the diagonal-tension cracking of the girders.

Oh and Kim (2004) experimentally explored the shear behavior of post-tensioned prestressed concrete girders. Girders were tested to failure while deflections, steel stirrup strains, cracking pattern, and average strains in the web were monitored. The stirrup strains showed a sudden increase immediately after cracking and continued to grow as the load increased. It was found that the angle of principal strain direction decreased as the applied load increased and that it approached approximately 23 to 25 degrees at the ultimate load stage. Hegger et al (2004) used laser-interferometry and photogrammetry devices to attempt to gain insight to the shear resistance mechanism of PC beams by studying pre- and post-cracking behavior. It was found that a nonlinear stress distribution was evident before the formation of visible cracks, thereby influencing the cracking angle. It was also shown that for beams with low or high shear reinforcement ratios, the amount of shear force transferred across cracks by shear friction was negligible.

Recupero et al. (2005) attempted to generalize a model for evaluating the shear strength of prestressed beams that was previously proposed for box and I-shaped reinforced concrete cross sections. After being modified, the model included the effect of prestressing tendons, and took into consideration variable-depth stress fields applied to the cross section. The method was validated by comparing its numerical results to the strength provided by tests on reinforced concrete beams and on thin-webbed prestressed concrete beams. The method was used in the design of a pretensioned bridge beam to evaluate the additional reinforcement necessary in the flanges, as a function of the reinforcement provided to the web. Cederwall (2006) summarized the results of experimental investigations of the shear capacity of composite prestressed concrete I-beams. On the basis of the test results, the relevance of the equation in the Swedish Code BBK-79 for shear capacity of homogeneous prestressed concrete beams is discussed, if applied to composite beams. The test series indicated a slight overestimation of the beneficial influence of

prestressing, which was greater for homogeneous beams than for composite beams. De Silva et al. (2007) experimentally explored the shear cracking behavior of prestressed reinforced concrete girders. Tests were conducted on three I-shaped RC beams and four I-shaped PC beams. The variables of interest were the prestressing force, side concrete cover, stirrup spacing, bond characteristics of the stirrups, and amount of longitudinal reinforcement. The influence on shear crack width from each of these parameters was observed. The study determined that the prestressing force significantly reduced the shear crack width in PC beams compared to RC beams. Furthermore, an equation was proposed to calculate the shear crack width of PC beams.

More recently, Pei et al. (2008), as reported in (FHWA OK-08-08), conducted analytical and experimental studies of shear capacities of prestressed concrete bridges in Oklahoma. The concern was to determine if older structures were adequate in shear. The study focused on precast pretensioned prestressed concrete girders, mainly AASHTO Type II girders, designed according to AASHTO Standard Specifications prior to the 1979 Interim provisions. In the study, actual girders removed from the I-244 Bridge and the Wild Horse Creek Bridge were tested. Camber measurements were taken to estimate the prestressing stress as well as flexural stiffness, as according to Sandburg (2007), the prestressing stress has a significant influence on shear carrying capacity. Results obtained from the tests were then compared to the performance standards provided by different design codes. Three different code provisions were compared on the basis of minimum shear reinforcement (Fig. 2.1); shear demand (Fig. 2.2), nominal shear strength (Figs. 2.3 and 2.4), and margin of safety (Figs. 2.5 and 2.6). The latter was defined as the ratio of the factored nominal shear capacity to design shear demand considering all loads and reduction factors. It was found that the actual tested capacity of the bridge girders exceeded the nominal capacity of each code.

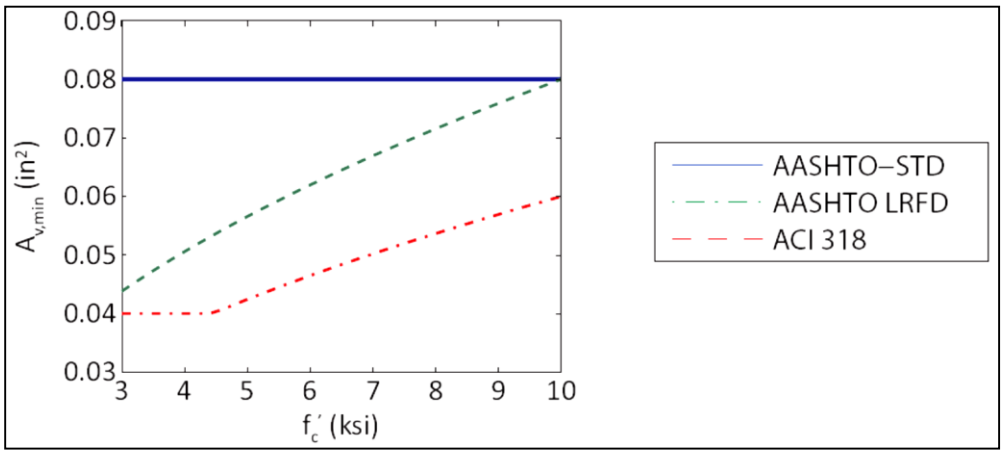

Figure 2.1. Minimum Shear Reinforcement Required With Varying Compressive Strength (Sandburg 2007).

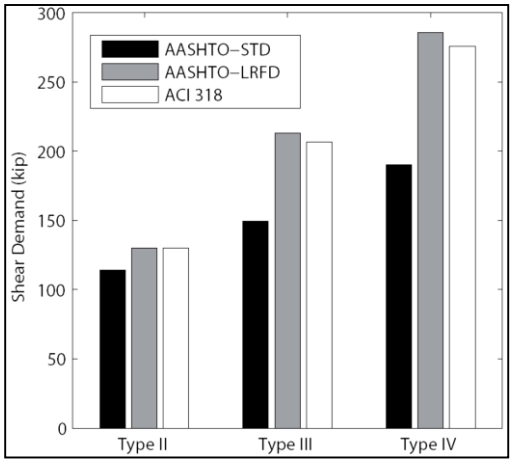

Figure 2.2. Comparison of Ultimate Shear Demands For Different AASHTO Girders (Sandburg 2007).

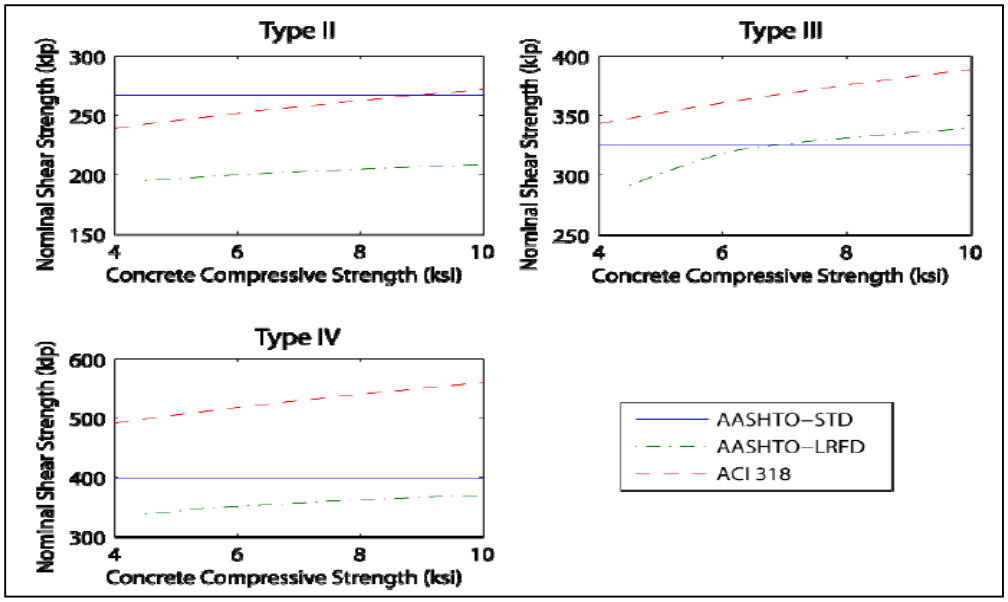

Figure 2.3. Nominal Shear Strength As Affected By Concrete Compressive Strength For AASHTO Types II, III And IV Prestressed Concrete Girders (Sandburg 2007).

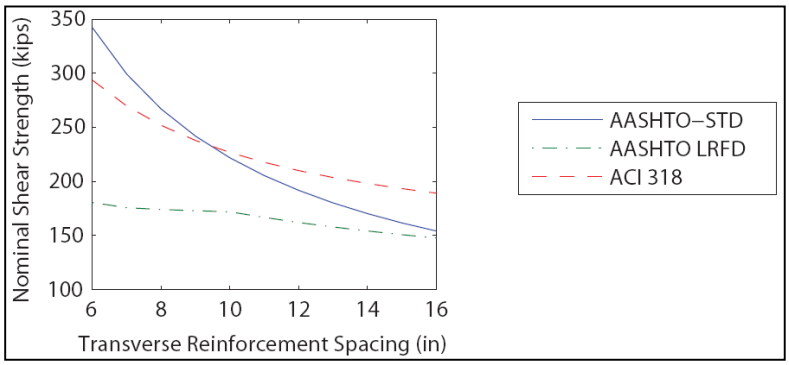

Figure 2.4. Nominal Shear Strength Of A Type II Girder With Varying Stirrup Spacing (Sandburg 2007).

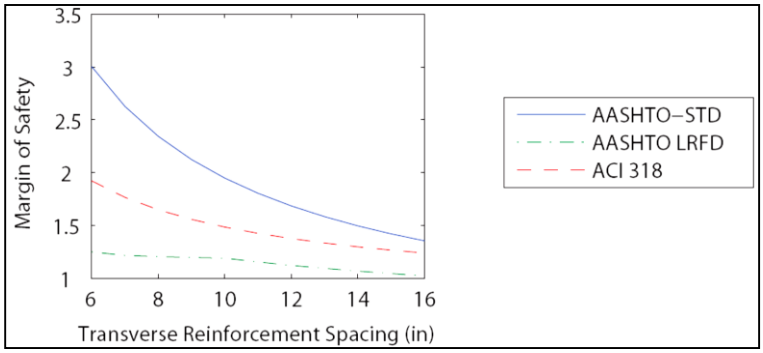

Figure 2.5. Margin Of Safety Of A Type II Girder With Varying Stirrup Spacing (Sandburg 2007).

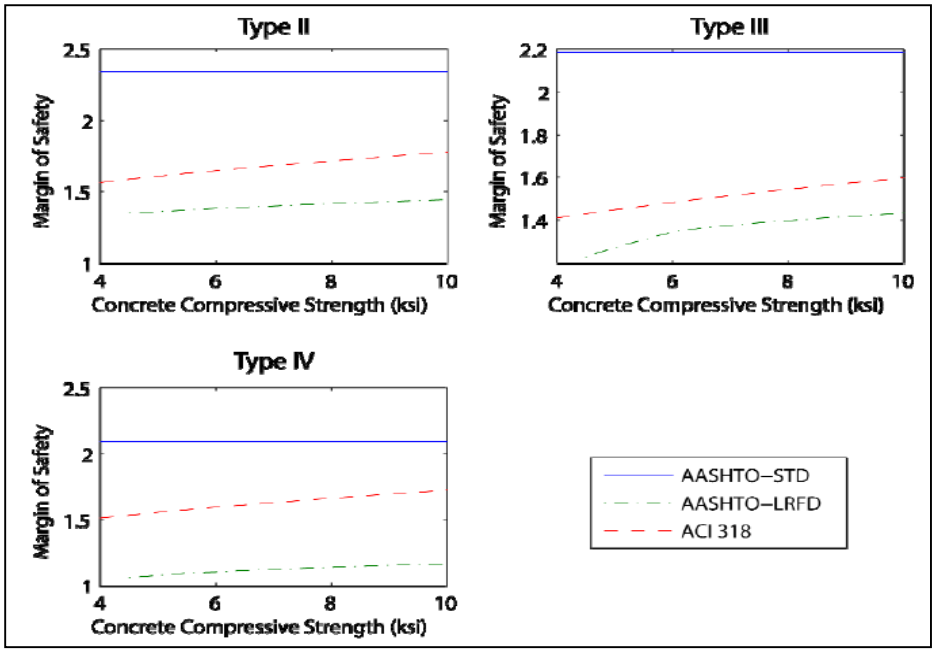

Figure 2.6. Margin Of Safety As Affected By Concrete Compressive Strength For AASHTO Types II, III And IV Prestressed Concrete Girders (Sandburg 2007).

A similar study was conducted by Runzell et al. (2007) for the Minnesota Department of Transportation. The scope of the study was to determine whether bridge girders designed according to the 1979 Interim provisions were underdesigned for shear according to current code provisions (such as AASHTO LRFD code). Two shear capacity tests were performed on opposite ends of a bridge girder removed from a highway bridge in Minnesota, which was designed according to the 1979 Interim shear provisions. The results from the shear tests indicated the girder was capable of holding the required shear demand because the applied shear at failure for both tests was larger than the factored shear strength required by the 2004 LRFD HL-93 and 2002 Standard HS20-44 loads (Table 2.2). The results of a parametric study, however, showed that some girders designed using the 1979 Interim Specifications would most likely be underdesigned for shear near the supports. The girders most likely to be underdesigned in this region had relatively smaller length to girder spacing ratios. Moreover, girders were most likely to be underdesigned for shear between 0.1*L* (*L* is the girder span length) and the support.

In this region, the $\frac{\phi V_n}{V_u}$ ratio for the girders varied between 0.73 and 1.09, and was proportional to the $\frac{L}{S_g}$ ratio, where S_g is girder spacing. Girders with a length-to-spacing ratio of more than 10 were determined to be safe, while those with ratios under 8.5 were determined to be under-designed in shear.

Similarly, Ross et al. (2011) evaluated the structural condition of prestressed concrete girders salvaged from a bridge in the Gulf of Mexico in Florida. The four salvaged girders were AASHTO type III from a bridge built in 1979. The girders were originally designed using the 1973 edition of the AASHTO Standard Specifications. Girders were tested using a three-point loading scheme with five different *a*/*d* (shear span-to-depth) ratios ranging from 1.2 to 5.4.
The results were presented according to the *a*/*d* used and the corresponding modes of failure: bond-shear failure, shear-compression failure, or flexural failure.

Table 2.2. Shear Test Rresults (Runzell et al. 2007).

		V_{pred} (kips) (Measured material properties)	V_{test} (kips) (Including dead load)	$\frac{V_{test}}{V_{pred}}$
Specimen I (with bridge deck)	2004 LRFD	259	392	1.51
	2002 Standard	316		1.24
	1979 Interim	189		2.07
	Strut and Tie	281		1.40
Specimen II (no bridge deck)	2004 LRFD	204	329	1.61
	2002 Standard	238		1.38
	1979 Interim	157		2.09
	Strut and Tie	246		1.34

Each of the three girders tested (Table 2.3) at an *a*/*d* of 3 or less (G1, G2, and G3) demonstrated bond-shear failure. Bond-shear failure was identified by the formation of flexural cracks in the strand development length and by slipping of the strands. Results of the tests indicate that capacity of the prestressing strands was limited by slipping and that additional capacity beyond this slip point might be possible with the use of vertical and horizontal mild steel reinforcement. Two girders were tested with an *a*/*d* of 4.1 (G4-1 and G4-2). Girder G4-1 failed in a shear-compression mode, whereas girder G4-2 failed in a bond-shear mode. Although the girders failed differently, their shear versus displacement behavior was similar. One girder was tested with an *a*/*d* of 5, and the failure was categorized as flexural. Overall, the 30-year-old girders performed well in the load tests. The full-scale testing gave no indication of reduced capacity or performance as a result of exposure or use. Testing confirmed visual ratings made during inspections before demolition.

Ma and Hu (2008) developed formulas that could determine the diagonal section strength of composite prestressed concrete beams (such as those where reaction powder concrete is applied in the unbonded prestressed composite beams without stirrups). The new formulas were found to be less conservative than the existing ones. Saqan and Frosch (2009) investigated the shear strength and behavior of partially prestressed reinforced concrete rectangular beams with prestressing strands and reinforcing bars, but without transverse reinforcement. Tests were conducted on nine large-scale beams, and the prestressing force was kept constant. Test variables were the amount of prestressing steel and the amount of mild steel. A strong correlation was

found between the flexural reinforcement and shear strength of PC beams. In general, the total amount of reinforcement controls the behavior and strength of the member until the first shear crack occurs.

Table 2.3. Comparison Of Calculated Shear Capacity To Experimental Results (Ross et al. 2011).

a/d	Test	*Vexp*	MCFT		STM		ACI detailed		Modified end region	
			Vn	*Vexp/Vn*	*Vn*	*Vexp/Vn*	*Vn*	*Vexp/Vn*	*Vner*	*Vexp/Vn*
1.2	G1	344	211	1.63	159	2.16	268	1.28	252	1.37
2.1	G2	255	231	1.10	108	2.36	243	1.05	255	1.00
3.1	G3	207	193	1.07	n.a.	n.a.	227	0.91	222	0.93
4.2	G4-1	180	181	0.99	n.a.	n.a.	181	0.99	n.a.	n.a.
4.2	G4-2	198	181	1.09	n.a.	n.a.	181	1.09	n.a.	n.a.
5.4	G5	158	167	0.95	n.a.	n.a.	160	0.99	n.a.	n.a.

Note: units in kips. *a/d*=shear span-to-depth ratio; MCFT=modified compression field theory; STM=strut-and-tie method; *Vexp* = experimental shear capacity; *Vn* = nominal shear capacity; *Vner* = nominal shear capacity of the end region.

Llanos et al. (2009) tested three types of concrete bridge girders: AASHTO Type IV, AASHTO Type III, and post-tensioned girders with a design established in the 1950s. For the AASHTO Type IV girders, it was found that capacity was not controlled by typical shear failure mechanisms, but rather was due to cracking and separation of the bottom bulb flange of the girder. This was a result of the unusual debonding pattern that placed the fully bonded strands in the bulb flange and the debonded strands under the web. A carbon fiber-reinforced plastic (CFRP) fabric strengthening system was tested to alleviate issues associated with the strand debonding pattern. The AASHTO Type III girders were tested at *a/d* ratios ranging from 1-5. For *a/d* ratios of 3 or less, the failure mode was strand slip, which was precipitated by the formation of cracks in the strand development length zone. While these cracks resulted in strand slip, transverse and longitudinal mild steel reinforcement at the girder end was engaged, which improved the capacity and ductility beyond the first strand slip. Unique features of the 1950s design included the presence of both straight and parabolic post-tension bars, and lack of shear reinforcement away from the end block. The girder tested with direct bearing on concrete displayed a 7% larger capacity and nearly half the displacement of a similar girder tested on a neoprene bearing pad.

Idriss and Liang (2010) measured in-service shear and moment girder distribution factors in simple-span prestressed concrete girders with a built-in optical fiber sensor system. This system was built into the I-25 Bridge in New Mexico during construction. The bridge is composed of six simple-span, high-performance prestressed concrete girders. Sensors were installed along the top and bottom flanges and at midspan and quarter spans. Pairs of crossed sensors in a rosette configuration were also embedded in the webs at the supports. The bridge was monitored for two years, from transfer of the prestressing force through service. The sensor data were analyzed to evaluate shear and moment girder distribution factors, in situ material properties, prestress losses, camber, dynamic load allowance, and bridge performance under traffic loads. Shear and moment girder distribution factors were obtained from a finite element model, sensor measurements under a live load test, as well as regular traffic loading and compared with the

values specified by the AASHTO standard specifications (2002) and the AASHTO load and resistance factor design specifications (2007).

Lee et al. (2010) investigated the shear deformation of large-scale reinforced I-shaped girders and post-tensioned prestressed concrete girders with a small shear span-depth ratio of 2.5. The test variables were the compressive strength of the concrete, the stirrup ratio, and the prestressing force. This large-scale experimental study enabled the investigation of diagonal cracking behavior, crack patterns, principal strain direction, and crack width, as well as ultimate shear capacity. From the experimental results, it was shown that the ultimate shear capacity of concrete girders increased with an increase in the concrete compressive strength, the stirrup ratio, and the prestressing force. The effect of concrete strength in the girders with stirrups and prestressing force, however, was not as much as in those without stirrups and prestress. It was also shown that the stirrup was highly effective for controlling diagonal crack width, whereas the prestressing force is only effective at delaying cracking load. It was found that the presence of stirrups was the dominant factor contributing to the arching action of a beam member with a short shear span-depth ratio.

Yoshitake et al. (2011) emphasized the difficulty of evaluating shear cracking load since many factors influence the behavior of RC and PC flexural members. The results showed that reinforcement had little influence on the shear cracking strength. On the other hand, tensile strength and Poisson ratio were strongly related to shear cracking strength. Burgueno and Sun (2011) investigated the effect of strand debonding and end zone cracking in MDOT prestressed concrete beams. It was observed that typical cracks are horizontal or diagonal with a positive slope, which can be clearly distinguished from shear cracks. A series of experimental studies using scaled beam specimens, as well as finite element modeling, was used to study the relationship between debonding and end zone cracking. It was found that debonding strands using flexible sheathing can crack the concrete along the debonded length, due to the expansion of the debonded strand at transfer. Cracking can be avoided by using oversized rigid sheathing, providing space for the strand to expand.

Numerical Modeling

Few studies in the technical literature are specifically focused on the numerical modeling of prestresssed concrete girder shear behavior. However, a review of numerical modeling-focused research is given below.

Laskar et al. (2010) discus development of the Cyclic Softened Membrane Model (CSMM), which has been efficiently used to predict the behavior of RC and PC beams critical in shear. CSMM has been implemented into the OpenSees (Open System for Earthquake Engineering Simulation) finite element framework, and is being implemented in the finite element program Simulation of Concrete Structures (SCS). To create SCS, five full scale prestressed girders were tested to study web shear and flexural shear behavior. The failure plane on each of the girders occurred at an angle of approximately 45 degrees, which was inconsistent with the provisions of AASHTO and ACI 318 codes (where angles of failure planes ranged from 22.3-35.7 degrees for AASHTO and 37.5 degrees for ACI code). To confirm the failure angle, the researchers used SCS. It was found that SCS was capable of predicting the shear behavior of beams under vertical loading well.

Mahesh and Surinder (2011) predicted the shear strength of RC and PC deep beams by using Support Vector Regression. Here, a back-propagation neural network and three empirical relations were used to model reinforced concrete deep beams. For prestressed deep beams, one empirical relation was used. Results suggest an improved performance could be obtained by use of SVR in terms of prediction capabilities in comparison to the existing empirical relations and the back propagation neural network. Parametric studies with SVR suggest the importance of concrete cylinder strength and ratio of shear span to effective depth when predicting the strength of deep beams. The SVR model was also used to perform parametric studies, which suggest that the shear strength of deep beams is in direct proportion with the concrete strength and inversely proportional to the shear span-to-depth ratio. However, it was found that the shear strength of deep beams is not affected by the variation in horizontal web reinforcement for shear a span-to-depth greater than 1. The results of the parametric studies using SVR were in agreement with previous work.

Liu et al. (2011) discus a method that uses inner transverse prestressing bars to enhance the shear capacity of concrete beams. Four transversely prestressed concrete beams and one ordinary reinforced concrete beam were modeled using a nonlinear finite element method. A parametric study was carried out to analyze the behavior of the PC beams. It was found that the transverse prestressing bars can increase the shear capacity and failure load of the reinforced concrete beam, where the increase in prestressing force directly increases the shear capacity of reinforced beams. It was found that bars with smaller diameters and smaller spacing can be more efficient in enhancing the shear capacity of transversely prestressed concrete beams.

NCHRP Reports

The NCHRP Reports most relevant to this project are discussed earlier in this Chapter (NCHRP 322; 368; and 549). However, a summary of additional report information is provided below.

The objective of NCHRP 368, *Calibration of LRFD Bridge Design Code* (Nowak 1999) was to develop the reliability-based calibration for the Load Resistance Factor Design bridge design code. Load and resistance factors were derived so that the reliability of bridges designed using the proposed provisions will be at the predefined target level. The report describes the calibration procedure and reviews proposed changes to load and resistance models. It was found that the AASHTO Standard Specifications resulted in PC beam designs in shear that generally had reliability indices lower than the target proposed for the AASHTO LRFD Specification, with least-reliable beams in the smaller girder spacing and spans. However, as noted above, this is due to girder distribution factor and design load discrepancies in the Standard Code rather than calculation of shear capacity.

NCHRP 454, *Calibration of Load Factors for LRFR Bridge Evaluation* (Moses 2001) presented the derivation of live load factors and associated checking criteria incorporated in the proposed *Manual for Condition Evaluation and Load and Resistance Factor Rating of Highway Bridges* prepared for NCHRP Project 12-46. A major goal in the study was to unify the reliability analyses and corresponding database used in the load and resistance factor rating (LRFR) and the recommendations for the Evaluation Manual compatible with the AASHTO LRFD bridge design

specifications. Although the report considers all types of bridges, it provides no particular insight for the shear design or behavior of prestressed concrete bridges.

NCHRP 485, *Bridge Software-Validation Guidelines and Examples* (Baker et al. 2003) developed a process for bridge design and analysis software validation. The study has resulted in a test-bed of bridges with well-defined parametric inputs and outputs. The Report allows comparison of the results of multiple software analysis packages and/or hand calculations to the same data. Various prestressed concrete sections were considered in the test-bed, and errors in some existing software for computing the shear in prestressed concrete girders were identified.

The objective of NCHRP 517, *Extending Span Ranges of Precast Prestressed Concrete Girders* (Castrodale and White 2004) was to address the limitations caused by the infrequent use of prestressed concrete girders for spans longer than 160 ft. The authors address this issue by extending the practical use of prestressed concrete girders to longer spans and to applications not normally associated with prestressed concrete girder construction. The major goal of the research was to provide the a design procedure for long span prestressed girders. Suggested design details and examples are presented. Particular attention was given to the effects of splicing long girders on shear and shear transfer through joints, with the interface shear at bent caps of interest.

NCHRP 549, *Simplified Shear Design of Structural Concrete Members* (Hawkins et al. 2005) developed simplified shear design provisions for the AASHTO LRFD Bridge Design Specifications that attempted to overcome perceived difficulties with using the previous shear design provisions. The detailed provisions recommended by this project were described earlier in this report.

NCHRP 579, *Application of LRFD Bridge Design Specifications to High-Strength Structural Concrete: Shear Provisions* (Hawkins and Kuchma 2007), proposed guidelines to allow the use of concrete strengths up to 18 ksi for shear design. It addressed the compression angle θ; the proper concrete strength contribution to shear strength; minimum shear reinforcement; and maximum shear limits. It was found that the existing LRFD values for θ, β, and minimum shear reinforcement were safe to use for high strength concrete, but the maximum shear stress limit requires restriction.

In NCHRP 654, *Evaluation and Repair Procedures for Precast/Prestressed Concrete Girders with Longitudinal Cracking in the Web* (Tadros et al. 2010), guidelines were established for the acceptance, repair, or rejection of precast/prestressed concrete girders with longitudinal web cracking. The cracks of concern occur in the end zone as a result of prestress transfer, and may result in debonding and increased corrosion. Experimental tests determined that girder shear capacities were larger than estimated by code design procedures even when longitudinal cracks were present. The report proposes revisions to the AASHTO LRFD Bridge Design Specifications and provides recommendations to develop improved crack control reinforcement details for use in new girders. To achieve this objective, guidelines were established for various cracking categories such as: cracks that are not required to be repaired, cracks that are required to be repaired, including the methods and materials of repair, and cracks that cause structural capacity to be compromised and thus may cause the girders to be rejected.

NCHRP 678, *Design of FRP Systems for Strengthening Concrete Girders in Shear* (Belarbi et al. 2011) develops recommendations for a design method that can be used to strengthening concrete girders in shear using externally bonded FRP systems. It was found that beams with existing shear cracks displayed stirrup yield at a lower shear force than beams that did not have cracks, and limiting stirrup stress to the yield stress will avoid fatigue failures in the girder.

NCHRP 700, *A Comparison of AASHTO Bridge Load Rating Methods* (Mlynarski et al. 2011) compared the load factor rating to load and resistance factor ratings for various design vehicles. It provides proposals for changes to the AASHTO *Manual for Bridge Evaluation* through the extensive data analysis of 1,500 bridges of varying material types and structure configurations. The bridges were analyzed using the AASHTO Virtis software. It was found that a significant number of the girders analyzed achieved favorable LFR ratings but had LRFR ratings less than 1.0. This occurred because LRFR included evaluation criteria not covered by LFR that in fact governed the rating, though these criteria did not include prestressed concrete girder shear strength checks. However, for concrete structures, the suggested evaluation provisions include a check for shear capacity when the factored load effects from the permit load exceed the factored load effects from the design load, which was not previously included under LFR. It was recommended that concrete bridges that show no visible signs of shear problems need not be checked for shear when rating for design or legal loads, however. Revisions to load factors for permit vehicles were suggested to increase the target reliability index to 3.5.

CHAPTER 3: FIELD STUDY OF PC BRIDGES

A field survey of bridges suspected to have diagonal cracks was conducted from January – March, 2012. The purpose of the investigation was to identify girders which may have shear distress and to determine, if possible, common characteristics for shear-distressed girders. Such information may suggest reasons why shear problems may be occurring. Twenty three structures to inspect in the Metro and University Regions were initially identified as shown in Tables 3.1 and 3.2, below.

Table 3.1. Initial List Of Bridges.

	BRIDGE	FACILITY	FEATURE	BUILT	STATUS
	METRO REGION				
1	7933	COOLIDGE ROAD	I-696	1985	INCLUDE
2	11114	I-94 WB	MERRIMAN RD	1993	box beam
3	11115	I-94 EB	MIDDLEBELT RD	1993	box beam
4	11116	I-94 WB	MIDDLEBELT RD	1993	box beam
	UNIVERSITY REGION				
5	1829	US-127 SB	M-21	1993	INCLUDE
6	1830	US-127 NB	M-21	1993	INCLUDE
7	2332	EATON HWY	I-69 NB & I-96 WB	1961/81	INCLUDE
8	3717	US-127 NB	SYCAMORE CREEK	1966	no access
9	3831	ZIMMER RD	I-96 WB	1962	no V cracks
10	3841	WALLACE RD	I-96	1962	no access
11	3848	US-127 SB	VINE ST	1970	no V cracks
12	3849	US-127 SB	SELLERS ST	1970/98	INCLUDE
13	3854	US-127 NB	VINE ST	1970	no V cracks
14	4447	E SOUTH ST	US-127	2001	no V cracks
15	7132	US-24	SWAN CREEK	1922/93	not visited
16	9728	M-52	SHIAWASSEE RIVER	1999	INCLUDE
17	10879	WARREN RD	US-23	1962	no access
18	12693	US-127 SB	LOOKING GLASS RIVER	1997	INCLUDE
19	12773	CENTERLINE ROAD	US-127	1993	INCLUDE
20	12774	TAFT ROAD	US-127	1993	no V cracks
21	12775	TOWNSEND ROAD	US-127	1993	no V cracks
22	12943	I-496 EB	GR RIV,I-96 BL, RIVER ST	2000	no V cracks
23	12944	I-496 EB SERV RD	GR RIV,I-96 BL, RIVER ST	2000	no V cracks

Of these, four structures were deemed inaccessible by the MDOT inspection crew (#8, 10, and 17), while three were later identified as box beam bridges, beyond the scope of the project (#2, 3, 4), and one was not visited due to its inconvenient distance (#16), per the judgment of the MDOT inspection crew. Thus, 16 structures were inspected. Of these, 8 were found to have no significant shear cracking. The 8 remaining structures (highlighted in Table 1) were found to have potentially significant shear cracking. These findings are summarized in Appendix A. In the Appendix, structures are presented in the order of visitation, with representative diagrams and pictures of the shear cracks. Note that some cracks did not photograph well, and non-illustrative pictures were not included. Examples of representative cracks found are given in Figures 3.1- 3.4.

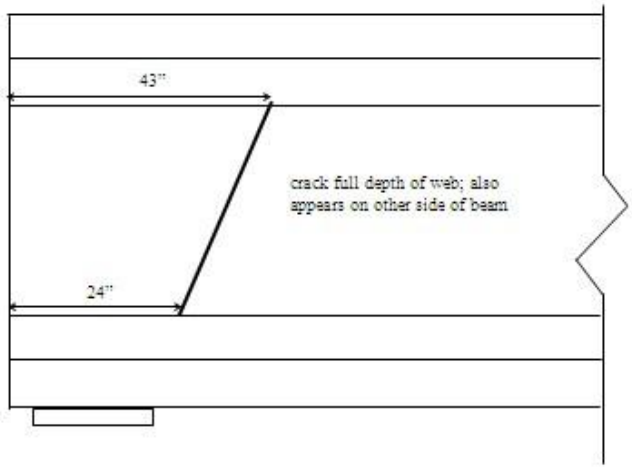

Figure 3.1. Crack Diagram For South Span Girder, North End, 4th Beam From East Side, West Face (Bridge 1, #7933).

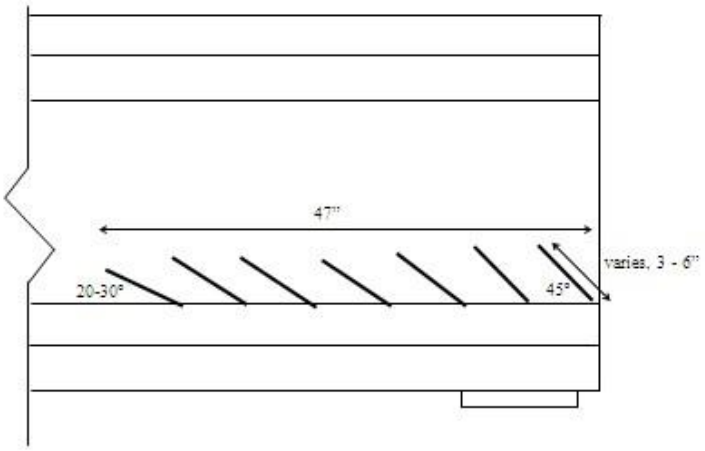

Figure 3.2. Crack Diagram For Exterior Girder, West Side, West Face, South Abutment (Bridge 16, #9728).

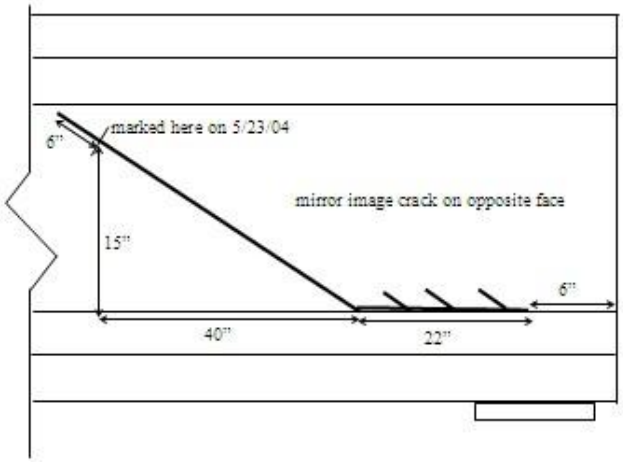

Figure 3.3. Crack Diagram For Girder 5th From West Side, West Face, South Abutment (Bridge 18, #12693).

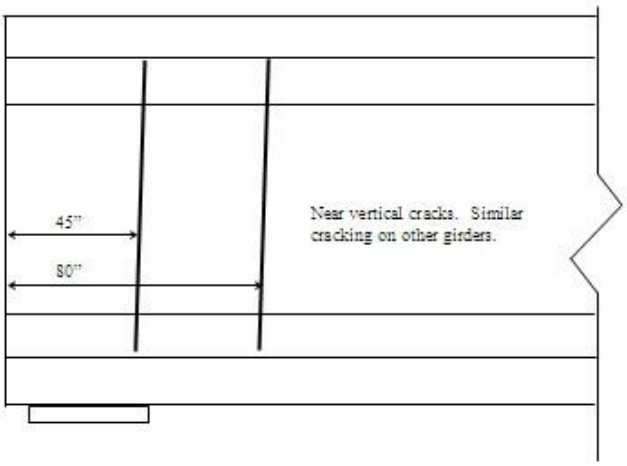

Figure 3.4. Crack Diagram For Girder 2nd From South Side, South Face, West Abutment (Bridge 19, #12773).

Table 3.2. Summary Of Inspector Comments.

	INSPECTOR COMMENT
1	Diagonal shear cracks at the beam web of the fascia beams of span 2s.
	Diag. shear cracks at the webs of Bm 2e, 3e, 4e, 5e, 6e, 8e.
2	Tight shear cracks at fascia beams at east abutment.
3	Tight shear cracks at fascia beam ends, typical.
4	Tight shear cracks at south fascia beam ends at abutments and at pier 1w.
5	Tight diagonal crack in web of each beam end.
6	Few diagonal cracks near beam ends at abutments.
7	Few tight shear cracks in fascia beams near bearing areas.
8	Diagonal cracks on south end of beam 1w span 2s.
9	Hairline vertical & diagonal cracks in beam ends.
10	Cracks in webs of a few beam ends.
11	Diagonal cracks at pier 1s: beam 7w span1s; beams 1,5,7w span 2s.
12	Diagonal and vertical cracks in beam 8w near north backwall.
13	Shear cracks: BM1,2 SP3 P2; BM1,2,3 SP2 P2; BM7 SP2,3; BM1,2,7S P2 P1 & BM1 SP1 P1
14	Beams 2 & 3 at east abutment and beam 2 at west abutment have tight shear cracks.
15	Tight diagonal cracks at the beam ends.
16	Minor tight diagonal cracks in fascia beam ends at abutments.
	Tight diagonal cracks in bottom flange of beam 5w span2s at pier.
17	Tight diagonal crack on south face of beam that extends along top flange,
	crack goes from the outside edge of the gravel shoulder to the yellow lane line.
18	Beam 5w at south abutment has tight diagonal crack in web.
19	Tight diagonal & vertical cracks near most beam ends.
20	Tight diagonal and vertical cracks near beam ends in various locations.
21	Tight diagonal cracks near beam ends over piers.
22	Most concrete I-beams have tight horizontal and diagonal cracks at ends over piers.
23	Tight diagonal and cracks in most beam ends over piers, cracks more defined in spans 1,2 and
	3W. Shear crack 0.020 inch wide in beam 5S at pier 1w span 1W, on both sides of beam.

Construction as-built plan sets were obtained for the 16 structures shown in Table 3.1, in addition to 4 LRFD-designed structures. Available structural characteristics that were thought to have possible influence on shear cracking are provided in Tables B1a-c. In Table B1a, Bridge ID cells shaded in red indicate girders with shear cracks. In Table 4.1b, *Strand Dist Proportion* refers to the proportion: (girder centriod - strand centroid) / (girder centroid), where centroids are measured from the bottom of the girder at the critical section; *Ac* is the area of the non-

composite section; *Girder Total Ps* is the total initial prestress force imparted to the girder, and *Girder sps* is the average stress in the non-composite girder due to the initial prestress force (i.e. total initial prestress / Ac). In Table B1c, *End Zone Steel Spacing* indicates the number of stirrups and spacing near the supports. *Lifetime Trucks* is an estimation of the total commercial truck traffic that passed over the structure during its lifetime, as calculated based on the ADTT estimates from the 2010 Sufficiency Report (MDOT 2010), multiplied by the number of years of bridge service. For most structures, however, no information on traffic is available.

There was no strong pattern revealed between a particular set of bridge characteristics and shear cracks, other than the observation that no structure with end blocks experienced cracking. Average applicable characteristics in Tables B1a-c are given in Table B1d, with slight differences between them. Cracked girders did tend to be associated with longer spans, larger girders, and higher average prestress stresses, however. Although the particular AASHTO code version used to design the structures is not apparent, as the age range of structures considered is from 2-33 years, with both cracked and non-cracked bridges appearing throughout the age range (with the exception of LRFD-designed bridges, which have no cracks), a particular code version used to design the structure does not appear to be directly linked to cracking.

Each different span of the structures in Table B1 (for 78 total cases) were analyzed for shear load and capacity according to the 2010 AASHTO LRFD Code; the 1979 Interim Specifications; and the 2002 Standard Code. Material strength values not provided on the plans were taken from the MDOT Bridge Analysis Guide. Results of this analysis is presented in Tables B2-B4. In the tables, V_c is the concrete contribution to shear capacity; V_s is the steel contribution, and V_p is the prestressing strand contribution. V_n is the total shear capacity ($V_n = V_c + V_s + V_p$), while *phi*V_n refers to ϕV_n, with ϕ specified per code used. V_u is the design shear force (i.e. factored total load including dead and live loads), while *V1* is the shear force due to all specified unfactored design loads (including dead load, truck load, impact, and lane load, if applicable). *V2* is the shear force due to a unfactored HS20 truck and dead load only.

Various ratios of shear capacity and shear loads are presented in Table B5a. As expected, all structures evaluated had design capacities greater than design loads for at least one code version (i.e. $\phi Vn / Vu \geq 1.0$), with one exception: Span 2 of Bridge 3854, which had a maximum ratio of 0.90. Of the 74 spans evaluated, 11 did not meet Standard requirements; 8 did not meet LRFD requirements, and only 1 did not meet 1979 Interim requirements.

Table B5b presents the average capacity/load ratios for cracked and uncracked spans. As shown, for most ratios, there is no significant difference between the cracked and uncracked structures. The ratio which shows the greatest proportional difference between the cases (1.1 for cracked, 1.3 for uncracked) is that of $V_c / V2$, with V_c evaluated with the 1979 Interim code.

To identify any patterns, the shear ratios in Table B5 were sorted by ratio magnitude. It was found that the best predictor of cracking resulted with the ratio of $V_n/V2$, with V_n found from the 1979 Interim Specifications. These results are presented in Table B6. Here, most structures that cracked had the lowest $V_n/V2$ ratios, where 8 of the 11 spans with cracked girders had $V_n/V2$ ratios of 3.3 or less (with a ratio range from 1.9 to 5.8). Moreover, 5 of the 11 cracked spans has $V_n/V2$ ratios of 2.4 or less. However, two of the structures, Bridges 7933 and 3849 spans 1&3b, had some of the highest $V_n/V2$ ratios. Both of these structures are somewhat special cases,

however. Bridge 7933 (Coolidge Road over 696) had nearly all girders with significant shear cracks, very much unlike the other structures, which may indicate a special case. Bridge 3849 was constructed with different girder sizes, as shown in Figure 3.5. It is notable that the cracked girder is on the exterior of the east side (to the left in the figure). Here, the cracked girder (AASHTO Type II) is adjacent to two smaller girders (AASHTO Type I), which have significantly less stiffness. It is expected that the more stiff exterior girder will attract more force than the less stiff adjacent girders, thereby causing it to absorb proportionally more load than expected if all girders were designed assuming the same girder distribution factor. Referring to Table B5b, the average ratio of V_n / *V2* (Interim) was found to be 3.2 for cracked and 3.9 for uncracked, approximately a 20% difference. Therefore, the V_n / *V2* ratio, with V_n evaluated with the 1979 Interim code, may be a reasonable predictor of shear crack potential for typical cases.

Additionally, the principal tension stress for a typical span from each structure was analyzed. Stress was calculated due to (unfactored) dead load, prestress force, and a HS20 truck, at the composite girder centroid at 1 ft and 2 ft away from the girder end (with dead load and prestress stresses calculated based on the noncomposite section). The factor needed to be multiplied to the HS20 truck weight in order for the principal tension stress to equal the concrete cracking strength, evaluated both as $3.5\sqrt{f_c'}$ (*ft1*) and $6.4\sqrt{f_c'}$ (*ft2*), was determined. Results are presented in Table B7. Results sorted based on factor magnitude are given in Table B8. Factors ranged from 1.9 – 5.2 for *ft1* and 3.7-7.8 for *ft2*. It was found that the cracked girders tended to fall towards the lower range of factors, with the lowest factor girders cracked and the highest factor girders remaining uncracked, in all sort cases. In each sort, the average factor is lower for the crack structures than the uncracked. In general, although some patterns have emerged, differences are not large. A similar result was found by Higgens et al. (2004), where over 400 reinforced concrete bridges were studied, and little difference was found in structural characteristics with regard to shear cracking potential.

There are several possible reasons why cracking is not clearly linked to computed shear capacity/load ratios. The first is that code methods for shear strength prediction were not particularly accurate for the beams considered. This can be seen from the experimental results of this study (see Table 4.8, Chapter 8) as well as the results of the finite element modeling (see Figures 7.1-7.3, Chapter 7). It is also likely that other critical factors are associated with crack development, such as girder manufacturing processes; girder transportation and construction loads; vehicular overloads; thermal, shrinkage, or other special loads; and differences in structural characteristics found from the construction documents and otherwise assumed and as built. Unfortunately, these data are unavailable.

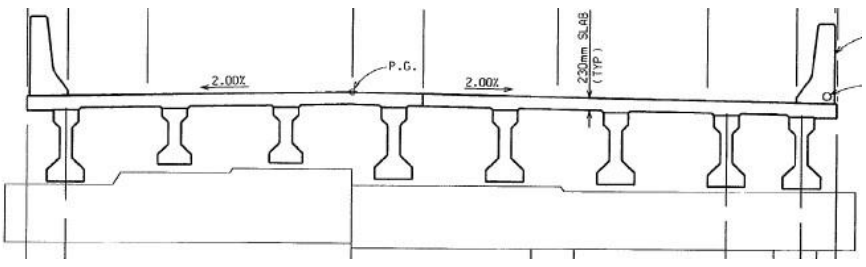

Figure 3.5. Bridge Section (Bridge 12 (#3849), M27 over Sellers Ave.)

To further check for patterns, additional shear analyses were conducted for the bridges using additional loads, as recommended by the research advisory panel: For LFR analyses, truck numbers 5-DL, 18-DL and 23-DL were used, as specified in the Bridge Analysis Guide. For bridges that did not have a Virtis file, Truck 18-D was used. For LRFR analyses, trucks 4-DL, 5-DL, 16-DL, 17-DL and 18-DL were used for bridges that have a Virtis file. For bridges that did not have a Virtis file available, Truck 4-DL was used for spans less than 50' and Truck 16-DL was used for spans greater than 50'.

Resuls are presented in Tables B9-B29. In the tables, the following notation is used with regard to loads: V_u is the total factored shear force. For V_u calculations, the truck-specific strength load factor taken from the MDOT Bridge Analysis Guide (BAG) was considered (5000 ADTT). *V1* is the shear force due to the unfactored truck, impact, lane and dead loads, while *V2* is the shear force due to unfactored truck (no impact) and dead loads only. Note for LRFD analysis, capacity *Vn* changes as a function of load applied. These capacities are provided in Tables B20-B29. As shown in the tables, using the additional load configurations revealed no new patterns.

CHAPTER 4: LABORATORY TESTING

To collect the experimental information necessary for development of a reliable numerical model, two full-scale AASHTO Type II girders were tested in controlled conditions under various load configurations. Each girder was tested three times in different regions of the span by adjusting support locations, to generate data for different critical shear span-to-depth ratios and stirrup spacings. The shear span is altered by adjusting the support locations. For each beam, the portion of the span which is to be preserved for subsequent testing is clamped with steel bars acting as external stirrups to prevent any significant damage in this region during the first two tests. A summary of the critical beam parameters is given in Table 4.1. Note that the numerical model (see Chapter 5) was first developed based on Beam 1 test results. Then, Beam 2 test parameters where chosen to represent configurations that the numerical model had most difficulty predicting well.

Table 4.1 Summary Of Test Beam Parameters.

	Test	*S* (in)	*a/d*
Beam 1	1	8.0	2.8
	2	8.0	3.4
	3	21.0	3.4
Beam 2	1	21.0	2.0
	2	21.0	2.8
	3	21.0	3.5

Beam 1

Beam 1 was cast on 1/28/2013 at Stress-Con Industries (Kalamazoo), and transported to the University of Michigan Civil and Environmental Engineering Structures Lab for testing. The casting specification sheet is given in Appendix C. The layout for Beam 1 is shown in Figure 4.1, where the load (*P1, P2, P3*) and support (*A, B, C, D*) positions for each test are summarized, as well as stirrup spacing and section geometry. Note all dimensions are given in inches. Beam tests 1-3 were carried out on 4/29, 5/3, and 5/20 (2013), respectively. The beam was instrumented with strain gages on transverse steel stirrups, an Optitrack camera grid for measuring displacements on the beam exterior in the critical shear region, as well as potentiometers at supports and near the load location at the bottom of the beam, as shown in Figures 4.2 and 4.3.

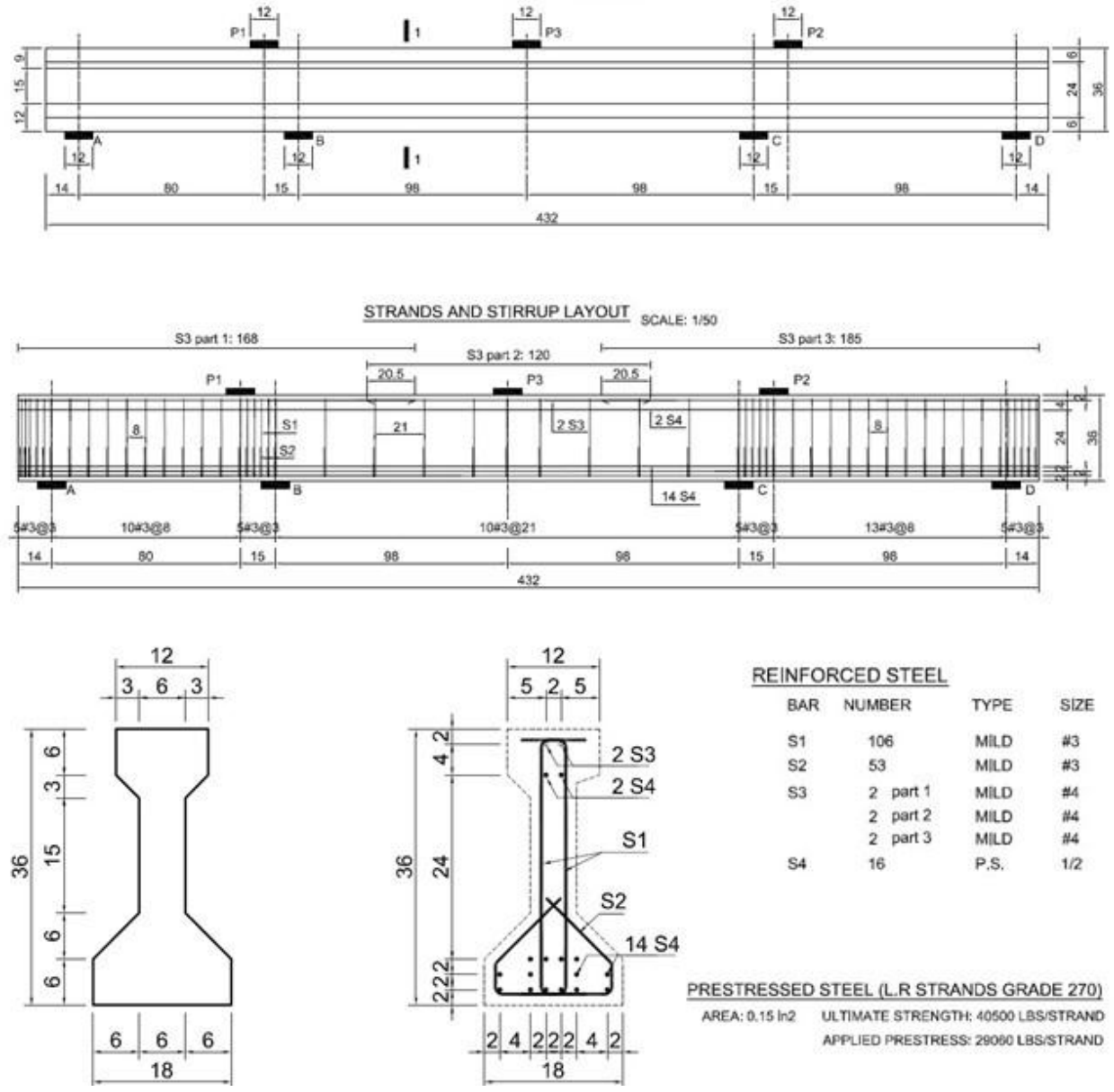

Figure 4.1. Beam 1 Layout (dimensions in inches).

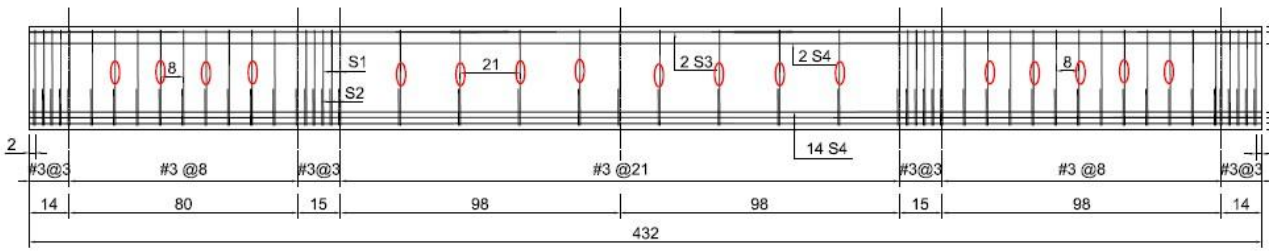

Figure 4.2. Strain Gage Location (dimensions in inches).

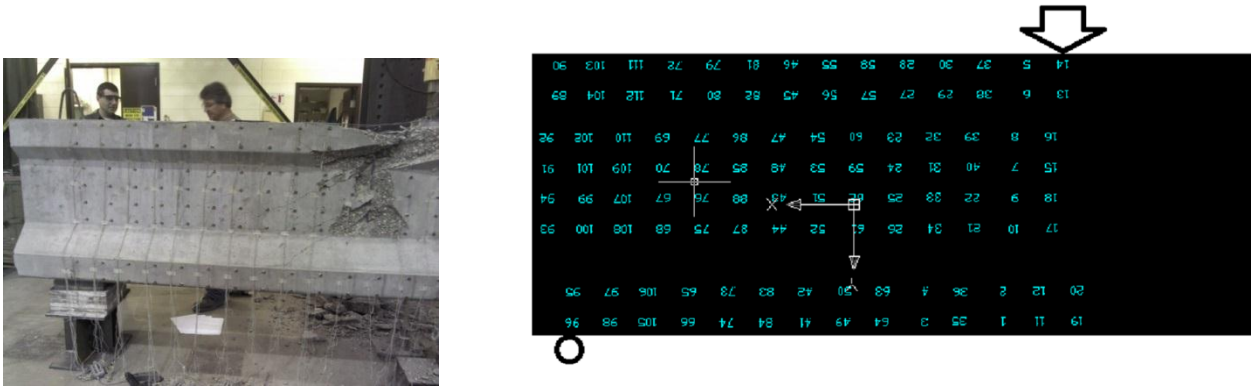

Figure 4.3. Optitrack Grid.

Beam 1, Test 1

For test 1, the beam was supported and loaded as shown in Figure 4.4.

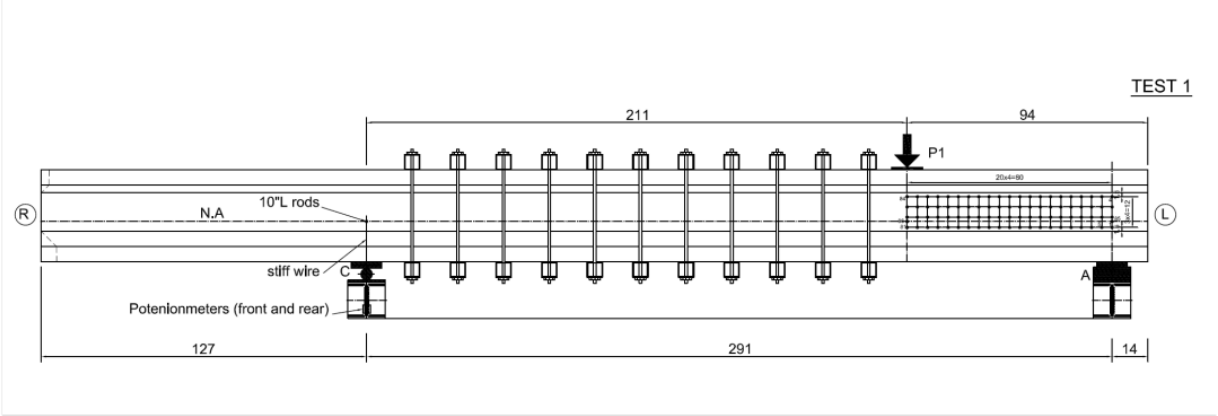

Figure 4.4. Beam 1 Test 1 Configuration (dimensions in inches).

Five concrete cylinders were tested on test day, with results shown in Table 4.2. Note that the mean strength (7.6 ksi) is substantially higher than the 5.5 ksi as specified in the design.

Table 4.2. Beam 1 Test 1 Cylinder Tests.

Cylinder	Failure Load (kips)	Stress (psi)	% from mean
1	76.1	6057	-20.8
2	115.9	9222	20.6
3	88.9	7072	-7.5
4	109.0	8670	13.4
5	90.7	7219	-5.6
Mean	96.1	7648	

The test results are summarized in Figures D1-D4 (Appendix D). First cracking load occurred at approximately 180 kips (Figure D1); flexural cracks appeared at approximately 280 kips (Figure D2); and failure occurred at approximately 300 kips (Figures D3 and D4).

Beam 1 Test 2

For test 2, the beam was supported and loaded as shown in Figure 4.5.

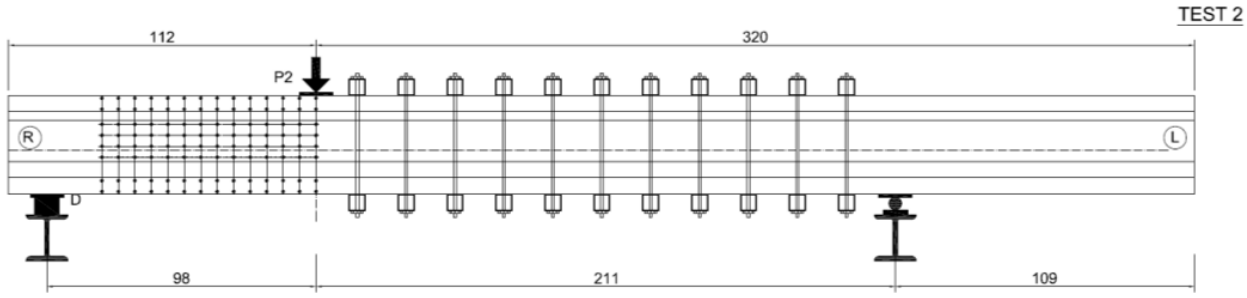

Figure 4.5. Beam 1 Test 2 Configuration (dimensions in inches).

Concrete cylinder strength test results on the test date are given in Table 4.3.

Table 4.3. Beam 1 Test 2 Cylinder Tests.

Cylinder	Failure Load (kips)	Stress (psi)	% from mean
1	81.5	6482	-17.7
2	120.3	9572	21.6
3	105.7	8414	6.9
4	86.3	6863	-12.8
5	101.0	8038	2.1
Mean	99	7874	

The test results are summarized in Figures D5-D7 (Appendix D). First cracking load occurred at approximately 200 kips (Figure D5). Figure 5.11 shows the beam response before failure, while failure occurred at approximately 265 kips (Figure D7).

Beam 1 Test 3

For test 3, the beam was supported and loaded as shown in Figure 4.6.

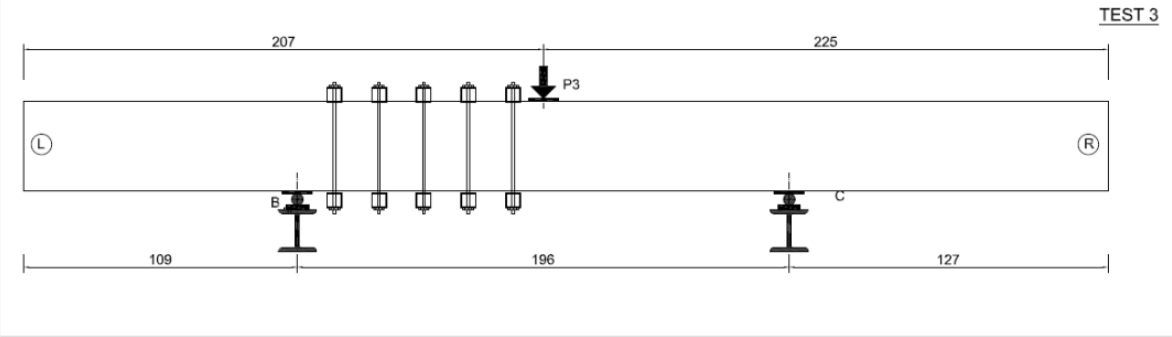

Figure 4.6. Beam 1 Test 3 Configuration (dimensions in inches).

Concrete cylinder strength test results on the test date are given in Table 4.4.

Table 4.4. Beam 1 Test 3 Cylinder Tests.

Cylinder	Failure Load (kips)	Stress (psi)	% from mean
1	106.3	8455	-1.9
2	112.3	8933	3.6
3	94.4	7513	-12.9
4	127.2	10125	17.4
5	101.6	8081	-6.3
Mean	108.3	8622	

The test results are summarized in Figures D8-D10 (Appendix D). First cracking load occurred at approximately 220 kips (Figure D8), while failure occurred at approximately 355 kips (Figures D9 and D10).

Beam 2

Beam 2 was cast on 8/30/2013. The casting specification sheet is given in Appendix C. The layout for Beam 2 is given in Figure 4.7, with geometry and properties otherwise similar to Beam 1. The beam was instrumented similar to Beam 1. Beam 2 tests 1-3 were carried out on 10/10, 10/17, and 10/29 (2013), respectively.

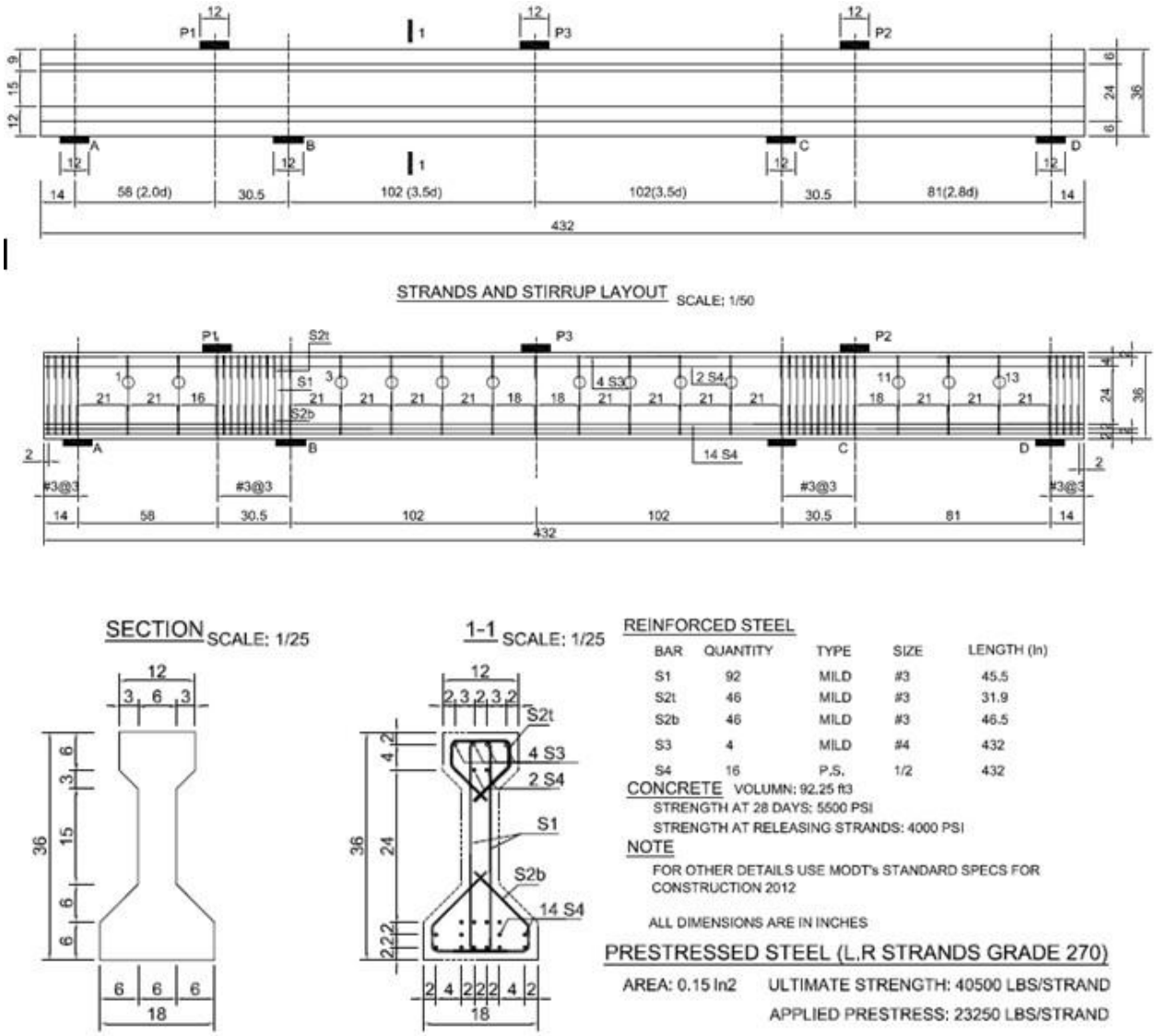

Figure 4.7. Beam 2 Layout (dimensions in inches).

Beam 2, Test 1

For test 2, the beam was supported and loaded as shown in Figure 4.8.

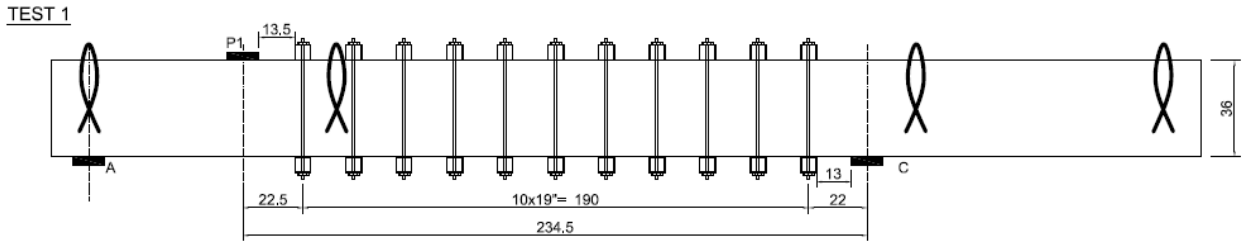

Figure 4.8. Beam 2 Test 1 Configuration (dimensions in inches).

Five concrete cylinders were tested on test day, with result shown in Table 4.5.

Table 4.5. Beam 2 Test 1 Cylinder Tests.

Cylinder	Failure Load (kips)	Stress (psi)	% from mean
1	120.4	9579.5	4.8
2	110.0	8754.2	-4.2
3	115.6	9196.0	0.8
4	123.0	9788.7	6.8
5	104.0	8274.5	-10.2
Mean	114.6	9118.6	-

The test results are summarized in Figures D11 and D12 (Appendix D). As with Beam 1, Test 1, first cracking load occurred at approximately 180 kips (Figure D11). For safety concerns, the test was stopped at 294 kips, due to localized concrete crushing under the load point, indicating impending failure based on previous test results (Figure D12).

Beam 2 Test 2

For test 2, the beam was supported and loaded as shown in Figure 4.9.

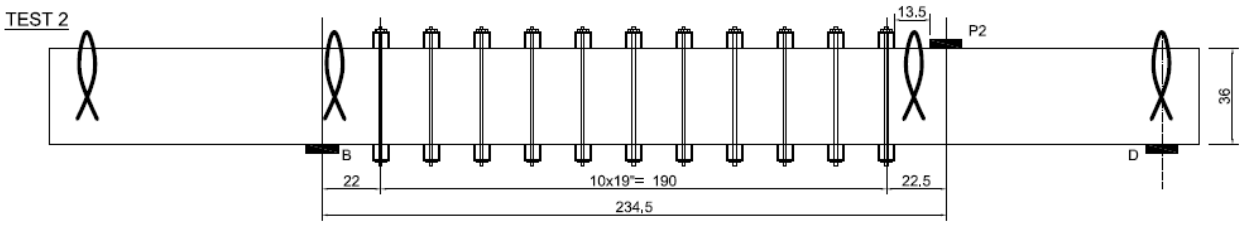

Figure 4.9. Beam 2 Test 2 Configuration (dimensions in inches).

Concrete cylinder strength test results on the test date are given in Table 4.6.

Table 4.6. Beam 2 Test 2 Cylinder Tests.

Cylinder	Failure Load (kips)	Stress (psi)	% from mean
1	126.5	10065	8.7
2	119.1	9475	3.0
3	101.2	8056	-14.0
4	130.6	10388	11.6
5	104.4	8307	-10.6
6	111.0	8835	-4.0
Mean	115	9188	

The test results are summarized in Figures D13-D16. First cracking load occurred at approximately 175 kips (Figure D13); flexural cracks appeared at approximately 200 kips (Figure D14); and failure occurred at approximately 267 kips (Figures D15 and D16).

Beam 2 Test 3

For test 3, the beam was supported and loaded as shown in Figure 4.10.

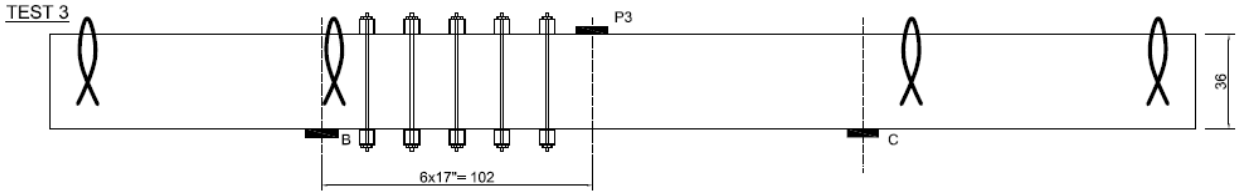

Figure 4.10. Beam 2 Test 3 Configuration (dimensions in inches).

Table 4.7. Beam 2 Test 3 Cylinder Tests.

Cylinder	Failure Load (kips)	Stress (psi)	% from mean
1	126.6	10074	8.6
2	112.1	8921	-3.3
3	108.6	8639	-6.6
Mean	116.8	9211	

The test results are summarized in Figures D17 and D18 below. First cracking load occurred at approximately 220 kips. For safety concerns, the test was stopped near impending failure at 273 kips.

A summary of all test results and the code-predicted capacity is given in Table 4.8. Note for the LRFD Code computation, the test beam failure load is taken as V_u. However, for comparison to the test beams, it was found that more accurate results can be obtained with the method by iterating until $V_n=V_u$ (see Appendix H).

Table 4.8. Summary of Test Results.

	Test	S (in)	a/d	f'_c (ksi)	Failure Load (kips)	Standard Code	1979 Interim	LRFD Code
Beam 1	1	8.0	2.8	7.5	299	167	154	147
	2	8.0	3.4	7.8	262	168	157	148
	3	21.0	3.4	8.6	356	141	112	105
Beam 2	1	21.0	2.0	9.2	294	143	117	108
	2	21.0	2.8	9.2	271	143	117	108
	3	21.0	3.5	9.2	273	143	117	108

CHAPTER 5: FINITE ELEMENT MODELING

This chapter discusses development and validation of a FEA model to predict the shear capacity of prestressed concrete bridge beams. Validation of the modeling approach was achieved by comparing numerical results to the test results presented in Chapter 4, as well as independent beam tests documented in the technical literature.

Methodology

The numerical tool chosen for model development is VecTor2, which was developed at the University of Toronto to model reinforced concrete shear behavior. VecTor2 is a program based on the Modified Compression Field Theory (Vecchio and Collins, 1986) and the Disturbed Stress Field Model (Vecchio, 2000). It allows nonlinear analysis of two-dimensional reinforced concrete structures. Cracked concrete behavior is modeled in VecTor2 as an orthotropic material with smeared, rotating cracks. This approach is applicable for reinforced concrete structures using a relatively fine mesh to model reinforcement details and local crack patterns.

Modified Compression Field Theory (MCFT)

The MCFT (Vecchio and Collins 1986) is an analytical model for predicting the load-deformation response of reinforced concrete membrane elements subjected to shear and normal stresses, as shown in Figure 5.1.

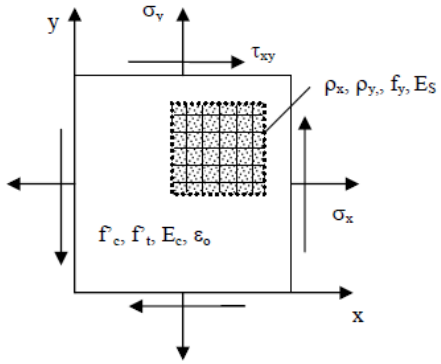

Figure 5.1. Reinforced Concrete Membrane Element Subject To In-Plane Stresses (Wong and Vecchio 2002).

The MCFT predicts the average and local strains and stresses of the concrete and reinforcement, as well as the widths and orientation of cracks throughout the load-deformation response of the element. Based on this information, the failure mode of the element can be determined (Wong and Vecchio 2002).

Disturbed Stress Field Model (DSFM)

The DSFM (Vecchio, 2000) addresses specific deficiencies of MCFT in predicting the response of certain structures and load scenarios. In particular, in lightly reinforced elements, where crack shear slip is significant, the rotation of the principal stress field tends to lag the greater rotation of

the principal strain field. For such cases, the shear stiffness and strength is generally overestimated by MCFT, which assumes that the rotations are equal. Conversely, in elements that exhibit limited rotation of the principal stress and strain fields, MCFT generally underestimates the shear stiffness and strength, partly because the concrete compression response calibrated for MCFT is overly softened for the effect of principal tensile strains.

The DSFM is conceptually similar to MCFT, but extends MCFT in several respects. Most importantly, DSFM augments the compatibility relationships of MCFT to include crack shear slip deformations. The strains due to these deformations are distinguished from the strains of the concrete continuum due to stress. As such, DSFM decouples the orientation of the principal stress field from that of the principal strain field, resulting in a smeared delayed rotating-crack model. Moreover, by explicitly calculating crack slip deformations, DSFM eliminates the crack shear check as required by the MCFT (Wong and Vecchio 2002).

More detail regarding MCFT and DSFM can be found in Wong and Vecchio (2002).

Material Models

The reinforcement steel constitutive models are illustrated in Figures 5.2 and 5.3. In the Figures, ε_s is the reinforcement strain, ε_y is the yield strain, ε_{sh} is the strain at the onset of strain hardening, ε_u is the ultimate strain, E_s is the elastic modulus, E_{sh} is the strain hardening modulus, f_y is the yield strength, and f_u is the ultimate strength, where

$$\varepsilon_u = \varepsilon_{sh} + \frac{(f_u - f_y)}{E_{sh}} \tag{5.1}$$

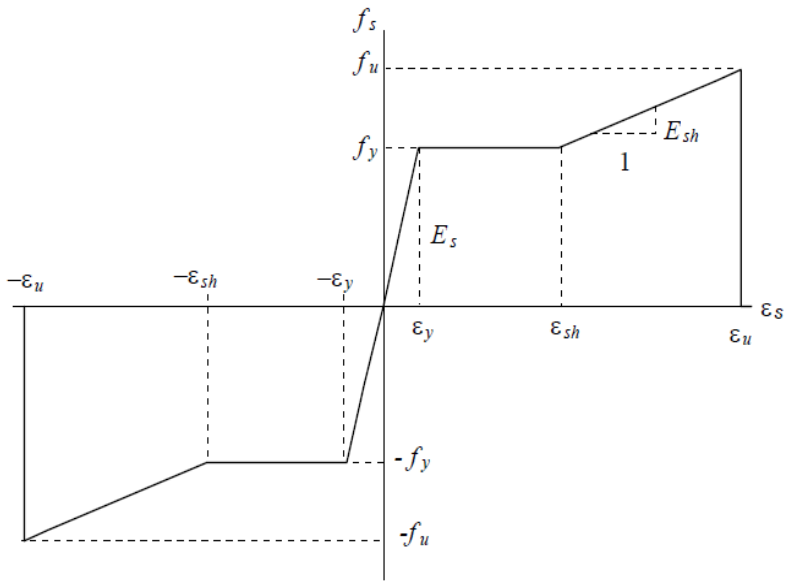

Figure 5.2. Ductile Steel Reinforcement Stress-Strain Response As Implemented In Wong and Vecchio (2002).

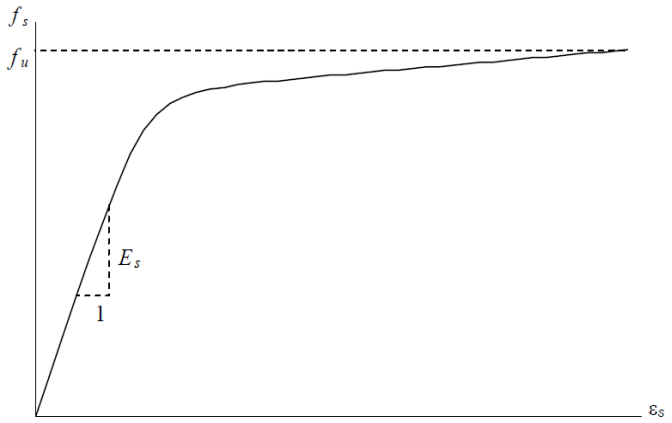

Figure 5.3. Prestressing Steel Reinforcement Stress-Strain Response As Implemented In Wong and Vecchio (2002).

The concrete model uses Hognestad's parabola for compressive pre-peak behavior, and modified Park-Kent relationship for post-peak (Figure 5.4). Compression softening is governed by Vecchio's *e1/e2*-Form approach (Vecchio 1992) and a modified Bentz model for tension stiffening (Bentz 2003). Linear tension softening is assumed, while confined strength is described by Kupfer/Richart (Kupfer et al. 1969) and dilation by the variable Kupfer model (Kupfer and Gerstle 1973). Mohr-Coulomb failure criteria is used to determine cracking stress, with stress calculated from DSFM/MCFT. Crack slip calculation is according to the Walraven (monotonic) approach (Walraven 1981), while crack width check is the *Agg*/2.5 Max Crack Width method, which reduces average compressive stresses when crack widths exceed a specified limit, and is useful for beams with minimal shear reinforcement (Vecchio, 2000). Concrete bond is given by Eligenhausen et al. (1983). Additional details can be found in Wong and Vecchio (2002).

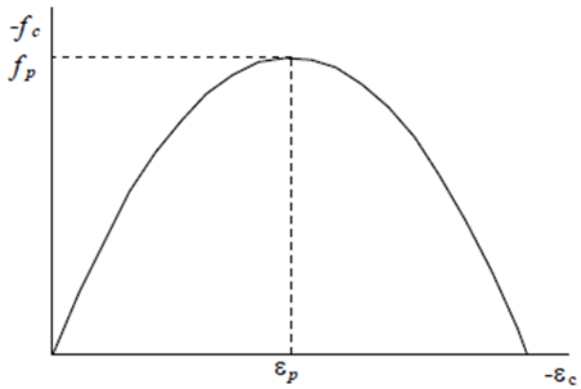

Figure 5.4. Hognestad Parabolic Pre- And Post-Peak Concrete Compression Response.

Verification Data Set 1: Saqan and Frosch Tests

The literature search revealed that very few prestressed beam shear tests were documented with sufficient detail that allows for model verification. Of the suitable sources describes a series of

tests conducted by Saqan and Frosch (2009), who documented several prestressed beam shear tests. Three beam tests were used for model verification. A description of the tests and the FEA model is given in Appendix E. A plot of the resulting load-deflection curves of the experimental results and the models is shown in Figure 5.5, with a numerical summary presented in Table 4.9. As shown in the figure, excellent results have been obtained for each of the three test beam with the FEA model, with very close response throughout the load-deflection profile as well as ultimate capacity.

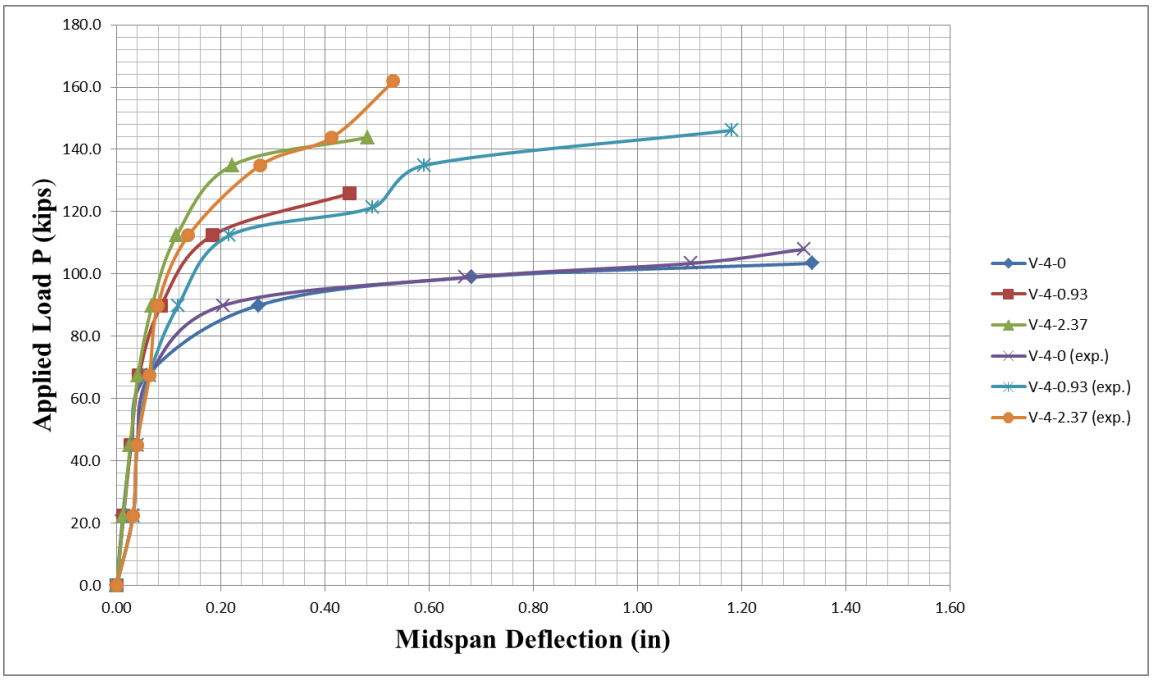

Figure 5.5. Load-Displacement Response For Test Beams (exp.) And FEA Models.

Table 4.9. Summary Of FEA And Experimental Results

Beam #	FEA (kips)	Exp. (kips)	FEA/Exp.
V-4-0	103	110	0.94
V-4-0.93	126	150	0.84
V-4-2.37	144	165	0.87

Verification Data Set 2: UM Test Beams

Finite element models were developed and compared to the results of the two beam tests discussed in Chapter 4. Details of the models and results are given in Appendix E. A summary of all model results is given in Table 5.1, while Figure 5.6 presents an example load displacement comparison. The final (modified) model results (M) well-matched the experimental results (E) with the exception of Test 3 for Beam 2, for which it is considerably conservative, under-predicting capacity by about 27%. However, because of the reasonably good match for the majority of the tests, the revised model was deemed adequate for use in the parametric analysis.

Table 5.1. Summary Of Model Results.

					Failure Load (Kips)				
	Test	S (in)	a/d	f'c (KSI)	Original Model	Modified Model	Exp.	% (M-E)	Failure Mode
Beam 1	1	8.0	2.8	7.5	265.3	266.4	298.9	-12.2	S-C
	1	8.0	2.8	9.2	277.6	278.8	298.9	-7.2	S-C
	2	8.0	3.4	7.8	239.4	239.4	262.4	-9.6	S-C
	2	8.0	3.4	9.5	245.1	243.9	262.4	-7.6	S-C
	3	21.0	3.4	8.6	279.9	337.2	355.7	-5.5	S
	3	21.0	3.4	10	299.0	352.9	355.7	-0.8	S
Beam 2	1	21.0	2.0	9.2	223.7	260.8	294.0	-12.7	S-C (stopped)
	2	21.0	2.8	9.2	179.8	213.6	271.0	-26.9	S
	3	21.0	3.5	9.2	239.4	275.4	273.0	0.9	S-C (stopped)

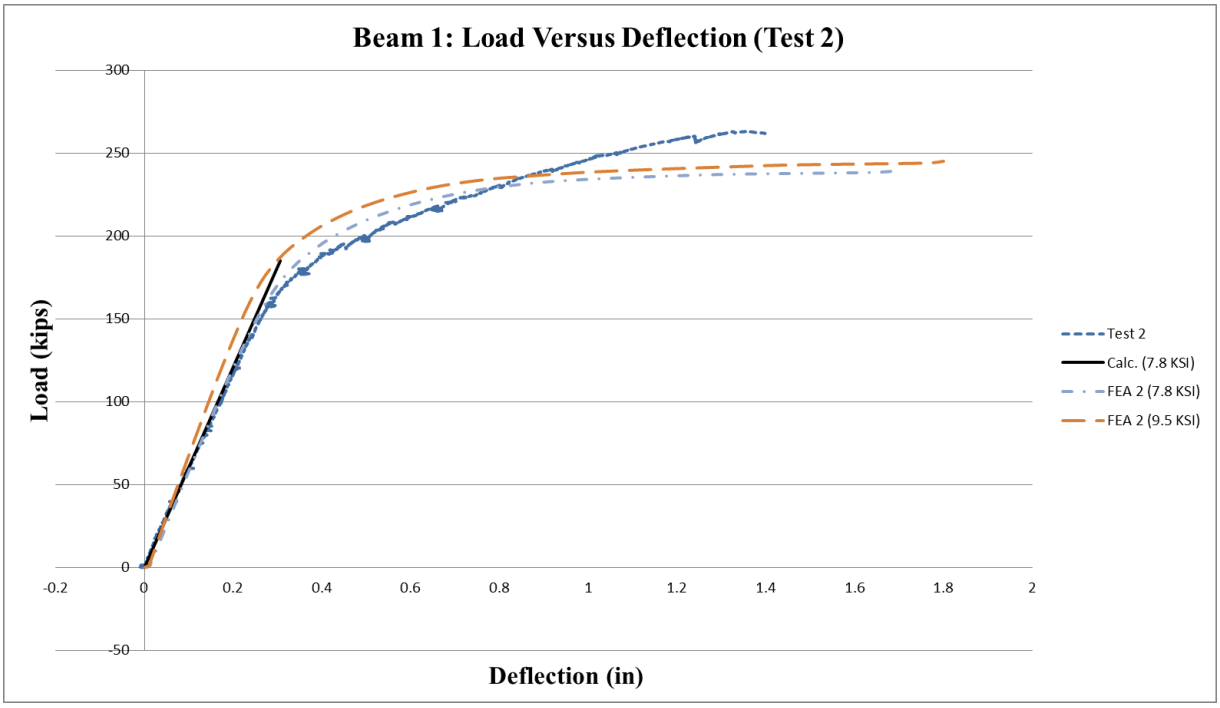

Figure 5.6. Example Load-Deflection Result (For Modified Model, Beam 1, Test 2).

Parametric Analysis

Using the FEA modeling technique developed above, a parametric analysis was conducted on a variety of prestressed bridge girder configurations. The range of parameters considered was chosen such that beams generally representing MDOT design practice were covered, as well as cases for which code procedures estimating shear capacity would be least conservative. The variety of parameters considered is given in Table 5.2.

Table 5.2. Analysis Beam Parameters.

Parameter	Values
Beam Type	II, III, IV, MI-1800
Load Position	*h/2*, LRFD, Worst position
Strand Geometry	Straight, Harped
Concrete Strength	5.5 ksi, 8.0 ksi
Section Axial Stress	0.5 ksi, 1.5 ksi, 2.5 ksi
Stirrup Spacing	3", 12", 24"
Long. Steel Reinf. Ratio	Tension control limit, 0.01

In the table, beam type refers to AASHTO Types II, III, IV, and the MI-1800 (~72") T-beam, respectively. Load position refers to the location from the support were a single point load was applied and increased until shear failure; "LRFD" refers to the critical section as specified by the AASHTO LRFD sectional method, while the "Worst position" is the position of the load which produces the smallest capacity from the FEA model, which was generally found to be near *L*/4 for the beams considered (note that this position depends on the span/depth ratio of the beam, as discussed later in this chapter, and is valid only for the beam depths and length considered for the parametric analysis). The sectional axial stress is found by taking the total prestress force applied to the beam and dividing by the gross cross-sectional area. Moreover, as it was found that the LFRD approach becomes generally less conservative as the (longitudinal) reinforcement ratio increases, two cases of relatively high reinforcement ratios were analyzed. The first case used a reinforcement ratio equal to that at the tension controlled limit, which was thought to be a reasonable upper limit used for most designs. The second case was that of a reinforcement ratio equal to 0.01, which is beyond the LRFD-specified tension controlled limit for the beams considered.

In total, 414 analyses with different parameter combinations were conducted. Note that the MI-1800 models included straight strands and tension controlled longitudinal prestressed steel ratios only. Specific parameter combinations considered are summarized in Appendix F, Tables F1-F3. All analyses were for a 20' beam span. FEA models are shown in Figures F1-F8 (Appendix F). Results are presented in Tables F4-F20 (Appendix F). The top half of the tables indicate the shear failure load (i.e. nominal shear capacity) predicted from the FEA model for three different load positions: *h*/2 (1); LRFD (2); and the worst position (3), as described above. Also presented in the tables are the code-calculated nominal shear capacities of the beams, using either the AASHTO Standard (4); the LRFD method where an iteration is conducted until $V_n = V_u$ (5); the 1979 Interim Specifications (6); the LRFD method where strain is set to the maximum allowed (7); and the LRFD method where Vu is set equal to a HL-93 design truck (8). The latter two results (7) and (8) are presented for interest. The bottom half of the tables present the ratios of the FEA results to the code predictions. For example, "(1/4)" refers to the ratio of the FEA-predicted shear capacity where load is applied at *h*/2 (1), to the AASHTO Standard code predicted shear capacity (4). Assuming that the FEA result represents the true shear capacity of the section, ratios greater than 1.0 are conservative. Also presented at the bottom of the tables are the mean FEA/code capacity ratios as well as the coefficient of variation (COV) of the results.

For every beam type, for all cases, the lowest mean FEA/code capacity ratio as well as lowest COV was found for the Standard code (case "(3/4)"), which indicates that the Standard

procedure is most accurate as well as consistent for the cases considered. Tables F7, F12, F16, and F20 present a summary of the mean values and COV of these results. Note that similar results were also found when the LRFD code predicted capacity was determined by setting V_u equal to the capacity value (i.e. ultimate load value) found from the FEA model, except that the LRFD prediction was significantly more conservative.

Additional Load Cases Considered

As discussed above, the parametric analyses were based on the application of a single point load. However, such a load configuration does not realistically appear in practice. Thus, to confirm shear capacity, loads on a selection of model beams were applied representative of vehicular traffic. For this purpose, two legal Michigan vehicle configurations shown in Figure 5.7 were considered: a Trucks 4 (single unit) and 23 (three-unit), as presented in the MDOT Bridge Analysis Guide.

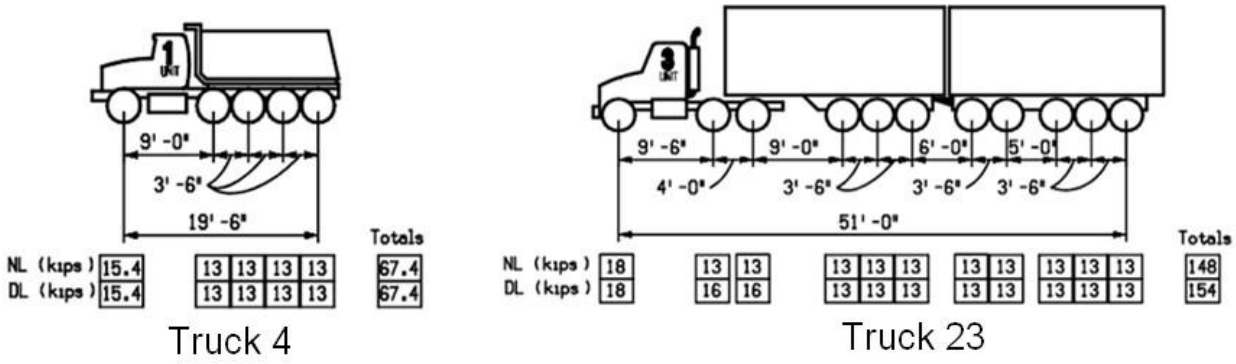

Figure 5.7 Model Trucks.

For each analysis, these vehicles were placed onto the bridge model (constructed with the same FEA procedure detailed earlier in this chapter), with one axle a distance of *h*/2 from the support, and axle loads proportionally increased until the beam reaches ultimate moment capacity or shear cracks develop. The model beams were Type II, with 3" stirrup spacing at the critical section, 0.007 longitudinal (prestress) steel reinforcing ratio, and 0.5 ksi axial stress (based on gross section area) due to prestress, and 5.5 ksi concrete strength. Note that actual transverse steel parameters are not critical, as in this analysis, a shear 'failure' is conservatively taken as the development of shear cracks, not ultimate shear capacity. Spans of 100' and 50' were considered for both vehicles. It was found for every analysis, moment failure occurred at a load level much below that required for a shear failure (i.e. development of shear cracks), as shown in Figures 5.8-5.11, below. Here, it was not possible to fail the beams in shear (before a moment failure) using reasonable vehicle configurations. Thus, as expected, typical vehicle configurations on a reasonably designed and undamaged prestressed concrete beam will generally result in moment failures rather than shear failures, especially for longer vehicles and spans.

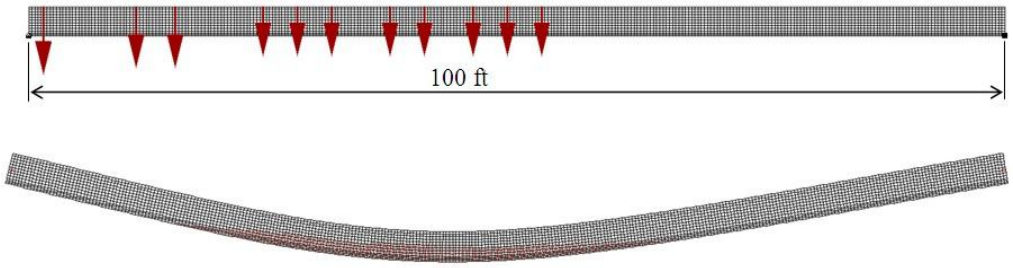

Figure 5.8. Moment Failure For 100’ Span, Truck 23.

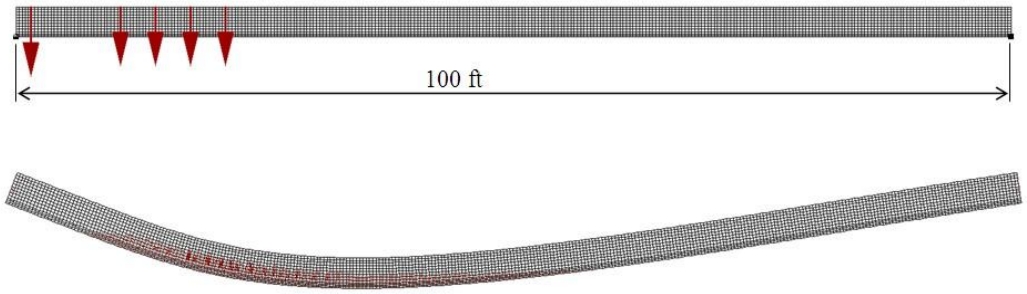

Figure 5.9. Moment Failure For 100’ Span, Truck 4.

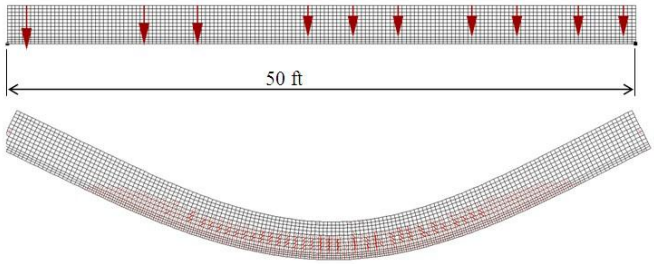

Figure 5.10. Moment Failure For 50’ Span, Truck 23.

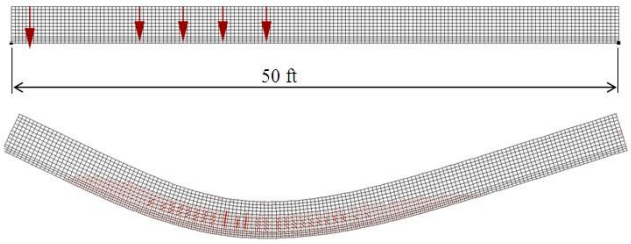

Figure 5.11. Moment Failure For 50’ Span, Truck 4.

An additional series of analyses were conducted to explore the possibility of a combined shear and moment failure. In these analyses, a point load (as it is clear from the analyses above that multiple point loads representative of vehicle configurations will not result in shear failures) was positioned on the model beam span at a position of *L*/4, as specified as the critical section in the 1979 Interim specifications, and increased until beam failure. Additionally, the position of the point load, farthest from the support, was determined that would result in a combined shear-moment failure (i.e. any indication of a shear failure, even if the section primarily failed in moment). For the 100' and 50' spans, placing the load at *L*/4 resulted in a moment failure, with no indication of a shear failure, as shown in Figures 5.12 and 5.13.

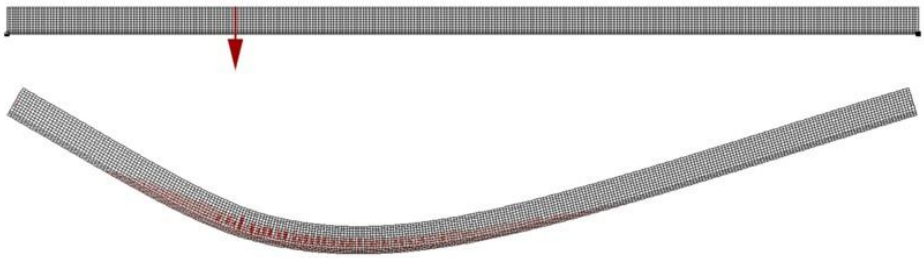

Figure 5.12. Moment Failure, 100' Span, Load at L/4.

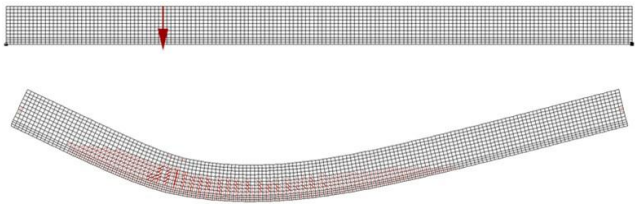

Figure 5.13. Moment Failure, 50' Span, Load at L/4.

For the 100' span, a combined shear and moment failure occurred when the load was placed a distance of *L*/36 (2.78'; approximately equal to beam depth) from the support, as shown in Figure 5.14. For the 50' span, a combined shear and moment failure occurred when the load was placed a distance of *L*/14 (3.57'; approximately equal to 1.5 times beam depth), as shown in Figure 5.15. For a 20' span, a combined shear and moment failure occurred when the load was placed at a distance of approximately *L*/4 (5' from the support; about equal to 2 times beam depth), as shown in Figure 5.16.

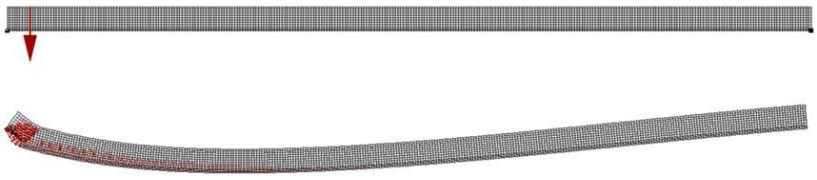

Figure 5.14. 100' Span, Combined Shear-Moment Failure At L/36.

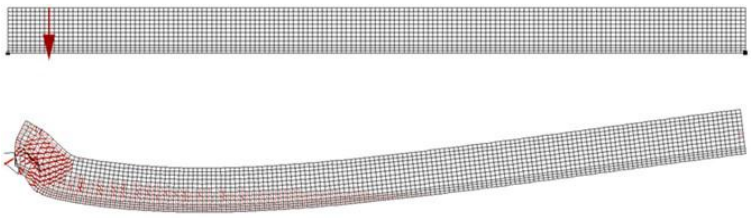

Figure 5.15. 50’ Span, Combined Shear-Moment Failure At L/14.

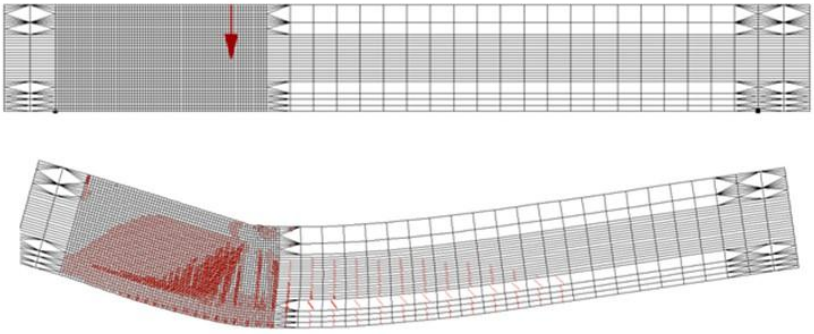

Figure 5.16. 20’ Span, Combined Shear-Moment Failure At L/4.

In summary, using a single point load, the onset of a shear-moment failure occurred over a range of load positions, as a function of the beam span-to-depth ratio. For a Type II beam spanning from 20’-100’, this range varied from approximately *L*/4-*L*/36, with corresponding shear span ratios (load position / beam depth *d*) between approximately 1 - 2.

Based on the results above, it appears that the developed FEA approach can reasonably model PC beam shear capacity. Moreover, for PC beams with reasonable shear/moment capacity ratios, it appears highly unlikely that a typical vehicle configuration could cause a shear failure before a moment failure.

CHAPTER 6: FIELD TESTING

The purpose of field testing was to determine the degree of moment continuity between adjoining spans of prestressed concrete bridges designed continuous for live load. Of secondary interest is determining the girder distribution factors associated with this type of structure.

Test Bridges

Two nearly identical bridges were tested. Each is two lane, no skew, with 2 live-load continuous middle spans of 106 ft, girder spacing of 6.4 ft with Type IV prestressed girders, and built in 1993. The structures are on Taft Road and Centerline Road over US-127, as shown in Figures 7.1-7.3.

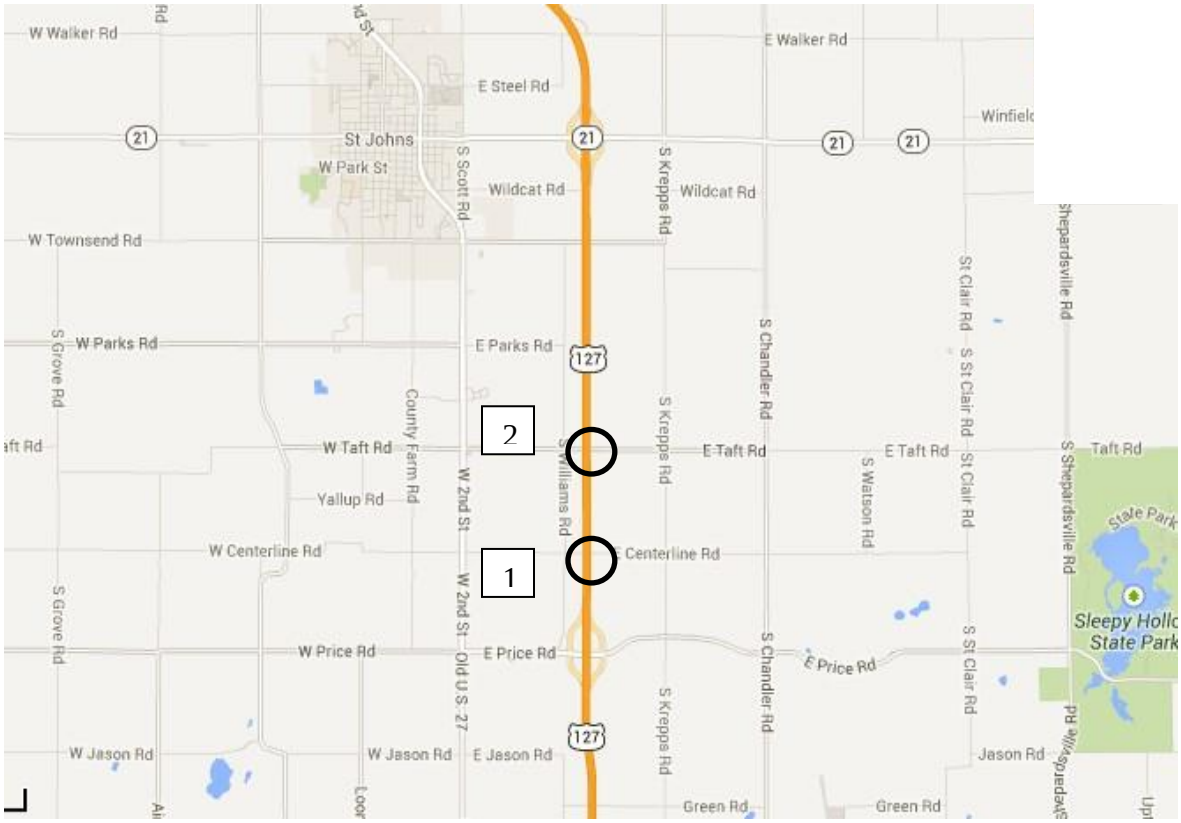

Figure 6.1. Test Bridge Locations.

Figure 6.2. Bridge 1, Centerline Road Over US-127.

Figure 6.3. Bridge 2, Taft Road Over US-127.

A cross-section of the bridges is given in Figure 6.4.

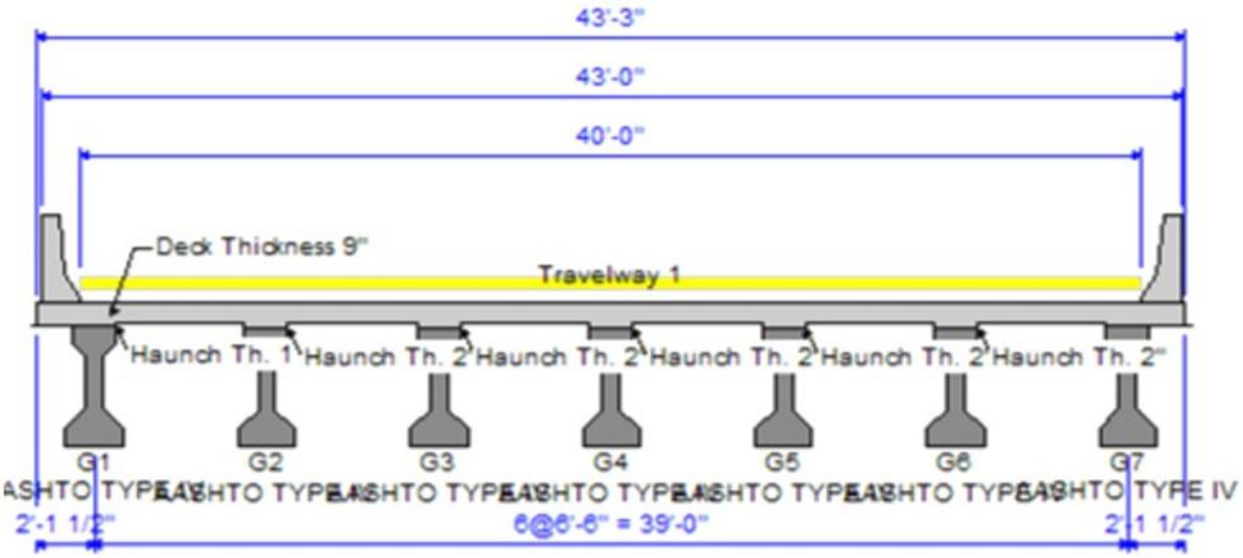

Figure 6.4. Test Bridge Cross-Section.

Instrumentation

A BDI Wireless Structural Testing System (STS-WiFi) was used to obtain strain data. Twenty-two sensors were available, and all were attached to the bottom surfaces of the girders, near midspan and near the continuous support of each span. The re-usable gages are bolted to metal tabs, with nuts tightened to 45 lb-in as recommended by the manufacturer. The metal tabs are then adhered to the girders with an epoxy. The locations of the sensors are indicated in the figure below. In Figure 6.5, open circles indicate gage placement, while darkened circles indicate that no gage was placed in that corresponding location.

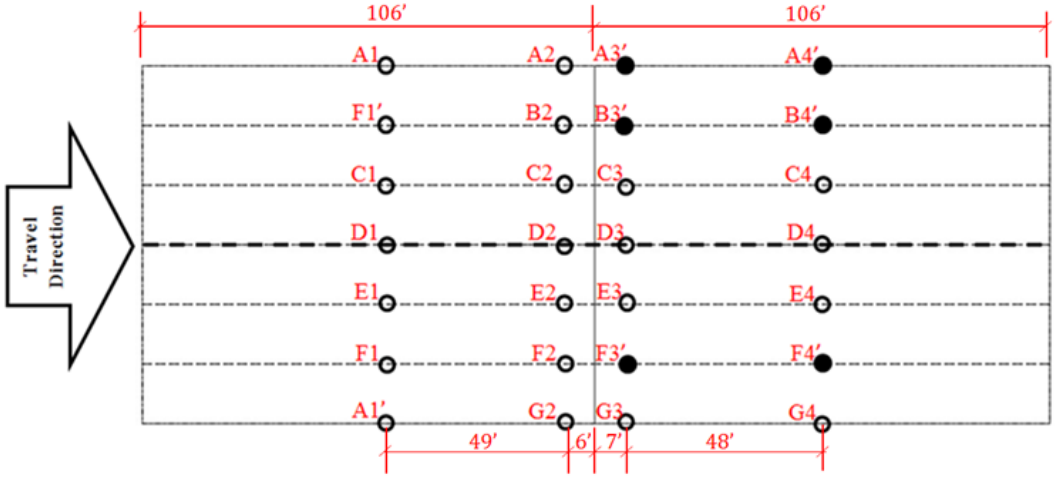

Figure 6.5. Bridge Instrumentation.

The BDI System setup is shown in Figure 6.6 below. The system is controlled by a laptop (PC), which transmits wireless signals to a Base Station. In turn, the Base Station receives wireless signals from a data acquisition Node. Up to four strain gages are hard wired to each Node. The installed system (on Bridge 1) is shown in Figures 6.7-6.10.

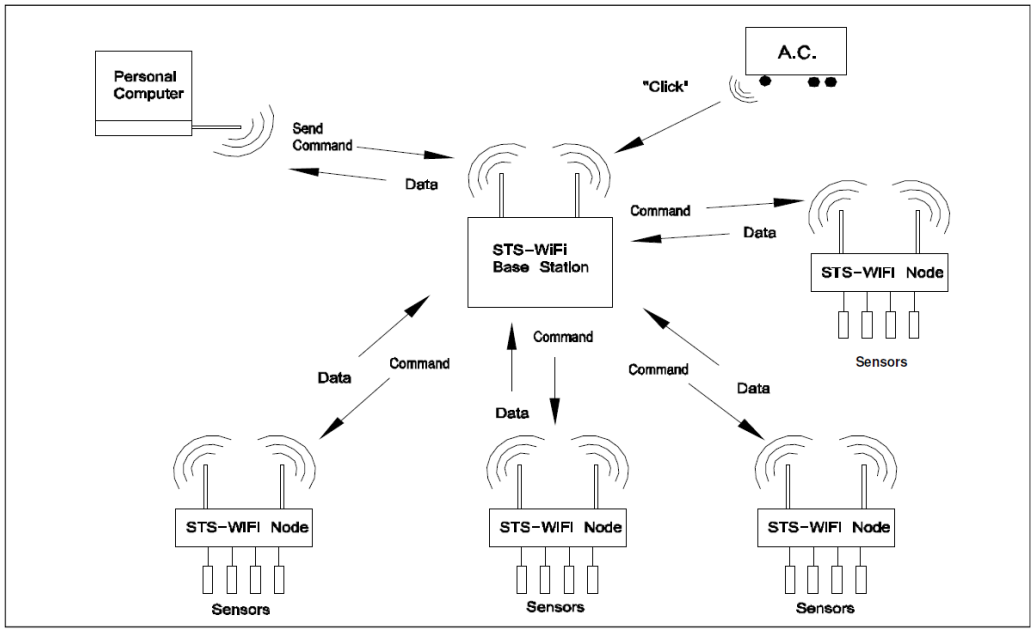

Figure 6.6. Diagram Of Wireless Instrumentation System

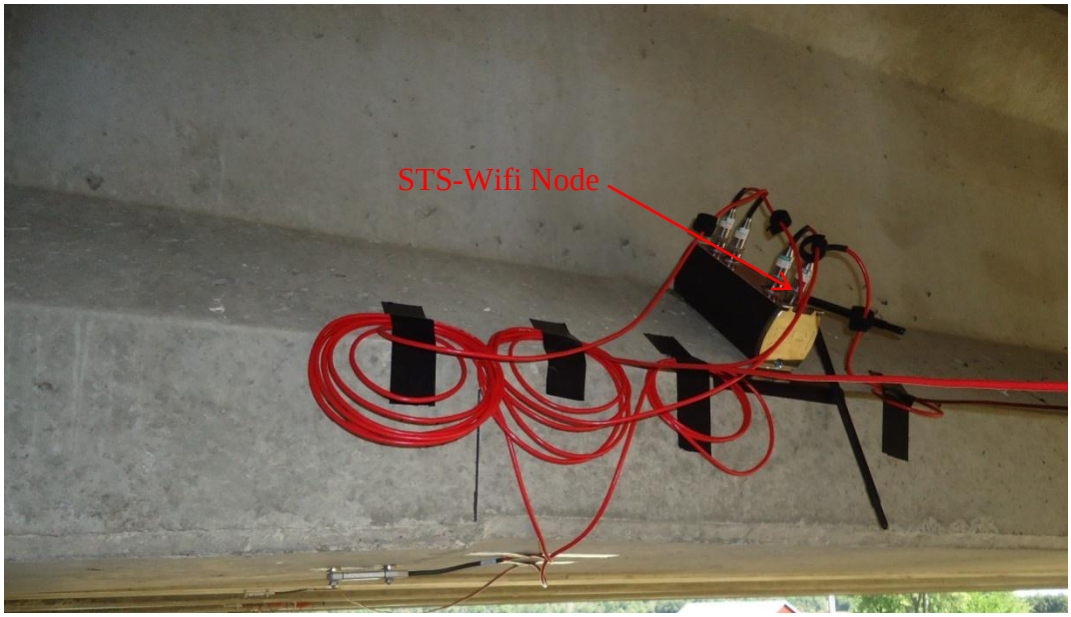

Figure 6.7. Node Attached To Girder.

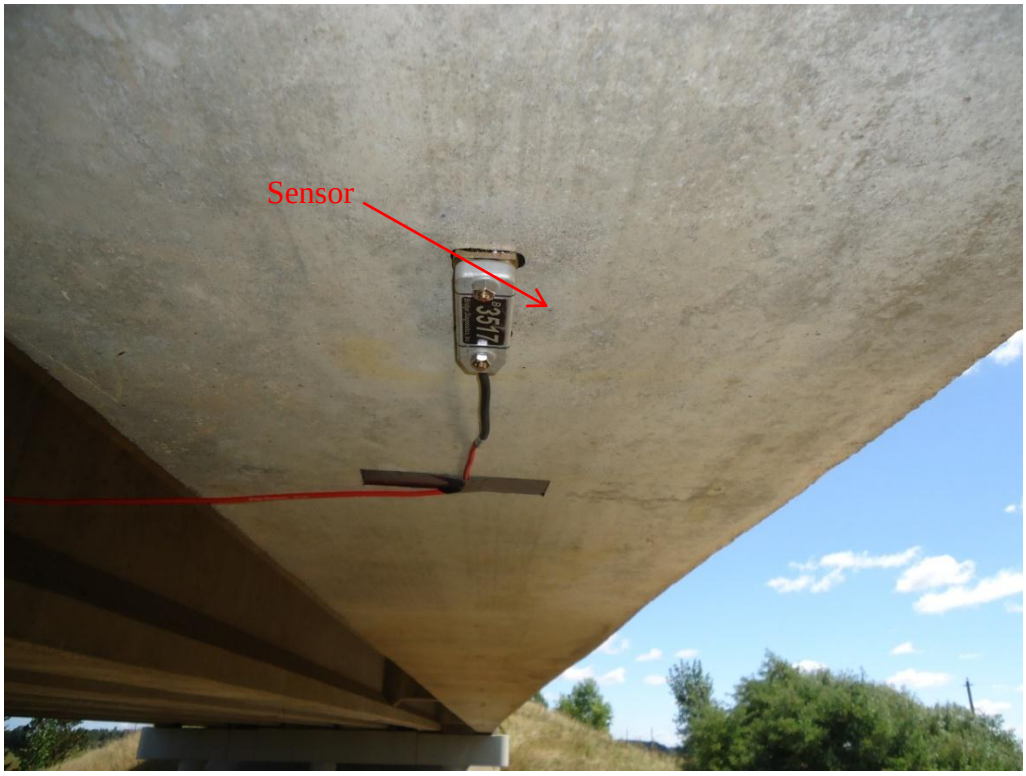

Figure 6.8. Gage Installed On Girder.


Figure 6.9. View Of Bridge With Gages Installed.

Figure 6.10. View Of Bridge With Base Station And Attached Gages.

Test Trucks

Two fully-loaded 11-axle trucks (approximately 147-154 kips each) were used to test the bridges. Trucks were driven across the bridge at crawling speed. The trucks have a configuration similar to that of Truck #23 from the MDOT Analysis Guide, as shown in Figures 6.12-6.15. Truck axle weights and spacings were recorded at the vehicle weigh station prior to the test. Transversely, front tires on the vehicles were spaced approximately 7.17 ft center to center, while rear tires were spaced approximately 6.08 ft center to center (to middle of double-tire wheel).

Test data were continuously recorded as the trucks moved across the bridge. Traffic was stopped such that no other vehicles were on the bridge during the tests. The lateral positions of the trucks on the bridge were carefully recorded during the tests. Pictures from the Centerline Road bridge testing are shown in Figures below.

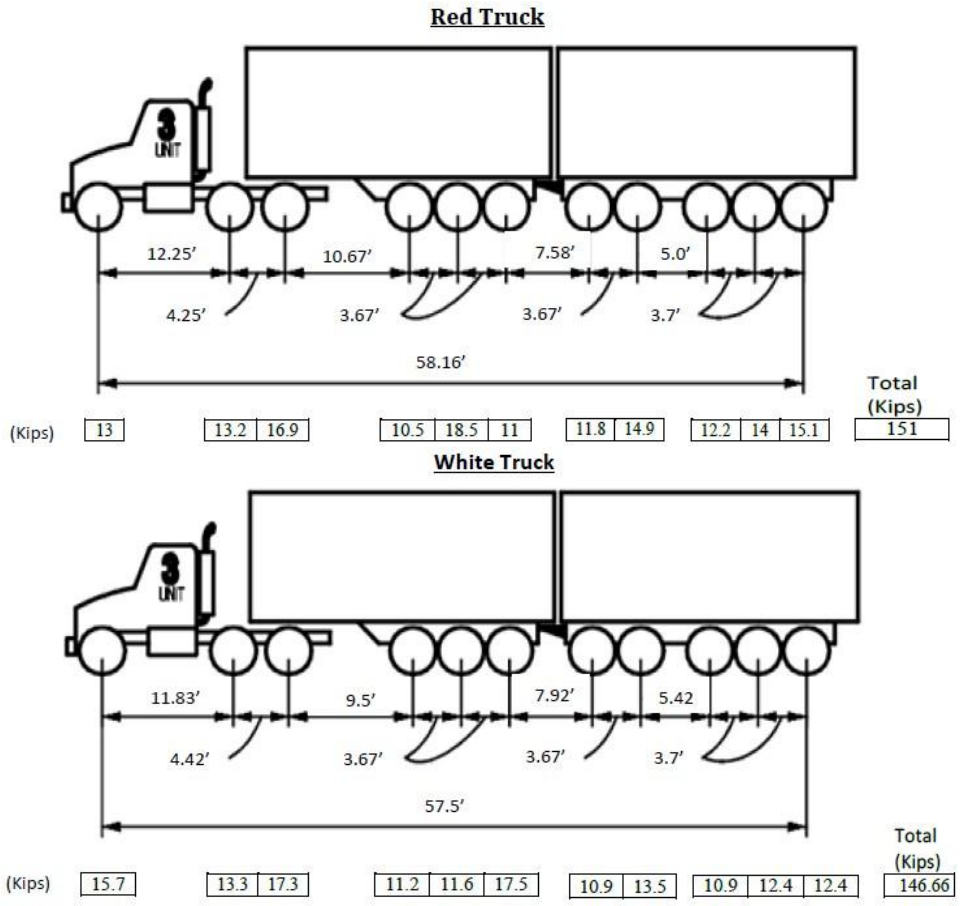

Figure 6.11. Bridge 1 (Centerline Rd.) Trucks.

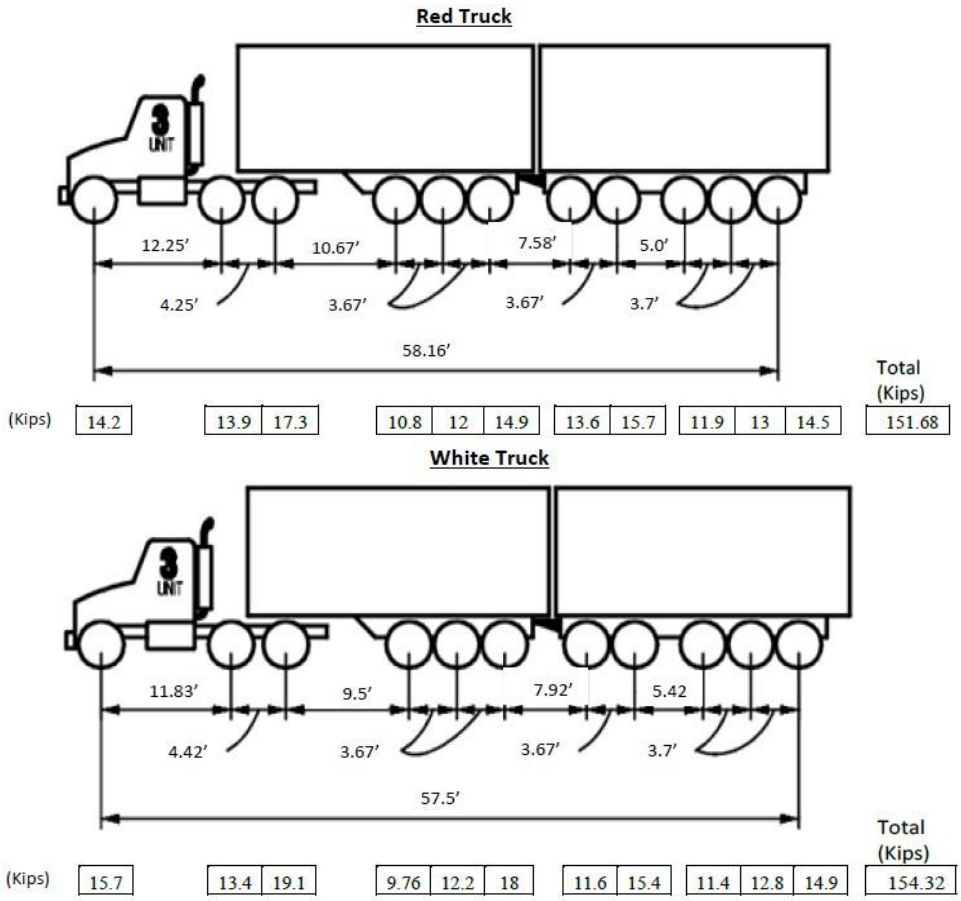

Figure 6.12. Bridge 2 (Taft Rd.) Trucks.

Figure 6.13. Following Test Trucks On Bridge.

Figure 6.14. Side-By-Side Test Trucks on Bridge.

Figure 6.15. Following Test Trucks In Center Of Bridge.

Test Plan

The specific test runs conducted are given below in Figure 6.16:

Run 1: Two trucks side by side, centered in each lane

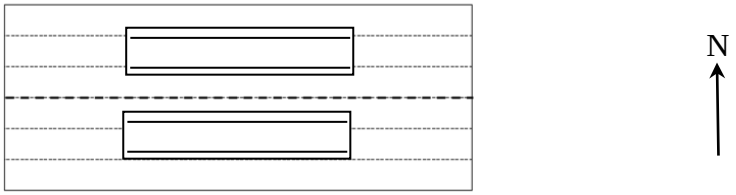

Run 2: Two trucks side by side, as close as possible in center of bridge

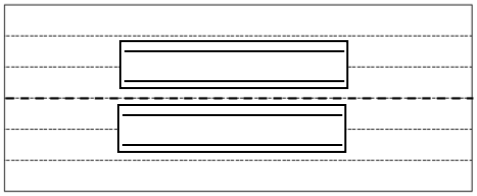

Run 3: Two trucks side by side, as close as possible to the left edge

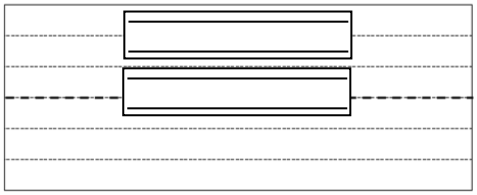

Run 4: Two trucks side by side, as close as possible to the right edge

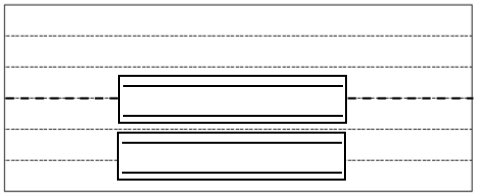

Run 5: Two trucks separated to provide maximum negative moment, center of bridge

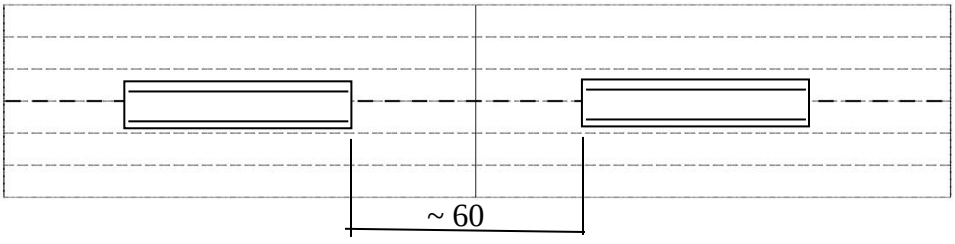

Run 6: Two trucks separated to provide maximum negative moment, left lane

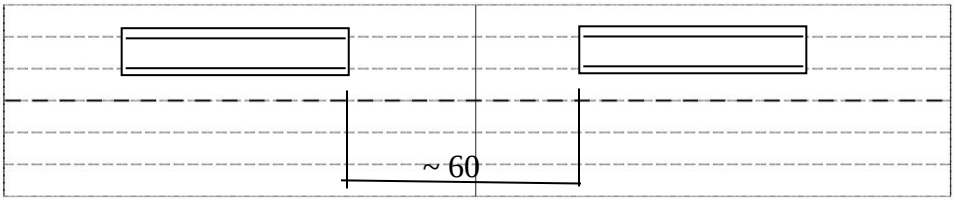

Run 7: Two trucks separated to provide maximum negative moment, right lane

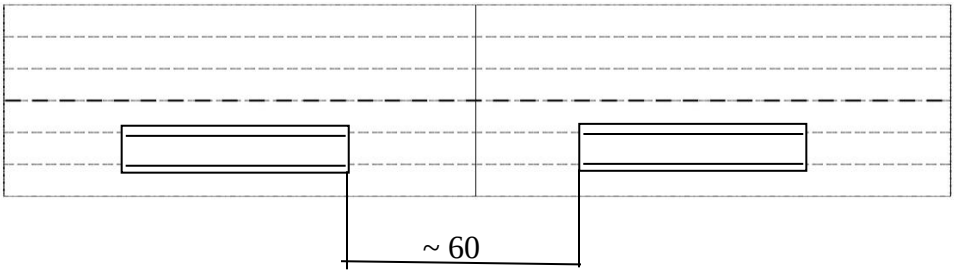

Run 8: Two trucks minimally separated, center of bridge

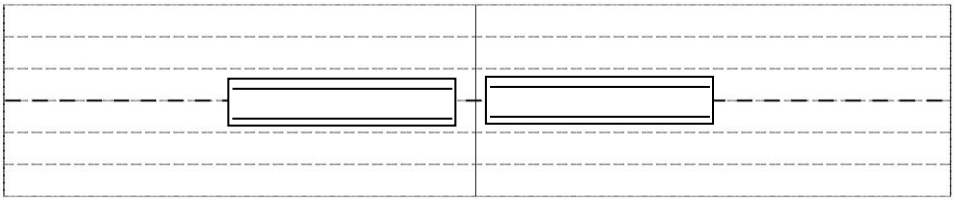

Run 9: Two trucks minimally separated, left lane

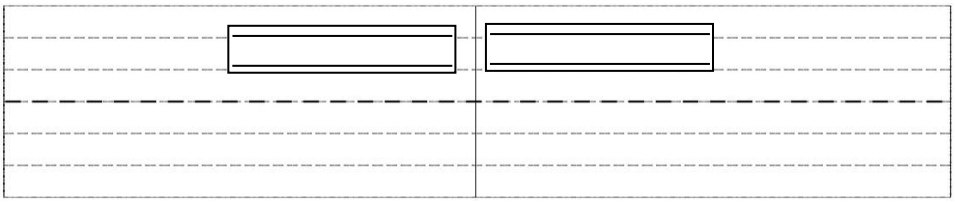

Run 10: Two trucks minimally separated, right lane

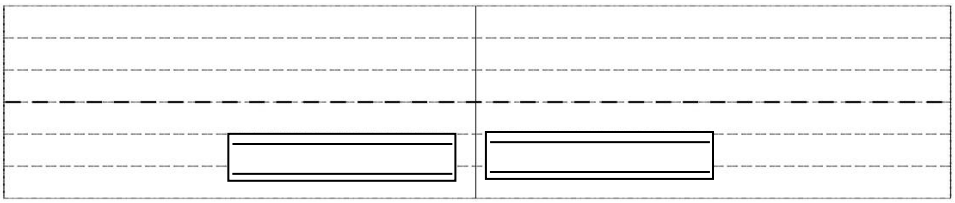

Run 11: One truck, center of bridge

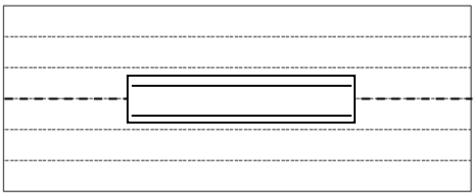

Run 12: One truck, centered in left lane

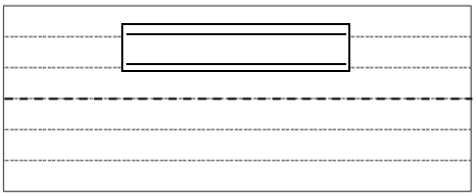

Run 13: One truck, as close as possible to left edge

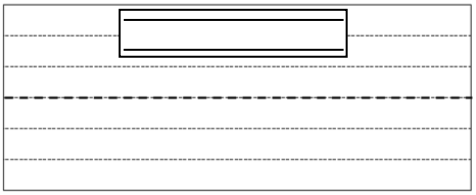

Run 14: One truck, centered in right lane

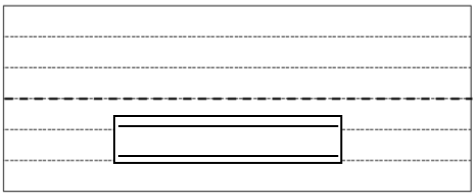

Run 15: One truck, as close as possible to right edge

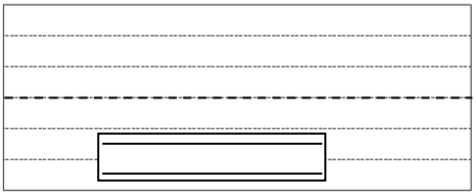

Figure 6.16. Test Plan.

Summary of Results

A representative selection of test results is summarized below. A diagram of Bridge 1 is given in Figure 6.17 for reference.

Bridge 1 (Centerline Road)

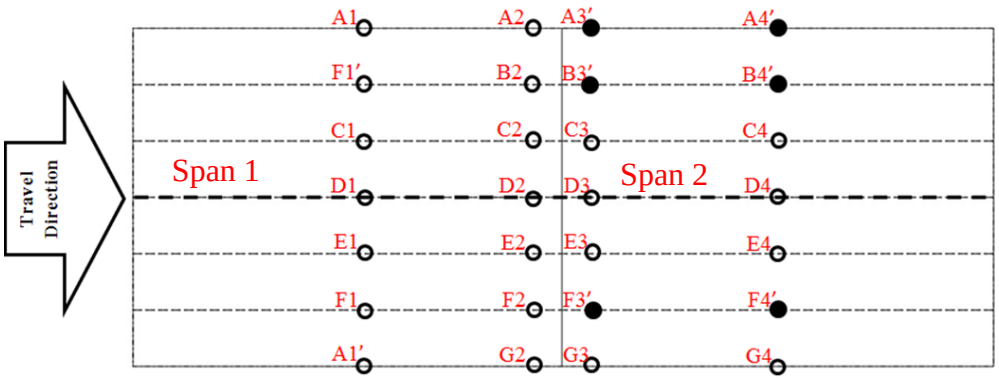

Figure 6.17. Bridge 1 Instrumentation.

Note that sensors A1' and F1' gave unreliable strain results for Test 1. Therefore, the results of these sensors were discarded and not shown. A selection of representative test run results are given below.

Bridge 1 Run 1: Two trucks side by side, centered in each lane

Comparison of Strains in the Transverse Span Direction

In this comparison, at a particular instant in time during the test, strains corresponding to gages located at the same positions on the girders (i.e. gages intersected by drawing a transverse line across the bridge) are considered. This allows estimation of girder distribution factors (GDF)s. For maximum positive moment (span 1) girder strain comparison, strains in gage line 1 are compared at a test time of 85 s, as shown by the vertical line on Figure 6.18. Figure 6.19 shows the resulting girder strains at this time. On the figures, tensile strain is reported as positive.

For maximum negative moment (span 1) girder strain comparison, strains along gage line 2 are compared at a time of 105 s, as shown by the vertical line on Figure 6.20. The resulting girder strains at this time are shown in Figure 6.21. Similar results are obtained for the positive and negative strains on Span 2, as shown in Appendix G, Figures G1-G4.

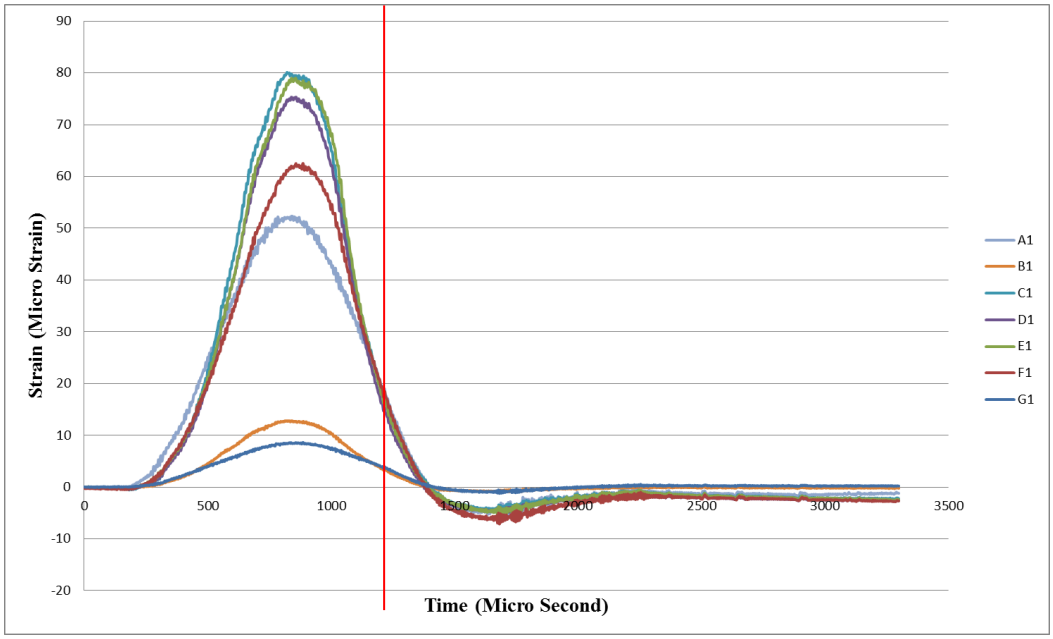

Figure 6.18. Bridge 1 Run 1 Girder Strains, Gage Line 1.

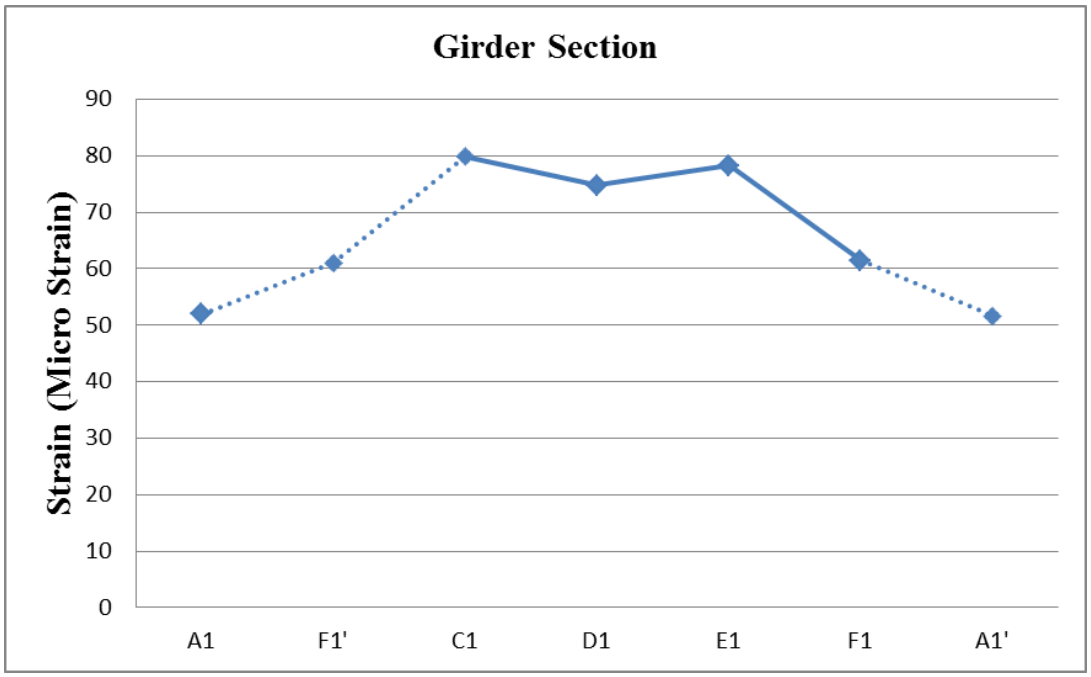

Figure 6.19. Bridge 1 Run 1 Girder Strains For Maximum Positive Moment.

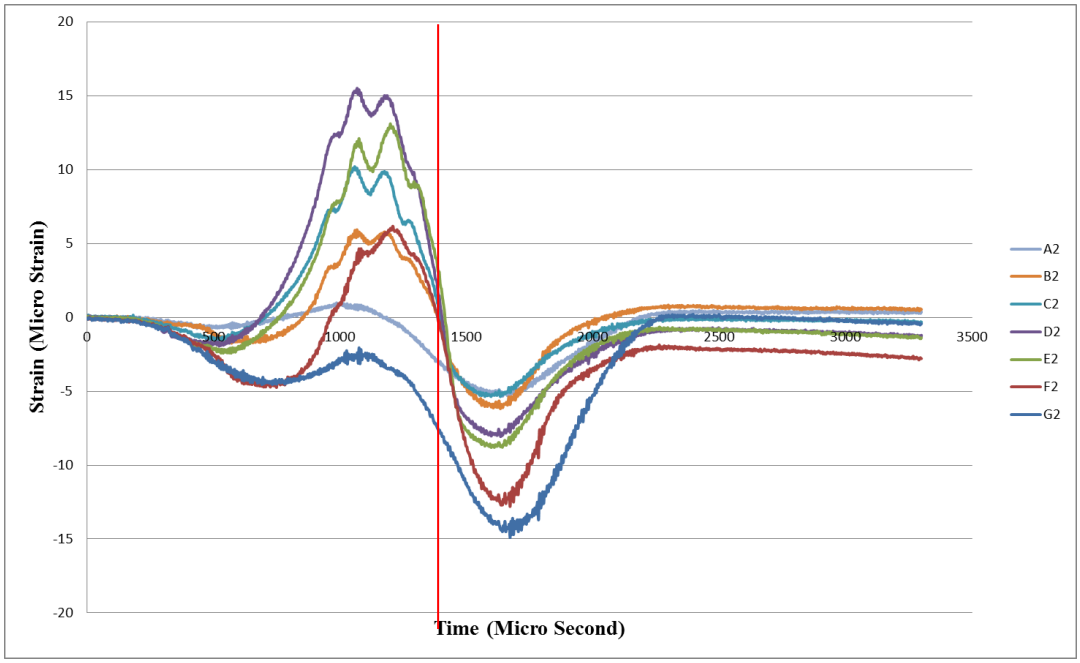

Figure 6.20. Bridge 1 Run 1 Girder Strains, Gage Line 2.

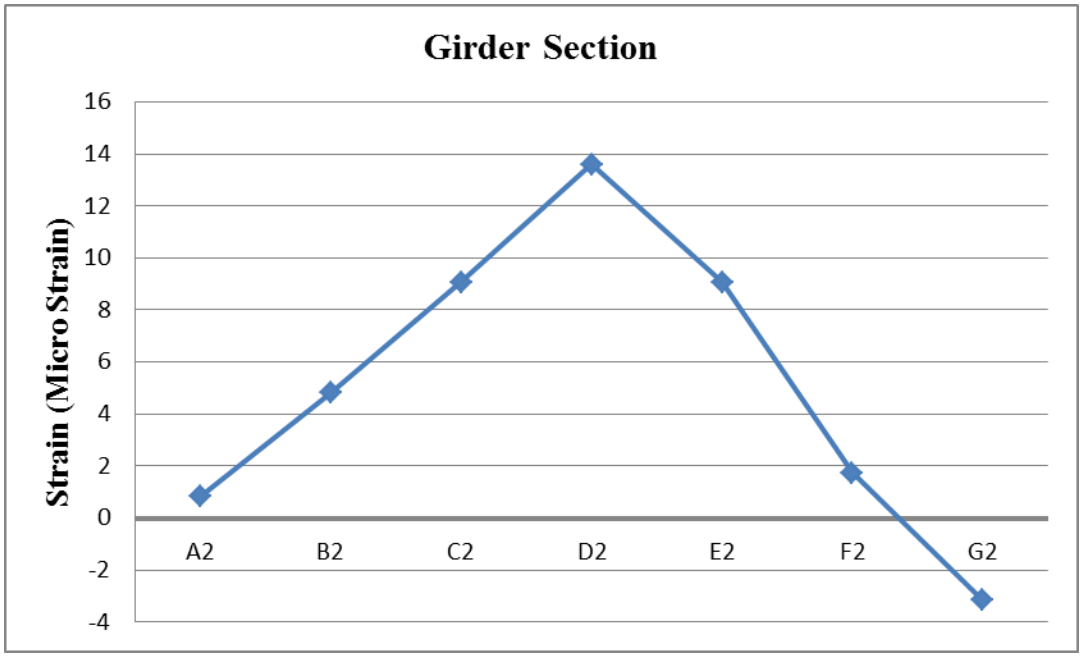

Figure 6.21. Bridge 1 Run 1 Girder Strains For Maximum Negative Moment.

Comparison of Srains in the Longitudinal Span Direction

In this comparison, at a particular instant in time during the test, strains corresponding to gages located along the same girder (i.e. gages intersected by drawing a longitudinal line along the bridge) are considered. This allows estimation of moment continuity over the center support. Figures G5-G18 in Appendix G show the strain variation on several girders during the test as a

function of time (i.e. vehicle longitudinal position), and the point in time for which strains are graphed for comparison.

This and similar data from the remaining test runs can be used to estimate moment continuity, as discussed below. A sample of data similar to that presented for Run 1 is given for some additional test runs presented in Appendix G, Figures G19-G34.

Bridge 2 (Taft Road)

The same 15 runs conducted for Bridge 1 were repeated for Bridge 2, with similar results. Here, an example result is shown for Run 1 in Appendix G, Figures G35-G38.

Comparison between Bridge 1 and Bridge 2 (Run 1)

An example comparison is given in Figures 6.22 and 6.33 for the time of maximum positive moment of span 1. It appears that the deck of Bridge 2 is less stiff in the transverse direction than is that of Bridge 1.

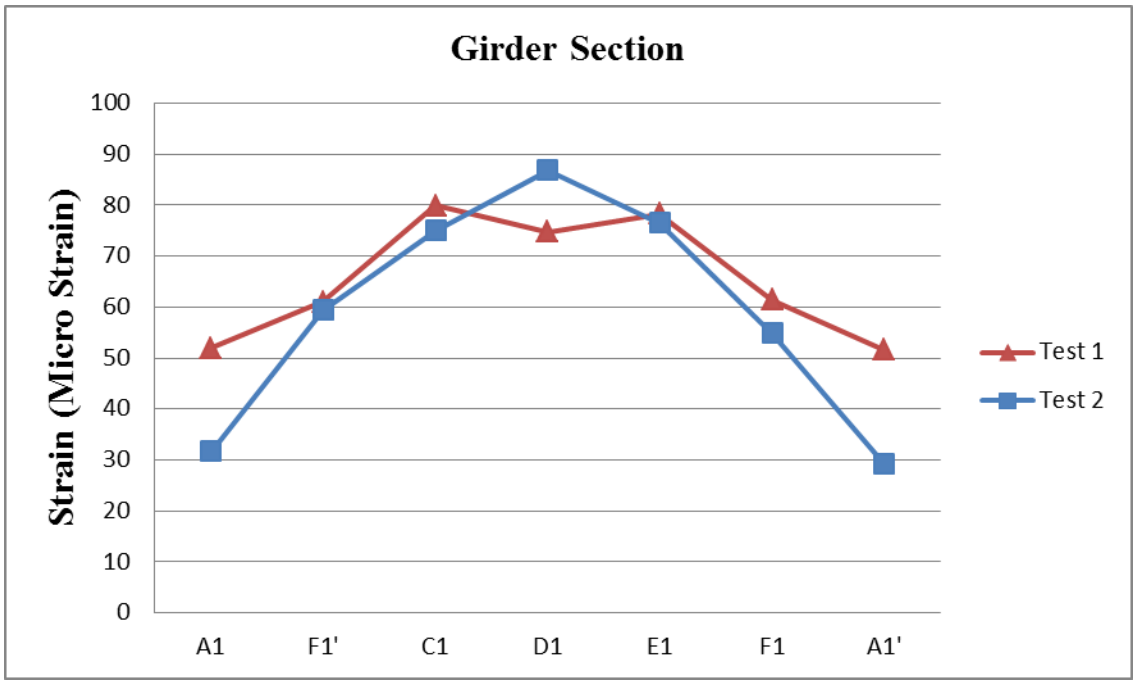

Figure 6.22. Bridge 1 And 2 Run 1 Girder Strains For Maximum Positive Moment.

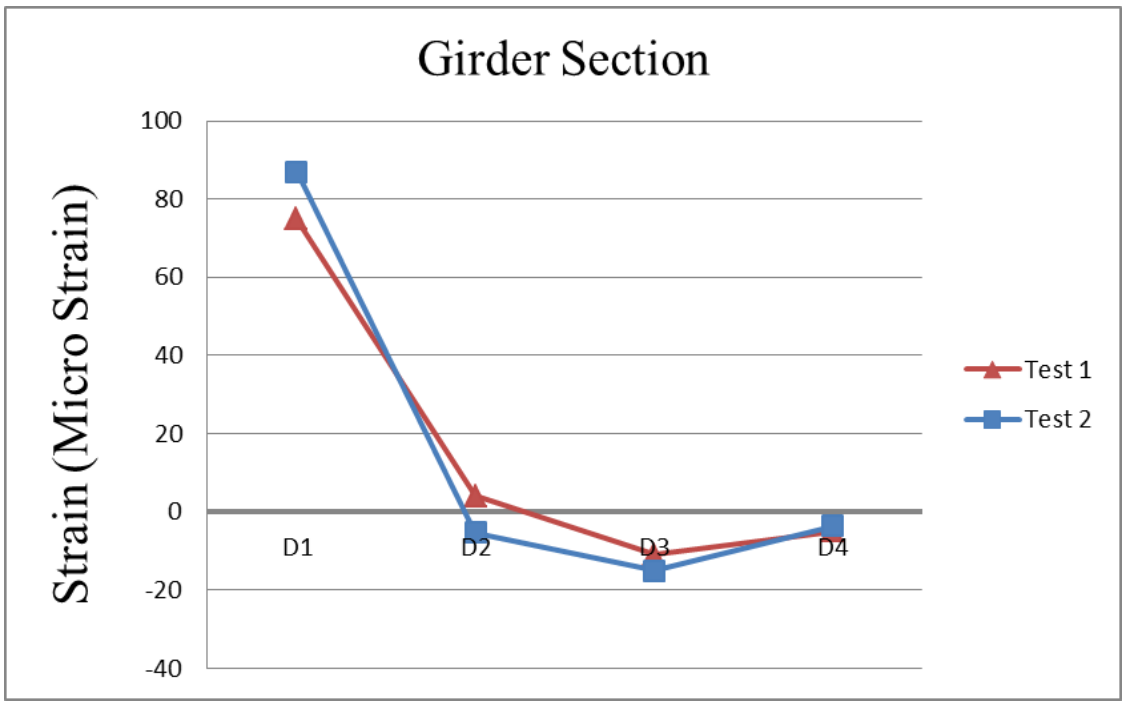

Figure 6.23. Bridge 1 And 2 Run 1 Girder D Strains For Maximum Positive Moment.

Girder Distribution Factors

Assuming that all girders have identical stiffness, the resulting girder distribution factors (GDF) are calculated based on the test results by dividing the maximum girder strain value by the sum of the girder strains along a given gage line. The GDF represents the proportion of the total truck live load that is carried by the most heavily-loaded girder. These results are shown in Tables 6.1 and 6.2, where the AASHTO LRFD and Standard GDFs are presented for comparison. Note for direct comparison to the test results, in Table 6.1, the AASHTO LRFD result is divided by 1.2 to remove the multiple presence factor. For Table 6.2, the AASHTO LRFD result is divided by 2 as the LRFD GDF is to be used with the weight of a single truck rather than two trucks. Similarly, the AASHTO Standard GDF (*S*/7 for 1 lane and *S*/5.5 for 2 lanes) is reduced by 1/2 in Table 6.1 and by 1/4 in Table 6.2 as it is to be used for a wheel line (i.e. 1/2 of a single truck weight). As shown in the tables, the AASHTO prediction is conservative for all positive moment cases. In some negative moment cases, the test value exceeds the AASHTO prediction. However, negative moment values are less reliable since strains are relatively low and other factors such as debris around the joints, variations in slab stiffness due to cracking, etc. more significantly influence results. It is therefore recommended that the negative moment GDFs are viewed with caution.

Table 6.1. One Lane Girder Distribution Factors.

Run	Bridge 1 (+)	Bridge 1 (-)	Bridge 2 (+)	Bridge 2 (-)
5	0.18	0.25	0.24	0.26
6	-	0.19	0.21	0.35
7	-	0.28	0.23	0.51
8	0.18	0.25	0.22	0.31
9	-	0.23	0.22	0.23
10	-	0.43	0.23	0.29
11	0.18	0.20	0.23	0.23
12	-	0.20	0.22	0.29
14	-	0.37	0.23	0.39
Average	0.18	0.27	0.23	0.32
Minimum	0.18	0.19	0.21	0.23
Maximum	0.18	0.43	0.24	0.51
LRFD/1.2	0.33	0.33	0.33	0.33
Standard/2	0.47	0.47	0.47	0.47

Table 6.2. Two Lane Girder Distribution Factors.

Run	Bridge 1 (+)	Bridge 1 (-)	Bridge 2 (+)	Bridge 2 (-)
1	0.17	0.25	0.21	0.24
2	0.18	0.33	0.22	0.27
3	-	0.22	0.23	0.43
4	-	0.53	0.22	0.55
Average	0.18	0.33	0.22	0.37
Minimum	0.17	0.25	0.21	0.24
Maximum	0.18	0.53	0.23	0.55
LRFD/2	0.28	0.28	0.28	0.28
Standard/4	0.30	0.30	0.30	0.30

Degree of Negative Moment at Middle Support

To evaluate the degree of span continuity over the middle support, a simple analytical model representing the tested bridge spans was considered using different support conditions and joint rotational stiffness at the middle support. The actual test truck loads were applied on the model at the location that produced the maximum positive moment at the first span, as shown in Figure 6.24.

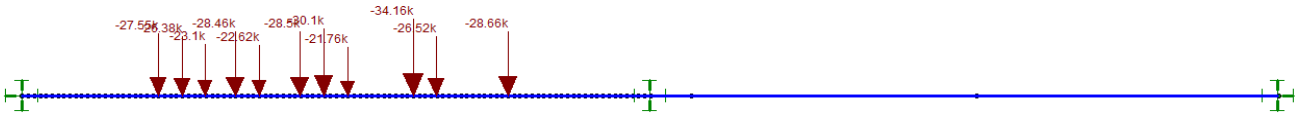

Figure 6.24. Bridge Joint Continuity Model.

Three cases were considered for analysis, as shown below.

Case 1: Full moment continuity.

This case corresponds to a continuous span over a interior roller support, as generally assumed for design, with a sample resulting moment diagram shown in Figure 6.25. Note moment diagrams in the figures are reversed from the standard sign convention.

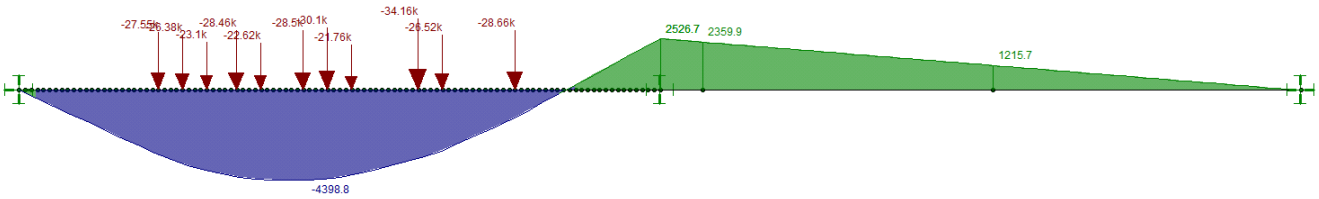

Figure 6.25. Case 1 Moment Diagram.

Case 2: Fixed support.

This case corresponds to a fixed support placed at the center support; i.e. the spans are independent structures. The resulting maximum positive moment diagram is shown in Figure 6.26.

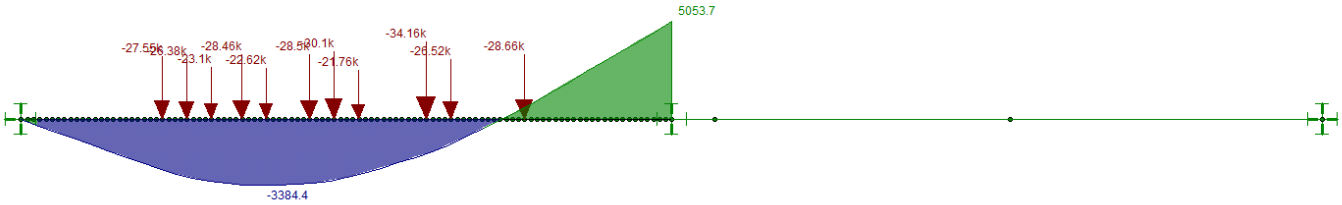

Figure 6.26. Case 2 Moment Diagram.

Case 3: Pinned support.

This case corresponds to a pinned center support; i.e. the spans are independent simple spans, with resulting maximum moment diagram shown in Figure 6.27.

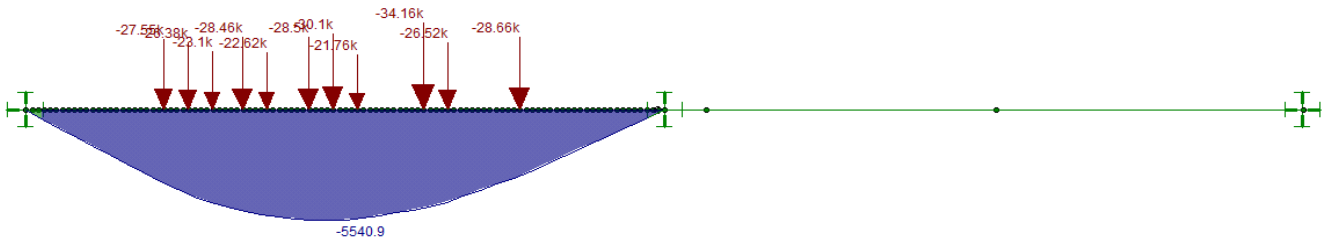

Figure 6.27. Case 3 Moment Diagram.

In addition to the cases above, to best-estimate the degree of continuity on the test structures, the rotational stiffness of the moment connection between the spans over the middle support was adjusted until the proportion of moments found along the span best matched the proportion of strains along the span (i.e. at D1, D2, D3, D4) found experimentally. A best-fit scale factor was then chosen to covert the analysis model moments to strains. Once this scale factor was determined, it was also used to convert the moments found from cases 1-3 above into strains for comparison. These results are given in Figure 6.28 (for Run 1). On the figure, "Actual" refers to the test values, while "Model" refers to the best-fit result found from adjusting the connection rotational stiffness. Note that the center support lies approximately midway between points D2 and D3 on the graph. As shown in Figure 6.28, for maximum positive moment, the best-fit model result falls somewhere between a simple span and continuous span, with results slightly closer to a simple span.

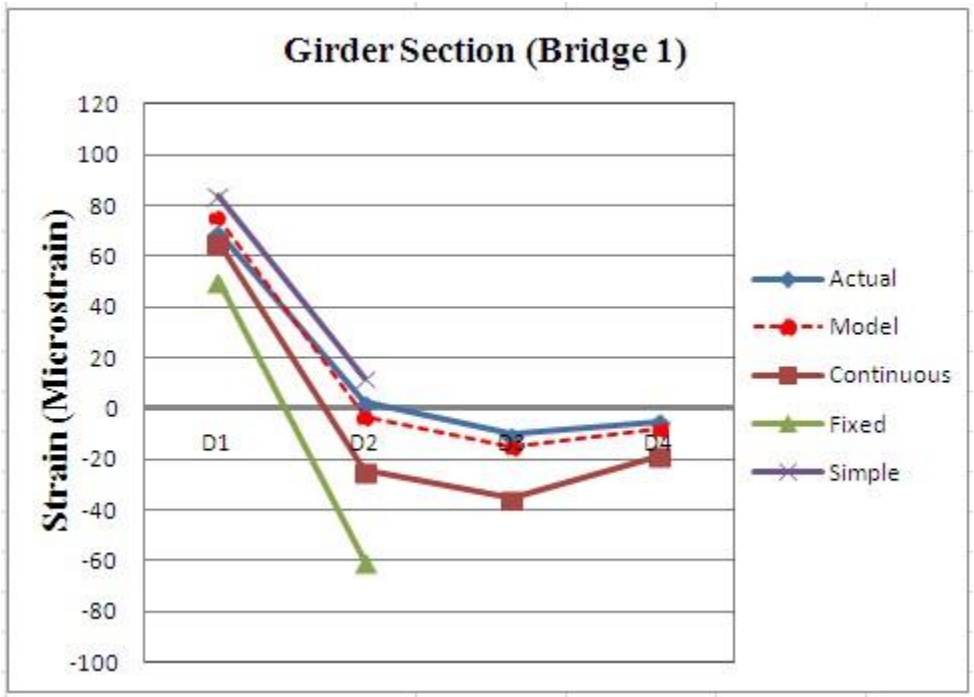

Figure 6.28a. Girder Strains For Different Joint Continuity Assumptions, Bridge 1.

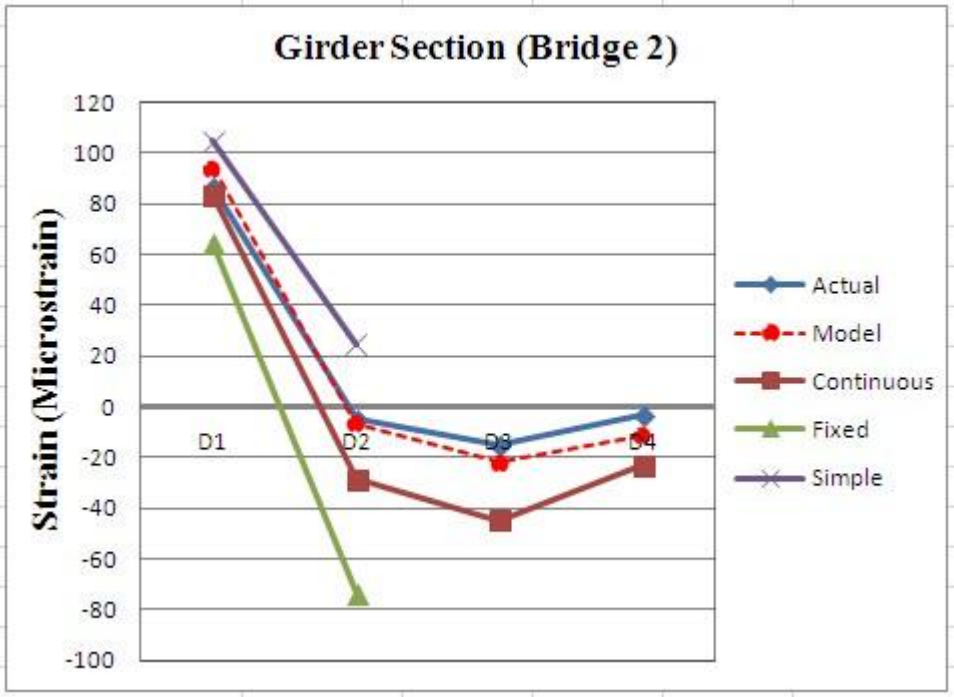

Figure 6.28b. Girder Strains For Different Joint Continuity Assumptions, Bridge 2.

Using the analysis models, the moments on the center girder found from the test truck positioned at a location that maximizes positive moment on Span 1 are given in Table 6.3.

Table 6.3a. Bridge 1 Moments.

	Girder Moment (k-ft)				Moment Ratios		
Location	Continuous	Fixed	Simple	Model	Cont./Model	Fixed/Model	Simple/Model
D1 (center of span 1)	4399	3403	5588	5038	0.87	0.68	1.11
D2 (interior support, span 1)	-1630	-3998	811	-214	7.6	18.6	-3.78
D3 (interior support, span 2)	-2360	-	-	-1026	2.3	-	-
D4 (center of span 2)	-1216	-	-	-529	2.3	-	-

Table 6.3b. Bridge 2 Moments.

	Girder Moment (k-ft)				Moment Ratios		
Location	Continuous	Fixed	Simple	Model	Cont./Model	Fixed/Model	Simple/Model
D1 (center of span 1)	4505	3488	5664	5096	0.88	0.68	1.11
D2 (interior support, span 1)	-1548	-3983	1333	-357	4.3	11.2	-3.74
D3 (interior support, span 2)	-2419	-	-	-1186	2.0	-	-
D4 (center of span 2)	-1246	-	-	-611	2.0	-	-

As shown in the Table, the maximum positive moment (location D1) found using the best-fit joint stiffness value is approximately 1/0.87 or 15% higher than that assumed from a continuous support, while negative moments are significantly lower than assumed from a continuous support.

Strain Comparison Based on Different Support Assumptions

For a selection of representative results, analyses were conducted that present expected girder strains assuming that the interior support is simple, continuous, and fixed, and compared to the actual test results, as shown in Figures 6.29-6.36. As seen in each case, with regard to positive moment, the test results ("Actual") are between a simple and continuous support condition.

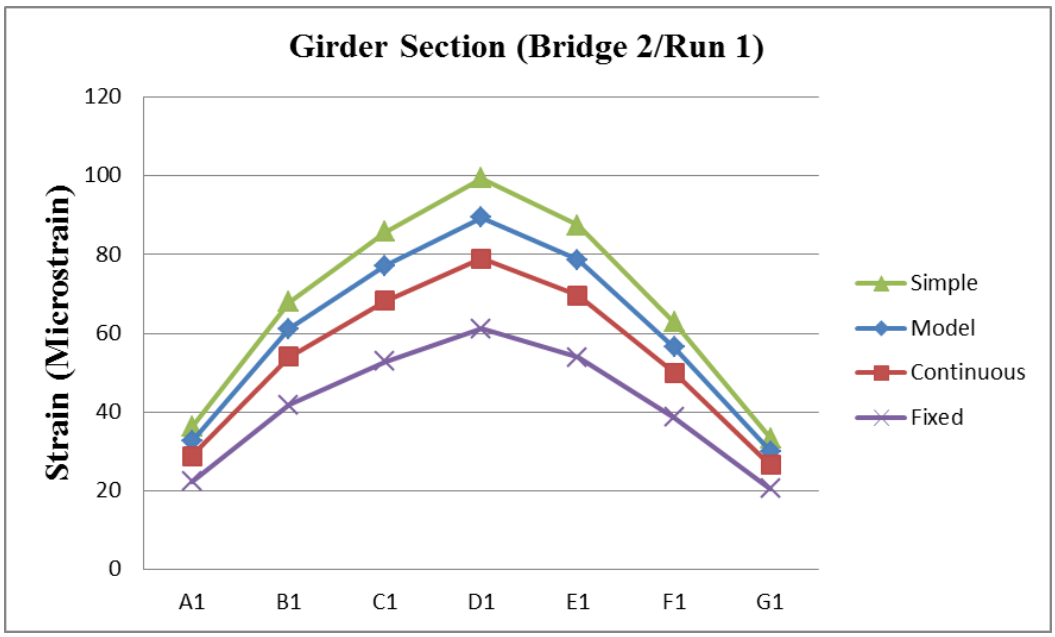

Figure 6.29. Bridge 2 Run 1 Girder Strain Comparison For Maximum Positive Moment.

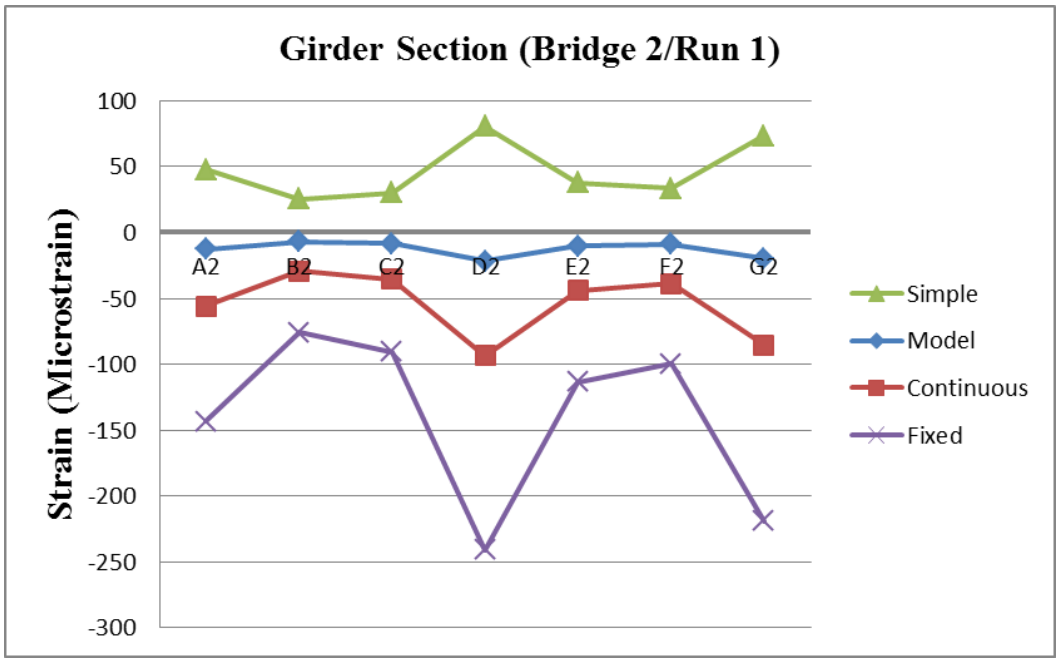

Figure 6.30. Bridge 2 Run 1 Girder Strain Comparison For Maximum Negative Moment.

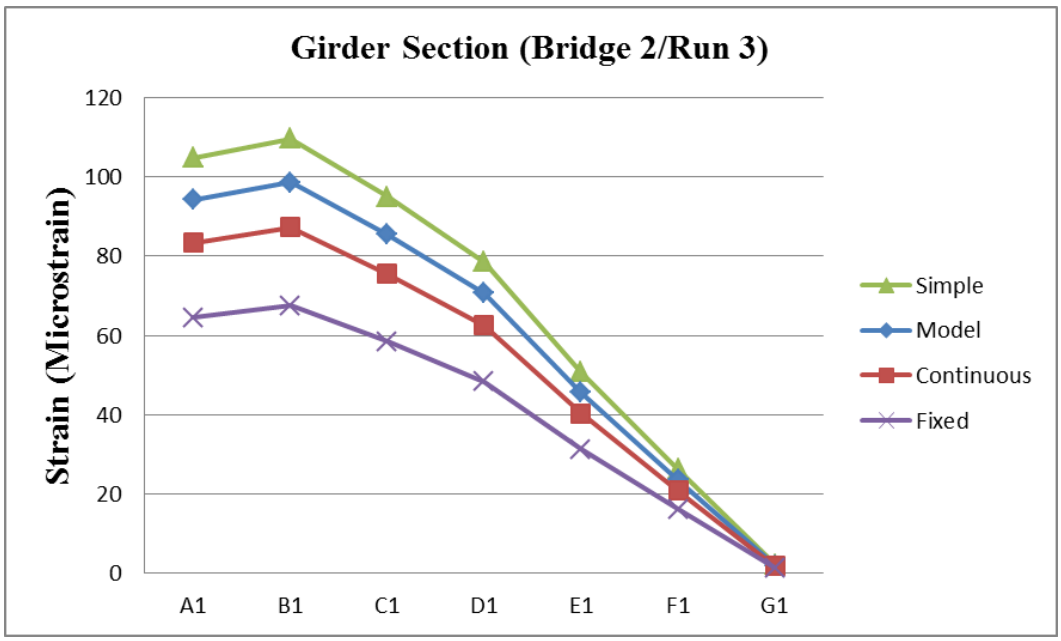

Figure 6.31. Bridge 2 Run 3 Girder Strain Comparison For Maximum Positive Moment.

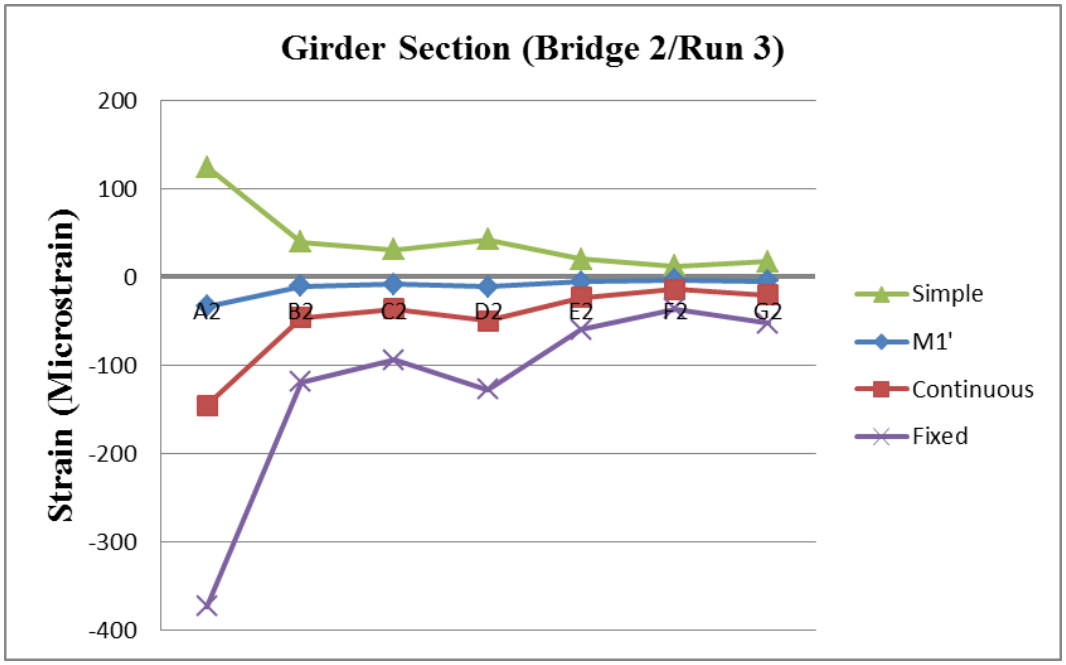

Figure 6.32. Bridge 2 Run 3 Girder Strain Comparison For Maximum Negative Moment.

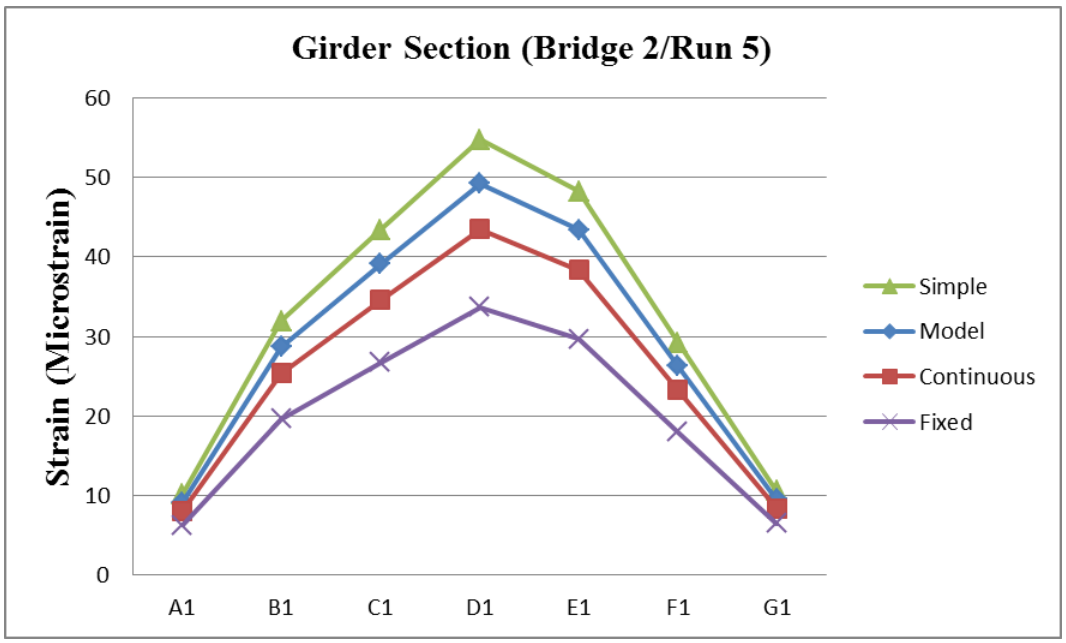

Figure 6.33. Bridge 2 Run 5 Girder Strain Comparison For Maximum Positive Moment.

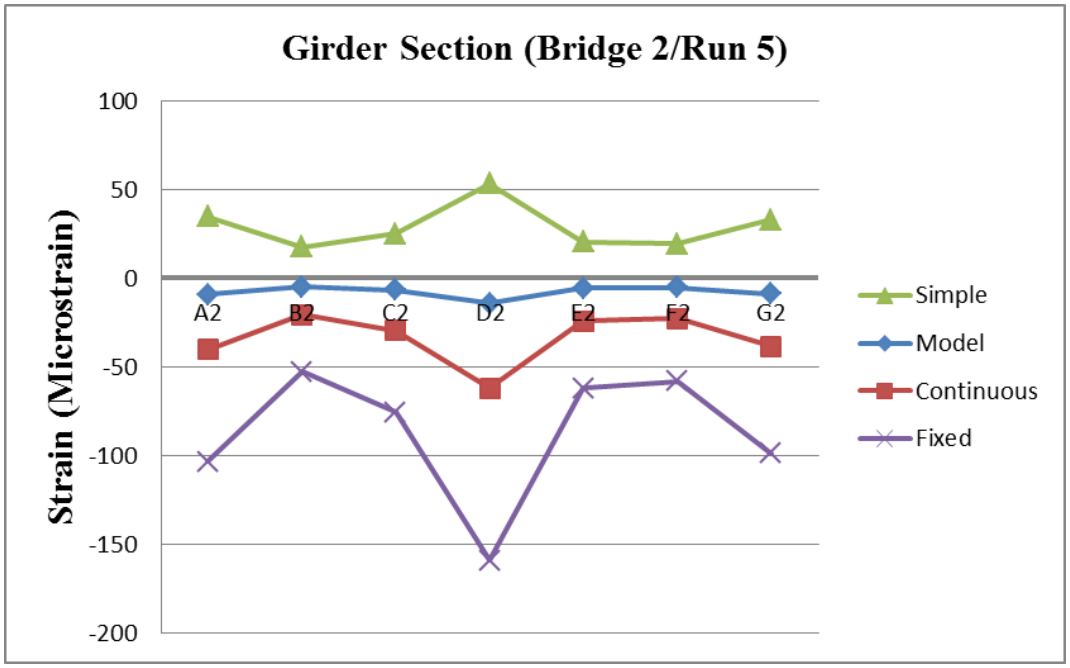

Figure 6.34. Bridge 2 Run 5 Girder Strain Comparison For Maximum Negative Moment.

Figure 6.35. Bridge 2 Run 11 Girder Strain Comparison For Maximum Positive Moment.

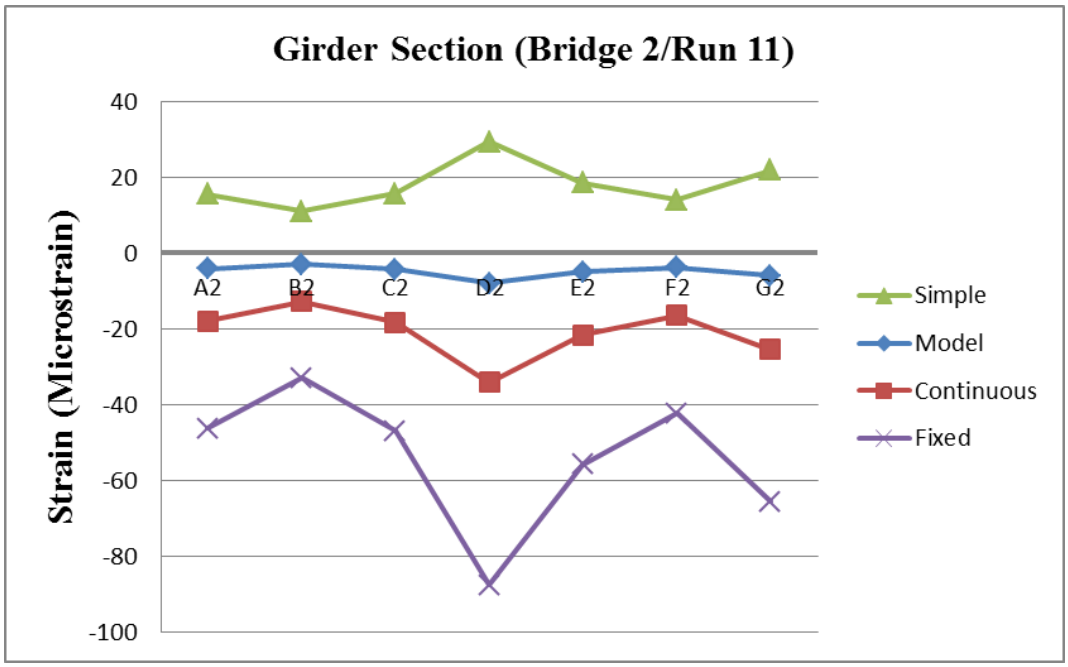

Figure 6.36. Bridge 2 Run 11 Girder Strain Comparison For Maximum Negative Moment.

Shear Analysis

To determine the effect of joint continuity on shear reactions, the analysis shown in Table 6.3 was repeated, but shears were recorded rather than moments. Here, a test truck was positioned on the analysis model to generate maximum shear either at the exterior or interior support, as shown in Figures 6.37 and 6.38, and the analysis was repeated for different joint continuity conditions. Results are given in Table 6.4. In the Table, V_c represents the reactions assuming a continuous interior joint; V' are the reactions based on the best-fit model of the actual joint continuity; and V_s represents the reactions assuming simple spans. As shown in the Table, as with moment results, the actual condition is between that of a continuous and simple span, with results slightly closer to the simple case. The V_s/V' ratio of 1.04 for both tested bridges indicates that actual interior shears are only about 4% higher than if a completely simple support were assumed.

Table 6.4. Shears Due To Different Interior Joint Stiffness Conditions.

(units in kips)	Bridge 1					Bridge 2				
Support	V_c	V'	V_s	V_c/V'	V_s/V'	V_c	V'	V_s	V_c/V'	V_s/V'
Exterior	207	215	223	0.96	1.04	213	221	229	0.97	1.04
Interior	-224	-211	-202	1.06	0.96	-229	-218	-207	1.05	0.95

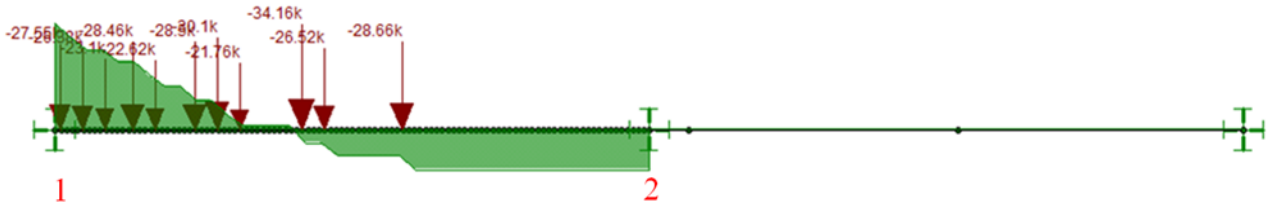

Figure 6.37. Truck load And Resulting Shear Diagram For Maximum Shear At Exterior Support.

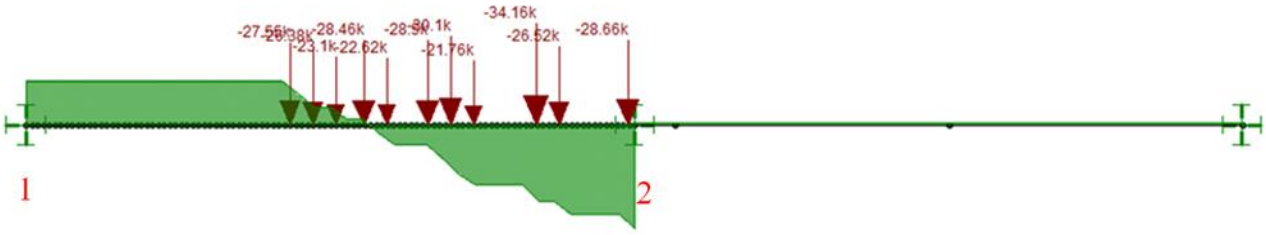

Figure 6.38. Truck Load And Resulting Shear Diagram For Maximum Shear At Interior Support.

In summary, it was found that for both moment and shear effects, the bridge tests and analysis revealed that the interior joint continuity behaves with stiffness between that of a continuous and simple condition, with overall results slightly closer to the simple case.

CHAPTER 7: SHEAR CAPACITY PREDICTION

LRFD Model

Using the computed ratios of the FEA-predicted shear capacity and the AASHTO LRFD nominal shear capacity for the beams modeled in Chapter 5, a regression analysis was performed. In the analysis, the FEA/LRFD ratios were taken as dependent variables while the parameters used in the FEA analyses; concrete compressive strength (f'_c), average stress due to prestress force (σ), stirrups spacing (s), and beam height (h), were considered independent variables. Both linear and nonlinear regression analyses were performed on 216 representative FEA/LRFD ratios, and best fit regression lines were developed. These lines were then adjusted by adding a constant value to them such that the predicted beam capacity (as compared to the FEA result) was never unconservative. These regression equations are given below.

$$\left(\frac{FEA}{LRFD}\right)_{Linear} = 0.009 f_c^{'} + 0.2\sigma + 0.035s + 0.018h + 0.01 \qquad (7.1)$$

$$\left(\frac{FEA}{LRFD}\right)_{Nonlinear} = 0.034 f_c^{'} + 0.942\sigma - 0.21\sigma^2 + 0.134s - 0.003s^2 - 0.002h - 0.25 \qquad (7.2)$$

Comparisons between the two regression models and the original FEA/LRFD ratios are shown in Figures 7.1 and 7.2. In the figures, the triangular symbols (blue) represent the original FEA/LRFD ratios while the circular (red) symbols represent the (FEA/LRFD) ratios adjusted by multiplying by the regression equation.

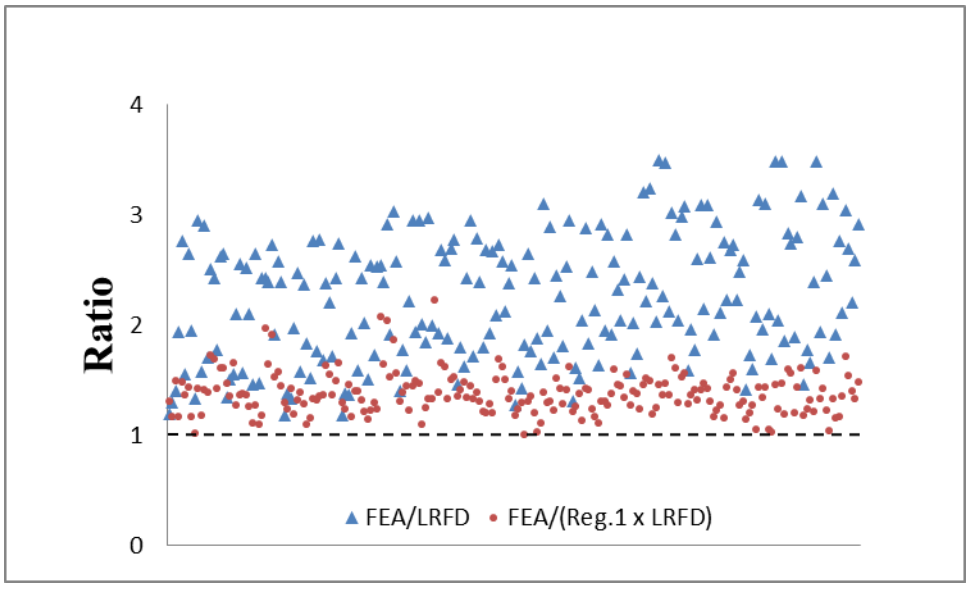

Figure 7.1. Results Of Linear Regression Model With LRFD Code.

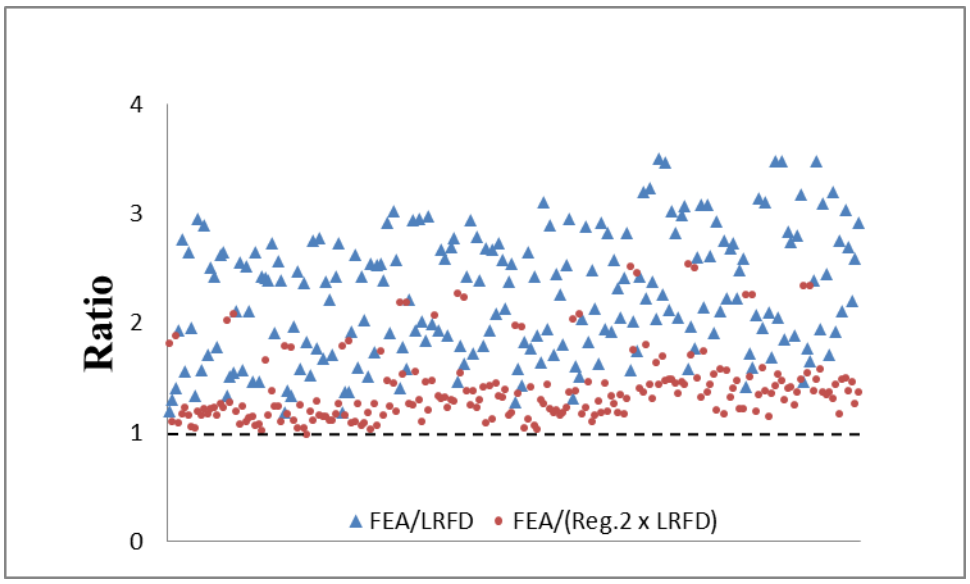

Figure 7.2. Results Of Nonlinear Regression Model With LRFD Code.

As shown in the figures, in both cases, the regression line, if used as an adjustment factor, produces a significant improvement in the accuracy of the code prediction, bringing the ratio of FEA/LRFD much closer, but not below, 1.0. Table 7.1 presents a summary of these results, where the simpler linear regression model (eq. 1) provides the best fit. Here, the linear regression model has a significantly lower mean FEA/LRFD ratio (1.37) and COV (0.14) as compared to the original LFRD approach (with mean FEA/LRFD ratio of 2.25 and COV of 0.26).

In practice, the model would be used by computing V_n from the LRFD sectional method then iterating until $V_n=V_u$ (see Appendix H), then multiplying the resulting capacity value by eq. 7.1; this produced the results presented in Figure 7.1 and Table 7.1. Results of the regression models for each beam considered are given in Table I1 (Appendix I).

Table 7.1. Statistical Analysis Of Regression Models With LRFD Code.

	FEA/ LRFD	Reg.1	Reg.2	FEA/ (Reg.1*LRFD)	FEA/ (Reg.2*LRFD)
Mean	2.25	1.64	1.70	1.37	1.39
STDEV.	0.59	0.37	0.55	0.19	0.32
COV	0.26	0.23	0.32	0.14	0.23

Standard Model

Following the same procedure used for the LRFD regression analyses, the process above was repeated using the Standard Code as a reference rather than LRFD. In this case, only the linear model was considered, and results are given by Eq. 7.3 and shown in Figure 7.3 and Table 7.2. Results for individual beams are given in Table I2 (Appendix I).

$$\left(\frac{FEA}{STD}\right)_{Linear} = 0.033 f_c^{'} + 0.13\sigma + 0.01s + 0.017h - 0.15 \qquad (7.3)$$

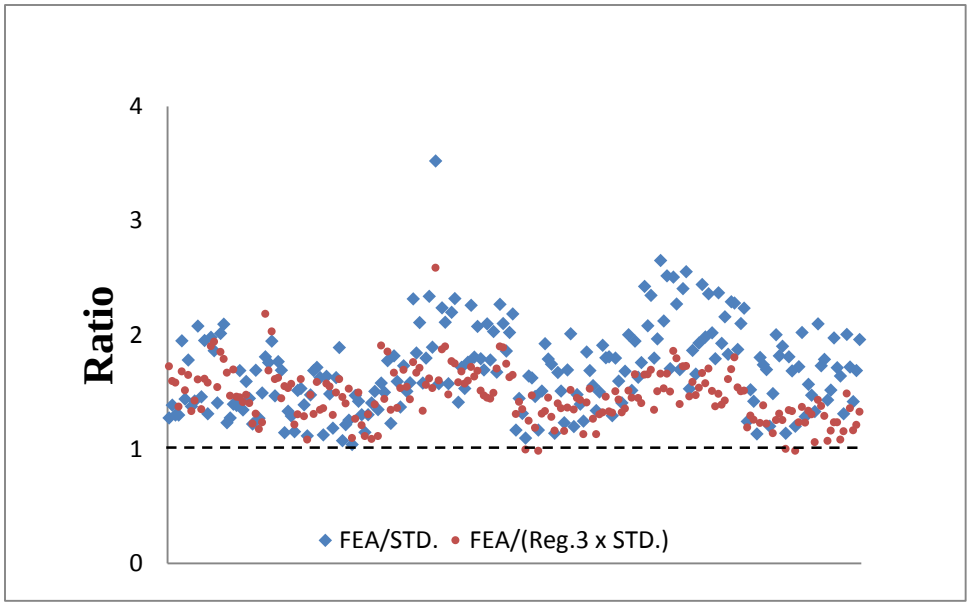

Figure 7.3. Results Of Linear Regression Model With Standard Code.

Table 7.2. Statistical Analysis Of Regression Models With Standard Code.

	(FEA/STD.)	Reg.	FEA/(Reg.*STD)
Mean	1.69	1.16	1.47
STDEV.	0.37	0.19	0.27
COV	0.22	0.16	0.18

As shown in Table 7.2, Standard Code results are similar to, but somewhat worse than, LRFD Code results, as both mean value as well as COV of the final result (last column in table) are higher

CHAPTER 8: RECOMMENDATIONS

Estimation of Shear Capacity

As discussed in Chapter 7, in all cases considered, it was found that the AASHO methods conservatively estimated shear capacity, sometimes significantly so. To best estimate shear capacity V_n of MDOT PC girders, it is recommended that the linear regression equation (eq. 7.1) is used in conjunction with the modified AASHTO LRFD procedure described in Chapter 7; this procedure is summarized by eq. 8.1. Specifically, V_n is first computed from the LRFD sectional method then an iteration is conducted until $V_n=V_u$, as described in Appendix H, to produce $V_{n\ mod\ LRFD}$. This result is then multiplied by the outcome of eq. 7.1, as a function of concrete compressive strength (f'c, ksi), average stress due to prestress force (σ = gross area of concrete beam / total prestress force, ksi), stirrups spacing (s, inches), and beam height (h, inches), to provide the best estimate for V_n:

$$V_n = V_{n\ \mathrm{mod}\,LRFD} \cdot k_{mL} \tag{8.1}$$

$$k_{mL} = \left(0.009 f_c^{'} + 0.2\sigma + 0.035s + 0.018h + 0.01\right);\ 1.18 \le k_{mL} \le 3.49$$

Eq. 8.1 provided the lowest deviation (mean ratio of estimation to FEA model predicted capacity = 1.37; COV 0.14) from the expected beam capacities, as determined from the FEA models, with no case unconservatively estimated. Note that if k_{mL} is computed outside of the limit provided (i.e. $1.18 \le k_{mL} \le 3.49$), then k_{mL} should be limited to that value; it does not mean that the adjustment is invalid. The lower limit (1.18) is added to improve results for some cases. As shown Table I1 (Appendix I), the minimum ratio of FEA/LRFD for any case is 1.18; however, the best-fit linear regression expression generates ratios lower than 1.18 for some cases, producing some over-conservative results. Imposing this limit ensures that a beam capacity analyzed with eq. 8.1 is at least given the minimum capacity increase factor k_{mL} found from all of the cases. The upper limit represents the maximum FEA/LRFD ratio found from all of the cases studied, and is imposed for safety.

Alternatively, a significantly simpler procedure can be obtained from using the Standard Code V_n for base capacity, as given by eq. 8.2:

$$V_n = V_{n\ S\tan dard} \cdot k_S \tag{8.2}$$

$$k_S = \left(0.033 f_c^{'} + 0.13\sigma + 0.01s + 0.017h - 0.15\right);\ 1.04 \le k_S \le 3.52$$

In this case, $V_{n\ S\tan dard}$ is the shear capacity as determined from the AASHTO Standard Code. However, use of this approach results in slightly greater inconsistency and average level of conservativeness (mean ratio of estimation to FEA model predicted capacity = 1.47; COV 0.18).

Note that the adjustment factors k_{mL} and k_S are empirical, and were verified acceptable for prestressed AASHTO Type beams with f'c from 5.5-8 ksi; σ from 0.5-2.5 ksi; s from 3-24 in; and h from 36-54 in. This does not necessarily mean that the adjustment factors are invalid for

beams exceeding these parameters, but rather that additional caution should be exercised with their use in such cases.

PC Beams Continuous for Live Load

For analysis of positive moments, as shown in Chapter 6 (Table 6.3), results fell between simple and continuous cases, with a slight bias toward simple. Therefore, based on the test results, a reasonably accurate way to estimate positive moment would be to average the results from a simple span and a continuous span assumption. An easier and more conservative estimation would be to take the simple span moment only. For negative moments, test results were approximately 50% less than the continuous case. Therefore, a reasonable estimation of negative moment would be to reduce the continuous span moment by half.

Similarly, for analysis of shears for both interior (pier) and end (abutment) supports, results fell between simple and continuous cases (see Chapter 6, Table 6.4), with an overall slight bias toward simple, although shears are less affected by a change in joint stiffness than moments. As with moments, this suggests that a reasonably accurate way to estimate shear effects would be to average the results from a simple span and a continuous span assumption. For end supports, a slightly conservative assumption would be to assume a simple span case, while for the interior support, a slightly conservative assumption would be to assume a continuous span case. However, it would be slightly unconservative (underestimating shears by about 5%) to assume a simple span for the interior support with regard to shear. Therefore, an easy to use alternative would be to treat the spans as simple, and increase the interior support shear (not exterior) found from the simple span analysis by approximately 5%. For the bridges studied, this procedure would provide reasonably accurate interior support shears and a slightly conservative estimation of end support shears.

Note that the above recommendations are based on a field test and analysis under service load levels only. At higher load levels close to ultimate, the joint stiffness may decrease further to even more closely resemble that of a simple condition.

Existing Shear Cracks

Based on the field study and analysis presented in Chapters 3 and 4 and the FEA results in Chapter 5, it appears highly unlikely that any diagonal cracks observed on the field study bridges were due to live load overloads, as not only are all code nominal shear capacities considerably conservative for the beams studied, but significant shear damage to the beam without the development of significant flexural cracks could not be predicted for any reasonable beam designs. Therefore, it appears highly likely that the existence of diagonal cracks is due to issues other than vehicular live load exceeding shear capacity, such as beam end design and prestress anchorage, mix design, or loads during manufacturing, construction, or transportation.

Consequently, it does not appear that the presence of these cracks, which were observed to be relatively tight where aggregate interlock is preserved, poses significant concern for significant loss of shear capacity. It is thus recommended that cracks are monitored and repaired if necessary to prevent penetration of water and corrosion of reinforcing steel. Various references

are available to guide this process, such as ACI 201.1R, *Guide for Making a Condition Survey of Concrete in Service*; ACI 224.1R, *Causes, Evaluation, and Repair of Cracks in Concrete*; ACI 503R, *Use of Epoxy Compounds with Concrete*; and ACI 546, *Concrete Repair Guide*. If crack growth and opening continues and strength loss becomes a concern, external strengthening may be achieved with the use of fiber reinforced composite fabric, an MDOT guideline for which is currently under development (see OR10-039, *Design and Construction Guidelines for Strengthening Bridges Using Fiber Reinforced Polymers*) and should be completed in 2014.

If MDOT is concerned about the existing shear capacity of a beam, and the capacity evaluation expressions presented earlier in this Chapter are deemed insufficiently adequate, a field load test may provide insight to the performance of the beam under heavy loading. This type of test can be conducted before or after repairs to the beam, and may take two forms: a monitoring test or a proof load test. With a monitoring test, the shear strains and crack width openings are monitored with appropriate gages, to determine the change in the existing conditions due to the application of a given vehicular load. Results from such a test can be used to determine the potential behavior under heavier loads than used in testing by analytical modeling and extrapolation from the test results. Such an effort is not straightforward, however. Alternatively, a proof load test can be used to confirm the needed capacity of a structure by loading it with the legal or permit loads which are desired to pass. This effort requires careful monitoring of the bridge structure during the test to ensure no damage occurs, as well as acquisition of the usually heavy loads desired. However, a successful proof load test provides definite confirmation of structural capacity. Several existing MDOT reports detail the field load testing of bridges.

REFERENCES

ACI 318-11: *Building Code Requirements for Structural Concrete and Commentary*. American Concrete Institute, Farmington Hills, MI, 2011.

AASHTO. *Standard Specifications for Highway Bridges*. 11th edition, 1973.

AASHTO. *Interim Revisions to Standard Specifications for Highway Bridges*, 1979.

AASHTO. *Standard Specifications for Highway Bridges*. 17th edition, 2002.

AASHTO *LRFD Bridge Design Specifications*. 2010.

ASTM Committee C09. *Standard Test Method for Compressive Strength of Cylindrical Concrete Specimens*. ASTM C39/C39M-01 edition, 2001.

Aboutaha, R., and Burns, N. "Shear Strengthening of Pretensioned Prestressed Concrete Composite Flexural Members". Federal Highway Administration, Austin, Texas. Report CTR-3-5-89/1-1210-2. p 92. March 1991

Baker, M., Thompson, P. D. "Bridge Software--Validation Guidelines and Examples". NCHRP Report 485. Transportation research Board, Washington, D.C., 2003.

Belarbi, A., and Hsu, T. C. "Consecutive laws of RC in Biaxial tension-Compression". Research report UHCEE 91-2. University of Houston, Texas. 1991.

Belarbi, A., and Hsu, T. C. "Softened Concrete in Biaxial Tension-Compression". *ACI Structural Journal*, v 92, n 5, 562-573. Sept-Oct 1995.

Belarbi, A., Bae, S-W., Ayoub, A., Kuchma, D., Mirmiran, A., and Okeil, A. "Design of FRP Systems for Strengthening Concrete Girders in Shear". NCHRP Report 678. Transportation Research Board, Washington, D.C., 2011.

Bennett, E.W., Abdul-Ahad, H.Y., and Neville, A.M. " Shear strength of reinforced and prestressed beams subject to moving loads". *Journal of the Prestressed Concrete Institute*, v 17, n 6, p 58-69, Nov-Dec 1972.

Bennett, E.W. and Mlingwa, G. "Cracking and Shear Strength of Beams with Prestressed Web Reinforcement." *Structural Engineering*, v 58, n 2, p 25-32.

Bentz, E.C., "Sectional Analysis of Reinforced Concrete Members", Ph.D. Thesis, Department of Civil Engineering, University of Toronto, 310 p. 2000.

Bentz, E. C., Vecchio, F. J., and Collins, M. P. "Simplified Modified Compression Field Theory for Calculating Shear Strength of Reinforced Concrete Elements". *ACI Structural Journal*, v 103 n 4, p 614– 624, July-August 2006.

Bresler, B., and Pister, K.S. "Strength of Concrete under Combined Stresses". *ACI Journal Proceedings*, v 55, n 9, 321-345, 1958.

Brown, M.D. and Bayrak, O. "Design of Deep Beams using Strut-and-Tie Models - Part I: Evaluating U.S. Provisions". *ACI Structural Journal*, v 105 n 4, p 395–404, July-August 2008.

Burgueno R. and Sun, Y. "Effects of Debonded Strands on the Production and Performance of Prestressed Concrete Beams" MDOT Report RC-1546. MSU Report No. CEE-RR - 2011/01, Michigan State University, Jan. 2011.

Castrodale, R. W., and White, C. D. "Extending Span Ranges of Precast Prestressed Concrete Girders". NCHRP Report 517. Transportation Research Board, Washington, D.C., 2004.

Cederwall, K. "Shear Capacity of Composite Prestressed Concrete Beams". Nordic Concrete Research, n 7, 28-40. December 2006.

Cladera, A., and Marif, A.R. "Shear design of prestressed and reinforced concrete beams". *Magazine of Concrete Research*, v 58, n 10, 713-22, Dec. 2006.

Collins, M. P., and Mitchell, D. “Prestressed Concrete Structures”. p 776. Englewood Cliffs, New Jersey: Prentice-Hall, Inc. 1991.

Colllins, M.P., Mitchell, D., Adebar, P., and Vecchio, F.J. "A General Shear Design Method." *ACI Structural Journal*, v 93, n 1, Jan-Feb 1996.

Cumming, D. A., French, C. E., and Shield, C. K. “Shear Capacity of High-Strength Concrete Prestressed Girders”. Minnesota Department of Transportation. p 396. May 1998.

De Silva, S., Mutsuyoshi, H., and Witchukreangkrai, E. “Evaluation of shear crack width in I-shaped prestressed reinforced concrete beams”. *Journal of Advanced Concrete Technology*, v 6, n 3, p 443-458, October 2008.

Dei Poli, S., Prisco, M. D., and Gambarova, P. G. “Stress Fields in Web of Reinforced Concrete Thin-Webbed Beams Failing in Shear”. *Journal of Structural Engineering*, v 116, n 9, 2496-2515. September 1990.

Duthinh, D. “Sensitivity of Shear Strength of RC and PC Beams to Shear Friction and Concrete Softening According to the MCFT”. National Institute of Standards and Technology. p 38. Gaithersburg, MD. August 1997.

Duthinh, D., and Dat. “Sensitivity of shear strength of reinforced concrete and prestressed concrete beams to shear friction and concrete softening according to modified compression field theory”. *ACI Structural Journal*, v 96, n 4, p 495-508, July/August 1999.

Eligehausen, R., Popov, E., and Bertero, V. “Local Bond Stress-Slip relationship of Deformed Bars under Generalized Excitations”, Report No. UCB/EERC-83/23, Earthquake Engineering Center, University of California, Berkeley, 1983.

Esfandiari, A., and Adebar, P. “Shear strength evaluation of concrete bridge girders”. *ACI Structural Journal*, v 106, n 4, 416-26, July-Aug. 2009.

Fagundo, F. E., Lybas, J. M., Basu, A., Shaw, T. J., White, D. “Effect of Confinement in Transfer Region on the Interaction between Bond and Shear Forces in Prestressed Concrete Girders”. Florida University, Gainesville, Dept. of Civil Engineering, 185 p, Dec 1995.

Fenwick, R.C., and Paulay, T. “Mechanisms of shear resistance of concrete beams“. *American Society of Civil Engineers Proceedings, Journal of the Structural Division*, v 94, n ST10, p 2325-2350, Oct 1968.

Gustafson, D. P., and Bruce, R. N. “Investigation of Shear Behavior of Prestressed Concrete Bridge Girders”. Tulane Univ., New Orleans, La. Dept. of Civil Engineering. Report: TR-101, 188 p, Oct 1966.

Hanson, J. M., and Hulsbos, C. L. “Shear Fatigue Tests of Prestressed Concrete I-Beams with Web Reinforcement”. Lehigh Univ., Bethlehem, Pa. Fritz Engineering Lab. Report: 223.29, 114 p, Jan 1969.

Hartmann, D. L., Breen, J. E., and Kreger, M. E. “Shear Capacity of High Strength Prestressed Concrete Girders”, University of Texas at Austin, Center for Transportation Research. Report: CTR-3-5-84-381-2, 271 p, Jan 1988.

Hawkins, N. M., and Kuchma, D. A. “Simplified Shear Design of Structural Concrete Members”. NCHRP Report 549. Transportation Research Board, Washington, D.C., 2005.

Hegger, J., Sherif, A., and Görtz, S. “Investigation of Pre- and Postcracking Shear Behavior of Prestressed Concrete Beams Using Innovative Measuring Techniques”. *ACI Structural Journal*, v 101, n 2, p 183-192, March/April 2004.

Higgins, C., Farrow, W.C., Potisuk, T., Miller, T.H., Yim, S.C., Holcomb, G.R., Cramer, S.D., Covino, B.S., Bullard, S.J., Ziomek-Moroz, M., and Matthes, S.A. "Shear Capacity Assessment Of Corrosion Damaged Reinforced Concrete Beams." Final Report SPR 326. Department of Civil Engineering, Oregon State University, Corvallis OR, December 2003.

Higgins, C., Yim, S.C., Miller, T.H., Robelo, M.J., and Potisuk, T. "Remaining Life Of Reinforced Concrete Beams With Diagonal-Tension Cracks." Final Report SPR 341. Department of Civil Engineering, Oregon State University, Corvallis OR, April 2004.

Hsu, T.C. "Softened Truss Model Theory for Shear and Torsion." *ACI Structural Journal*, Nov/Dec 1988.

Idriss, Rola L., and Liang, Zhiyong. "In-service shear and moment girder distribution factors in simple-span prestressed concrete girder bridge: Measured with built-in optical fiber sensor system". *Transportation Research Record*, n 2172, p 142-150, January 12, 2010.

Kollegger, J., and Melhorn, G. "Material Model for Cracked Reinforced Concrete". IABSE Colloquium on Computational Mechanics of Concrete Structures: Advances and Applications, Delft, n 54, p 63-74, 1987.

Kollegger, J., and Melhorn, G. "Material Model for Analysis of Reinforced Concrete Surface Structures". *Computational Mechanics*, n 6, p 341-357. 1990.

Kuchma, D. A., Hawkins, N. M., et al. "Simplified Shear Provisions of the AASHTO LRFD Bridge Design Specifications". *PCI Journal*, v 53 n 3, p 53–73, May-June 2008.

Kuchma, D. A., and Hawkins, N. M. "Application of LRFD Bridge Design Specifications to High-Strength Structural Concrete: Shear Provisions". NCHRP Report 579. Transportation Research Board, Washington, D.C., 2007.

Kuchma, D., Kang, S. K., Nagle, T. J., and Hawkins, N. M. "Shear Tests on High-Strength Prestressed Bulb-Tee Girders: Strength and Key Observations". *ACI Structural Journal*, v 105, n 3, p 358-67, May-June 2008.

Kupfer, H. and Bulicek, H. "A Consistent Model for Design of Shear Reinforcement in Slender Beams with I- or Box-Shaped Cross Section". *Proceedings, Symposium on Concrete Shear in Earthquake*, p 256-265. Houston, Texas, 1992.

Kupfer, H., Mang, R., and Karavesyroglou, M. "Ultimate Limit State of Shear Zone of Reinforced and Prestressed Concrete Girders-An Analysis Taking Aggregate Interlock into Account". *Bauingenieur* 58, p 143-149, 1983.

Kupfer, H., Hilsdorf, H.K.and Rusch, H.. "Behavior of Concrete under Biaxial Stress", ACI Journal, v 87, n 2, p 656-666, 1969.

Kupfer, H.B., and Gerstle, K.H., "Behaviour of Concrete under Biaxial Stresses", *ASCE Journal of Engineering Mechanics*, v 99, EM4, p 853-866, 1973.

Laskar, A., Hsu, T. C., Mo, Y.L. "Shear strengths of prestressed concrete beams part 1: Experiments and shear design equations". *ACI Structural Journal*, v 107, n 3, p 330-339, May-June 2010.

Laskar, A., Howser, R., Mo, Y.L., Hsu, T.T.C. "Modeling of prestressed concrete bridge girders*". Proceedings of the 12th International Conference on Engineering, Science, Construction, and Operations in Challenging Environments - Earth and Space 2010*, p 2870-2887, 2010.

Lee, S-C., J-Y Cho, J-Y., Oh, B-H. "Shear Behavior of Large-Scale Post-Tensioned Girders with Small Shear Span-Depth Ratio". *ACI Structural Journal*, v 107, n 2, p 137-45, March-April 2010.

Libby, J. R., Konczak, L. Z. "Designing for shear in continuous prestressed concrete bridges". S*tructural Engineers Assoc of California Conference: Proceedings.* Convention of Structural Engineers Association of California, p 97-109, 1985.

Lin, T. Y., and Burns, N. H. "*Design of Prestressed Concrete Structures*". John Wiley & Sons, 1981.

Liu, C., Wu, B., and Xu, K.Y. "Parametric Study on Reinforced Concrete Beams with Transversely Prestressed Bars." *Applied Mechanics and Materials*, v 105-107, p 912-917, 2012.

Llanos, G., Ross, B. E., Hamilton, H. R. "Shear Performance of Existing Prestressed Concrete Bridge Girders ". Florida University, Gainesville. Dept. of Civil and Coastal Engineering. Report: BD545-56, 160 p, May 2009.

Ma, Y., and Hu, J. "Shear Strength of the RPC Prestressed Composite Beam". *Journal of Highway and Transportation Research and Development,* v 24, n 12, 85-88. December 2008.

MacGregor, J.G. "Strength and Behavior of Prestressed Concrete Beams with Web Reinforcement," PhD Thesis, University of Illinois, Urbana, July 1960.

MacGregor, J.G., Sozen, M.A., Siess, C.P. "Strength of Prestressed Concrete Beams with Web Reinforcement," *Journal of the American Concrete Institute*, p 1503-1518, December 1965.

Mahesh, P., Surinder, D. "Support vector regression based shear strength modeling of deep beams". *Computers and Structures*, v 89, p 1430-1439, April 2011.

Maruyama, K., and Rizkalla, S. H. "Shear Design Consideration for Pretensioned Prestressed Beams". *ACI Structural Journal*, v 85, n 5, p 492-498, Sep-Oct 1988.

Mast, P.E. "Shortcuts for shear analysis of standard prestressed concrete members". *Journal of the Prestressed Concrete Institute*, v 9, n 5, p 15-47, Oct, 1964.

Mau, S. T. and Hsu, T. T. Discussion of paper by Walraven, Frenay, and Pruijssers "Influence of Concrete Strength and Load History on Shear Friction Capacity of Concrete Members". *PCI Journal*, v 22, n 1, p 166-170. Jan-Feb 1998.

MDOT *Bridge Analysis Guide*, 2005 Ed, with 2009 Interim Update, Parts 1 and 2. MDOT Construction and Technology Support Area, 2009.

MDOT 2010 *Sufficiency Report, University Region*, 2010.

Mikame, A., Uchida, K., and Noguchi, H. "A Study of Compressive Deterioration of Cracked Concrete". *Proceedings, International Workshop on FEA of RC*, Columbia University, New York. 1991.

Mindess, S., Young, J. F., and Darwin, D. *Concrete*. Prentice Hall, 2nd edition, 2003.

Miyahara, T., Kawakami, T., and Maekawa, K. "Nonlinear Behavior of Cracked Reinforced Concrete Plate Element under Uniaxial Compression". *Proceedings, Japan Society of Civil Engineers*, v 11, p 306-319, 1988.

Milynarski, M., Wassef, W. G., and Nowak, A. S. "A Comparison of AASHTO Bridge Load Rating Methods". NCHRP Project 700. Transportation Research Board, Washington, D.C., 2011.

Moses, F. "Calibration of Load Factors for LRFR Bridge Evaluation". NCHRP Report 454. Transportation Research Board, Washington, D.C., 2011.

Mörsch, E. Reinforced Concrete Construction Theory and Application. 5th ed. V 1, part 1. Stuttgart, Germany: Konrad Wittwer. 1920.

Nazir, C.P. and Wilby, C.B. "Shear Strength of Uniformly Loaded Prestressed Concrete Beams." *Civil Engineering*, v 59, n 693, p 457-463.

Ning, Z. and Tan, K-H. "Direct Strut-and-Tie Model for Single Span and Continuous Deep Beams." *Engineering Structures*, v 29, n 11, p 2987-3001, Nov 2007.

Nowak, A.S. "Calibration of LRFD Bridge Design Code." NCHRP Report 368. Transportation Research Board, Washington, D.C., 1999.

Oesterle, R.G., Glikin, J.D., and Larson, S.C. "Design of Precast Prestressed Bridge Girders Made Continuous." NCHRP Report 322. Transportation Research Board, Washington, D.C., 1989.

Oh, B. H., Kim, Kwang S. "Shear Behavior of Full-Scale Post-Tensioned Prestressed Concrete Bridge Girders". *ACI Structural Journal*, v 101, n 2, p 176-182, March/April 2004.

Okamura, H., and Maekawa, K. "Nonlinear Analysis of Reinforced Concrete". *Proceedings of JSCE*, n 360, p 1-10. August, 1987.

Palermo, D., and Vecchio, F.J., "Behaviour and Analysis of Reinforced Concrete Walls Subjected to Reversed Cyclic Loading", Publication No. 2002-01, Department of Civil Engineering, University of Toronto, 351 p., 2002.

Pei, J. S., Martin, R. D., Sandburg, C. J., and Kang, T. H. "Rating Precast Prestressed Concrete Bridges for Shear". FHWA-OK-08-08. December 2008.

Rabbat, B.G., Collins, M.P. "The computer aided design of structural concrete sections subjected to combined loading". *Computers and Structures*, v 7, n 2, 229-36, April 1977.

Ramirez, J. A., Breen, J. E. "Evaluation of a modified truss-model approach for beams in shear". *ACI Structural Journal*, v 88, n 5, p 562-571, Sep-Oct 1991.

Ranasinghe, K., Mutsuyoshi, H., Ashraf, M. "Effect of bond on shear behavior of RC and PC beams: Experiments and FEM analysis". *Transactions of the Japan Concrete Institute*, v 23, p 407-412, 2001.

Recupero, A., D'Aveni, A., and Ghersi, A. "Bending Moment-Shear Force Interaction Domains for Prestressed Concrete Beams". *Journal of Structural Engineering*, v 131, n 9, p 1413-1421. September 2005.

Reineck, K. H. "Models for Design of Reinforced and Prestressed Concrete Members". *CEB Bulletin d'Information*, n 146-Shear in Prestressed Concrete, 1982.

Reineck, K. H. "Modeling of Members with Transverse Reinforcement". IABSE Colloquium on Structural Concrete, Stuttgart. *IABSE Report*, v 62, p 481-488. 1991.

Richart, F.E. "An Investigation of Web Stresses in Reinforced Concrete Beams," *Bulletin No. 166*, University of Illinois Engineering Experiment Station, 105 p, 1927.

Ritter, W. "Construction Techniques of Hennebique". *Schweizerische Bauzeitung*, v 33, n 7, p 59-61, 1899.

Ross, b. E., Ansley, M., Hamilton, H. R. "Load testing of 30-year-old AASHTO Type III highway bridge girders". *PCI Journal*, p 152-163, 2011.

Runzell, B., Shield, C. K., French, C. W. "Shear Capacity of Prestressed Concrete Beams". MN/RC 2007-47. March 2008.

Sandburg, C. J. "Shearing Capacity of Prestressed Concrete AASHTO Girders". Master's thesis, University of Oklahoma, School of Civil Engineering and Environmental Science, May 2007.

Saqan, E., Frosch, R. J. "Influence of flexural reinforcement on shear strength of prestressed concrete beams". *ACI Structural Journal*, v 106, n 1, p 60-68, Jan-Feb 2009.

Schlaich, J.K., Schafer, M.J. "Toward a Consistent Design of Structural Concrete." *PCI Journal*, Special Report, v 32, n 3.

Scott, B.D., Park, R., and Priestley, M.J.N. "Stress-Strain Behavior of Concrete Confined by Overlapping Hoops at Low and High Strain Rates", ACI Journal, v 79, n 1, p13-27, 1982.

Shahawy, M. A., Cui, C. S. "New approach to shear design of prestressed concrete members". *PCI Journal*, v 44, n 4, p 92-117, July/August 1999.

Shirai, S., and Noguchi, H. "Compressive Deterioration of Cracked Concrete". Proceedings, Structures Congress-Design, Analysis, and Testing, ASCE: New York. p 1-10, 1989.

Tadros, M. K., Badie, S. S., and Tuan, C. Y. "Evaluation and Repair Procedures for Precast/Prestressed Concrete Girders with Longitudinal Cracking in the Web". NCHRP Report 654. Transportation Research Board, Washington, D.C., 2010.

Tuchscherer, R. G., Birrcher, D. B., and Bayrak , O. "Strut-and-tie model design provisions". *PCI Journal*, v 56, n 1, p 155-170, Winter 2011.

Tureyen, A.K., and Frosch, R.J. "Concrete Shear Strength: Another Perspective". *ACI Structural Journal*, v 100, n 5, p 609-615, 2003.

Ueda, M., Noguchi, H., Shirai, N., and Morita, S. "Introduction to Activity of new Reinforced Concrete". *Proceedings, International Workshop on FEA of reinforced Concrete*: Columbia University, New York, 1991.

Vecchio, F.J. "Finite Element Modeling of Concrete Expansion and Confinement", *ASCE Journal of Structural Engineering*, v 118, n 9, p. 2390-2406, 1992.

Vecchio, F.J. and Collins, M.P. "The Modified Compression-Field Theory for Reinforced Concrete Elements Subjected to Shear." ACI Journal, March-April 1986.

Vecchio, F.J. and Collins, M.P. "Compression Response of Cracked reinforced Concrete". ASCE Journal of Structural Engineering, v 119, n 12, p 3590-3610. December 1993.

Vecchio, F.J. "Analysis of Shear-Critical Reinforced Concrete Beams", ACI Structural Journal, v 97, n1, p. 102-110, 2000.

Walraven, J. C. "Fundamental Analysis of Aggregate Interlock". *Journal of Structural Division, ASCE*, v 107, n ST11, p 2245-2270, 1981.

Walraven, J. C., and Reinhardt, H. W. "Theory and Experiments on Mechanical Behavior of Cracks in Plain and reinforced Concrete Subjected to Shear Loading". *Heron*, v 26, n 1A, 68p, 1981.

Wang, G., Meng, S-P. "Modified strut-and-tie model for prestressed concrete deep beams". *Engineering Structures*, v 30, n 12, p 3489-3496, December 2008.

Wight, J.K. and MacGregor, J.G. "Reinforced Concrete Mechanics and Design", 6th Ed. Pearson, New Jersey, 2012.

Wilby, C.B., Nazir, C.P. "Shear strength of uniformly loaded prestressed concrete beams". *Civil Engineering (London)*, v 59, n 693, p 457-463, Apr, 1964.

Wong, P. S., and Vecchio, F. J. _2002_. "VecTor2 and FormWorks user's manual." Technical Rep., Dept. of Civil Engineering, Univ. of Toronto, Toronto, Canada, _http://www.civ.utoronto.ca/vector/_.

Yang, K.-H., Ashour, A.F., Lee, J.-K. "Shear strength of reinforced concrete dapped-end beams using mechanism analysis". *Magazine of Concrete Research*, v 63, n 2, p 81-97, February 1, 2011.

Yoshitake. "Simplified Test of Cracking Strength of Concrete Element Subjected to Pure Shear". *Journal of Materials in Civil Engineering*, v 23, n 7, p 999-1006, July, 2011.

Zhang, N. and Tan, K-H. "Direct strut-and-tie model for single span and continuous deep beams". *Engineering Structures*, v 29, n 11, p 2987-3001, November 2007.

APPENDIX A: SUMMARY OF FIELD SURVEY FINDINGS

Bridge 1

This structure (#7933) carries Coolidge Road over I-696 (Southfield/Detroit area), and was built in 1985. Significant diagonal cracks near the ends of most of its girders were observed, as shown in Figures A2- A37.

Figure A1. Bridge 1 (#7933).

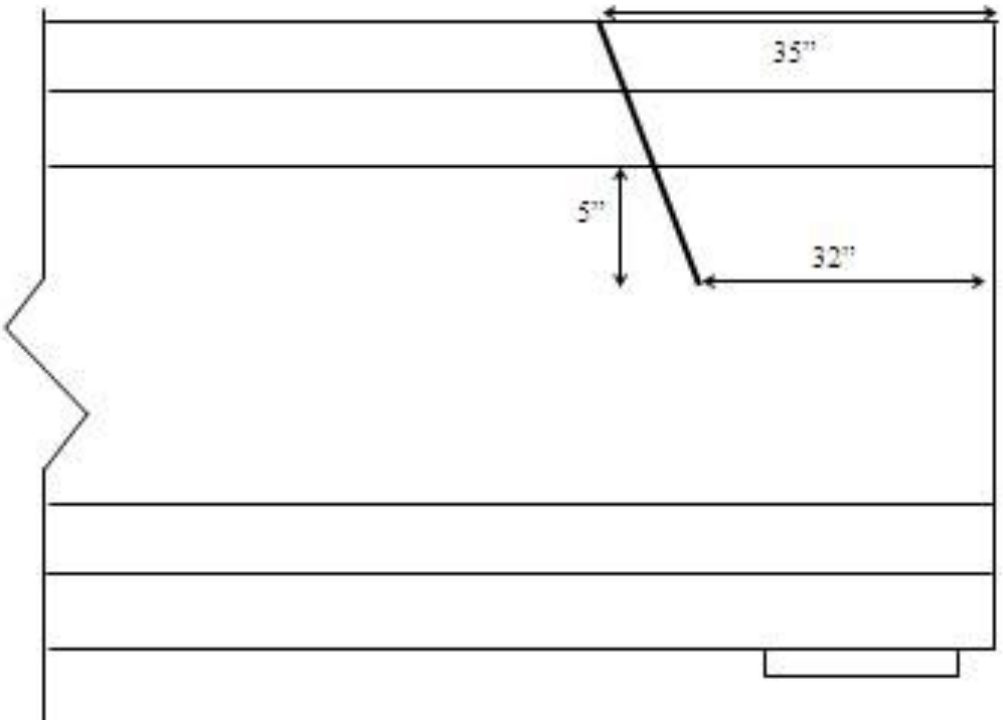

Figure A2. Crack diagram, exterior girder of north span, south end, east side, interior face (#7933).

Figure A3. Cracks, exterior girder of north span, south end, east side, interior face (#7933).

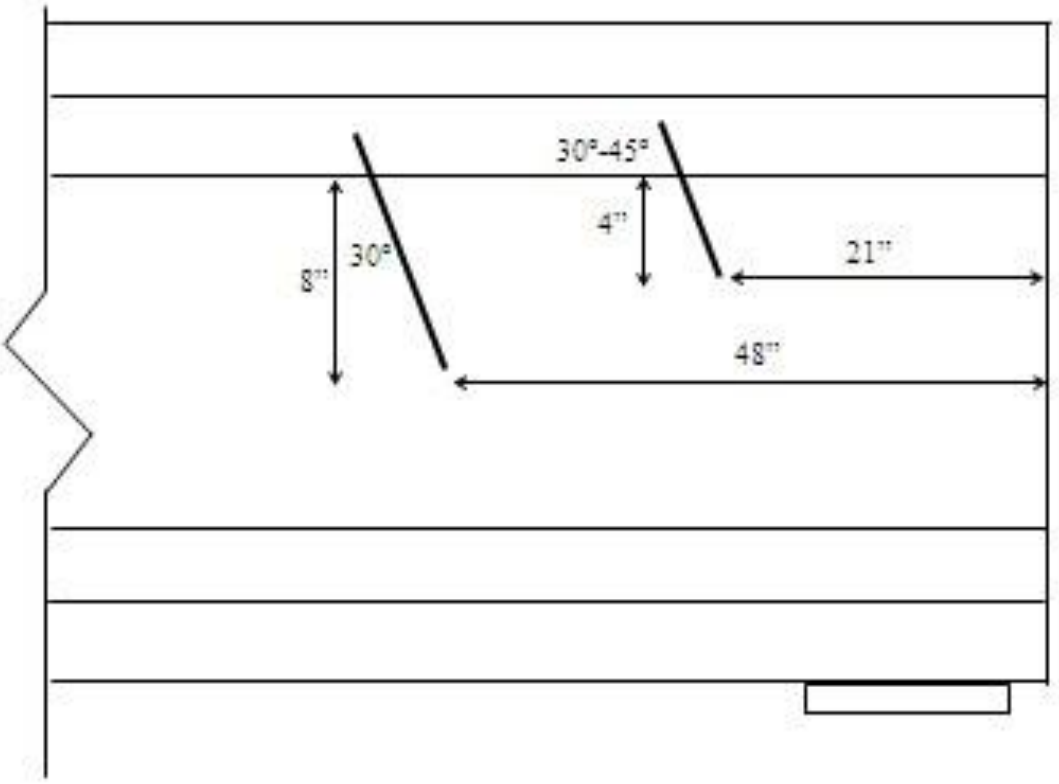

Figure A4. Crack diagram, girder at south span, north end, 4th beam from west side, west face (#7933).

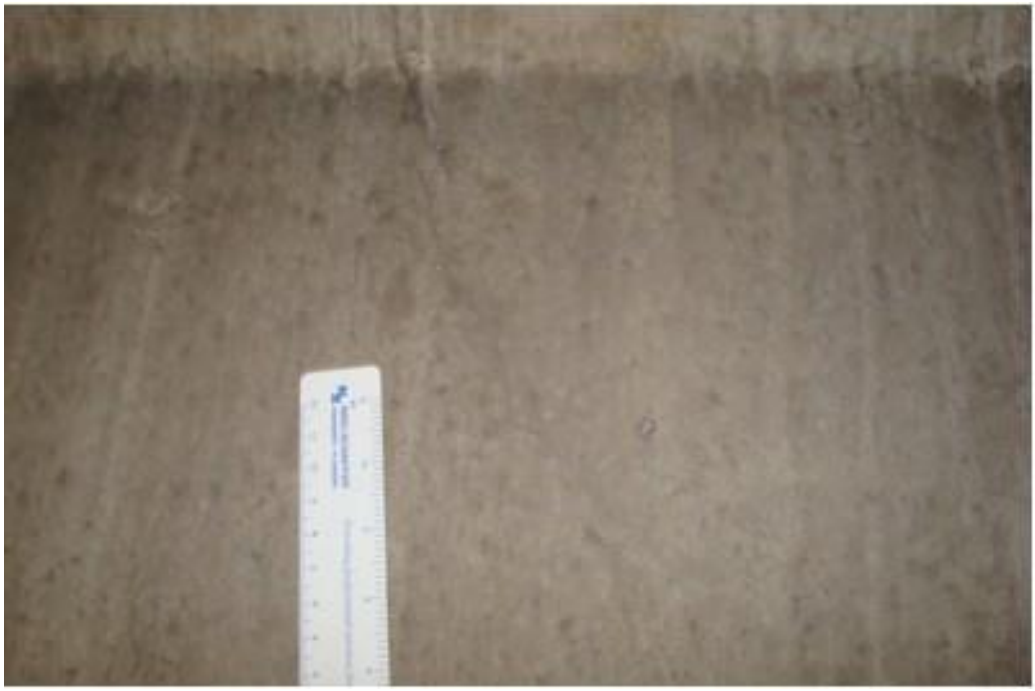

Figure A5. Cracks, girder at south span, north end, 4th beam from west side, west face (#7933).

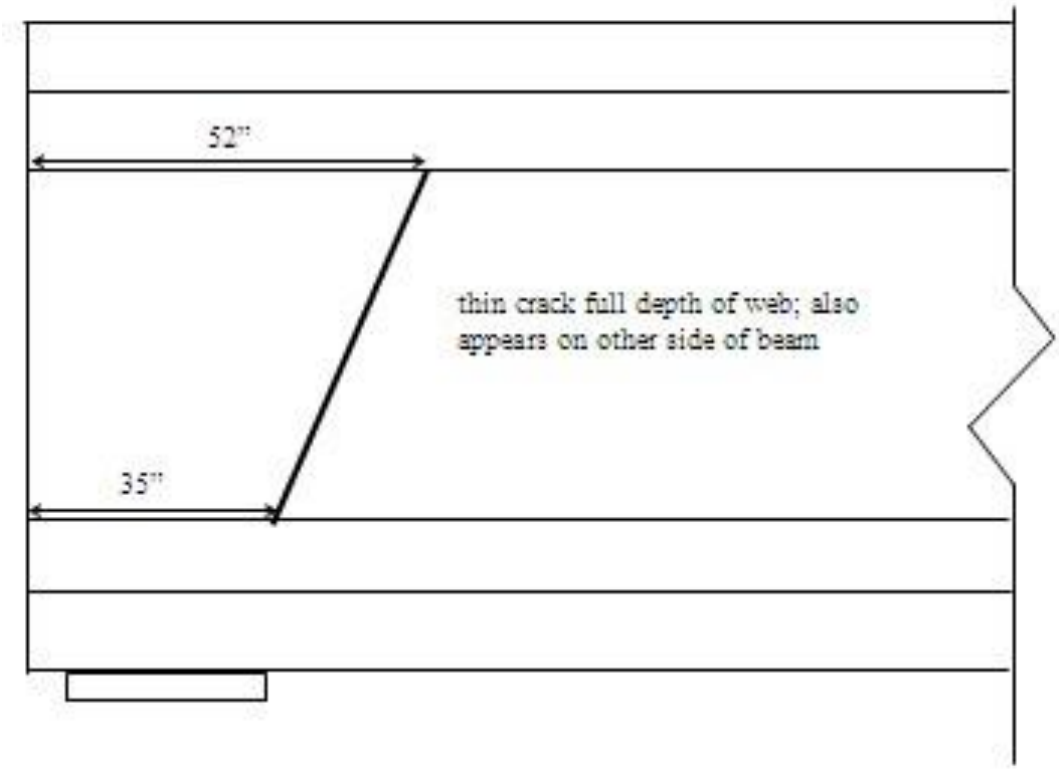

Figure A6. Crack diagram for girder on south span, north end, 6th beam from east side, west face (#7933).

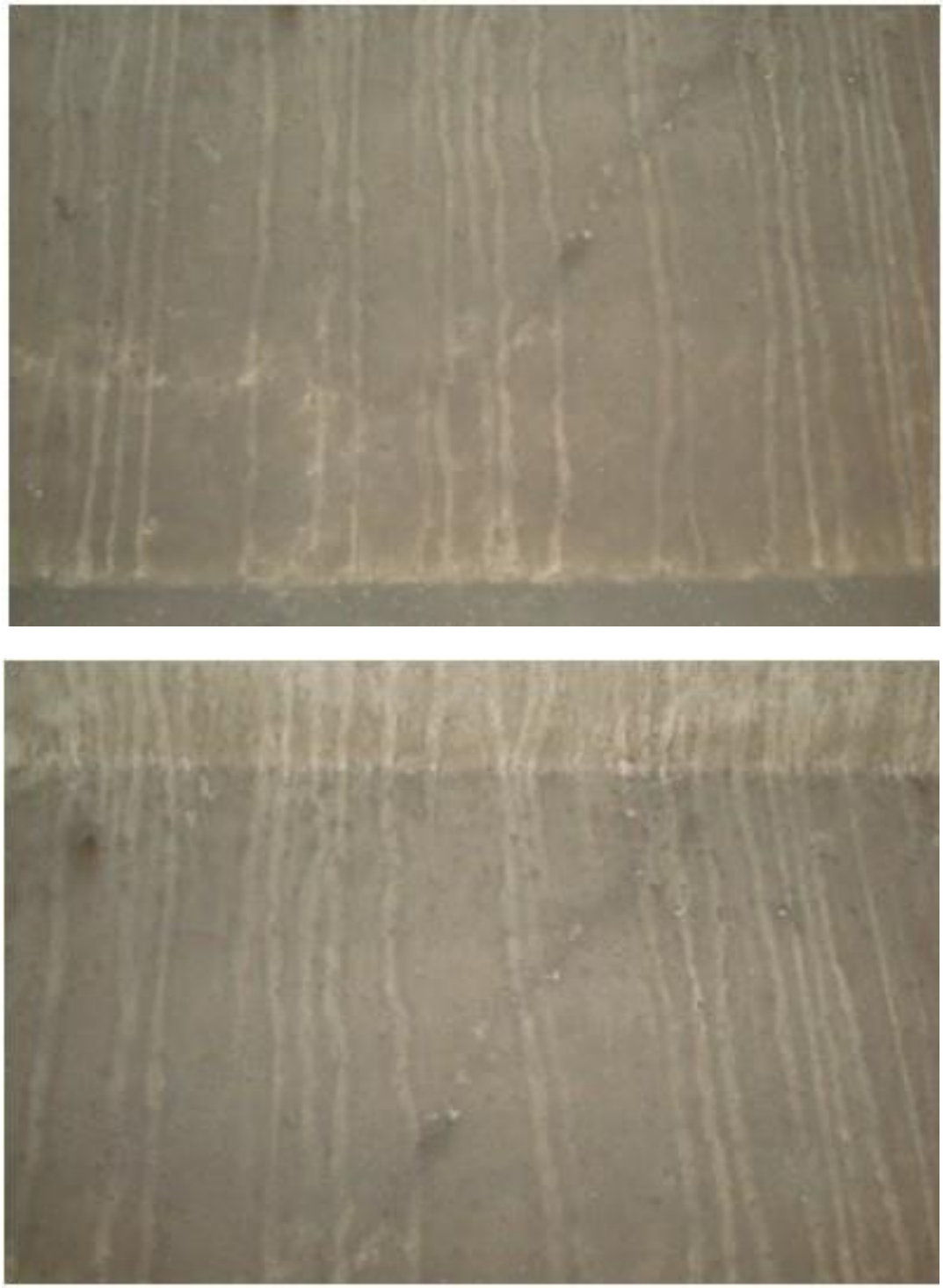

Figure A7. Cracks on south span girder, north end, 6th beam from east side, west face (#7933).

Figure A8. Cracks on south span girder, north end, 6th beam from east side, east face (#7933).

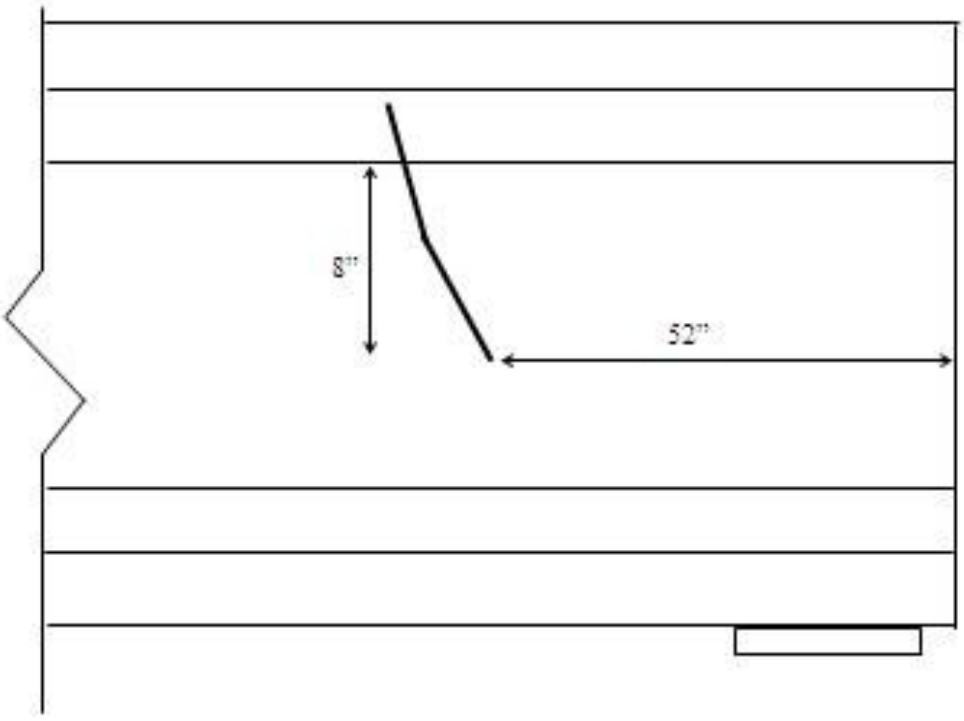

Figure A9. Crack diagram for south span girder, north end, 5th beam from east side, east face (#7933).

Figure A10. Cracks on south span girder, north end, 5th beam from east side, east face (#7933).

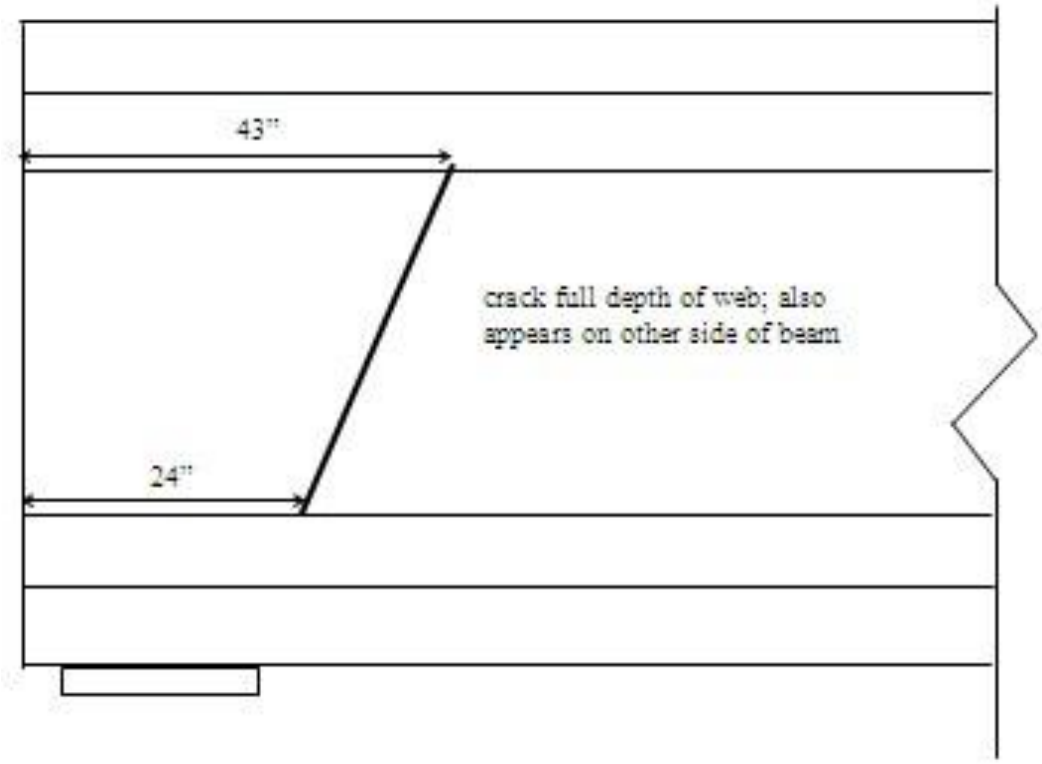

Figure A11. Crack diagram for south span girder, north end, 4th beam from east side, west face (#7933).

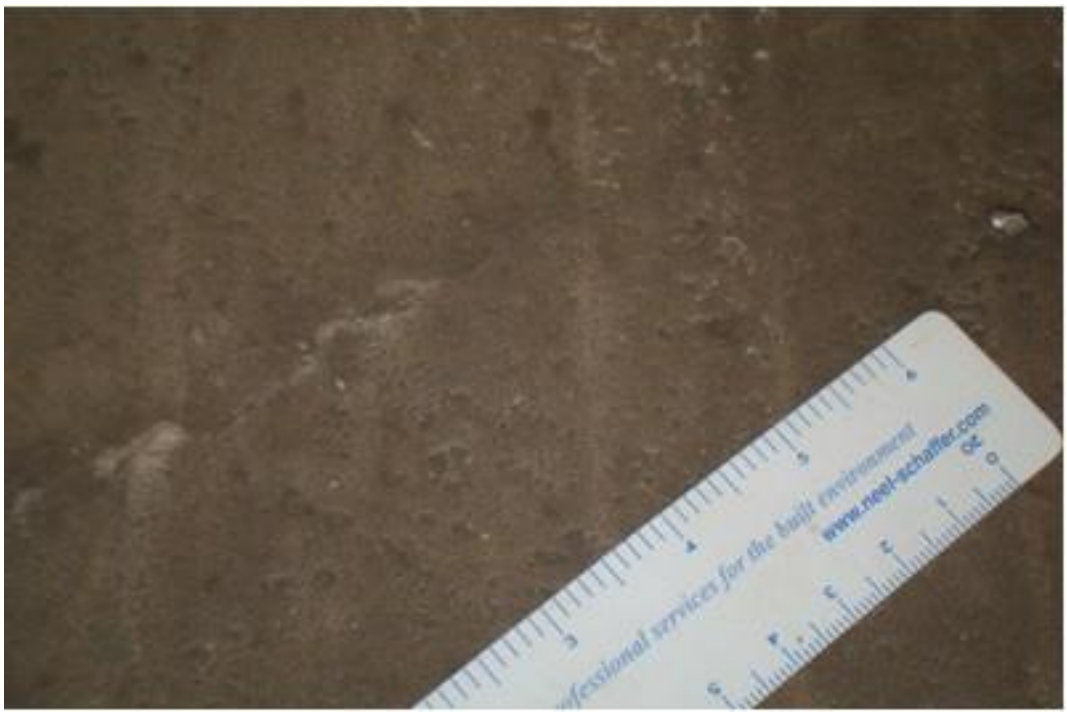

Figure A12. Cracks on south span girder, north end, 4th beam from east side, west face (#7933).

Figure A13. Cracks on south span girder, north end, 4th beam from east side, east face (#7933).

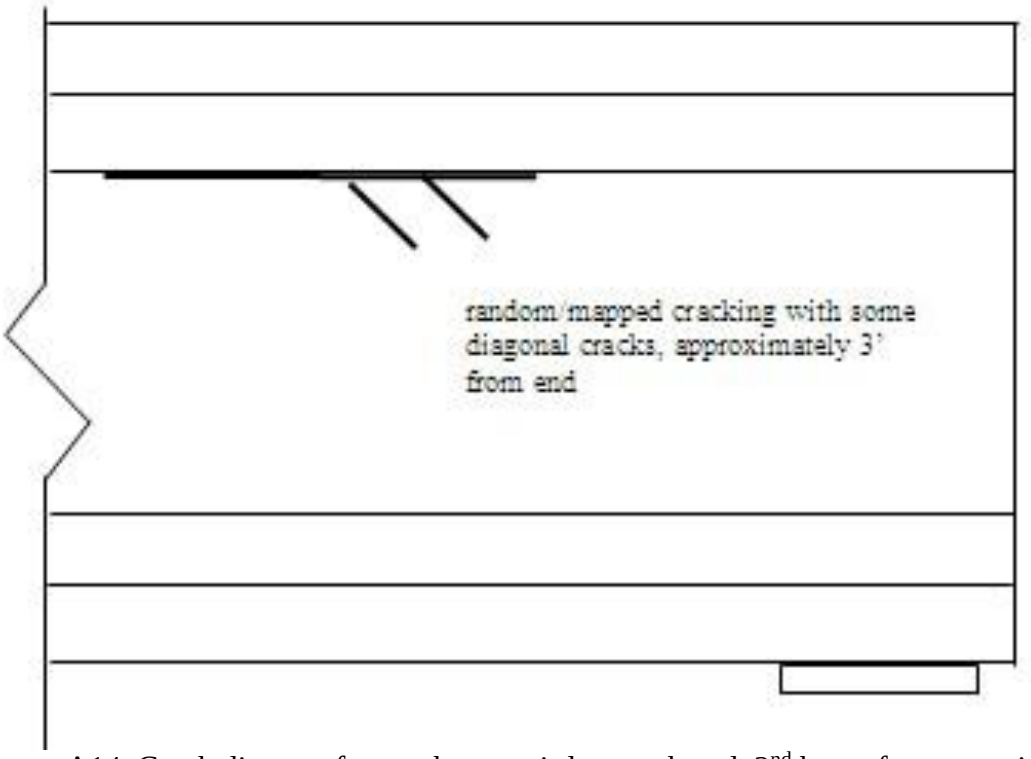

Figure A14. Crack diagram for south span girder, north end, 2nd beam from east side, east face (#7933).

Figure A15. Cracks on south span girder, north end, 2nd beam from east side, east face (#7933).

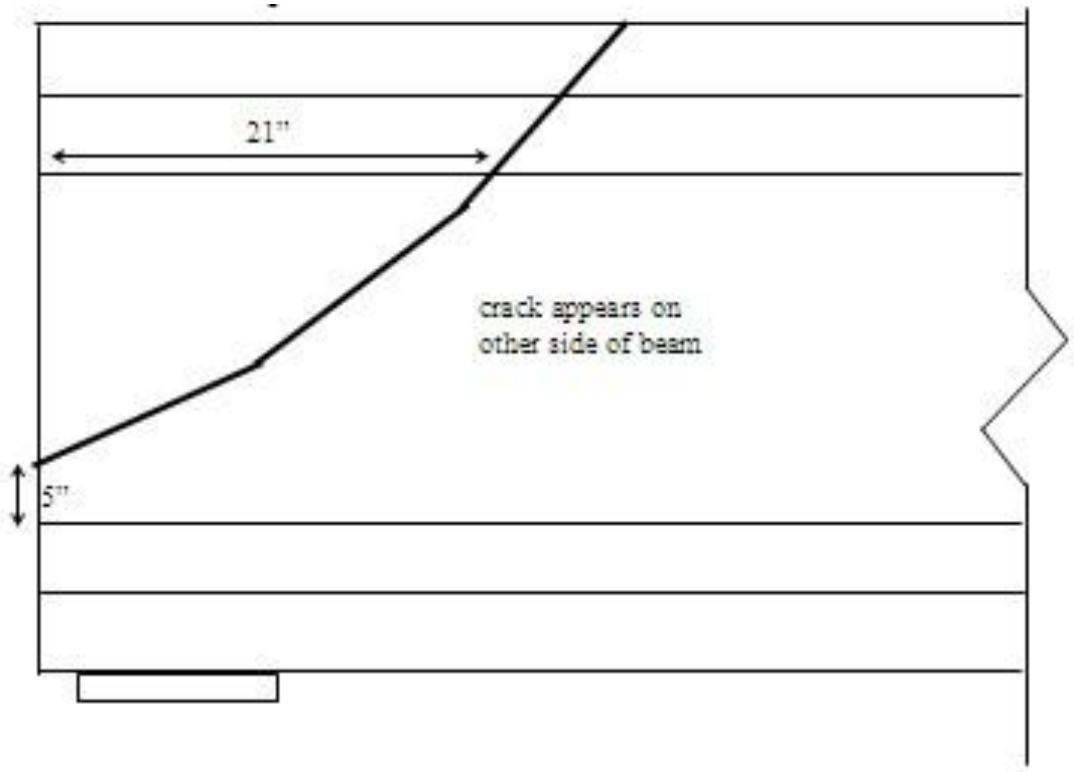

Figure A16. Crack diagram for south span girder, exterior beam, west side, interior face (#7933).

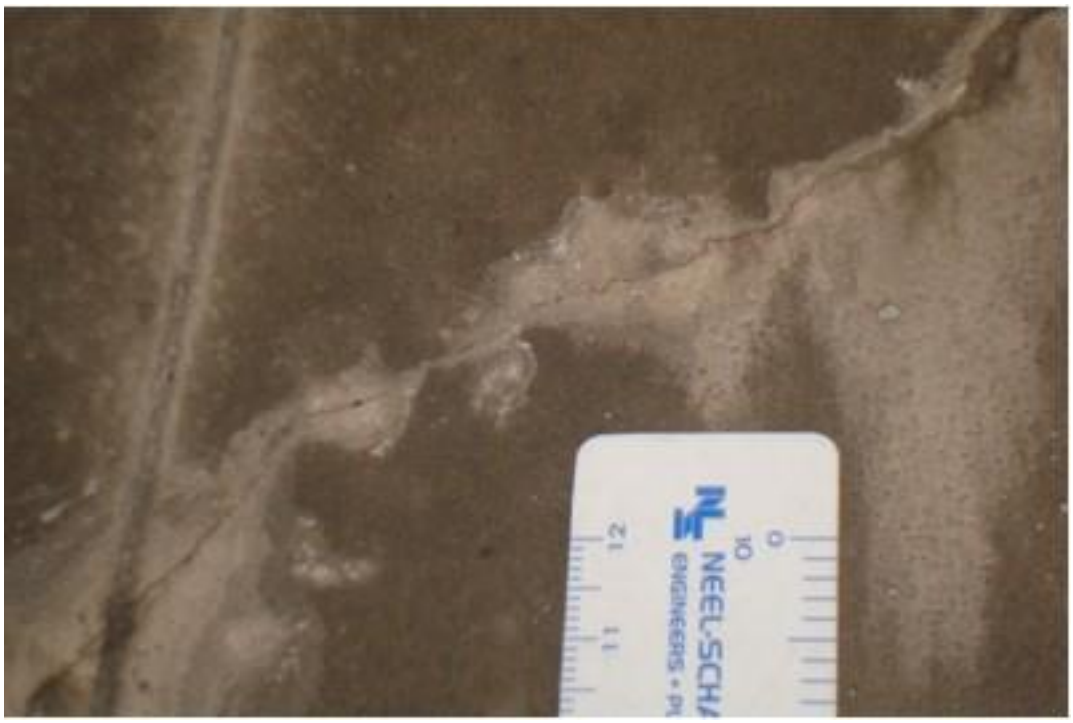

Figure A17. Cracks on south span girder, exterior beam, west side, interior face (#7933).

Figure A18. Cracks on south span girder, exterior beam, west side, exterior face (#7933).

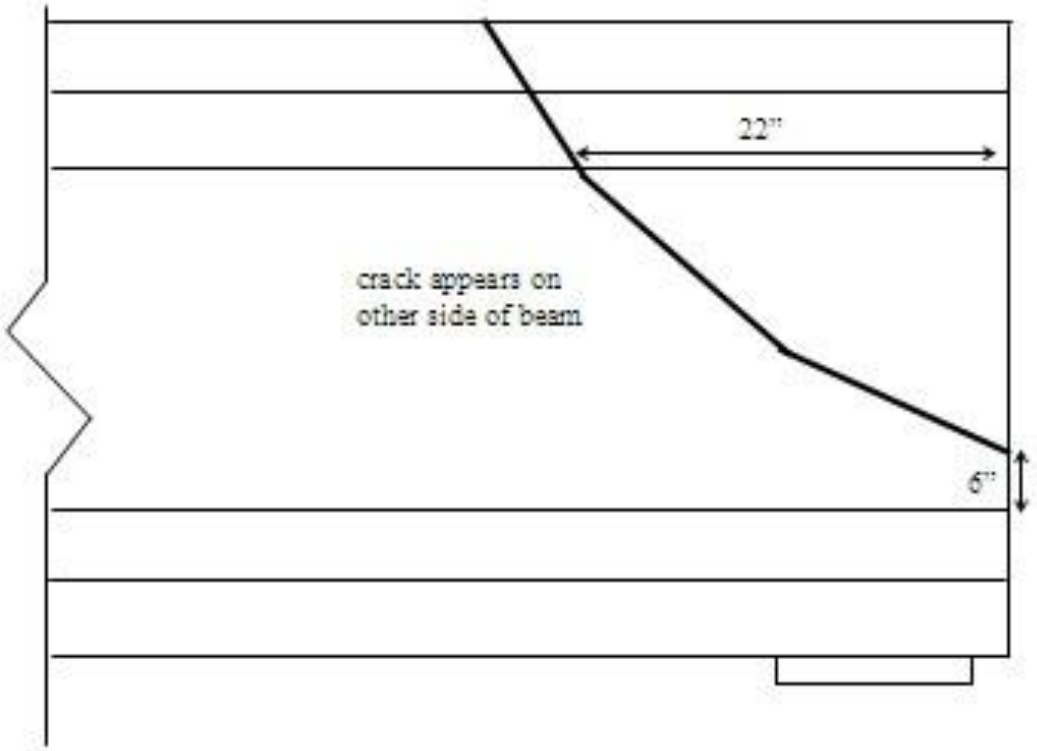

Figure A19. Crack diagram for north span girder, exterior beam, east face, north abutment (#7933).

Figure A20. Cracks on north span girder, exterior beam, east face, north abutment (#7933).

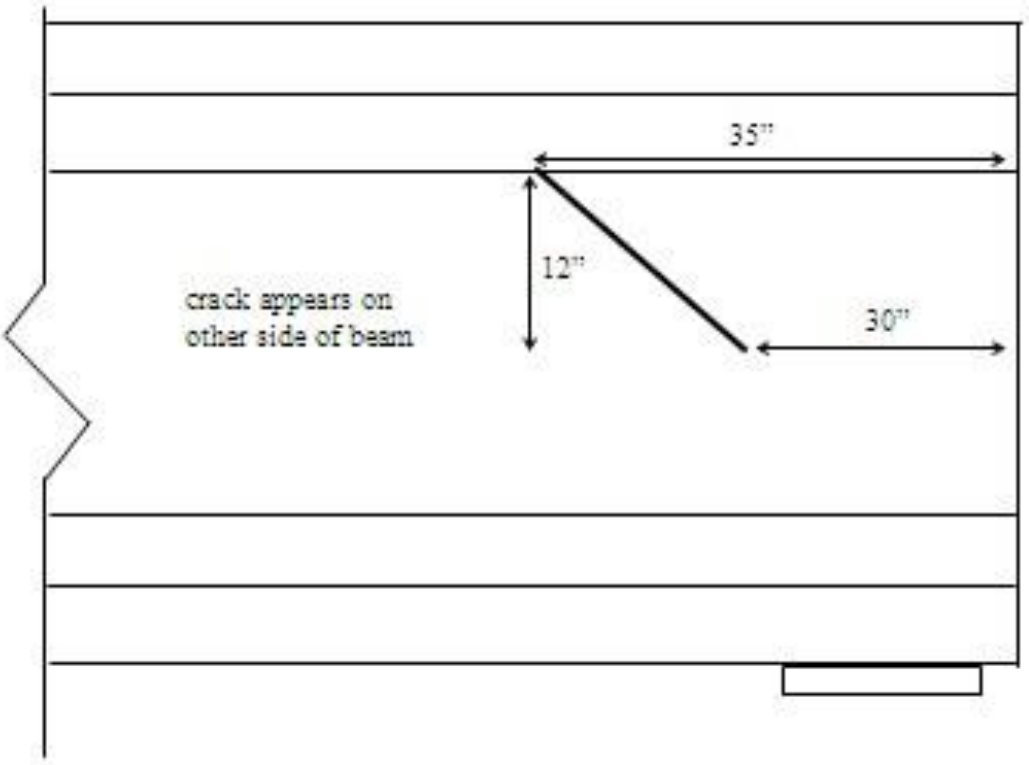

Figure A21. Crack diagram for north span girder, 2nd beam from east side, east face, north abutment (#7933).

Figure A22. Cracks on north span girder, 2nd beam from east side, east face, north abutment (#7933).

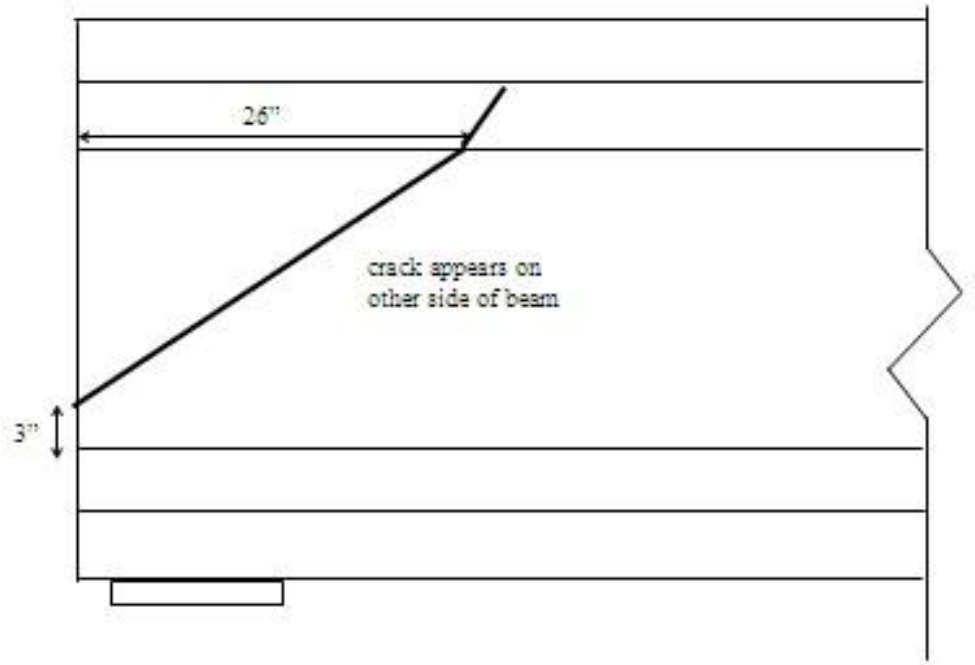

Figure A23. Crack diagram for north span, exterior girder on west side, west face, north abutment (#7933).

Figure A24. Cracks on north span, exterior girder on west side, west face, north abutment (#7933).

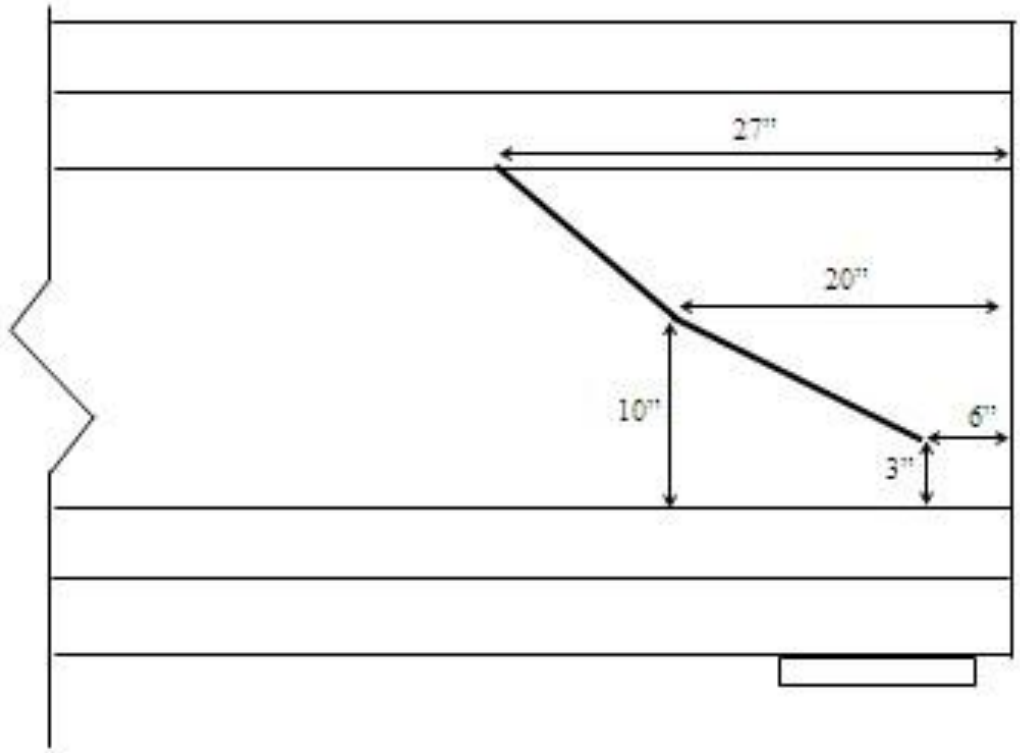

Figure A25. Crack diagram for south span girder, 3rd beam from west side, west face, south abutment (#7933).

Figure A26. Cracks on south span girder, 3rd beam from west side, west face, south abutment (#7933).

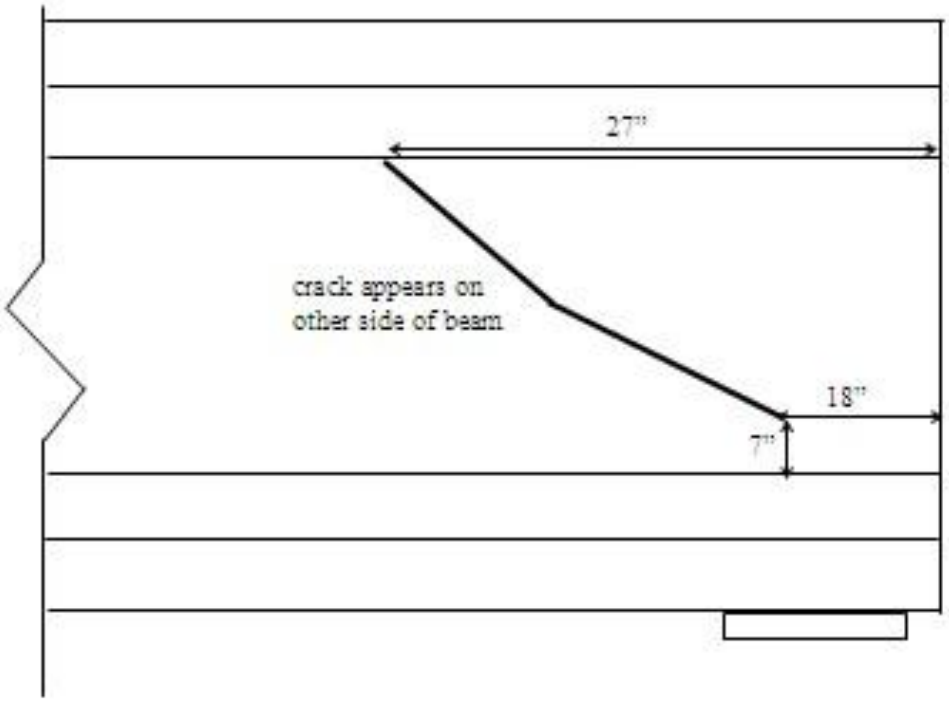

Figure A27. Crack diagram for south span girder, 6th beam from west side, west face, south abutment (#7933).

Figure A28. Cracks on south span girder, 6th beam from west side, west face, south abutment (#7933).

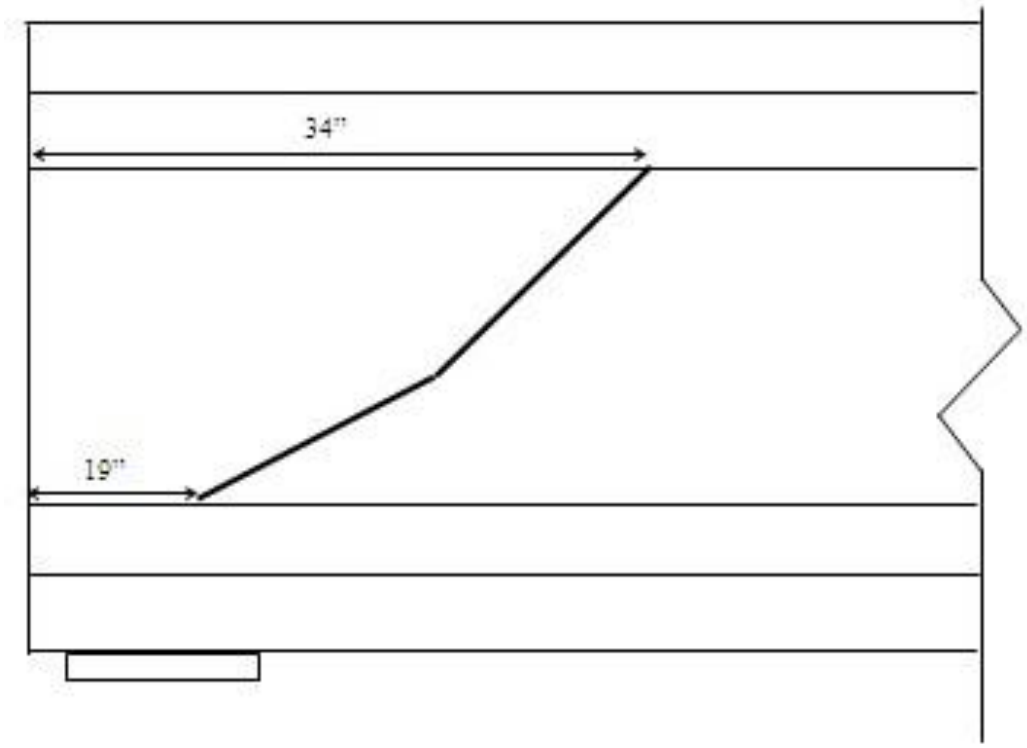

Figure A29. Crack diagram for south span girder, 7th beam from west side, east face, south abutment (#7933).

Figure A30. Cracks on south span girder, 7th beam from west side, east face, south abutment (#7933).

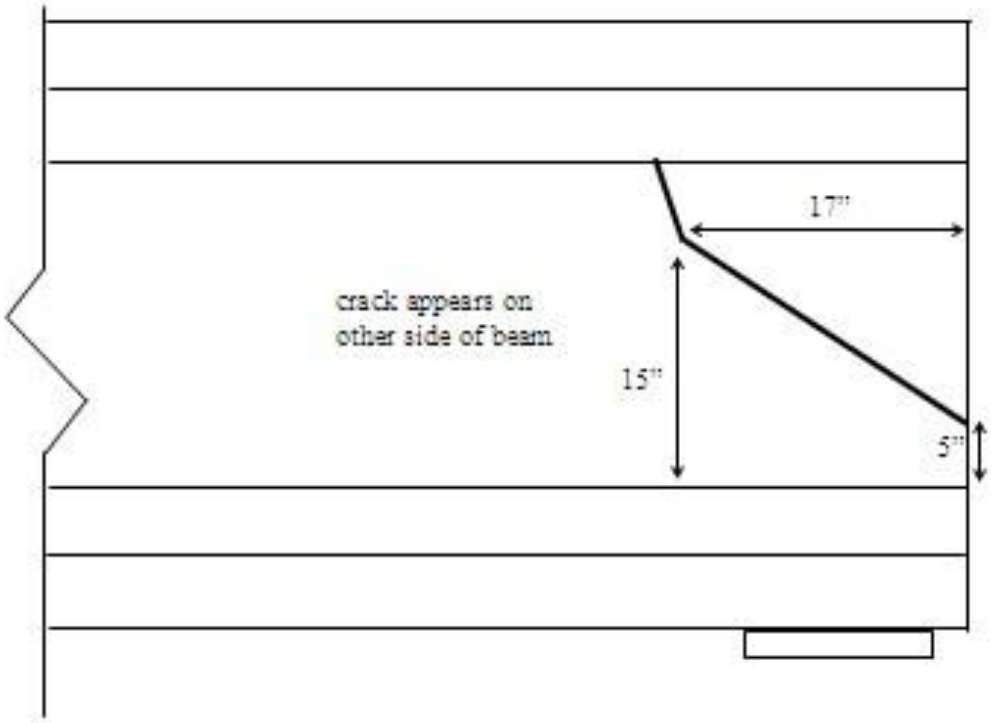

Figure A31. Crack diagram for south span girder, 4th beam from east side, west face, south abutment (#7933).

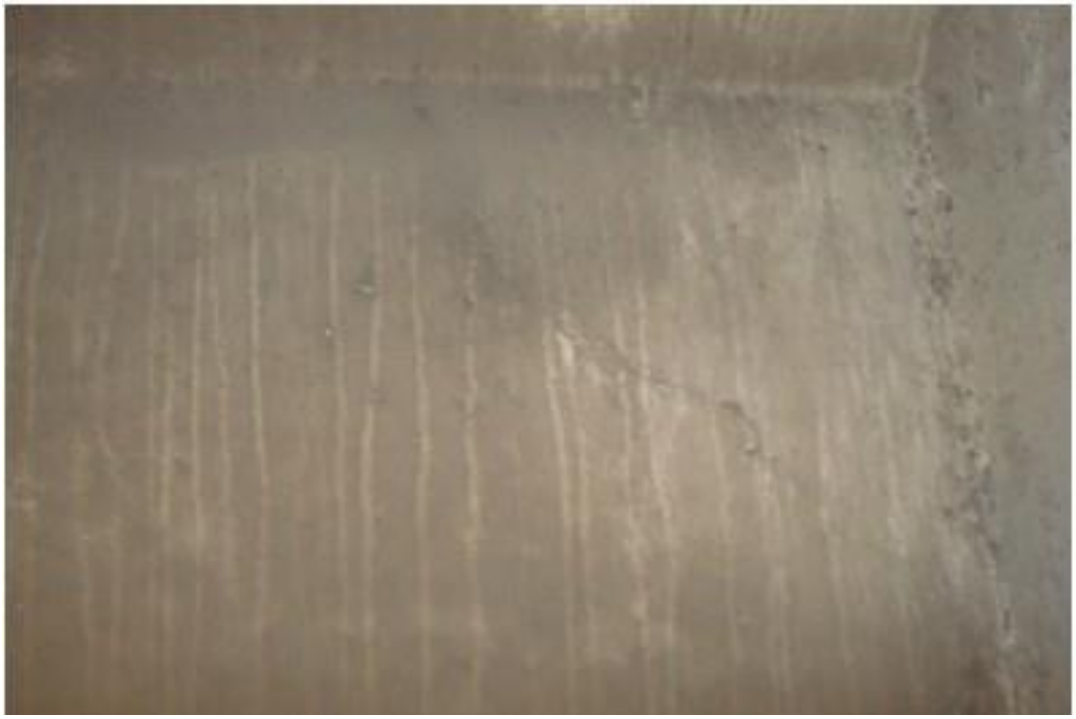

Figure A32. Cracks on south span girder, 4th beam from east side, west face, south abutment (#7933).

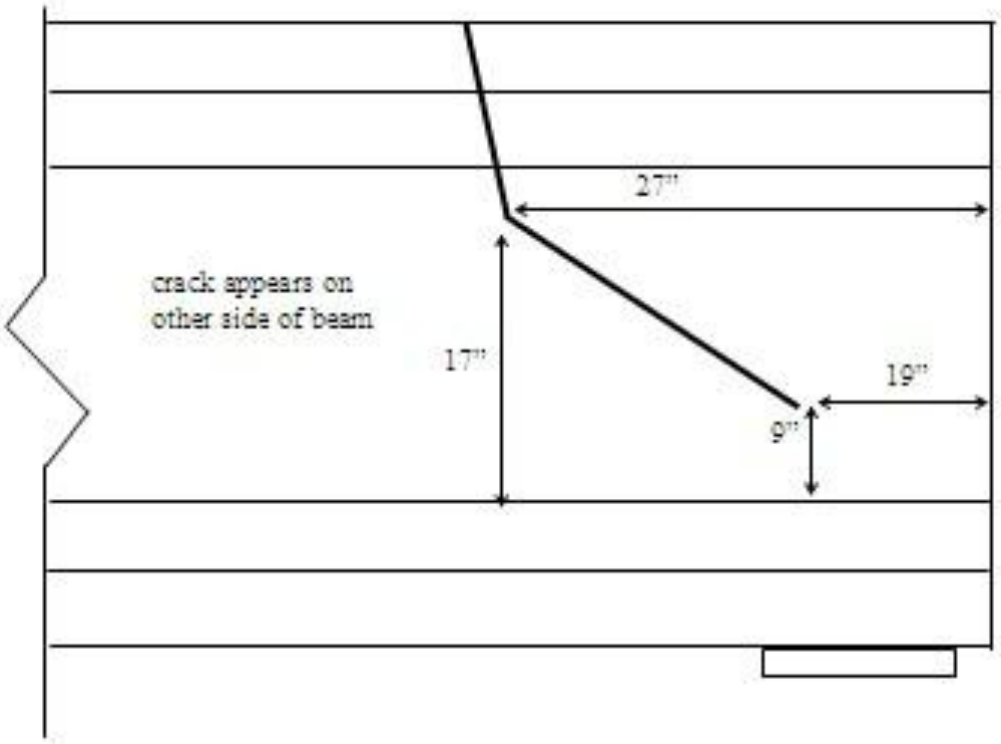

Figure A33. Crack diagram for south span girder, 3rd from east side, west face, south abutment (#7933).

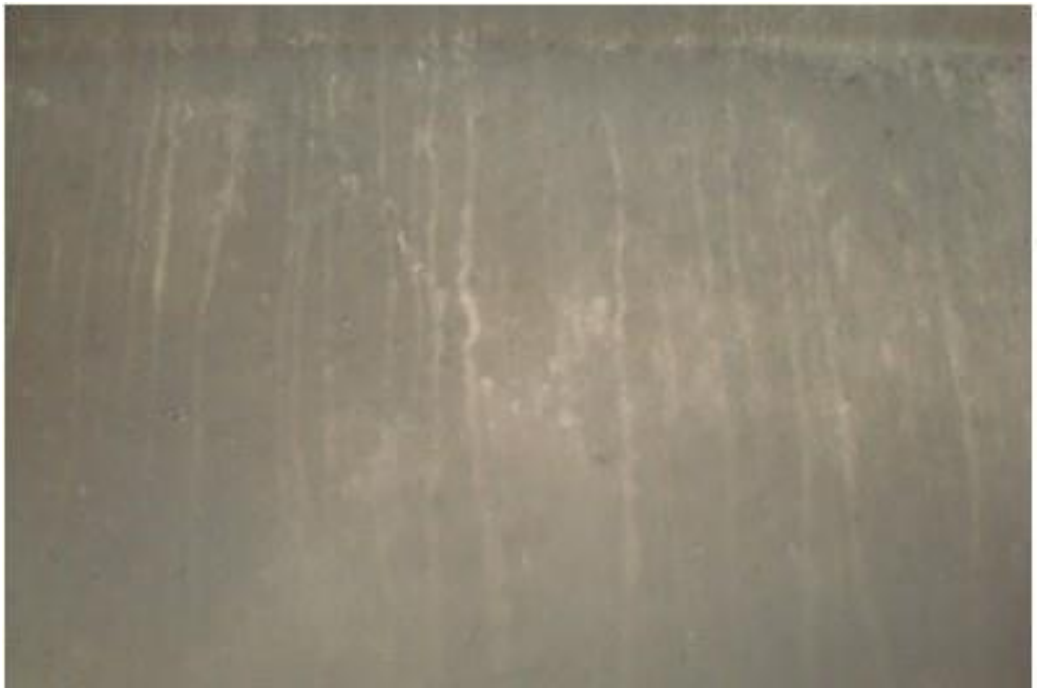

Figure A34. Cracks on south span girder, 3rd from east side, west face, south abutment (#7933).

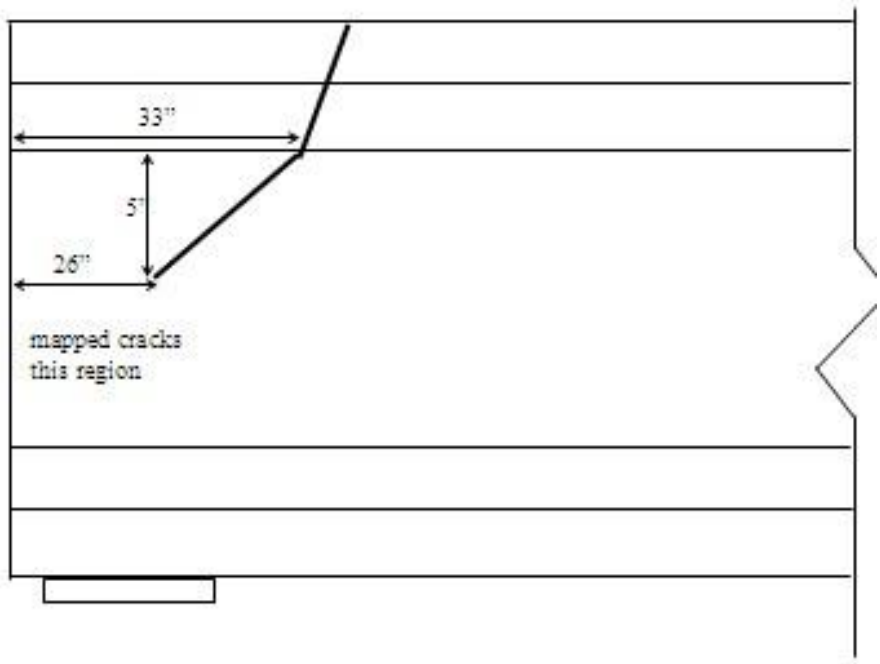

Figure A35. Crack diagram for south span girder, 2nd beam from east side, east face, south abutment (#7933).

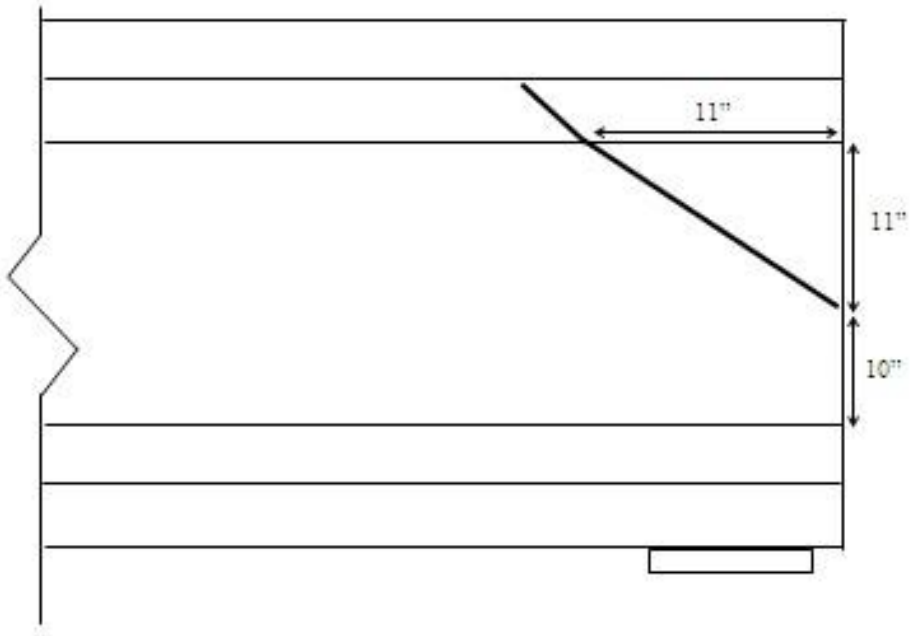

Figure A36. Crack diagram for south span, exterior girder, east side, interior face, south abutment (#7933).

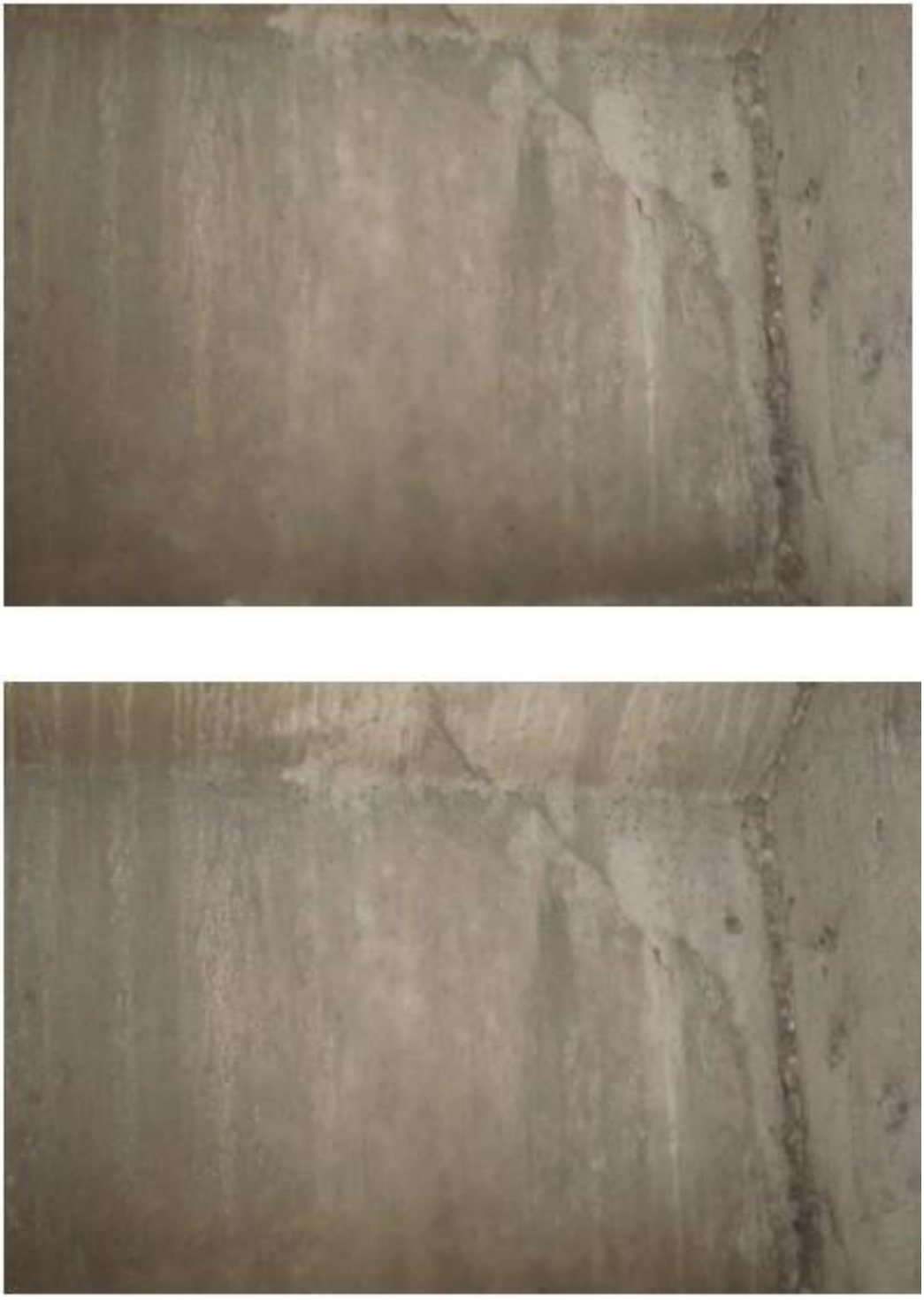

Figure A37. Cracks on south span, exterior girder, east side, interior face, south abutment (#7933).

Bridge 5

This structure (#1829) carries US-127 South over M-21 (north of Lansing, just east of St. Johns), and was built in 1993. Some minor diagonal cracks were found near the ends of some girders, as shown in Figures A39-A49.

Figure A38. Bridge #5 (#1829).

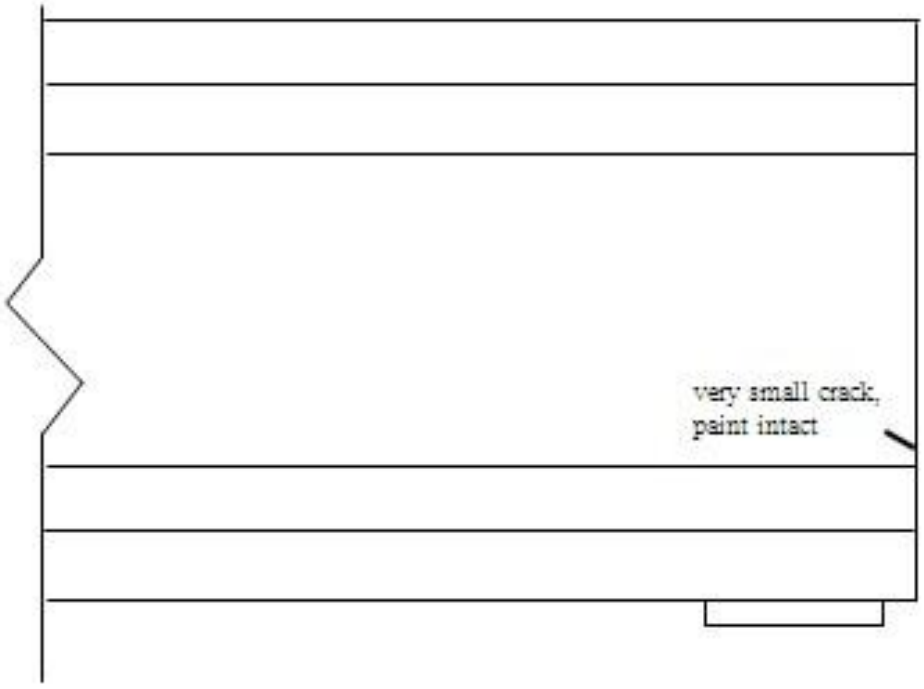

Figure A39. Crack diagram, exterior girder on east side, east face, north abutment (#1829).

Figure A40. Cracks on exterior girder on east side, east face, north abutment (#1829).

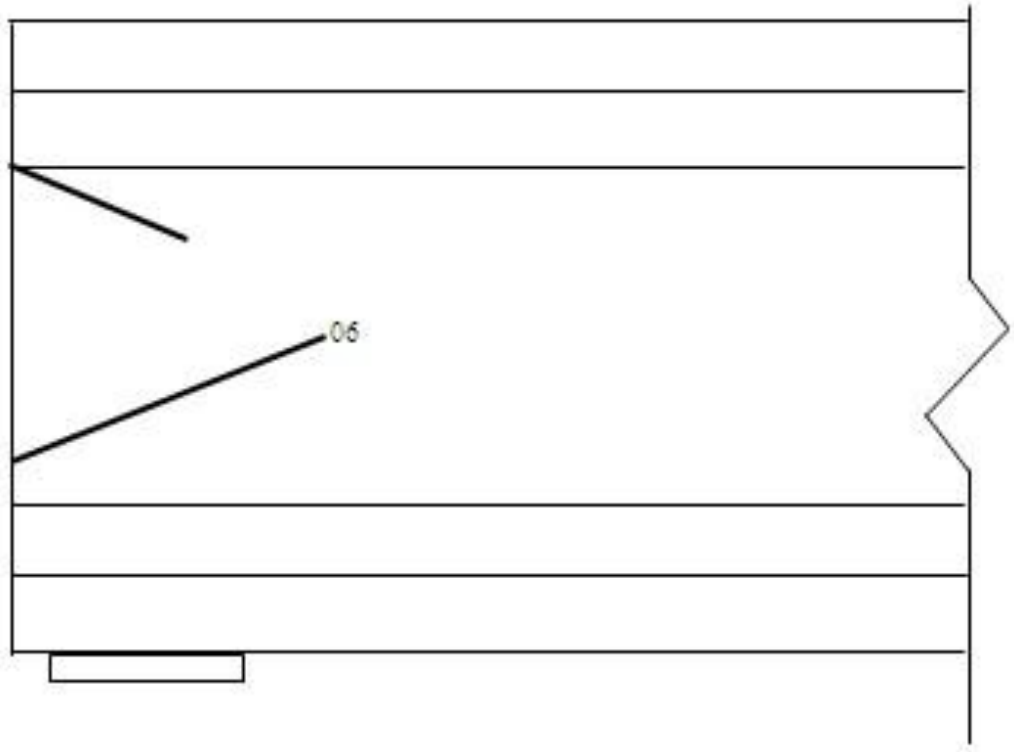

Figure A41. Crack diagram for exterior girder on east side, west face, north abutment (#1829).

Figure A42. Cracks on exterior girder on east side, west face, north abutment (#1829).

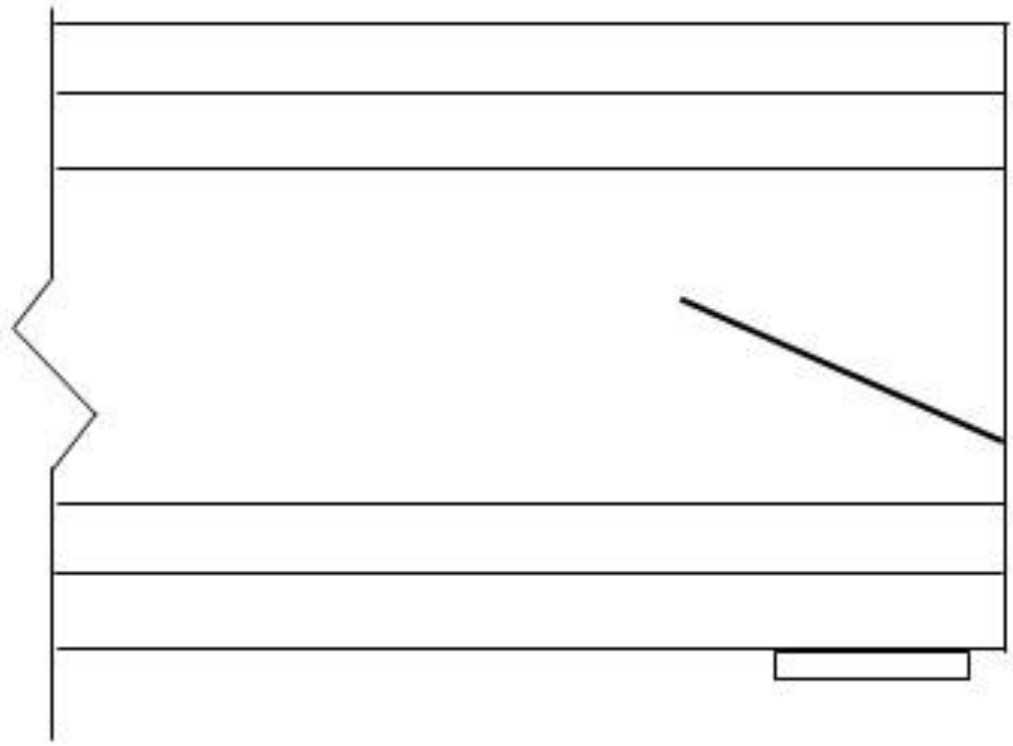

Figure A43. Crack diagram for girder 2nd from east side, east face, north abutment (#1829).

Figure A44. Cracks on girder 2nd from east side, east face, north abutment (#1829).

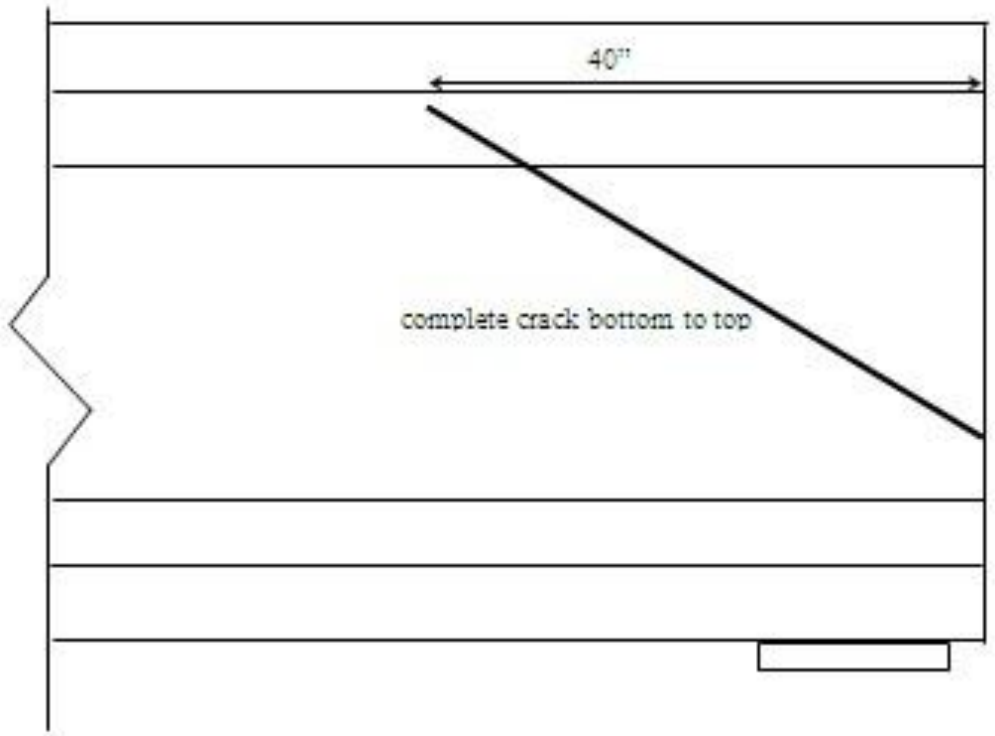

Figure A45. Crack diagram for girder 4th from east side, east face, north abutment (#1829).

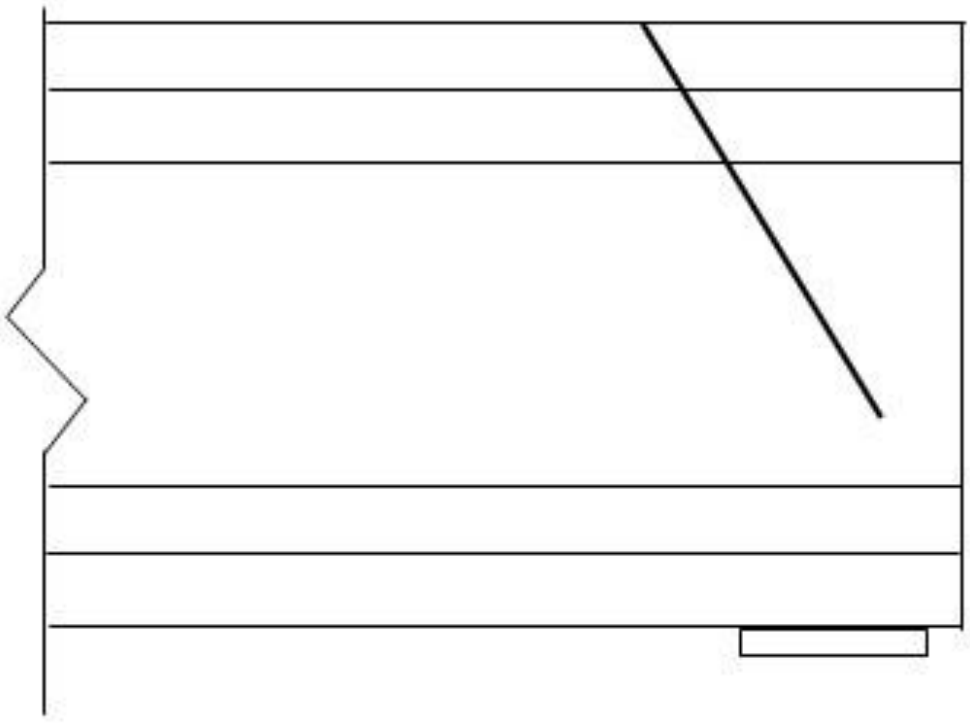

Figure A46. Crack diagram for exterior girder, west side, west face, south abutment (#1829).

Figure A47. Cracks on exterior girder, west side, west face, south abutment (#1829).

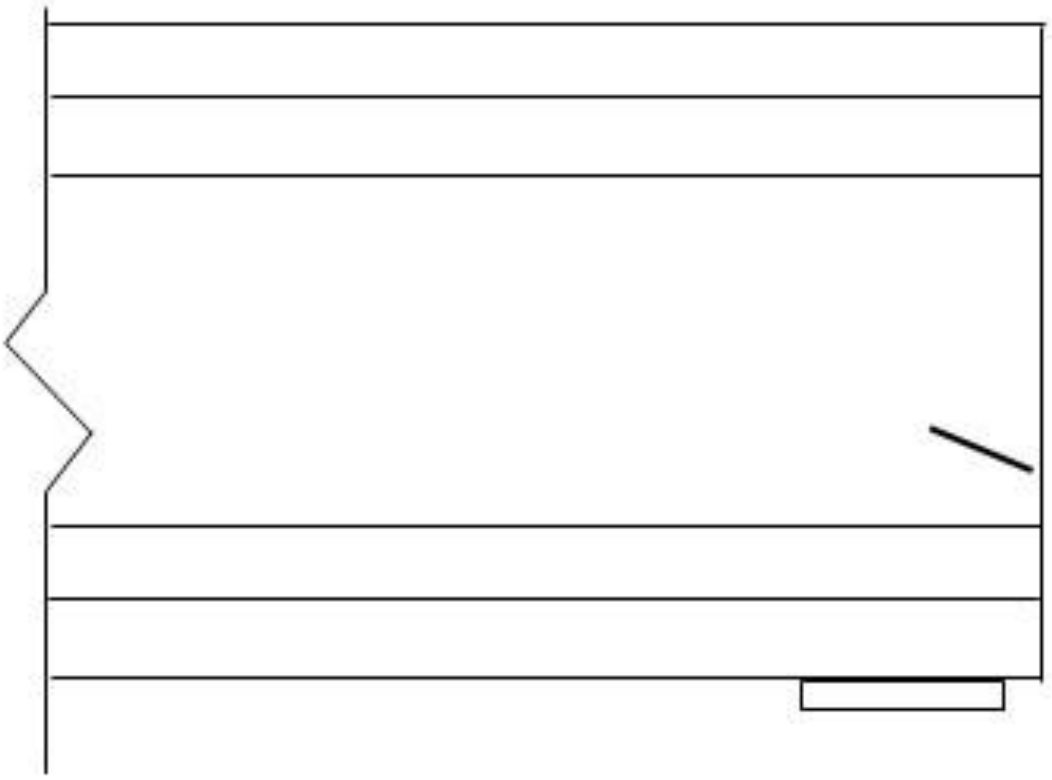

Figure A48. Crack diagram for girder 2nd from west side, west face, south abutment (#1829).

Figure A49. Cracks on girder 2nd from west side, west face, south abutment (#1829).

Bridge 6

This structure (#1830) is adjacent to Bridge #5 (see Figure 3.38), and carries US-127 North over M-21 (north of Lansing, just east of St. Johns), and was built in 1993. Some potentially significant diagonal cracks were found near the ends of some girders, as shown in Figures A50-A59.

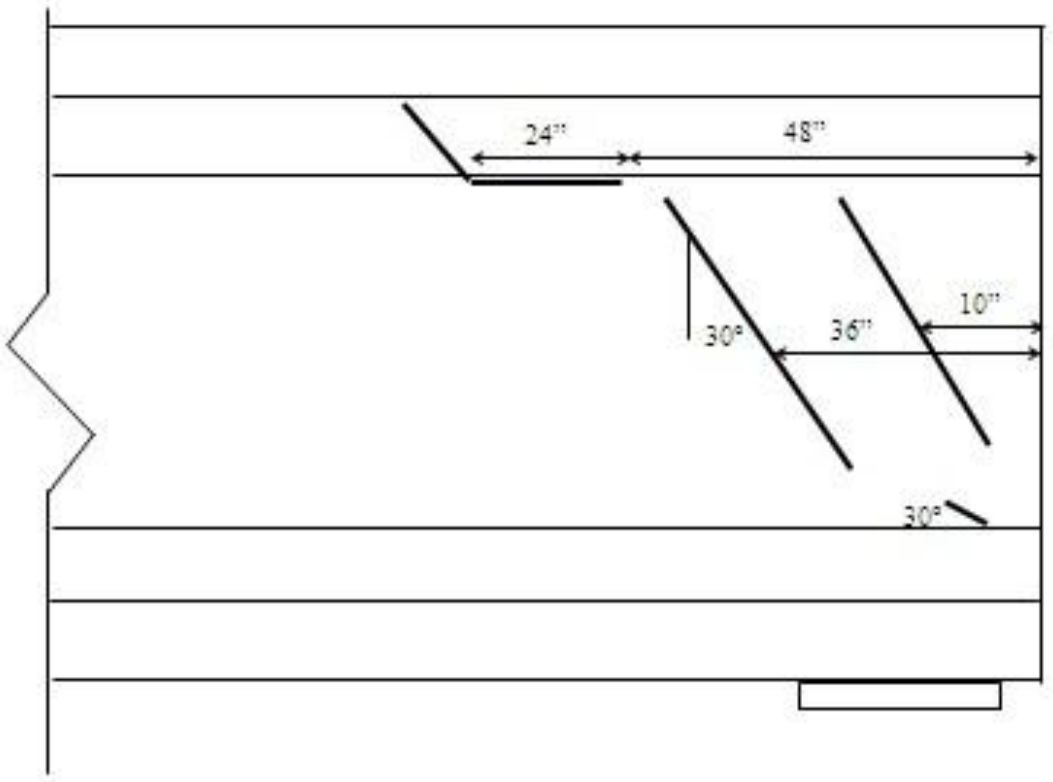

Figure A50. Crack diagram for east-most exterior girder, east face, north abutment (#1830).

Figure A51. Cracks on east-most exterior girder, east face, north abutment (#1830).

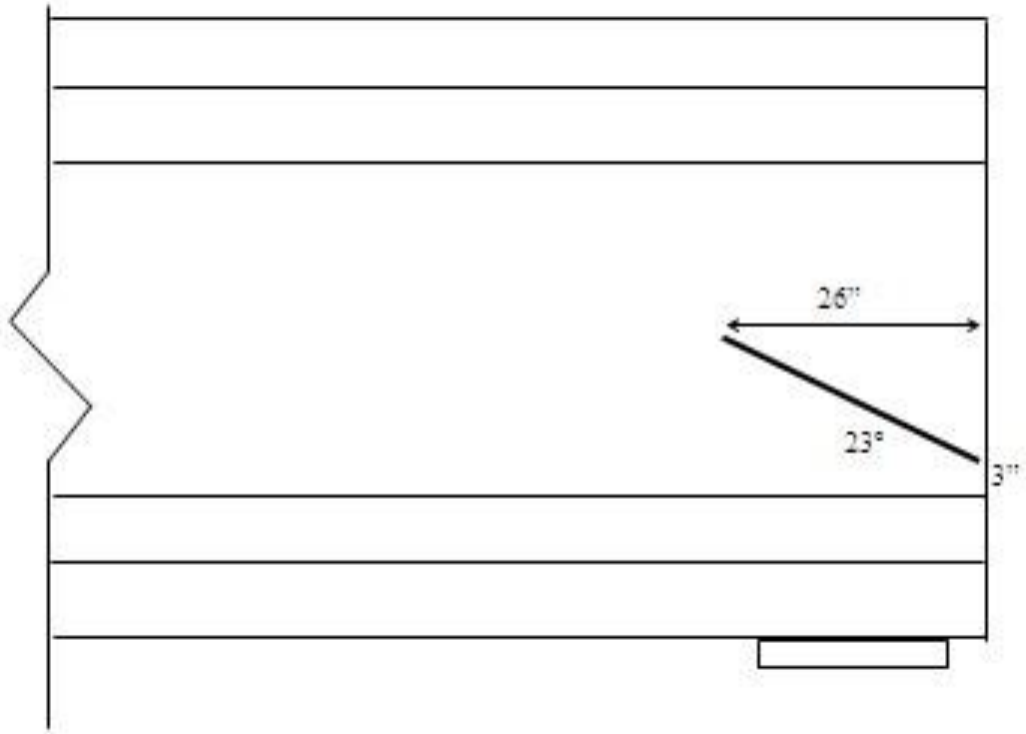

Figure A52. Crack diagram for girder 4th from east side, east face, north abutment (#1830).

Figure A53. Cracks on girder 4th from east side, east face, north abutment (#1830).

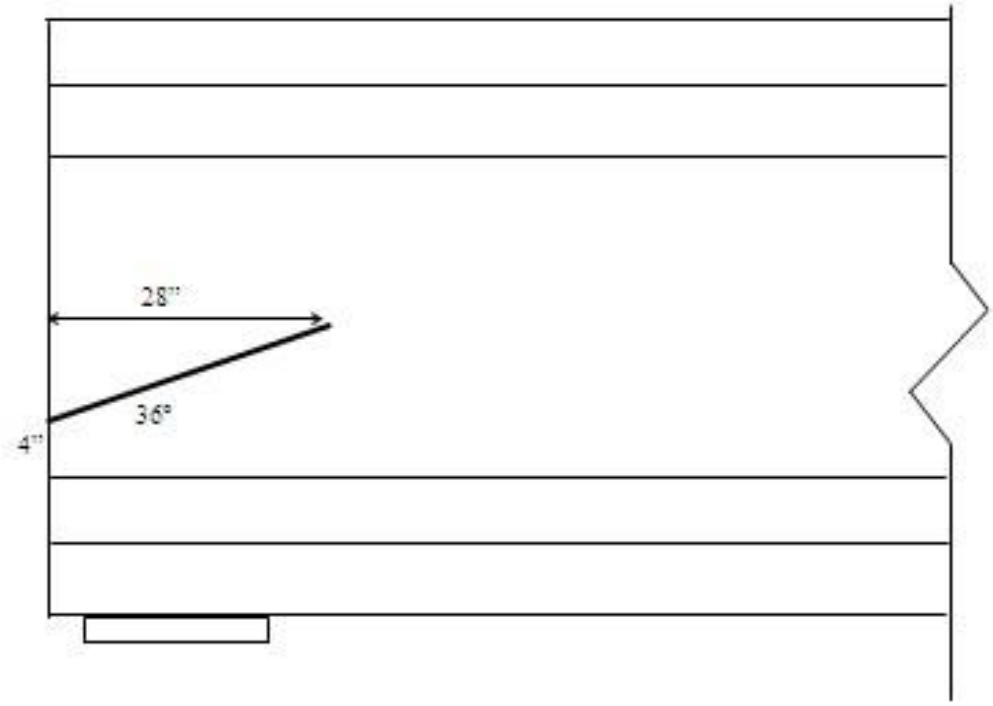

Figure A54. Crack diagram for girder 3rd from east side, west face, north abutment (#1830).

Figure A55. Cracks on girder 3rd from east side, west face, north abutment (#1830).

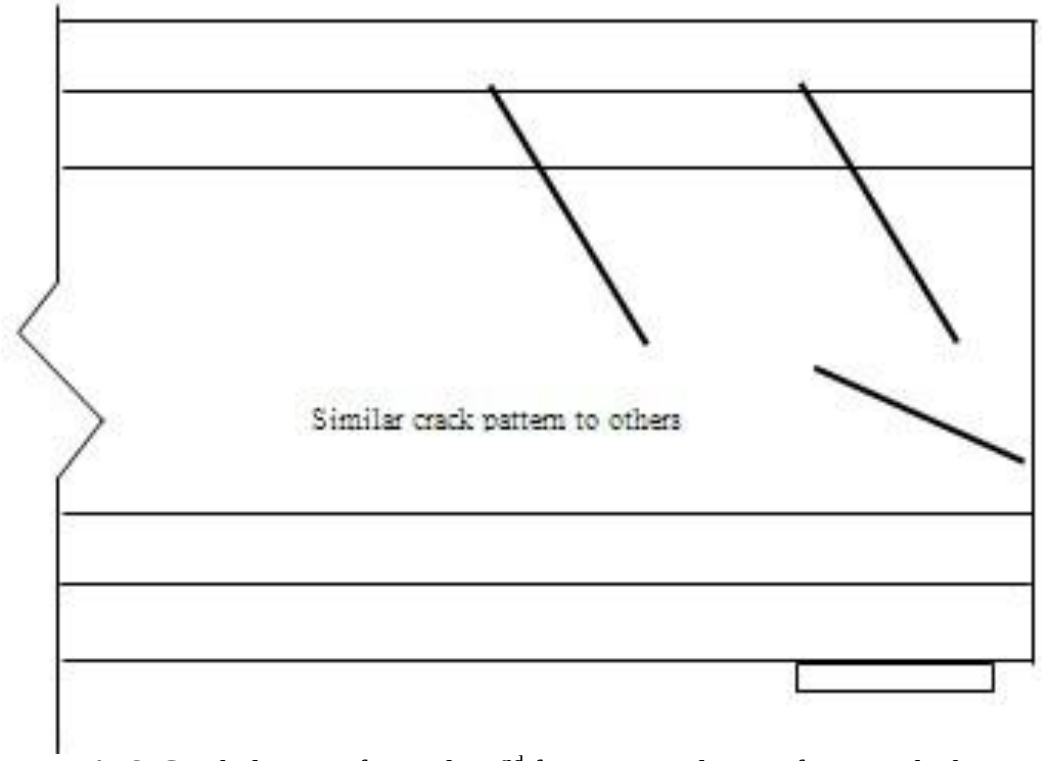

Figure A56. Crack diagram for girder 2nd from west side, east face, north abutment (#1830).

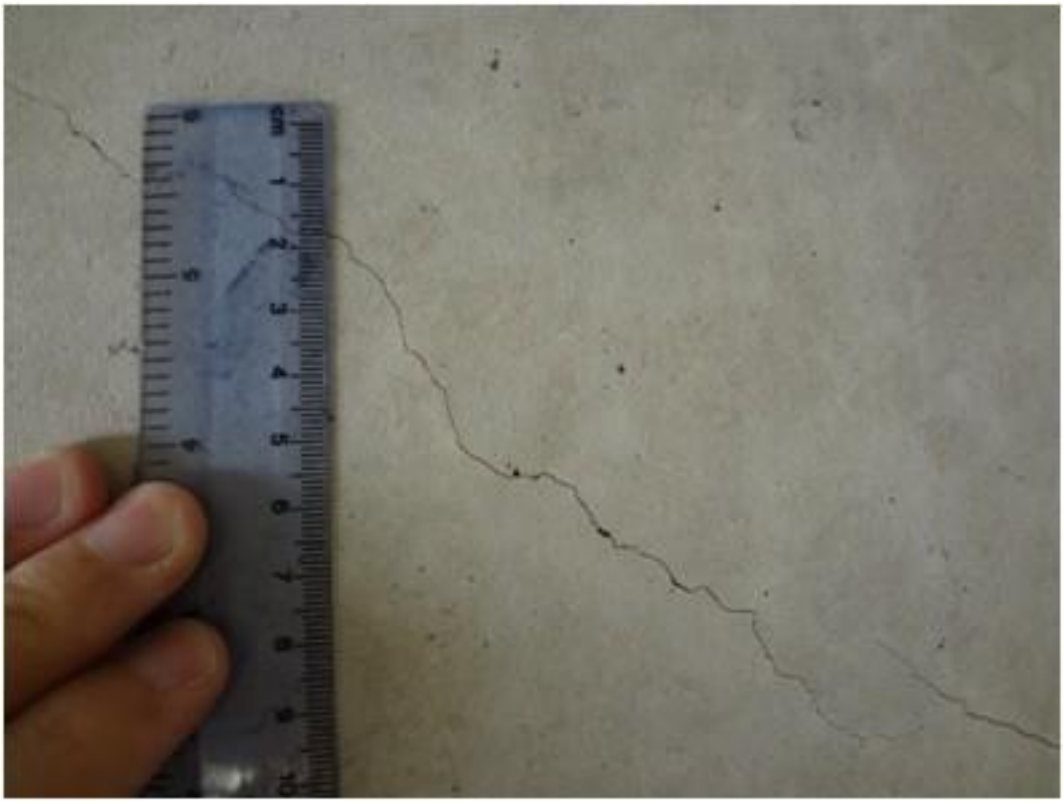

Figure A57. Cracks on girder 2nd from west side, east face, north abutment (#1830).

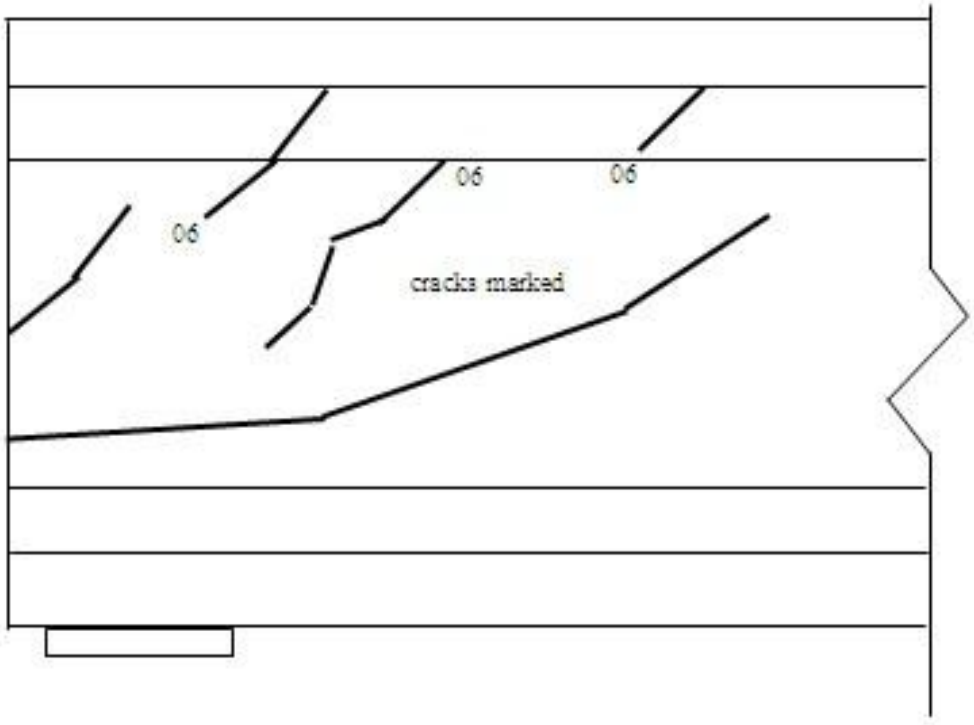

Figure A58. Crack diagram for exterior girder on west side, west face, north abutment (#1830).

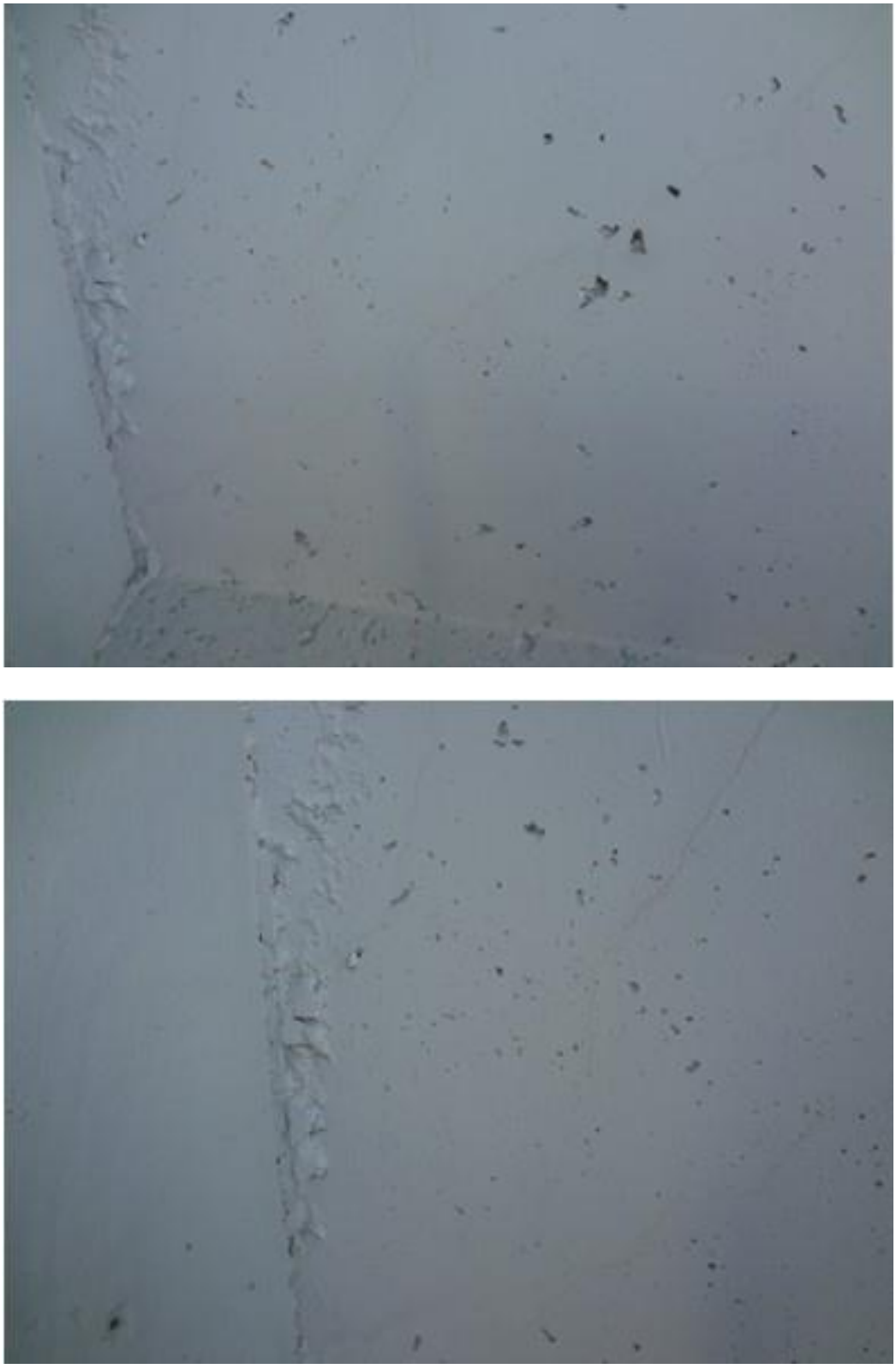

Figure A59. Cracks on exterior girder on west side, west face, north abutment (#1830).

Bridge 7

This structure (#2332) carries Eaton Highway over I-69 North / I -96 West (northwest of Lansing, just west of the Capital Region International Airport). It was originally built in 1961 and renovated in 1981. Some minor diagonal cracks were found near the ends of some girders, as shown in Figure A60.

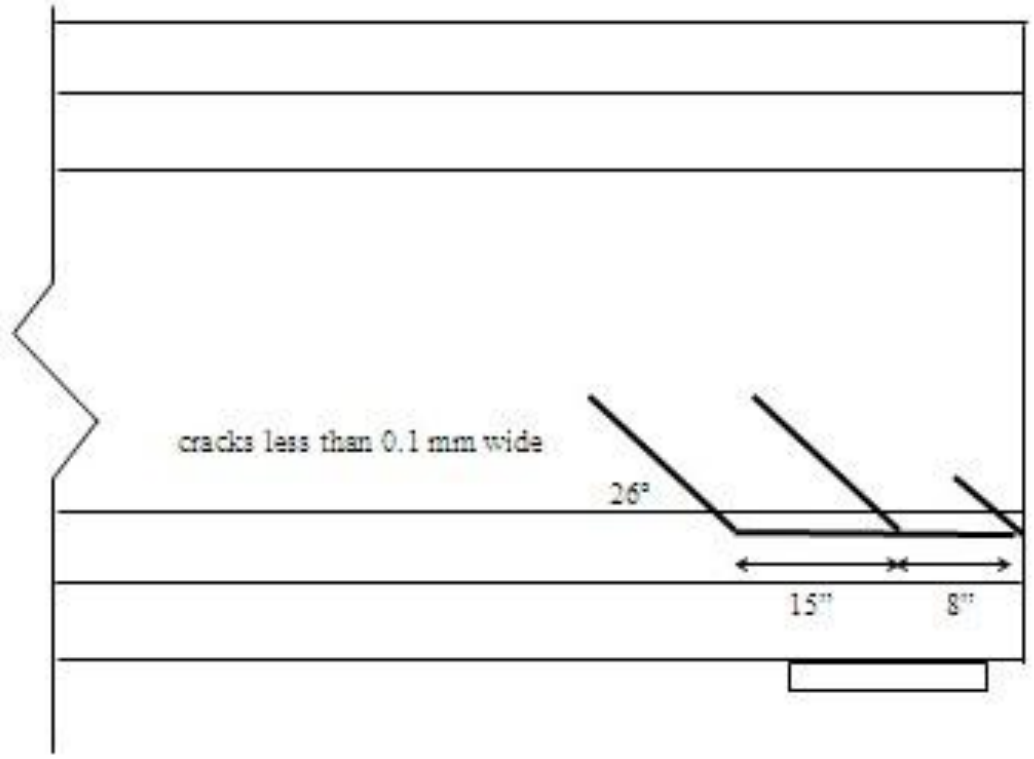

Figure A60. Crack diagram for exterior girder, south side, south face, at interior pier (#2332).

Bridge 12

This structure (#3849) carries US-127 South over Sellers Avenue (within Lansing, between Highways 43 and 143). It was originally built in 1970 and renovated in 1998. Some potentially significant diagonal cracks were found near the ends of some girders, as shown in Figures A61 and A62.

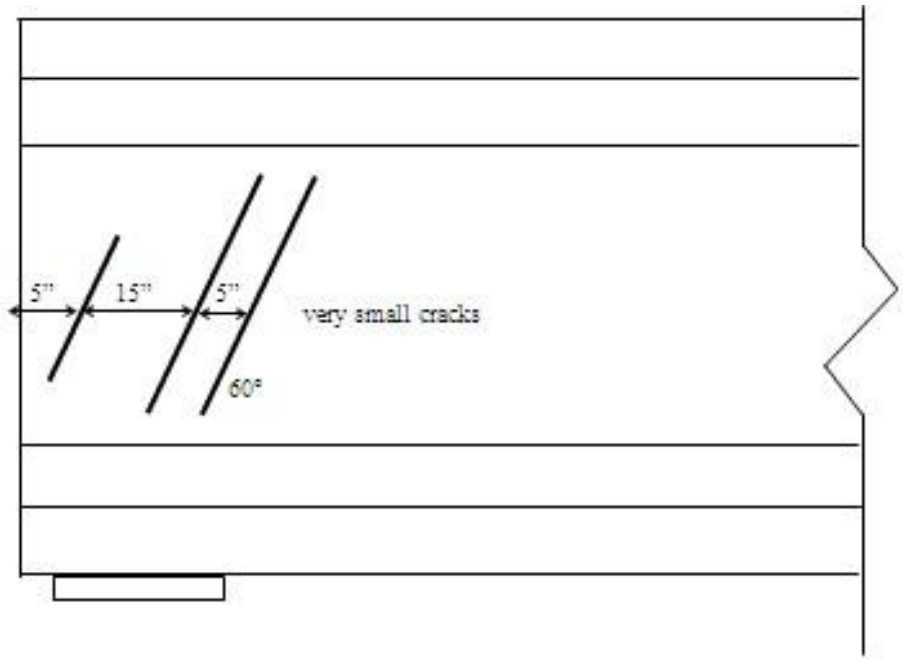

Figure A61. Crack diagram for exterior girder on east side, interior face, north abutment (#3849).

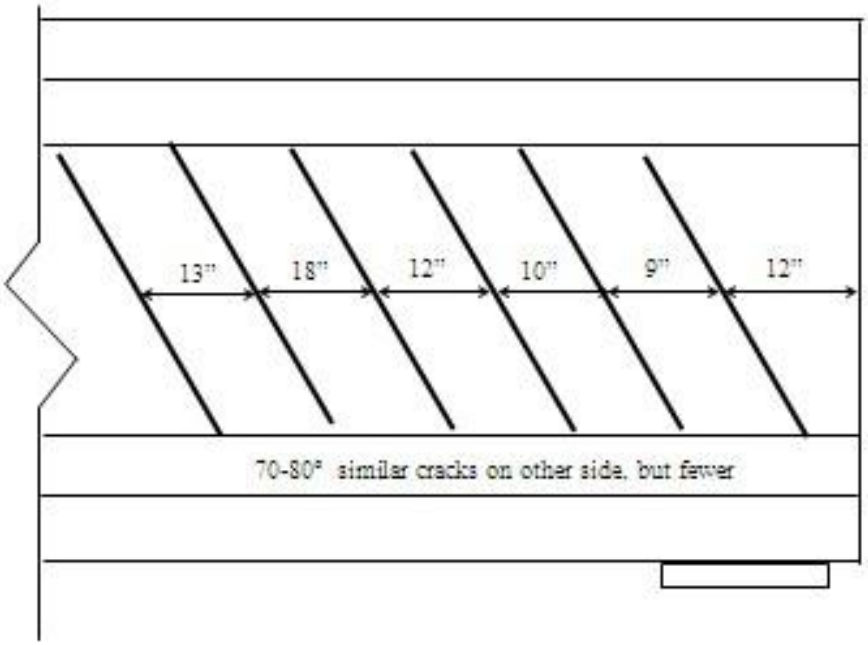

Figure A62. Crack diagram for exterior girder on east side, exterior face, south abutment (#3849).

Bridge 16

This structure (#9728) carries M-52 over Shiawassee River (by Henderson Road, north of Owosso), and was built in 1999. Some potentially significant diagonal cracks were found near the ends of some girders, as shown in Figures A64-A71.

Figure A63. Bridge 16 (#9728).

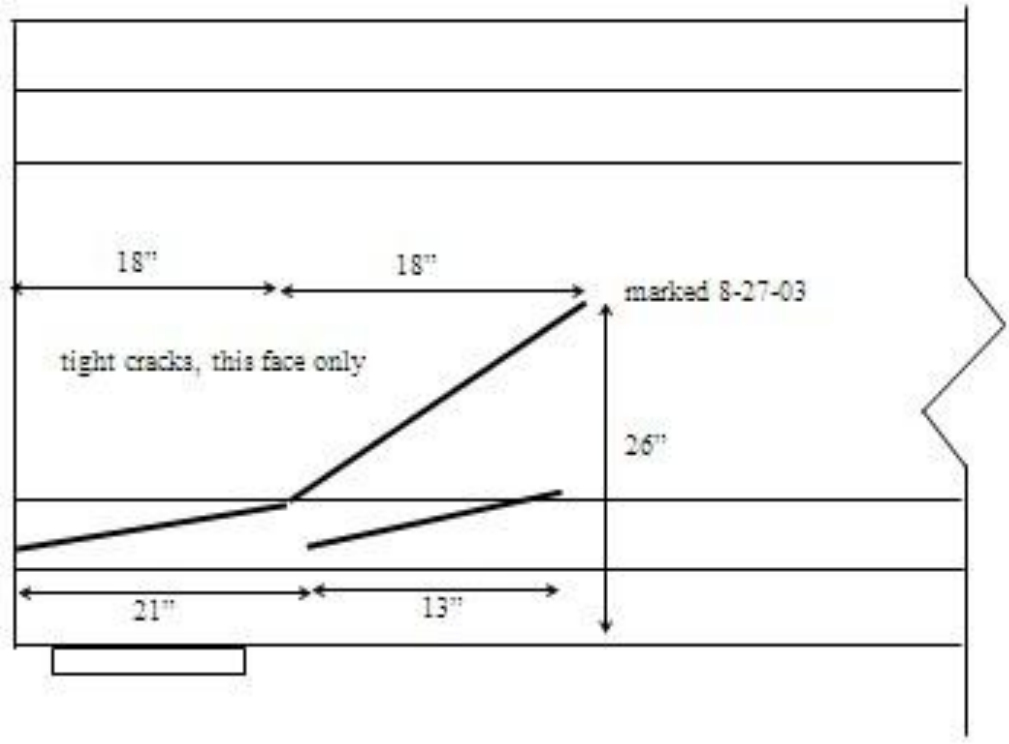

Figure A64. Crack diagram, exterior girder, west side, west face, north abutment (#9728).

Figure A65. Cracks on exterior girder, west side, west face, north abutment (#9728).

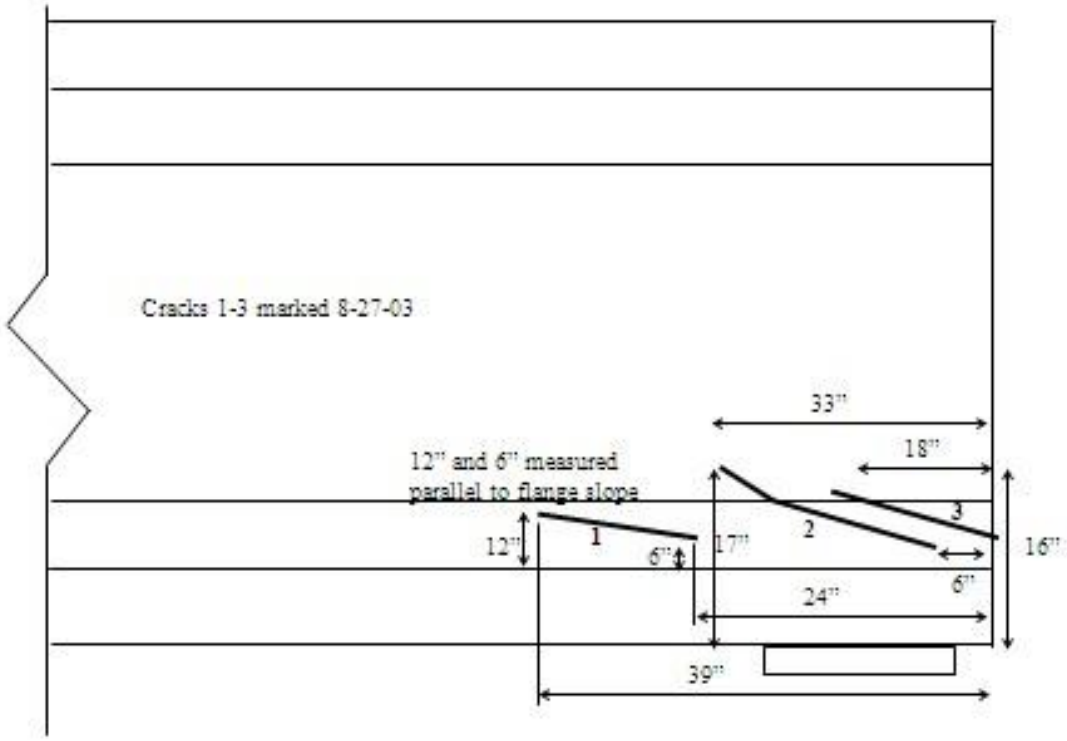

Figure A66. Crack diagram, exterior girder, east side, east face, north abutment (#9728).

Figure A67. Cracks on exterior girder, east side, east face, north abutment (#9728).

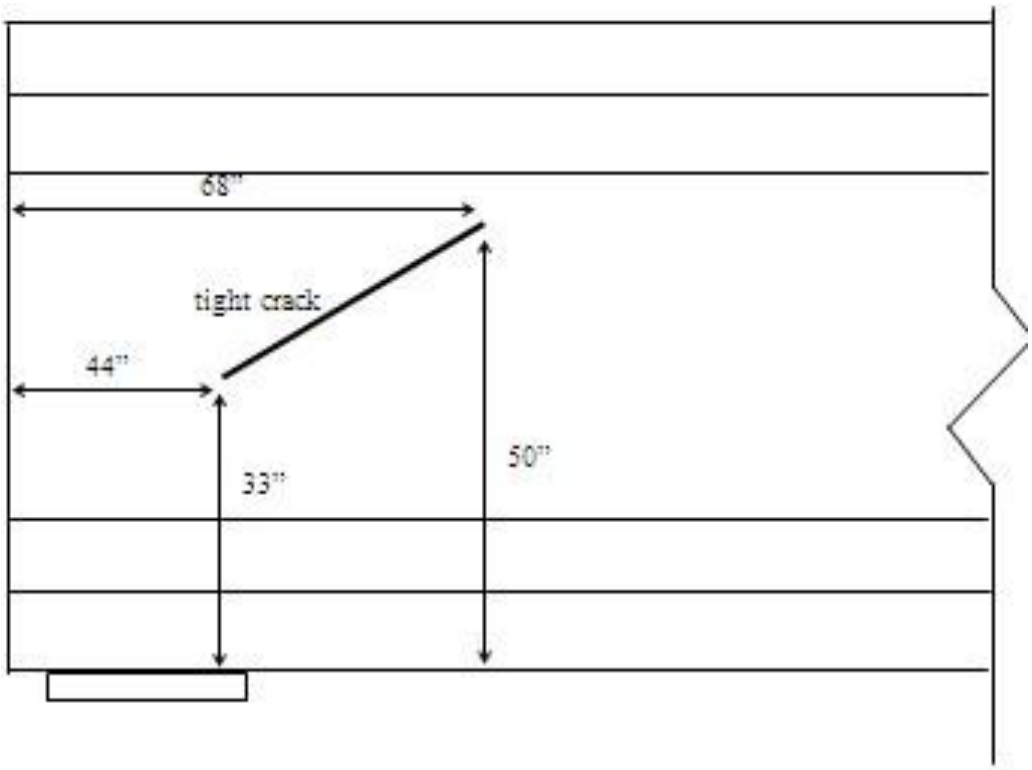

Figure A68. Crack diagram for exterior girder, east side, east face, south abutment (#9728).

Figure A69. Cracks on exterior girder, east side, east face, south abutment (#9728).

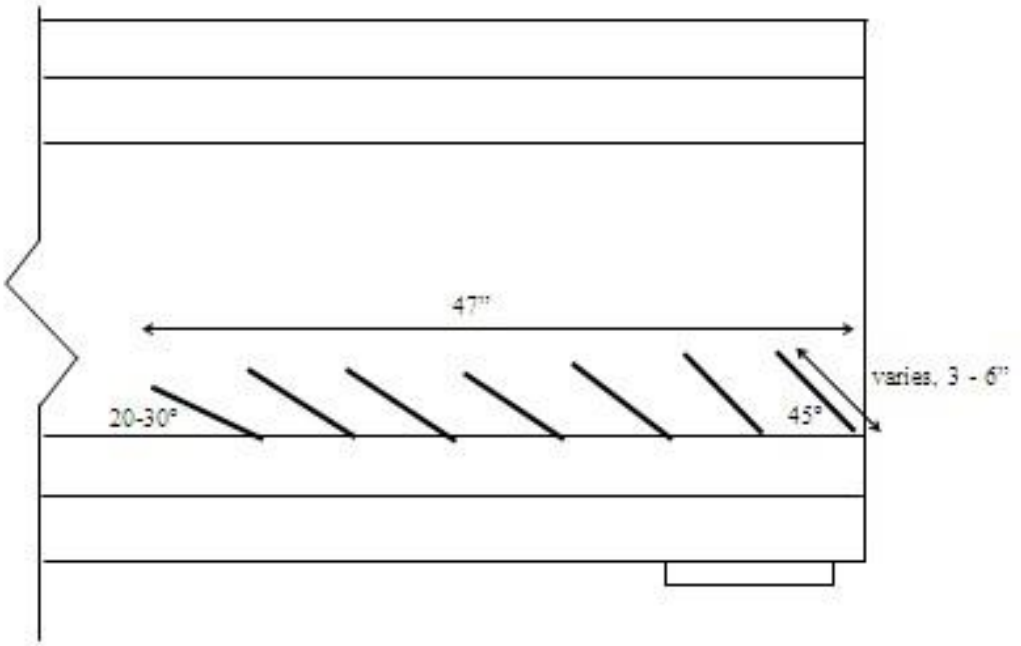

Figure A70. Crack diagram, exterior girder, west side, west face, south abutment (#9728).

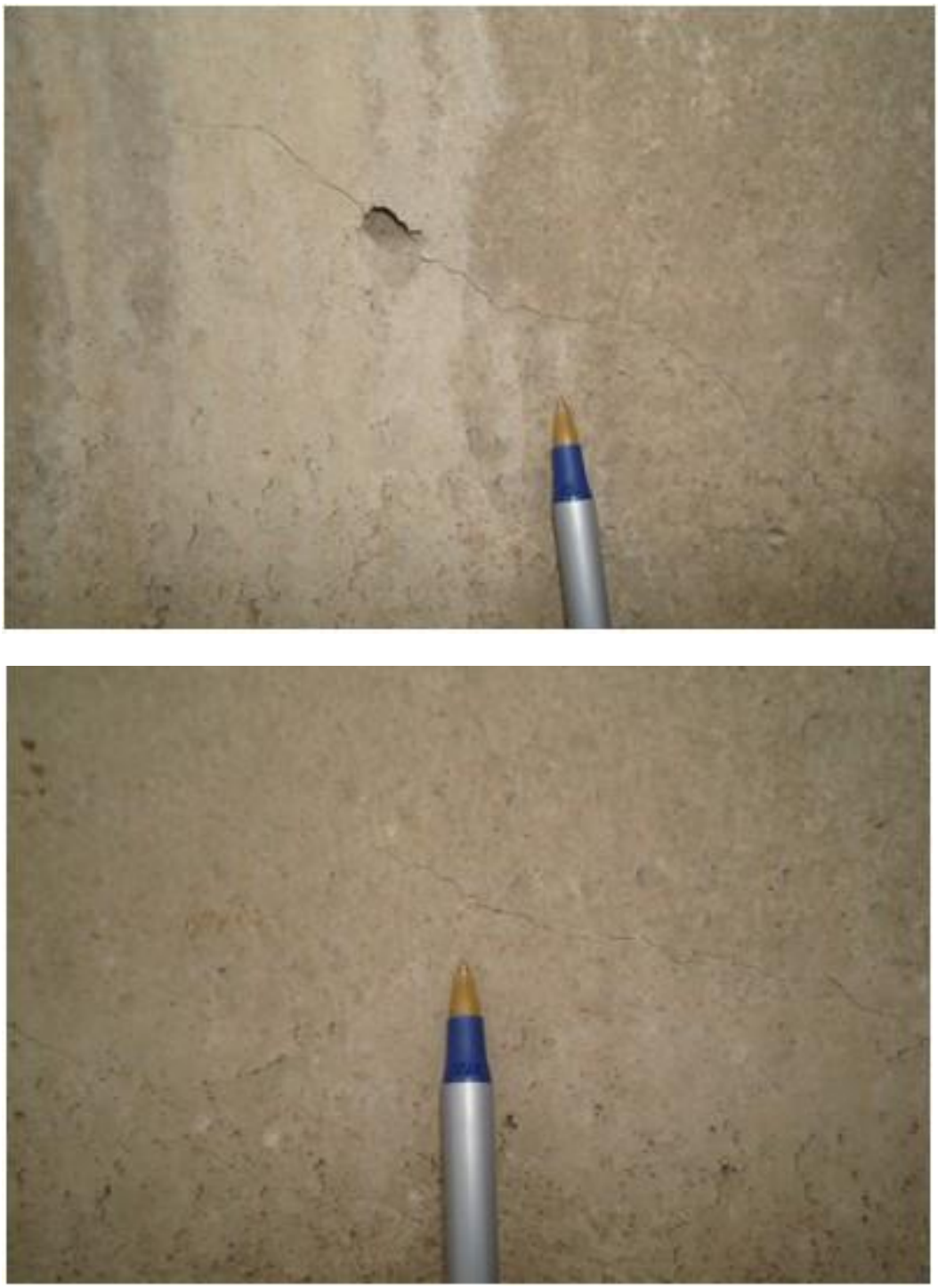

Figure A71. Cracks on exterior girder, west side, west face, south abutment (#9728).

Bridge 18

This structure (#12693) carries US-127 South over Looking Glass River (north of Highway 69, just south of West Cutler Road), and was built in 1997. Some potentially significant diagonal cracks were found near the ends of some girders, as shown in Figures A73 and A74.

Figure A72. Bridge 18 (#12693).

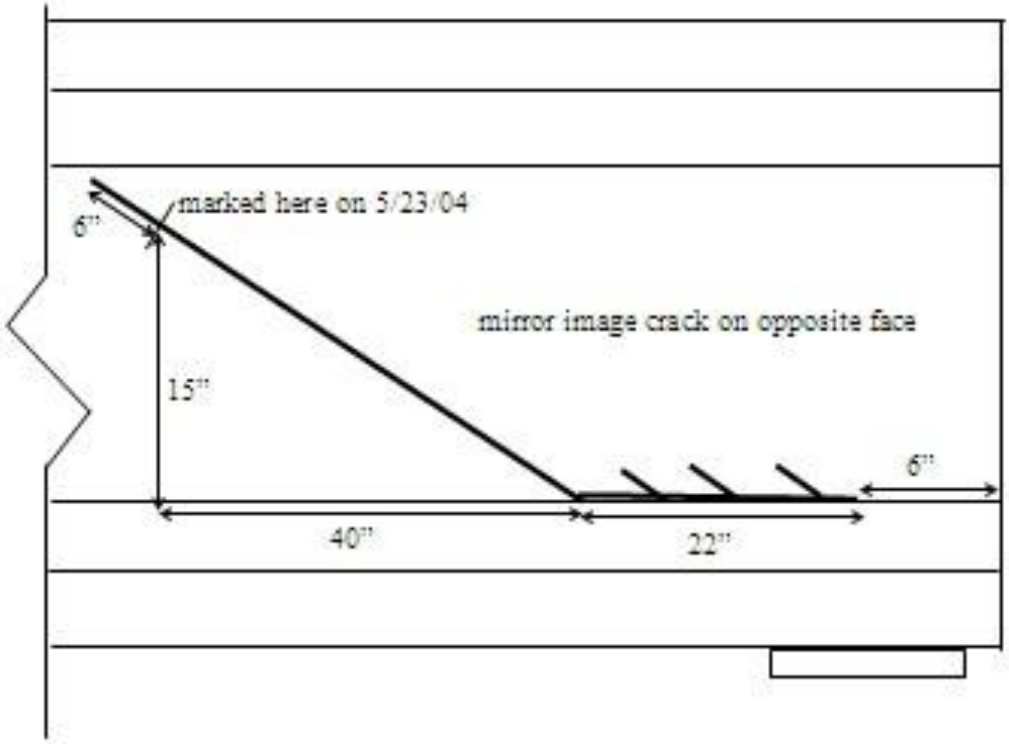

Figure A73. Crack diagram for Girder 5th from west side, west face, south abutment (#12693).


K 5'28'04

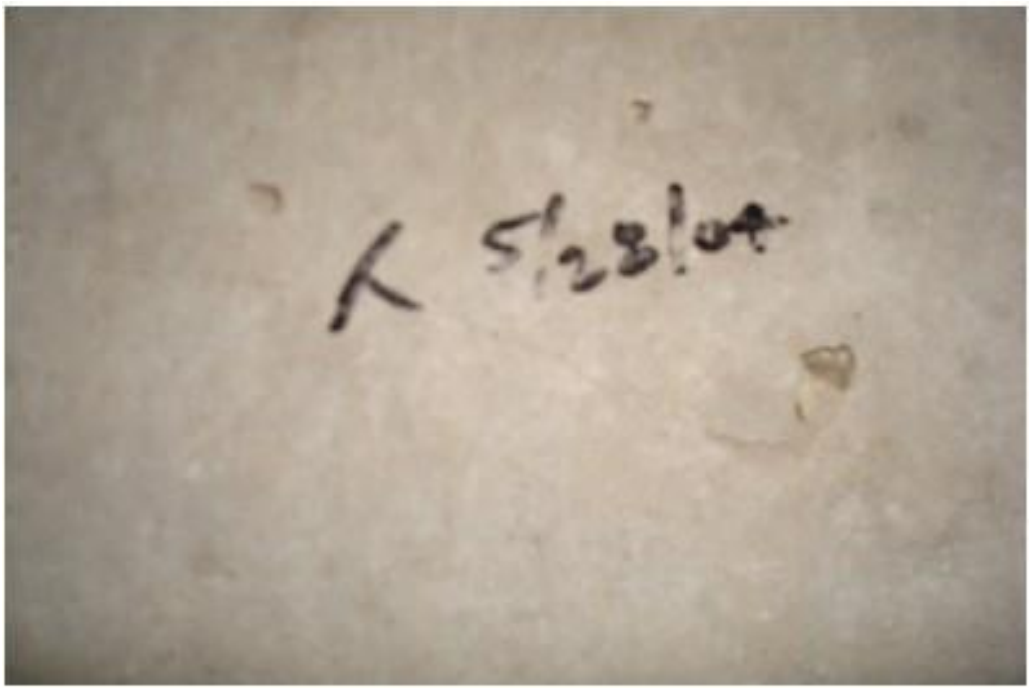
K 5'28'04

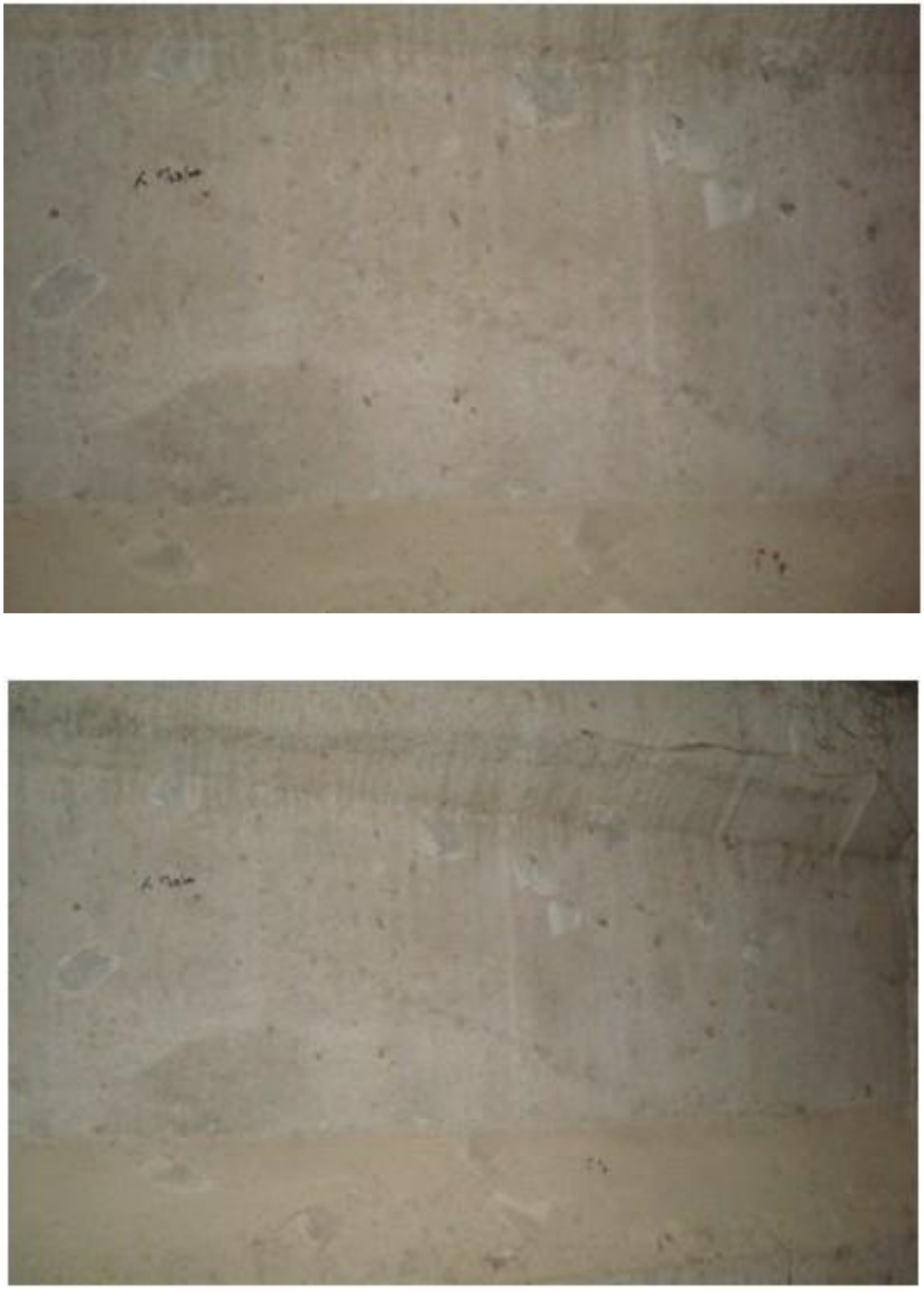

Figure A74. Cracks on Girder 5th from west side, west face, south abutment (#12693).

Bridge 19

This structure (#12773) carries Centerline Road over US-127, and was built in 1993. Some minor diagonal cracks were found near the ends of some girders, as shown in Figures A76 and A77.

Figure A75. Bridge 19 (#12773).

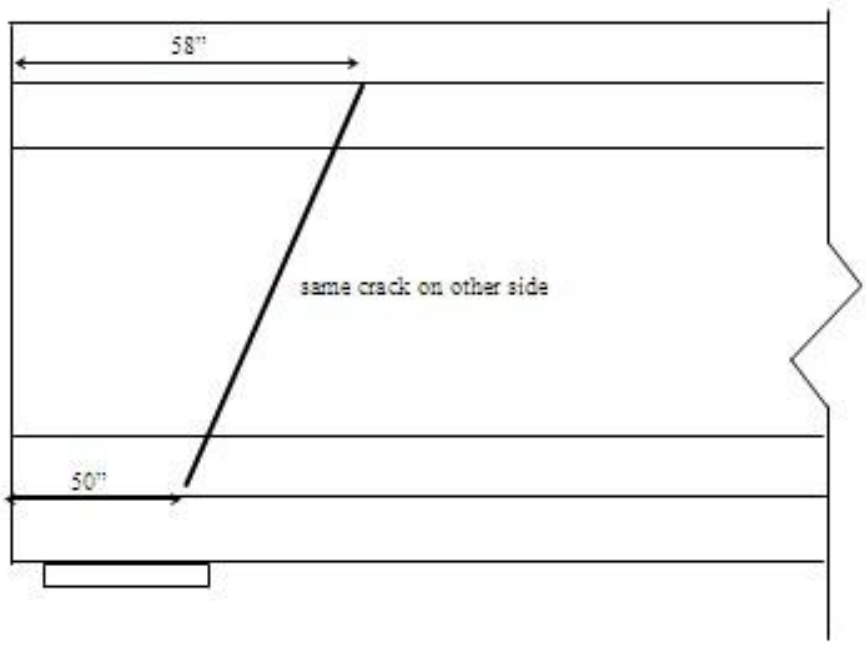

Figure A76. Crack diagram for girder on exterior of south side, south face, west abutment (#12773).

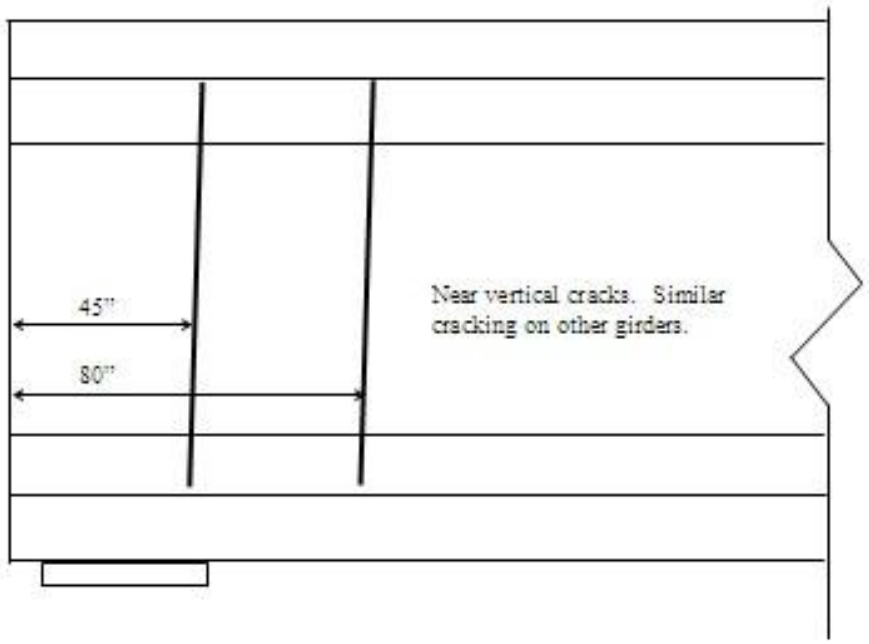

Figure A77. Crack diagram for girder 2nd from south side, south face, west abutment (#12773).

APPENDIX B: ANALYSIS OF FIELD STRUCTURES

Table B1a. Bridge Characteristics (cont).

ID	Bridge	Girder Span (ft)	Girder Spacing (ft)	Girder Type	Web Thk(in)	Girder Ht (ft)	Span/Ht Ratio
1	7933	77	8	Type IV	8	4.5	17.1
5, 6	1829, 1830	64.5	7.2	Wisconsin	6	5.83	11.1
18	12693	102	7.9	Type IV	8	4.5	22.7
19	12773 s 1, 4	35.5	9.6	Type IV	8	4.5	7.9
	s 2, 3	106	6.4	Type IV	8	4.5	23.6
12	3849 s 1, 3 a	29.5	6.4	Type I	6	2.33	12.7
	s 1, 3 b	29.5	6.4	Type II	6	3	9.8
	s 2	52.5	6.4	Type II	6	3	17.5
16	9728	140	7.4	MI-1800	5.9	5.92	23.6
7	2332 s 1	40	5.5	Type III	7	3.75	10.7
	s 2, 3	71	5.5	Type III	7	3.75	18.9
	s 4	35.5	5.5	Type III	7	3.75	9.5
20	12774 s 1, 4	35.5	9.8	Type IV	8	4.5	7.9
	s 2, 3	106	6.5	Type IV	8	4.5	23.6
21	12775 s 1	35.5	9.6	Type IV	8	4.5	7.9
	s 2, 3	106	6.4	Type IV	8	4.5	23.6
	s 4	40	9.6	Type IV	8	4.5	8.9
11	3848 s 1, 3 a	29.5	6.3	Type I	6	2.33	12.7
	s 1, 3 b	29.5	6.3	Type II	6	3	9.8
	s 2	53.5	6.3	Type II	6	3	17.8
13	3854 s 1, 3 a	29.5	6.3	Type I	6	2.33	12.7
	s 1, 3 b	29.5	4.6	Type I	6	2.33	12.7
	s 1, 3 c	29.5	5.5	Type II	6	3	9.8
	s 2 a	53.5	6.3	Type II	6	3	17.8
	s 2 b	53.5	4.6	Type I	6	2.33	23
9	3831 s 1, 3 a	37.5	5	Type I	6	2.33	16.1
	s 1, 3 b	37.5	5	Type II	6	3	12.5
	s 2, a	58	5	Type I	6	2.33	24.9
	s 2, b	58	5	Type II	6	3	19.3
14	4447 s 1	107	7.5	Type IV	8	4.5	23.8
	s 2	106	7.5	Type IV	8	4.5	23.6
22	12943 s 1	91.5	10	Type IV	8	4.5	20.3
	s 2	91.5	10	Type IV	8	4.5	20.3
	s 3	91.5	10	Type IV	8	4.5	20.3
	s 4 a	81.55	10	Type IV	8	4.5	18.1
	s 4 b	81.55	10	Type IV	8	4.5	18.1
	s 4 c	81.55	10	Type IV	8	4.5	18.1
	s 4 d	81.55	10	Type IV	8	4.5	18.1
	s 4 e	81.55	10	Type IV	8	4.5	18.1
	s 5	71.75	10	Type IV	8	4.5	15.9
	s 6	91.5	10	Type IV	8	4.5	20.3
	s 7	75.18	10	Type IV	8	4.5	16.7
	s 8 a	58.73	10	Type IV	8	4.5	13.1
	s 8 b	58.73	10	Type IV	8	4.5	13.1
	s 8 c	58.73	10	Type IV	8	4.5	13.1
	s 8 d	58.73	10	Type IV	8	4.5	13.1
	s 8 e	58.73	10	Type IV	8	4.5	13.1

Table B1a. Bridge Characteristics (cont).

ID	Bridge	Girder Span (ft)	Girder Spacing (ft)	Girder Type	Web Thk(in)	Girder Ht (ft)	Span/Ht Ratio
23	12944 s 1	91.5	8.3	Type IV	8	4.5	20.3
	s 2	91.5	8.3	Type IV	8	4.5	20.3
	s 3	91.5	8.3	Type IV	8	4.5	20.3
	s 4 a	67.04	8.3	Type IV	8	4.5	14.9
	s 4 b	67.04	8.3	Type IV	8	4.5	14.9
	s 4 c	67.04	8.3	Type IV	8	4.5	14.9
	s 4 d	67.04	8.3	Type IV	8	4.5	14.9
	s 4 e	67.04	8.3	Type IV	8	4.5	14.9
	s 4 f	67.04	8.3	Type IV	8	4.5	14.9
	s 5	71.75	8.3	Type IV	8	4.5	15.9
	s 6	91.5	8.3	Type IV	8	4.5	20.3
	s 7	75.18	8.3	Type IV	8	4.5	16.7
	s 8 a	65.34	8.3	Type IV	8	4.5	14.5
	s 8 b	65.34	8.3	Type IV	8	4.5	14.5
	s 8 c	65.34	8.3	Type IV	8	4.5	14.5
	s 8 d	65.34	8.3	Type IV	8	4.5	14.5
	s 8 e	65.34	8.3	Type IV	8	4.5	14.5
	s 8 f	65.34	8.3	Type IV	8	4.5	14.5
24	B03 s 1	60	4.9	Type II	6	3	20
25	B09 s 1	60	4.9	Type II	6	3	20
26	B05 s 1	20	4.9	Type I	6	2.33	8.6
27	B08 s 1	20	4.9	Type I	6	2.33	8.6

Table B1b. Bridge Characteristics (cont).

ID	Strands Harped	Strand Dist Proportion	f'c (ksi) transfer	f'c (ksi) service	Ac (si)	Girder Total Ps (k)	Girder sps (ksi)
1	no	0.74	3.5	5	789	796	1.01
5, 6	some	0.66	5.7	7	773	1488	1.92
18	some	0.72	5.1	6	789	1364	1.73
19	no	0.92	3.5	5	789	186	0.24
	some	0.65	4.6	6	789	1240	1.57
12	all	0.63	3.6	5	276	263	0.95
	all	0.71	3.6	5	369	263	0.71
	all	0.65	4.5	6.4	369	526	1.43
16	no	0.89	6	7	874	1927	2.2
7	no	0.92	3.5	5	560	173	0.31
	some	0.68	3.5	5	560	578	1.03
	no	0.92	3.5	5	560	173	0.31
20	no	0.89	3.5	5	789	248	0.31
	some	0.65	4.6	6	789	1240	1.57
21	no	0.92	3.5	5	789	186	0.24
	some	0.65	4.6	6	789	1240	1.57
	no	0.92	3.5	5	789	248	0.31

Table B1b. Bridge Characteristics (cont).

ID	Strands Harped	Strand Dist Proportion	f'c (ksi) transfer	f'c (ksi) service	Ac (si)	Girder Total Ps (k)	Girder sps (ksi)
11	no	0.68	3.6	5	276	290	1.05
	no	0.67	3.6	5	369	250	0.68
	some	0.45	3.6	5	369	432	1.17
13	no	0.58	3.6	5	276	290	1.05
	no	0.52	3.7	5	276	176	0.64
	no	0.46	3.6	5	369	245	0.66
	some	0.46	3.6	5	369	432	1.17
	some	0.45	5.8	5.9	276	528	1.91
9	no	0.56	3.5	5	276	267	0.97
	no	0.7	3.5	5	369	191	0.52
	no	0.56	3.5	5	276	267	0.97
	some	0.38	3.5	5	369	458	1.24
14	some	0.65	6	7	789	1664	2.11
	some	0.65	6	7	789	1664	2.11
22	some	0.62	5.5	6.5	789	1294	1.64
	some	0.64	5.8	7.1	789	1375	1.74
	some	0.64	5.8	7.1	789	1375	1.74
	some	0.69	4.3	5	789	1051	1.33
	some	0.74	5.8	6	789	1132	1.43
	some	0.73	4.8	5.5	789	1051	1.33
	some	0.71	4.3	5	789	970	1.23
	some	0.7	3.6	5	789	728	0.92
	some	0.7	3.6	5	789	728	0.92
	some	0.64	5.8	7.1	789	1375	1.74
	some	0.72	4	5	789	889	1.13
	no	0.92	3.6	5	789	323	0.41
	no	0.92	3.6	5	789	404	0.51
	no	0.91	3.6	5	789	485	0.61
	no	0.92	3.6	5	789	485	0.61
	no	0.92	3.6	5	789	404	0.51
23	some	0.73	4.5	5.5	789	1051	1.33
	some	0.62	4.8	5.5	789	1132	1.43
	some	0.62	4.8	5.5	789	1132	1.43
	some	0.66	3.6	5	789	566	0.72
	some	0.68	3.6	5	789	647	0.82
	some	0.66	3.6	5	789	566	0.72
	no	0.91	3.6	5	789	485	0.61
	no	0.91	3.6	5	789	485	0.61
	no	0.92	3.6	5	789	323	0.41
	some	0.68	3.6	5	789	647	0.82
	some	0.62	4.8	5.5	789	1132	1.43
	some	0.7	3.6	5	789	728	0.92
	no	0.92	3.6	5	789	323	0.41
	no	0.91	3.6	5	789	485	0.61
	no	0.91	3.6	5	789	485	0.61
	no	0.91	3.6	5	789	485	0.61
	some	0.66	3.6	5	789	566	0.72
	no	0.92	3.6	5	789	404	0.51
24	no	0.57	6	7	369	704	1.91
25	no	0.57	6	7	369	704	1.91
26	no	0.27	6	7	276	704	2.55
27	no	0.27	6	7	276	704	2.55

Table B1c. Bridge Characteristics.

ID	Continuous for LL	Debonded Strands	End Zone (in) Steel Spacing	Steel Bar Size	Lifetime Trucks	Year Built	End Blocks
1	no	some	5a3, 14a9	5	no info	1985	no
5, 6	no	some	8a3, 21a7	4	15200	1993	no
18	YES	some	5a3, 12a9	5	no info	1997	no
19	no	some	5a3, 3a16	4	no info	1993	no
	YES	some	6a3, 6a10	4	no info	1993	no
12	no	some	3a3, 12a7	4	12600	1998	no
	no	some	3a3, 12a7	4	12600	1998	no
	no	some	3a3, 12a7	4	12600	1998	no
16	no	some	13a3, 4a10.5	5	3380	1999	no
7	no	none	5a3, 19a23	4	no info	1981	no
	no	none	5a3, 36a23	4	no info	1981	no
	no	none	5a3, 17a23	4	no info	1981	no
20	no	some	5a3, 4a18	4	no info	1993	no
	YES	some	6a3, 6a10	4	no info	1993	no
21	no	some	5a3, 3a20	4	no info	1993	no
	YES	some	6a3, 6a10	4	no info	1993	no
	no	some	5a3, 4a15	4	no info	1993	no
11	no	none	21 at 15.72	4	37800	1970	no
	no	none	21 at 15.72	4	37800	1970	no
	no	none	36a17	4	37800	1970	no
13	no	none	3a3, 21 a 13.5	4	37800	1970	YES
	no	none	2a3, 16 a20.2	4	37800	1970	YES
	no	none	4a3, 21 a13.5	4	37800	1970	YES
	no	none	4a3, 36a17	4	37800	1970	YES
	no	none	3a3, 3a16	4	37800	1970	YES
9	no	none	6a3, 6a12	4	no info	1962	YES
	no	none	6a3, 6a12	4	no info	1962	YES
	no	none	6a3 , 6a12	4	no info	1962	YES
	no	none	6a3 , 6a12	4	no info	1962	YES
14	YES	some	8a3, 14a7	4	no info	2001	no
	YES	some	8a3, 22a6	4	no info	2001	no
22	YES	some	7a3, 22a5	4	8040	2000	no
	YES	some	7a3, 42a4	4	8040	2000	no
	YES	some	7a3, 36a5	4	8040	2000	no
	YES	some	6a3, 29a5.5	4	8040	2000	no
	YES	some	6a3, 89a4	4	8040	2000	no
	YES	some	6a3, 72a4	4	8040	2000	no
	YES	some	5a3, 47a4	4	8040	2000	no
	YES	some	4a3, 17a7	4	8040	2000	no
	YES	some	4a3, 37a5	4	8040	2000	no
	YES	some	7a3, 42a4	4	8040	2000	no
	YES	some	5a3, 55a5	4	8040	2000	no
	YES	some	2a3, 12a9.5	4	8040	2000	no
	YES	some	2a3, 31a5.5	4	8040	2000	no
	YES	some	3a3, 38a5	4	8040	2000	no
	YES	some	3a3, 38a5	4	8040	2000	no
	YES	some	2a3, 15a9	4	8040	2000	no

Table B1c. Bridge Characteristics (cont).

ID	Continuous for LL	Debonded Strands	End Zone (in) Steel Spacing	Steel Bar Size	Lifetime Trucks	Year Built	End Blocks
23	YES	some	6a3, 18a6	4	8040	2000	no
	YES	some	6a3, 31a5.5	4	8040	2000	no
	YES	some	6a3, 31a5.5	4	8040	2000	no
	YES	some	3a3, 5a12.5	4	8040	2000	no
	YES	some	4a3, 22a6	4	8040	2000	no
	YES	some	3a3, 24a6	4	8040	2000	no
	YES	some	3a3, 23a7	4	8040	2000	no
	YES	some	3a3, 20a7	4	8040	2000	no
	YES	some	2a3, 4a16.5	4	8040	2000	no
	YES	some	4a3, 21a6	4	8040	2000	no
	YES	some	6a3, 29a5.5	4	8040	2000	no
	YES	some	4a3, 22a6	4	8040	2000	no
	YES	some	2a3, 5a15	4	8040	2000	no
	YES	some	3a3, 25a6	4	8040	2000	no
	YES	some	3a3, 45a6	4	8040	2000	no
	YES	some	3a3, 26a6	4	8040	2000	no
	YES	some	3a3, 26a6	4	8040	2000	no
	YES	some	2a3, 7a13	4	8040	2000	no
24	no	none	4a3, 10a6	5	?	2011	no
25	no	none	4a3, 10a6	5	?	2011	no
26	no	none	5a1.5, 14a3	4	?	2011	no
27	no	none	5a1.5, 14a3	4	?	2011	no

Table B1d. Average Bridge Characteristics.

Characteristic	Cracked	Uncracked
Girder Span (ft)	72	61
Girder Spacing (ft)	7.2	7.6
Girder Type	III, IV	IV
Girder Height (ft)	4.5	3.8
Strand Dist Proport.	0.74	0.69
f'c Transfer (ksi)	4.3	4.1
f'c Service (ksi)	5.7	5.4
Ac (in^2)	693	613
Girder Total Ps (k)	892	621
Girder sps (ksi)	1.2	1.0
Year Built	1992	1991

Table B2. Bridge Designs According to AASHTO Standard Specifications (kips).

BRIDGE	SPAN	LOAD	Vc	Vs	Vp	Vu	V1	V2	phiVn	Vn
7933	1	HS 20	138	236	0	213	127	116	336	373
1829	1	HS 25	221	154	12	321	204	183	337	375
1830	1	HS 25	204	154	10	321	204	183	322	358
2332		H 15	74	30	6	64	38	52	94	104
	1	H 15	103	30	9	68	41	55	119	133
		H 15	95	35	0	61	38	49	117	130
	2&3	H 15	146	57	14	101	66	82	183	203
		H 15	117	32	5	92	60	75	135	150
		H 15	76	39	7	59	35	48	103	115
	4	H 15	102	29	10	62	38	50	117	131
		H 15	95	35	0	56	34	45	117	130
3831	1&3	H 15	47	38	0	53	32	43	76	84
		H 15	62	48	0	55	34	44	99	110
	2	H 15	50	38	0	71	45	58	79	88
		H 15	93	43	10	74	48	60	122	136
3848	1&3	HS 20	39	49	0	95	50	41	79	87
		HS 20	62	59	0	94	50	41	109	121
	2	HS 20	94	50	9	130	72	63	129	143
3849	1&3	HS 25	41	83	0	117	61	44	112	124
		HS 25	56	102	0	116	61	44	143	158
	2	HS 25	68	100	0	159	87	67	151	168
3854		HS 20	29	26	0	101	55	46	63	70
	1&3	HS 25	49	38	0	88	47	34	78	87
		HS 20	52	33	0	89	49	42	92	102
	2	HS 20	80	37	10	145	83	74	106	117
		HS 25	65	50	5	121	68	53	101	112
4447	1	HS 25	213	186	10	325	190	159	359	399
	2	HS 25	213	217	10	324	189	158	387	430
9728	1&2	HS 25	205	218	0	322	204	182	381	423
12693	1	HS 25	176	156	5	277	167	143	298	332
	2	HS 25	176	175	5	261	159	138	316	351
	3	HS 25	176	175	5	277	167	143	316	351
12773	1&4	HS 20	125	62	0	164	90	77	168	187
	2&3	HS 20	196	88	10	223	141	132	256	284
12774	1&4	HS 20	122	54	0	166	91	78	158	176
	2&3	HS 20	195	88	9	226	142	134	255	283
12775	1	HS 20	125	49	0	164	90	77	157	174
	2&3	HS 20	196	88	10	223	140	132	256	284
	4 (s9)	HS 20	123	98	0	176	98	84	265	294
	4 (s15)	HS 20	123	66	0	176	98	84	170	188
12943	1	HS 25	189	191	13	316	188	159	342	380
	2	HS 25	194	231	13	292	177	151	383	425
	3	HS 25	194	193	13	297	179	153	348	387
	4-A	HS 25	142	169	7	267	160	136	280	311
	4-B	HS 25	150	241	7	267	160	136	352	391
	4-C	HS 25	142	241	8	267	160	136	345	383
	4-D	HS 25	140	238	8	267	160	136	341	379
	4-E	HS 25	147	132	10	267	160	136	251	279
	5	HS 25	143	198	10	252	148	124	307	341
	6	HS 25	194	231	13	300	180	154	383	425

Table B2. Bridge Designs According to AASHTO Standard Specifications (kips) (cont).

BRIDGE	SPAN	LOAD	Vc	Vs	Vp	Vu	V1	V2	phiVn	Vn
12943	7	HS 25	138	200	9	276	161	134	304	338
	8-A	HS 25	125	108	0	263	147	117	210	233
	8-B	HS 25	119	185	0	263	147	117	274	304
	8-C	HS 25	114	215	0	263	147	117	297	330
	8-D	HS 25	114	215	0	263	147	117	297	330
	8-E	HS 25	119	118	0	263	147	117	213	237
12944	1	HS 25	155	149	7	270	162	138	274	304
	2	HS 25	180	163	14	251	153	132	309	343
	3	HS 25	180	163	14	253	154	142	309	343
	4-F	HS 25	151	72	10	195	117	99	201	223
	4-G	HS 25	149	146	10	195	117	99	266	296
	4-H	HS 25	151	145	11	195	117	99	267	296
	4-J	HS 25	123	143	0	195	117	99	239	266
	4-K	HS 25	123	143	0	195	117	99	239	266
	4-L	HS 25	131	61	0	195	117	99	173	192
	5	HS 25	151	146	10	219	130	109	267	297
	6	HS 25	180	163	14	188	124	113	309	343
	7	HS 25	150	147	9	236	139	116	267	297
	8-F	HS 25	130	68	0	236	135	109	178	198
	8-G	HS 25	123	160	0	236	135	109	255	283
	8-H	HS 25	123	160	0	236	135	109	255	283
	8-J	HS 25	123	160	0	236	135	109	255	283
	8-K	HS 25	151	145	11	236	135	109	266	296
	8-L	HS 25	126	76	0	236	135	109	182	202
B03	1	1.2HL93-HS20	93	240	0	116	67	60	300	333
B09	1	1.2HL93-HS20	93	240	0	116	67	60	300	333
B05	1	1.2HL93-Mil	100	237	0	81	42	32	303	337
B08	1	1.2HL93-Mil	100	237	0	81	42	32	303	337

Table B3. Bridge Designs According to AASHTO LRFD Specifications (kips).

BRIDGE	SPAN	Vc	Vs	Vp	Vu	V1	V2	phiVn	Vn
7933	1	89	567	0	223	145	112	504	560
1829	1	101	405	13	365	244	179	467	519
1830	1	101	405	10	365	244	179	465	517
2332		85	64	6	68	45	54	139	154
	1	122	65	9	70	46	55	176	195
		122	68	0	64	42	51	171	190
	2&3	157	119	14	115	78	86	261	290
		145	65	6	106	72	79	193	215
		85	85	7	62	40	50	159	177
	4	122	65	10	63	41	50	177	197
		122	68	0	58	38	46	171	190
3831	1&3	75	72	0	60	39	48	132	146
		82	91	0	60	40	48	155	173
	2	42	82	0	84	56	63	112	124
		109	92	10	86	58	66	190	211
3848	1&3	36	113	0	93	57	42	134	149
		76	120	0	93	57	42	177	196
	2	46	127	10	142	88	66	164	182
3849	1&3	31	122	0	118	72	45	138	153
		43	167	0	115	70	44	189	210
	2	43	156	0	175	109	70	179	199
3854		43	91	0	98	61	46	121	134
	1&3	24	48	0	98	60	38	65	73
		89	99	0	90	56	43	169	188
	2	52	97	10	152	97	75	143	159
		40	102	5	146	91	59	132	147
4447	1	105	457	11	359	231	154	516	573
	2	105	546	11	357	230	153	596	662
9728	1&2	77	284	0	382	254	182	325	361
12693	1	94	374	5	351	225	143	426	473
	2	94	420	5	330	214	136	468	520
	3	94	420	5	351	225	143	468	520
12773	1&4	78	78	0	142	89	69	140	156
	2&3	122	270	8	283	186	147	360	400
12774	1&4	87	89	0	144	91	70	159	176
	2&3	122	272	8	284	187	147	363	403
12775	1	78	63	0	142	89	69	126	140
	2&3	103	223	8	284	186	147	300	334
	4 (s9)	81	248	0	158	100	77	323	359
	4 (s15)	81	109	0	158	100	77	171	190
12943	1	102	412	13	395	253	162	474	527
	2	112	574	13	367	237	152	629	699
	3	112	491	13	373	240	155	555	616
	4-A	90	371	7	338	217	139	421	468
	4-B	102	577	7	338	217	139	618	686
	4-C	101	553	8	338	217	139	596	662
	4-D	93	527	8	338	217	139	566	629
	4-E	94	299	10	338	217	139	363	403
	5	95	473	10	315	200	128	520	578
	6	110	568	13	373	240	155	623	692

Table B3. Bridge Designs According to AASHTO LRFD Specifications (kips) (cont).

BRIDGE	SPAN	Vc	Vs	Vp	Vu	V1	V2	phiVn	Vn
12943	7	93	446	9	347	220	140	492	547
	8-A	103	259	0	256	162	110	326	362
	8-B	102	444	0	256	162	110	492	546
	8-C	102	426	0	256	162	110	475	528
	8-D	102	501	0	256	162	110	542	603
	8-E	102	274	0	256	162	110	339	377
12944	1	92	327	7	347	222	159	384	426
	2	94	389	14	325	210	151	447	497
	3	94	396	14	327	211	152	454	504
	4-F	103	187	10	257	164	115	270	300
	4-G	101	372	10	257	164	115	435	483
	4-H	103	375	11	257	164	115	439	488
	4-J	90	275	0	257	163	115	329	366
	4-K	90	275	0	257	163	115	329	366
	4-L	95	119	0	257	163	115	192	214
	5	96	294	10	280	178	125	360	401
	6	94	408	14	328	211	152	464	516
	7	92	319	9	307	194	136	378	420
	8-F	91	92	0	227	146	106	165	183
	8-G	101	339	0	228	146	106	396	440
	8-H	101	339	0	228	146	106	396	440
	8-J	101	339	0	228	146	106	396	440
	8-K	126	338	11	228	146	106	427	474
	8-L	91	129	0	227	146	106	198	220
B03	1	52	554	0	154	97	65	348	387
B09	1	52	554	0	154	97	65	348	387
B05	1	40	545	0	121	71	32	265	295
B08	1	40	545	0	121	71	32	265	295

Table B4. Bridge Designs According to AASHTO 1979 Interim Specifications (kips).

BRIDGE	SPAN	Vc	Vs	Vp	Vu	V1	V2	phiVn	Vn
7933	1	124	424	0	213	127	116	494	549
1829	1	155	276	12	321	204	183	399	444
1830	1	155	276	10	321	204	183	397	442
2332		62	54	6	64	38	52	110	122
	1	86	53	9	68	41	55	133	148
		98	64	0	61	38	49	146	162
	2&3	82	102	14	101	66	82	178	197
		90	58	5	92	60	75	138	154
		61	71	7	59	35	48	125	139
	4	83	52	10	62	38	50	130	145
		98	64	0	56	34	45	146	162
3831	1&3	52	68	0	53	32	43	108	120
		66	86	0	55	34	44	137	152
	2	52	68	0	71	45	58	108	120
		58	77	10	74	48	60	131	145
3848	1&3	53	88	0	95	50	41	127	141
		65	106	0	94	50	41	154	171
	2	59	89	9	130	72	63	142	158
3849	1&3	56	149	0	117	61	44	184	204
		69	184	0	116	61	44	227	252
	2	81	179	0	159	87	67	234	260
3854		58	74	0	101	55	46	119	132
	1&3	53	68	0	88	47	34	109	121
		72	91	0	89	49	42	146	162
	2	66	67	10	145	83	74	128	143
		60	84	5	121	68	53	134	149
4447	1	167	335	10	306	190	159	461	512
	2	167	391	10	324	189	158	511	568
9728	1&2	170	392	0	322	204	182	506	563
12693	1	148	281	5	277	167	143	390	434
	2	148	316	5	261	159	138	422	469
	3	148	316	5	277	167	143	422	469
12773	1&4	136	111	0	164	90	77	222	246
	2&3	145	158	10	223	141	132	282	313
12774	1&4	134	97	0	166	91	78	208	231
	2&3	145	158	9	226	142	134	281	312
12775	1	136	89	0	164	90	77	202	224
	2&3	145	158	10	223	140	132	282	313
	4 (s9)	136	176	0	176	98	84	280	312
	4 (s15)	136	118	0	176	98	84	228	254
12943	1	162	344	13	316	188	159	467	519
	2	178	416	13	292	177	151	546	607
	3	178	347	13	297	179	153	484	538
	4-A	130	304	7	267	160	136	397	441
	4-B	159	433	7	267	160	136	539	599
	4-C	144	433	8	267	160	136	526	584
	4-D	131	429	8	267	160	136	512	569
	4-E	131	237	10	267	160	136	340	377
	5	131	356	10	252	148	124	447	497
	6	178	416	13	300	180	154	546	607

Table B4. Bridge Designs According to AASHTO 1979 Interim Specifications (kips) (cont).

BRIDGE	SPAN	Vc	Vs	Vp	Vu	V1	V2	phiVn	Vn
12943	7	132	360	9	276	161	134	451	501
	8-A	142	194	0	263	147	117	303	337
	8-B	142	333	0	263	147	117	428	475
	8-C	142	388	0	263	147	117	477	530
	8-D	142	388	0	263	147	117	477	530
	8-E	142	212	0	263	147	117	319	354
12944	1	143	269	7	270	162	138	377	419
	2	136	293	14	251	153	132	398	442
	3	136	293	14	253	154	142	398	442
	4-F	128	130	10	195	117	99	241	268
	4-G	129	263	10	195	117	99	362	402
	4-H	128	261	11	195	117	99	359	399
	4-J	141	257	0	195	117	99	358	398
	4-K	141	257	0	195	117	99	358	398
	4-L	142	110	0	195	117	99	227	252
	5	129	263	10	219	130	109	362	402
	6	136	293	14	188	124	113	398	442
	7	130	265	9	236	139	116	364	404
	8-F	142	122	0	236	135	109	237	263
	8-G	141	289	0	236	135	109	387	430
	8-H	141	289	0	236	135	109	387	430
	8-J	141	289	0	236	135	109	387	430
	8-K	128	261	11	236	135	109	360	400
	8-L	142	136	0	236	135	109	250	278
B03	1	89	432	0	116	67	60	469	521
B09	1	89	432	0	116	67	60	469	521
B05	1	69	427	0	81	42	32	446	496
B08	1	69	427	0	81	42	32	446	496

Table B5a. Shear Capacity/Load Ratios.

		phi Vn / Vu			Vn / V1			Vn / V2			Vc / V2		
Bridge	Span	STD	LRFD	INT	STD	LRFD	INT	STD	LRFD	INT	STD	LRFD	INT
7933	1	1.6	2.3	2.3	2.9	3.9	4.3	3.2	5	4.7	1.2	0.8	1.1
1829	1	1.1	1.3	1.2	1.8	2.1	2.2	2	2.9	2.4	1.2	0.6	0.8
1830	1	1	1.3	1.2	1.8	2.1	2.2	2	2.9	2.4	1.1	0.6	0.8
2332		1.5	2	1.7	2.7	3.5	3.2	2	2.8	2.3	1.4	1.6	1.2
	1	1.8	2.5	2	3.2	4.2	3.6	2.4	3.5	2.7	1.9	2.2	1.6
		1.9	2.7	2.4	3.5	4.5	4.3	2.6	3.7	3.3	1.9	2.4	2
	2&3	1.8	2.3	1.8	3.1	3.7	3	2.5	3.4	2.4	1.8	1.8	1
		1.5	1.8	1.5	2.5	3	2.6	2	2.7	2.1	1.6	1.8	1.2
		1.7	2.6	2.1	3.3	4.4	3.9	2.4	3.6	2.9	1.6	1.7	1.3
	4	1.9	2.8	2.1	3.5	4.8	3.9	2.6	3.9	2.9	2	2.4	1.7
		2.1	3	2.6	3.8	5	4.8	2.9	4.1	3.6	2.1	2.6	2.2
3831	1&3	1.4	2.2	2	2.6	3.7	3.7	2	3.1	2.8	1.1	1.6	1.2
		1.8	2.6	2.5	3.3	4.4	4.5	2.5	3.6	3.4	1.4	1.7	1.5
	2	1.1	1.3	1.5	2	2.2	2.7	1.5	2	2.1	0.9	0.7	0.9
		1.6	2.2	1.8	2.8	3.6	3	2.3	3.2	2.4	1.5	1.7	1
3848	1&3	0.8	1.4	1.3	1.8	2.6	2.9	2.1	3.6	3.4	0.9	0.9	1.3
		1.2	1.9	1.6	2.4	3.4	3.4	2.9	4.6	4.1	1.5	1.8	1.6
	2	1	1.2	1.1	2	2.1	2.2	2.3	2.8	2.5	1.5	0.7	0.9
3849	1&3	1	1.2	1.6	2	2.1	3.4	2.8	3.4	4.7	1	0.7	1.3
		1.2	1.6	2	2.6	3	4.1	3.6	4.7	5.8	1.3	1	1.6
	2	1	1	1.5	1.9	1.8	3	2.5	2.8	3.9	1	0.6	1.2
3854		0.6	1.2	1.2	1.3	2.2	2.4	1.5	2.9	2.9	0.6	0.9	1.3
	1&3	0.9	0.7	1.2	1.9	1.2	2.6	2.5	1.9	3.5	1.4	0.6	1.5
		1	1.9	1.6	2.1	3.4	3.3	2.4	4.4	3.9	1.2	2.1	1.7
	2	0.7	0.9	0.9	1.4	1.6	1.7	1.6	2.1	1.9	1.1	0.7	0.9
		0.8	0.9	1.1	1.7	1.6	2.2	2.1	2.5	2.8	1.2	0.7	1.1
4447	1	1.1	1.4	1.5	2.1	2.5	2.7	2.5	3.7	3.2	1.3	0.7	1.1
	2	1.2	1.7	1.6	2.3	2.9	3	2.7	4.3	3.6	1.3	0.7	1.1
9728	1&2	1.2	0.9	1.6	2.1	1.4	2.8	2.3	2	3.1	1.1	0.4	0.9
12693	1	1.1	1.2	1.4	2	2.1	2.6	2.3	3.3	3	1.2	0.7	1
	2	1.2	1.4	1.6	2.2	2.4	2.9	2.5	3.8	3.4	1.3	0.7	1.1
	3	1.1	1.3	1.5	2.1	2.3	2.8	2.5	3.6	3.3	1.2	0.7	1
12773	1&4	1	1	1.4	2.1	1.7	2.8	2.4	2.3	3.2	1.6	1.1	1.8
	2&3	1.1	1.3	1.3	2	2.2	2.2	2.1	2.7	2.4	1.5	0.8	1.1
12774	1&4	1	1.1	1.3	1.9	1.9	2.5	2.3	2.5	3	1.6	1.2	1.7
	2&3	1.1	1.3	1.2	2	2.2	2.2	2.1	2.7	2.3	1.5	0.8	1.1
12775	1	1	0.9	1.2	1.9	1.6	2.5	2.3	2	2.9	1.6	1.1	1.8
	2&3	1.1	1.1	1.3	2	1.8	2.2	2.2	2.3	2.4	1.5	0.7	1.1
	4(s9)	1.5	2	1.6	3	3.6	3.2	3.5	4.7	3.7	1.5	1.1	1.6
	4(s15)	1	1.1	1.3	1.9	1.9	2.6	2.2	2.5	3	1.5	1.1	1.6
12943	1	1.1	1.2	1.5	2	2.1	2.8	2.4	3.2	3.3	1.2	0.6	1
	2	1.3	1.7	1.9	2.4	3	3.4	2.8	4.6	4	1.3	0.7	1.2
	3	1.2	1.5	1.6	2.2	2.6	3	2.5	4	3.5	1.3	0.7	1.2
	4-A	1.1	1.2	1.5	1.9	2.2	2.8	2.3	3.4	3.2	1	0.6	1
	4-B	1.3	1.8	2	2.4	3.2	3.7	2.9	4.9	4.4	1.1	0.7	1.2
	4-C	1.3	1.8	2	2.4	3.1	3.7	2.8	4.8	4.3	1	0.7	1.1
	4-D	1.3	1.7	1.9	2.4	2.9	3.6	2.8	4.5	4.2	1	0.7	1
	4-E	0.9	1.1	1.3	1.7	1.9	2.4	2	2.9	2.8	1.1	0.7	1
	5	1.2	1.7	1.8	2.3	2.9	3.3	2.8	4.5	4	1.2	0.7	1.1

Table B5a. Shear Capacity/Load Ratios (cont).

		phi Vn / Vu			Vn / V1			Vn / V2			Vc / V2		
Bridge	Span	STD	LRFD	INT	STD	LRFD	INT	STD	LRFD	INT	STD	LRFD	INT
12943	6	1.3	1.7	1.8	2.4	2.9	3.4	2.8	4.5	3.9	1.3	0.7	1.2
	7	1.1	1.4	1.6	2.1	2.5	3.1	2.5	3.9	3.7	1	0.7	1
	8-A	0.8	1.3	1.2	1.6	2.2	2.3	2	3.3	2.9	1.1	0.9	1.2
	8-B	1	1.9	1.6	2.1	3.4	3.2	2.6	5	4.1	1	0.9	1.2
	8-C	1.1	1.9	1.8	2.2	3.3	3.6	2.8	4.8	4.5	1	0.9	1.2
	8-D	1.1	2.1	1.8	2.2	3.7	3.6	2.8	5.5	4.5	1	0.9	1.2
	8-E	0.8	1.3	1.2	1.6	2.3	2.4	2	3.4	3	1	0.9	1.2
12944	1	1	1.1	1.4	1.9	1.9	2.6	2.2	2.7	3	1.1	0.6	1
	2	1.2	1.4	1.6	2.2	2.4	2.9	2.6	3.3	3.3	1.4	0.6	1
	3	1.2	1.4	1.6	2.2	2.4	2.9	2.4	3.3	3.1	1.3	0.6	1
	4-F	1	1.1	1.2	1.9	1.8	2.3	2.3	2.6	2.7	1.5	0.9	1.3
	4-G	1.4	1.7	1.9	2.5	3	3.4	3	4.2	4.1	1.5	0.9	1.3
	4-H	1.4	1.7	1.8	2.5	3	3.4	3	4.2	4.1	1.5	0.9	1.3
	4-J	1.2	1.3	1.8	2.3	2.2	3.4	2.7	3.2	4	1.2	0.8	1.4
	4-K	1.2	1.3	1.8	2.3	2.2	3.4	2.7	3.2	4	1.2	0.8	1.4
	4-L	0.9	0.7	1.2	1.6	1.3	2.2	1.9	1.9	2.6	1.3	0.8	1.4
	5	1.2	1.3	1.7	2.3	2.2	3.1	2.7	3.2	3.7	1.4	0.8	1.2
	6	1.6	1.4	2.1	2.8	2.4	3.6	3	3.4	3.9	1.6	0.6	1.2
	7	1.1	1.2	1.5	2.1	2.2	2.9	2.6	3.1	3.5	1.3	0.7	1.1
	8-F	0.8	0.7	1	1.5	1.3	2	1.8	1.7	2.4	1.2	0.9	1.3
	8-G	1.1	1.7	1.6	2.1	3	3.2	2.6	4.1	3.9	1.1	1	1.3
	8-H	1.1	1.7	1.6	2.1	3	3.2	2.6	4.1	3.9	1.1	1	1.3
	8-J	1.1	1.7	1.6	2.1	3	3.2	2.6	4.1	3.9	1.1	1	1.3
	8-K	1.1	1.9	1.5	2.2	3.2	3	2.7	4.5	3.7	1.4	1.2	1.2
	8-L	0.8	0.9	1.1	1.5	1.5	2.1	1.9	2.1	2.5	1.2	0.9	1.3
B03	1	2.6	2.3	4	5	4	7.7	5.5	6	8.7	1.6	0.8	1.5
B09	1	2.6	2.3	4	5	4	7.7	5.5	6	8.7	1.6	0.8	1.5
B05	1	3.7	2.2	5.5	8	4.1	11.8	10.5	9.2	15.5	3.1	1.2	2.1
B08	1	3.7	2.2	5.5	8	4.1	11.8	10.5	9.2	15.5	3.1	1.2	2.1

Table B5b. Average Shear Capacity/Load Ratios.

	phi Vn / Vu			Vn / V1			Vn / V2			Vc / V2		
Bridges	STD	LRFD	INT	STD	LRFD	INT	STD	LRFD	INT	STD	LRFD	INT
Cracked	1.3	1.5	1.6	2.3	2.5	2.9	2.5	3.2	3.2	1.4	1.0	1.1
Uncracked	1.3	1.6	1.8	2.5	2.8	3.4	2.8	3.7	3.9	1.4	1.0	1.3

Table B6. Results of Table B5a Sorted By Ratio Magnitude.

Bridge	INTERIM Vn / V2	Bridge	INTERIM Vn / V2
3854, 2a	1.9	12693, 2	3.4
2332, 2&3b	2.1	3848, 1&3a	3.4
3831, 2a	2.1	3831, 1&3b	3.4
12774, 2&3	2.3	12994, 7	3.5
2332, 1a	2.3	12934, 3	3.5
12773, 2&3	2.4	3854, 1&3b	3.5
12775, 2&3	2.4	2332, 4c	3.6
2332, 2&3a	2.4	4447, 2	3.6
3831, 2b	2.4	12994, 8k	3.7
1830	2.4	12775, 4s9	3.7
12994, 8f	2.4	12994, 5	3.7
1829	2.4	12934, 7	3.7
3848, 2	2.5	3849, 2	3.9
12994, 8l	2.5	3854, 1&3c	3.9
12994, 4l	2.6	12994, 6	3.9
2332, 1b	2.7	12934, 6	3.9
12994, 4f	2.7	12994, 8g	3.9
12934, 4e	2.8	12994, 8h	3.9
3831, 1&3a	2.8	12994, 8j	3.9
3854, 2b	2.8	12934, 2	4.0
3854, 1&3a	2.9	12934, 5	4.0
2332, 4b	2.9	12994, 4j	4.0
2332, 4a	2.9	12994, 4k	4.0
12934, 8a	2.9	12994, 4h	4.1
12775, 1	2.9	12934, 8b	4.1
12774, 1&4	3.0	12994, 4g	4.1
12775, 4s15	3.0	3848, 1&3b	4.1
12693, 1	3.0	12934, 4d	4.2
12944, 1	3.0	12934, 4c	4.3
12934, 8e	3.0	12934, 4b	4.4
9728	3.1	12934, 8c	4.5
12994, 3	3.1	12934, 8d	4.5
12773, 1&4	3.2	3849 1&3a	4.7
4447, 1	3.2	7933	4.7
12934, 4a	3.2	3849 1&3b	5.8
12943, 1	3.3	B03	8.7
12693, 3	3.3	B05	8.7
12773, 3	3.3	B09	15.5
2332, 1c	3.3	B08	15.5
12994, 2	3.3		

Table B7. Crack Load Factors Based on Principal Tension Stress.

Bridge	$f_{t1} = 3.5\sqrt{f_c'}$		$f_{t2} = 6.4\sqrt{f_c'}$	
	1 ft	2 ft	1 ft	2 ft
7933	2.5	2.6	4.5	4.6
1829	3.4	3.5	6.3	6.4
1830	3.4	3.5	6.3	6.4
2332	2.5	2.7	4.5	4.7
3831	4.6	4.8	7.4	7.8
3848	2.6	2.8	4.2	4.4
3849	2.3	2.6	3.9	4.2
3854	4.4	4.7	7.1	7.6
4447	4.3	4.4	7.0	7.1
9728	2.7	2.8	5.2	5.2
12693	4.2	4.3	6.8	7.0
12773	1.9	2.1	3.7	3.9
12774	2.1	2.3	3.9	4.1
12775	1.9	2.1	3.7	3.9
12943	3.7	3.8	6.3	6.5
12944	2.9	3.0	5.1	5.3
B03	3.4	3.5	5.5	5.6
B09	3.4	3.5	5.5	5.6
B05	5.2	5.2	7.5	7.6
B08	5.2	5.2	7.5	7.6

Table B8. Bridges Sorted By Crack Load Factor Magnitude.

ft1, 1 ft		ft1, 2 ft		ft2, 1 ft		ft2, 2 ft	
Bridge	Factor	Bridge	Factor	Bridge	Factor	Bridge	Factor
12773	1.9	12773	2.1	12773	3.7	12773	3.9
12775	1.9	12775	2.1	12775	3.7	12775	3.9
12774	2.1	12774	2.3	3849	3.9	12774	4.1
3849	2.3	3849	2.6	12774	3.9	3849	4.2
7933	2.5	7933	2.6	3848	4.2	3848	4.4
2332	2.5	2332	2.7	2332	4.5	7933	4.6
3848	2.6	9728	2.8	7933	4.5	2332	4.7
9728	2.7	3848	2.8	12944	5.1	9728	5.2
12944	2.9	12944	3.0	9728	5.2	12944	5.3
1829	3.4	1829	3.5	B03	5.5	B03	5.6
1830	3.4	1830	3.5	B09	5.5	B09	5.6
B03	3.4	B03	3.5	1829	6.3	1829	6.4
B09	3.4	B09	3.5	1830	6.3	1830	6.4
12943	3.7	12943	3.8	12943	6.3	12943	6.5
12693	4.2	12693	4.3	12693	6.8	12693	7.0
4447	4.3	4447	4.4	4447	7.0	4447	7.1
3854	4.4	3854	4.7	3854	7.1	3854	7.6
3831	4.6	3831	4.8	3831	7.4	B05	7.6
B05	5.2	B05	5.2	B05	7.5	B08	7.6
B08	5.2	B08	5.2	B08	7.5	3831	7.8
Averages:							
Cracked	2.9		3.0		5.1		5.3
Uncracked	3.6		3.8		5.9		6.1

Table B9. Bridge Shear Forces Vu.

		Vu, LFR			Vu, LRFR				
BRIDGE	SPAN	5-DL	18-DL	23-DL	4-DL	5-DL	16-DL	17-DL	18-DL
7933	1		155				223		
1829	1		259				318		
1830	1	228	259	258	287	302	318	320	320
2332			63		101				
	1		67		100				
			60		91				
	2&3		105				163		
			108				147		
			57		92				
	4		60		91				
			54		88				
3831	1 &3		51		82				
			53		83				
	2		75				114		
			79				117		
3848	1 & 3		47		83				
			47		83				
	2		81				126		
3849	1 & 3		50		86				
			50		86				
	2		85				86		
3854		64	78	72	87	79	78	76	76
	1 & 3	52	64	59	65	59	59	57	57
		51	60	56	77	70	70	68	68
	2	92	109	105	131	135	139	137	135
		74	90	86	96	99	102	101	99
4447	1		193		235	249	264	266	265
	2		191		233	247	263	265	264
9728	1 & 2		245		291	307	322	328	328
12693	1	167	193	192	238	253	268	270	269
	2	167	193	192	239	253	268	270	269
	3	167	194	192	238	253	268	270	269
12773	1 & 4	77	89	84	142	135	131	130	129
	2 & 3	154	176	175	213	224	237	239	238
12774	1 & 4	78	90	85	145	137	133	132	131
	2 & 3	154	174	173	212	223	234	235	234
12775	1	77	89	84	142	134	131	130	129
	2 & 3	154	176	174	212	224	237	238	238
	4 (s=9')	87	99	95	155	152	149	146	144
	4 (s=15')	87	99	95	155	152	149	146	144
12943	1	202	244	241	274	290	308	309	308
	2	202	244	241	274	290	308	309	308
	3	202	244	241	274	290	308	309	308
	4-A	186	227	224	256	272	288	290	288
	4-B	186	227	224	256	272	288	290	288
	4-C	186	227	224	256	272	288	290	288
	4-D	186	227	224	256	272	288	290	288
	4-E	186	227	224	256	272	288	290	288
	5	168	203	199	235	247	260	260	258

Table B9. Bridge Shear Forces Vu (cont).

		Vu, LFR			Vu, LRFR				
BRIDGE	SPAN	5-DL	18-DL	23-DL	4-DL	5-DL	16-DL	17-DL	18-DL
12943	6	202	244	241	274	290	308	309	308
	7	174	211	207	242	255	268	269	267
	8-A	142	168	163	206	213	218	216	213
	8-B	142	168	163	206	213	218	216	213
	8-C	142	168	163	206	213	218	216	213
	8-D	142	168	163	206	213	218	216	213
	8-E	142	168	163	206	213	218	216	213
12944	1	170	200	198	235	249	263	265	264
	2	170	200	198	235	249	263	265	264
	3	170	200	198	235	249	263	265	264
	4-F	133	160	157	195	205	216	216	215
	4-G	133	160	157	195	205	216	216	215
	4-H	133	160	157	195	205	216	216	215
	4-J	133	160	157	195	205	216	216	215
	4-K	133	160	157	195	205	216	216	215
	4-L	133	160	157	195	205	216	216	215
	5	139	166	162	201	211	222	222	220
	6	170	200	198	235	249	263	265	264
	7	145	172	169	207	218	229	230	228
	8-F	128	151	147	188	196	203	202	200
	8-G	128	151	147	188	196	203	202	200
	8-H	128	151	147	188	196	203	202	200
	8-J	128	151	147	188	196	203	202	200
	8-K	128	151	147	188	196	203	202	200
	8-L	128	151	147	188	196	203	202	200
B03	1	67	80	78	108	113	118	117	116
B09	1	67	80	78	108	113	118	117	116
B05	1	31	35	34	67	61	57	54	54
B08	1	31	35	34	67	61	57	54	54

Table B10. Bridge Shear Forces V1.

		V1, LFR			V1, LRFR				
BRIDGE	SPAN	5-DL	18-DL	23-DL	4-DL	5-DL	16-DL	17-DL	18-DL
7933	1		119				175		
1829	1		199				250		
1830	1	175	199	189	204	214	250	258	258
2332			49		64				
	1		51		66				
			46		59				
	2&3		81				128		
			83				115		
			44		56				
	4		46		58				
			42		55				
3831	1 & 3		39		52				
			41		53				
	2		58				89		
			60				91		
3848	1 & 3		36		51				
			36		51				
	2		62				98		
3849	1 & 3		38		54		61		
			38		54		61		
	2		49				67		
3854		49	60	55	55	51	61	62	62
	1 & 3	40	50	46	41	38	46	46	46
		39	46	43	49	46	55	55	55
	2	71	84	81	86	90	109	111	110
		57	69	66	63	66	80	81	81
4447	1		148		162	172	207	215	215
	2		147		161	171	206	214	214
9728	1 & 2		189		206	217	253	263	264
12693	1	129	149	147	164	174	210	218	218
	2	129	149	147	164	174	210	218	218
	3	129	149	148	164	174	210	218	218
12773	1 & 4	59	68	65	90	87	103	105	105
	2 & 3	119	136	134	148	156	186	193	193
12774	1 & 4	60	69	66	92	89	104	107	107
	2 & 3	119	134	133	148	155	184	189	189
12775	1	59	68	65	90	87	103	105	105
	2 & 3	118	135	134	148	156	186	192	192
	4 (s=9')	67	76	73	99	99	116	118	118
	4 (s=15')	67	76	73	99	99	116	118	118
12943	1	155	188	185	186	197	241	250	250
	2	155	188	185	186	197	241	250	250
	3	155	188	185	186	197	241	250	250
	4-A	143	175	184	172	183	226	234	234
	4-B	143	175	184	172	183	226	234	234
	4-C	143	175	184	172	183	226	234	234
	4-D	143	175	184	172	183	226	234	234
	4-E	143	175	184	172	183	226	234	234
	5	129	156	176	156	165	204	210	209
	6	155	188	185	186	197	241	250	250

Table B10. Bridge Shear Forces V1 (cont).

		V1, LFR			V1, LRFR				
BRIDGE	SPAN	5-DL	18-DL	23-DL	4-DL	5-DL	16-DL	17-DL	18-DL
12943	7	134	162	178	162	171	210	217	217
	8-A	109	129	163	135	141	171	175	173
	8-B	109	129	163	135	141	171	175	173
	8-C	109	129	163	135	141	171	175	173
	8-D	109	129	163	135	141	171	175	173
	8-E	109	129	163	135	141	171	175	173
12944	1	130	154	152	160	170	207	214	214
	2	130	154	152	160	170	207	214	214
	3	130	154	152	160	170	207	214	214
	4-F	103	123	121	129	137	169	175	175
	4-G	103	123	121	129	137	169	175	175
	4-H	103	123	121	129	137	169	175	175
	4-J	103	123	121	129	137	169	175	175
	4-K	103	123	121	129	137	169	175	175
	4-L	103	123	121	129	137	169	175	175
	5	107	127	125	135	142	174	179	179
	6	130	154	152	160	170	207	214	214
	7	111	132	130	139	147	180	186	185
	8-F	99	116	113	125	131	159	164	163
	8-G	99	116	113	125	131	159	164	163
	8-H	99	116	113	125	131	159	164	163
	8-J	99	116	113	125	131	159	164	163
	8-K	99	116	113	125	131	159	164	163
	8-L	99	116	113	125	131	159	164	163
B03	1	52	61	60	71	75	92	95	95
B09	1	52	61	60	71	75	92	95	95
B05	1	24	27	26	41	38	44	44	44
B08	1	24	27	26	41	38	44	44	44

Table B11. Bridge Shear Forces V2.

		V2, LFR			V2, LRFR				
BRIDGE	SPAN	5-DL	18-DL	23-DL	4-DL	5-DL	16-DL	17-DL	18-DL
7933	1		110				151		
1829	1		190				226		
1830	1	170	190	189	191	199	226	231	232
2332			43		127				
	1		45		129				
			41		118				
	2&3		74				217		
			75				197		
			38		114				
	4		41		116				
			37		112				
3831	1 & 3		34		44				
			36		45				
	2		52				75		
			55				78		
3848	1 & 3		31		42				
			31		43				
	2		55				82		
3849	1 & 3		33		45				
			34		45				
	2		59		33		51		
3854		42	50	47	47	44	52	52	52
	1 & 3	34	41	38	35	33	39	39	39
		34	40	37	42	40	46	47	47
	2	64	75	72	76	79	93	95	94
		51	60	58	55	57	68	69	69
4447	1		140		149	156	183	188	188
	2		139		148	155	182	187	187
9728	1 & 2		181		192	200	227	236	236
12693	1	123	140	138	150	157	184	190	190
	2	123	140	138	150	157	185	190	190
	3	123	140	139	150	157	184	190	190
12773	1 & 4	54	60	58	78	75	87	89	89
	2 & 3	114	128	127	137	143	165	170	170
12774	1 & 4	54	61	58	79	76	88	90	90
	2 & 3	114	127	126	137	142	163	168	168
12775	1	54	60	58	78	75	87	89	89
	2 & 3	114	128	127	136	142	165	170	170
	4 (s=9')	61	68	66	86	85	99	100	99
	4 (s=15')	61	68	66	86	85	99	100	99
12943	1	146	172	170	168	177	210	216	216
	2	146	172	170	168	177	210	216	216
	3	146	172	170	168	177	210	216	216
	4-A	133	159	157	154	163	195	201	201
	4-B	133	159	157	154	163	195	201	201
	4-C	133	159	157	154	163	195	201	201
	4-D	133	159	157	154	163	195	201	201
	4-E	133	159	157	154	163	195	201	201
	5	119	141	138	140	146	175	180	179
	6	146	172	170	168	177	210	216	216

Table B11. Bridge Shear Forces V2 (cont).

		V2, LFR			V2, LRFR				
BRIDGE	SPAN	5-DL	18-DL	23-DL	4-DL	5-DL	16-DL	17-DL	18-DL
12943	7	124	147	144	145	152	181	187	186
	8-A	100	116	112	119	124	146	149	148
	8-B	100	116	112	119	124	146	149	148
	8-C	100	116	112	119	124	146	149	148
	8-D	100	116	112	119	124	146	149	148
	8-E	100	116	112	119	124	146	149	148
12944	1	123	143	141	146	153	180	186	186
	2	123	143	141	146	153	180	186	186
	3	123	143	141	146	153	180	186	186
	4-F	95	112	110	115	121	145	150	149
	4-G	95	112	110	115	121	145	150	149
	4-H	95	112	110	115	121	145	150	149
	4-J	95	112	110	115	121	145	150	149
	4-K	95	112	110	115	121	145	150	149
	4-L	95	112	110	115	121	145	150	149
	5	100	116	114	121	126	150	154	154
	6	123	143	141	146	153	180	186	186
	7	104	121	119	125	131	156	160	160
	8-F	92	105	103	112	116	137	141	140
	8-G	92	105	103	112	116	137	141	140
	8-H	92	105	103	112	116	137	141	140
	8-J	92	105	103	112	116	137	141	140
	8-K	92	105	103	112	116	137	141	140
	8-L	92	105	103	112	116	137	141	140
B03	1	48	55	54	63	65	79	81	80
B09	1	48	55	54	63	65	79	81	80
B05	1	21	23	22	34	32	36	36	36
B08	1	21	23	22	34	32	36	36	36

Table B12. Shear Capacity/Load Ratio Tables, Standard Code.

		Phi Vn/Vu, LFR			phi Vn/Vu, LRFR				
BRIDGE	SPAN	5-DL	18-DL	23-DL	4-DL	5-DL	16-DL	17-DL	18-DL
7933	1	0	2.2	0			1.5		
1829	1	0	1.3	0			1.1		
1830	1	1.5	1.3	1.3	1.2	1.1	1.1	1.1	1.1
2332			1.5		0.9				
	1		1.8		1.2				
			2		1.3				
	2&3		1.7				1.1		
			1.3				0.9		
			1.8		1.1				
	4		2		1.3				
			2.2		1.3				
3831	1 &3		1.5		0.9				
			1.9		1.2				
	2		1.1				0.7		
			1.6				1		
3848	1 & 3		1.7		1				
			2.3		1.3				
	2		1.6				1		
3849	1 & 3		2.2		1.3				
			2.8		1.7				
	2		1.8				1.8		
3854		1	0.8	0.9	0.7	0.8	0.8	0.8	0.8
	1 & 3	1.5	1.2	1.3	1.2	1.3	1.3	1.4	1.4
		1.8	1.5	1.6	1.2	1.3	1.3	1.4	1.4
	2	1.1	1	1	0.8	0.8	0.8	0.8	0.8
		1.4	1.1	1.2	1	1	1	1	1
4447	1		1.9				1.4		
	2		2				1.5		
9728	1 & 2		1.6				1.2		
12693	1	1.8	1.5	1.6	1.3	1.2	1.1	1.1	1.1
	2	1.9	1.6	1.6	1.3	1.2	1.2	1.2	1.2
	3	1.9	1.6	1.6	1.3	1.3	1.2	1.2	1.2
12773	1 & 4	2.2	1.9	2	1.2	1.2	1.3	1.3	1.3
	2 & 3	1.7	1.5	1.5	1.2	1.1	1.1	1.1	1.1
12774	1 & 4	2	1.8	1.9	1.1	1.2	1.2	1.2	1.2
	2 & 3	1.7	1.5	1.5	1.2	1.1	1.1	1.1	1.1
12775	1	2	1.8	1.9	1.1	1.2	1.2	1.2	1.2
	2 & 3	1.7	1.5	1.5	1.2	1.1	1.1	1.1	1.1
	4 (s=9')	3	2.7	2.8	1.7	1.7	1.8	1.8	1.8
	4 (s=15')	1.9	1.7	1.8	1.1	1.1	1.1	1.2	1.2
12943	1	1.7	1.4	1.4	1.3	1.2	1.1	1.1	1.1
	2	1.9	1.6	1.6	1.4	1.3	1.2	1.2	1.2
	3	1.7	1.4	1.4	1.3	1.2	1.1	1.1	1.1
	4-A	1.5	1.2	1.3	1.1	1	1	1	1
	4-B	1.9	1.5	1.6	1.4	1.3	1.2	1.2	1.2
	4-C	1.9	1.5	1.5	1.3	1.3	1.2	1.2	1.2
	4-D	1.8	1.5	1.5	1.3	1.3	1.2	1.2	1.2
	4-E	1.3	1.1	1.1	1	0.9	0.9	0.9	0.9
	5	1.8	1.5	1.5	1.3	1.2	1.2	1.2	1.2

Table B12. Shear Capacity/Load Ratio Tables, Standard Code (cont).

		Phi Vn/Vu, LFR			phi Vn/Vu, LRFR				
BRIDGE	SPAN	5-DL	18-DL	23-DL	4-DL	5-DL	16-DL	17-DL	18-DL
12943	6	1.9	1.6	1.6	1.4	1.3	1.2	1.2	1.2
	7	1.8	1.4	1.5	1.3	1.2	1.1	1.1	1.1
	8-A	1.5	1.2	1.3	1	1	1	1	1
	8-B	1.9	1.6	1.7	1.3	1.3	1.3	1.3	1.3
	8-C	2.1	1.8	1.8	1.4	1.4	1.4	1.4	1.4
	8-D	2.1	1.8	1.8	1.4	1.4	1.4	1.4	1.4
	8-E	1.5	1.3	1.3	1	1	1	1	1
12944	1	1.6	1.4	1.4	1.2	1.1	1	1	1
	2	1.8	1.5	1.6	1.3	1.2	1.2	1.2	1.2
	3	1.8	1.5	1.6	1.3	1.2	1.2	1.2	1.2
	4-F	1.5	1.3	1.3	1	1	0.9	0.9	0.9
	4-G	2	1.7	1.7	1.4	1.3	1.2	1.2	1.2
	4-H	2	1.7	1.7	1.4	1.3	1.2	1.2	1.2
	4-J	1.8	1.5	1.5	1.2	1.2	1.1	1.1	1.1
	4-K	1.8	1.5	1.5	1.2	1.2	1.1	1.1	1.1
	4-L	1.3	1.1	1.1	0.9	0.8	0.8	0.8	0.8
	5	1.9	1.6	1.6	1.3	1.3	1.2	1.2	1.2
	6	1.8	1.5	1.6	1.3	1.2	1.2	1.2	1.2
	7	1.8	1.6	1.6	1.3	1.2	1.2	1.2	1.2
	8-F	1.4	1.2	1.2	0.9	0.9	0.9	0.9	0.9
	8-G	2	1.7	1.7	1.4	1.3	1.3	1.3	1.3
	8-H	2	1.7	1.7	1.4	1.3	1.3	1.3	1.3
	8-J	2	1.7	1.7	1.4	1.3	1.3	1.3	1.3
	8-K	2.1	1.8	1.8	1.4	1.4	1.3	1.3	1.3
	8-L	1.4	1.2	1.2	1	0.9	0.9	0.9	0.9
B03	1	4.5	3.8	3.9	2.8	2.7	2.5	2.6	2.6
B09	1	4.5	3.8	3.9	2.8	2.7	2.5	2.6	2.6
B05	1	9.7	8.6	9	4.6	5	5.4	5.6	5.6
B08	1	9.7	8.6	9	4.6	5	5.4	5.6	5.6

Table B13. Vn/V1 Shear Capacity/Load Ratio Tables, Standard Code.

		Vn/V1, LFR			Vn/V1, LRFR				
BRIDGE	SPAN	5-DL	18-DL	23-DL	4-DL	5-DL	16-DL	17-DL	18-DL
7933	1		3.1				2.1		
1829	1		1.9	0			1.5		
1830	1	2.1	1.9	2	1.8	1.8	1.5	1.5	1.5
2332			2.1	0	1.6				
	1		2.6	0	2				
			2.8	0	2.2				
	2&3		2.5	0			1.6		
			1.8	0			1.3		
			2.6	0	2.1				
	4		2.8	0	2.3				
			3.1	0	2.4				
3831	1 &3		2.2	0	1.6				
			2.7	0	2.1				
	2		1.5	0			1		
			2.2	0			1.5		
3848	1 & 3		2.4	0	1.7				
			3.3	0	2.4				
	2		2.3	0			1.5		
3849	1 & 3		3.2	0	2.3				
			4.2	0	3				
	2		3.4	0			2.5		
3854		1.4	1.2	55.4	1.3	1.4	1.1	1.1	1.1
	1 & 3	2.2	1.8	45.7	2.1	2.3	1.9	1.9	1.9
		2.6	2.2	43	2.1	2.2	1.9	1.9	1.9
	2	1.7	1.4	80.9	1.4	1.3	1.1	1.1	1.1
		2	1.6	66.3	1.8	1.7	1.4	1.4	1.4
4447	1		2.7	0			1.9		
	2		2.9	0			2.1		
9728	1 & 2		2.2	0			1.7		
12693	1	2.6	2.2	147.4	2	1.9	1.6	1.5	1.5
	2	2.7	2.4	147.4	2.1	2	1.7	1.6	1.6
	3	2.7	2.4	147.6	2.1	2	1.7	1.6	1.6
12773	1 & 4	3.1	2.7	64.8	2.1	2.1	1.8	1.8	1.8
	2 & 3	2.4	2.1	134.5	1.9	1.8	1.5	1.5	1.5
12774	1 & 4	2.9	2.5	65.6	1.9	2	1.7	1.6	1.6
	2 & 3	2.4	2.1	132.9	1.9	1.8	1.5	1.5	1.5
12775	1	2.9	2.6	64.8	1.9	2	1.7	1.7	1.7
	2 & 3	2.4	2.1	134.1	1.9	1.8	1.5	1.5	1.5
	4 (s=9')	4.4	3.8	73.3	3	3	2.5	2.5	2.5
	4 (s=15')	2.8	2.5	73.3	1.9	1.9	1.6	1.6	1.6
12943	1	2.4	2	185.2	2	1.9	1.6	1.5	1.5
	2	2.7	2.3	185.2	2.3	2.2	1.8	1.7	1.7
	3	2.5	2.1	185.2	2.1	2	1.6	1.5	1.5
	4-A	2.2	1.8	183.7	1.8	1.7	1.4	1.3	1.3
	4-B	2.7	2.2	183.7	2.3	2.1	1.7	1.7	1.7
	4-C	2.7	2.2	183.7	2.2	2.1	1.7	1.6	1.6
	4-D	2.6	2.2	183.7	2.2	2.1	1.7	1.6	1.6
	4-E	1.9	1.6	183.7	1.6	1.5	1.2	1.2	1.2
	5	2.6	2.2	175.8	2.2	2.1	1.7	1.6	1.6

Table B13. Vn/V1 Shear Capacity/Load Ratio Tables, Standard Code (cont).

		Vn/V1, LFR			Vn/V1, LRFR				
BRIDGE	SPAN	5-DL	18-DL	23-DL	4-DL	5-DL	16-DL	17-DL	18-DL
12943	6	2.7	2.3	185.2	2.3	2.2	1.8	1.7	1.7
	7	2.5	2.1	177.7	2.1	2	1.6	1.6	1.6
	8-A	2.1	1.8	163.1	1.7	1.7	1.4	1.3	1.3
	8-B	2.8	2.4	163.1	2.3	2.2	1.8	1.7	1.8
	8-C	3	2.5	163.1	2.4	2.3	1.9	1.9	1.9
	8-D	3	2.5	163.1	2.4	2.3	1.9	1.9	1.9
	8-E	2.2	1.8	163.1	1.8	1.7	1.4	1.4	1.4
12944	1	2.3	2	152.2	1.9	1.8	1.5	1.4	1.4
	2	2.6	2.2	152.2	2.1	2	1.7	1.6	1.6
	3	2.6	2.2	152.2	2.1	2	1.7	1.6	1.6
	4-F	2.2	1.8	120.8	1.7	1.6	1.3	1.3	1.3
	4-G	2.9	2.4	120.8	2.3	2.2	1.7	1.7	1.7
	4-H	2.9	2.4	120.8	2.3	2.2	1.8	1.7	1.7
	4-J	2.6	2.2	120.8	2.1	1.9	1.6	1.5	1.5
	4-K	2.6	2.2	120.8	2.1	1.9	1.6	1.5	1.5
	4-L	1.9	1.6	120.8	1.5	1.4	1.1	1.1	1.1
	5	2.8	2.3	124.9	2.2	2.1	1.7	1.7	1.7
	6	2.6	2.2	152.2	2.1	2	1.7	1.6	1.6
	7	2.7	2.2	129.8	2.1	2	1.7	1.6	1.6
	8-F	2	1.7	113	1.6	1.5	1.2	1.2	1.2
	8-G	2.9	2.4	113	2.3	2.2	1.8	1.7	1.7
	8-H	2.9	2.4	113	2.3	2.2	1.8	1.7	1.7
	8-J	2.9	2.4	113	2.3	2.2	1.8	1.7	1.7
	8-K	3	2.6	113	2.4	2.3	1.9	1.8	1.8
	8-L	2	1.7	113	1.6	1.5	1.3	1.2	1.2
B03	1	6.4	5.4	59.8	4.7	4.5	3.6	3.5	3.5
B09	1	6.4	5.4	59.8	4.7	4.5	3.6	3.5	3.5
B05	1	14.1	12.4	25.9	8.3	8.9	7.6	7.6	7.6
B08	1	14.1	12.4	25.9	8.3	8.9	7.6	7.6	7.6

Table B14. Vn/V2 Shear Capacity/Load Ratio Tables, Standard Code.

		Vn/V2, LRFR					Vn/V2, LRFR		
BRIDGE	SPAN	5-DL	18-DL	23-DL	4-DL	5-DL	16-DL	17-DL	18-DL
7933	1		3.4				2.5		
1829	1	0	2	0			1.7		
1830	1	2.2	2	2	2	1.9	1.7	1.6	1.6
2332			2.4		0.8				
	1		2.9		1				
			3.2		1.1				
	2&3		2.7				0.9		
			2				0.8		
			3		1				
	4		3.2		1.1				
			3.5		1.2				
3831	1 &3		2.4		1.9				
			3.1		2.4				
	2		1.7				1.2		
			2.5				1.7		
3848	1 & 3		2.8		2.1				
			3.9		2.8				
	2		2.6				1.7		
3849	1 & 3		3.7		2.8				
			4.7		3.5				
	2		2.9				3.3		
3854		1.7	1.4	1.5	1.5	1.6	1.4	1.4	1.4
	1 & 3	2.5	2.1	2.3	2.5	2.6	2.3	2.2	2.2
		3	2.6	2.7	2.4	2.5	2.2	2.2	2.2
	2	1.8	1.6	1.6	1.5	1.5	1.3	1.2	1.3
		2.2	1.9	1.9	2	1.9	1.6	1.6	1.6
4447	1		2.9				2.2		
	2		3.1				2.4		
9728	1 & 2		2.3				1.9		
12693	1	2.7	2.4	2.4	2.2	2.1	1.8	1.7	1.7
	2	2.9	2.5	2.5	2.3	2.2	1.9	1.8	1.8
	3	2.9	2.5	2.5	2.3	2.2	1.9	1.8	1.8
12773	1 & 4	3.5	3.1	3.2	2.4	2.5	2.1	2.1	2.1
	2 & 3	2.5	2.2	2.2	2.1	2	1.7	1.7	1.7
12774	1 & 4	3.2	2.9	3	2.2	2.3	2	2	2
	2 & 3	2.5	2.2	2.2	2.1	2	1.7	1.7	1.7
12775	1	3.2	2.9	3	2.2	2.3	2	2	2
	2 & 3	2.5	2.2	2.2	2.1	2	1.7	1.7	1.7
	4 (s=9')	4.8	4.3	4.5	3.4	3.4	3	2.9	3
	4 (s=15')	3.1	2.8	2.9	2.2	2.2	1.9	1.9	1.9
12943	1	2.6	2.2	2.2	2.3	2.2	1.8	1.8	1.8
	2	2.9	2.5	2.5	2.5	2.4	2	2	2
	3	2.7	2.2	2.3	2.3	2.2	1.8	1.8	1.8
	4-A	2.3	2	2	2	1.9	1.6	1.5	1.5
	4-B	2.9	2.5	2.5	2.5	2.4	2	1.9	1.9
	4-C	2.9	2.4	2.4	2.5	2.4	2	1.9	1.9
	4-D	2.8	2.4	2.4	2.5	2.3	1.9	1.9	1.9
	4-E	2.1	1.8	1.8	1.8	1.7	1.4	1.4	1.4
	5	2.9	2.4	2.5	2.4	2.3	2	1.9	1.9

Table B14. Vn/V2 Shear Capacity/Load Ratio Tables, Standard Code (cont).

		Vn/V2, LRFR			Vn/V2, LRFR				
BRIDGE	SPAN	5-DL	18-DL	23-DL	4-DL	5-DL	16-DL	17-DL	18-DL
12943	6	2.9	2.5	2.5	2.5	2.4	2	2	2
	7	2.7	2.3	2.3	2.3	2.2	1.9	1.8	1.8
	8-A	2.3	2	2.1	2	1.9	1.6	1.6	1.6
	8-B	3.1	2.6	2.7	2.6	2.5	2.1	2	2.1
	8-C	3.3	2.9	2.9	2.8	2.7	2.3	2.2	2.2
	8-D	3.3	2.9	2.9	2.8	2.7	2.3	2.2	2.2
	8-E	2.4	2	2.1	2	1.9	1.6	1.6	1.6
12944	1	2.5	2.1	2.2	2.1	2	1.7	1.6	1.6
	2	2.8	2.4	2.4	2.4	2.2	1.9	1.8	1.8
	3	2.8	2.4	2.4	2.4	2.2	1.9	1.8	1.8
	4-F	2.3	2	2	1.9	1.8	1.5	1.5	1.5
	4-G	3.1	2.6	2.7	2.6	2.4	2	2	2
	4-H	3.1	2.7	2.7	2.6	2.4	2	2	2
	4-J	2.8	2.4	2.4	2.3	2.2	1.8	1.8	1.8
	4-K	2.8	2.4	2.4	2.3	2.2	1.8	1.8	1.8
	4-L	2	1.7	1.8	1.7	1.6	1.3	1.3	1.3
	5	3	2.6	2.6	2.5	2.4	2	1.9	1.9
	6	2.8	2.4	2.4	2.4	2.2	1.9	1.8	1.8
	7	2.9	2.5	2.5	2.4	2.3	1.9	1.9	1.9
	8-F	2.2	1.9	1.9	1.8	1.7	1.4	1.4	1.4
	8-G	3.1	2.7	2.7	2.5	2.4	2.1	2	2
	8-H	3.1	2.7	2.7	2.5	2.4	2.1	2	2
	8-J	3.1	2.7	2.7	2.5	2.4	2.1	2	2
	8-K	3.2	2.8	2.9	2.6	2.5	2.2	2.1	2.1
	8-L	2.2	1.9	2	1.8	1.7	1.5	1.4	1.4
B03	1	6.9	6	6.1	5.3	5.1	4.2	4.1	4.1
B09	1	6.9	6	6.1	5.3	5.1	4.2	4.1	4.1
B05	1	16.3	14.6	15.3	10.1	10.7	9.3	9.3	9.3
B08	1	16.3	14.6	15.3	10.1	10.7	9.3	9.3	9.3

Table B15. Vc/V2 Shear Capacity/Load Ratio Tables, Standard Code.

		Vc/V2, LFR			Vc/V2, LRFR				
BRIDGE	SPAN	5-DL	18-DL	23-DL	4-DL	5-DL	16-DL	17-DL	18-DL
7933	1	0	1.3	0			0.9		
1829	1	0	1.2	0			1		
1830	1	1.3	1.2	1.2	1.2	1.1	1	1	1
2332			1.7		0.6				
	1		2.3		0.8				
			2.3		0.8				
	2&3		2				0.7		
			1.6				0.6		
			2		0.7				
	4		2.5		0.9				
			2.6		0.8				
3831	1 &3		1.4		1.1				
			1.7		1.4				
	2		1				0.7		
			1.7				1.2		
3848	1 & 3		1.3		0.9				
			2		1.5				
	2		1.7				1.1		
3849	1 & 3		1.2		0.9				
			1.7		1.2				
	2		1.2				1.3		
3854		0.7	0.6	0.6	0.6	0.7	0.6	0.6	0.6
	1 & 3	1.4	1.2	1.3	1.4	1.5	1.3	1.3	1.3
		1.5	1.3	1.4	1.2	1.3	1.1	1.1	1.1
	2	1.2	1.1	1.1	1.1	1	0.9	0.8	0.9
		1.3	1.1	1.1	1.2	1.1	1	0.9	0.9
4447	1		1.5				1.2		
	2		1.5				1.2		
9728	1 & 2		1.1				0.9		
12693	1	1.4	1.3	1.3	1.2	1.1	1	0.9	0.9
	2	1.4	1.3	1.3	1.2	1.1	1	0.9	0.9
	3	1.4	1.3	1.3	1.2	1.1	1	0.9	0.9
12773	1 & 4	2.3	2.1	2.2	1.6	1.7	1.4	1.4	1.4
	2 & 3	1.7	1.5	1.5	1.4	1.4	1.2	1.2	1.2
12774	1 & 4	2.2	2	2.1	1.5	1.6	1.4	1.4	1.4
	2 & 3	1.7	1.5	1.5	1.4	1.4	1.2	1.2	1.2
12775	1	2.3	2.1	2.2	1.6	1.7	1.4	1.4	1.4
	2 & 3	1.7	1.5	1.5	1.4	1.4	1.2	1.2	1.2
	4 (s=9')	2	1.8	1.9	1.4	1.4	1.2	1.2	1.2
	4 (s=15')	2	1.8	1.9	1.4	1.4	1.2	1.2	1.2
12943	1	1.3	1.1	1.1	1.1	1.1	0.9	0.9	0.9
	2	1.3	1.1	1.1	1.2	1.1	0.9	0.9	0.9
	3	1.3	1.1	1.1	1.2	1.1	0.9	0.9	0.9
	4-A	1.1	0.9	0.9	0.9	0.9	0.7	0.7	0.7
	4-B	1.1	0.9	1	1	0.9	0.8	0.7	0.7
	4-C	1.1	0.9	0.9	0.9	0.9	0.7	0.7	0.7
	4-D	1.1	0.9	0.9	0.9	0.9	0.7	0.7	0.7
	4-E	1.1	0.9	0.9	1	0.9	0.8	0.7	0.7
	5	1.2	1	1	1	1	0.8	0.8	0.8

Table B15. Vc/V2 Shear Capacity/Load Ratio Tables, Standard Code (cont).

		Vc/V2, LFR			Vc/V2, LRFR				
BRIDGE	SPAN	5-DL	18-DL	23-DL	4-DL	5-DL	16-DL	17-DL	18-DL
12943	6	1.3	1.1	1.1	1.2	1.1	0.9	0.9	0.9
	7	1.1	0.9	1	1	0.9	0.8	0.7	0.7
	8-A	1.3	1.1	1.1	1.1	1	0.9	0.8	0.8
	8-B	1.2	1	1.1	1	1	0.8	0.8	0.8
	8-C	1.1	1	1	1	0.9	0.8	0.8	0.8
	8-D	1.1	1	1	1	0.9	0.8	0.8	0.8
	8-E	1.2	1	1.1	1	1	0.8	0.8	0.8
12944	1	1.3	1.1	1.1	1.1	1	0.9	0.8	0.8
	2	1.5	1.3	1.3	1.2	1.2	1	1	1
	3	1.5	1.3	1.3	1.2	1.2	1	1	1
	4-F	1.6	1.4	1.4	1.3	1.2	1	1	1
	4-G	1.6	1.3	1.4	1.3	1.2	1	1	1
	4-H	1.6	1.4	1.4	1.3	1.2	1	1	1
	4-J	1.3	1.1	1.1	1.1	1	0.8	0.8	0.8
	4-K	1.3	1.1	1.1	1.1	1	0.8	0.8	0.8
	4-L	1.4	1.2	1.2	1.1	1.1	0.9	0.9	0.9
	5	1.5	1.3	1.3	1.2	1.2	1	1	1
	6	1.5	1.3	1.3	1.2	1.2	1	1	1
	7	1.4	1.2	1.3	1.2	1.1	1	0.9	0.9
	8-F	1.4	1.2	1.3	1.2	1.1	0.9	0.9	0.9
	8-G	1.3	1.2	1.2	1.1	1.1	0.9	0.9	0.9
	8-H	1.3	1.2	1.2	1.1	1.1	0.9	0.9	0.9
	8-J	1.3	1.2	1.2	1.1	1.1	0.9	0.9	0.9
	8-K	1.6	1.4	1.5	1.3	1.3	1.1	1.1	1.1
	8-L	1.4	1.2	1.2	1.1	1.1	0.9	0.9	0.9
B03	1	1.9	1.7	1.7	1.5	1.4	1.2	1.2	1.2
B09	1	1.9	1.7	1.7	1.5	1.4	1.2	1.2	1.2
B05	1	4.8	4.3	4.5	3	3.2	2.7	2.7	2.7
B08	1	4.8	4.3	4.5	3	3.2	2.7	2.7	2.7

Table B16. Shear Capacity/Load Ratio Tables, 1979 Interim.

			phi Vn/Vu, LFR				phi Vn/Vu, LRFR		
BRIDGE	SPAN	5-DL	18-DL	23-DL	4-DL	5-DL	16-DL	17-DL	18-DL
7933	1		3.2				2.2		
1829	1		1.9				1.3		
1830	1	1.8	1.9	1.5	1.4	1.3	1.3	1.2	1.2
2332			7.8		1.1				
	1		7.4		1.3				
			8.2		1.6				
	2&3		4.7				1.1		
			4.6				0.9		
			8.7		1.4				
	4		8.2		1.4				
			9.1		1.6				
3831	1 & 3		9.7		1.3				
			9.4		1.6				
	2		6.6				0.9		
			6.3				1.1		
3848	1 & 3		10.6		1.5				
			10.4		1.9				
	2		6.1				1.1		
3849	1 & 3		9.9		2.1				
			9.8		2.6				
	2		5.8				2.7		
3854		1.9	6.3	1.7	1.4	1.5	1.5	1.6	1.6
	1 & 3	2.1	7.7	1.8	1.7	1.8	1.9	1.9	1.9
		2.9	8.3	2.6	1.9	2.1	2.1	2.1	2.2
	2	1.4	4.5	1.2	1	0.9	0.9	0.9	1
		1.8	5.5	1.6	1.4	1.4	1.3	1.3	1.4
4447	1		2.6				1.7		
	2		2.6				1.9		
9728	1 & 2		2				1.6		
12693	1	2.3	2.6	2	1.6	1.5	1.5	1.4	1.5
	2	2.5	2.6	2.2	1.8	1.7	1.6	1.6	1.6
	3	2.5	2.5	2.2	1.8	1.7	1.6	1.6	1.6
12773	1 & 4	2.9	5.6	2.6	1.6	1.6	1.7	1.7	1.7
	2 & 3	1.8	2.8	1.6	1.3	1.3	1.2	1.2	1.2
12774	1 & 4	2.7	5.5	2.4	1.4	1.5	1.6	1.6	1.6
	2 & 3	1.8	2.8	1.6	1.3	1.3	1.2	1.2	1.2
12775	1	2.6	5.6	2.4	1.4	1.5	1.5	1.6	1.6
	2 & 3	1.8	2.8	1.6	1.3	1.3	1.2	1.2	1.2
	4 (s=9')	3.2	5	2.9	1.8	1.8	1.9	1.9	1.9
	4 (s=15')	2.6	5	2.4	1.5	1.5	1.5	1.6	1.6
12943	1	2.3	2	1.9	1.7	1.6	1.5	1.5	1.5
	2	2.7	2	2.3	2	1.9	1.8	1.8	1.8
	3	2.4	2	2	1.8	1.7	1.6	1.6	1.6
	4-A	2.1	2.2	1.8	1.6	1.5	1.4	1.4	1.4
	4-B	2.9	2.2	2.4	2.1	2	1.9	1.9	1.9
	4-C	2.8	2.2	2.3	2.1	1.9	1.8	1.8	1.8
	4-D	2.7	2.2	2.3	2	1.9	1.8	1.8	1.8
	4-E	1.8	2.2	1.5	1.3	1.3	1.2	1.2	1.2
	5	2.7	2.4	2.2	1.9	1.8	1.7	1.7	1.7

Table B16. Shear Capacity/Load Ratio Tables, 1979 Interim (cont).

		phi Vn/Vu, LFR			phi Vn/Vu, LRFR				
BRIDGE	SPAN	5-DL	18-DL	23-DL	4-DL	5-DL	16-DL	17-DL	18-DL
12943	6	2.7	2	2.3	2	1.9	1.8	1.8	1.8
	7	2.6	2.3	2.2	1.9	1.8	1.7	1.7	1.7
	8-A	2.1	2.9	1.9	1.5	1.4	1.4	1.4	1.4
	8-B	3	2.9	2.6	2.1	2	2	2	2
	8-C	3.4	2.9	2.9	2.3	2.2	2.2	2.2	2.2
	8-D	3.4	2.9	2.9	2.3	2.2	2.2	2.2	2.2
	8-E	2.2	2.9	2	1.5	1.5	1.5	1.5	1.5
12944	1	2.2	2.5	1.9	1.6	1.5	1.4	1.4	1.4
	2	2.3	2.5	2	1.7	1.6	1.5	1.5	1.5
	3	2.3	2.5	2	1.7	1.6	1.5	1.5	1.5
	4-F	1.8	3.1	1.5	1.2	1.2	1.1	1.1	1.1
	4-G	2.7	3.1	2.3	1.9	1.8	1.7	1.7	1.7
	4-H	2.7	3.1	2.3	1.8	1.8	1.7	1.7	1.7
	4-J	2.7	3.1	2.3	1.8	1.7	1.7	1.7	1.7
	4-K	2.7	3.1	2.3	1.8	1.7	1.7	1.7	1.7
	4-L	1.7	3.1	1.4	1.2	1.1	1	1	1.1
	5	2.6	3	2.2	1.8	1.7	1.6	1.6	1.6
	6	2.3	2.5	2	1.7	1.6	1.5	1.5	1.5
	7	2.5	2.9	2.2	1.8	1.7	1.6	1.6	1.6
	8-F	1.8	3.3	1.6	1.3	1.2	1.2	1.2	1.2
	8-G	3	3.3	2.6	2.1	2	1.9	1.9	1.9
	8-H	3	3.3	2.6	2.1	2	1.9	1.9	1.9
	8-J	3	3.3	2.6	2.1	2	1.9	1.9	1.9
	8-K	2.8	3.3	2.4	1.9	1.8	1.8	1.8	1.8
	8-L	1.9	3.3	1.7	1.3	1.3	1.2	1.2	1.3
B03	1	7	6.2	6	4.3	4.1	4	4	4
B09	1	7	6.2	6	4.3	4.1	4	4	4
B05	1	14.3	14	13.3	6.7	7.4	7.9	8.2	8.3
B08	1	14.3	14	13.3	6.7	7.4	7.9	8.2	8.3

Table B17. Vn/V1 Shear Capacity/Load Ratio Tables, 1979 Interim.

		Vn/V1, LFR			Vn/V1, LRFR				
BRIDGE	SPAN	5-DL	18-DL	23-DL	4-DL	5-DL	16-DL	17-DL	18-DL
7933	1		4.6				3.1		
1829	1		2.2				1.8		
1830	1	3.1	2.2	2.4	2.2	2.1	1.8	1.7	1.7
2332			2.5		1.9				
	1		2.9		2.2				
			3.5		2.7				
	2&3		2.4				1.5		
			1.9				1.3		
			3.2		2.5				
	4		3.1		2.5				
			3.9		3				
3831	1 & 3		3.1		2.3				
			3.8		2.9				
	2		2.1				1.3		
			2.4				1.6		
3848	1 & 3		3.9		2.8				
			4.7		3.3				
	2		2.5				1.6		
3849	1 & 3		5.3		3.8				
			6.7		4.7				
	2		5.3				3.9		
3854		11.1	2.2	2.4	2.4	2.6	2.2	2.1	2.1
	1 & 3	13.6	2.4	2.6	2.9	3.1	2.6	2.6	2.6
		14.1	3.5	3.8	3.3	3.5	3	2.9	2.9
	2	7.8	1.7	1.8	1.7	1.6	1.3	1.3	1.3
		9.7	2.2	2.3	2.4	2.3	1.9	1.8	1.9
4447	1		3.5				2.5		
	2		3.9				2.8		
9728	1 & 2		3				2.2		
12693	1	4.3	2.9	2.9	2.6	2.5	2.1	2	2
	2	4.3	3.1	3.2	2.9	2.7	2.2	2.2	2.1
	3	4.3	3.1	3.2	2.9	2.7	2.2	2.2	2.2
12773	1 & 4	9.2	3.6	3.8	2.7	2.8	2.4	2.3	2.3
	2 & 3	4.6	2.3	2.3	2.1	2	1.7	1.6	1.6
12774	1 & 4	9.1	3.3	3.5	2.5	2.6	2.2	2.2	2.2
	2 & 3	4.6	2.3	2.4	2.1	2	1.7	1.7	1.7
12775	1	9.2	3.3	3.5	2.5	2.6	2.2	2.1	2.1
	2 & 3	4.6	2.3	2.3	2.1	2	1.7	1.6	1.6
	4 (s=9')	8.2	4.1	4.2	3.1	3.2	2.7	2.6	2.6
	4 (s=15')	8.2	3.3	3.5	2.6	2.6	2.2	2.1	2.2
12943	1	3.5	2.8	2.8	2.8	2.6	2.2	2.1	2.1
	2	3.5	3.2	3.3	3.3	3.1	2.5	2.4	2.4
	3	3.5	2.9	2.9	2.9	2.7	2.2	2.2	2.2
	4-A	3.8	2.5	2.4	2.6	2.4	2	1.9	1.9
	4-B	3.8	3.4	3.3	3.5	3.3	2.7	2.6	2.6
	4-C	3.8	3.3	3.2	3.4	3.2	2.6	2.5	2.5
	4-D	3.8	3.2	3.1	3.3	3.1	2.5	2.4	2.4
	4-E	3.8	2.2	2.1	2.2	2.1	1.7	1.6	1.6
	5	4.3	3.2	2.8	3.2	3	2.4	2.4	2.4

Table B17. Vn/V1 Shear Capacity/Load Ratio Tables, 1979 Interim (cont).

		Vn/V1, LFR			Vn/V1, LRFR				
BRIDGE	SPAN	5-DL	18-DL	23-DL	4-DL	5-DL	16-DL	17-DL	18-DL
12943	6	3.5	3.2	3.3	3.3	3.1	2.5	2.4	2.4
	7	4.1	3.1	2.8	3.1	2.9	2.4	2.3	2.3
	8-A	5	2.6	2.1	2.5	2.4	2	1.9	1.9
	8-B	5	3.7	2.9	3.5	3.4	2.8	2.7	2.8
	8-C	5	4.1	3.2	3.9	3.8	3.1	3	3.1
	8-D	5	4.1	3.2	3.9	3.8	3.1	3	3.1
	8-E	5	2.7	2.2	2.6	2.5	2.1	2	2
12944	1	4.2	2.7	2.8	2.6	2.5	2	2	2
	2	4.2	2.9	2.9	2.8	2.6	2.1	2.1	2.1
	3	4.2	2.9	2.9	2.8	2.6	2.1	2.1	2.1
	4-F	5.4	2.2	2.2	2.1	2	1.6	1.5	1.5
	4-G	5.4	3.3	3.3	3.1	2.9	2.4	2.3	2.3
	4-H	5.4	3.2	3.3	3.1	2.9	2.4	2.3	2.3
	4-J	5.4	3.2	3.3	3.1	2.9	2.3	2.3	2.3
	4-K	5.4	3.2	3.3	3.1	2.9	2.3	2.3	2.3
	4-L	5.4	2	2.1	1.9	1.8	1.5	1.4	1.4
	5	5.1	3.2	3.2	3	2.8	2.3	2.2	2.2
	6	4.2	2.9	2.9	2.8	2.6	2.1	2.1	2.1
	7	4.9	3.1	3.1	2.9	2.7	2.2	2.2	2.2
	8-F	5.6	2.3	2.3	2.1	2	1.7	1.6	1.6
	8-G	5.6	3.7	3.8	3.4	3.3	2.7	2.6	2.6
	8-H	5.6	3.7	3.8	3.4	3.3	2.7	2.6	2.6
	8-J	5.6	3.7	3.8	3.4	3.3	2.7	2.6	2.6
	8-K	5.6	3.4	3.5	3.2	3	2.5	2.4	2.5
	8-L	5.6	2.4	2.5	2.2	2.1	1.7	1.7	1.7
B03	1	10.6	8.5	8.7	7.3	7	5.6	5.5	5.5
B09	1	10.6	8.5	8.7	7.3	7	5.6	5.5	5.5
B05	1	22.9	18.3	19.2	12.2	13.1	11.2	11.2	11.2
B08	1	22.9	18.3	19.2	12.2	13.1	11.2	11.2	11.2

Table B18. Vn/V2 Shear Capacity/Load Ratio Tables, 1979 Interim.

		Vn/V2, LFR			Vn/V2, LRFR				
BRIDGE	SPAN	5-DL	18-DL	23-DL	4-DL	5-DL	16-DL	17-DL	18-DL
7933	1		5				3.6		
1829	1		2.3				2		
1830	1	2.6	2.3	2.4	2.3	2.2	2	1.9	1.9
2332			2.9		1				
	1		3.3		1.1				
			3.9		1.4				
	2&3		2.7				0.9		
			2				0.8		
			3.6		1.2				
	4		3.6		1.2				
			4.4		1.4				
3831	1 & 3		3.5		2.7				
			4.2		3.3				
	2		2.3				1.6		
			2.7				1.9		
3848	1 & 3		4.6		3.3				
			5.5		4				
	2		2.9				1.9		
3849	1 & 3		6.2		4.5				
			7.5		5.6				
	2		4.4				5.1		
3854		3.1	2.6	2.8	2.8	3	2.6	2.5	2.5
	1 & 3	3.5	2.9	3.2	3.4	3.6	3.1	3.1	3.1
		4.7	4.1	4.4	3.8	4.1	3.5	3.5	3.5
	2	2.2	1.9	2	1.9	1.8	1.5	1.5	1.5
		3	2.5	2.6	2.7	2.6	2.2	2.2	2.2
4447	1		3.7				2.8		
	2		4.1				3.1		
9728	1 & 2		3.1				2.5		
12693	1	3.5	3.1	3.1	2.9	2.8	2.4	2.3	2.3
	2	3.8	3.4	3.4	3.1	3	2.5	2.5	2.5
	3	3.8	3.4	3.4	3.1	3	2.5	2.5	2.5
12773	1 & 4	4.6	4.1	4.3	3.2	3.3	2.8	2.8	2.8
	2 & 3	2.7	2.4	2.5	2.3	2.2	1.9	1.8	1.8
12774	1 & 4	4.3	3.8	4	2.9	3	2.6	2.6	2.6
	2 & 3	2.7	2.5	2.5	2.3	2.2	1.9	1.9	1.9
12775	1	4.2	3.7	3.9	2.9	3	2.6	2.5	2.5
	2 & 3	2.7	2.5	2.5	2.3	2.2	1.9	1.8	1.8
	4 (s=9')	5.1	4.6	4.7	3.6	3.7	3.2	3.1	3.1
	4 (s=15')	4.2	3.7	3.9	3	3	2.6	2.5	2.6
12943	1	3.6	3	3.1	3.1	2.9	2.5	2.4	2.4
	2	4.2	3.5	3.6	3.6	3.4	2.9	2.8	2.8
	3	3.7	3.1	3.2	3.2	3	2.6	2.5	2.5
	4-A	3.3	2.8	2.8	2.9	2.7	2.3	2.2	2.2
	4-B	4.5	3.8	3.8	3.9	3.7	3.1	3	3
	4-C	4.4	3.7	3.7	3.8	3.6	3	2.9	2.9
	4-D	4.3	3.6	3.6	3.7	3.5	2.9	2.8	2.8
	4-E	2.8	2.4	2.4	2.4	2.3	1.9	1.9	1.9
	5	4.2	3.5	3.6	3.6	3.4	2.8	2.8	2.8

Table B18. Vn/V2 Shear Capacity/Load Ratio Tables, 1979 Interim (cont).

		Vn/V2, LFR			Vn/V2, LRFR				
BRIDGE	SPAN	5-DL	18-DL	23-DL	4-DL	5-DL	16-DL	17-DL	18-DL
12943	6	4.2	3.5	3.6	3.6	3.4	2.9	2.8	2.8
	7	4	3.4	3.5	3.5	3.3	2.8	2.7	2.7
	8-A	3.4	2.9	3	2.8	2.7	2.3	2.3	2.3
	8-B	4.8	4.1	4.2	4	3.8	3.3	3.2	3.2
	8-C	5.3	4.6	4.7	4.4	4.3	3.6	3.6	3.6
	8-D	5.3	4.6	4.7	4.4	4.3	3.6	3.6	3.6
	8-E	3.6	3.1	3.2	3	2.9	2.4	2.4	2.4
12944	1	3.4	2.9	3	2.9	2.7	2.3	2.3	2.3
	2	3.6	3.1	3.1	3	2.9	2.4	2.4	2.4
	3	3.6	3.1	3.1	3	2.9	2.4	2.4	2.4
	4-F	2.8	2.4	2.4	2.3	2.2	1.8	1.8	1.8
	4-G	4.2	3.6	3.7	3.5	3.3	2.8	2.7	2.7
	4-H	4.2	3.6	3.6	3.5	3.3	2.7	2.7	2.7
	4-J	4.2	3.6	3.6	3.4	3.3	2.7	2.7	2.7
	4-K	4.2	3.6	3.6	3.4	3.3	2.7	2.7	2.7
	4-L	2.6	2.3	2.3	2.2	2.1	1.7	1.7	1.7
	5	4	3.5	3.5	3.3	3.2	2.7	2.6	2.6
	6	3.6	3.1	3.1	3	2.9	2.4	2.4	2.4
	7	3.9	3.3	3.4	3.2	3.1	2.6	2.5	2.5
	8-F	2.9	2.5	2.6	2.4	2.3	1.9	1.9	1.9
	8-G	4.7	4.1	4.2	3.8	3.7	3.1	3.1	3.1
	8-H	4.7	4.1	4.2	3.8	3.7	3.1	3.1	3.1
	8-J	4.7	4.1	4.2	3.8	3.7	3.1	3.1	3.1
	8-K	4.4	3.8	3.9	3.6	3.4	2.9	2.8	2.9
	8-L	3	2.6	2.7	2.5	2.4	2	2	2
B03	1	10.8	9.4	9.6	8.3	7.9	6.6	6.4	6.5
B09	1	10.8	9.4	9.6	8.3	7.9	6.6	6.4	6.5
B05	1	24	21.6	22.5	14.8	15.7	13.7	13.7	13.7
B08	1	24	21.6	22.5	14.8	15.7	13.7	13.7	13.7

Table B19. Vc/V2 Shear Capacity/Load Ratio Tables, 1979 Interim.

		Vc/V2, LFR			Vc/V2, LRFR				
BRIDGE	SPAN	5-DL	18-DL	23-DL	4-DL	5-DL	16-DL	17-DL	18-DL
7933	1		1.1				0.8		
1829	1		0.8				0.7		
1830	1	0.9	0.8	0.8	0.8	0.8	0.7	0.7	0.7
2332			1.5		0.5				
	1		1.9		0.7				
			2.4		0.8				
	2&3		1.1				0.4		
			1.2				0.5		
			1.6		0.5				
	4		2.1		0.7				
			2.7		0.9				
3831	1 & 3		1.5		1.2				
			1.8		1.4				
	2		1				0.7		
			1.1				0.7		
3848	1 & 3		1.7		1.3				
			2.1		1.5				
	2		1.1				0.7		
3849	1 & 3		1.7		1.2				
			2		1.5				
	2		1.4				1.6		
3854		1.4	1.2	1.2	1.2	1.3	1.1	1.1	1.1
	1 & 3	1.5	1.3	1.4	1.5	1.6	1.4	1.4	1.4
		2.1	1.8	1.9	1.7	1.8	1.5	1.5	1.5
	2	1	0.9	0.9	0.9	0.8	0.7	0.7	0.7
		1.2	1	1	1.1	1.1	0.9	0.9	0.9
4447	1		1.2				0.9		
	2		1.2				0.9		
9728	1 & 2		0.9				0.7		
12693	1	1.2	1.1	1.1	1	0.9	0.8	0.8	0.8
	2	1.2	1.1	1.1	1	0.9	0.8	0.8	0.8
	3	1.2	1.1	1.1	1	0.9	0.8	0.8	0.8
12773	1 & 4	2.5	2.2	2.3	1.7	1.8	1.6	1.5	1.5
	2 & 3	1.3	1.1	1.1	1.1	1	0.9	0.9	0.9
12774	1 & 4	2.5	2.2	2.3	1.7	1.8	1.5	1.5	1.5
	2 & 3	1.3	1.1	1.2	1.1	1	0.9	0.9	0.9
12775	1	2.5	2.2	2.3	1.7	1.8	1.6	1.5	1.5
	2 & 3	1.3	1.1	1.1	1.1	1	0.9	0.9	0.9
	4 (s=9')	2.2	2	2.1	1.6	1.6	1.4	1.4	1.4
	4 (s=15')	2.2	2	2.1	1.6	1.6	1.4	1.4	1.4
12943	1	1.1	0.9	1	1	0.9	0.8	0.7	0.7
	2	1.2	1	1	1.1	1	0.8	0.8	0.8
	3	1.2	1	1	1.1	1	0.8	0.8	0.8
	4-A	1	0.8	0.8	0.8	0.8	0.7	0.6	0.6
	4-B	1.2	1	1	1	1	0.8	0.8	0.8
	4-C	1.1	0.9	0.9	0.9	0.9	0.7	0.7	0.7
	4-D	1	0.8	0.8	0.8	0.8	0.7	0.7	0.7
	4-E	1	0.8	0.8	0.8	0.8	0.7	0.6	0.6
	5	1.1	0.9	0.9	0.9	0.9	0.7	0.7	0.7

Table B19. Vc/V2 Shear Capacity/Load Ratio Tables, 1979 Interim (cont).

		Vc/V2, LFR			Vc/V2, LRFR				
BRIDGE	SPAN	5-DL	18-DL	23-DL	4-DL	5-DL	16-DL	17-DL	18-DL
12943	6	1.2	1	1	1.1	1	0.8	0.8	0.8
	7	1.1	0.9	0.9	0.9	0.9	0.7	0.7	0.7
	8-A	1.4	1.2	1.3	1.2	1.2	1	1	1
	8-B	1.4	1.2	1.3	1.2	1.2	1	1	1
	8-C	1.4	1.2	1.3	1.2	1.1	1	1	1
	8-D	1.4	1.2	1.3	1.2	1.1	1	1	1
	8-E	1.4	1.2	1.3	1.2	1.2	1	1	1
12944	1	1.2	1	1	1	0.9	0.8	0.8	0.8
	2	1.1	1	1	0.9	0.9	0.8	0.7	0.7
	3	1.1	1	1	0.9	0.9	0.8	0.7	0.7
	4-F	1.3	1.1	1.2	1.1	1.1	0.9	0.9	0.9
	4-G	1.4	1.2	1.2	1.1	1.1	0.9	0.9	0.9
	4-H	1.3	1.1	1.2	1.1	1.1	0.9	0.9	0.9
	4-J	1.5	1.3	1.3	1.2	1.2	1	0.9	0.9
	4-K	1.5	1.3	1.3	1.2	1.2	1	0.9	0.9
	4-L	1.5	1.3	1.3	1.2	1.2	1	0.9	0.9
	5	1.3	1.1	1.1	1.1	1	0.9	0.8	0.8
	6	1.1	1	1	0.9	0.9	0.8	0.7	0.7
	7	1.2	1.1	1.1	1	1	0.8	0.8	0.8
	8-F	1.5	1.3	1.4	1.3	1.2	1	1	1
	8-G	1.5	1.3	1.4	1.3	1.2	1	1	1
	8-H	1.5	1.3	1.4	1.3	1.2	1	1	1
	8-J	1.5	1.3	1.4	1.3	1.2	1	1	1
	8-K	1.4	1.2	1.2	1.1	1.1	0.9	0.9	0.9
	8-L	1.5	1.3	1.4	1.3	1.2	1	1	1
B03	1	1.8	1.6	1.6	1.4	1.4	1.1	1.1	1.1
B09	1	1.8	1.6	1.6	1.4	1.4	1.1	1.1	1.1
B05	1	3.3	3	3.1	2	2.2	1.9	1.9	1.9
B08	1	3.3	3	3.1	2	2.2	1.9	1.9	1.9

Table B20. Design Shear Capacity, LFRD.

		phiVn, LFR			phiVn, LRFR				
BRIDGE	SPAN	5-DL	18-DL	23-DL	4-DL	5-DL	16-DL	17-DL	18-DL
7933	1		555				562		
1829	1		473				439		
1830	1	591	473	506	510	476	439	423	422
9728	1 & 2		312			0	310		
4447	1		708			0	681		
	2		786			0	759		
B03	1	652	639	634	618	613	504	491	490
B09	1	652	639	634	618	613	504	491	490

Table B21. Nominal Shear Capacity, LFRD.

		Vn, LFR			Vn, LRFR				
BRIDGE	SPAN	5-DL	18-DL	23-DL	4-DL	5-DL	16-DL	17-DL	18-DL
7933	1		617				624		
1829	1	525	525				488		
1830	1	657	525	563	566	529	488	470	469
9728	1 & 2		347				345		
4447	1		786				756		
	2		873				843		
B03	1	725	710	705	686	681	560	545	544
B09	1	725	710	705	686	681	560	545	544

Table B22. Nominal Concrete Shear Capacity, LFRD.

		Vc, LFR			Vc, LRFR				
BRIDGE	SPAN	5-DL	18-DL	23-DL	4-DL	5-DL	16-DL	17-DL	18-DL
7933	1		114				104		
1829	1	101	101				98		
1830	1	199	101	105	109	101	98	94	92
9728	1 & 2		68				63		
4447	1		256				226		
	2		256				226		
B03	1	104	89	83	65	59	50	49	48
B09	1	104	89	83	65	59	50	49	48

Table B23. Design Shear Load, LFRD.

		Vu, LFR			Vu, LRFR				
BRIDGE	SPAN	5-DL	18-DL	23-DL	4-DL	5-DL	16-DL	17-DL	18-DL
7933	1		145				165		
1829	1		266				321		
1830	1	211	266	239	282	300	321	325	325
9728	1 & 2		236				333		
4447	1		172				274		
	2		171				278		
B03	1	70	85	82	120	126	134	134	132
B09	1	70	85	82	124	130	137	136	135

Table B24. Shear Load V1, LFRD.

		V1, LFR			V1, LRFR				
BRIDGE	SPAN	5-DL	18-DL	23-DL	4-DL	5-DL	16-DL	17-DL	18-DL
7933	1		112				129		
1829	1		205				253		
1830	1	162	205	184	198	210	253	262	263
9728	1 & 2		182				262		
4447	1		143				215		
	2		142				218		
B03	1	54	65	63	77	81	105	109	108
B09	1	54	65	63	80	84	107	111	110

Table B25. Shear Load V2, LFRD.

		V2, LFR			V2, LRFR				
BRIDGE	SPAN	5-DL	18-DL	23-DL	4-DL	5-DL	16-DL	17-DL	18-DL
7933	1		103				115		
1829	1		195				225		
1830	1	157	195	175	183	193	225	232	233
9728	1 & 2		174				232		
4447	1		135				187		
	2		134				190		
B03	1	49	58	56	66	70	88	91	90
B09	1	49	58	56	69	73	90	93	92

Table B26. Shear Capacity/Load Ratios, LFRD.

		phi Vn/Vu, LFR			phi Vn/Vu, LRFR				
BRIDGE	SPAN	5-DL	18-DL	23-DL	4-DL	5-DL	16-DL	17-DL	18-DL
7933	1		3.8				3.4		
1829	1		1.8				1.4		
1830	1	2.8	1.8	2.1	1.8	1.6	1.4	1.3	1.3
9728	1 & 2		1.3				0.9		
4447	1		4.1				2.5		
	2		4.6				2.7		
B03	1	9.4	7.6	7.7	5.2	4.9	3.8	3.7	3.7
B09	1	9.4	7.6	7.7	5.0	4.7	3.7	3.6	3.6

Table B27. Vn/V1 Shear Capacity/Load Ratios, LFRD.

		Vn/V1, LFR			Vn/V1, LRFR				
BRIDGE	SPAN	5-DL	18-DL	23-DL	4-DL	5-DL	16-DL	17-DL	18-DL
7933	1		5.5				4.8		
1829	1		2.6				1.9		
1830	1	4.0	2.6	3.1	2.9	2.5	1.9	1.8	1.8
9728	1 & 2		1.9				1.3		
4447	1		5.5				3.5		
	2		6.1				3.9		
B03	1	13.5	10.9	11.1	9.0	8.4	5.3	5.0	5.0
B09	1	13.5	10.9	11.1	8.6	8.1	5.2	4.9	5.0

Table B28. Vn/V2 Shear Capacity/Load Ratios, LFRD.

		Vn/V2, LFR			Vn/V2, LRFR				
BRIDGE	SPAN	5-DL	18-DL	23-DL	4-DL	5-DL	16-DL	17-DL	18-DL
7933	1		6.0				5.4		
1829	1		2.7				2.2		
1830	1	4.2	2.7	3.2	3.1	2.7	2.2	2.0	2.0
9728	1 & 2		2.0				1.5		
4447	1		5.8				4.0		
	2		6.5				4.4		
B03	1	14.8	12.3	12.5	10.4	9.8	6.4	6.0	6.0
B09	1	14.8	12.3	12.5	9.9	9.4	6.2	5.9	5.9

Table B29. Vc/V2 Shear Capacity/Load Ratios, LFRD.

		Vc/V2, LFR			Vc/V2, LRFR				
BRIDGE	SPAN	5-DL	18-DL	23-DL	4-DL	5-DL	16-DL	17-DL	18-DL
7933	1		1.1				0.9		
1829	1		0.5				0.4		
1830	1	1.3	0.5	0.6	0.6	0.5	0.4	0.4	0.4
9728	1 & 2		0.4				0.3		
4447	1		1.9				1.2		
	2		1.9				1.2		
B03	1	2.1	1.5	1.5	1.0	0.9	0.6	0.5	0.5
B09	1	2.1	1.5	1.5	0.9	0.8	0.6	0.5	0.5

APPENDIX C: BEAM CASTING SHEETS

Beam 1 Casting Sheet

Stress-con Pour Report		Job Name: US-31 NB OVER ELMER SELTENRIGHT DITCH				Q.C. Inspector: Brian C			
Pour Date: 1-28-13	Bed ID: Gilbert	Job Number: 12080				Lead Man:			
Pour Number: 1		County:				Foreman:			
Piece Number	Piece Length	Mix Design: 775				Inspector:			
Test Beam		Heat o Steam o Heaters o Ambient Heat o				Test Results			
		Required Cylinder Strengths					1st	2nd	3rd
		Release Strength: 5000 psi				Time:	10:15	:	:
		28-Day Strength: 7000 psi				Slump:	7 3/4 "	"	"
		Cylinder Strength Results				Temp:	60 °F	°F	°F
			1st Set	2nd Set	3rd Set	Air %:	6.0 %	%	%
		Release	7369	7434		Vsi	0		
		28-Day				Temp: 40	Cond: Rain (light)		
		Early Ship							

Reel Numbers: 170402.78264

					Hercules	Calibration Date
Strand Size: 1/2"	Initial Force	Net Elongation	Total Force		o Simms 12486	10-3-12
Strand Usage:	4000	5 13/16 "	31,446	lbs	Time 11 : 15	Temp: 40 °F
Actual Usage:	(+5%)	6 2/16 "	33,018	lbs	Time :	Temp: °F
Waste:	(-5%)	5 5/16 "	29,874	lbs	Time :	Temp: °F

Measured Elongation & Gauge Pressure Witnessed

Strand Diagram

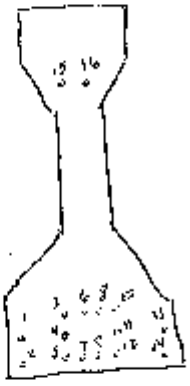

1	6 "	3240	24	"	
2	6 "	3210	25	"	
3	6 "	3200	26	"	
4	5 7/8 "	3210	27	"	
6	6 "	3200	28	"	
8	6 1/16 "	3240	29	"	
7	5 7/8 "	3210	30	"	
8	6 "	3240	31	"	
9	6 "	3200	32	"	
10	6 1/16 "	3240	33	"	
11	5 15/16 "	3210	34	"	
12	6 1/16 "	3240	35	"	
13	6 "	3210	36	"	
14	5 7/8 "	3200	37	"	
15	6 1/8 "	3240	38	"	
16	6 1/16 "	3240	39	"	
17	"		40	"	
18	"		41	"	
19	"		42	"	
20	"		43	"	
21	"		44	"	
22	"		45	"	
23	"		46	"	

Comments: Pour Inside

Beam 2 Casting Sheet

STRESS-CON POUR REPORT

Pour Date: 8/30/13	Pour # 1	Job Name: U of M	
Bed ID: C-floor		Job Number: 13063	Q.C Inspector: Brian
Piece Number	Piece Length	County:	Lead Man:
Test beam #2		Mix Design: 775	Foreman:
		Heat o Steam o Heaters o Ambient Heat	3rd Party Inspector

Required Cylinder Strengths		
Release Strength:	4000	PSI
28-Day Strength	5500	PSI

Cylinder Strength Results	1st Set	2nd Set	3rd Set
Release			
28-Day			
Early Ship			

Test Results	1st Test	2nd Test	Extra
Time:	1 : 10	:	:
Slump:	8 "	"	"
Temperature	81 °F	°F	°F
Air %	5.4 %	%	%
VSI	0		
Temp and Cond:			

Reel #: 120140389764

Strand Size:	1/2"
Strand Usage:	
Actual Usage:	
Waste:	

	Initial Force:	Net Elongation	Total Force
	4000 lbs	4 1/2"	25586 lbs
	(+5%)	4 3/4"	26865 lbs
	(-5%)	4 5/16"	24307 lbs

o Hercules
o Simms

Date of Calibration		
Time:	8 : 45	Temp: 68 °F
Time:	:	Temp: °F
Time:	:	Temp: °F

Measured Elongation Pull and Gauge Pressure Witnessed

1	9 3/8"	25600 lbs	11	9 1/2"	lb	21	"	lb	31	"	lb	51	"	lb
2	9 1/2"	lbs	12	9 1/2"	lb	22	"	lb	32	"	lb	52	"	lb
3	9 1/2"	lbs	13	9 3/8"	lb	23	"	lb	33	"	lb	53	"	lb
4	9 1/2"	lbs	14	9 1/2"	lb	24	"	lb	34	"	lb	54	"	lb
5	9 3/8"	lbs	15	9 5/8"	lb	25	"	lb	35	"	lb	55	"	lb
6	9 1/2"	lbs	16	9 5/8"	lb	26	"	lb	36	"	lb	56	"	lb
7	9 1/2"	lbs	17	"	lb	27	"	lb	37	"	lb	57	"	lb
8	9 1/2"	lbs	18	"	lb	28	"	lb	38	"	lb	58	"	lb
9	9 1/2"	lbs	19	"	lb	29	"	lb	39	"	lb	59	"	lb
10	9 3/8"	lbs	20	"	lb	30	"	lb	40	"	lb	60	"	lb
									41	"	lb	61	"	lb
									42	"	lb	62	"	lb
									43	"	lb	63	"	lb
									44	"	lb	64	"	lb
									45	"	lb	65	"	lb
									46	"	lb	66	"	lb
									47	"	lb	67	"	lb
									48	"	lb	68	"	lb
									49	"	lb	69	"	lb
									50	"	lb	70	"	lb

Strand Diagram

15 16

13 11 12 14

9 7 8 10

5 3 1 2 4 6

Strand Location

( ) @

( ) @

Comments:

APPENDIX D: BEAM TEST RESULTS

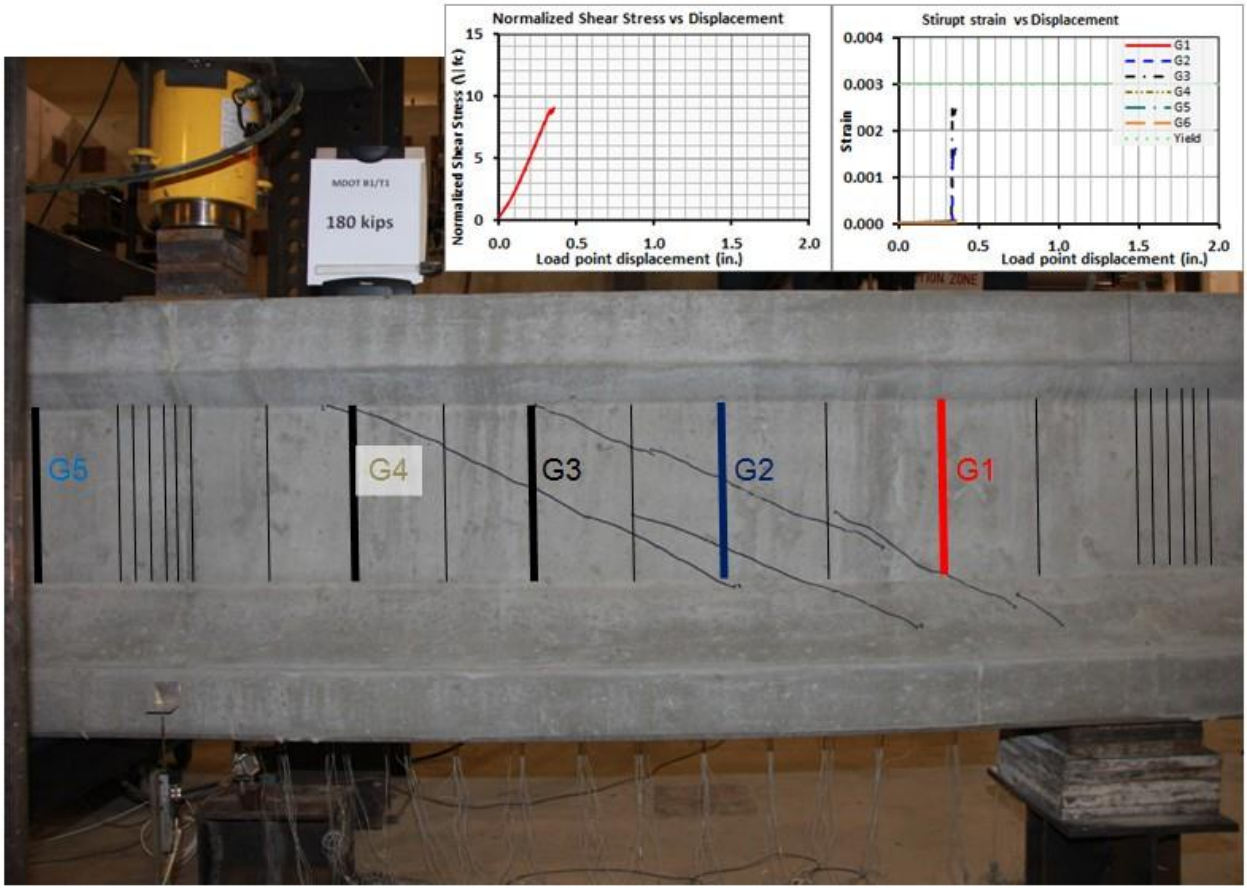

Figure D1. Beam 1 Test 1 First Cracking Load.

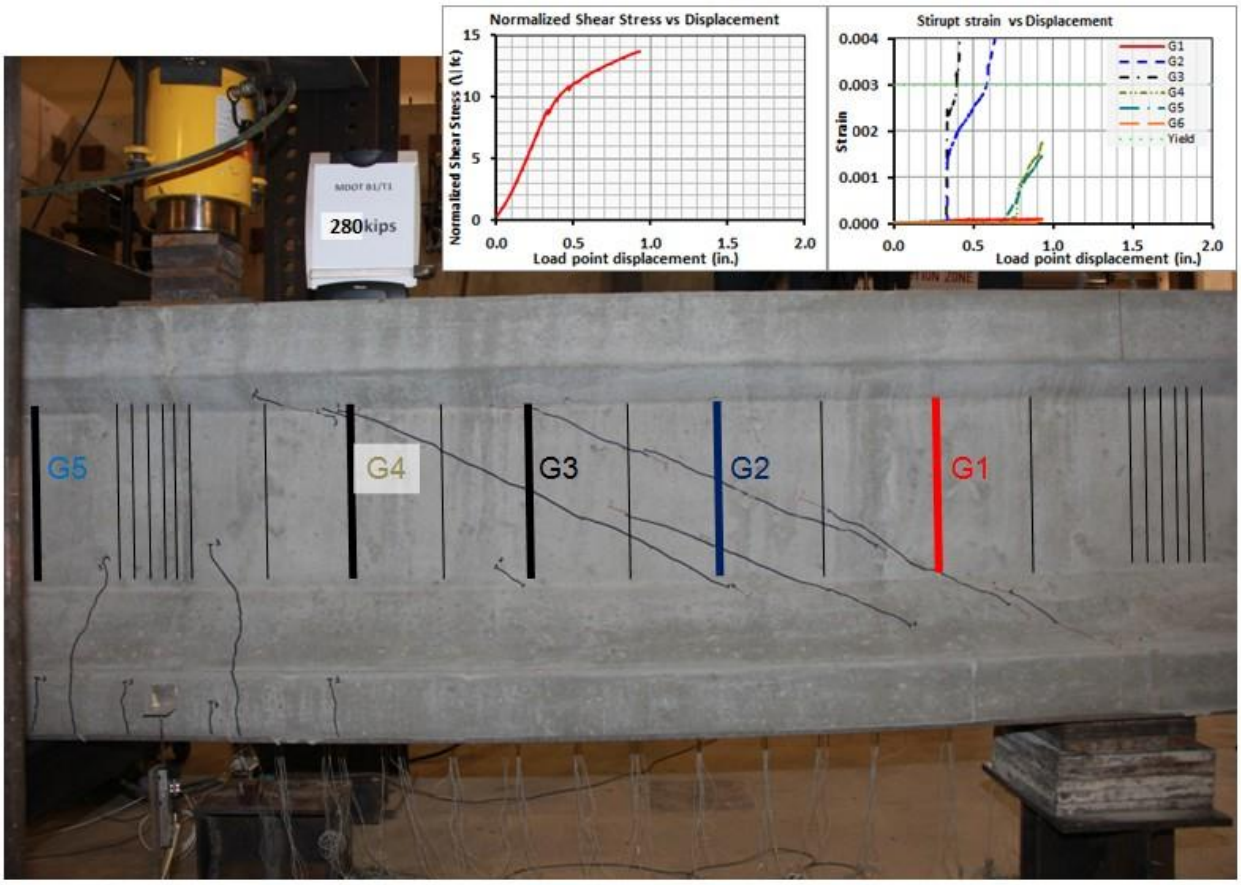

Figure D2. Beam 1 Test 1 Flexural Cracks.

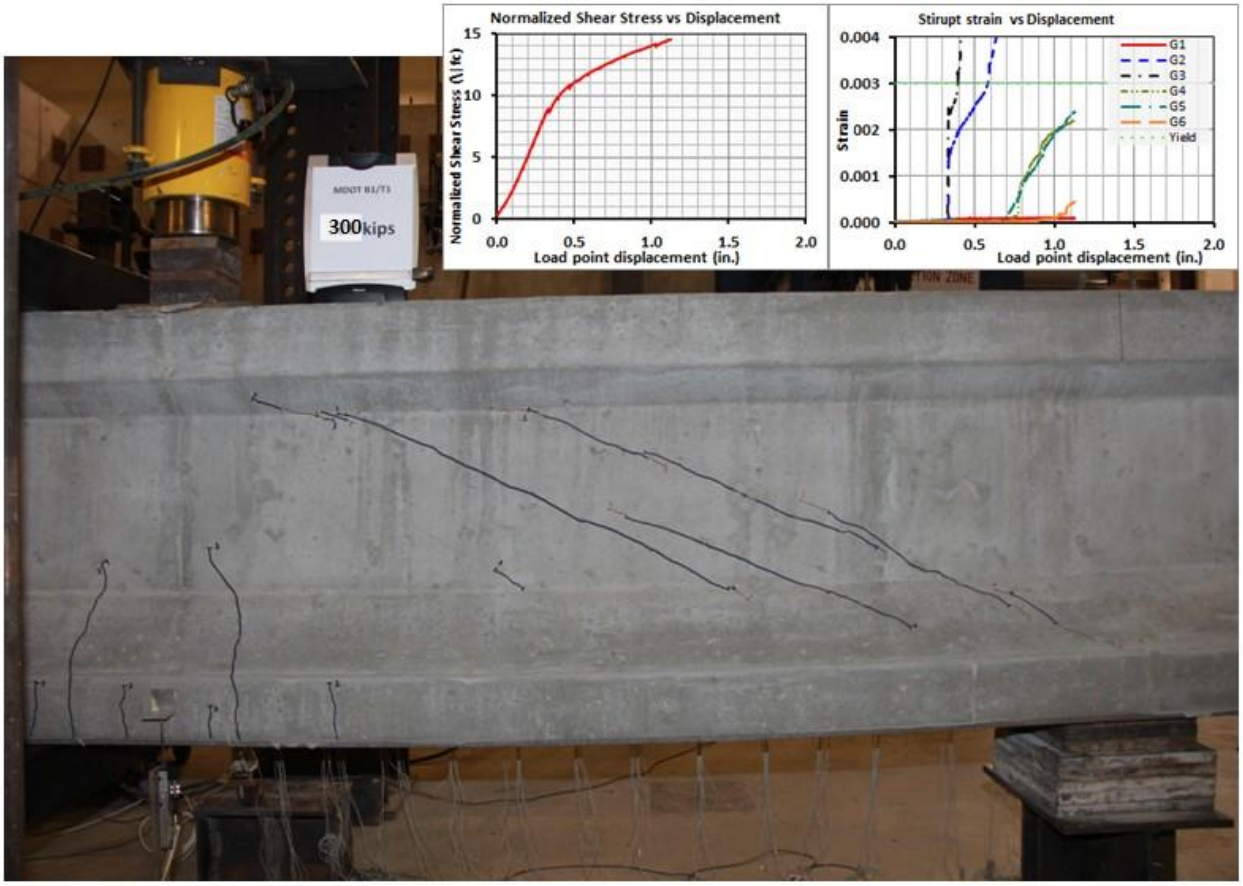

Figure D3. Beam 1 Test 1 Peak Load Before Failure.

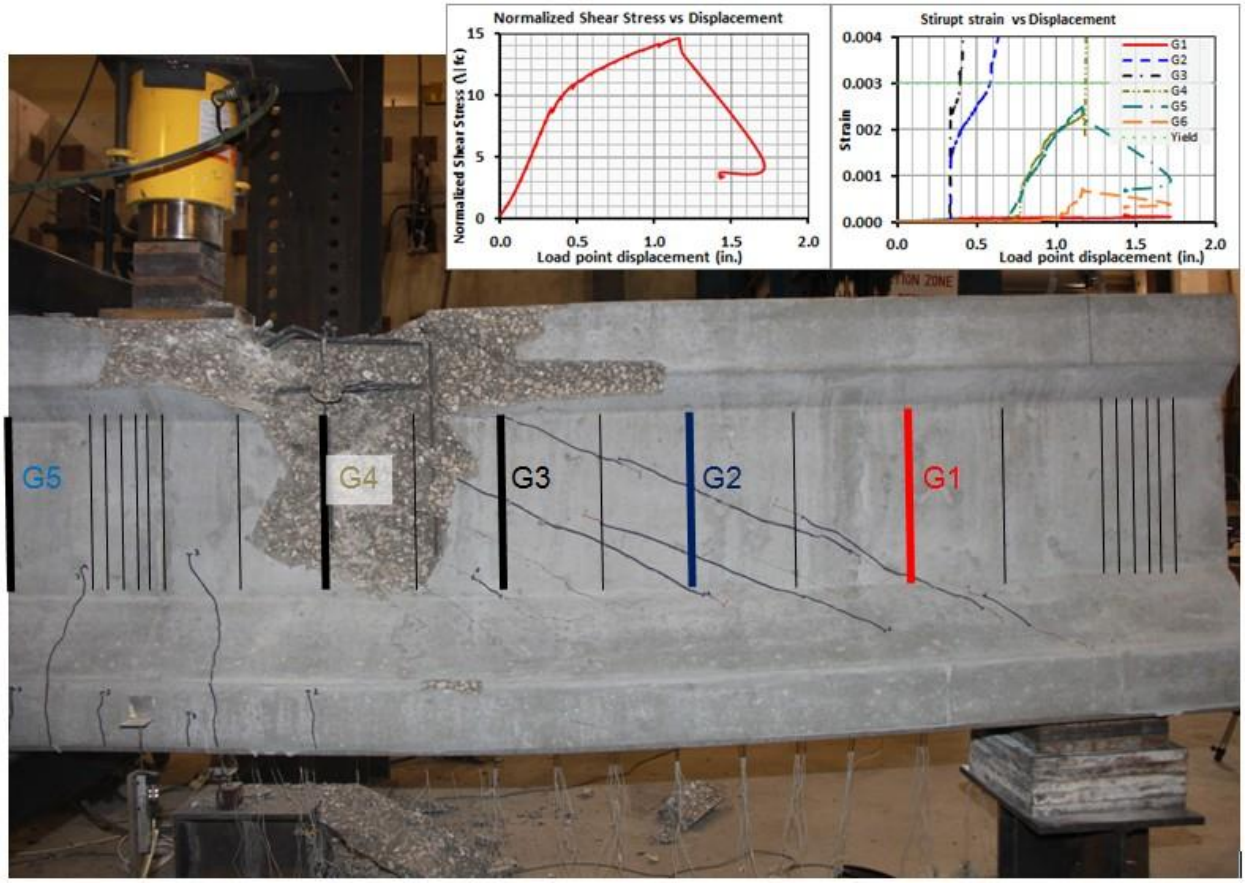

Figure D4. Beam 1 Test 1 Failure.

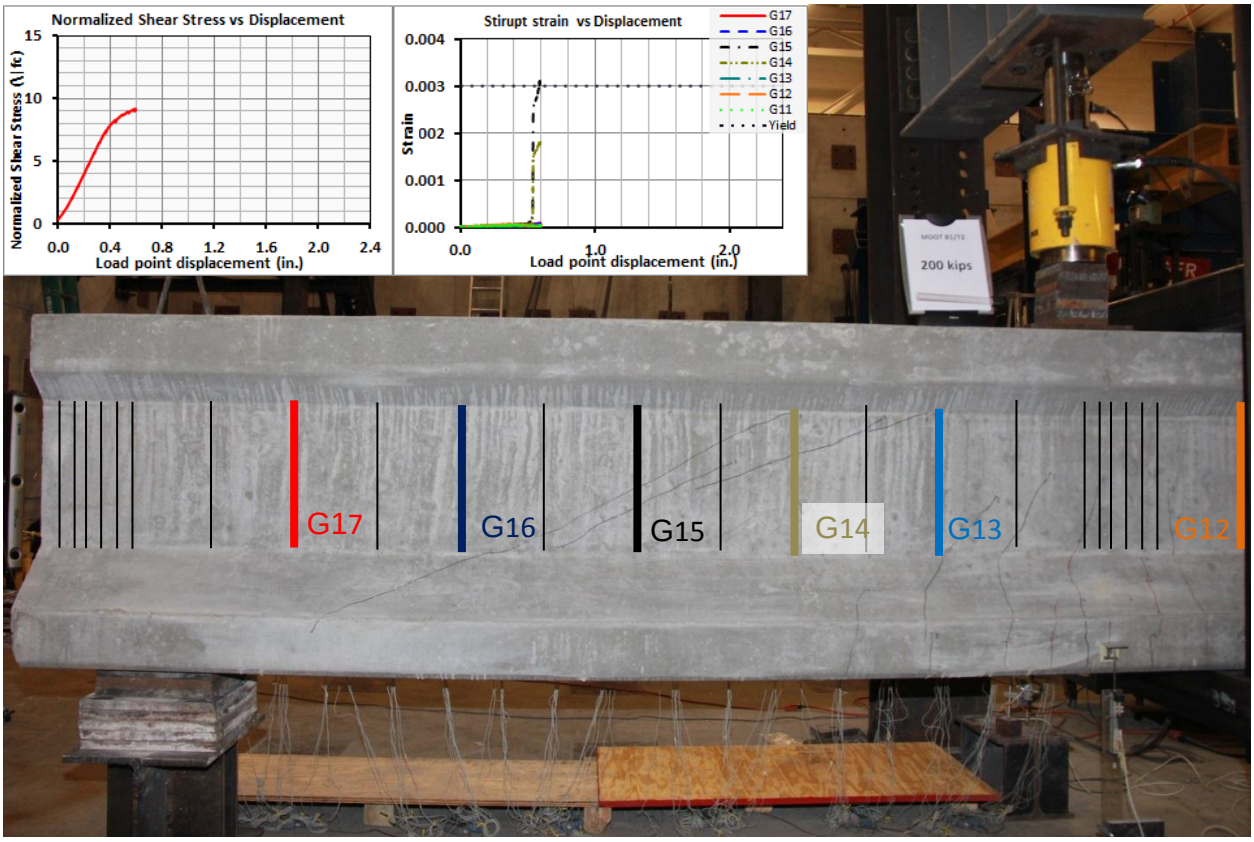

Figure D5. Beam 1 Test 2 First Cracking Load.

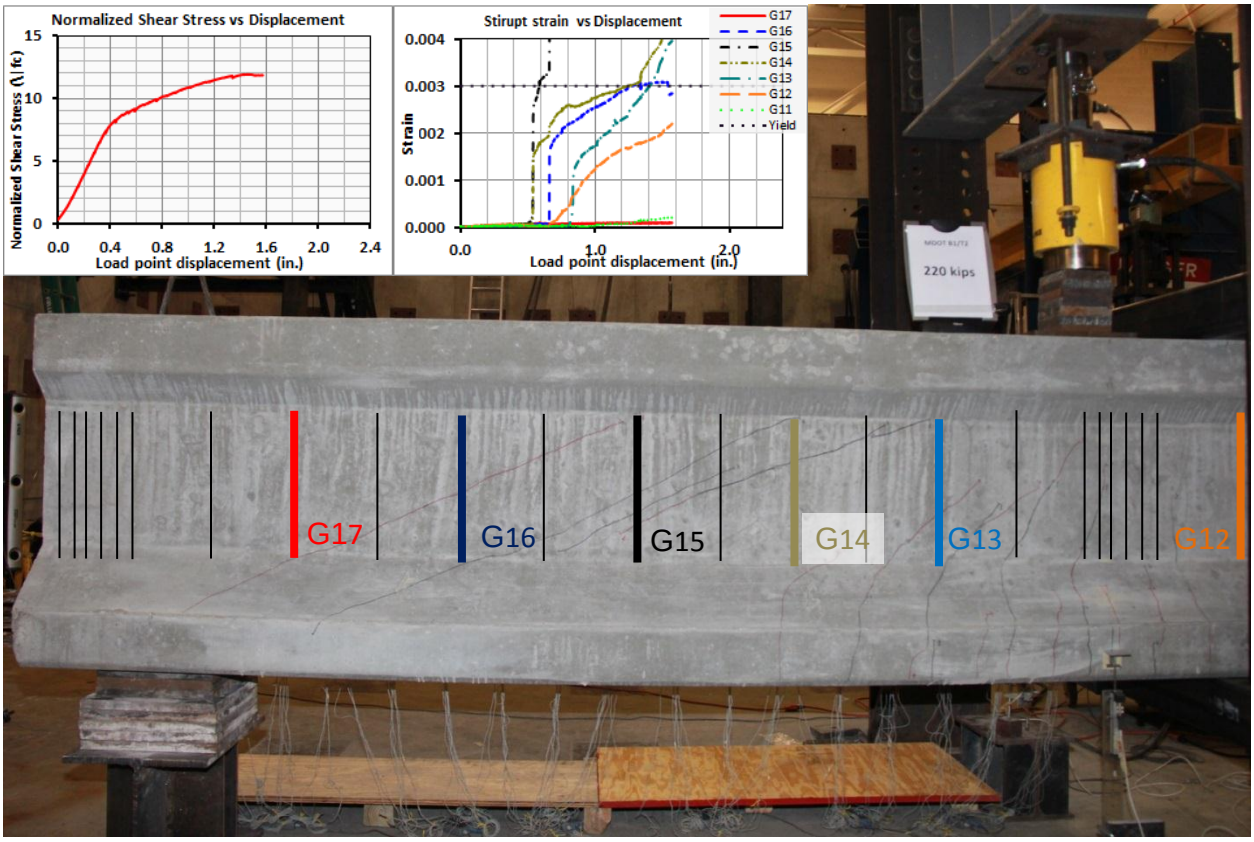

Figure D6. Beam 1 Test 2 at 260 kips.

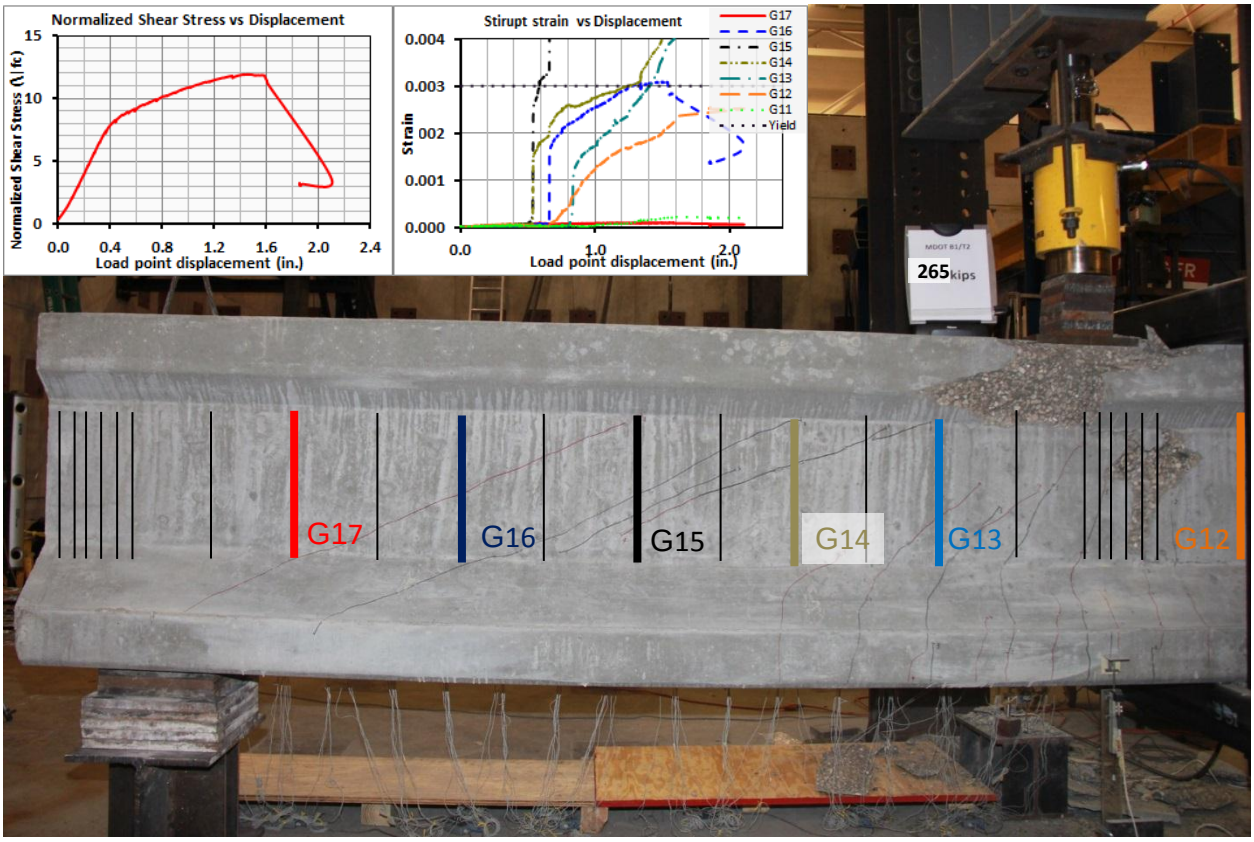

Figure D7. Beam 1 Test 2 Failure.

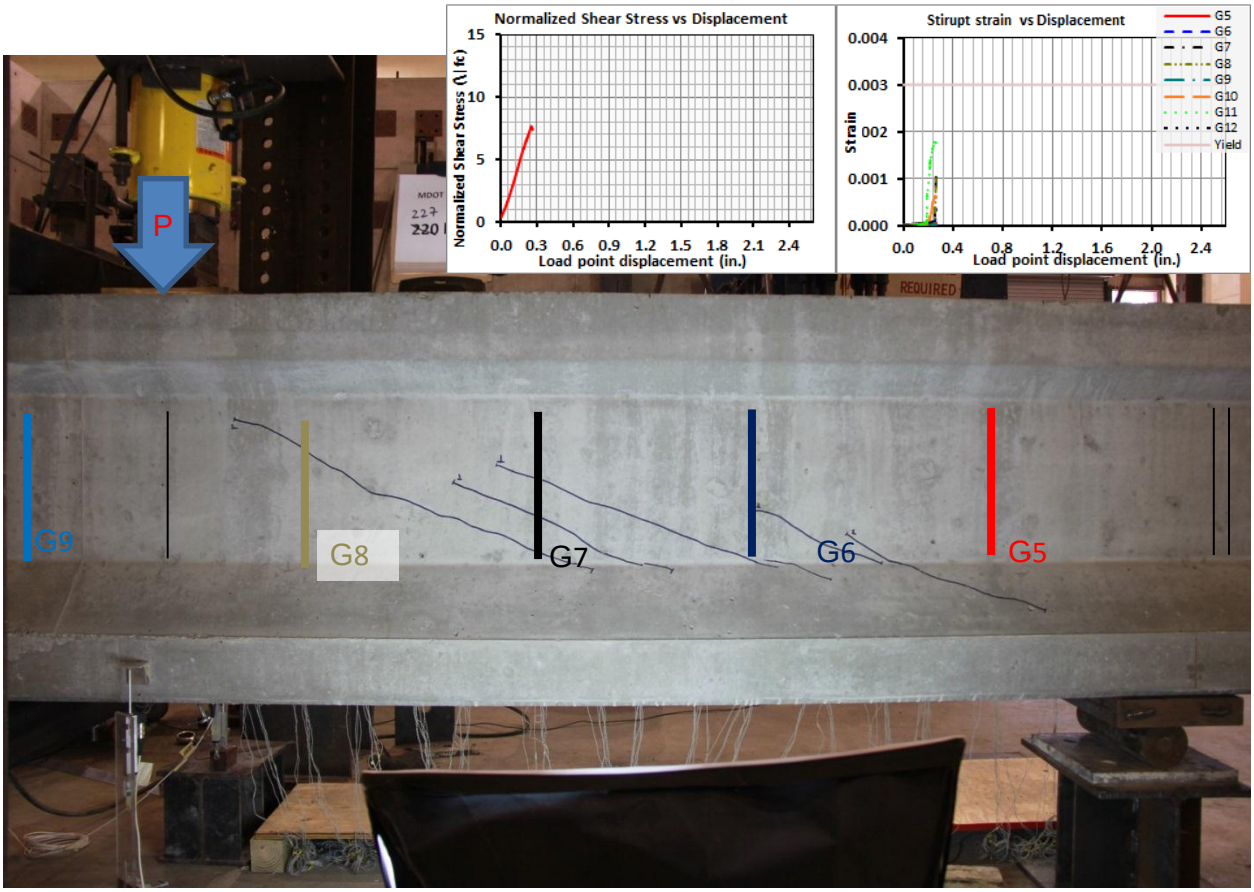

Figure D8. Beam 1 Test 3 First Cracking Load.

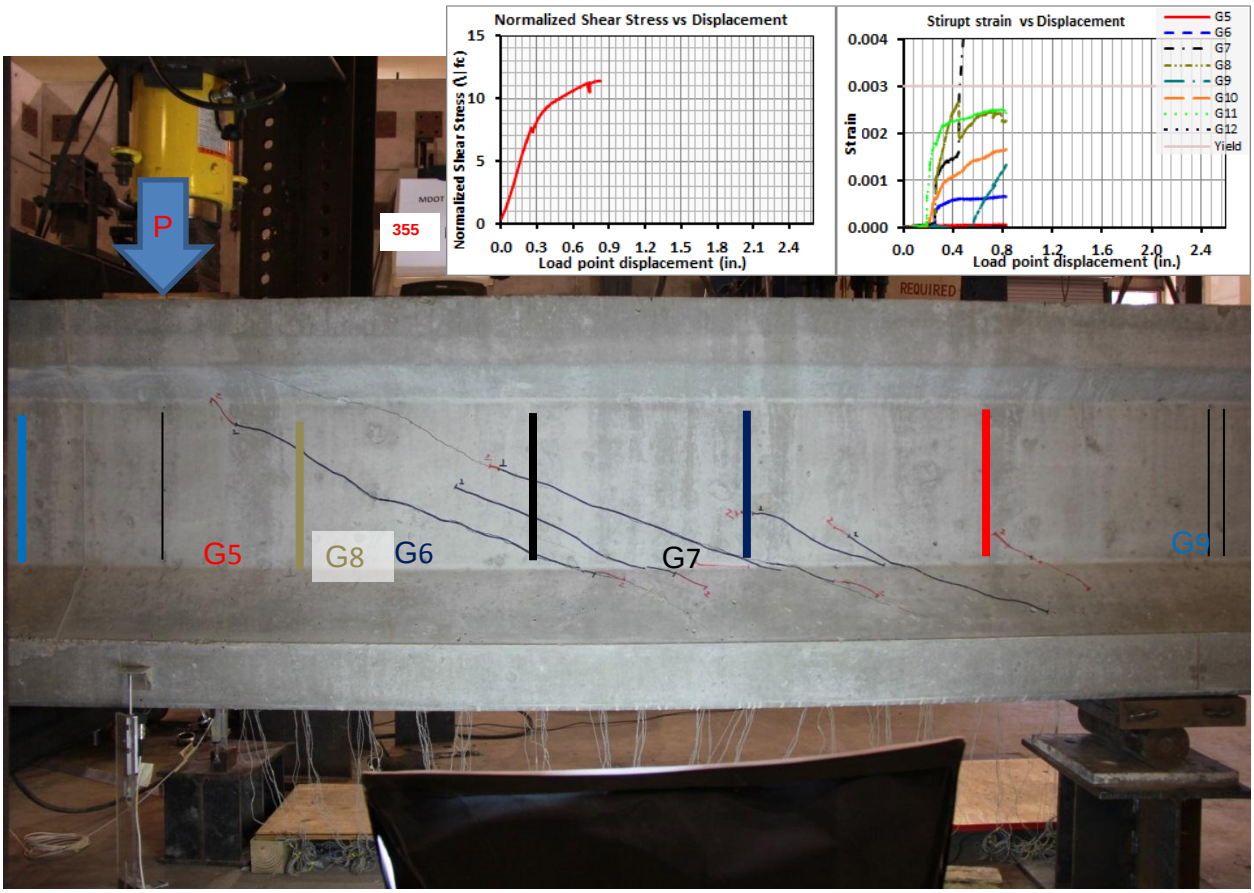

Figure D9. Beam 1 Test 3 Peak Load Before Failure.

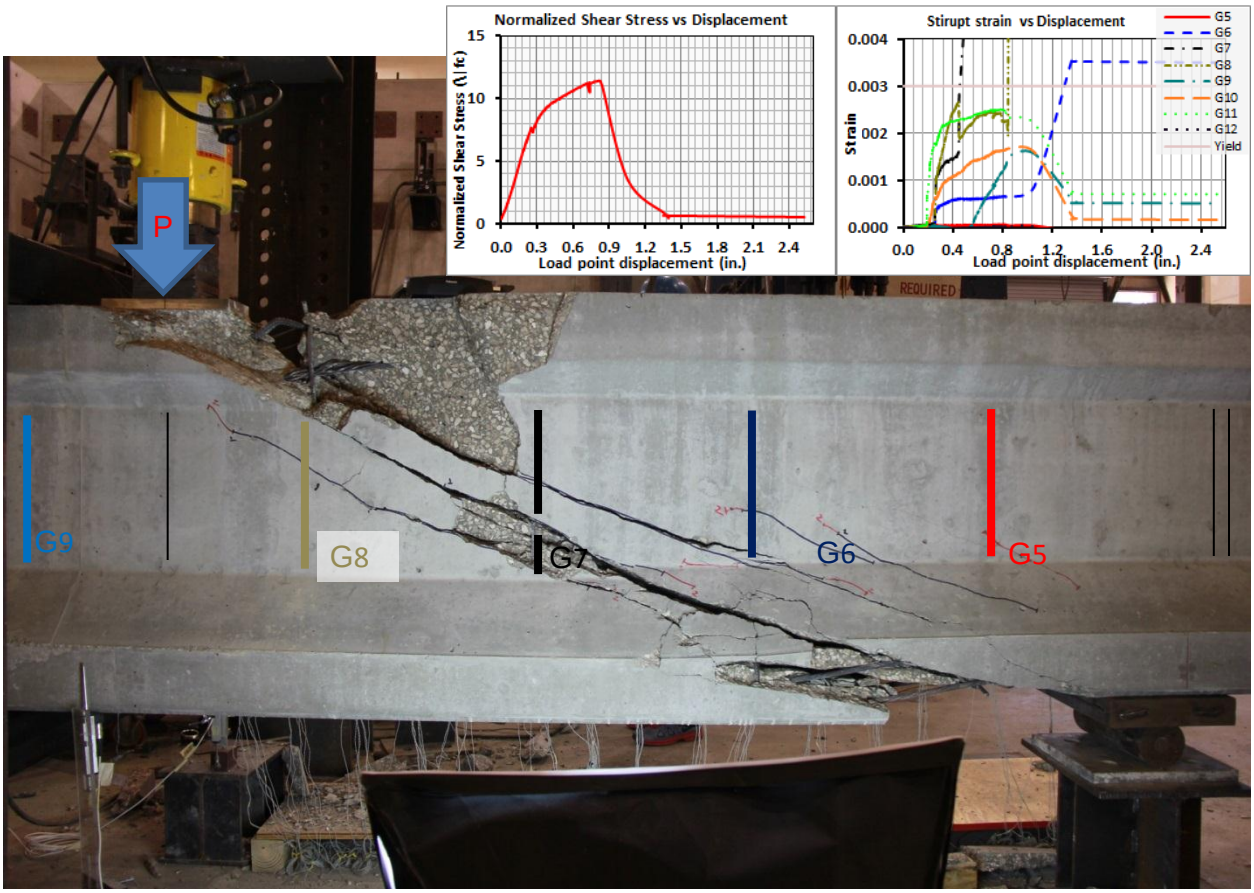

Figure D10. Beam 1 Test 3 Failure.

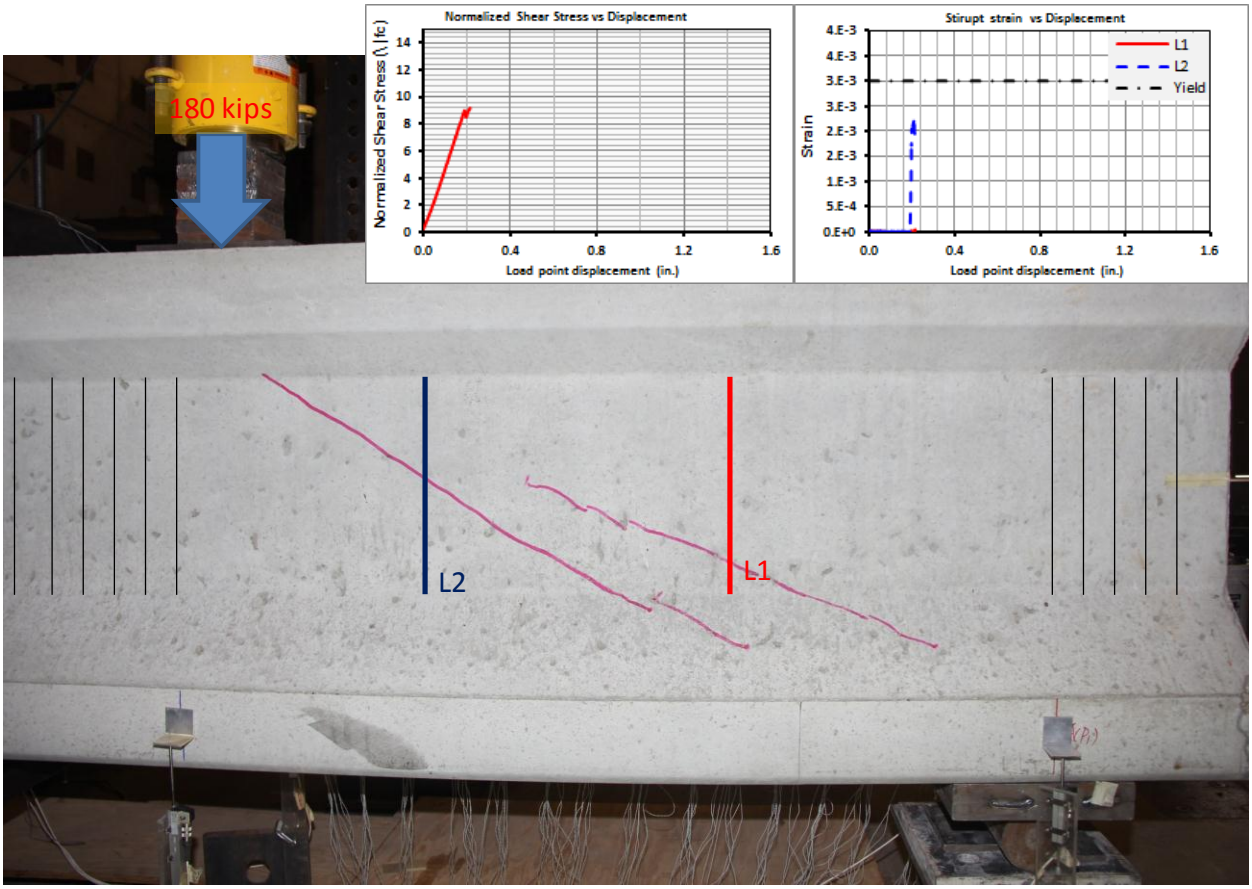

Figure D11. Beam 2 Test 1 First Cracking Load.

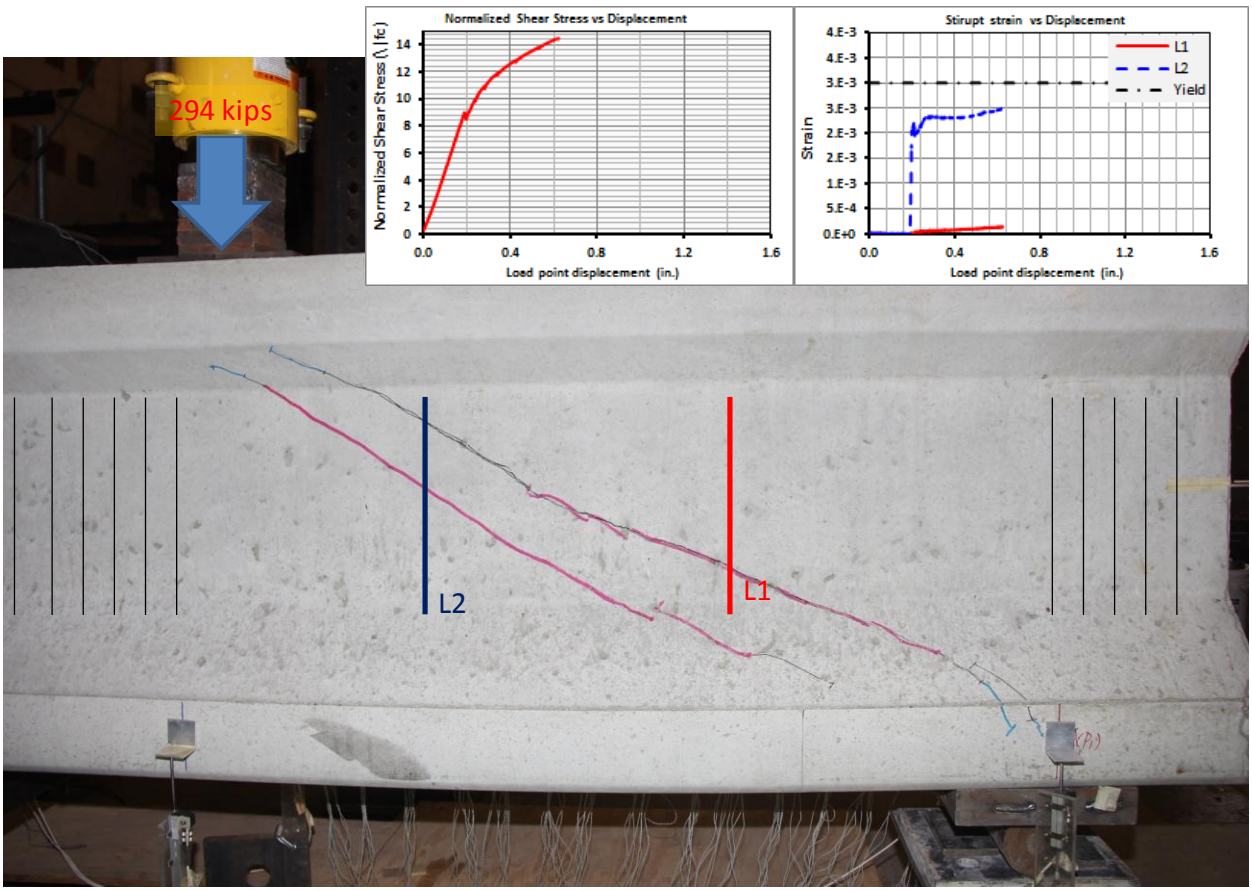

Figure D12. Beam 2 Test 1 Peak Load Before Failure.

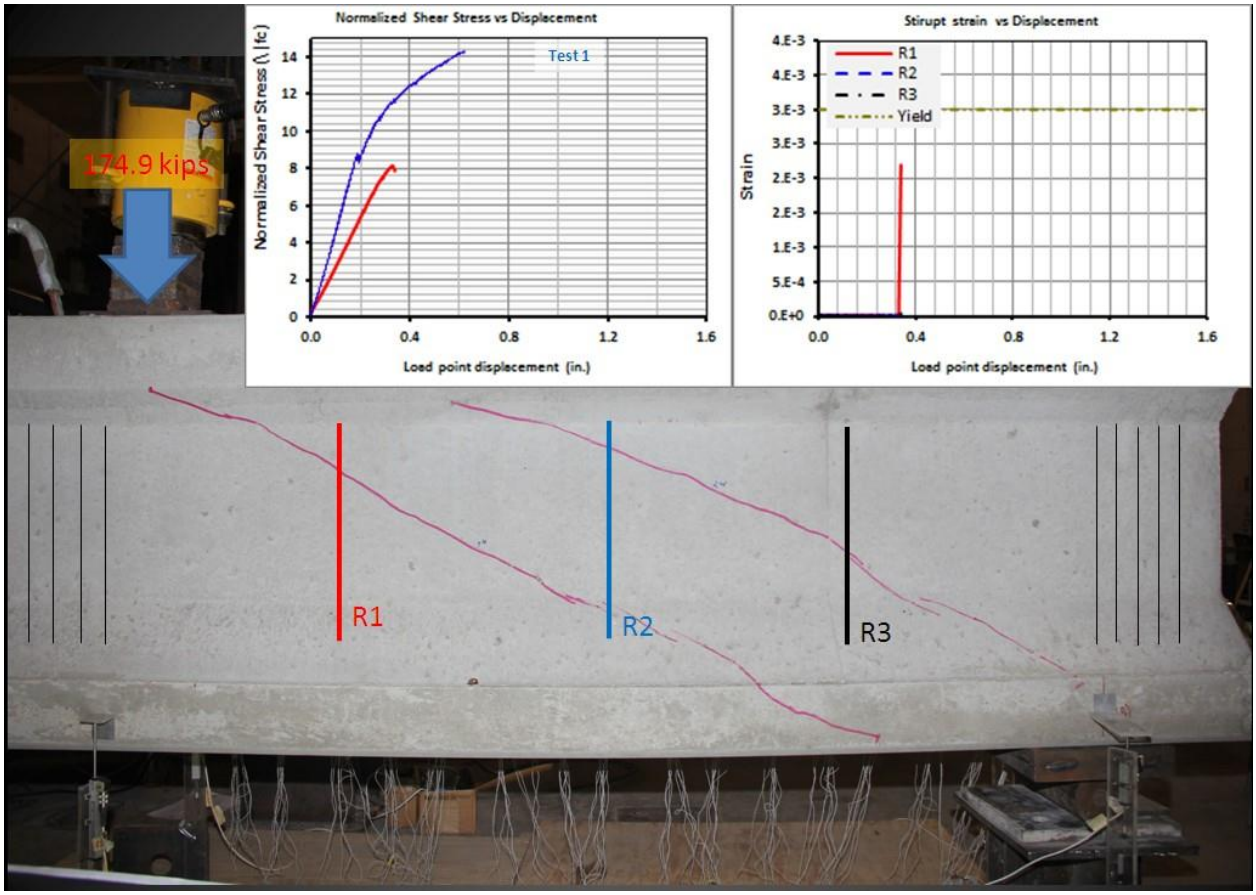

Figure D13. Beam 2 Test 2 First Cracking Load.

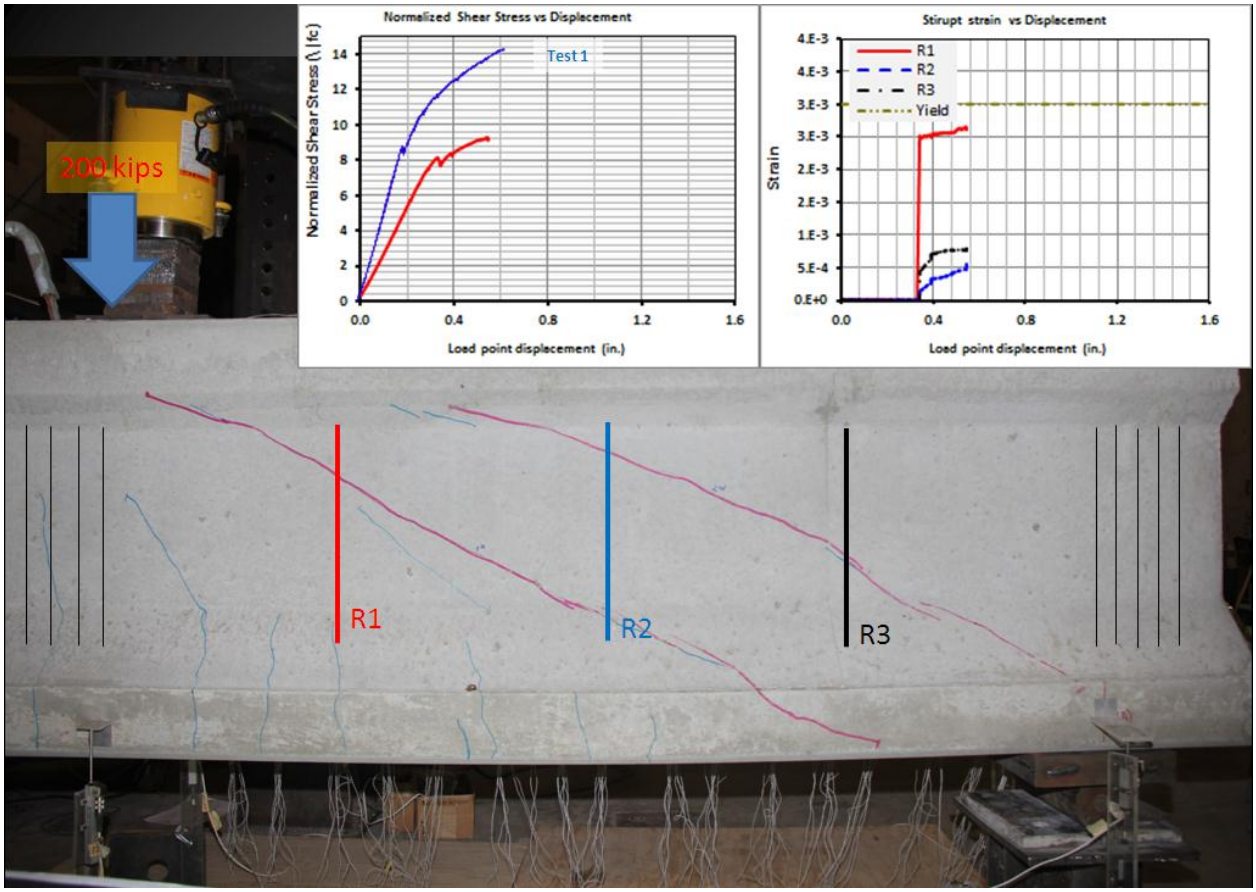

Figure D14. Beam 2 Test 2 Flexural Cracks.

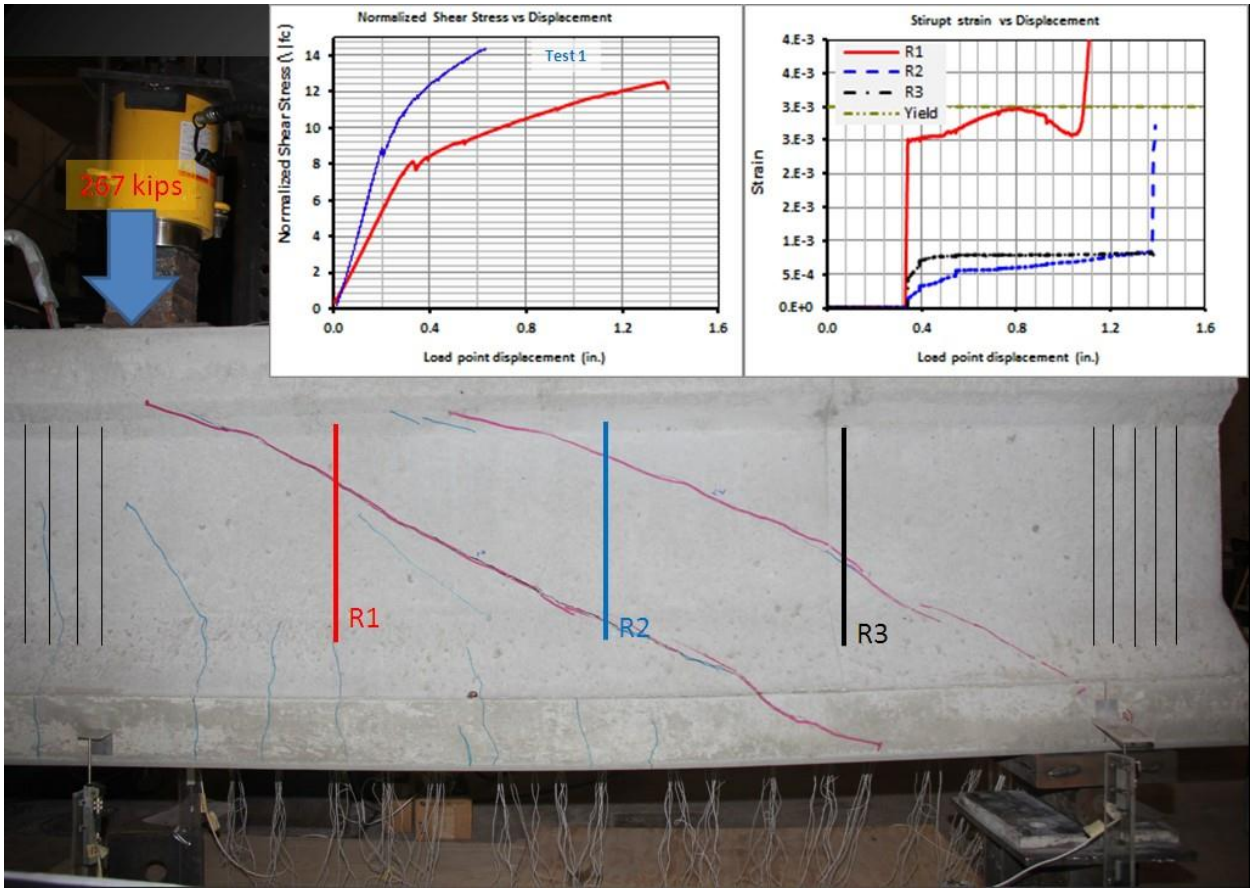

Figure D15. Beam 2 Test 2 Peak Load Before Failure.

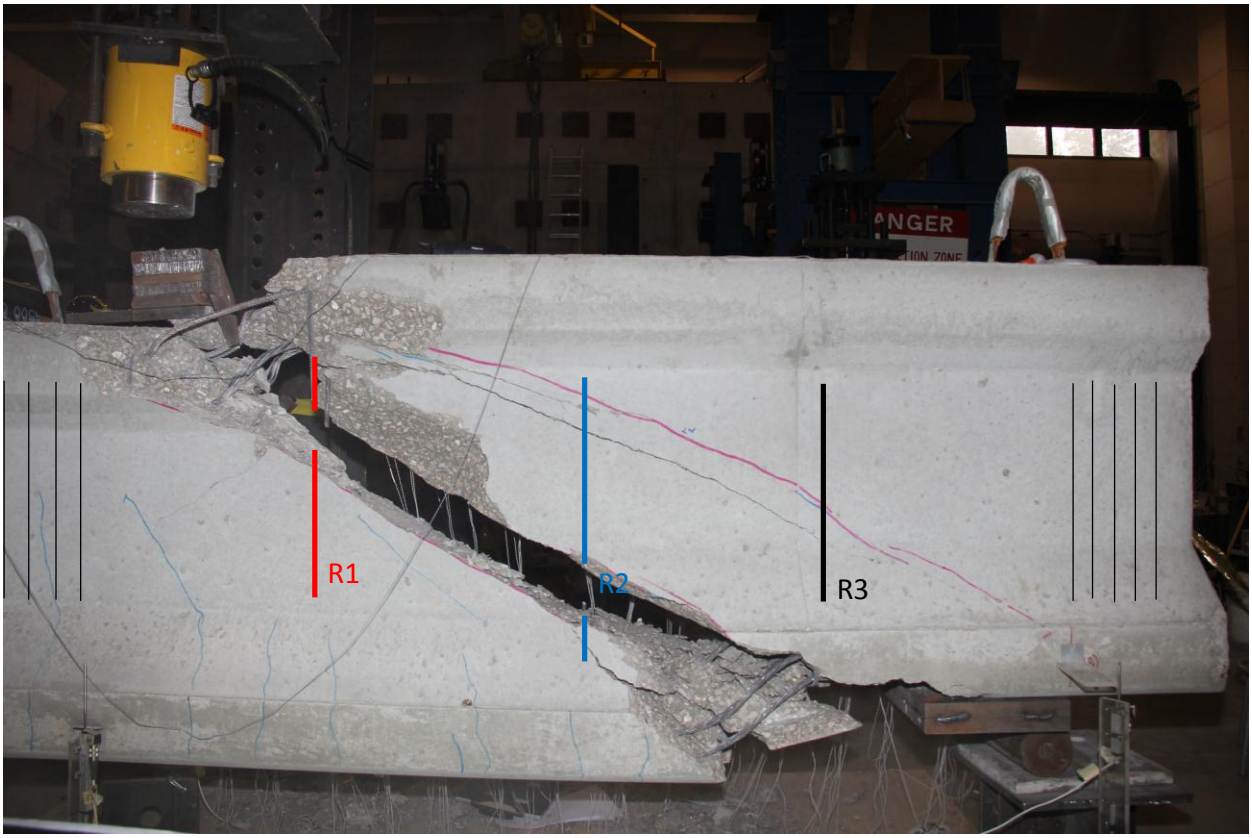

Figure D16. Beam 2 Test 2 Failure.

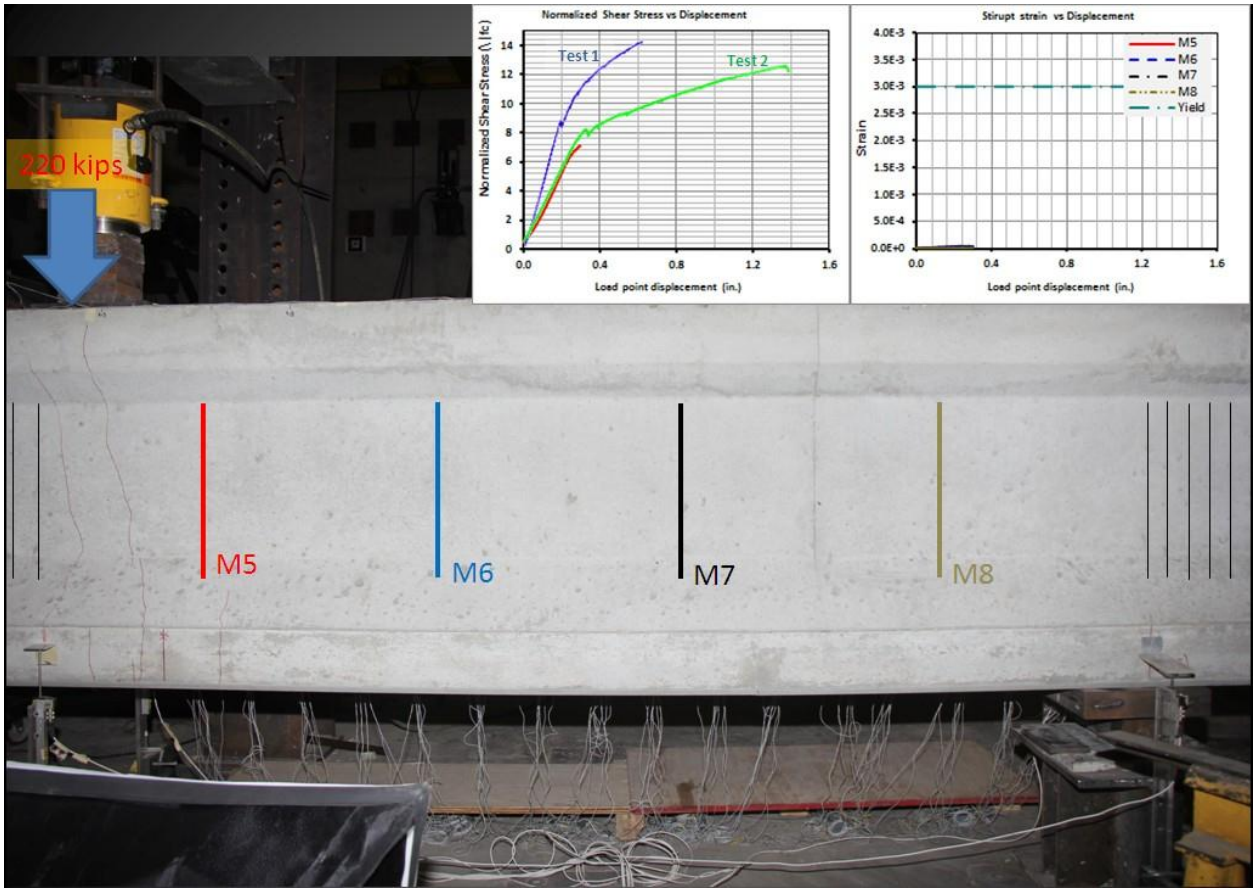

Figure D17. Beam 2 Test 3 First Cracking Load.

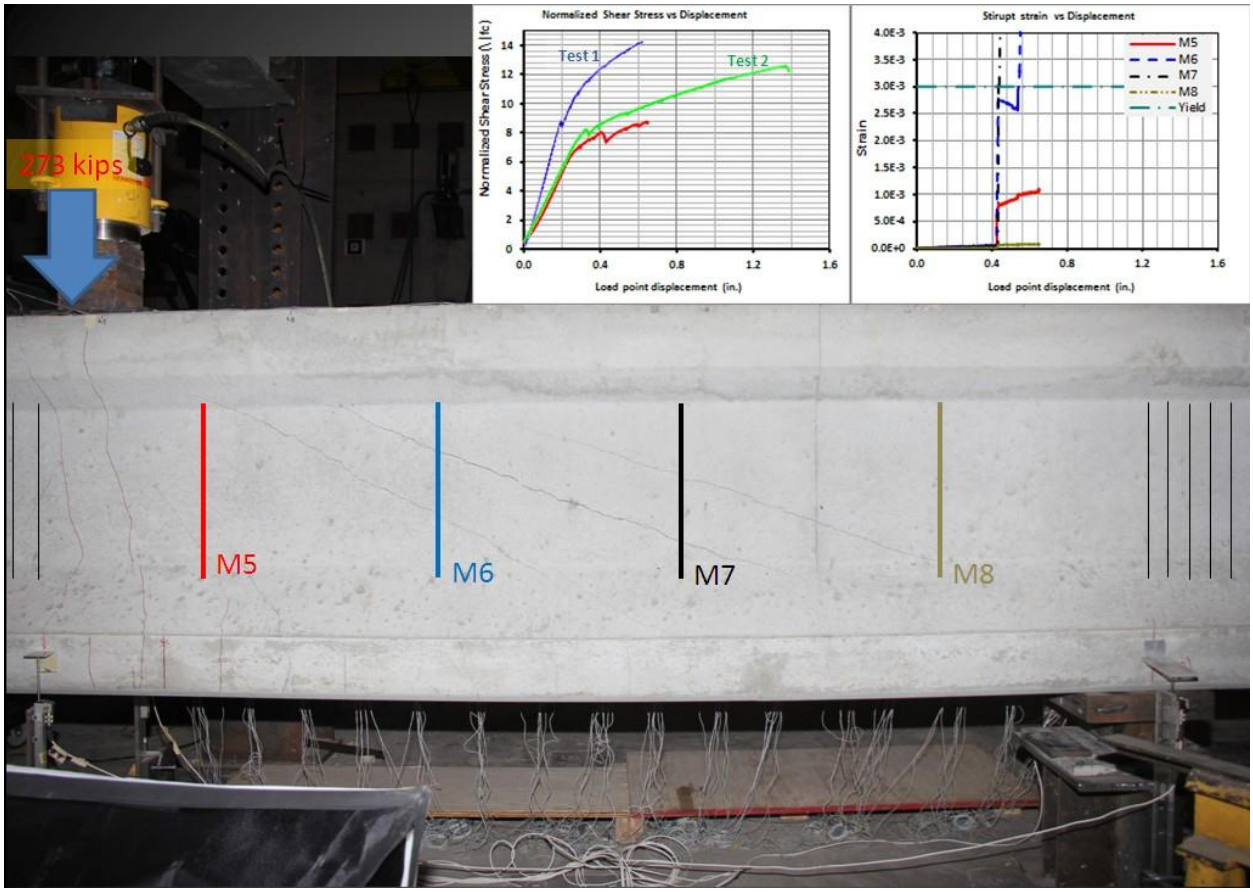

Figure D18. Beam 2 Test 3 Peak Load Before Failure.

APPENDIX E: FEA MODEL VERIFICATION

Verification Data Set 1: Saqan and Frosch Tests

Test Beams

Test beam characteristics used for model verification are shown in Table E1, while beam cross-sections are shown in Figure E1.

Table E1. Specimens details (Saqan and Frosch 2009).

Series	Specimen	Prestressed strand 1/2 in. (No. 13)	Mild reinforcement		Width b_w, in. (mm)	Effective depth of strands d_p, in. (mm)	Effective depth of bars d, in. (mm)
			Bars	Area, in.^{2} (mm^2)			
1	V-4-0	4	—	0	14.25 (362)	24 (610)	-
	V-4-0.93	4	Three No. 5 (Three No. 16)	0.93 (600)	14.50 (368)	24 (610)	26.40 (671)
	V-4-2.37	4	Three No. 8 (Three No. 25)	2.37 (1529)	14.68 (373)	24 (610)	26.00 (660)

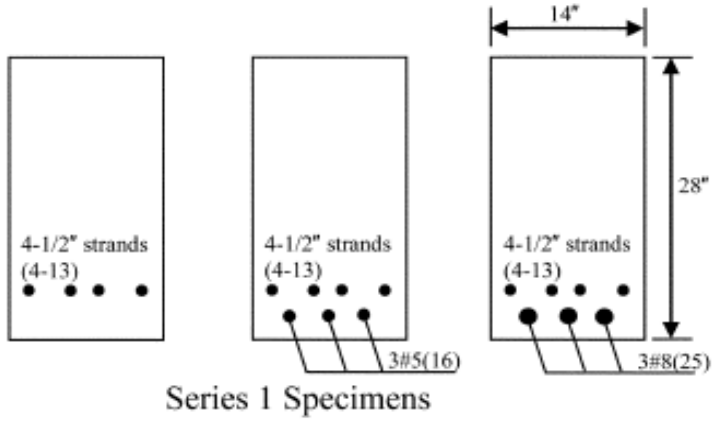

Figure E1. Test Beam Cross-Sections (Saqan and Frosch 2009).

Beam reinforcement consisted of ASTM A416, 1/2 in seven-wire Grade 270 low-relaxation prestressing strands and ASTM A615, Grade 60 reinforcing bars. The concrete had a nominal design strength of 6000 psi (7550 psi at 28 days). Cement was specified as ASTM C150, Type I. The coarse aggregate maximum-size is 3/4 in. The effective prestress force that was applied to each beam was 108 kips. The experimental tests consisted of a simply supported beam with a concentrated load applied at mid-span. The beam length, loading and boundary conditions are shown in Figure E2. These conditions are the same for all the tested beams.

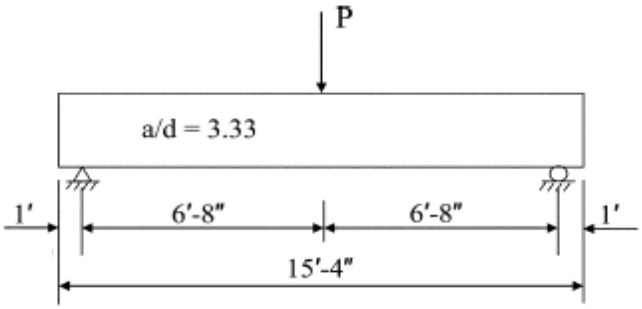

Figure E2. Test Setup (Saqan and Frosch 2009).

FEA Model

The dimensions and reinforcement details used to model the beams are given in Figures E3-E5 and Table E2.

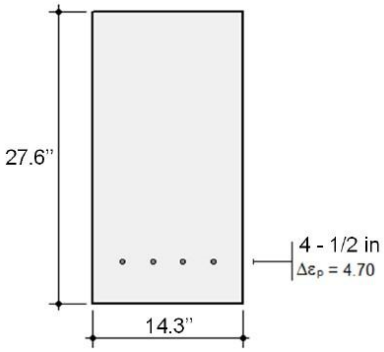

Figure E3. Test Beam V-4-0.

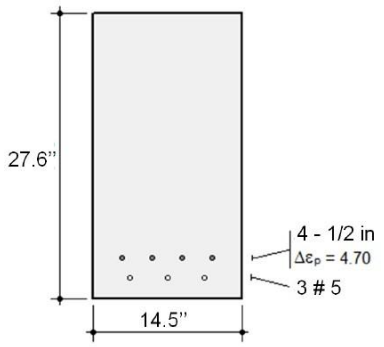

Figure E4. Test Beam V-4-0.93.

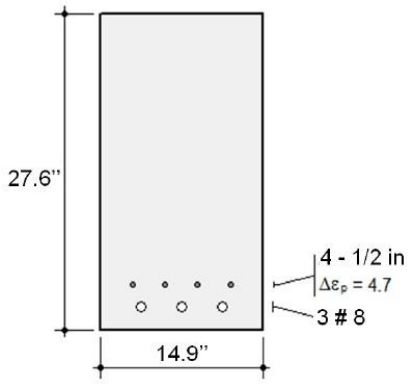

Figure E5. Test Beam V-4-2.37.

In the analysis, prestress strands are modeled with truss elements while the concrete is modeled with plane stress quadrilateral elements. The reinforcement is assumed perfectly bonded over the entire beam length and a prestress force of 108 kips was applied as a prestrain to the prestress steel truss elements. Steel properties used in the models are given in Table E2. For concrete, compressive strength $f_c' = 7550\ psi$; tensile strength $f_t' = 0.345\ ksi$; cylinder strain at $f_c', eo = 2.1\ me$; Poisson's ratio $u = 0.15$; and maximum aggregate size $a = 3/4\ in$.

Table E2. Steel Material Properties.

	Prestressing Steel	Mild Steel
Yield stress (Fy) (ksi)	220	60
Ultimate Stress (Fu) (ksi)	270	90
Elastic Modulus (Es) (ksi)	27992	29000
Strain hardening (esh)	10 me (milli-strain)	10 me
Prestrain (Dep)	4.7 me (milli-strain)	0

Models had approximately 2600-2800 plane stress and 180 truss elements. Since both the load and the supports are symmetrical about mid-span, only half of each beam is modeled, with symmetry boundary conditions imposed. The node at the support (left side) was restrained against the displacement in the transverse direction (Y direction) while the nodes at the mid span slice (right side) were restrained against displacement in the longitudinal direction (X direction), as shown in Figure E6.

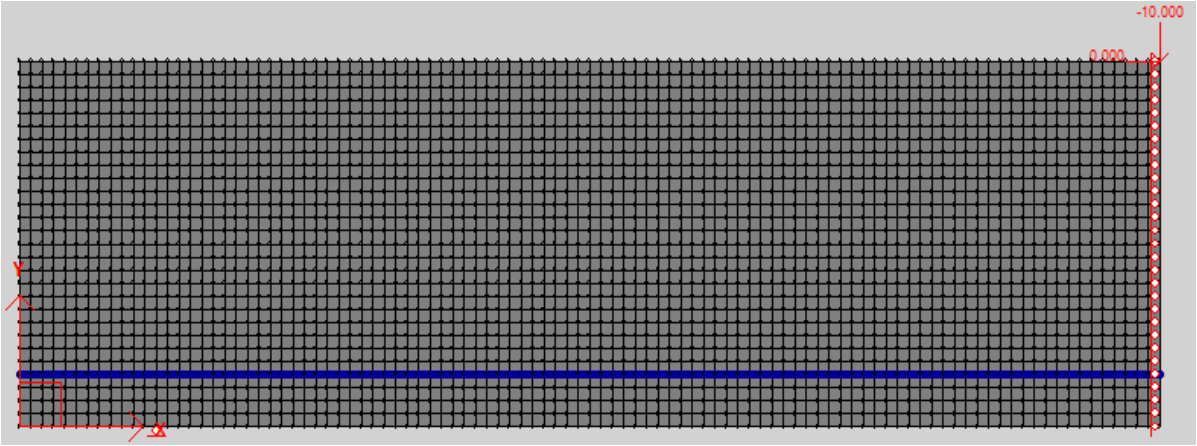

Figure E6. Mesh of Left Half of Symmetric FEA Model (Beam V-4-0.93).

A concentrated load of 2.2 kips was applied at the mid-span top node (Figure E6) in the negative Y direction. The load was increased at a rate of 2.2 kips per analysis step until the failure point was reached for each beam.

Results

The deformed shapes of the beams (exaggerated) at ultimate capacity are shown in Figures E7-E9. Damaged elements, indicating concrete crack locations, are shown in red.

- Test set up:

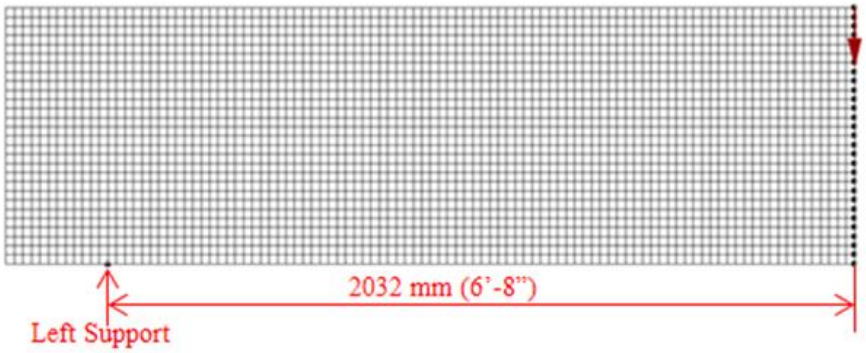

- Beam deformation at 89.9 kips:

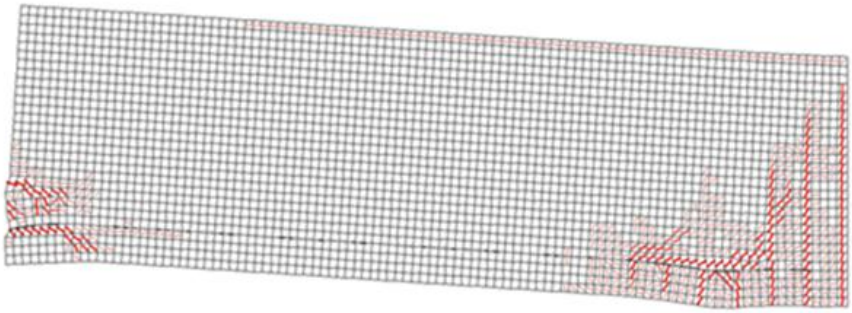

- Beam reached ultimate capacity at 103.4 kips:

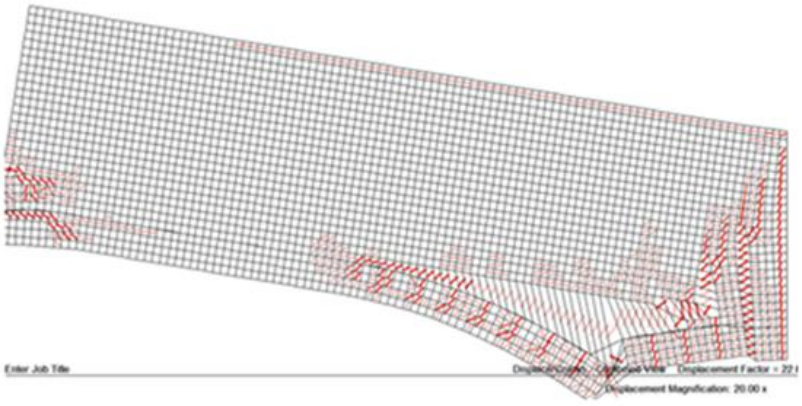

Figure E7. FEA Model for Beam V-4-0.

- Beam deformation at 98.9 kips:

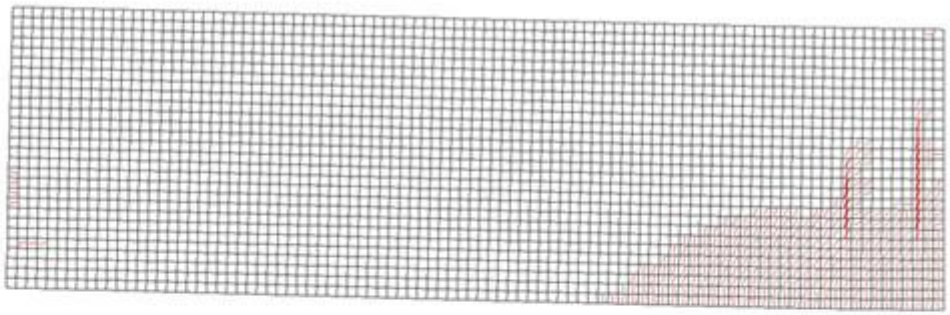

- Beam reached ultimate capacity at 125.9 kips:

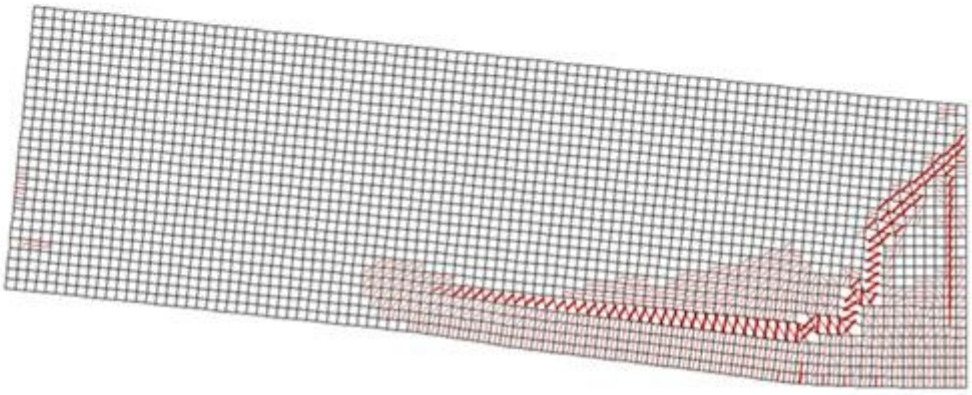

Figure E8. FEA Model for Beam V-4-0.93.

- Beam deformation at 107.9 kips:

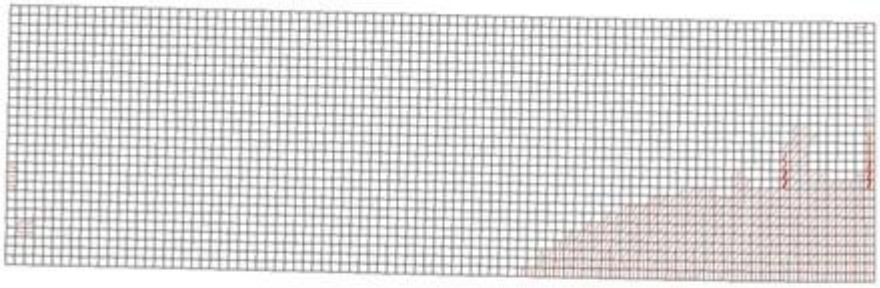

- Beam reached ultimate capacity at 143.9 kips:

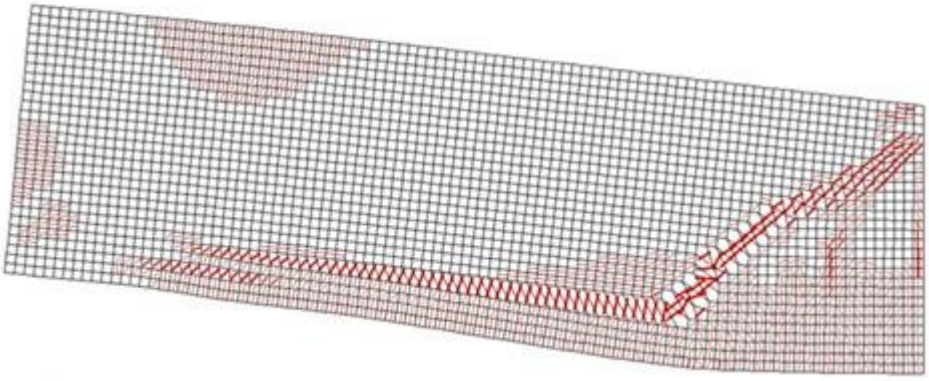

Figure E9. FEA Model For Beam V-4-2.37.

Verification Data Set 2: UM Test Beams

Beam 1

As noted in Chapter 4, beam 1 reinforcement consisted of sixteen 1/2 in seven-wire Grade 270 low-relaxation prestressing strands and two Grade 60 reinforcing bars. Concrete had an average compressive strength of approximately 7500 psi for Test 1, 7900 psi for Test 2, and 8620 psi for Test 3, with a coarse aggregate maximum-size of 3/4 in. The average prestress force that was applied to each strand is 32.2 kips (average stress of 1.4 ksi in the concrete cross section). Figure E10 presents the initial beam model used for Beam 1 in VecTor2.

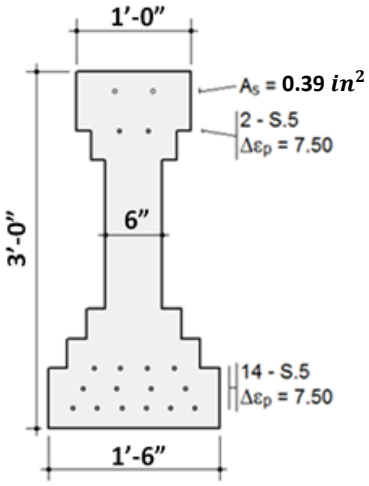

Figure E10. Initial Beam 1 Model Cross Section

It is assumed that the truss reinforcement is perfectly bonded over the entire beam length and a prestress force of 32.2 kips was applied as a prestrain (7.52 *me*) to each strand. Steel input properties are given in Table E3. Concrete compressive strength was taken from 6-9 ksi (minimum, mean, and maximum found from cylinder tests) for different model runs, with corresponding tensile strength from 0.33-0.39 ksi and cylinder strain at $f_c', eo = 2.55\, me$. Concrete Poisson ratio is taken as 0.15, with maximum aggregate size set to 1 in.

Table E3. Beam 1 Steel Material Model Parameters.

	Prestressing Steel	Mild Steel
Yield stress (Fy) (ksi)	243	60
Ultimate Stress (Fu) (ksi)	270	90
Elastic Modulus (Es) (ksi)	28500	29000
Strain hardening (esh)	10 me	10 me
Prestrain (Dep)	7.52	0

Beam 1 Test 1

In Test 1, only the left part of the full beam between supports A and C was modeled (Figure E11). The boundary conditions were modeled as a roller at support A and pinned at support C. No clamps were applied to the FEA model. Instead, the amount of transverse reinforcement at the clamped section was significantly increased (approximately 3 times) to prevent any cracking along that section. Due to a limitation in the number of elements allowed (6000) in the currently available version of the VecTor2 preprocessor (FormWorks, version 3.5), a fine mesh was applied only at the section of interest where critical shear cracks are expected to occur. A 6 in. line load was applied at P1 (Figure E11) in the negative Y direction, to prevent local element crushing and distortion. The load was increased monotonically at a rate of 4.5 kips/step until beam failure (the same load scenario was used for the other two tests as well). To prevent cracks at the zero-width supports, a higher-strength concrete material was modeled in the elements just above these locations.

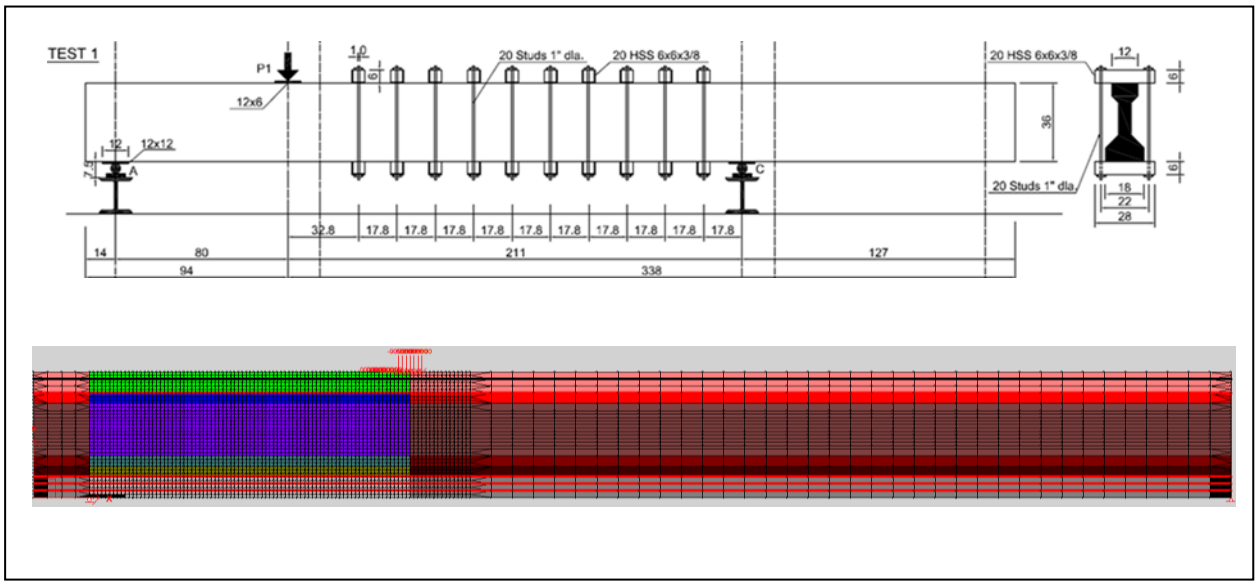

Figure E11. Beam 1 Test 1 Model (dimensions in inches).

At the beginning of the analysis, the left end of the beam cracked immediately as shown in Figure E12a. These cracks appeared to be as a result of the reinforcement prestrain at that location. In order to prevent the left face from prematurely cracking, a coarse mesh was applied at that section, which reduced crack potential, as shown in Figure E12b. Note that as this coarse mesh is outside of the beam span (i.e. to the left of the leftmost support), diagonal cracking potential is not affected. This adjustment was applied to all models. The results of the adjusted model are shown in Table E4 and Figure E13. Figure E14 shows intermediate deformation results with f'c = 7.5 ksi.

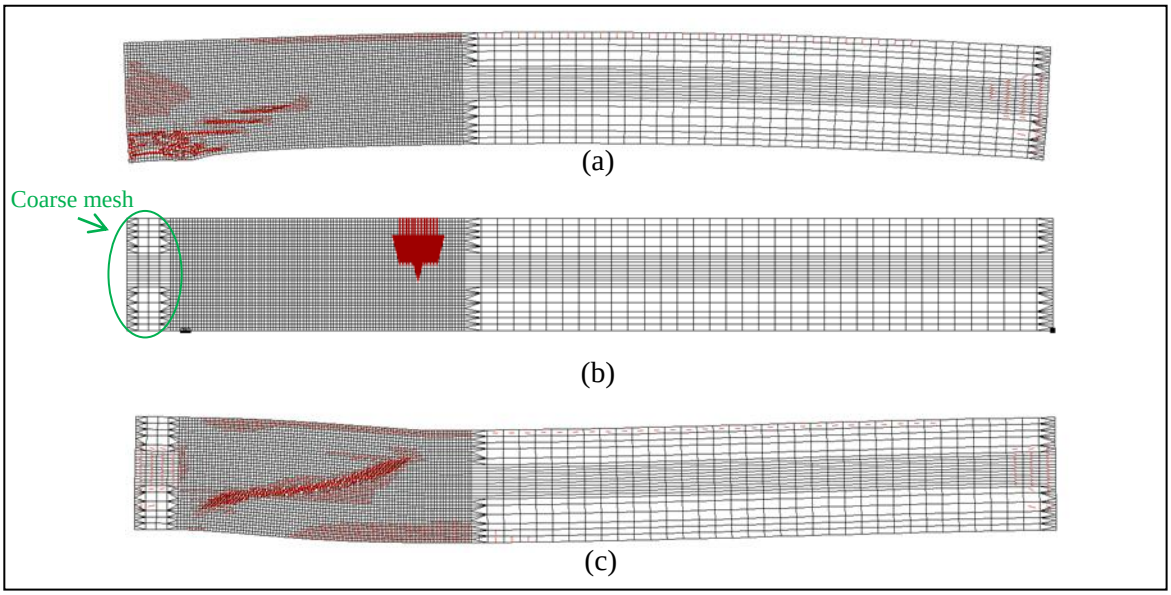

Figure E12. Beam 1 Test 1 Model Results: (a) Fine mesh at the left face (b) Coarse mesh at the left face (c) Deformation shape at failure.

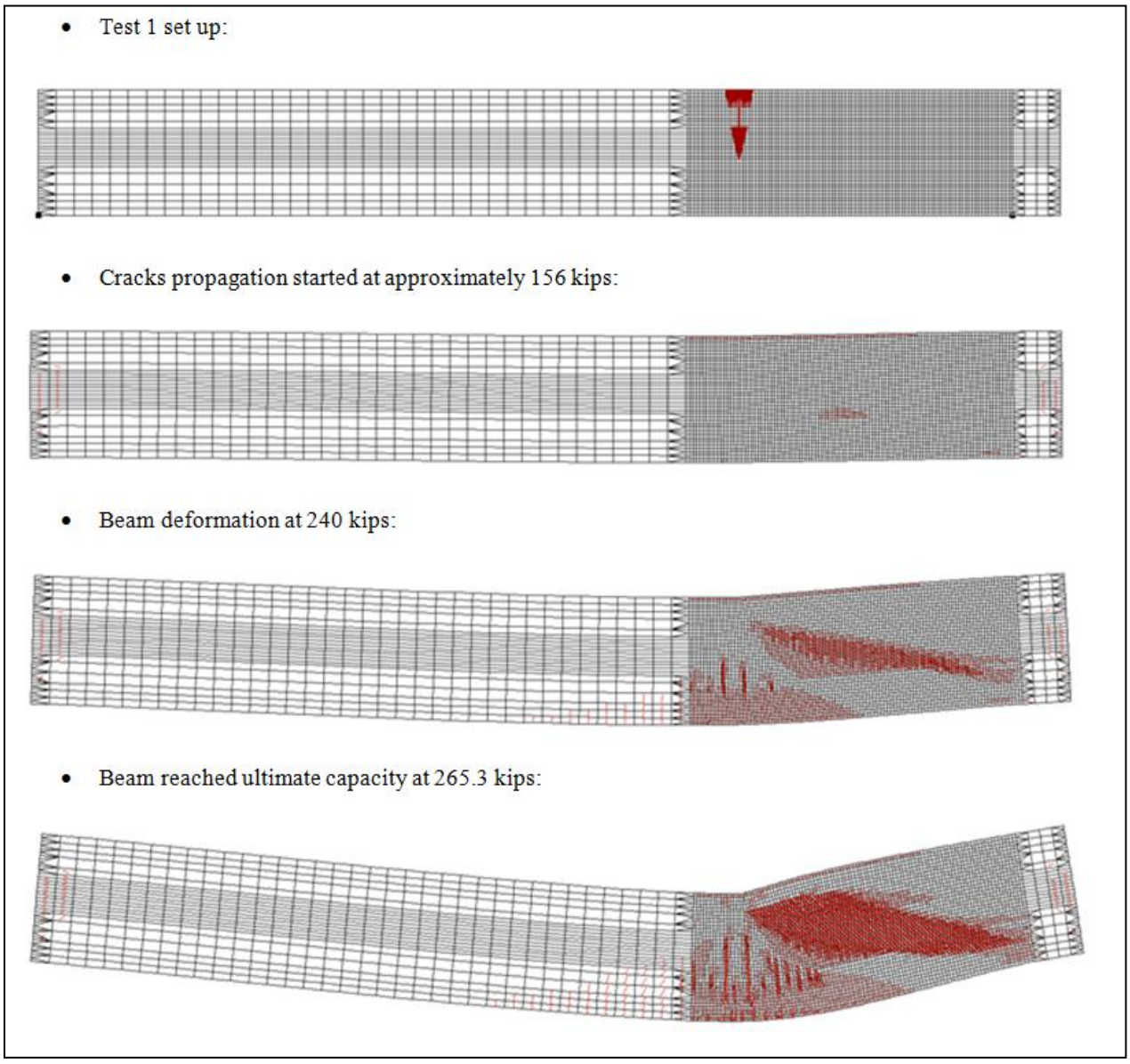

Figure E13. Beam 1 Test 1 Model Results.

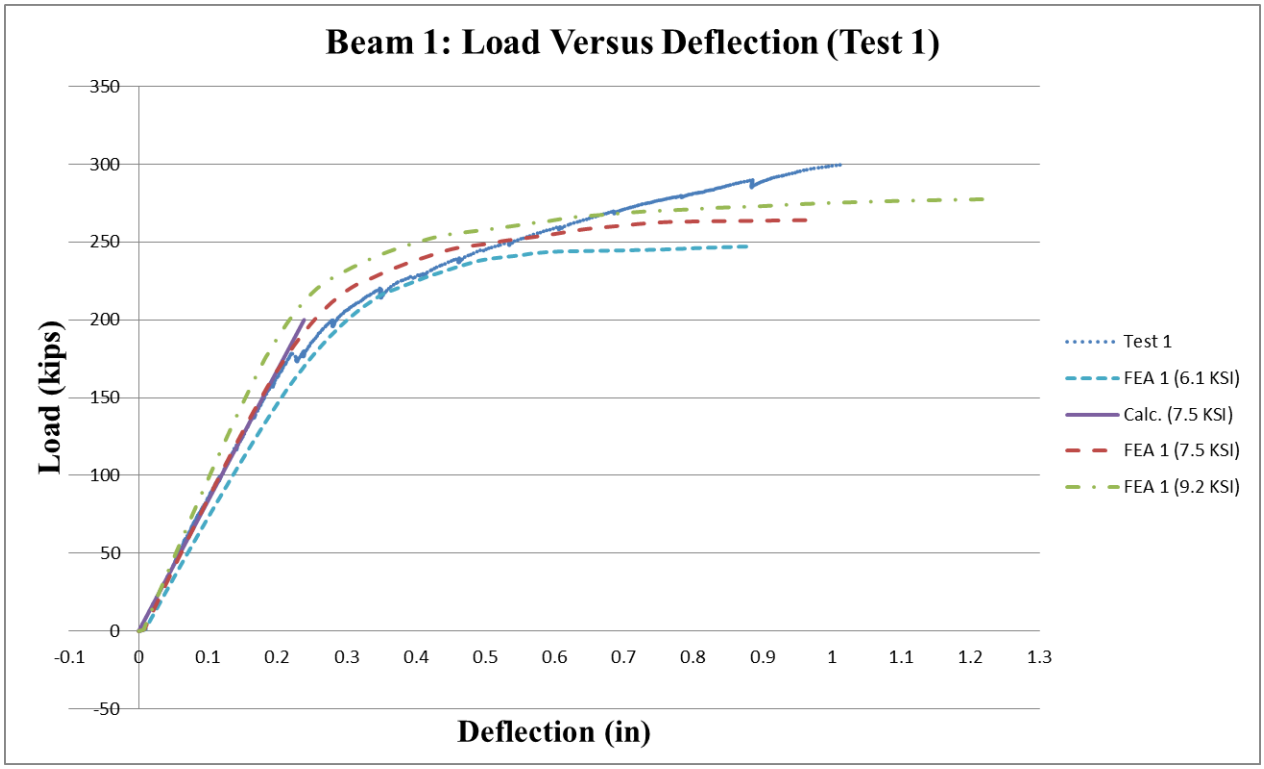

Figure E14. Beam 1 Test 1 Load-Deflection Results.

Table E4. Beam 1 Test 1 Model Results.

f'_c (ksi)	Shear cracking load (Kips)	Ultimate failure load (Kips)
Test	180	299
6.1	147	248
7.5	156	265
9.2	166	278

Beam 1 Test 2

In Test 2, only the portion of the beam between supports B and D was modeled. The boundary conditions consisted of a pin at support B (left) and a roller at support D (right). The transverse reinforcement at the clamped section (Figure E15) was increased as in the Test 1 model to prevent any cracking along that section. Results are shown in Table E5 and Figure E16. Figure E17 shows intermediate deformation results with f'_c = 7.8 ksi.

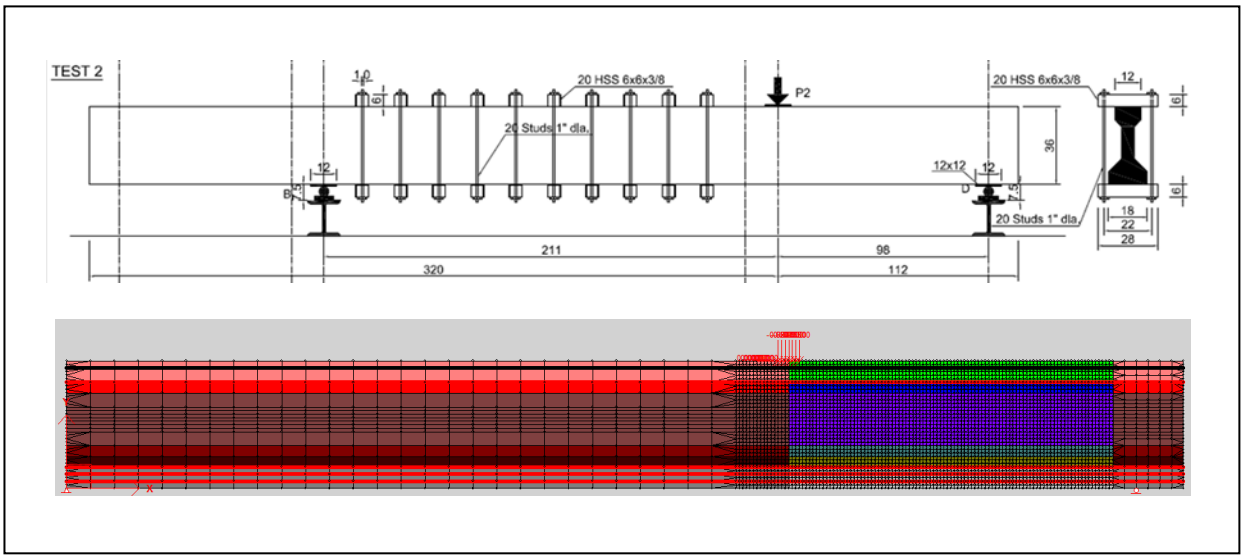

Figure E15. Beam 1 Test 2 Model (dimensions in inches).

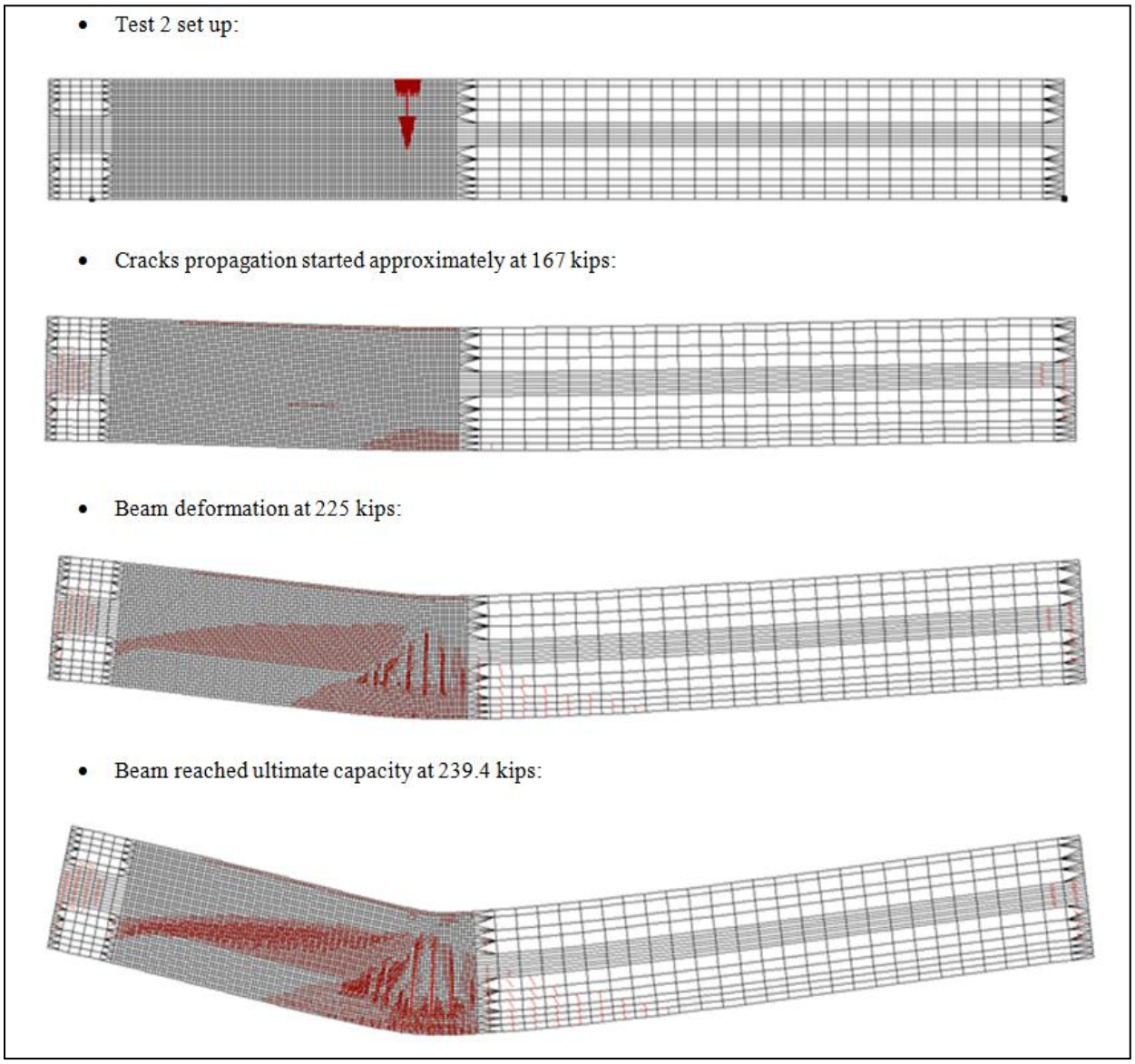

Figure E16. Beam 1 Test 2 Model Results.

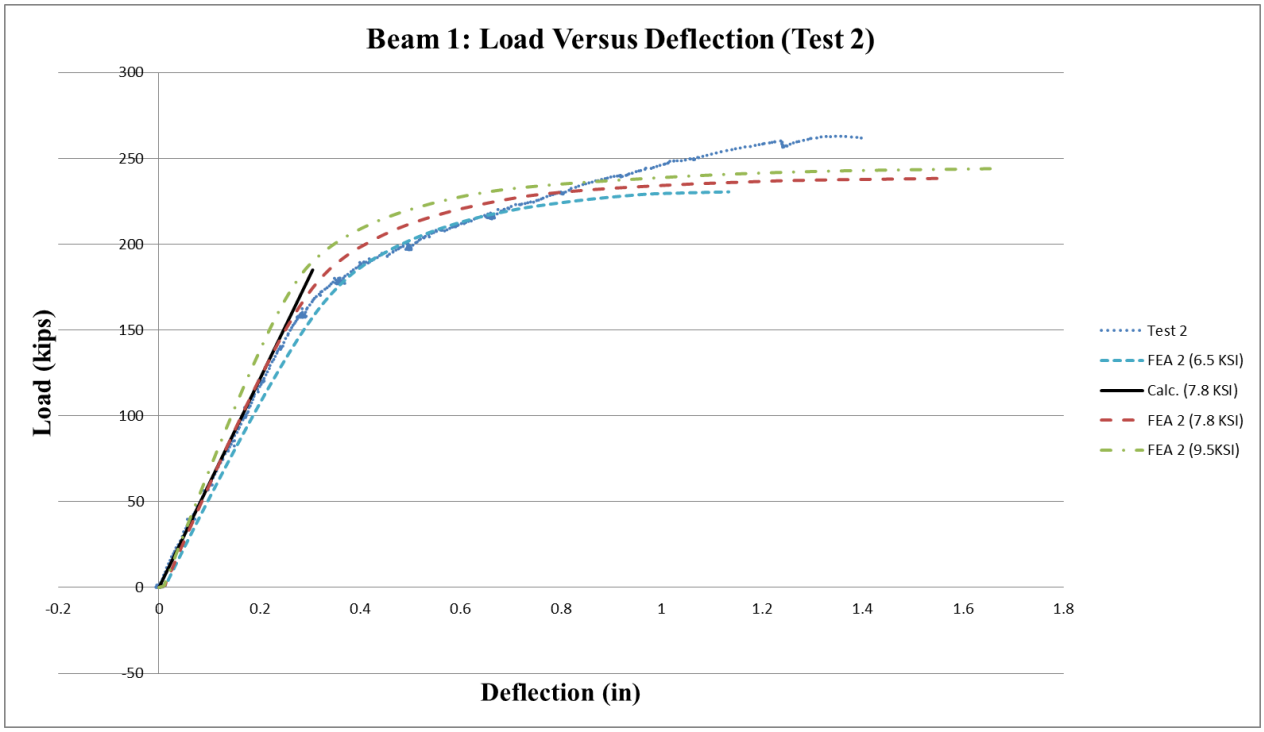

Figure E17. Beam 1 Test 2 Load-Deflection Results.

Table E5. Beam 1 Test 2 Model Results.

f'_c (ksi)	Shear cracking load (Kips)	Ultimate failure load (Kips)
Test	190	262
6.5	157	232
7.8	167	239
9.5	175	245

Beam 1 Test 3

In Test 3, the portion of the beam between supports B and C was modeled, as shown in Figure E18.

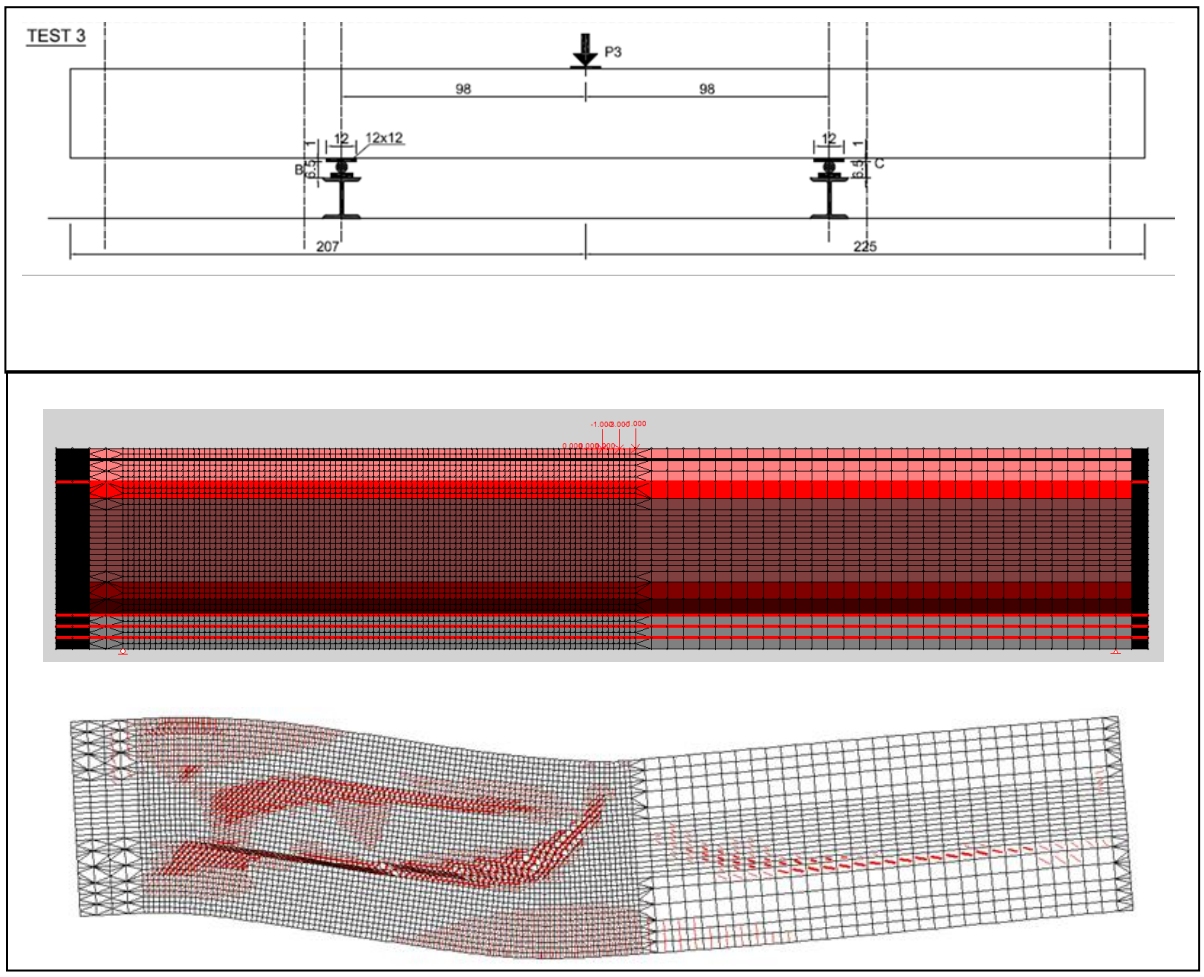

Figure E18. Beam 1 Test 3 Model (dimensions in inches).

The results of the model are shown in Table E6 and Figure E19. Figure E19 shows intermediate deformation results with f'_c = 8.6 ksi. As seen in Figures E19 and E20, a long horizontal crack appeared in the FEA model, which caused a beam failure significantly under the test result. It was determined that this crack was caused by artificially high stress concentrations that occurred at the abrupt, step-like width change of the idealized model, as a result of the prestress force (as shown in Figure E10). To avoid this problem, the modeling approach was again adjusted as shown in Figure E21. As shown in the figure, this method eliminated the section width change in the middle of the web, which was prone to shear cracking, and modeled the section with an "I" shape. In this method, the areas of the sloped, triangular web regions of the original section were distributed into a constant-width web of equal area as the original beam, resulting in a new modeled web width of 7.86" rather than the original 6.0", as shown in Figure E21. This

modified approach left the cracking load unchanged, but resulted in a substantial increase in predicted ultimate capacity, which was much closer to test results.

To verify the validity of the new "I" shaped modeling approach, it was applied to previous test results as well, as summarized in the load-displacement plots in Figures E22-E24 and in the ultimate capacity results shown in Tables E7-E9. Table E10 presents a summary of the critical beam test parameters. Figure E25 shows the final deformed shapes of the FEA models using the latest model. Good agreement with all test results were realized.

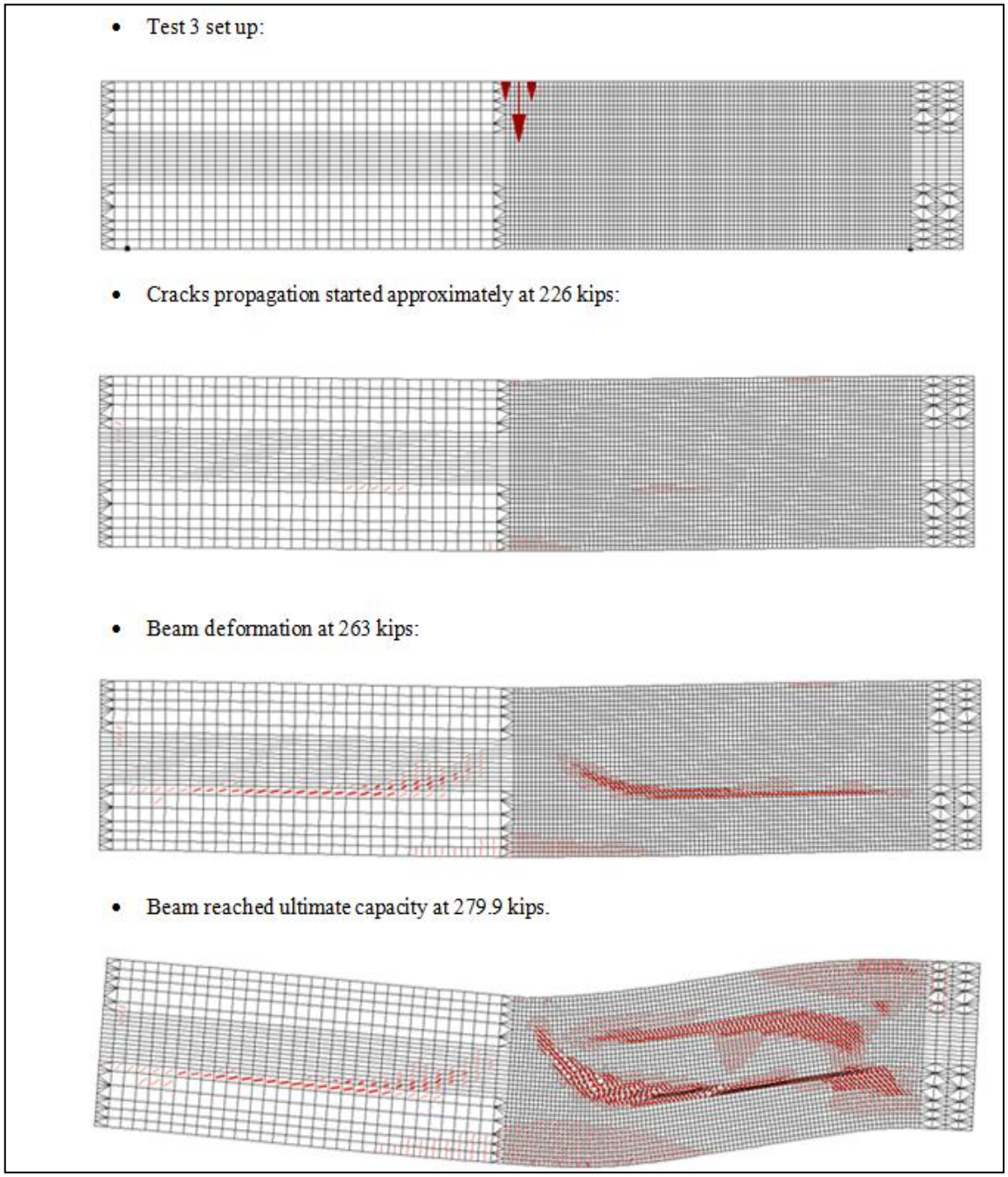

Figure E19. Beam 1 Test 3 Results.

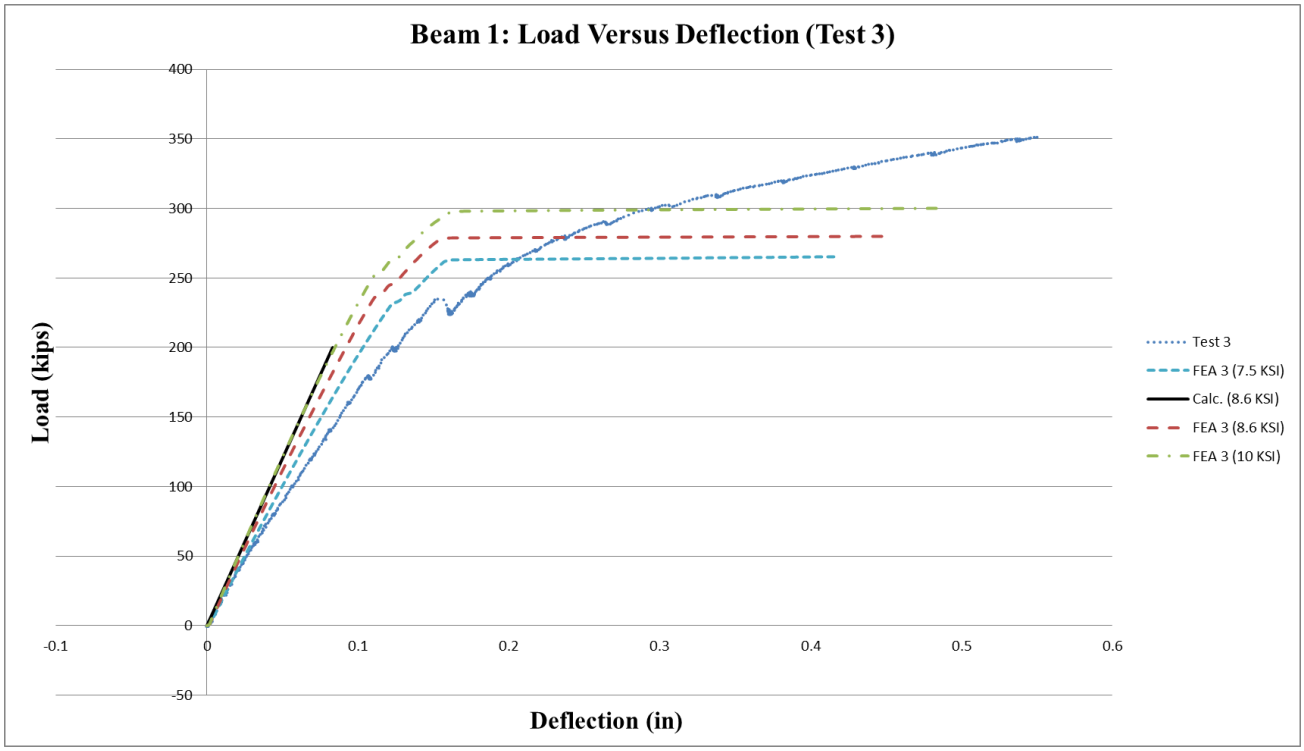

Figure E20. Beam 1 Test 3 Load-Deflection Results.

Table E6. Beam 1 Test 3 Model Results.

f'_c (ksi)	Shear cracking load (Kips)*	Ultimate failure load (Kips)
Test	227	356
7.5	225	264
8.6	226	280
8.6 Modified Model	245	337
10.0	242	299

*Shear cracking load in Test 3 was less than the FEA model results due to the existing cracks in the beam from Test 1 and Test 2.

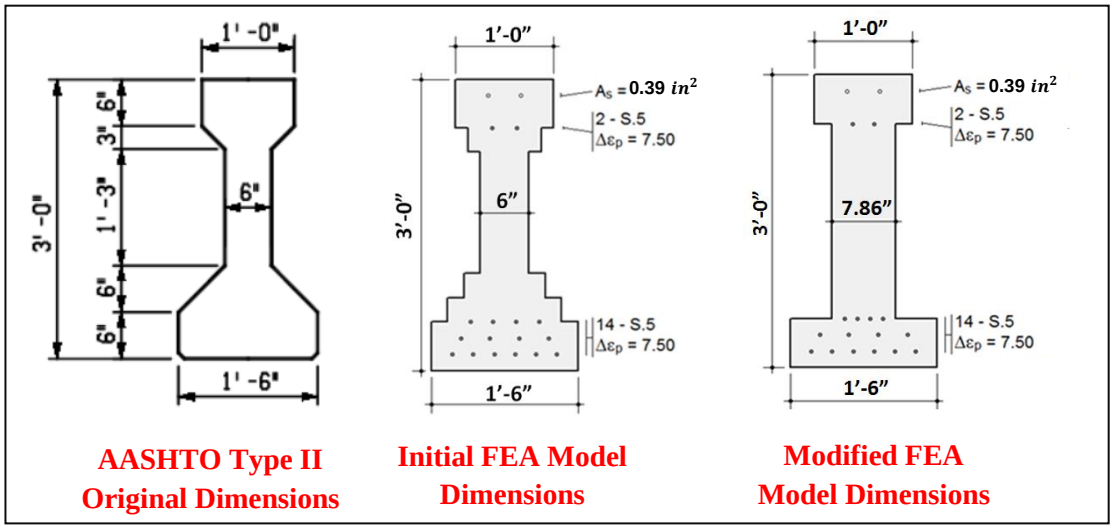

Figure E21. Modified FEA Model

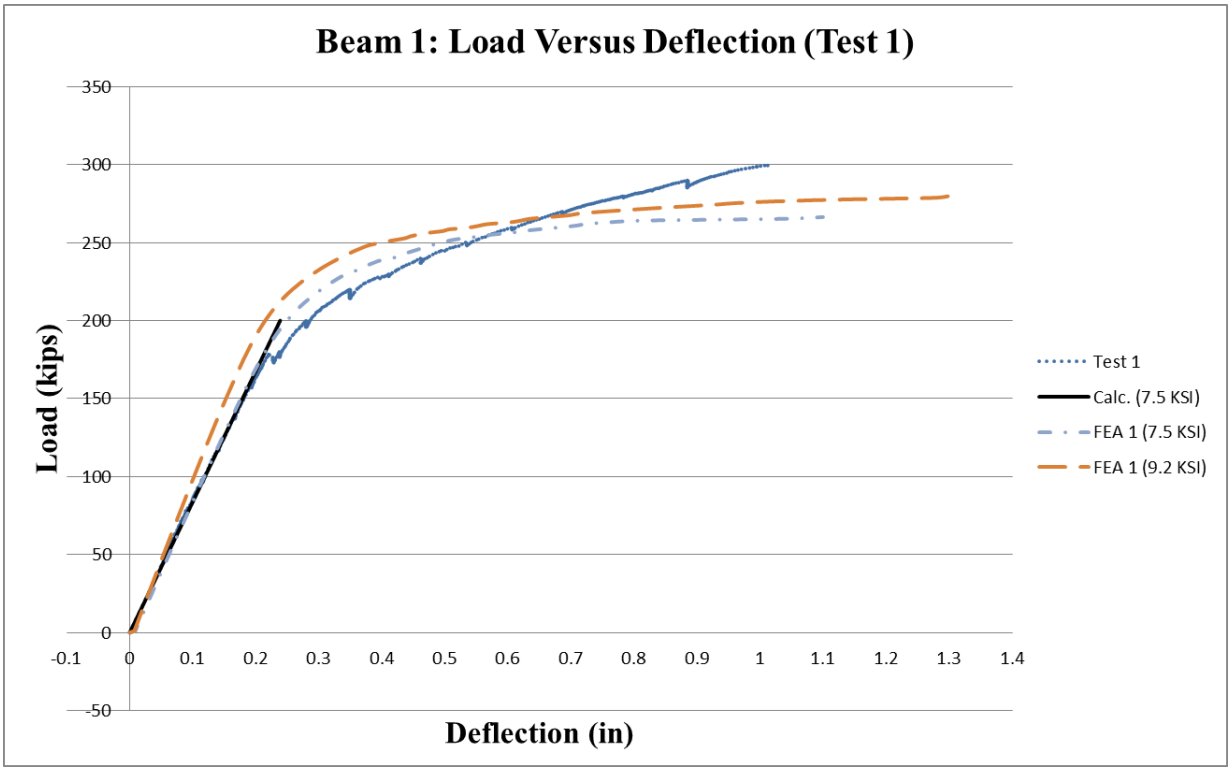

Figure E22. Modified Model Beam 1 Test 1 Load-Deflection Results

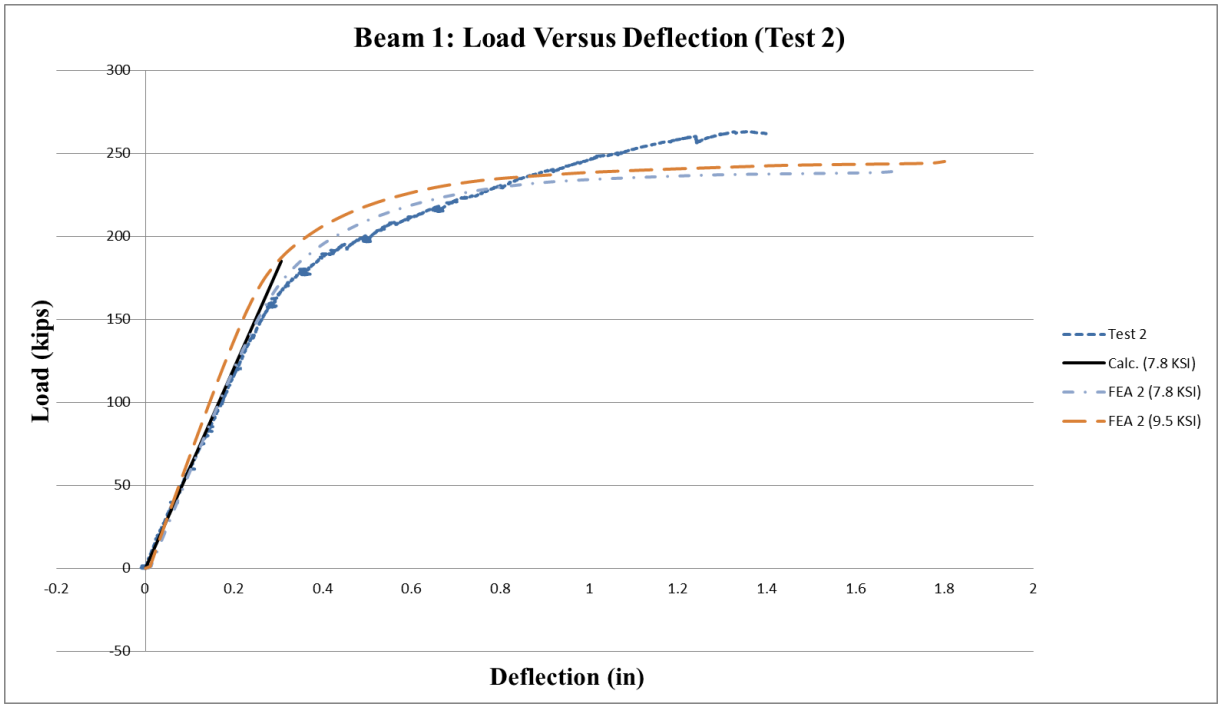

Figure E23. Modified Model Beam 1 Test 2 Load-Deflection Results.

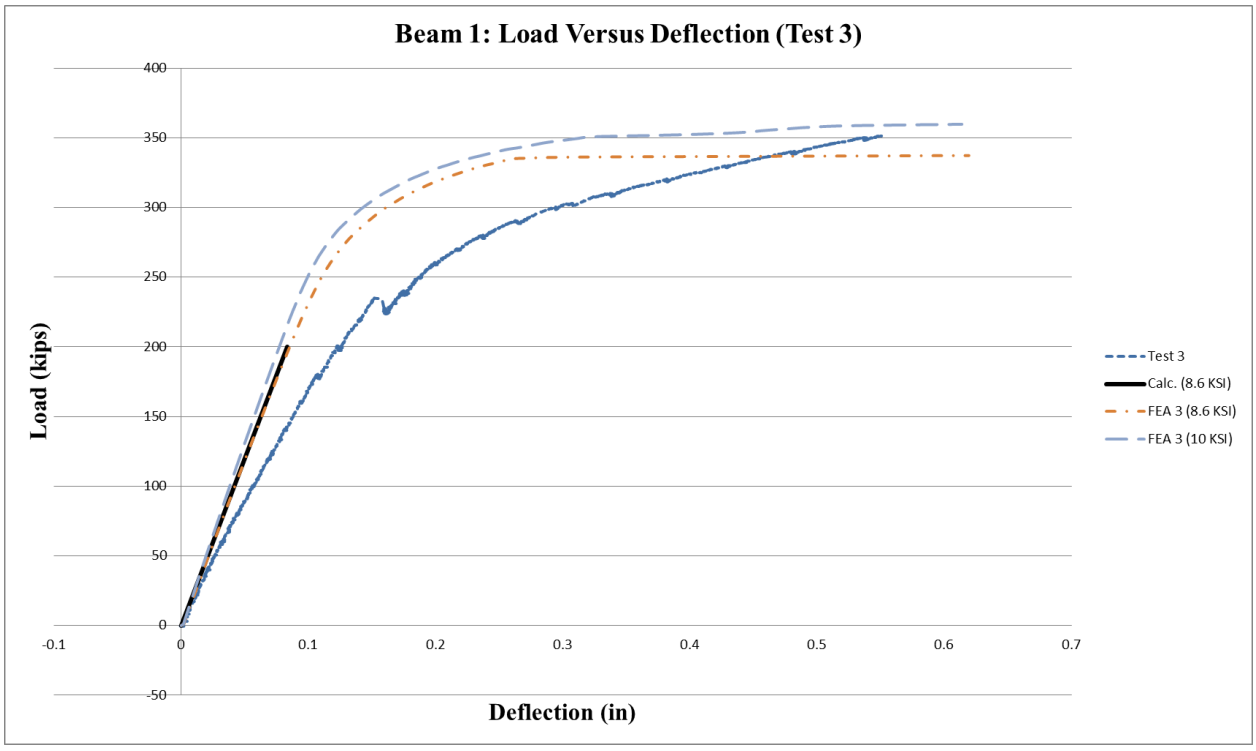

Figure E24. Modified Model Beam 1 Test 3 Load-Deflection Results.

Table E7. Modified Model Results for Beam 1 Test 1.

	Ultimate failure load (Kips)
Test 1	299
f'_c = 7.5 ksi	266
f'_c = 9.2 ksi	279

Table E8. Modified Model Results for Beam 1 Test 2.

	Ultimate failure load (Kips)
Test 2	262
f'_c = 7.8 ksi	239
f'_c = 9.5 ksi	244

Table E9. Modified Model Results for Beam 1 Test 3.

	Ultimate failure load (Kips)
Test 3	356
f'_c = 8.6 ksi	337
f'_c = 10.0 ksi	353

Table E10. Summary of Beam 1 Test Parameters.

Design	Stirrups spacing (in)	*a/d* ratio
Test 1	8	2.8
Test 2	8	3.4
Test 3	21	3.4

Test 1-Modified Model (7.5 KSI):

- Beam reached ultimate capacity at 266.4 kips:

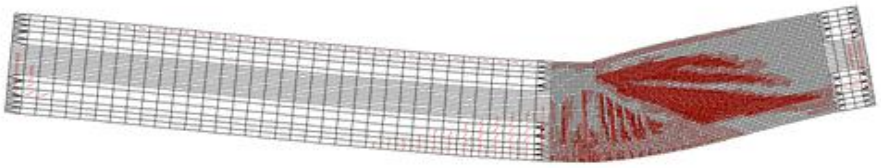

Test 2 Modified Model (7.8 KSI):

- Beam reached ultimate capacity at 239.4 kips:

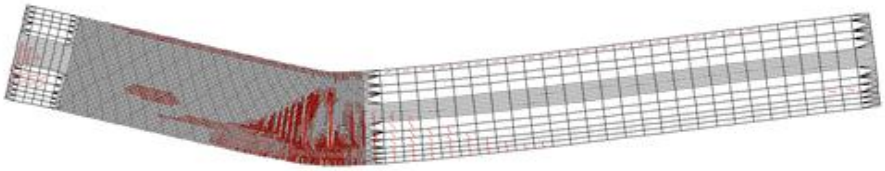

Test 3 Modified Model (8.6 KSI):

- Beam reached ultimate capacity at 337.2 kips.

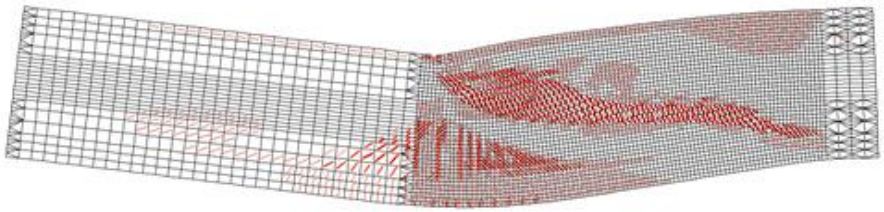

Figure E25. Beam 1 Modified Model Failure Results

Beam 2

As discussed in Chapter 4, similar to Beam 1, three tests were performed on Beam 2. The layout for Beam 2 is shown in Figure E26. Only the final, most successful FEA modeling approach used to model Beam 1 was used for Beam 2. The same material model parameters used for Beam 1 were used for Beam 2, with the exception of the prestrain value, taken as Dep = 5.43 *me*, and differing concrete strengths, to correspond to the test cylinders, as discussed below. A

typical value was $f_c' = 9200\ psi$, with corresponding tensile strength $f_t' = 381\ psi$ and cylinder strain at $f_c', eo = 2.70\ me$.

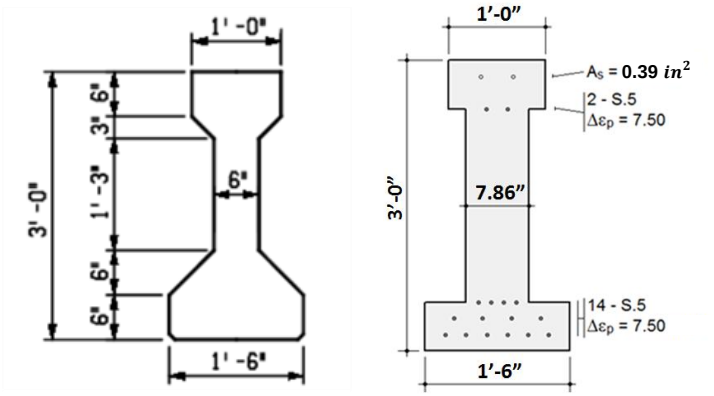

Figure E26. Beam 2 Section and FEA Model.

Beam 2 Test 1

Using the same approach taken for Beam 1, Beam 2 was modeled and loaded as shown in Figure E27 for Test 1. Results are summarized in Figures E28 and E29.

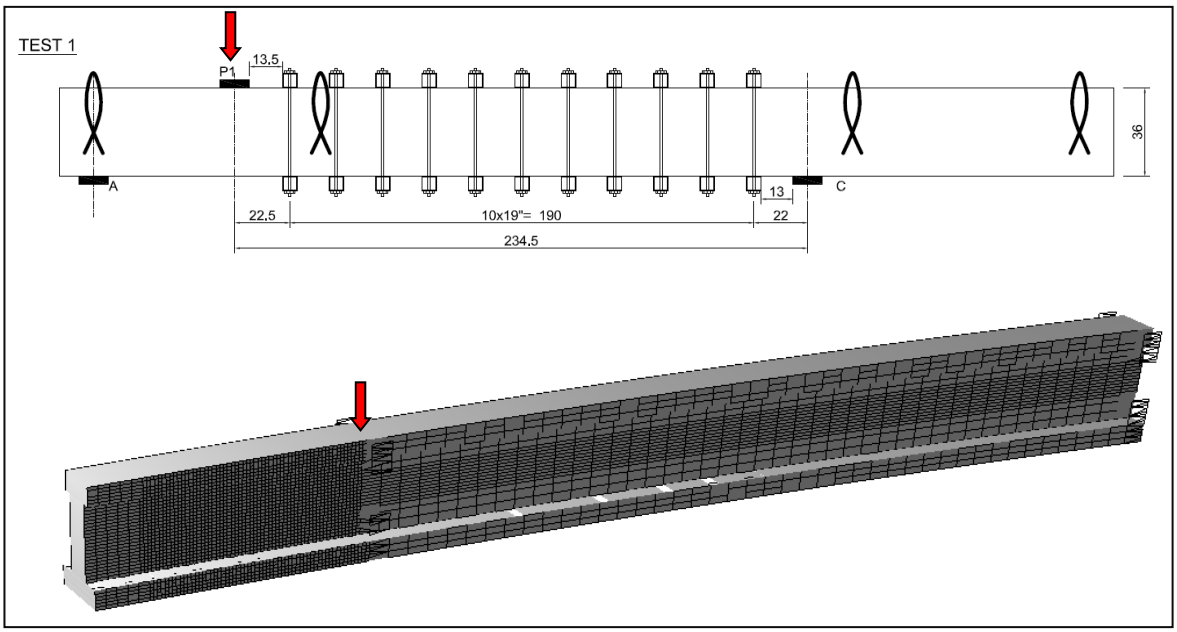

Figure E27. Beam 2 Test 1 Model (dimensions in inches).

Test 1 (f'_c = 9.2 ksi)

- Test 1 set up:

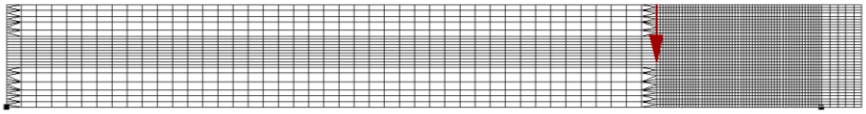

- Beam deformation at 204.6 kips:

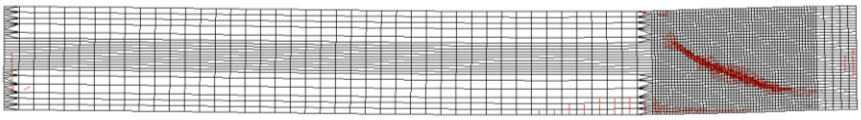

- Beam reached ultimate capacity at 260.8 kips:

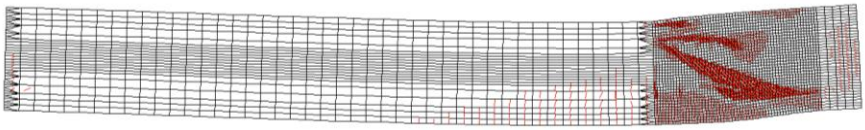

Figure E28. Beam 2 Test 1 Model Results.

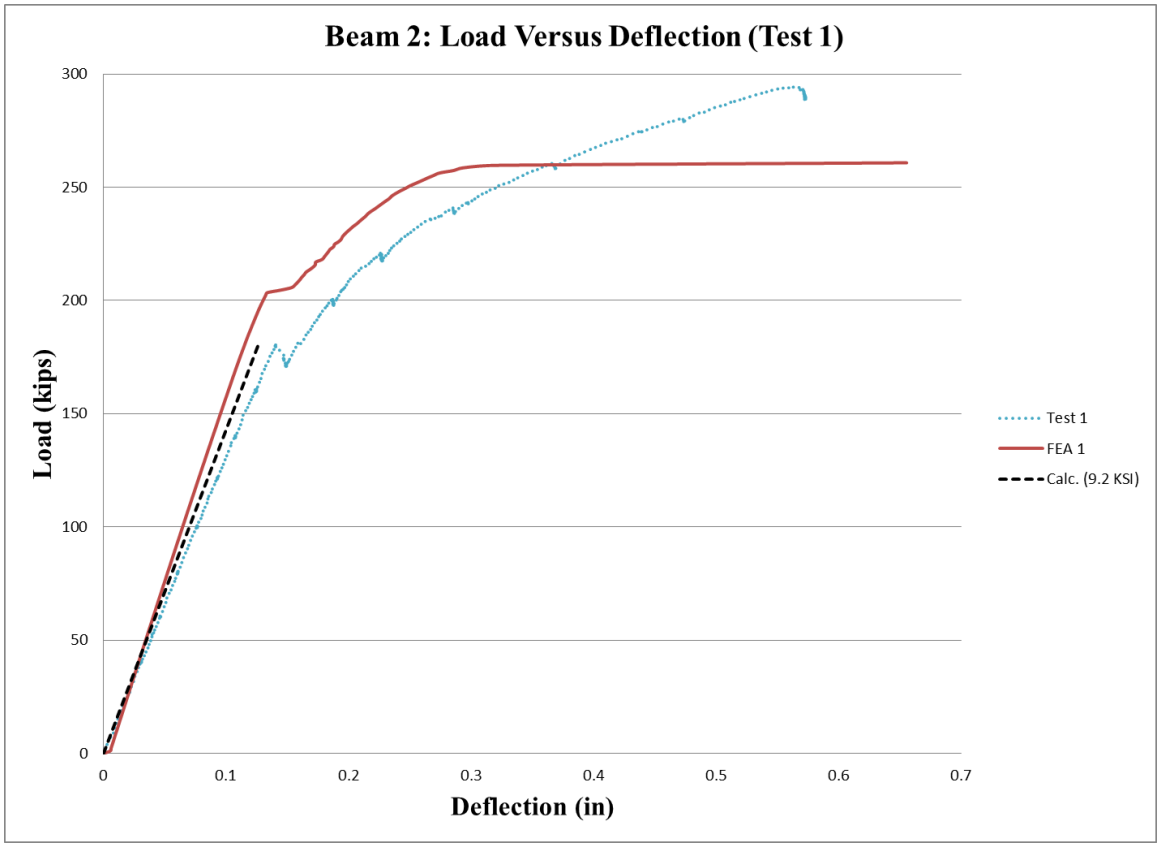

Figure E29. Beam 2 Test 2 Load-Displacement Results.

Test 2

For Test 2, the beam was supported and loaded as shown in Figure E30, and results summarized in Figures E31 and E32.

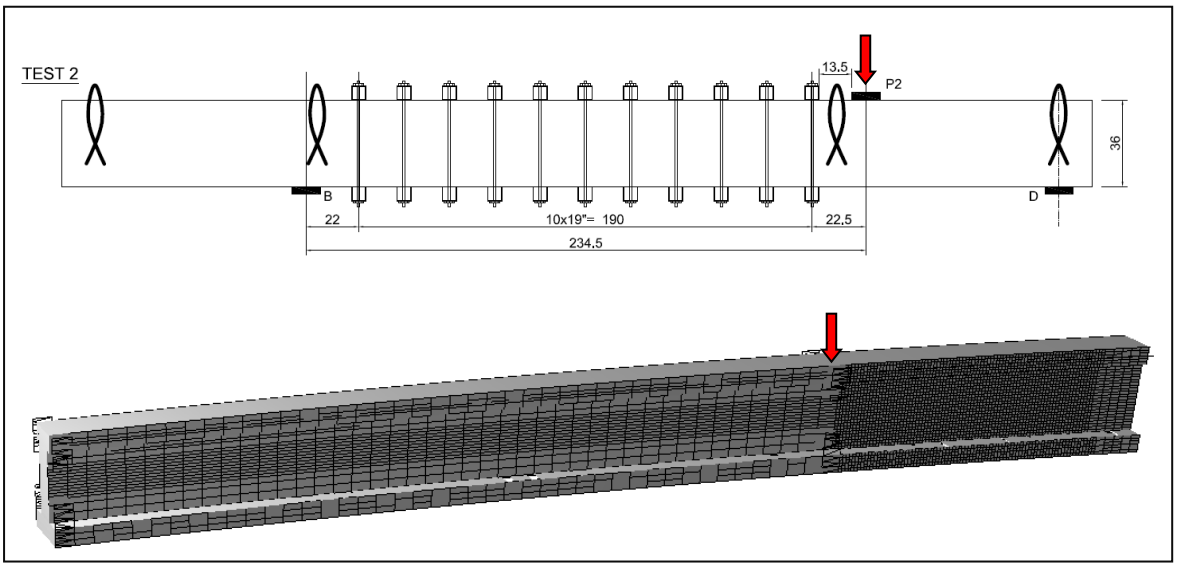

Figure E30. Beam 2 Test 2 Model (dimensions in inches).

Test 2 (f'_c = 9.2 ksi)

- Test 1 set up:

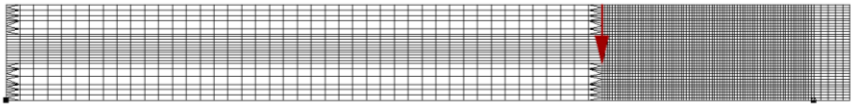

- Beam deformation at 202.3 kips:

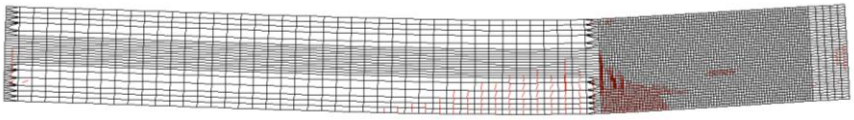

- Beam reached ultimate capacity at 213.6 kips:

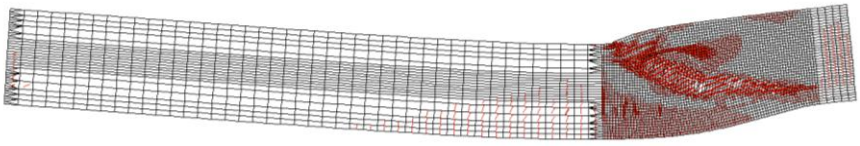

Figure E31. Beam 2 Test 2 Model Results.

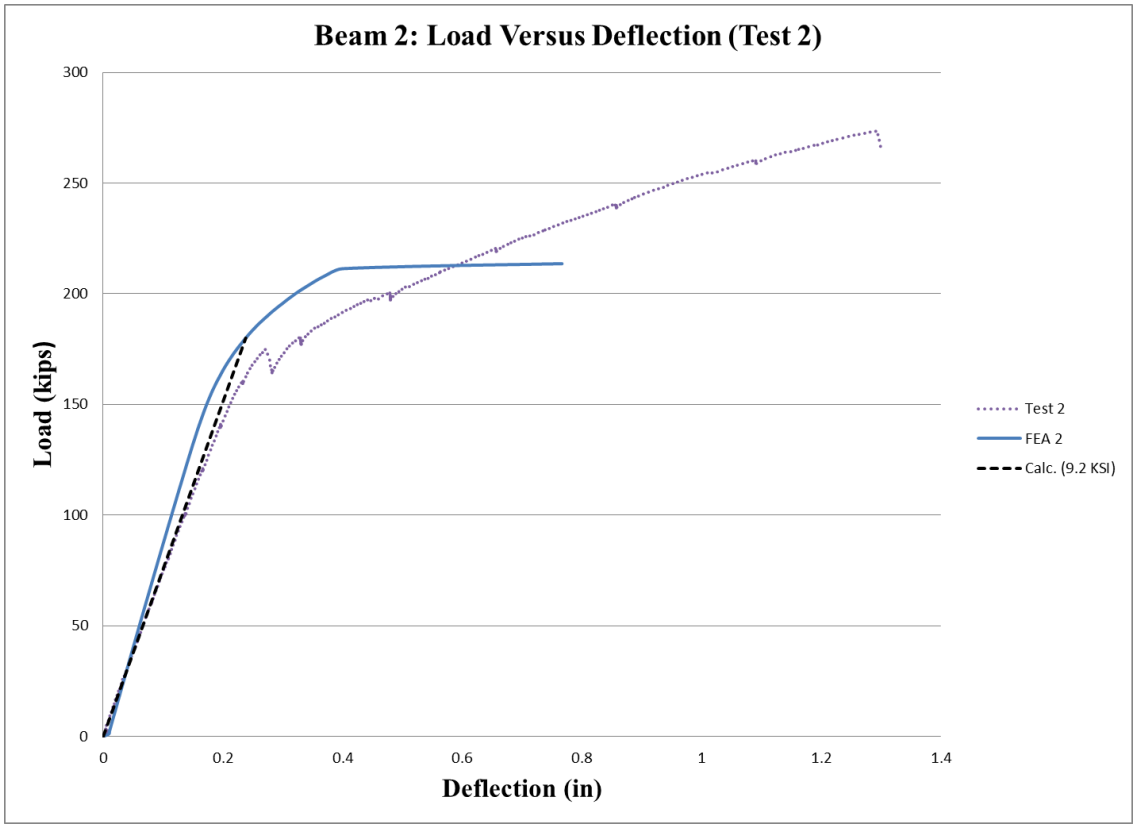

Figure E32. Beam 2 Test 2 Load-Displacement Results.

Test 3

For Test 3, the beam was supported and loaded as shown in Figure E33, with results summarized in Figures E34 and E35.

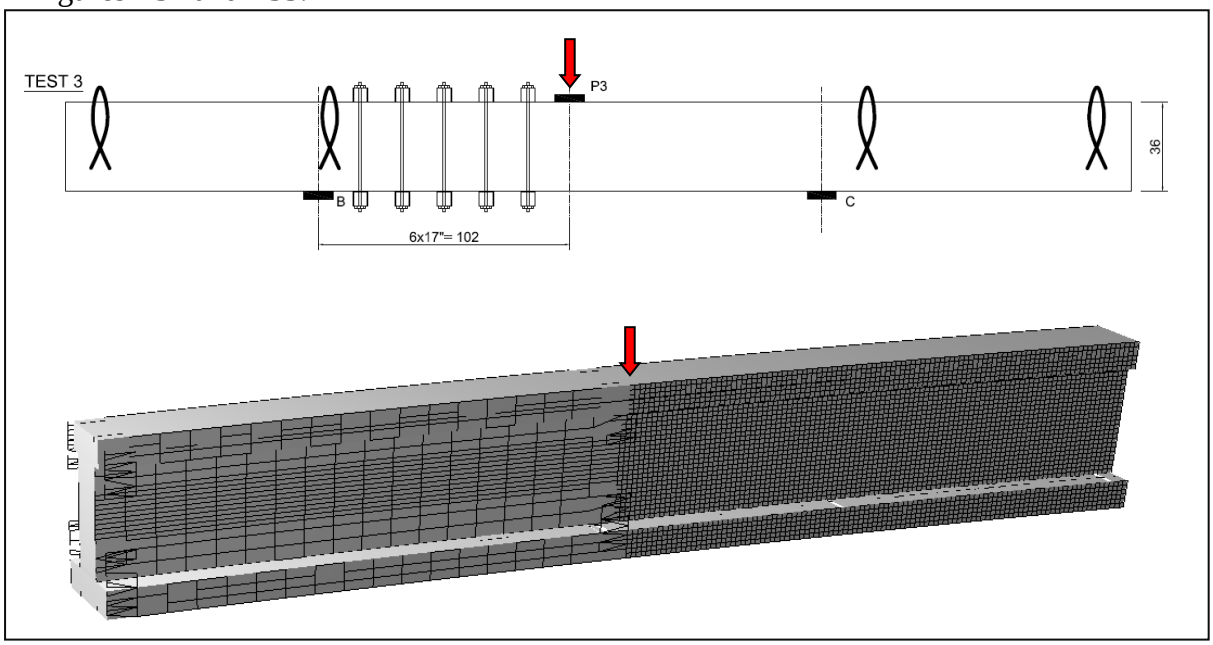

Figure E33. Beam 2 Test 3 Model (dimensions in inches).

Test 3 (f'_c = 9.2 ksi)

- Test 3 set up:

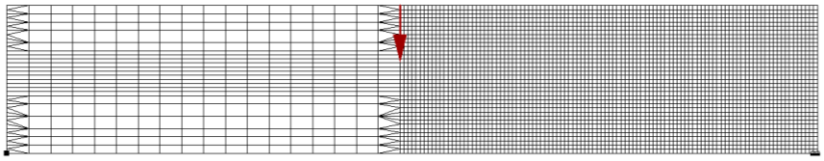

- Beam deformation at 258.5 kips:

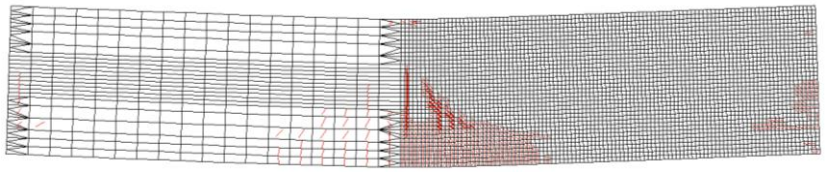

- Beam reached ultimate capacity at 275.4 kips:

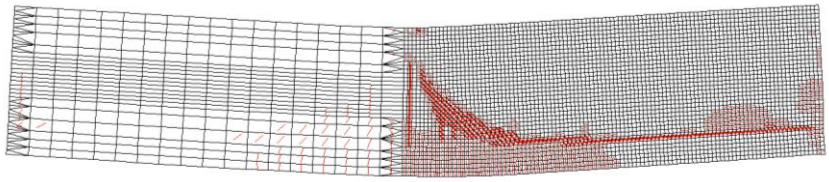

Figure E34. Beam 2 Test 3 Model Results.

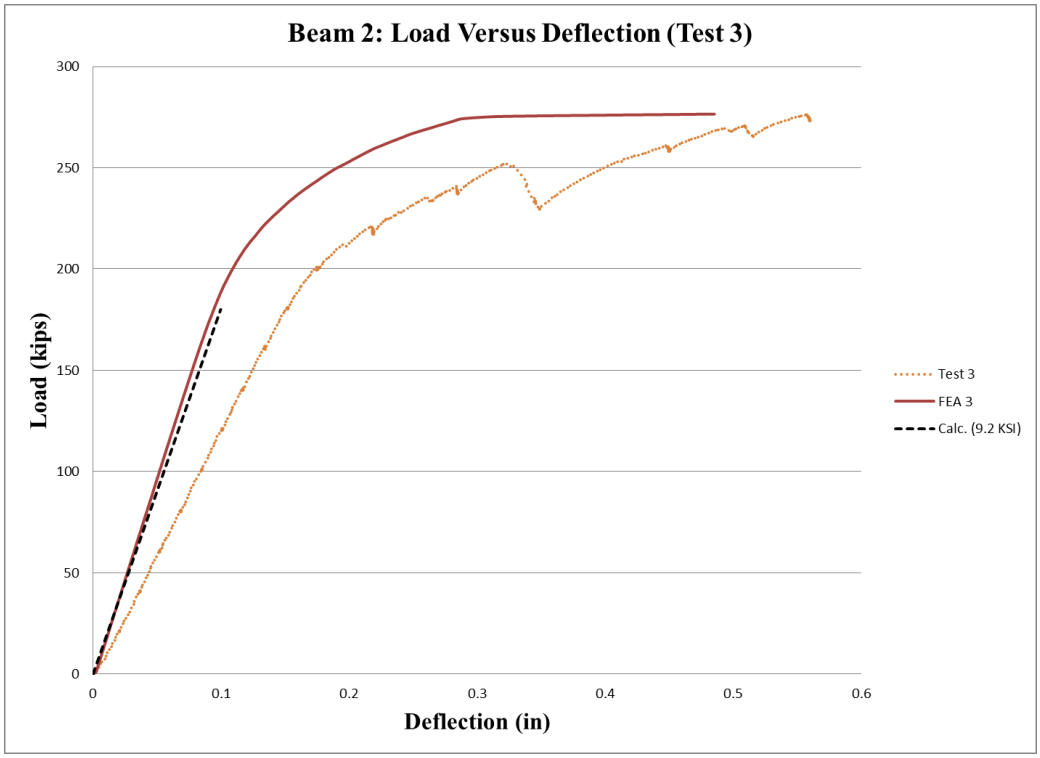

Figure E35. Beam 2 Test 3 Load-Displacement Results.

APPENDIX F: PARAMETRIC ANALYSIS

Table F1. Variables used in Tables F2 and F3.

Variable #	Avg. Stress (ksi)	Concrete f'c (ksi)	Strand Profile	Load Location	Stirrups Spacing (in)
1	0.5	5.5	Straight/Harped	h/2 (Standard)	3 (min)
2	1.5	8	Straight/Harped	LRFD CS	24 (max)
3	2.5	-	Straight/Harped	L/4 (Interim 1979)	12 (avg)

Table F2. Parameter combinations for beam types II, III, and IV.

Combination #	Beam Type	Avg. Stress	Concrete f'c	Load Location	Stirrups Spacing	Strand Profile
1	II,III,IV	1	1	1	1	S/H
2	II,III,IV	2	1	1	1	S/H
3	II,III,IV	1	2	1	1	S/H
4	II,III,IV	1	1	1	2	S/H
5	II,III,IV	2	2	1	2	S/H
6	II,III,IV	2	2	1	1	S/H
7	II,III,IV	2	1	1	2	S/H
8	II,III,IV	1	2	1	2	S/H
9	II,III,IV	3	1	1	1	S/H
10	II,III,IV	3	2	1	2	S/H
11	II,III,IV	3	2	1	1	S/H
12	II,III,IV	3	1	1	2	S/H
13	II,III,IV	1	1	1	3	S/H
14	II,III,IV	2	2	1	3	S/H
15	II,III,IV	2	1	1	3	S/H
16	II,III,IV	1	2	1	3	S/H
17	II,III,IV	3	1	1	3	S/H
18	II,III,IV	3	2	1	3	S/H
19	II,III,IV	1	1	2	1	S/H
20	II,III,IV	2	1	2	1	S/H
21	II,III,IV	1	2	2	1	S/H
22	II,III,IV	1	1	2	2	S/H
23	II,III,IV	2	2	2	2	S/H
24	II,III,IV	2	2	2	1	S/H
25	II,III,IV	2	1	2	2	S/H
26	II,III,IV	1	2	2	2	S/H
27	II,III,IV	3	1	2	1	S/H
28	II,III,IV	3	2	2	2	S/H
29	II,III,IV	3	2	2	1	S/H
30	II,III,IV	3	1	2	2	S/H
31	II,III,IV	1	1	2	3	S/H
32	II,III,IV	2	2	2	3	S/H
33	II,III,IV	2	1	2	3	S/H
34	II,III,IV	1	2	2	3	S/H
35	II,III,IV	3	1	2	3	S/H
36	II,III,IV	3	2	2	3	S/H
37	II,III,IV	1	1	3	1	S/H
38	II,III,IV	2	1	3	1	S/H
39	II,III,IV	1	2	3	1	S/H
40	II,III,IV	1	1	3	2	S/H
41	II,III,IV	2	2	3	2	S/H
42	II,III,IV	2	2	3	1	S/H
43	II,III,IV	2	1	3	2	S/H
44	II,III,IV	1	2	3	2	S/H
45	II,III,IV	3	1	3	1	S/H
46	II,III,IV	3	2	3	2	S/H
47	II,III,IV	3	2	3	1	S/H
48	II,III,IV	3	1	3	2	S/H
49	II,III,IV	1	1	3	3	S/H
50	II,III,IV	2	2	3	3	S/H
51	II,III,IV	2	1	3	3	S/H
52	II,III,IV	1	2	3	3	S/H
53	II,III,IV	3	1	3	3	S/H
54	II,III,IV	3	2	3	3	S/H

Table F3. Models combinations for beam MI-1800.

Combination #	Beam Type	Avg. Stress	Concrete f'c	Load Location	Stirrups Spacing	Strand Profile
1	MI-1800	1	1	1	1	S
2	MI-1800	2	1	1	1	S
3	MI-1800	1	2	1	1	S
4	MI-1800	1	1	1	2	S
5	MI-1800	2	2	1	2	S
6	MI-1800	2	2	1	1	S
7	MI-1800	2	1	1	2	S
8	MI-1800	1	2	1	2	S
9	MI-1800	1	1	1	3	S
10	MI-1800	2	2	1	3	S
11	MI-1800	2	1	1	3	S
12	MI-1800	1	2	1	3	S
13	MI-1800	1	1	2	1	S
14	MI-1800	2	1	2	1	S
15	MI-1800	1	2	2	1	S
16	MI-1800	1	1	2	2	S
17	MI-1800	2	2	2	2	S
18	MI-1800	2	2	2	1	S
19	MI-1800	2	1	2	2	S
20	MI-1800	1	2	2	2	S
21	MI-1800	1	1	2	3	S
22	MI-1800	2	2	2	3	S
23	MI-1800	2	1	2	3	S
24	MI-1800	1	2	2	3	S
25	MI-1800	1	1	3	1	S
26	MI-1800	2	1	3	1	S
27	MI-1800	1	2	3	1	S
28	MI-1800	1	1	3	2	S
29	MI-1800	2	2	3	2	S
30	MI-1800	2	2	3	1	S
31	MI-1800	2	1	3	2	S
32	MI-1800	1	2	3	2	S
33	MI-1800	1	1	3	3	S
34	MI-1800	2	2	3	3	S
35	MI-1800	2	1	3	3	S
36	MI-1800	1	2	3	3	S

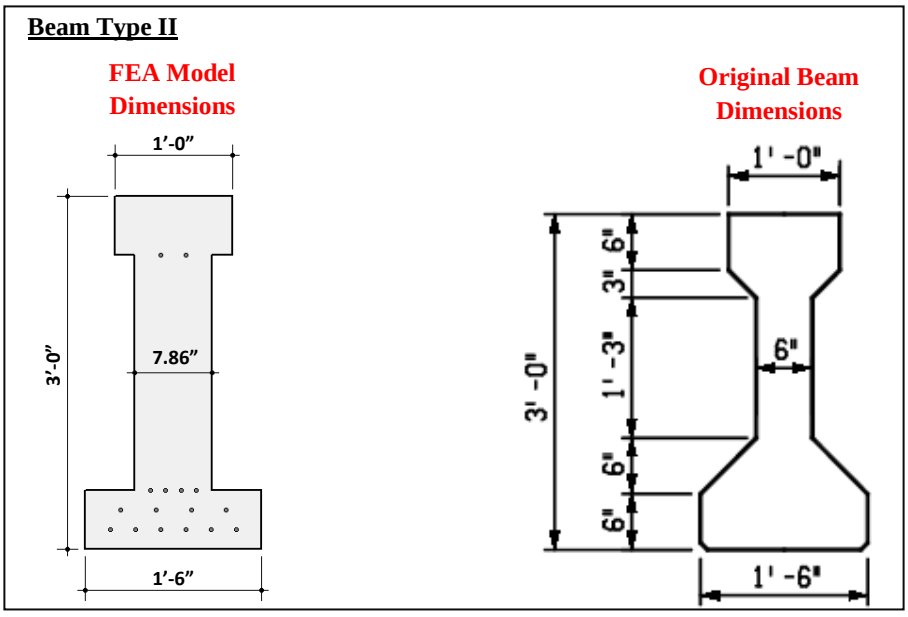

Figure F1. Beam type II Model Dimensions.

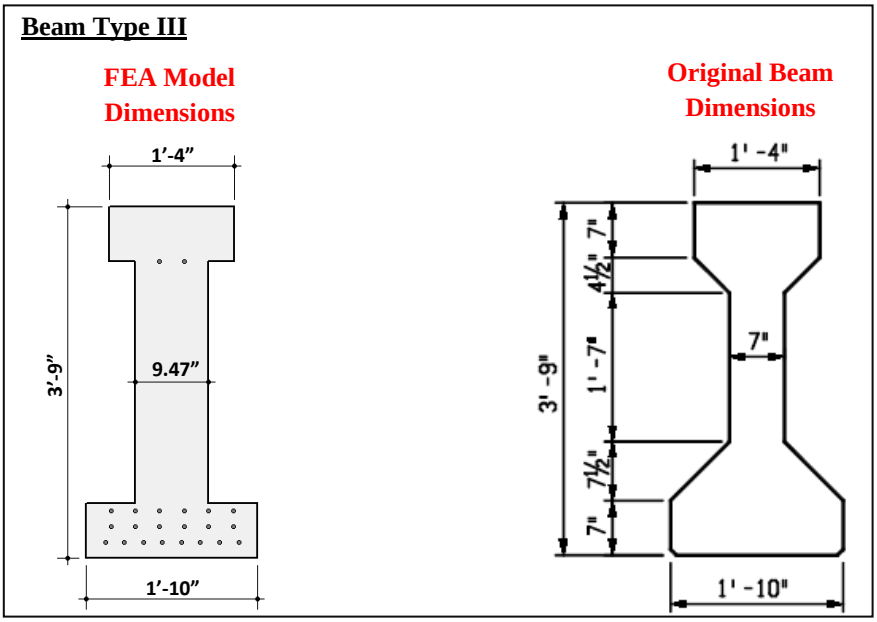

Figure F2. Beam Type III Model Dimensions.

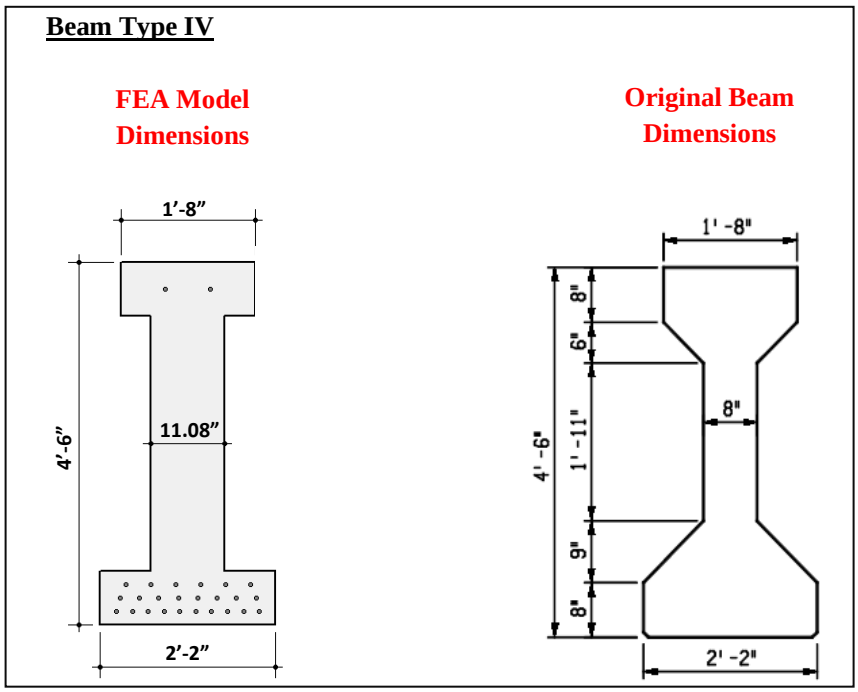

Figure F3. Beam Type IV Model Dimensions.

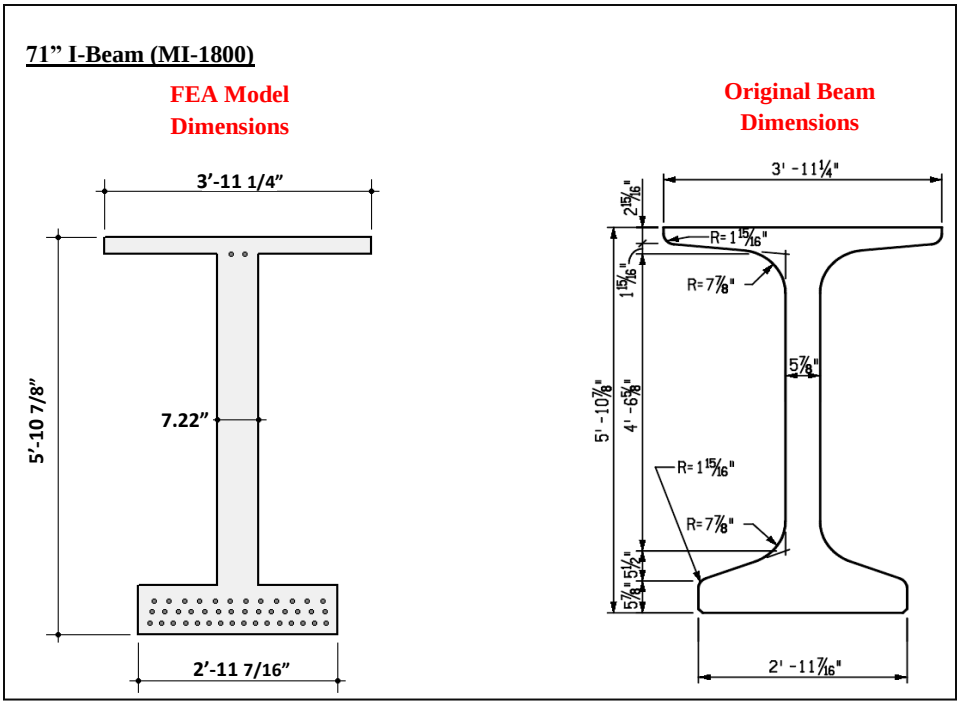

Figure F4. MI-1800 Beam Model Dimensions.

Beam Type II-Straight Strands

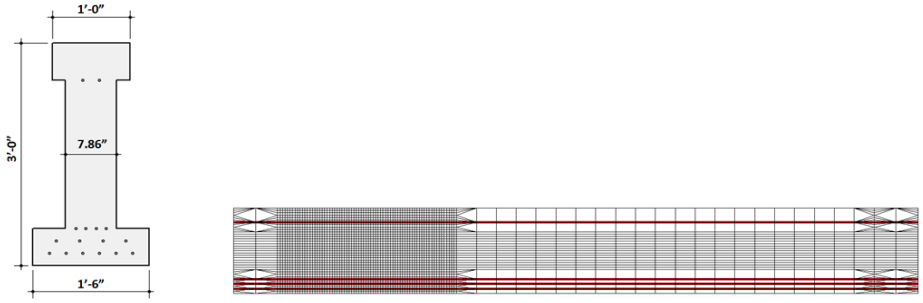

Load at H/2: Failure Load = 517.1 kips

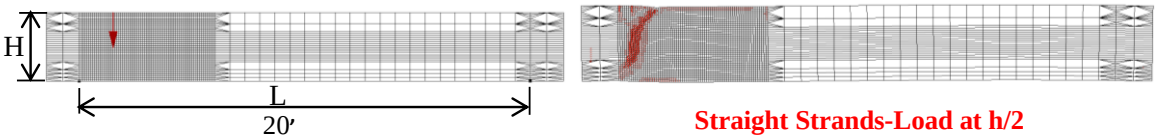

Straight Strands-Load at h/2

Load at LRFD Critical Section: Failure Load = 445.1 kips

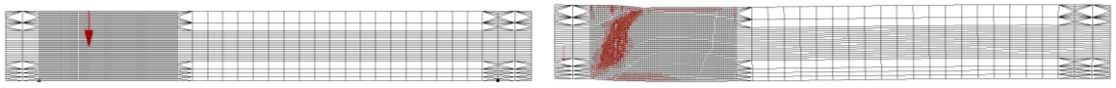

Straight Strands-Load at LRFD CS

Load at L/4: Failure Load = 310.2 kips

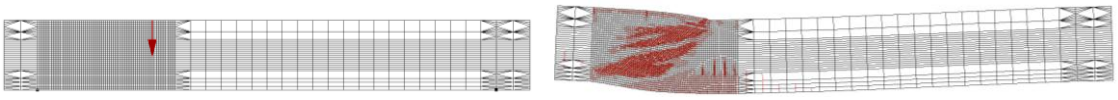

Straight Strands-Load at L/4

Beam Type II- Harped Strands: Load at L/4

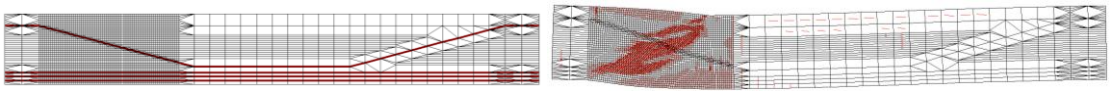

Harped Strands-Load at L/4

Figure F5. Example of Beam Type II Failure.

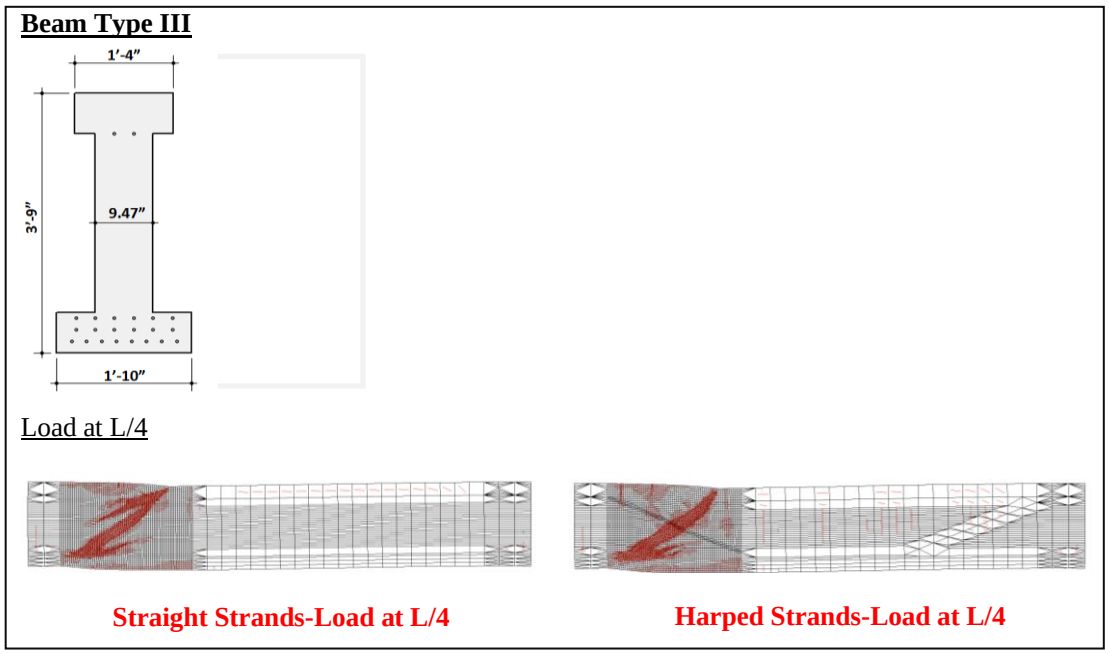

Figure F6. Example of Beam Type III Failure.

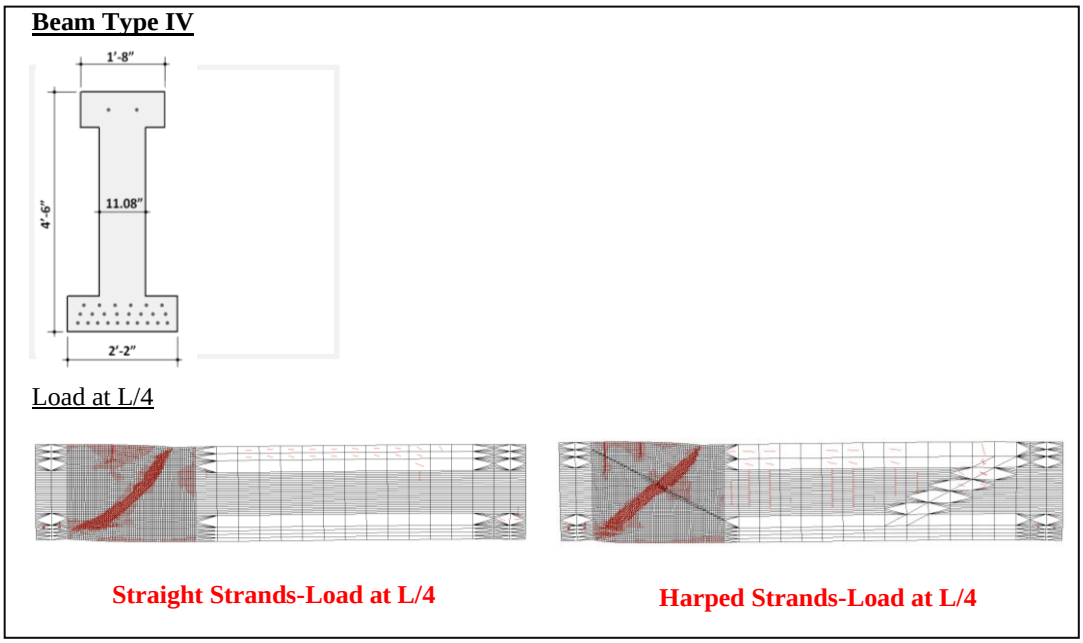

Figure F7. Example of Beam Type IV Failure.

MI-1800

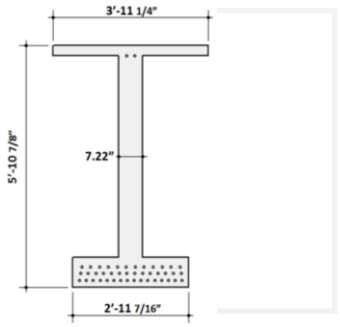

Load at L/4

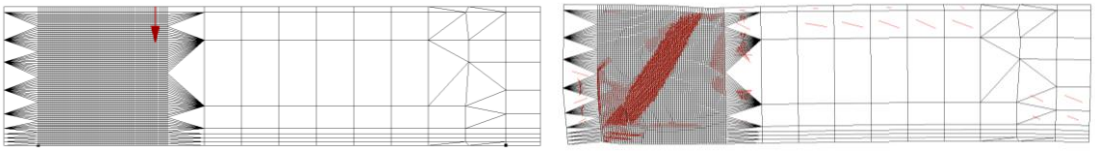

Straight Strands-Load at L/4

Figure F8. Example of MI-1800 Beam Failure.

Table F4. Results for Beam Type II, Straight Strands, Aps at Tension Controlled Limit.

		FEA			Code (Vn)			
II	1	2	3	4	5	6	7	8
Combination #	h/2	LRFD	L/4	Standard	LRFD	Interim 1979	LRFD (εx_max)	LRFD (HL-93)
1	346.2	323.7	310.2	243.3	260.1	282.2	106.8	270.9
2	404.7	427.1	337.2	243.3	260.1	282.2	106.8	270.9
3	431.6	400.2	328.2	252.6	235.0	305.7	108.9	281.8
4	314.7	274.3	170.9	131.3	88.6	80.5	24.3	86.4
5	490.1	445.1	274.3	140.6	99.3	104.0	24.3	86.4
6	508.1	517.1	364.2	252.6	235.0	305.7	108.9	281.8
7	391.2	364.2	233.8	131.3	88.6	80.5	24.3	86.4
8	355.2	305.7	193.3	140.6	99.3	104.0	24.3	86.4
9	463.1	458.6	346.2	243.3	260.1	282.2	106.8	270.9
10	521.6	454.1	292.3	140.6	99.3	104.0	24.3	86.4
11	526.1	530.5	368.7	252.6	235.0	305.7	108.9	281.8
12	418.1	386.7	256.3	131.3	88.6	80.5	24.3	86.4
13	319.2	287.8	193.3	147.3	113.6	109.3	34.3	112.7
14	517.1	445.1	310.2	156.6	124.2	132.8	36.4	124.1
15	404.7	382.2	274.3	147.3	113.6	109.3	34.3	112.7
16	355.2	332.7	220.3	156.6	124.2	132.8	36.4	124.1
17	436.1	395.7	296.7	147.3	113.6	109.3	34.3	112.7
18	521.6	467.6	328.2	156.6	124.2	132.8	36.4	124.1

Comparison #	(1/4)	(2/5)	(3/6)	(3/4)	(3/5)	(3/7)	(2/8)	(3/8)
1	1.42	1.24	1.10	1.27	1.19	2.90	1.20	1.15
2	1.66	1.64	1.20	1.39	1.30	3.16	1.58	1.24
3	1.71	1.70	1.07	1.30	1.40	3.01	1.42	1.16
4	2.40	3.09	2.12	1.30	1.93	7.03	3.17	1.98
5	3.49	4.48	2.64	1.95	2.76	11.29	5.15	3.17
6	2.01	2.20	1.19	1.44	1.55	3.34	1.83	1.29
7	2.98	4.11	2.90	1.78	2.64	9.62	4.22	2.71
8	2.53	3.08	1.86	1.38	1.95	7.96	3.54	2.24
9	1.90	1.76	1.23	1.42	1.33	3.24	1.69	1.28
10	3.71	4.57	2.81	2.08	2.94	12.03	5.26	3.38
11	2.08	2.26	1.21	1.46	1.57	3.38	1.88	1.31
12	3.18	4.36	3.18	1.95	2.89	10.55	4.48	2.97
13	2.17	2.53	1.77	1.31	1.70	5.64	2.55	1.71
14	3.30	3.58	2.34	1.98	2.50	8.53	3.59	2.50
15	2.75	3.37	2.51	1.86	2.42	8.00	3.39	2.43
16	2.27	2.68	1.66	1.41	1.77	6.05	2.68	1.78
17	2.96	3.48	2.71	2.01	2.61	8.65	3.51	2.63
18	3.33	3.76	2.47	2.10	2.64	9.02	3.77	2.65
Mean	2.55	3.00	2.00	1.63	2.06	6.85	3.05	2.09
STDEV.	0.692	1.049	0.719	0.316	0.609	3.110	1.270	0.749
COV	0.272	0.350	0.360	0.194	0.296	0.454	0.416	0.359

Table F5. Results for Beam Type III, Straight Strands, Aps at Tension Controlled Limit.

		FEA			Code (Vn)		
III	1	2	3	4	5	6	7
Combination #	h/2	LRFD	L/4	Standard	LRFD	Interim 1979	LRFD (ε$_x$ max)
1	499.1	499.1	458.6	334.8	327.7	381.9	142.5
2	589.0	616.0	580.0	334.8	327.7	381.9	142.5
3	589.0	593.5	526.1	349.0	332.8	417.9	145.7
4	422.6	373.2	296.7	187.6	134.5	117.0	31.4
5	660.9	607.0	467.6	201.9	159.2	153.0	34.6
6	737.4	714.9	643.0	349.0	332.8	417.9	145.7
7	562.0	499.1	395.7	187.6	134.5	117.0	31.4
8	512.6	422.6	319.2	201.9	159.2	153.0	34.6
9	625.0	629.5	602.5	334.8	327.7	381.9	142.5
10	705.9	602.5	472.1	201.9	159.2	153.0	34.6
11	714.9	737.4	660.9	349.0	332.8	417.9	145.7
12	589.0	539.5	660.9	187.6	134.5	117.0	31.4
13	440.6	391.2	328.2	208.6	170.9	154.9	47.3
14	674.4	616.0	499.1	222.9	186.9	190.9	50.5
15	566.5	508.1	440.6	208.6	170.9	154.9	47.3
16	481.1	449.6	350.7	222.9	186.9	190.9	50.5
17	580.0	539.5	458.6	208.6	170.9	154.9	47.3
18	687.9	620.5	517.1	222.9	186.9	190.9	50.5

Comparison #	(1/4)	(2/5)	(3/6)	(3/4)	(3/5)	(3/7)
1	1.49	1.52	1.20	1.37	1.40	3.22
2	1.76	1.88	1.52	1.73	1.77	4.07
3	1.69	1.78	1.26	1.51	1.58	3.61
4	2.25	2.78	2.54	1.58	2.21	9.45
5	3.27	3.81	3.06	2.32	2.94	13.52
6	2.11	2.15	1.54	1.84	1.93	4.41
7	3.00	3.71	3.38	2.11	2.94	12.60
8	2.54	2.66	2.09	1.58	2.01	9.23
9	1.87	1.92	1.58	1.80	1.84	4.23
10	3.50	3.79	3.08	2.34	2.97	13.65
11	2.05	2.22	1.58	1.89	1.99	4.54
12	3.14	4.01	5.65	3.52	4.92	21.05
13	2.11	2.29	2.12	1.57	1.92	6.94
14	3.03	3.29	2.61	2.24	2.67	9.89
15	2.72	2.97	2.84	2.11	2.58	9.32
16	2.16	2.41	1.84	1.57	1.88	6.95
17	2.78	3.16	2.96	2.20	2.68	9.70
18	3.09	3.32	2.71	2.32	2.77	10.24
Mean	2.47	2.76	2.42	1.98	2.39	8.70
STDEV.	0.608	0.783	1.062	0.500	0.805	4.607
COV	0.246	0.284	0.439	0.253	0.337	0.529

Table F6. Results for Beam Type IV, Straight Strands, Aps at Tension Controlled Limit.

		FEA			Code (Vn)		
IV	1	2	3	4	5	6	7
Combination #	h/2	LRFD	L/4	Standard	LRFD	Interim 1979	LRFD (ε_x max)
1	634.0	638.5	634.0	418.2	405.4	482.9	177.7
2	728.4	800.3	813.8	418.2	405.4	482.9	177.7
3	737.4	741.9	714.9	438.2	412.0	533.4	182.2
4	535.0	445.1	418.1	237.5	172.5	157.6	41.3
5	827.3	723.9	625.0	257.5	195.7	208.1	45.8
6	908.2	926.2	912.7	438.2	412.0	533.4	182.2
7	683.4	643.0	557.5	237.5	172.5	157.6	41.3
8	607.0	535.0	463.1	257.5	195.7	208.1	45.8
9	782.3	791.3	822.8	418.2	405.4	482.9	177.7
10	867.8	741.9	683.4	257.5	195.7	208.1	45.8
11	939.7	935.2	930.7	438.2	412.0	533.4	182.2
12	741.9	651.9	598.0	237.5	172.5	157.6	41.3
13	526.1	508.1	449.6	263.3	212.7	204.1	60.8
14	863.3	750.9	710.4	283.4	235.8	254.6	65.3
15	687.9	643.0	598.0	263.3	212.7	204.1	60.8
16	616.0	580.0	481.1	283.4	235.8	254.6	65.3
17	741.9	669.9	634.0	263.3	212.7	204.1	60.8
18	876.8	800.3	723.9	283.4	235.8	254.6	65.3

Comparison #	(1/4)	(2/5)	(3/6)	(3/4)	(3/5)	(3/7)
1	1.52	1.57	1.31	1.52	1.56	3.57
2	1.74	1.97	1.69	1.95	2.01	4.58
3	1.68	1.80	1.34	1.63	1.74	3.92
4	2.25	2.58	2.65	1.76	2.42	10.13
5	3.21	3.70	3.00	2.43	3.19	13.66
6	2.07	2.25	1.71	2.08	2.22	5.01
7	2.88	3.73	3.54	2.35	3.23	13.51
8	2.36	2.73	2.23	1.80	2.37	10.12
9	1.87	1.95	1.70	1.97	2.03	4.63
10	3.37	3.79	3.28	2.65	3.49	14.93
11	2.14	2.27	1.74	2.12	2.26	5.11
12	3.12	3.78	3.79	2.52	3.47	14.49
13	2.00	2.39	2.20	1.71	2.11	7.40
14	3.05	3.18	2.79	2.51	3.01	10.89
15	2.61	3.02	2.93	2.27	2.81	9.84
16	2.17	2.46	1.89	1.70	2.04	7.37
17	2.82	3.15	3.11	2.41	2.98	10.43
18	3.09	3.39	2.84	2.55	3.07	11.09
Mean	2.44	2.76	2.43	2.11	2.56	8.93
STDEV.	0.587	0.731	0.771	0.365	0.606	3.840
COV	0.240	0.265	0.317	0.173	0.237	0.430

Table F7. Summary of Results for Beam Types II-IV, Straight Strands, Aps at Tension Controlled Limit.

Mean

Comparison #	(1/4)	(2/5)	(3/6)	(3/4)	(3/5)	(3/7)
II	2.55	3.00	2.00	1.63	2.06	6.85
III	2.47	2.76	2.42	1.98	2.39	8.70
IV	2.44	2.76	2.43	2.11	2.56	8.93
Mean	2.49	2.84	2.28	1.91	2.33	8.16

COV

Comparison #	(1/4)	(2/5)	(3/6)	(3/4)	(3/5)	(3/7)
II	0.272	0.350	0.360	0.194	0.296	0.454
III	0.246	0.284	0.439	0.253	0.337	0.529
IV	0.240	0.265	0.317	0.173	0.237	0.430
Mean	0.253	0.300	0.372	0.207	0.290	0.471
STDEV	0.0166	0.0449	0.0619	0.0412	0.0503	0.0519
COV	0.066	0.150	0.166	0.200	0.173	0.110

Table F8. Results for MI-1800 Beam, Straight Strands, Aps at Tension Controlled Limit.

		FEA			Code (Vn)		
MI-1800	1	2	3	4	5	6	7
Combination #	h/2	LRFD	L/4	Standard	LRFD	Interim 1979	LRFD (£x_max)
1	732.9	791.3	791.3	583.8	628.8	651.2	247.7
2	687.9	854.3	854.3	583.8	628.8	651.2	247.7
3	899.2	989.2	989.2	604.9	650.3	704.5	252.4
4	732.9	687.9	687.9	324.2	258.3	184.0	51.1
5	944.2	917.2	917.2	345.3	276.3	237.3	55.9
6	944.2	1038.6	1038.6	604.9	650.2	704.5	55.9
7	741.9	777.8	777.8	324.2	258.3	184.0	51.1
8	876.8	849.8	849.8	345.3	276.3	237.3	55.9
9	-	-	-	-	-	-	-
10	-	-	-	-	-	-	-
11	-	-	-	-	-	-	-
12	-	-	-	-	-	-	-
13	723.9	696.9	696.9	362.3	311.4	251.4	79.2
14	944.2	921.7	921.7	383.4	330.1	304.8	83.9
15	638.5	553.0	553.0	362.3	311.4	251.4	79.2
16	858.8	863.3	863.3	383.4	330.1	304.8	83.9
17	-	-	-	-	-	-	-
18	-	-	-	-	-	-	-

Comparison #	(1/4)	(2/5)	(3/6)	(3/4)	(3/5)	(3/7)
1	1.3	1.3	1.2	1.4	1.3	3.2
2	1.2	1.4	1.3	1.5	1.4	3.4
3	1.5	1.5	1.4	1.6	1.5	3.9
4	2.3	2.7	3.7	2.1	2.7	13.5
5	2.7	3.3	3.9	2.7	3.3	16.4
6	1.6	1.6	1.5	1.7	1.6	18.6
7	2.3	3.0	4.2	2.4	3.0	15.2
8	2.5	3.1	3.6	2.5	3.1	15.2
9	-	-	-	-	-	-
10	-	-	-	-	-	-
11	-	-	-	-	-	-
12	-	-	-	-	-	-
13	2.0	2.2	2.8	1.9	2.2	8.8
14	2.5	2.8	3.0	2.4	2.8	11.0
15	1.8	1.8	2.2	1.5	1.8	7.0
16	2.2	2.6	2.8	2.3	2.6	10.3
17	-	-	-	-	-	-
18	-	-	-	-	-	-
Mean	1.98	2.27	2.64	1.99	2.27	10.54
STDEV.	0.521	0.736	1.095	0.446	0.736	5.357
COV	0.263	0.324	0.415	0.224	0.324	0.508

Table F9. Results for Beam Type II, Harped Strands, Aps at Tension Controlled Limit.

		FEA			Code		
II (Harped)	1	2	3	4	5	6	7
Combination #	h/2	LRFD	L/4	Standard	LRFD	Interim 1979	LRFD (ε_x max)
1	368.7	-	314.7	255.1	236.1	288.0	112.7
2	463.1	-	355.2	278.5	236.1	299.7	124.4
3	431.6	-	368.7	264.4	239.0	311.5	114.8
4	332.7	-	197.8	143.0	94.3	86.3	28.1
5	512.6	-	296.7	175.7	116.4	121.5	41.9
6	553.0	-	386.7	287.8	247.5	323.2	126.5
7	436.1	-	265.3	166.4	105.7	98.1	39.8
8	386.7	-	220.3	152.3	105.0	109.8	30.2
9	467.6	-	368.7	301.9	253.0	311.5	136.1
10	539.5	-	337.2	199.2	127.9	133.3	53.6
11	566.5	-	395.7	311.2	270.8	334.9	138.2
12	445.1	-	283.3	189.9	117.1	109.8	51.5
13	373.2	-	287.8	159.0	119.2	115.2	40.2
14	526.1	-	337.2	191.7	141.3	150.4	54.0
15	454.1	-	355.2	182.4	130.6	126.9	51.9
16	368.7	-	247.3	168.3	129.9	138.6	42.2
17	476.6	-	364.2	205.9	142.0	138.6	63.6
18	548.5	-	364.2	215.2	152.7	162.1	65.7

Comparison #	(1/4)	(3/6)	(3/4)	(3/5)	(3/7)
1	1.45	1.09	1.23	1.33	2.79
2	1.66	1.19	1.28	1.50	2.86
3	1.63	1.18	1.39	1.54	3.21
4	2.33	2.29	1.38	2.10	7.05
5	2.92	2.44	1.69	2.55	7.09
6	1.92	1.20	1.34	1.56	3.06
7	2.62	2.71	1.59	2.51	6.67
8	2.54	2.01	1.45	2.10	7.31
9	1.55	1.18	1.22	1.46	2.71
10	2.71	2.53	1.69	2.64	6.29
11	1.82	1.18	1.27	1.46	2.86
12	2.34	2.58	1.49	2.42	5.50
13	2.35	2.50	1.81	2.41	7.17
14	2.74	2.24	1.76	2.39	6.25
15	2.49	2.80	1.95	2.72	6.85
16	2.19	1.78	1.47	1.90	5.85
17	2.32	2.63	1.77	2.56	5.73
18	2.55	2.25	1.69	2.38	5.55
Mean	2.23	1.99	1.53	2.09	5.27
STDEV.	0.450	0.641	0.223	0.486	1.795
COV	0.202	0.322	0.146	0.233	0.341

Table F10. Results for Beam Type III, Harped Strands, Aps at Tension Controlled Limit.

		FEA			Code (Vn)		
III (Harped)	1	2	3	4	5	6	7
Combination #	h/2	LRFD	L/4	Standard	LRFD	Interim 1979	LRFD (εx_max)
1	517.1	-	485.6	343.7	334.1	390.9	151.5
2	629.5	-	620.5	361.6	346.8	408.8	169.4
3	616.0	-	548.5	358.0	339.2	426.9	154.7
4	449.6	-	346.2	196.5	143.0	126.0	40.3
5	696.9	-	517.1	228.7	176.0	179.8	61.4
6	755.4	-	678.9	375.8	395.8	444.8	172.6
7	607.0	-	445.1	214.4	160.2	143.8	58.2
8	512.6	-	377.7	210.8	158.7	162.0	43.5
9	634.0	-	643.0	379.5	359.8	426.6	187.2
10	746.4	-	517.1	246.5	193.2	197.7	79.3
11	777.8	-	701.4	393.7	364.7	462.6	190.4
12	625.0	-	472.1	232.3	177.3	161.7	76.1
13	445.1	-	364.2	217.6	174.9	163.8	56.2
14	705.9	-	566.5	249.7	207.9	217.7	77.3
15	593.5	-	494.6	235.4	192.1	181.7	74.1
16	526.1	-	404.7	217.6	190.7	163.8	59.4
17	584.5	-	512.6	253.3	215.8	199.6	92.0
18	741.9	-	584.5	267.6	230.6	235.6	95.2

Comparison #	(1/4)	(3/6)	(3/4)	(3/5)	(3/7)
1	1.50	1.24	1.41	1.45	3.21
2	1.74	1.52	1.72	1.79	3.66
3	1.72	1.28	1.53	1.62	3.55
4	2.29	2.75	1.76	2.42	8.58
5	3.05	2.88	2.26	2.94	8.42
6	2.01	1.53	1.81	1.72	3.93
7	2.83	3.09	2.08	2.78	7.65
8	2.43	2.33	1.79	2.38	8.68
9	1.67	1.51	1.69	1.79	3.43
10	3.03	2.62	2.10	2.68	6.52
11	1.98	1.52	1.78	1.92	3.68
12	2.69	2.92	2.03	2.66	6.20
13	2.05	2.22	1.67	2.08	6.48
14	2.83	2.60	2.27	2.73	7.33
15	2.52	2.72	2.10	2.58	6.68
16	2.42	2.47	1.86	2.12	6.81
17	2.31	2.57	2.02	2.37	5.57
18	2.77	2.48	2.18	2.53	6.14
Mean	2.32	2.24	1.89	2.25	5.92
STDEV.	0.487	0.622	0.248	0.452	1.901
COV	0.209	0.278	0.131	0.201	0.321

Table F11. Results for Beam Type IV, Harped Strands, Aps at Tension Controlled Limit.

		FEA			Code		
IV (Harped)	1	2	3	4	5	6	7
Combination #	h/2	LRFD	L/4	Standard	LRFD	Interim 1979	LRFD (ε$_x$ max)
1	669.9	-	660.9	432.3	418.5	497.0	191.8
2	719.4	-	858.8	460.6	439.0	525.2	220.1
3	782.3	-	750.9	452.3	425.1	547.5	196.3
4	557.5	-	485.6	251.6	187.2	171.7	55.4
5	858.8	-	732.9	299.9	238.0	250.4	88.1
6	867.8	-	953.2	480.6	445.5	575.7	224.5
7	701.4	-	660.9	279.8	214.8	199.9	83.6
8	710.4	-	548.5	271.6	210.5	222.2	59.9
9	791.3	-	876.8	488.8	459.7	553.4	248.3
10	881.3	-	777.8	328.1	265.6	278.6	116.3
11	944.2	-	980.2	508.8	466.1	603.9	252.8
12	741.9	-	665.4	308.1	242.3	228.1	111.8
13	602.5	-	508.1	277.5	228.4	218.2	74.9
14	890.2	-	746.4	325.7	279.2	296.9	107.6
15	773.3	-	696.9	305.7	255.9	246.4	103.1
16	705.9	-	557.5	297.5	251.6	268.7	79.4
17	795.8	-	701.4	333.9	283.5	274.6	131.3
18	894.7	-	791.3	353.9	306.7	325.1	135.8

Comparison #	(1/4)	(3/6)	(3/4)	(3/5)	(3/7)
1	1.55	1.33	1.53	1.58	3.45
2	1.56	1.64	1.86	1.96	3.90
3	1.73	1.37	1.66	1.77	3.82
4	2.22	2.83	1.93	2.59	8.77
5	2.86	2.93	2.44	3.08	8.32
6	1.81	1.66	1.98	2.14	4.25
7	2.51	3.31	2.36	3.08	7.91
8	2.62	2.47	2.02	2.61	9.16
9	1.62	1.58	1.79	1.91	3.53
10	2.69	2.79	2.37	2.93	6.69
11	1.86	1.62	1.93	2.10	3.88
12	2.41	2.92	2.16	2.75	5.95
13	2.17	2.33	1.83	2.22	6.79
14	2.73	2.51	2.29	2.67	6.94
15	2.53	2.83	2.28	2.72	6.76
16	2.37	2.08	1.87	2.22	7.03
17	2.38	2.55	2.10	2.47	5.34
18	2.53	2.43	2.24	2.58	5.83
Mean	2.23	2.29	2.04	2.41	6.02
STDEV.	0.434	0.615	0.260	0.444	1.880
COV	0.195	0.269	0.128	0.184	0.312

Table F12. Summary of Results for Beam Types II-IV, Harped Strands, Aps at Tension Controlled Limit.

Mean

Comparison #	(1/4)	(3/6)	(3/4)	(3/5)	(3/7)
II	2.23	1.99	1.53	2.09	5.27
III	2.32	2.24	1.89	2.25	5.92
IV	2.23	2.29	2.04	2.41	6.02
Mean	2.26	2.17	1.82	2.25	5.73

COV

Comparison #	(1/4)	(3/6)	(3/4)	(3/5)	(3/7)
II	0.202	0.322	0.146	0.233	0.341
III	0.209	0.278	0.131	0.201	0.321
IV	0.195	0.269	0.128	0.184	0.312
Mean	0.202	0.290	0.135	0.206	0.325
STDEV	0.0074	0.0286	0.0098	0.0248	0.0146
COV	0.037	0.099	0.072	0.121	0.045

Table F13. Results for Beam Type II, Straight Strands, High Aps.

	FEA		Code (Vn)			
II	3	4	5	6	7	8
Combination #	**L/4**	**Standard**	**LRFD**	**Interim 1979**	**LRFD (£x max)**	**LRFD (HL-93)**
1	328.2	286.5	278.3	289.9	109.7	285.1
2	382.2	286.5	278.3	289.9	109.7	285.1
3	382.2	296.0	288.8	314.0	111.9	295.8
4	197.8	171.4	100.8	82.7	22.8	93.3
5	274.3	180.9	111.1	106.8	25.0	104.9
6	454.1	296.0	288.8	314.0	111.9	295.8
7	238.3	171.4	100.8	82.7	22.8	93.3
8	202.3	180.9	111.1	106.8	25.0	104.9
9	422.6	286.5	278.3	289.9	109.7	285.1
10	305.7	180.9	111.1	106.8	25.0	104.9
11	508.1	296.0	288.8	314.0	111.9	295.8
12	278.8	171.4	100.8	82.7	22.8	93.3
13	211.3	187.8	126.5	112.3	35.2	120.7
14	323.7	197.4	136.8	136.4	37.4	132.2
15	278.8	187.8	126.5	112.3	35.2	120.7
16	233.8	197.4	136.8	136.4	37.4	132.2
17	305.7	187.8	126.5	112.3	35.2	120.7
18	373.2	197.4	136.8	136.4	37.4	132.2

Comparison #	**(3/6)**	**(3/4)**	**(3/5)**	**(3/7)**	**(3/8)**
1	1.13	1.15	1.18	2.99	1.15
2	1.32	1.33	1.37	3.48	1.34
3	1.22	1.29	1.32	3.42	1.29
4	2.39	1.15	1.96	8.67	2.12
5	2.57	1.52	2.47	10.99	2.61
6	1.45	1.53	1.57	4.06	1.54
7	2.88	1.39	2.36	10.44	2.55
8	1.89	1.12	1.82	8.10	1.93
9	1.46	1.48	1.52	3.85	1.48
10	2.86	1.69	2.75	12.25	2.91
11	1.62	1.72	1.76	4.54	1.72
12	3.37	1.63	2.77	12.22	2.99
13	1.88	1.13	1.67	6.00	1.75
14	2.37	1.64	2.37	8.66	2.45
15	2.48	1.48	2.20	7.91	2.31
16	1.71	1.18	1.71	6.25	1.77
17	2.72	1.63	2.42	8.68	2.53
18	2.74	1.89	2.73	9.98	2.82
Mean	2.12	1.44	2.00	7.36	2.07
STDEV.	0.676	0.235	0.521	3.133	0.595
COV	0.319	0.163	0.261	0.426	0.287

Table F14. Results for Beam Type III, Straight Strands, High Aps.

	FEA		Code (Vn)		
III	3	4	5	6	7
Combination #	L/4	Standard	LRFD	Interim 1979	LRFD (Ɛx_max)
1	490.1	419.9	386.7	388.2	144.9
2	607.0	419.9	386.7	388.2	144.9
3	571.0	434.4	401.4	424.8	148.1
4	296.7	270.3	163.5	119.0	31.9
5	467.6	284.8	177.1	155.5	35.2
6	705.9	434.4	401.4	424.8	148.1
7	395.7	270.3	163.5	119.0	31.9
8	332.7	284.8	177.1	155.5	35.2
9	634.0	419.9	386.7	388.2	144.9
10	548.5	284.8	177.1	155.5	35.2
11	777.8	434.4	401.4	424.8	148.1
12	472.1	270.3	163.5	119.0	31.9
13	332.7	291.7	195.6	157.4	48.0
14	512.6	306.2	209.4	194.0	51.3
15	440.6	291.7	195.6	157.4	48.0
16	377.7	306.2	209.4	194.0	51.3
17	494.6	291.7	195.6	157.4	48.0
18	616.0	306.2	209.4	194.0	51.3

Comparison #	(3/6)	(3/4)	(3/5)	(3/7)
1	1.26	1.17	1.27	3.38
2	1.56	1.45	1.57	4.19
3	1.34	1.31	1.42	3.86
4	2.49	1.10	1.82	9.30
5	3.01	1.64	2.64	13.30
6	1.66	1.62	1.76	4.77
7	3.33	1.46	2.42	12.40
8	2.14	1.17	1.88	9.46
9	1.63	1.51	1.64	4.38
10	3.53	1.93	3.10	15.60
11	1.83	1.79	1.94	5.25
12	3.97	1.75	2.89	14.79
13	2.11	1.14	1.70	6.92
14	2.64	1.67	2.45	9.99
15	2.80	1.51	2.25	9.17
16	1.95	1.23	1.80	7.36
17	3.14	1.70	2.53	10.29
18	3.18	2.01	2.94	12.01
Mean	2.42	1.51	2.11	8.69
STDEV.	0.813	0.278	0.554	3.903
COV	0.336	0.184	0.262	0.449

Table F15. Results for Beam Type IV, Straight Strands, High Aps.

	FEA		Code (Vn)		
IV	3	4	5	6	7
Combination #	L/4	Standard	LRFD	Interim 1979	LRFD (εx_max)
1	687.9	553.0	489.0	493.4	181.6
2	840.8	553.0	489.0	493.4	181.6
3	813.8	573.4	511.1	545.0	186.2
4	418.1	368.4	201.8	161.0	42.2
5	701.4	388.8	223.9	212.6	46.8
6	998.2	573.4	511.1	545.0	186.2
7	625.0	368.4	201.8	161.0	42.2
8	467.6	388.8	223.9	212.6	46.8
9	822.8	553.0	489.0	493.4	181.6
10	778.6	388.8	223.9	212.6	46.8
11	1043.1	573.4	511.1	545.0	186.2
12	700.5	368.4	201.8	161.0	42.2
13	449.6	394.7	243.2	208.5	62.1
14	750.9	415.2	265.3	260.1	66.7
15	665.4	394.7	243.2	208.5	62.1
16	499.1	415.2	265.3	260.1	66.7
17	680.1	394.7	243.2	208.5	62.1
18	840.1	415.2	265.3	260.1	66.7

Comparison #	(3/6)	(3/4)	(3/5)	(3/7)
1	1.39	1.24	1.41	3.79
2	1.70	1.52	1.72	4.63
3	1.49	1.42	1.59	4.37
4	2.60	1.14	2.07	9.91
5	3.30	1.80	3.13	15.00
6	1.83	1.74	1.95	5.36
7	3.88	1.70	3.10	14.82
8	2.20	1.20	2.09	10.00
9	1.67	1.49	1.68	4.53
10	3.66	2.00	3.48	16.65
11	1.91	1.82	2.04	5.60
12	4.35	1.90	3.47	16.61
13	2.16	1.14	1.85	7.24
14	2.89	1.81	2.83	11.26
15	3.19	1.69	2.74	10.72
16	1.92	1.20	1.88	7.48
17	3.26	1.72	2.80	10.95
18	3.23	2.02	3.17	12.60
Mean	2.59	1.59	2.39	9.53
STDEV.	0.902	0.301	0.690	4.378
COV	0.348	0.190	0.289	0.459

Table F16. Summary of Results for Beam Types II-IV, Straight Strands, High Aps.

Mean

Comparison #	(3/6)	(3/4)	(3/5)	(3/7)
II	2.12	1.44	2.00	7.36
III	2.42	1.51	2.11	8.69
IV	2.59	1.59	2.39	9.53
Mean	2.38	1.51	2.17	8.53

COV

Comparison #	(3/6)	(3/4)	(3/5)	(3/7)
II	0.319	0.163	0.261	0.426
III	0.336	0.184	0.262	0.449
IV	0.348	0.190	0.289	0.459
Mean	0.334	0.179	0.271	0.445
STDEV	0.0143	0.0139	0.0159	0.0173
COV	0.043	0.077	0.059	0.039

Table F17. Results for Beam Type II, Harped Strands, High Aps.

	FEA		Code (Vn)		
II (Harped)	3	4	5	6	7
Combination #	L/4	Standard	LRFD	Interim 1979	LRFD (Ɛx_max)
1	332.7	309.1	283.1	294.8	114.7
2	400.2	328.8	292.6	304.6	124.5
3	400.2	318.7	293.5	318.9	116.8
4	202.3	194.0	105.5	87.6	27.8
5	328.2	223.3	125.4	121.6	39.8
6	481.1	338.4	303.1	328.8	126.7
7	278.8	213.7	115.1	97.5	37.6
8	233.8	203.6	115.9	111.7	29.9
9	454.1	348.6	302.1	314.5	134.4
10	341.7	243.0	135.0	131.5	49.6
11	539.5	358.1	312.6	338.6	136.5
12	314.7	233.5	124.6	107.3	47.5
13	332.7	210.5	131.3	117.2	40.2
14	359.7	239.7	151.1	151.2	52.2
15	409.2	230.2	140.8	127.1	50.0
16	269.8	220.0	141.6	141.3	42.3
17	454.1	249.9	150.3	136.9	59.9
18	413.6	259.5	160.7	161.1	62.0

Comparison #	(3/6)	(3/4)	(3/5)	(3/7)
1	1.13	1.08	1.18	2.90
2	1.31	1.22	1.37	3.21
3	1.25	1.26	1.36	3.43
4	2.31	1.04	1.92	7.29
5	2.70	1.47	2.62	8.26
6	1.46	1.42	1.59	3.80
7	2.86	1.30	2.42	7.41
8	2.09	1.15	2.02	7.82
9	1.44	1.30	1.50	3.38
10	2.60	1.41	2.53	6.89
11	1.59	1.51	1.73	3.95
12	2.93	1.35	2.53	6.63
13	2.84	1.58	2.53	8.28
14	2.38	1.50	2.38	6.89
15	3.22	1.78	2.91	8.18
16	1.91	1.23	1.91	6.38
17	3.32	1.82	3.02	7.58
18	2.57	1.59	2.57	6.67
Mean	2.22	1.39	2.12	6.05
STDEV.	0.713	0.219	0.569	1.984
COV	0.322	0.157	0.269	0.328

Table F18. Results for Beam Type III, Harped Strands, High Aps.

	FEA		Code (Vn)		
III (Harped)	3	4	5	6	7
Combination #	L/4	Standard	LRFD	Interim 1979	LRFD (Ɛx_max)
1	512.6	426.9	393.4	395.2	151.9
2	651.9	441.0	406.6	409.3	165.9
3	616.0	441.4	408.1	431.8	155.1
4	346.2	277.4	170.1	126.0	38.9
5	566.5	305.9	197.1	176.6	56.2
6	768.8	455.5	421.4	445.8	169.2
7	454.1	291.4	183.3	140.0	53.0
8	391.2	291.9	183.8	162.6	42.2
9	683.4	455.0	420.0	423.3	180.0
10	611.5	319.9	210.4	190.6	70.3
11	845.3	469.5	434.8	459.9	183.2
12	553.0	305.4	196.5	154.1	67.0
13	386.7	298.7	202.2	164.4	55.1
14	589.0	327.3	229.4	215.1	72.4
15	499.1	312.8	215.5	178.5	69.1
16	440.6	313.2	216.1	201.0	58.3
17	549.8	326.8	228.7	192.5	83.2
18	683.4	341.3	242.8	229.1	86.4

Comparison #	(3/6)	(3/4)	(3/5)	(3/7)
1	1.30	1.20	1.30	3.37
2	1.59	1.48	1.60	3.93
3	1.43	1.40	1.51	3.97
4	2.75	1.25	2.04	8.89
5	3.21	1.85	2.87	10.08
6	1.72	1.69	1.82	4.54
7	3.24	1.56	2.48	8.57
8	2.41	1.34	2.13	9.27
9	1.61	1.50	1.63	3.80
10	3.21	1.91	2.91	8.70
11	1.84	1.80	1.94	4.61
12	3.59	1.81	2.81	8.25
13	2.35	1.29	1.91	7.02
14	2.74	1.80	2.57	8.14
15	2.80	1.60	2.32	7.22
16	2.19	1.41	2.04	7.56
17	2.86	1.68	2.40	6.61
18	2.98	2.00	2.81	7.91
Mean	2.43	1.59	2.17	6.80
STDEV.	0.711	0.243	0.501	2.180
COV	0.292	0.153	0.231	0.320

Table F19. Results for Beam Type IV, Harped Strands, High Aps.

	FEA		Code (Vn)		
IV (Harped)	3	4	5	6	7
Combination #	L/4	Standard	LRFD	Interim 1979	LRFD (Ɛx_max)
1	723.9	562.6	498.3	503.0	191.3
2	912.7	581.9	517.0	522.3	210.6
3	858.8	583.1	520.4	554.6	195.9
4	503.6	378.0	211.1	170.7	51.8
5	876.8	417.8	252.0	241.6	75.7
6	1043.1	602.4	539.1	574.0	215.2
7	710.4	397.3	229.8	190.0	71.1
8	571.0	398.4	233.3	222.3	56.4
9	912.7	601.2	535.6	541.6	229.9
10	863.3	437.1	270.8	260.9	95.0
11	1065.6	621.7	557.8	593.3	234.5
12	683.4	416.6	248.5	209.3	90.4
13	530.5	404.4	252.6	218.2	71.7
14	890.2	444.1	293.4	289.1	95.6
15	728.4	423.7	271.3	237.5	91.0
16	602.5	424.8	274.7	269.8	76.3
17	749.0	443.0	289.9	256.8	110.4
18	908.2	463.4	312.2	308.4	114.9

Comparison #	(3/6)	(3/4)	(3/5)	(3/7)
1	1.44	1.29	1.45	3.78
2	1.75	1.57	1.77	4.33
3	1.55	1.47	1.65	4.38
4	2.95	1.33	2.39	9.72
5	3.63	2.10	3.48	11.58
6	1.82	1.73	1.93	4.85
7	3.74	1.79	3.09	9.99
8	2.57	1.43	2.45	10.12
9	1.69	1.52	1.70	3.97
10	3.31	1.98	3.19	9.09
11	1.80	1.71	1.91	4.54
12	3.27	1.64	2.75	7.56
13	2.43	1.31	2.10	7.39
14	3.08	2.00	3.03	9.31
15	3.07	1.72	2.69	8.00
16	2.23	1.42	2.19	7.89
17	2.92	1.69	2.58	6.79
18	2.95	1.96	2.91	7.90
Mean	2.56	1.65	2.40	7.29
STDEV.	0.748	0.251	0.599	2.455
COV	0.292	0.152	0.249	0.337

Table F20. Summary of Results for Beam Types II-IV, Harped Strands, High Aps.

AVERAGE

Comparison #	(3/6)	(3/4)	(3/5)	(3/7)
II	2.22	1.39	2.12	6.05
III	2.43	1.59	2.17	6.80
IV	2.56	1.65	2.40	7.29
Mean	2.41	1.54	2.23	6.71

COV

Comparison #	(3/6)	(3/4)	(3/5)	(3/7)
II	0.322	0.157	0.269	0.328
III	0.292	0.153	0.231	0.320
IV	0.292	0.152	0.249	0.337
Mean	0.302	0.154	0.250	0.328
STDEV	0.0172	0.0028	0.0190	0.0082
COV	0.057	0.018	0.076	0.025

APPENDIX G: FIELD TEST RESULTS

Bridge 1 Run 1: Two trucks side by side, centered in each lane

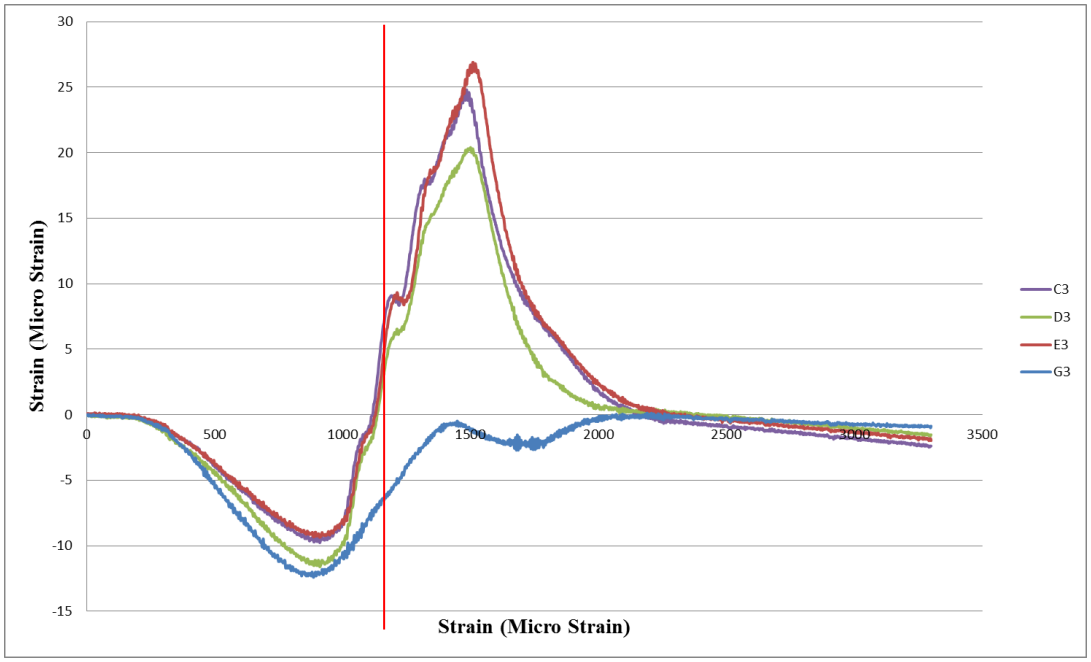

Figure G1. Bridge 1 Run 1 Girder Strains, Gage Line 3.

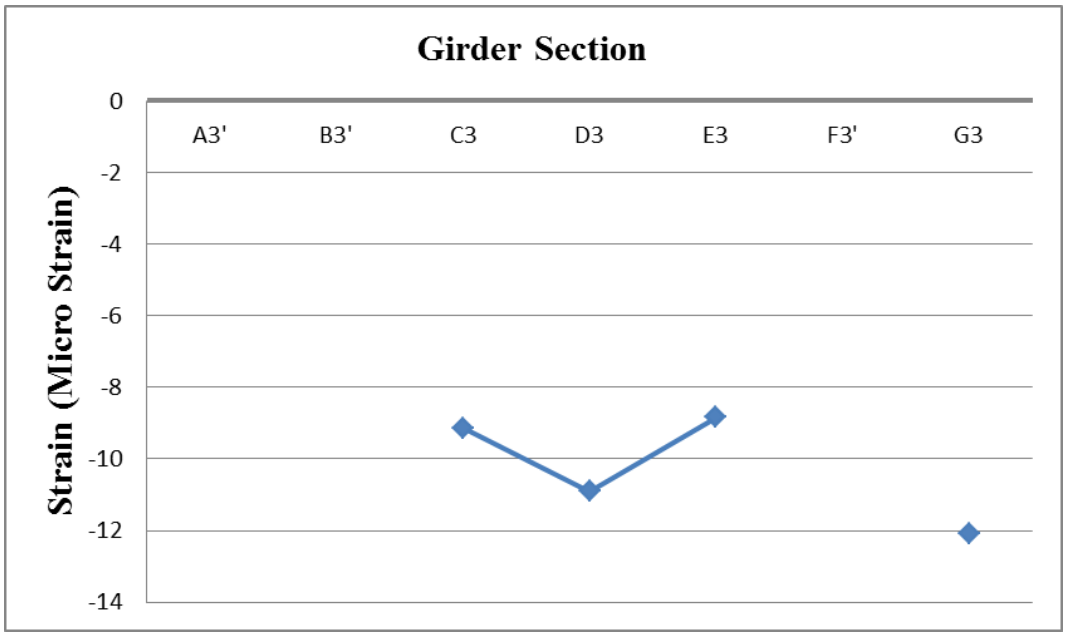

Figure G2. Bridge 1 Run 1 Girder Strains for Maximum Negative Moment, Span 2.

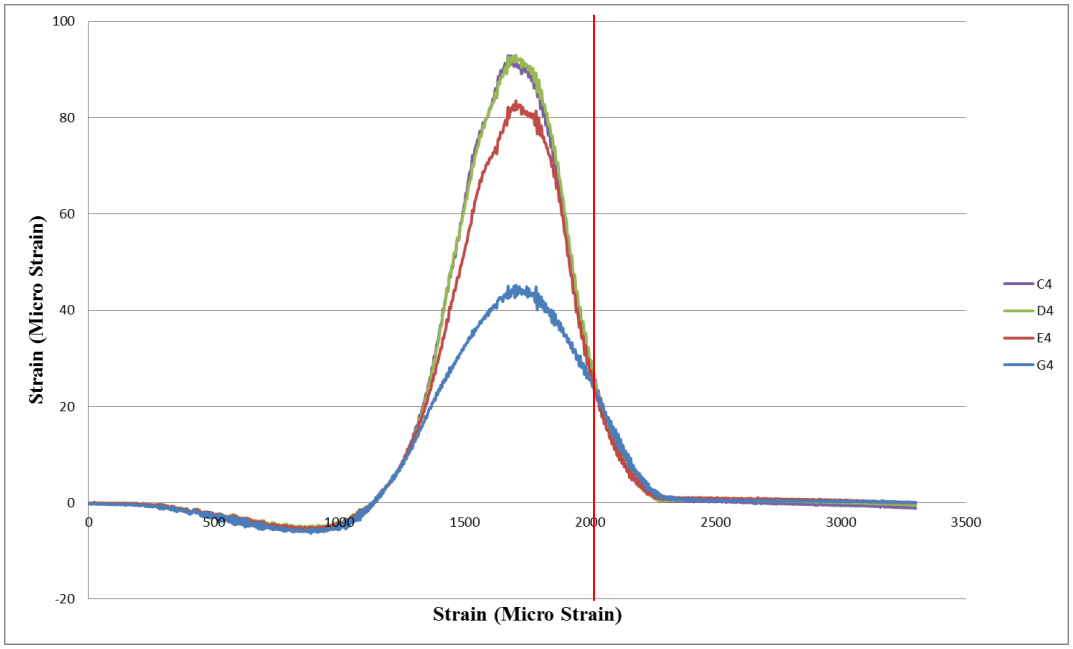

Figure G3. Bridge 1 Run 1 Girder Strains, Gage Line 4.

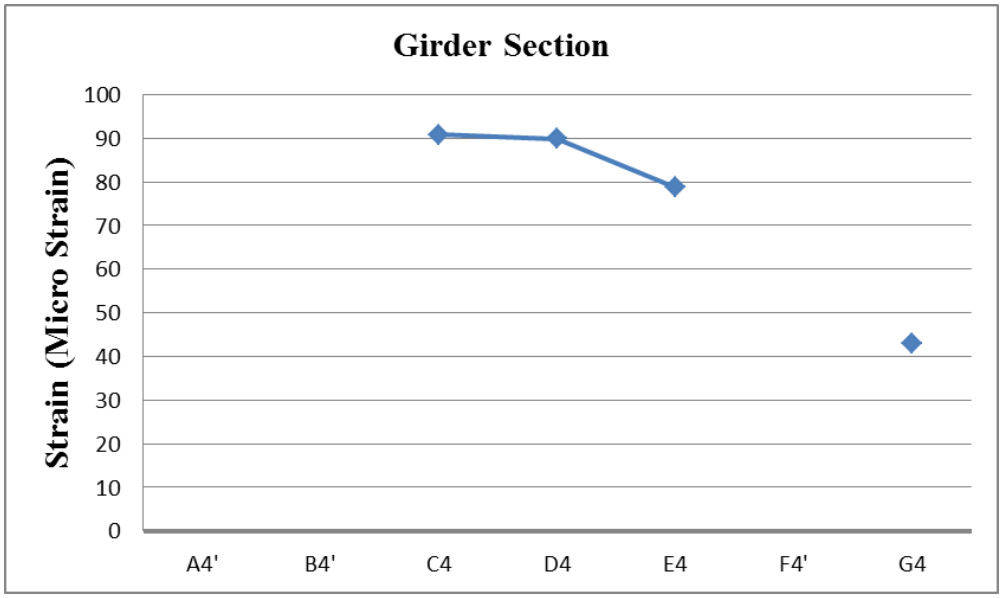

Figure G4. Bridge 1 Run 1 Girder Strains for Maximum Positive Moment, Span 2.

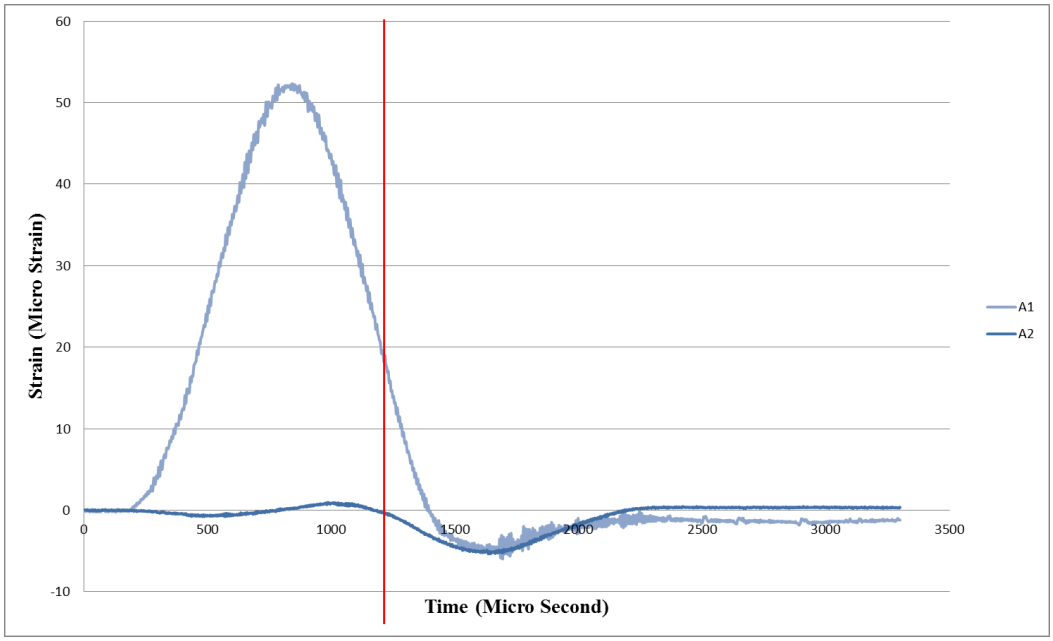

Figure G5. Bridge 1 Run 1 Girder Strains Along Girder A.

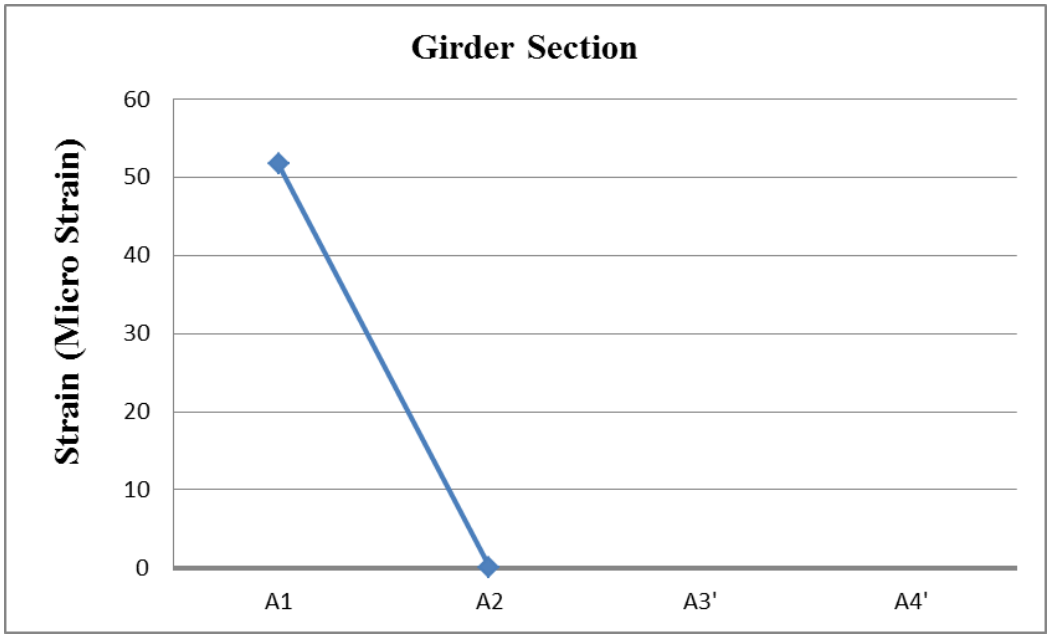

Figure G6. Girder A Strains For Maximum Positive Moment.

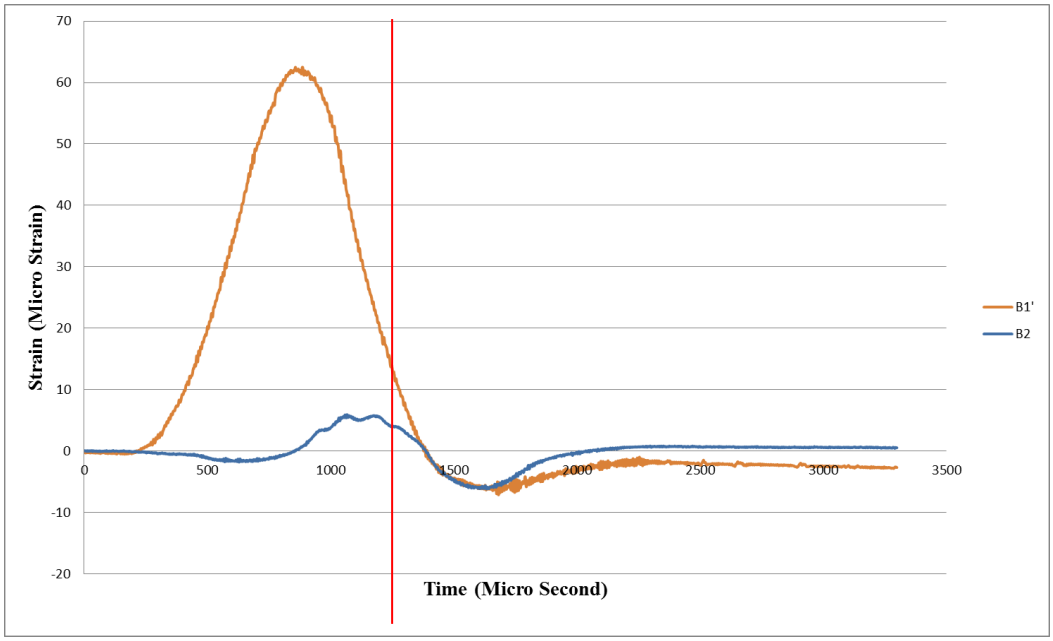

Figure G7. Bridge 1 Run 1 Girder Strains Along Girder B.

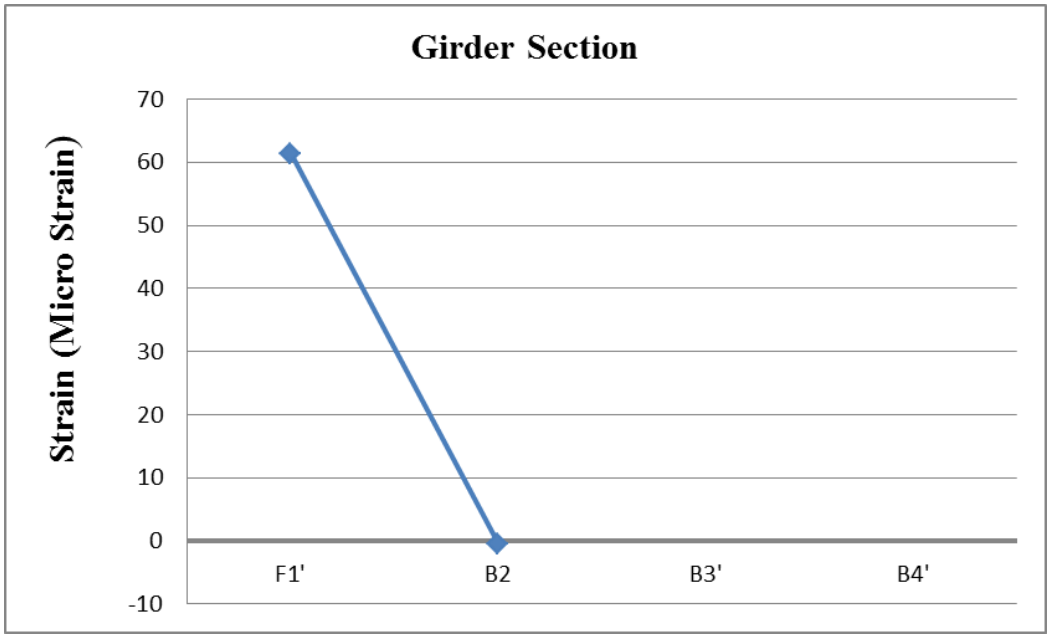

Figure G8. Girder B Strains for Maximum Positive Moment.

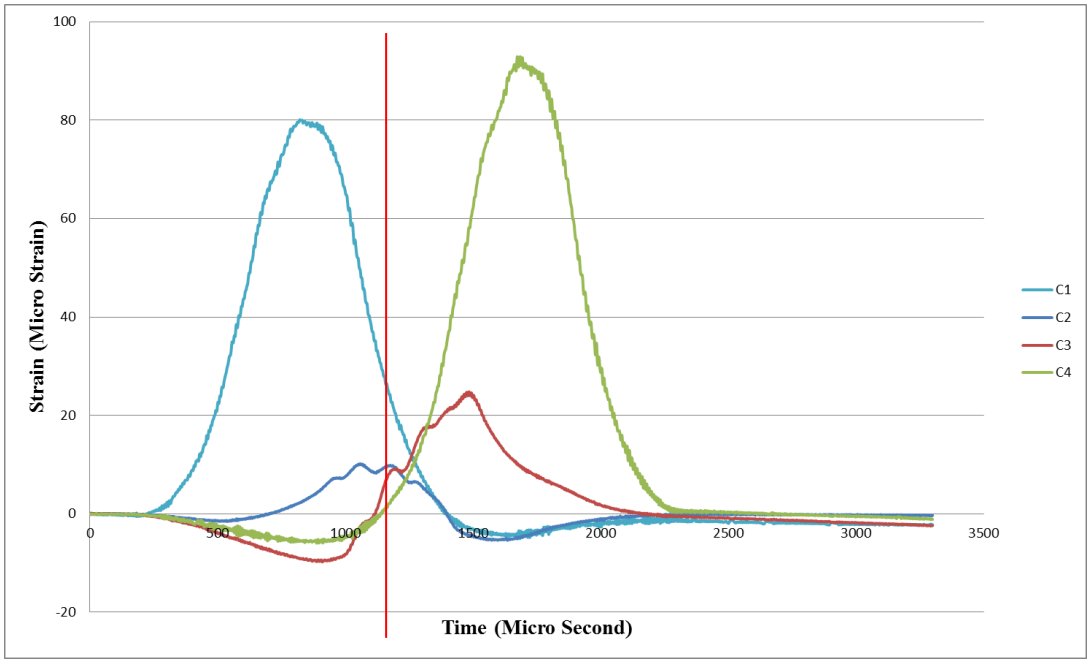

Figure G9. Girder Strains Along Girder C.

Figure G10. Girder C Strains For Maximum Positive Moment.

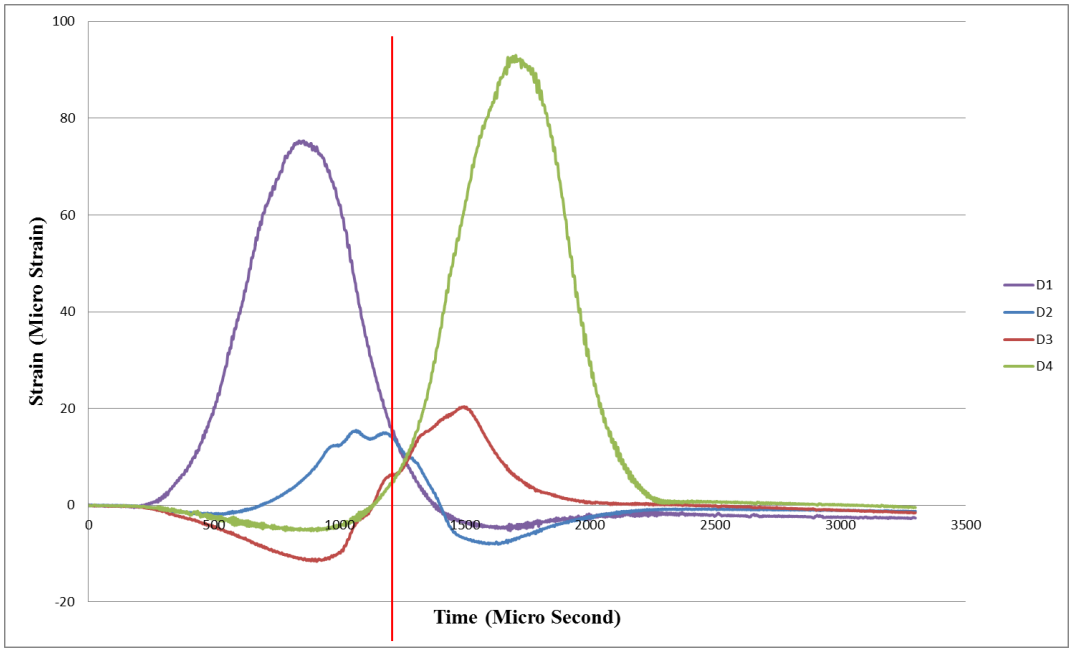

Figure G11. Girder Strains Along Girder D.

Figure G12. Girder D Strains For Maximum Positive Moment.

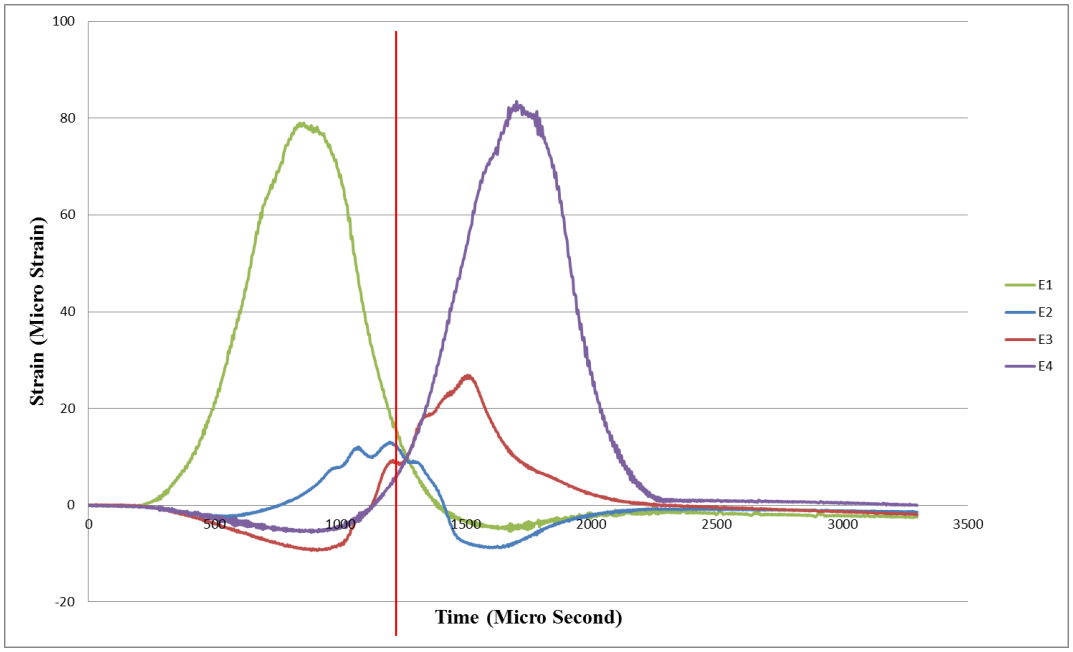

Figure G13. Girder Strains Along Girder E.

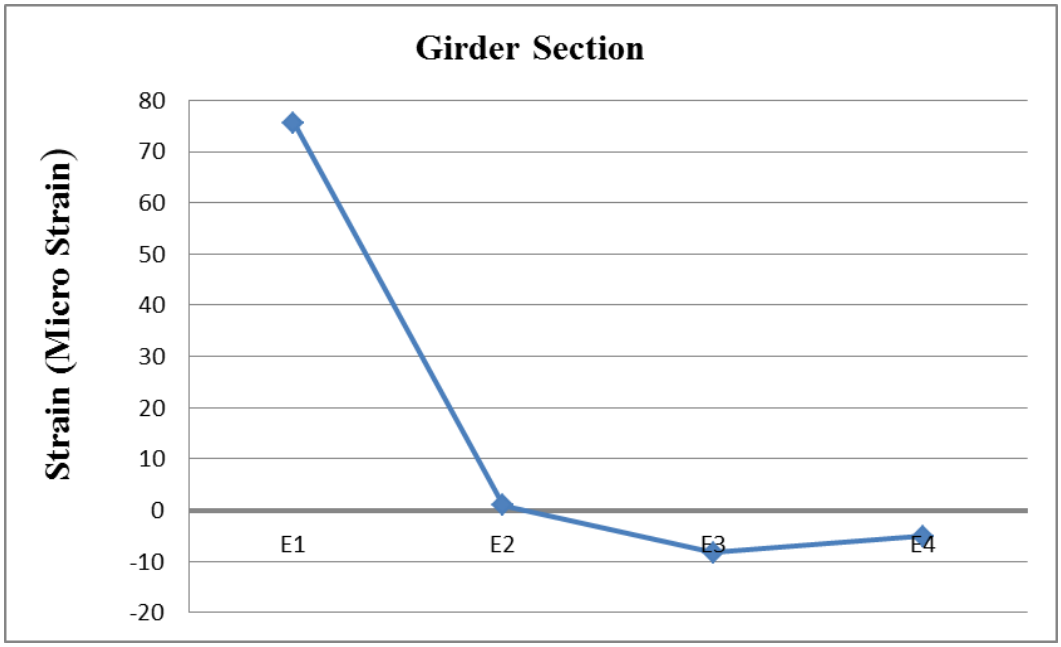

Figure G14. Girder E Strains For Maximum Positive Moment.

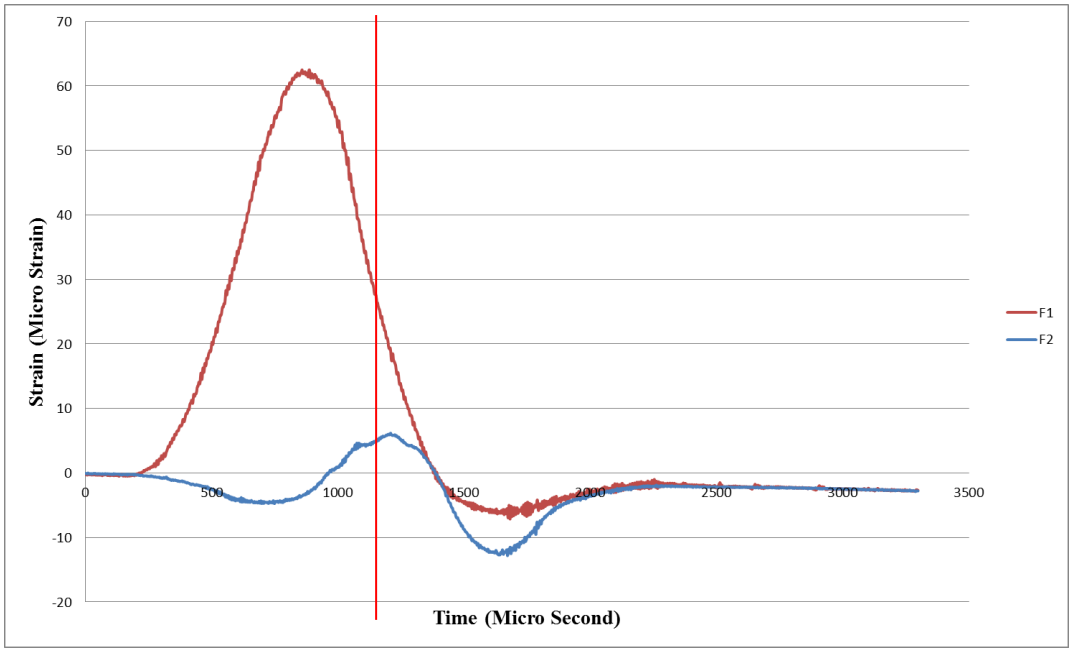

Figure G15. Girder Strains Along Girder F.

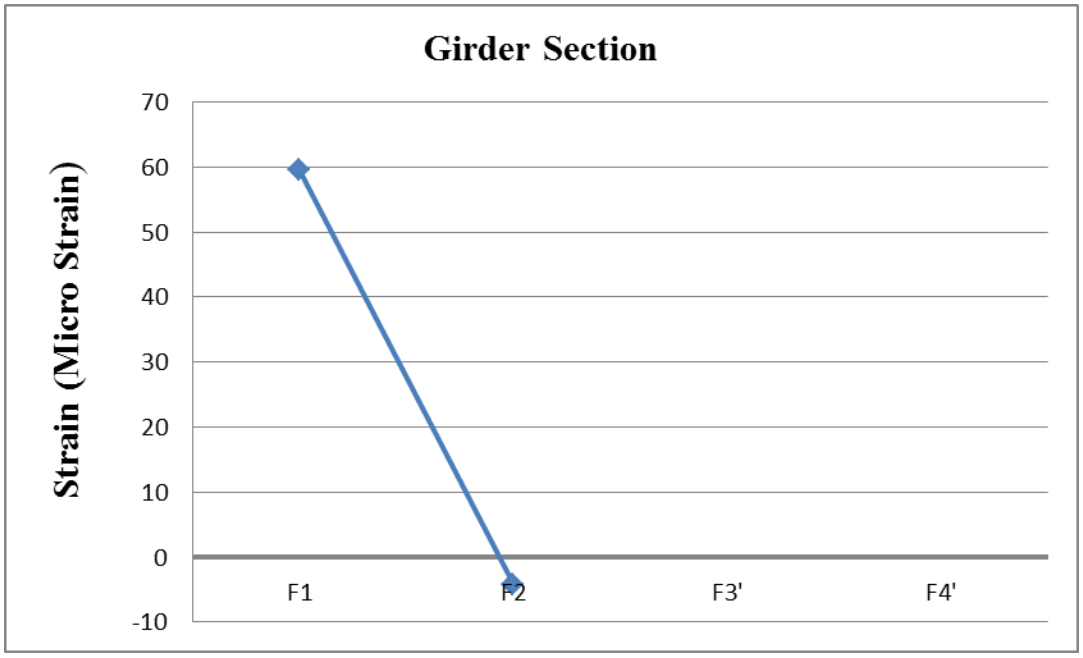

Figure G16. Girder F Strains for Maximum Positive Moment.

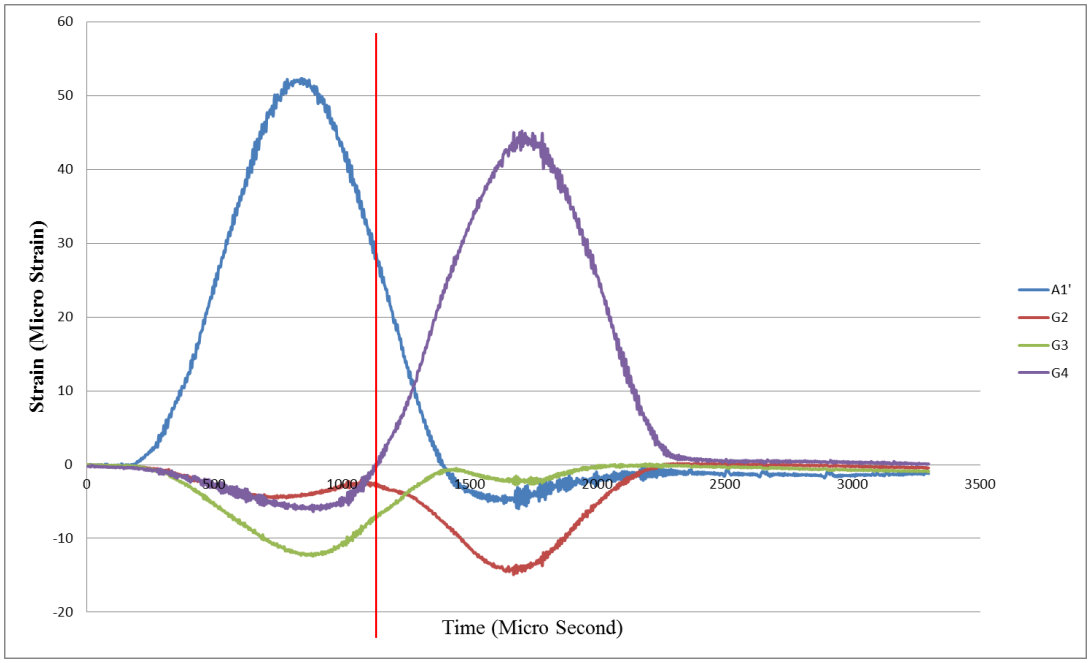

Figure G17. Girder Strains Along Girder Line G.

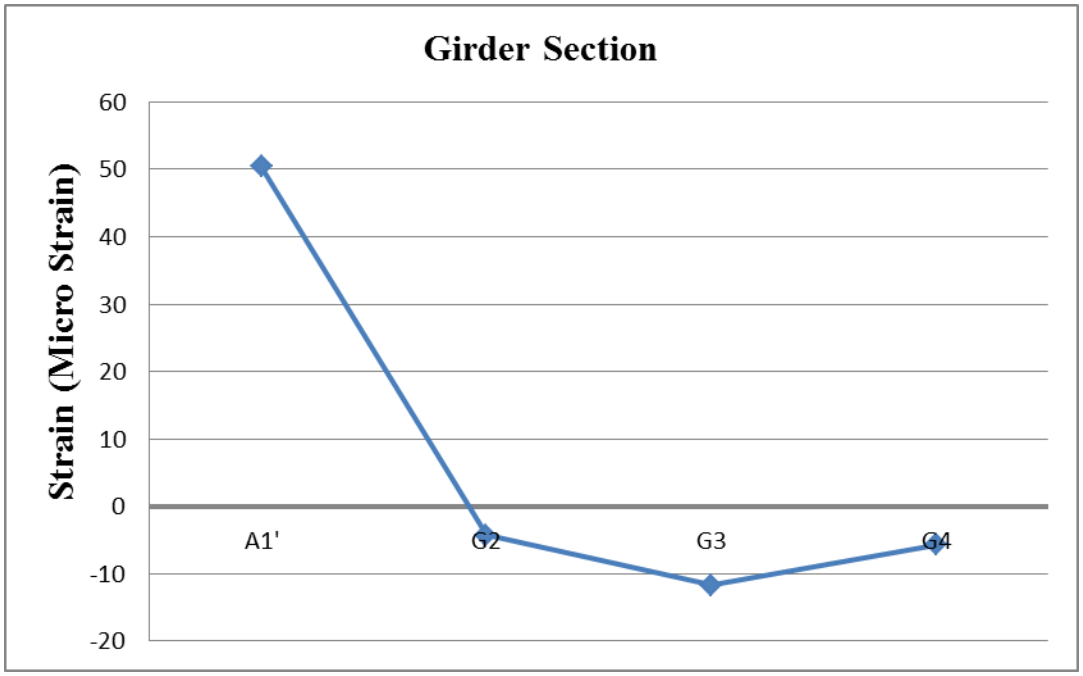

Figure G18. Girder G Strains for Maximum Positive Moment.

Bridge 1 Run 3: Two trucks side by side, as close as possible to the left edge.

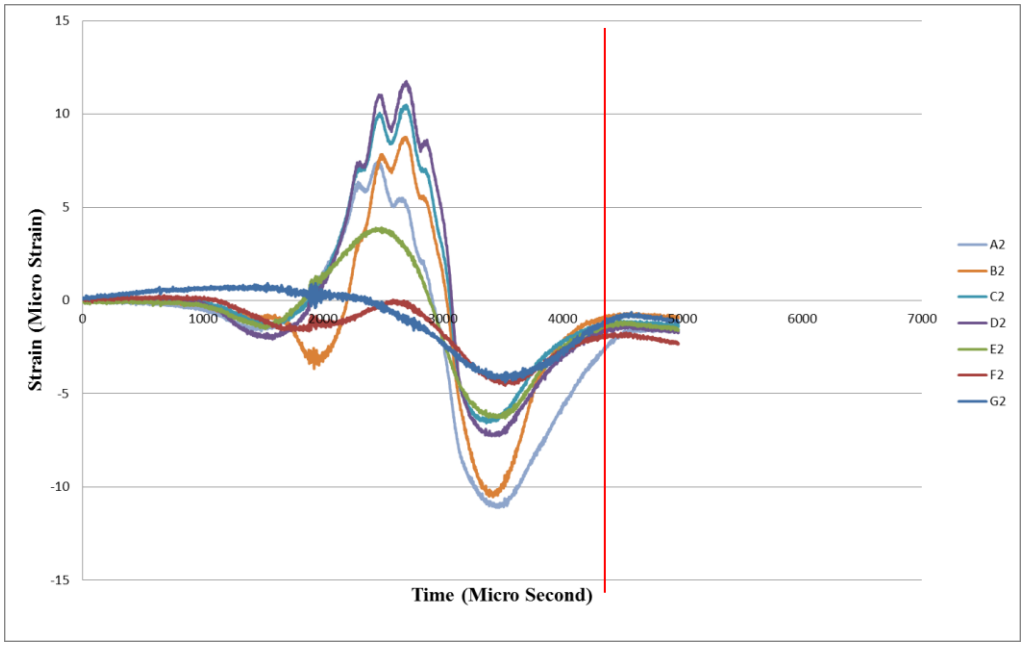

Figure G19. Bridge 1 Run 3 Girder Strains, Gage Line 2.

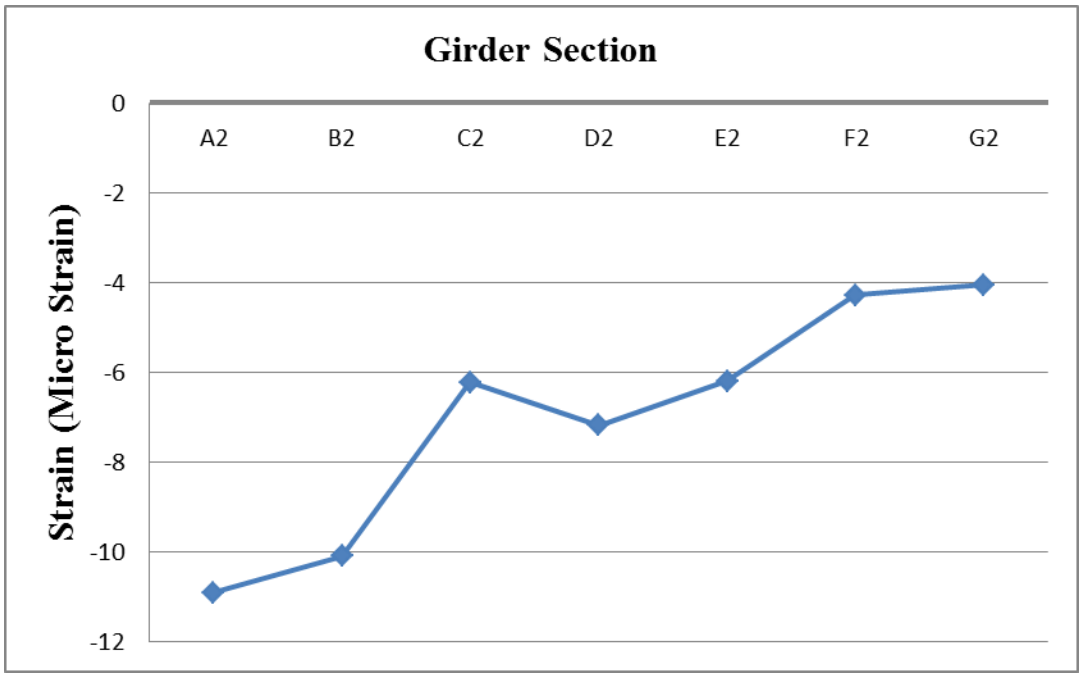

Figure G20. Bridge 1 Run 3 Girder Strains for Maximum Negative Moment.

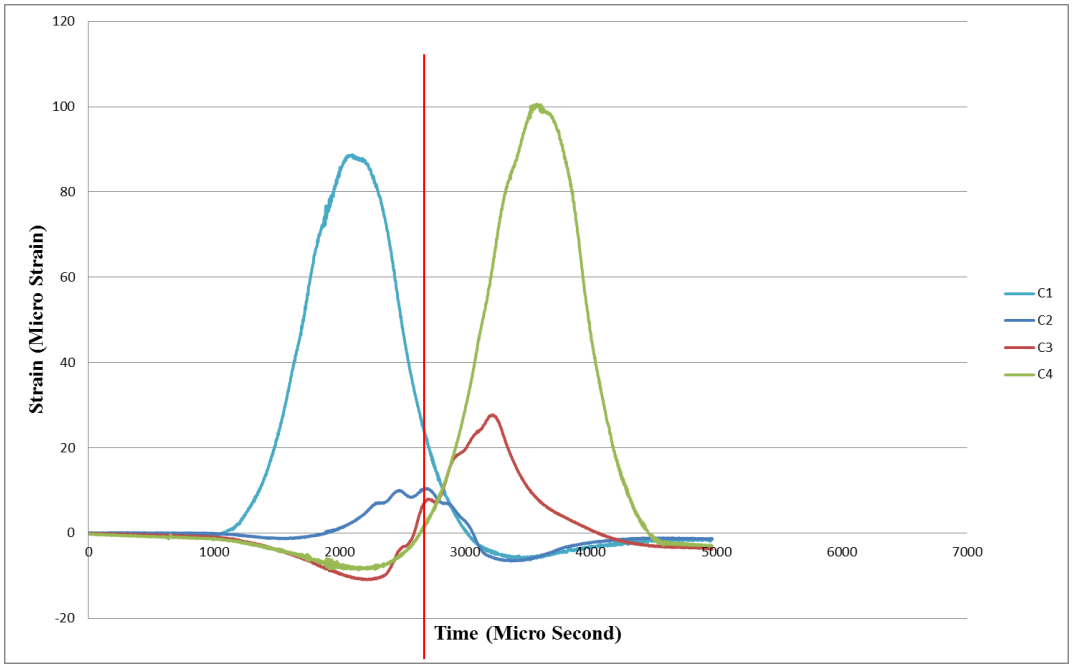

Figure G21. Bridge 1 Run 3 Girder Strains Along Girder C.

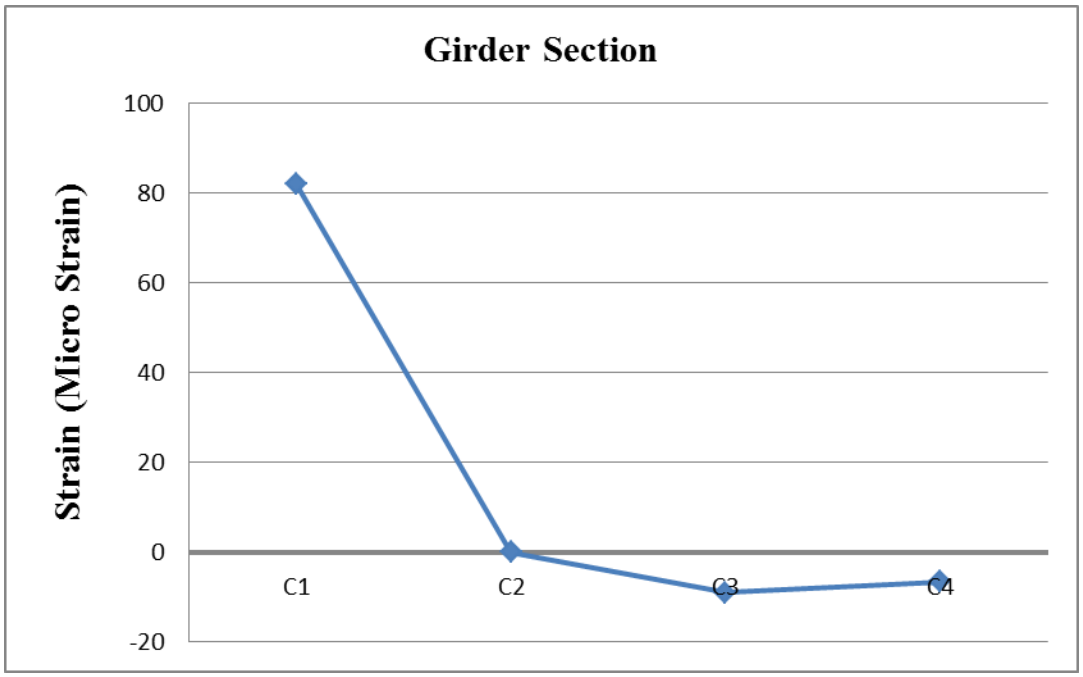

Figure G22. Girder C Strains for Maximum Positive Moment.

Bridge 1 Run 5: Two trucks separated to provide maximum negative moment, center of bridge.

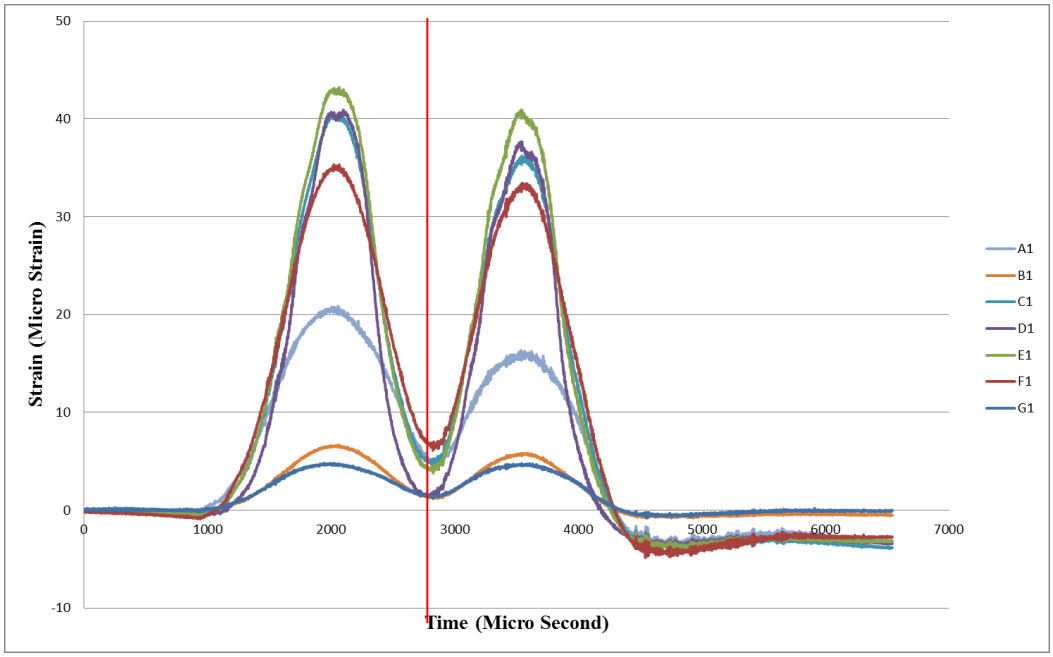

Figure G23. Bridge 1 Run 5 Girder Strains, Gage Line 1.

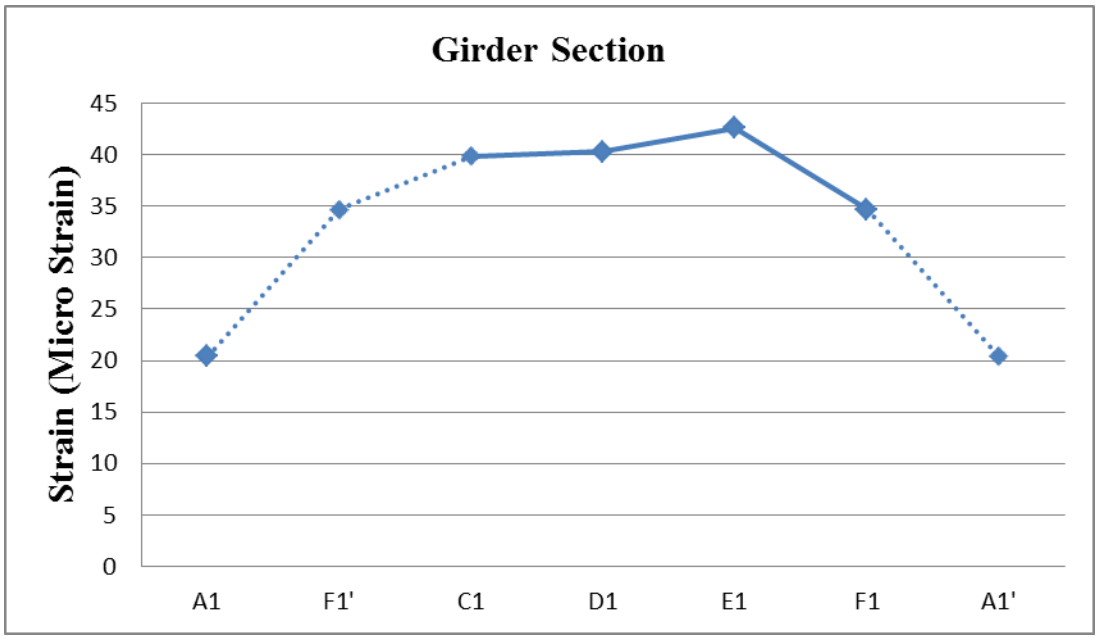

Figure G24. Bridge 1 Run 5 Girder Strains for Maximum Positive Moment.

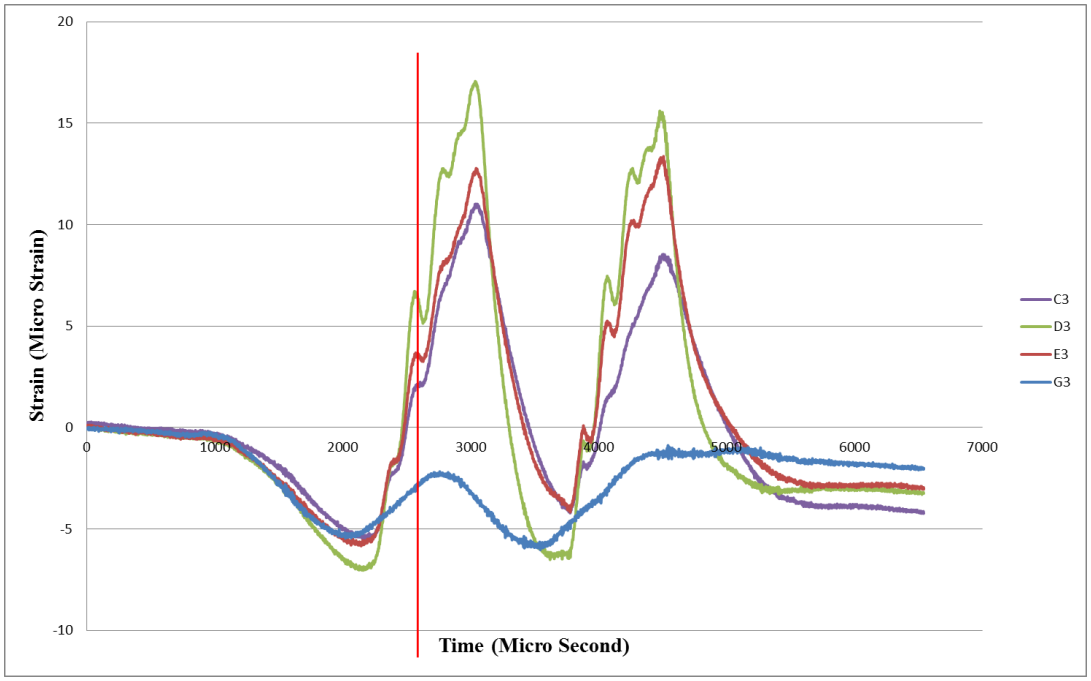

Figure G25. Bridge 1 Run 5 Girder Strains gage Line 3.

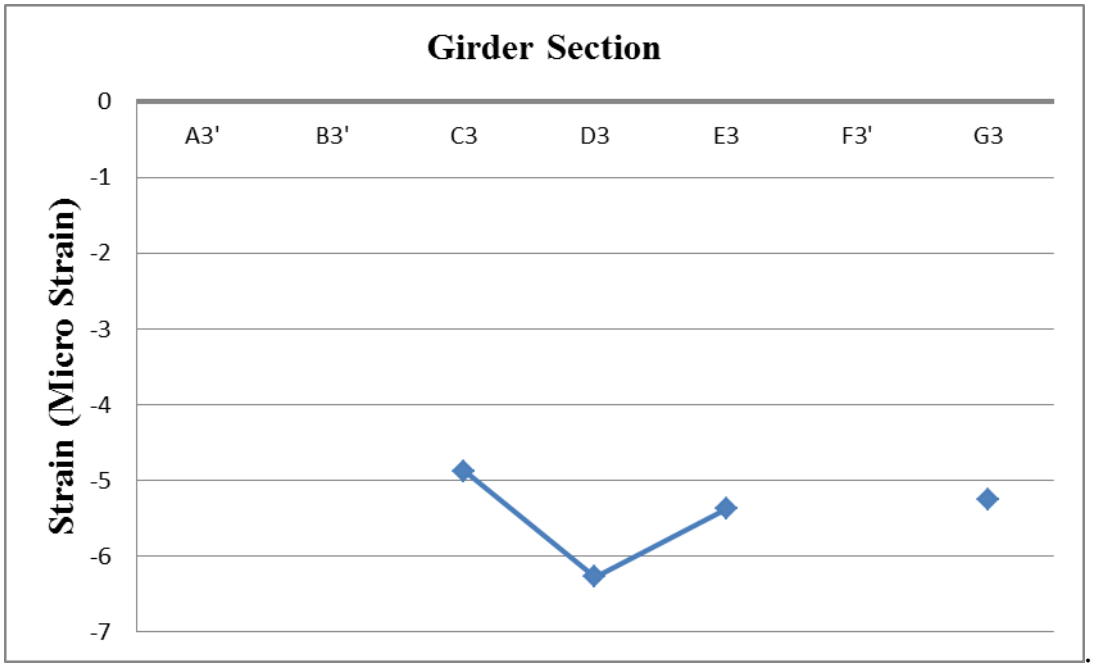

Figure G26. Bridge 1 Run 5 Girder Strains for Maximum Negative Moment.

Bridge 1 Run 8: Two trucks minimally separated, center of bridge.

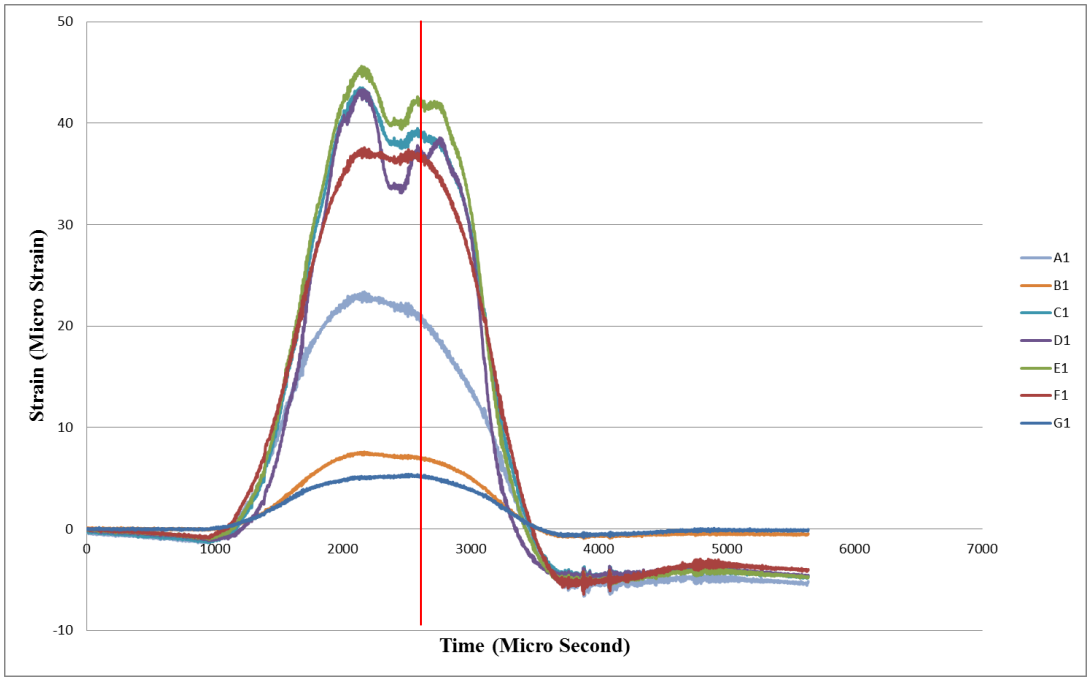

Figure G27. Bridge 1 Run 8 Girder Strains, Gage Line 1.

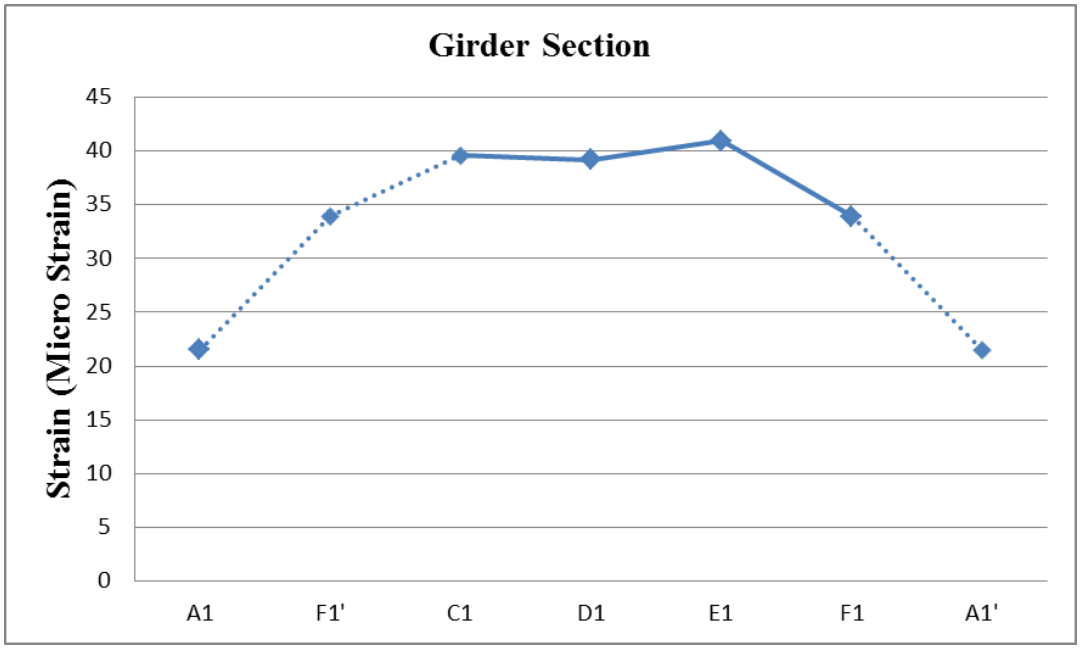

Figure G28. Bridge 1 Run 8 Girder Strains for Maximum Positive Moment.

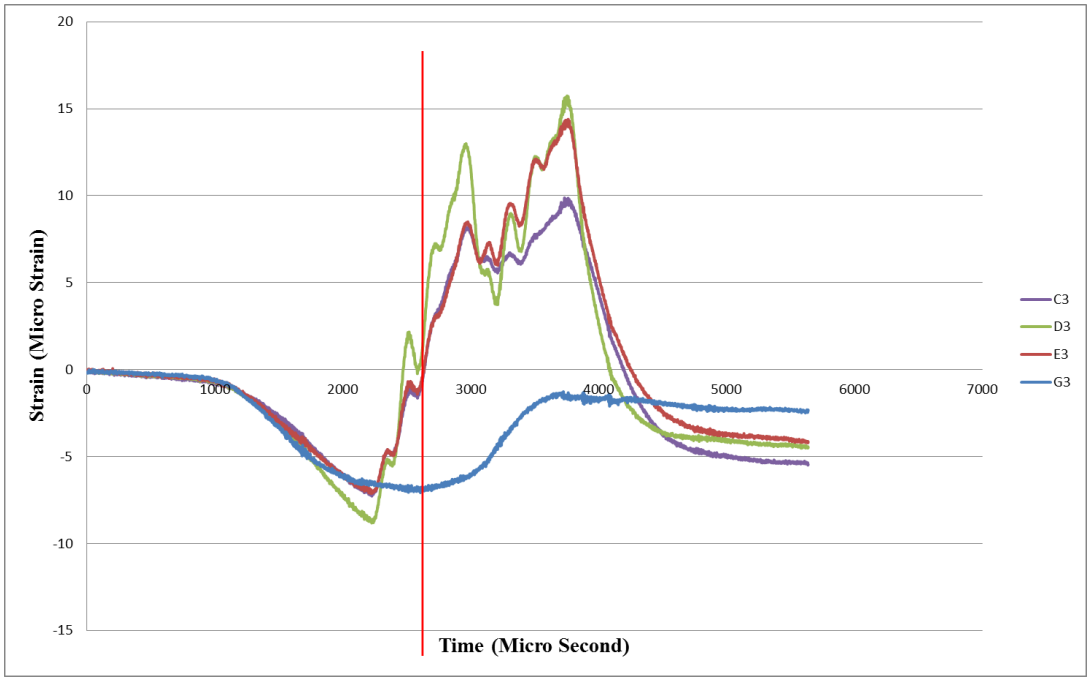

Figure G29. Bridge 1 Run 8 Girder Strains, Gage Line 3.

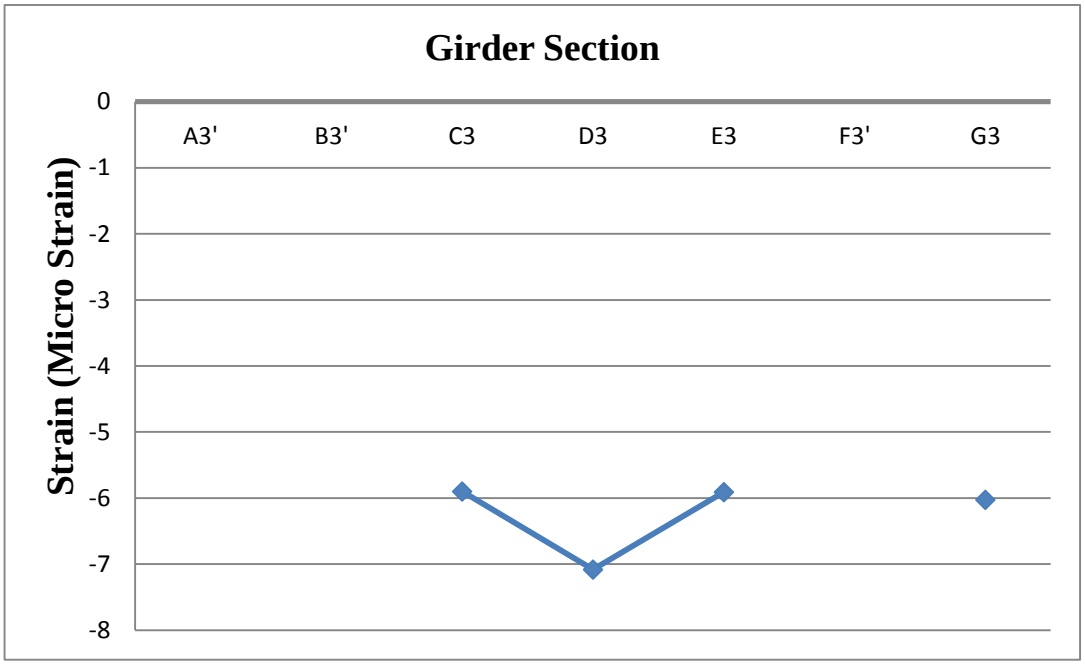

Figure G30. Bridge 1 Run 8 Girder Strains for Maximum Negative Moment.

Bridge 1 Run 11: One truck, center of bridge.

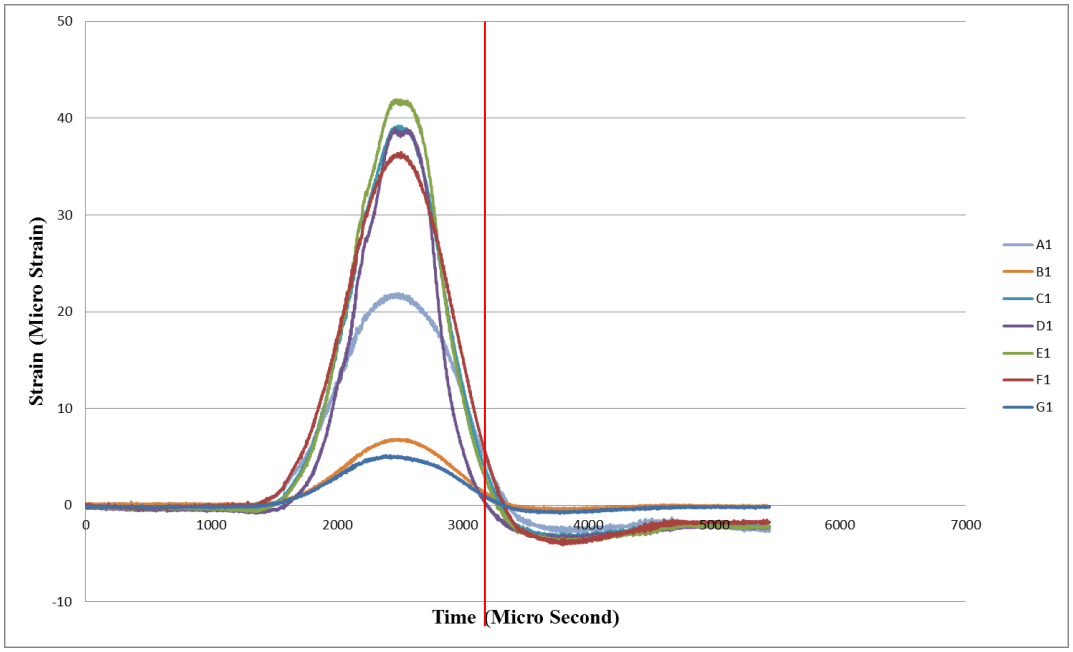

Figure G31. Bridge 1 Run 11 Girder Strains, Gage Line 1.

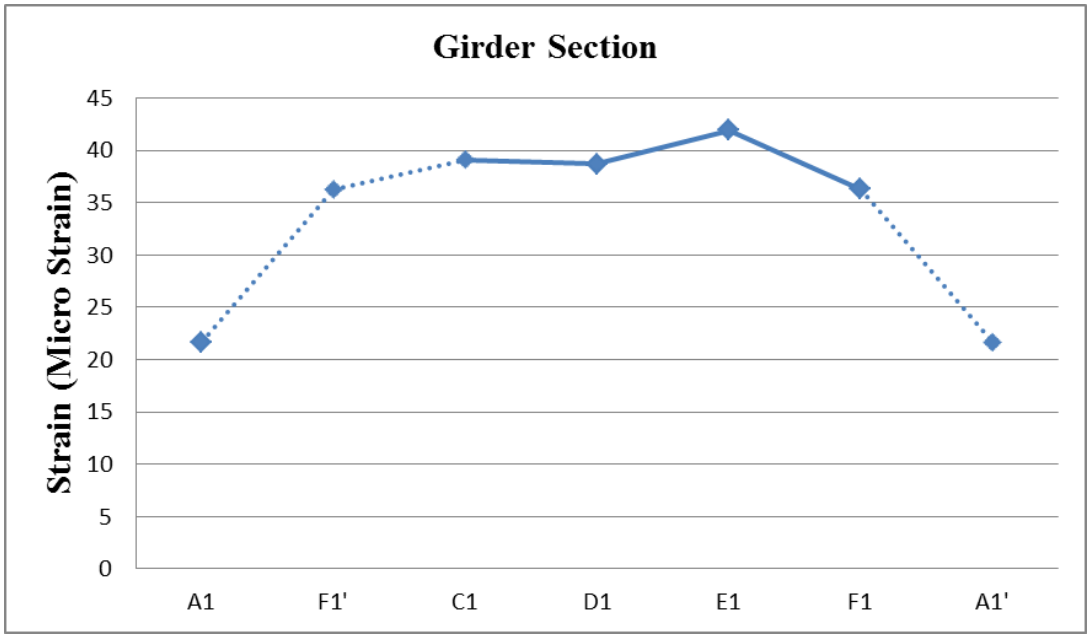

Figure G32. Bridge 1 Run 11 Girder Strains for Maximum Positive Moment.

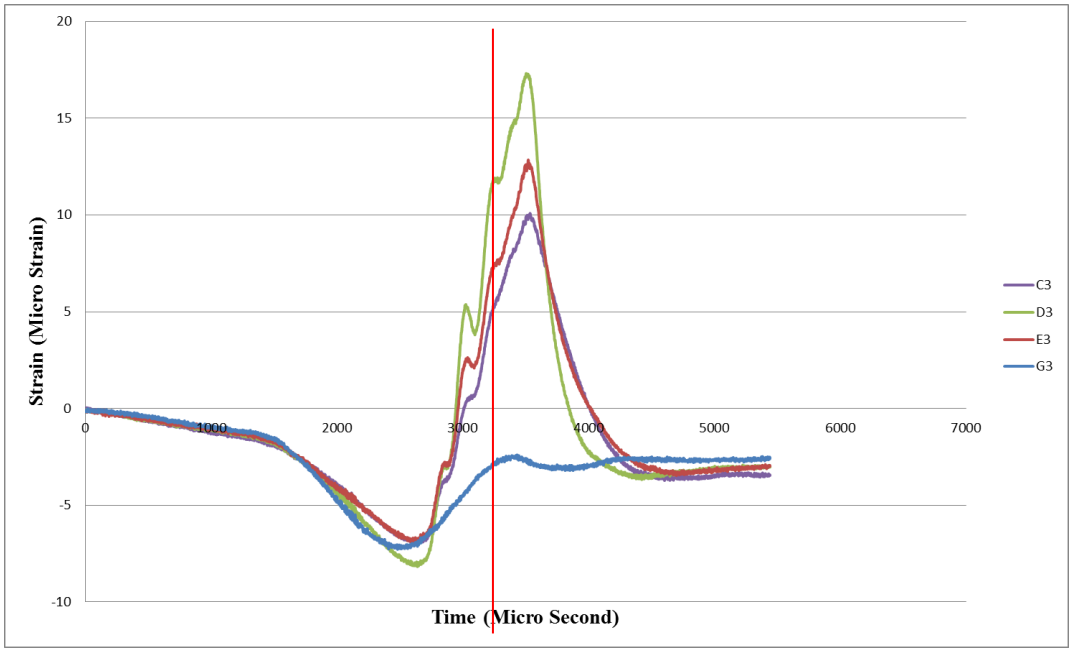

Figure G33. Bridge 1 Run 11 Girder Strains, Gage Line 3.

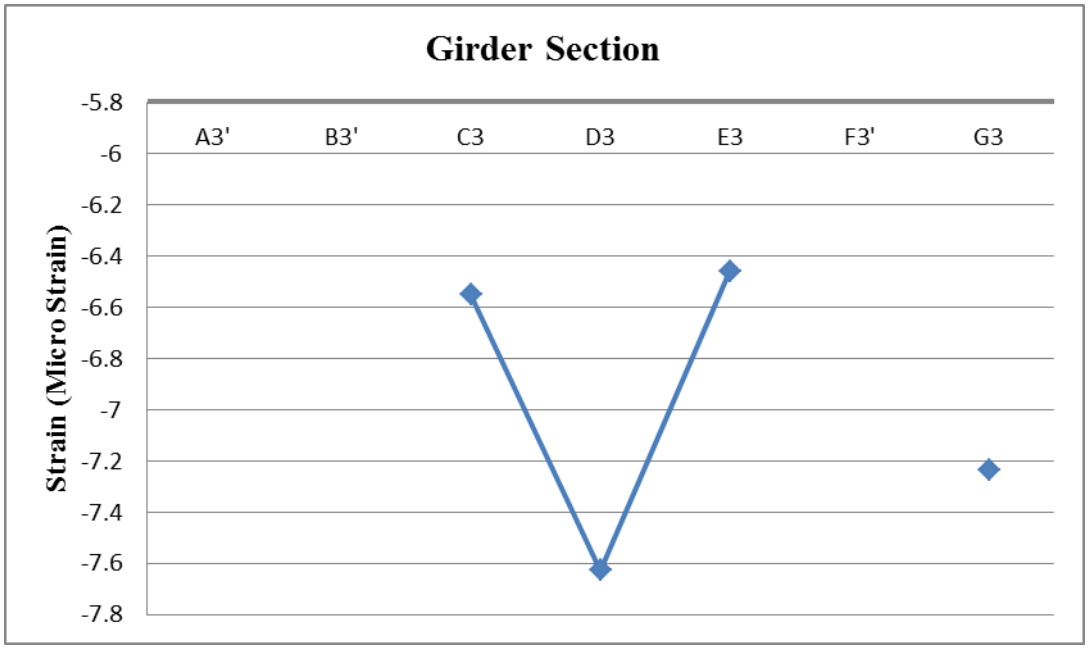

Figure G34. Bridge 1 Run 11 Girder Strains for Maximum Negative Moment.

Bridge 2 Run 1: Two trucks side by side, centered in each lane.

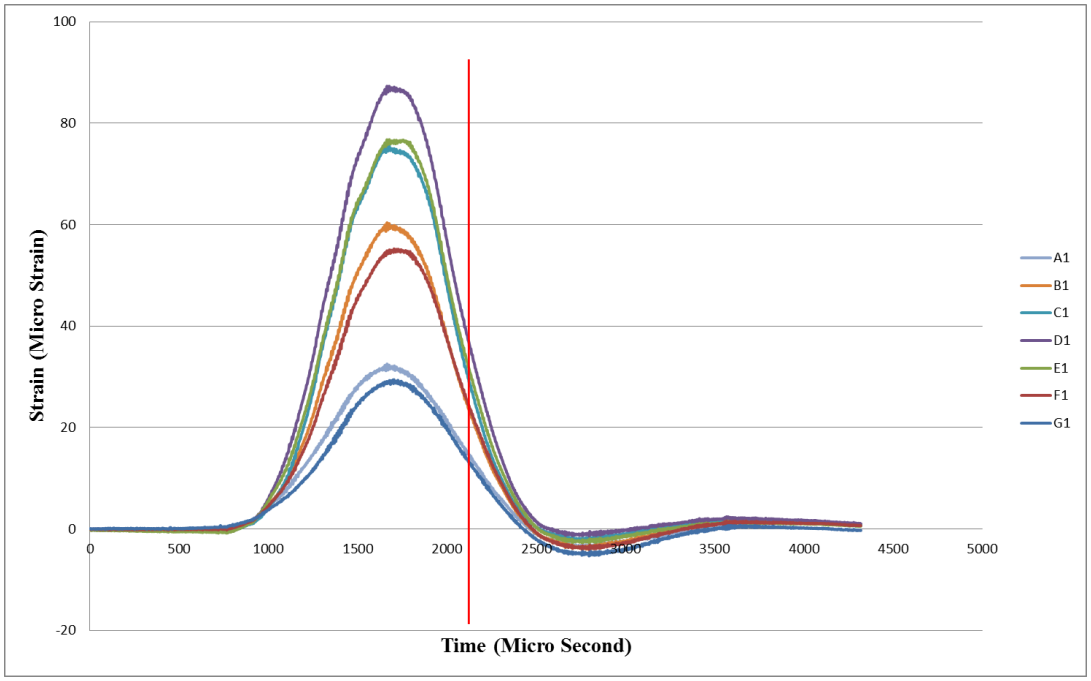

Figure G35. Bridge 2 Run 1 Girder Strains, Gage Line 1.

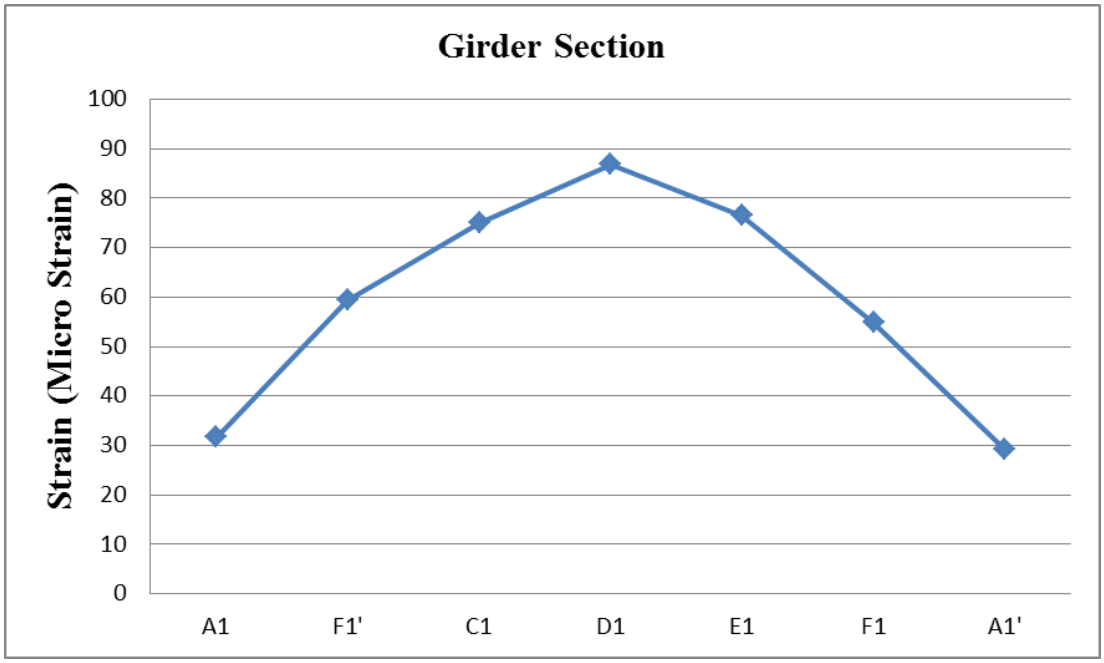

Figure G36. Bridge 2 Run 1 Girder Strains for Maximum Positive Moment.

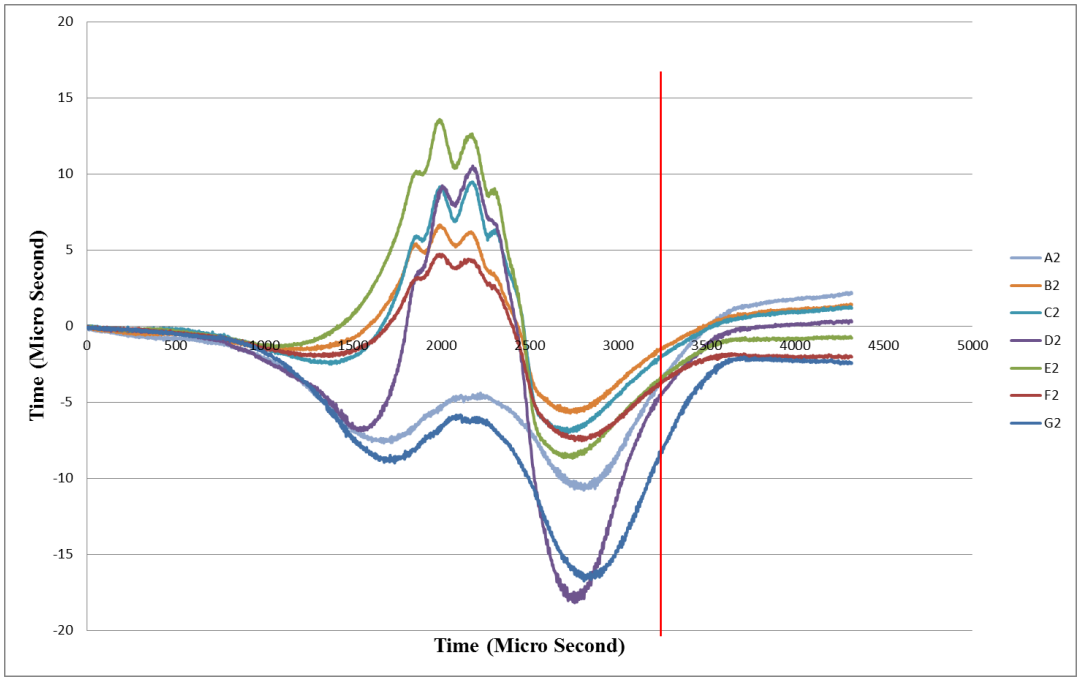

Figure G37. Bridge 2 Run 1 Girder Strains, Gage Line 2.

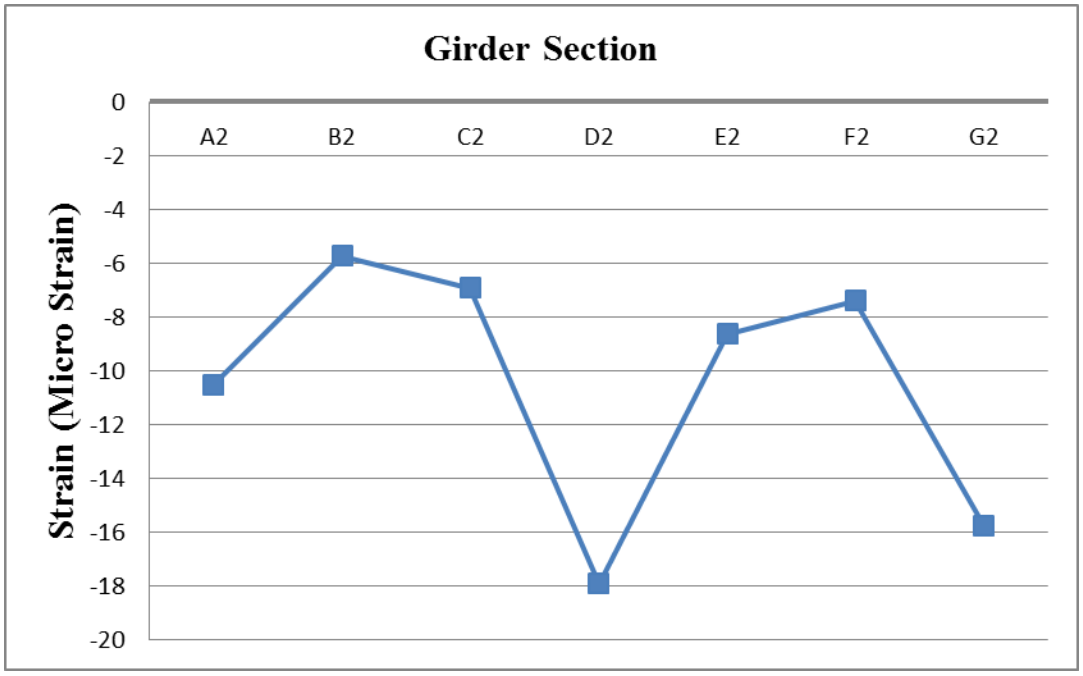

Figure G38. Bridge 2 Run 1 Girder Strains for Maximum Negative Moment.

APPENDIX H: V_n=V_u SECTIONAL METHOD ITERATION PROCEURE

The following example calculation is performed on an AASHTO Type II beam (modeled after Beam 1- Test 2 in Chapter 4) to illustrate how to determine the nominal shear capacity (Vn) using the general LRFD method by iteration to achieve $V_u=V_n$. Note this procedure is not how the general method as outlined in the LRFD Code is applied in design, where $V_u=V_n$ is not enforced. The beam characteristics are given in Table H1.

Table H1. Beam Parameters.

Variable	Value	Unit(s)
Beam type	AASHTO II	-
Area (Ac)	369	in^2
Clear span	14.83	ft
Weight	384	lb/ft
Flange width (be)	12	in
Web Thicknes (bv)	6	in
Yt	20.17	in
Yb	15.83	in
St	2530	in^3
Sb	3220	in^3
I	51000	in^4
Height (in)	36	in
f'c (28)	8.6	ksi
Ec beam	5622.12	ksi
f's (ksi)	270	ksi
# of Strands	16	#
Diameter	0.5	in
Nominal area	0.15	in^2
fpe	23.25	kips/strand
fpc	1.01	ksi
Bar size	3	#
# beams	1	#
Ep	28500	ksi
Av	0.221	in^2
fy	60	ksi
Stirrups spacing	21	in
vu	0.746	ksi
vu/f'c	0.008	<0.125
S_max	20.9	in (<24 in)
k	0.28	-
dp	29.0	in
c	9.07	in
Aps	2.1	in^2
fpu	270	ksi
f'c slab	8.6	ksi
β1	0.65	-
be	12	in
a	5.897509328	in
de	29	in
de-a/2	26.05124534	in
0.9de	26.1	in
0.72h	25.92	in
dv	26.10	in

The iteration process starts by assuming a value for V_u. In this example, the iteration is started by assuming that V_u=200 kips. V_n is then calculated with the standard LRFD procedure; results are shown in column 1 in Table H2. Since the calculated V_n at the first iteration (100 kips) is smaller than the assumed V_u, a smaller value of V_u is then taken in the second iteration. This process is repeated until convergrence at $V_u = V_n$ (at approximately 105.2 kips). In Table H2, this has been achieved at the fifth iteration, as shown below.

Table H2. Results of Iteration.

Iteraion #	1	2	3	4	5
Vu (kips)	200.00	150.00	100.00	105.00	105.20
Mu (ft-kips)	376.50	283.70	190.89	200.17	200.55
ε_x (original)	-0.0003976	-0.0019459	-0.0034943	-0.0033394	-0.0033332
ε_x (alternative)	-0.0000115	-0.0000561	-0.0001008	-0.0000963	-0.0000962
θ (degrees)	28.96	28.80	28.65	28.66	28.66
β	4.84	5.01	5.19	5.17	5.17
Vc (kips)	70.26	72.72	75.36	75.08	75.07
Vs (kips)	29.75	29.94	30.14	30.12	30.12
Vn (kips)	100.01	102.66	105.49	105.20	105.19

where:

$$\varepsilon_s = \frac{|M_u| + 0.5N_u + |(V_u - V_p)| - A_{ps}f_{po}}{(E_s A_s + E_p A_{ps})}$$

When ε_x is negative, it is taken as either zero or recalculated as the following:

$$\varepsilon_s = \frac{|M_u| + 0.5N_u + |(V_u - V_p)| - A_{ps}f_{po}}{(E_s A_s + E_p A_{ps} + E_c A_{ct})}$$

$$S_{xe} = \frac{1.38\, S_x}{0.63 + a_g}$$ (for members having less than the minimum shear reinforcement)

$$S_{xe} = S_{ze} = 12$$ (for members having at least the minimum shear reinforcement)

<u>For the first iteration</u>:

$$\beta 1 = \frac{4.8}{(1 + 750\varepsilon_s)} = \frac{4.8}{1 + 750(-0.0000115)} = 4.84$$

$$\theta 1 = 29 + 3500\varepsilon_s = 29 + 3500(-0.0000115) = 28.96^0$$

$$V_c 1 = 0.0316\, \beta \sqrt{f'_c}\, b_v d_v = 0.0316\,(4.84)(6)(\sqrt{8.6})(26.10) = 70.26 \text{ kips}$$

$$V_s 1 = \frac{A_v f_y d_v (\cot\theta + \cot\alpha)\sin\alpha}{S} = \frac{(0.221)(60)(26.1)(\cot 28.96)}{21} = 29.75 \text{ kips}$$

$$V_n1 = V_c1 + V_s1 + V_p = 70.26 + 29.75 + 0 = 100.01 \text{ kips}$$

This process is continued for the remaining iterations, as shown in Table H2.

APPENDIX I: REGRESSION ANALYSIS

Table I1. LRFD Model Regression Analysis Results.

#	f'c (ksi)	Stress (ksi)	Stirrups Spacing(in)	h (in)	(FEA/LRFD)	Reg.1	Reg.2	FEA/(Reg.1*LRFD)	FEA/(Reg.2*LRFD)
1	5.5	0.5	3	36	1.19	0.91	0.66	1.31	1.81
2	5.5	1.5	3	36	1.30	1.11	1.18	1.17	1.10
3	8	0.5	3	36	1.40	0.94	0.74	1.49	1.88
4	5.5	0.5	24	36	1.93	1.65	1.77	1.17	1.09
5	8	1.5	24	36	2.76	1.87	2.38	1.48	1.16
6	8	1.5	3	36	1.55	1.14	1.27	1.37	1.22
7	5.5	1.5	24	36	2.64	1.85	2.29	1.43	1.15
8	8	0.5	24	36	1.95	1.67	1.86	1.17	1.05
9	5.5	2.5	3	36	1.33	1.31	1.28	1.01	1.04
10	8	2.5	24	36	2.94	2.07	2.48	1.42	1.19
11	8	2.5	3	36	1.57	1.34	1.37	1.18	1.15
12	5.5	2.5	24	36	2.89	2.05	2.40	1.41	1.21
13	5.5	0.5	12	36	1.70	1.23	1.46	1.39	1.17
14	8	1.5	12	36	2.50	1.45	2.07	1.72	1.21
15	5.5	1.5	12	36	2.42	1.43	1.98	1.69	1.22
16	8	0.5	12	36	1.77	1.25	1.54	1.42	1.15
17	5.5	2.5	12	36	2.61	1.63	2.08	1.61	1.25
18	8	2.5	12	36	2.64	1.65	2.17	1.60	1.22
19	5.5	0.5	3	36	1.33	0.91	0.66	1.46	2.02
20	5.5	1.5	3	36	1.50	1.11	1.18	1.35	1.27
21	8	0.5	3	36	1.54	0.94	0.74	1.65	2.07
22	5.5	0.5	24	36	2.10	1.65	1.77	1.27	1.18
23	8	1.5	24	36	2.55	1.87	2.38	1.36	1.07
24	8	1.5	3	36	1.56	1.14	1.27	1.38	1.23
25	5.5	1.5	24	36	2.51	1.85	2.29	1.36	1.09
26	8	0.5	24	36	2.10	1.67	1.86	1.26	1.13
27	5.5	2.5	3	36	1.46	1.31	1.28	1.11	1.14
28	8	2.5	24	36	2.64	2.07	2.48	1.27	1.06
29	8	2.5	3	36	1.46	1.34	1.37	1.09	1.07
30	5.5	2.5	24	36	2.42	2.05	2.40	1.18	1.01
31	5.5	0.5	12	36	2.41	1.23	1.46	1.97	1.65
32	8	1.5	12	36	2.39	1.45	2.07	1.65	1.15
33	5.5	1.5	12	36	2.72	1.43	1.98	1.90	1.37
34	8	0.5	12	36	1.90	1.25	1.54	1.52	1.23
35	5.5	2.5	12	36	2.56	1.63	2.08	1.58	1.23
36	8	2.5	12	36	2.38	1.65	2.17	1.45	1.10
37	5.5	0.5	3	36	1.18	0.91	0.66	1.29	1.79
38	5.5	1.5	3	36	1.37	1.11	1.18	1.23	1.16
39	8	0.5	3	36	1.32	0.94	0.74	1.42	1.78
40	5.5	0.5	24	36	1.96	1.65	1.77	1.19	1.11
41	8	1.5	24	36	2.47	1.87	2.38	1.32	1.04
42	8	1.5	3	36	1.57	1.14	1.27	1.39	1.24
43	5.5	1.5	24	36	2.36	1.85	2.29	1.28	1.03
44	8	0.5	24	36	1.82	1.67	1.86	1.09	0.98
45	5.5	2.5	3	36	1.52	1.31	1.28	1.16	1.18
46	8	2.5	24	36	2.75	2.07	2.48	1.33	1.11
47	8	2.5	3	36	1.76	1.34	1.37	1.32	1.29
48	5.5	2.5	24	36	2.77	2.05	2.40	1.35	1.15
49	5.5	0.5	12	36	1.67	1.23	1.46	1.36	1.14
50	8	1.5	12	36	2.37	1.45	2.07	1.63	1.15

Table I1. LRFD Model Regression Analysis Results (cont).

#	f'c (ksi)	Stress (ksi)	Stirrups Spacing(in)	h (in)	(FEA/LRFD)	Reg.1	Reg.2	FEA/(Reg.1*LRFD)	FEA/(Reg.2*LRFD)
51	5.5	1.5	12	36	2.20	1.43	1.98	1.54	1.11
52	8	0.5	12	36	1.71	1.25	1.54	1.37	1.11
53	5.5	2.5	12	36	2.42	1.63	2.08	1.48	1.16
54	8	2.5	12	36	2.73	1.65	2.17	1.65	1.26
55	5.5	0.5	3	36	1.18	0.91	0.66	1.29	1.78
56	5.5	1.5	3	36	1.37	1.11	1.18	1.23	1.16
57	8	0.5	3	36	1.36	0.94	0.74	1.46	1.83
58	5.5	0.5	24	36	1.92	1.65	1.77	1.16	1.08
59	8	1.5	24	36	2.62	1.87	2.38	1.40	1.10
60	8	1.5	3	36	1.59	1.14	1.27	1.40	1.25
61	5.5	1.5	24	36	2.42	1.85	2.29	1.31	1.06
62	8	0.5	24	36	2.02	1.67	1.86	1.21	1.09
63	5.5	2.5	3	36	1.50	1.31	1.28	1.15	1.17
64	8	2.5	24	36	2.53	2.07	2.48	1.22	1.02
65	8	2.5	3	36	1.73	1.34	1.37	1.29	1.26
66	5.5	2.5	24	36	2.53	2.05	2.40	1.23	1.05
67	5.5	0.5	12	36	2.53	1.23	1.46	2.06	1.74
68	8	1.5	12	36	2.38	1.45	2.07	1.64	1.15
69	5.5	1.5	12	36	2.91	1.43	1.98	2.04	1.47
70	8	0.5	12	36	1.91	1.25	1.54	1.52	1.23
71	5.5	2.5	12	36	3.02	1.63	2.08	1.86	1.45
72	8	2.5	12	36	2.57	1.65	2.17	1.56	1.19
73	5.5	0.5	3	45	1.40	1.07	0.64	1.30	2.19
74	5.5	1.5	3	45	1.77	1.27	1.16	1.39	1.52
75	8	0.5	3	45	1.58	1.10	0.73	1.44	2.18
76	5.5	0.5	24	45	2.21	1.81	1.75	1.22	1.26
77	8	1.5	24	45	2.94	2.03	2.36	1.45	1.24
78	8	1.5	3	45	1.93	1.30	1.25	1.49	1.55
79	5.5	1.5	24	45	2.94	2.01	2.28	1.46	1.29
80	8	0.5	24	45	2.01	1.83	1.84	1.09	1.09
81	5.5	2.5	3	45	1.84	1.47	1.26	1.25	1.45
82	8	2.5	24	45	2.97	2.23	2.46	1.33	1.20
83	8	2.5	3	45	1.99	1.50	1.35	1.33	1.47
84	5.5	2.5	24	45	4.92	2.21	2.38	2.22	2.07
85	5.5	0.5	12	45	1.92	1.39	1.44	1.38	1.33
86	8	1.5	12	45	2.67	1.61	2.05	1.66	1.30
87	5.5	1.5	12	45	2.58	1.59	1.96	1.62	1.31
88	8	0.5	12	45	1.88	1.41	1.53	1.33	1.23
89	5.5	2.5	12	45	2.68	1.79	2.07	1.50	1.30
90	8	2.5	12	45	2.77	1.81	2.15	1.53	1.29
91	5.5	0.5	3	45	1.45	1.07	0.64	1.35	2.27
92	5.5	1.5	3	45	1.79	1.27	1.16	1.40	1.54
93	8	0.5	3	45	1.62	1.10	0.73	1.47	2.23
94	5.5	0.5	24	45	2.42	1.81	1.75	1.34	1.38
95	8	1.5	24	45	2.94	2.03	2.36	1.45	1.24
96	8	1.5	3	45	1.72	1.30	1.25	1.32	1.37
97	5.5	1.5	24	45	2.78	2.01	2.28	1.38	1.22
98	8	0.5	24	45	2.38	1.83	1.84	1.30	1.29
99	5.5	2.5	3	45	1.79	1.47	1.26	1.21	1.41
100	8	2.5	24	45	2.68	2.23	2.46	1.20	1.09
101	8	2.5	3	45	1.92	1.50	1.35	1.28	1.42

Table I1. LRFD Model Regression Analysis Results (cont).

#	f'c (ksi)	Stress (ksi)	Stirrups Spacing(in)	h (in)	(FEA/LRFD)	Reg.1	Reg.2	FEA/(Reg.1*LRFD)	FEA/(Reg.2*LRFD)
102	5.5	2.5	24	45	2.66	2.21	2.38	1.20	1.12
103	5.5	0.5	12	45	2.08	1.39	1.44	1.50	1.44
104	8	1.5	12	45	2.73	1.61	2.05	1.69	1.33
105	5.5	1.5	12	45	2.58	1.59	1.96	1.62	1.31
106	8	0.5	12	45	2.12	1.41	1.53	1.50	1.39
107	5.5	2.5	12	45	2.37	1.79	2.07	1.33	1.15
108	8	2.5	12	45	2.53	1.81	2.15	1.40	1.18
109	5.5	0.5	3	45	1.27	1.07	0.64	1.18	1.98
110	5.5	1.5	3	45	1.57	1.27	1.16	1.23	1.35
111	8	0.5	3	45	1.42	1.10	0.73	1.30	1.96
112	5.5	0.5	24	45	1.82	1.81	1.75	1.00	1.04
113	8	1.5	24	45	2.64	2.03	2.36	1.30	1.12
114	8	1.5	3	45	1.76	1.30	1.25	1.36	1.41
115	5.5	1.5	24	45	2.42	2.01	2.28	1.20	1.06
116	8	0.5	24	45	1.88	1.83	1.84	1.03	1.02
117	5.5	2.5	3	45	1.64	1.47	1.26	1.11	1.30
118	8	2.5	24	45	3.10	2.23	2.46	1.39	1.26
119	8	2.5	3	45	1.94	1.50	1.35	1.29	1.44
120	5.5	2.5	24	45	2.89	2.21	2.38	1.31	1.21
121	5.5	0.5	12	45	1.70	1.39	1.44	1.22	1.18
122	8	1.5	12	45	2.45	1.61	2.05	1.52	1.19
123	5.5	1.5	12	45	2.25	1.59	1.96	1.42	1.15
124	8	0.5	12	45	1.80	1.41	1.53	1.28	1.18
125	5.5	2.5	12	45	2.53	1.79	2.07	1.41	1.22
126	8	2.5	12	45	2.94	1.81	2.15	1.62	1.37
127	5.5	0.5	3	45	1.30	1.07	0.64	1.21	2.03
128	5.5	1.5	3	45	1.60	1.27	1.16	1.26	1.38
129	8	0.5	3	45	1.51	1.10	0.73	1.38	2.08
130	5.5	0.5	24	45	2.04	1.81	1.75	1.13	1.16
131	8	1.5	24	45	2.87	2.03	2.36	1.41	1.22
132	8	1.5	3	45	1.82	1.30	1.25	1.41	1.46
133	5.5	1.5	24	45	2.48	2.01	2.28	1.23	1.09
134	8	0.5	24	45	2.13	1.83	1.84	1.16	1.16
135	5.5	2.5	3	45	1.63	1.47	1.26	1.10	1.29
136	8	2.5	24	45	2.91	2.23	2.46	1.30	1.18
137	8	2.5	3	45	1.94	1.50	1.35	1.30	1.44
138	5.5	2.5	24	45	2.81	2.21	2.38	1.27	1.18
139	5.5	0.5	12	45	1.91	1.39	1.44	1.38	1.33
140	8	1.5	12	45	2.57	1.61	2.05	1.59	1.25
141	5.5	1.5	12	45	2.32	1.59	1.96	1.46	1.18
142	8	0.5	12	45	2.04	1.41	1.53	1.44	1.34
143	5.5	2.5	12	45	2.40	1.79	2.07	1.34	1.16
144	8	2.5	12	45	2.81	1.81	2.15	1.55	1.31
145	5.5	0.5	3	54	1.56	1.24	0.62	1.26	2.51
146	5.5	1.5	3	54	2.01	1.44	1.14	1.40	1.75
147	8	0.5	3	54	1.74	1.26	0.71	1.38	2.45
148	5.5	0.5	24	54	2.42	1.97	1.74	1.23	1.40
149	8	1.5	24	54	3.19	2.19	2.34	1.46	1.36
150	8	1.5	3	54	2.22	1.46	1.23	1.52	1.80
151	5.5	1.5	24	54	3.23	2.17	2.26	1.49	1.43
152	8	0.5	24	54	2.37	1.99	1.82	1.19	1.30

Table I1. LRFD Model Regression Analysis Results (cont).

#	f'c (ksi)	Stress (ksi)	Stirrups Spacing(in)	h (in)	(FEA/LRFD)	Reg.1	Reg.2	FEA/(Reg.1*LRFD)	FEA/(Reg.2*LRFD)
153	5.5	2.5	3	54	2.03	1.64	1.25	1.24	1.63
154	8	2.5	24	54	3.49	2.39	2.44	1.46	1.43
155	8	2.5	3	54	2.26	1.66	1.33	1.36	1.70
156	5.5	2.5	24	54	3.47	2.37	2.36	1.46	1.47
157	5.5	0.5	12	54	2.11	1.55	1.42	1.36	1.49
158	8	1.5	12	54	3.01	1.77	2.03	1.70	1.48
159	5.5	1.5	12	54	2.81	1.75	1.95	1.61	1.45
160	8	0.5	12	54	2.04	1.57	1.51	1.30	1.35
161	5.5	2.5	12	54	2.98	1.95	2.05	1.53	1.46
162	8	2.5	12	54	3.07	1.97	2.13	1.55	1.44
163	5.5	0.5	3	54	1.58	1.24	0.62	1.28	2.54
164	5.5	1.5	3	54	1.96	1.44	1.14	1.36	1.71
165	8	0.5	3	54	1.77	1.26	0.71	1.40	2.50
166	5.5	0.5	24	54	2.59	1.97	1.74	1.32	1.49
167	8	1.5	24	54	3.08	2.19	2.34	1.40	1.31
168	8	1.5	3	54	2.14	1.46	1.23	1.47	1.74
169	5.5	1.5	24	54	3.08	2.17	2.26	1.42	1.36
170	8	0.5	24	54	2.61	1.99	1.82	1.31	1.43
171	5.5	2.5	3	54	1.91	1.64	1.25	1.17	1.53
172	8	2.5	24	54	2.93	2.39	2.44	1.22	1.20
173	8	2.5	3	54	2.10	1.66	1.33	1.27	1.58
174	5.5	2.5	24	54	2.75	2.37	2.36	1.16	1.16
175	5.5	0.5	12	54	2.22	1.55	1.42	1.43	1.56
176	8	1.5	12	54	2.67	1.77	2.03	1.51	1.32
177	5.5	1.5	12	54	2.72	1.75	1.95	1.55	1.40
178	8	0.5	12	54	2.22	1.57	1.51	1.41	1.47
179	5.5	2.5	12	54	2.47	1.95	2.05	1.27	1.21
180	8	2.5	12	54	2.58	1.97	2.13	1.31	1.21
181	5.5	0.5	3	54	1.41	1.24	0.62	1.14	2.26
182	5.5	1.5	3	54	1.72	1.44	1.14	1.20	1.50
183	8	0.5	3	54	1.59	1.26	0.71	1.26	2.25
184	5.5	0.5	24	54	2.07	1.97	1.74	1.05	1.19
185	8	1.5	24	54	3.13	2.19	2.34	1.43	1.34
186	8	1.5	3	54	1.95	1.46	1.23	1.34	1.59
187	5.5	1.5	24	54	3.10	2.17	2.26	1.43	1.37
188	8	0.5	24	54	2.09	1.99	1.82	1.05	1.15
189	5.5	2.5	3	54	1.68	1.64	1.25	1.03	1.35
190	8	2.5	24	54	3.48	2.39	2.44	1.45	1.42
191	8	2.5	3	54	2.04	1.66	1.33	1.23	1.53
192	5.5	2.5	24	54	3.47	2.37	2.36	1.46	1.47
193	5.5	0.5	12	54	1.85	1.55	1.42	1.19	1.30
194	8	1.5	12	54	2.83	1.77	2.03	1.60	1.39
195	5.5	1.5	12	54	2.74	1.75	1.95	1.56	1.41
196	8	0.5	12	54	1.88	1.57	1.51	1.19	1.25
197	5.5	2.5	12	54	2.80	1.95	2.05	1.43	1.37
198	8	2.5	12	54	3.17	1.97	2.13	1.60	1.48
199	5.5	0.5	3	54	1.45	1.24	0.62	1.17	2.33
200	5.5	1.5	3	54	1.77	1.44	1.14	1.23	1.54
201	8	0.5	3	54	1.65	1.26	0.71	1.31	2.33
202	5.5	0.5	24	54	2.39	1.97	1.74	1.21	1.37
203	8	1.5	24	54	3.48	2.19	2.34	1.59	1.48
204	8	1.5	3	54	1.93	1.46	1.23	1.33	1.57

Table I1. LRFD Model Regression Analysis Results (cont).

#	f'c (ksi)	Stress (ksi)	Stirrups Spacing(in)	h (in)	(FEA/LRFD)	Reg.1	Reg.2	FEA/(Reg.1*LRFD)	FEA/(Reg.2*LRFD)
205	5.5	1.5	24	54	3.09	2.17	2.26	1.42	1.37
206	8	0.5	24	54	2.45	1.99	1.82	1.23	1.34
207	5.5	2.5	3	54	1.70	1.64	1.25	1.04	1.37
208	8	2.5	24	54	3.19	2.39	2.44	1.33	1.30
209	8	2.5	3	54	1.91	1.66	1.33	1.15	1.43
210	5.5	2.5	24	54	2.75	2.37	2.36	1.16	1.17
211	5.5	0.5	12	54	2.10	1.55	1.42	1.35	1.48
212	8	1.5	12	54	3.03	1.77	2.03	1.71	1.49
213	5.5	1.5	12	54	2.69	1.75	1.95	1.53	1.38
214	8	0.5	12	54	2.19	1.57	1.51	1.39	1.45
215	5.5	2.5	12	54	2.58	1.95	2.05	1.32	1.26
216	8	2.5	12	54	2.91	1.97	2.13	1.47	1.36
				Mean	2.25	1.64	1.70	1.37	1.39
				STDEV.	0.59	0.37	0.55	0.19	0.32
				COV	0.26	0.23	0.32	0.14	0.23

Table I2. Standard Code Regression Analysis Results.

#	f'c (ksi)	Stress (ksi)	Stirrups Spacing(in)	h (in)	(FEA/STD.)	Reg.3	FEA/(Reg.3*LRFD)
1	5.5	0.5	3	36	1.27	0.74	1.73
2	5.5	1.5	3	36	1.39	0.87	1.60
3	8	0.5	3	36	1.30	0.82	1.58
4	5.5	0.5	24	36	1.30	0.95	1.37
5	8	1.5	24	36	1.95	1.16	1.68
6	8	1.5	3	36	1.44	0.95	1.52
7	5.5	1.5	24	36	1.78	1.08	1.65
8	8	0.5	24	36	1.38	1.03	1.33
9	5.5	2.5	3	36	1.42	1.00	1.42
10	8	2.5	24	36	2.08	1.29	1.61
11	8	2.5	3	36	1.46	1.08	1.35
12	5.5	2.5	24	36	1.95	1.21	1.62
13	5.5	0.5	12	36	1.31	0.83	1.58
14	8	1.5	12	36	1.98	1.04	1.90
15	5.5	1.5	12	36	1.86	0.96	1.94
16	8	0.5	12	36	1.41	0.91	1.54
17	5.5	2.5	12	36	2.01	1.09	1.85
18	8	2.5	12	36	2.10	1.17	1.79
19	5.5	0.5	3	36	1.23	0.74	1.67
20	5.5	1.5	3	36	1.28	0.87	1.47
21	8	0.5	3	36	1.39	0.82	1.70
22	5.5	0.5	24	36	1.38	0.95	1.46
23	8	1.5	24	36	1.69	1.16	1.45
24	8	1.5	3	36	1.34	0.95	1.41
25	5.5	1.5	24	36	1.59	1.08	1.48
26	8	0.5	24	36	1.45	1.03	1.40
27	5.5	2.5	3	36	1.22	1.00	1.22
28	8	2.5	24	36	1.69	1.29	1.31
29	8	2.5	3	36	1.27	1.08	1.18
30	5.5	2.5	24	36	1.49	1.21	1.23
31	5.5	0.5	12	36	1.81	0.83	2.18
32	8	1.5	12	36	1.76	1.04	1.69
33	5.5	1.5	12	36	1.95	0.96	2.03
34	8	0.5	12	36	1.47	0.91	1.61
35	5.5	2.5	12	36	1.77	1.09	1.63
36	8	2.5	12	36	1.69	1.17	1.45
37	5.5	0.5	3	36	1.15	0.74	1.55
38	5.5	1.5	3	36	1.33	0.87	1.54
39	8	0.5	3	36	1.29	0.82	1.57
40	5.5	0.5	24	36	1.15	0.95	1.22
41	8	1.5	24	36	1.52	1.16	1.31
42	8	1.5	3	36	1.53	0.95	1.61
43	5.5	1.5	24	36	1.39	1.08	1.29
44	8	0.5	24	36	1.12	1.03	1.08
45	5.5	2.5	3	36	1.48	1.00	1.48
46	8	2.5	24	36	1.69	1.29	1.31
47	8	2.5	3	36	1.72	1.08	1.59
48	5.5	2.5	24	36	1.63	1.21	1.35
49	5.5	0.5	12	36	1.13	0.83	1.36
50	8	1.5	12	36	1.64	1.04	1.58

Table I2. Standard Code Regression Analysis Results (cont).

#	f'c (ksi)	Stress (ksi)	Stirrups Spacing(in)	h (in)	(FEA/STD.)	Reg.3	FEA/(Reg.3*LRFD)
51	5.5	1.5	12	36	1.48	0.96	1.55
52	8	0.5	12	36	1.18	0.91	1.30
53	5.5	2.5	12	36	1.63	1.09	1.50
54	8	2.5	12	36	1.89	1.17	1.61
55	5.5	0.5	3	36	1.08	0.74	1.46
56	5.5	1.5	3	36	1.22	0.87	1.40
57	8	0.5	3	36	1.26	0.82	1.53
58	5.5	0.5	24	36	1.04	0.95	1.10
59	8	1.5	24	36	1.47	1.16	1.27
60	8	1.5	3	36	1.42	0.95	1.49
61	5.5	1.5	24	36	1.30	1.08	1.21
62	8	0.5	24	36	1.15	1.03	1.11
63	5.5	2.5	3	36	1.30	1.00	1.30
64	8	2.5	24	36	1.41	1.29	1.09
65	8	2.5	3	36	1.51	1.08	1.39
66	5.5	2.5	24	36	1.35	1.21	1.12
67	5.5	0.5	12	36	1.58	0.83	1.91
68	8	1.5	12	36	1.50	1.04	1.44
69	5.5	1.5	12	36	1.78	0.96	1.85
70	8	0.5	12	36	1.23	0.91	1.35
71	5.5	2.5	12	36	1.82	1.09	1.67
72	8	2.5	12	36	1.59	1.17	1.36
73	5.5	0.5	3	45	1.37	0.89	1.54
74	5.5	1.5	3	45	1.73	1.02	1.70
75	8	0.5	3	45	1.51	0.97	1.55
76	5.5	0.5	24	45	1.58	1.10	1.44
77	8	1.5	24	45	2.32	1.31	1.76
78	8	1.5	3	45	1.84	1.10	1.67
79	5.5	1.5	24	45	2.11	1.23	1.71
80	8	0.5	24	45	1.58	1.18	1.34
81	5.5	2.5	3	45	1.80	1.15	1.56
82	8	2.5	24	45	2.34	1.44	1.62
83	8	2.5	3	45	1.89	1.23	1.53
84	5.5	2.5	24	45	3.52	1.36	2.59
85	5.5	0.5	12	45	1.57	0.98	1.60
86	8	1.5	12	45	2.24	1.19	1.88
87	5.5	1.5	12	45	2.11	1.11	1.90
88	8	0.5	12	45	1.57	1.06	1.48
89	5.5	2.5	12	45	2.20	1.24	1.77
90	8	2.5	12	45	2.32	1.32	1.75
91	5.5	0.5	3	45	1.41	0.89	1.58
92	5.5	1.5	3	45	1.72	1.02	1.68
93	8	0.5	3	45	1.53	0.97	1.57
94	5.5	0.5	24	45	1.76	1.10	1.60
95	8	1.5	24	45	2.26	1.31	1.72
96	8	1.5	3	45	1.81	1.10	1.64
97	5.5	1.5	24	45	2.08	1.23	1.69
98	8	0.5	24	45	1.79	1.18	1.51
99	5.5	2.5	3	45	1.69	1.15	1.47
100	8	2.5	24	45	2.10	1.44	1.45
101	8	2.5	3	45	1.78	1.23	1.44

Table I2. Standard Code Regression Analysis Results (cont).

#	f'c (ksi)	Stress (ksi)	Stirrups Spacing(in)	h (in)	(FEA/STD.)	Reg.3	FEA/(Reg.3*LRFD)
102	5.5	2.5	24	45	2.03	1.36	1.49
103	5.5	0.5	12	45	1.67	0.98	1.71
104	8	1.5	12	45	2.27	1.19	1.90
105	5.5	1.5	12	45	2.10	1.11	1.89
106	8	0.5	12	45	1.86	1.06	1.75
107	5.5	2.5	12	45	2.02	1.24	1.63
108	8	2.5	12	45	2.18	1.32	1.65
109	5.5	0.5	3	45	1.17	0.89	1.31
110	5.5	1.5	3	45	1.45	1.02	1.42
111	8	0.5	3	45	1.31	0.97	1.35
112	5.5	0.5	24	45	1.10	1.10	1.00
113	8	1.5	24	45	1.64	1.31	1.25
114	8	1.5	3	45	1.62	1.10	1.47
115	5.5	1.5	24	45	1.46	1.23	1.19
116	8	0.5	24	45	1.17	1.18	0.99
117	5.5	2.5	3	45	1.51	1.15	1.31
118	8	2.5	24	45	1.93	1.44	1.33
119	8	2.5	3	45	1.79	1.23	1.45
120	5.5	2.5	24	45	1.75	1.36	1.28
121	5.5	0.5	12	45	1.14	0.98	1.16
122	8	1.5	12	45	1.67	1.19	1.40
123	5.5	1.5	12	45	1.51	1.11	1.36
124	8	0.5	12	45	1.23	1.06	1.16
125	5.5	2.5	12	45	1.70	1.24	1.37
126	8	2.5	12	45	2.01	1.32	1.52
127	5.5	0.5	3	45	1.20	0.89	1.35
128	5.5	1.5	3	45	1.48	1.02	1.45
129	8	0.5	3	45	1.40	0.97	1.43
130	5.5	0.5	24	45	1.25	1.10	1.13
131	8	1.5	24	45	1.85	1.31	1.41
132	8	1.5	3	45	1.69	1.10	1.53
133	5.5	1.5	24	45	1.56	1.23	1.27
134	8	0.5	24	45	1.34	1.18	1.13
135	5.5	2.5	3	45	1.50	1.15	1.30
136	8	2.5	24	45	1.91	1.44	1.32
137	8	2.5	3	45	1.80	1.23	1.46
138	5.5	2.5	24	45	1.81	1.36	1.33
139	5.5	0.5	12	45	1.29	0.98	1.32
140	8	1.5	12	45	1.80	1.19	1.51
141	5.5	1.5	12	45	1.60	1.11	1.44
142	8	0.5	12	45	1.41	1.06	1.32
143	5.5	2.5	12	45	1.68	1.24	1.36
144	8	2.5	12	45	2.00	1.32	1.51
145	5.5	0.5	3	54	1.52	1.04	1.45
146	5.5	1.5	3	54	1.95	1.17	1.66
147	8	0.5	3	54	1.63	1.13	1.45
148	5.5	0.5	24	54	1.76	1.25	1.40
149	8	1.5	24	54	2.43	1.47	1.65
150	8	1.5	3	54	2.08	1.26	1.66
151	5.5	1.5	24	54	2.35	1.38	1.70
152	8	0.5	24	54	1.80	1.34	1.34

Table I2. Standard Code Regression Analysis Results (cont).

#	f'c (ksi)	Stress (ksi)	Stirrups Spacing(in)	h (in)	(FEA/STD.)	Reg.3	FEA/(Reg.3*LRFD)
153	5.5	2.5	3	54	1.97	1.30	1.51
154	8	2.5	24	54	2.65	1.60	1.66
155	8	2.5	3	54	2.12	1.39	1.53
156	5.5	2.5	24	54	2.52	1.51	1.66
157	5.5	0.5	12	54	1.71	1.13	1.50
158	8	1.5	12	54	2.51	1.35	1.86
159	5.5	1.5	12	54	2.27	1.26	1.80
160	8	0.5	12	54	1.70	1.22	1.40
161	5.5	2.5	12	54	2.41	1.39	1.73
162	8	2.5	12	54	2.55	1.48	1.73
163	5.5	0.5	3	54	1.53	1.04	1.46
164	5.5	1.5	3	54	1.86	1.17	1.59
165	8	0.5	3	54	1.66	1.13	1.47
166	5.5	0.5	24	54	1.93	1.25	1.54
167	8	1.5	24	54	2.44	1.47	1.67
168	8	1.5	3	54	1.98	1.26	1.58
169	5.5	1.5	24	54	2.36	1.38	1.71
170	8	0.5	24	54	2.02	1.34	1.51
171	5.5	2.5	3	54	1.79	1.30	1.38
172	8	2.5	24	54	2.37	1.60	1.48
173	8	2.5	3	54	1.93	1.39	1.39
174	5.5	2.5	24	54	2.16	1.51	1.43
175	5.5	0.5	12	54	1.83	1.13	1.61
176	8	1.5	12	54	2.29	1.35	1.70
177	5.5	1.5	12	54	2.28	1.26	1.80
178	8	0.5	12	54	1.87	1.22	1.54
179	5.5	2.5	12	54	2.10	1.39	1.51
180	8	2.5	12	54	2.24	1.48	1.51
181	5.5	0.5	3	54	1.24	1.04	1.19
182	5.5	1.5	3	54	1.52	1.17	1.29
183	8	0.5	3	54	1.42	1.13	1.26
184	5.5	0.5	24	54	1.14	1.25	-
185	8	1.5	24	54	1.80	1.47	1.23
186	8	1.5	3	54	1.74	1.26	1.38
187	5.5	1.5	24	54	1.70	1.38	1.23
188	8	0.5	24	54	1.20	1.34	-
189	5.5	2.5	3	54	1.49	1.30	1.14
190	8	2.5	24	54	2.00	1.60	1.25
191	8	2.5	3	54	1.82	1.39	1.31
192	5.5	2.5	24	54	1.90	1.51	1.26
193	5.5	0.5	12	54	1.14	1.13	1.00
194	8	1.5	12	54	1.81	1.35	1.34
195	5.5	1.5	12	54	1.69	1.26	1.33
196	8	0.5	12	54	1.20	1.22	0.99
197	5.5	2.5	12	54	1.72	1.39	1.24
198	8	2.5	12	54	2.02	1.48	1.37
199	5.5	0.5	3	54	1.29	1.04	1.23
200	5.5	1.5	3	54	1.57	1.17	1.34
201	8	0.5	3	54	1.47	1.13	1.31
202	5.5	0.5	24	54	1.33	1.25	1.06
203	8	1.5	24	54	2.10	1.47	1.43
204	8	1.5	3	54	1.73	1.26	1.38

Table I2. Standard Code Regression Analysis Results (cont).

#	f'c (ksi)	Stress (ksi)	Stirrups Spacing(in)	h (in)	(FEA/STD.)	Reg.3	FEA/(Reg.3*LRFD)
205	5.5	1.5	24	54	1.79	1.38	1.29
206	8	0.5	24	54	1.43	1.34	1.07
207	5.5	2.5	3	54	1.52	1.30	1.16
208	8	2.5	24	54	1.98	1.60	1.24
209	8	2.5	3	54	1.71	1.39	1.24
210	5.5	2.5	24	54	1.64	1.51	1.08
211	5.5	0.5	12	54	1.31	1.13	1.16
212	8	1.5	12	54	2.00	1.35	1.49
213	5.5	1.5	12	54	1.72	1.26	1.36
214	8	0.5	12	54	1.42	1.22	1.17
215	5.5	2.5	12	54	1.69	1.39	1.21
216	8	2.5	12	54	1.96	1.48	1.33
				Mean	1.69	1.16	1.47
				STDEV.	0.43	0.24	0.33
				COV	0.26	0.21	0.22